VOLUME 75 SEPTEMBER 16, 1971 NUMBER 19

JPCHAx

THE JOURNAL OF PHYSICAL CHEMISTRY

PUBLISHED BIWEEKLY BY THE AMERICAN CHEMICAL SOCIETY

Keep pace with the new...

through these basic research journals of the American Chemical Society

The Journal of the American Chemical Society
The premier American chemistry journal publishing original research papers in every field. Biweekly.

*ACS members:	U.S. $22.00	Canada, PUAS $26.50	Other nations $27.50
Nonmembers:	U.S. $44.00	Canada, PUAS $48.50	Other nations $49.50

The Journal of Organic Chemistry
Embraces the field, from synthesis to structure to behavior. Biweekly publication.

*ACS members:	U.S. $20.00	Canada, PUAS $24.50	Other nations $25.50
Nonmembers:	U.S. $40.00	Canada, PUAS $44.50	Other nations $45.50

The Journal of Physical Chemistry
Maintains a balance between classical areas of chemistry and modern structural quantum oriented areas. Biweekly.

*ACS members:	U.S. $20.00	Canada, PUAS $24.00	Other nations $25.00
Nonmembers:	U.S. $40.00	Canada, PUAS $44.00	Other nations $45.00

Biochemistry
Covers enzymes, proteins, carbohydrates, lipids, nucleic acids and their metabolism, genetics, biosynthesis. Biweekly.

*ACS members:	U.S. $20.00	Canada, PUAS $23.00	Other nations $23.50
Nonmembers:	U.S. $40.00	Canada, PUAS $43.00	Other nations $43.50

The Journal of Agricultural and Food Chemistry
Places special emphasis on the chemical aspects of agricultural and food chemistry. Bimonthly.

*ACS members:	U.S. $10.00	Canada, PUAS $13.00	Other nations $13.50
Nonmembers:	U.S. $20.00	Canada, PUAS $23.00	Other nations $23.50

The Journal of Medicinal Chemistry
Emphasis is on synthesis, mode of action and pharmacology of medicinal agents. Monthly.

*ACS members:	U.S. $15.00	Canada, PUAS $18.00	Other nations $18.50
Nonmembers:	U.S. $30.00	Canada, PUAS $33.00	Other nations $33.50

The Journal of Chemical and Engineering Data
Quarterly journal presenting data on properties and behavior of both new and known chemical systems.

*ACS members:	U.S. $15.00	Canada, PUAS $18.00	Other nations $18.50
Nonmembers:	U.S. $30.00	Canada, PUAS $33.00	Other nations $33.50

Inorganic Chemistry
Publishes original research, both experimental and theoretical, in all phases of inorganic chemistry.

*ACS members:	U.S. $18.00	Canada, PUAS $21.00	Other nations $21.50
Nonmembers:	U.S. $36.00	Canada, PUAS $39.00	Other nations $39.50

Macromolecules
Presents original research on all fundamental aspects of polymer chemistry. Bimonthly publication.

*ACS members:	U.S. $12.00	Canada, PUAS $15.00	Other nations $15.50
Nonmembers:	U.S. $24.00	Canada, PUAS $27.00	Other nations $27.50

American Chemical Society / 1155 Sixteenth Street, N.W., Washington, D.C. 20036
Please enter a one year subscription for the following journals:

1 _____ 2 _____ 3 _____

4 _____ 5 _____ 6 _____

7 _____ 8 _____ 9 _____

name _____ position _____

address _____

city _____ state/country _____ zip _____

your company _____ nature of company's business _____

☐ I am an ACS member ☐ I am not an ACS member ☐ Bill me for $ _____

☐ Payment enclosed (*payable to American Chemical Society*) in the amount of $_____. Payment must be made in U.S. currency, by international money order, UNESCO coupons, or U.S. bank draft, or order through your book dealer.

* NOTE: Subscriptions at ACS member rates are for personal use only.

72A

THE JOURNAL OF

PHYSICAL CHEMISTRY

AMERICAN CHEMICAL SOCIETY, *1155 Sixteenth St., N.W., Washington, D. C. 20036*
FREDERICK T. WALL, *Executive Director*

Books and Journals Division
JOHN K CRUM, *Director (Acting)*
JOSEPH H. KUNEY, *Head, Business Operations Department*
RUTH REYNARD, *Assistant to the Director*

 Published biweekly by the American Chemical Society at 20th and Northampton Sts., Easton, Pa. 18042. Second-class postage paid at Washington, D. C., and at additional mailing offices.

All manuscripts should be sent to *The Journal of Physical Chemistry*, Department of Chemistry, University of Minnesota, Minneapolis, Minn. 55455.

Additions and Corrections are published once yearly in the final issue. See Volume 74, Number 26 for the proper form.

Extensive or unusual alterations in an article after it has been set in type are made at the author's expense, and it is understood that by requesting such alterations the author agrees to defray the cost thereof.

The American Chemical Society and the Editor of *The Journal of Physical Chemistry* assume no responsibility for the statements and opinions advanced by contributors.

Correspondence regarding accepted copy, proofs, and reprints should be directed to Editorial Production Office, American Chemical Society, 20th and Northampton Sts., Easton, Pa. 18042. Manager: CHARLES R. BERTSCH. Assistant Editor: EDWARD A. BORGER. Editorial Assistant: EVELYN J. UHLER.

Advertising Office: Century Communications Corporation, 142 East Avenue, Norwalk, Conn. 06851.

Business and Subscription Information

Remittances and orders for subscriptions and for single copies, notices of changes of address and new professional connections, and claims for missing numbers should be sent to the Subscription Service Department, American Chemical Society, 1155 Sixteenth St., N.W., Washington, D. C. 20036. Allow 4 weeks for changes of address. Please include an old address label with the notification.

Claims for missing numbers will not be allowed (1) if received more than sixty days from date of issue, (2) if loss was due to failure of notice of change of address to be received before the date specified in the preceding paragraph, or (3) if the reason for the claim is "missing from files."

Subscription rates (1971): members of the American Chemical Society, $20.00 for 1 year; to nonmembers, $40.00 for 1 year. Those interested in becoming members should write to the Admissions Department, American Chemical Society, 1155 Sixteenth St., N.W., Washington, D. C. 20036. Postage to Canada and countries in the Pan-American Union, $4.00; all other countries, $5.00. Single copies for current year: $2.00. Rates for back issues from Volume 56 to date are available from the Special Issues Sales Department, 1155 Sixteenth St., N.W., Washington, D. C. 20036.

This publication and the other ACS periodical publications are now available on microfilm. For information write to: MICROFILM, Special Issues Sales Department, 1155 Sixteenth St., N.W., Washington, D. C. 20036.

Notice to Authors last printed in the issue of June 10, 1971

REACTIONS UNDER PLASMA CONDITIONS

Volumes I and II

Edited by Mundiyath Venugopalan, *Western Illinois University*

Reactions Under Plasma Conditions is the first comprehensive survey of the fundamental physical theories and properties of the plasma state of matter, the types of reactions that can be achieved in this medium, and the practical methods that can be applied for their investigation in both natural and laboratory plasmas. All topics covered are of major significance to plasma chemists and plasma physicists. In Volume I emphasis is placed on plasma physics and plasma diagnostics; in Volume II the chemical physics of plasmas is stressed. Together, both volumes provide the plasma scientist with a timely source of coordinated information.

Volume I:	1971	599 pages	179 illus.	$29.95
Volume II:	1971	608 pages	127 illus.	$29.95

THERMODYNAMIC THEORY OF STRUCTURE, STABILITY AND FLUCTUATIONS

By P. Glansdorff and I. Prigogine, *both at the Universite Libre de Bruxelles, Belgium, and the University of Texas*

"The great importance of thermodynamic and hydrodynamic methods is that they provide us with a 'reduced description', a 'simplified language' with which to describe macroscopic systems. In many cases of interest such a reduced description is all that is needed. . . .

"How far can we proceed with such methods? What is the class of phenomena which may be investigated? These are some of the problems we shall deal with in this book." —*from the Preface*

1971	339 pages	$13.20

PERSPECTIVES IN STRUCTURAL CHEMISTRY

Volume III

Edited by J. D. Dunitz, *Laboratorium für Organischule, Zurich* and J. A. Ibers, *Northwestern University*

CONTENTS: Preface. Crystallographic Shear, and the Niobium Oxides and Oxide Fluorides in the Composition Region MX_x, $2.4<x<2.7$—*A. D. Wadsley and Sten Andersson.* Molecular Crystals: Intermolecular Potentials and Equilibrium Structures—*R. Mason.* Structural Studies on Transition—metal Complexes Containing σ-Bonded Carbon Atoms—*Melvyn R. Churchill.* Stereochemical Aspects of Organophosphorous Compounds—*J. J. Daly.* Author Index. Cumulative Subject Index for Volumes I, II, and III.

1970	259 pages	$14.95

ADVANCES IN CHEMICAL PHYSICS

Volumes 19 and 20

Edited by I. Prigogine, *University of Brussels, Belgium* and Stuart A. Rice, *University of Chicago*

VOLUME 19 CONTENTS: Quantum Theories of Chemical Kinetics—*J. C. Light.* A Review of Ion-Molecule Reactions—*L. Friedman and B. G. Reuben.* Ion Cyclotron Resonance—*G. A. Gray.* Stability and Dissipative Structures in Open Systems Far From Equilibrium—*G. Nicolis.* Statistical-Mechanical Theories in Biology—*E. H. Kerner.* Photochemical Reaction Centers and Photosynthetic Membranes—*R. K. Clayton.* Author Index. Subject Index.

1971	424 pages	66 illus.	$22.50

VOLUME 20 CONTENTS: Multipolar Interactions in Molecular Crystals—*T. Kihara.* The Computation of Virial Coefficients—*J. E. Kilpatrick.* The Origin of Hysteresis in Simple Magnetic Systems—*T. Erber et al.* The Linear Gas—*M. R. Hoare.* Low-Energy Electron Diffraction—*G. A. Somorjai and H. H. Farrell.* High-Resolution Electronic Spectra of Large Polyatomic Molecules—*I. G. Ross.* Author Index. Subject Index.

1971	132 pages	135 illus.	$22.50

CHEMICAL DYNAMICS

Papers in Honor of Henry Eyring

Edited by Joseph O. Hirschfelder, *University of Wisconsin, Madison* and Douglas Henderson, *IBM Research Laboratory, San Jose*

Volume 21 in the series, Advances in Chemical Physics, edited by I. Prigogine and S. Rice

For more than four decades Henry Eyring has played a leading role in the development of theoretical chemistry and its application to many fields. *Chemical Dynamics* contains more than fifty papers by his students and associates—most of them previously unpublished—which were brought together in honor of his seventieth birthday.

1971	816 pages	275 illus.	$22.50

MOLECULAR COMPLEXES

A Lecture and Reprint Volume

By Robert S. Mulliken, *University of Chicago and Florida State University,* and Willis B. Person, *University of Florida*

Molecular Complexes has been compiled to serve as an outline of several major aspects of the subject and to delineate some of the important unsolved problems. The first section, compromised of eighteen chapters adapted from lecturers, treats subjects ranging from "Simplified Resonance-Structure Theory" to "The Geometrical Configurations of Complexes". The second section contains fifteen reprints of articles originally published in professional journals that bear on the subject. A list of general references, a partial glossary of symbols, and an index conclude the volume.

1969	498 pages	176 illus.	$19.50

—Interscience Physical Chemistry list

the latest volumes in
Physical Methods of Chemistry
Edited by Arnold Weissberger and Bryant W. Rossiter, *both at Eastman Kodak Company*

PART IIA: ELECTROCHEMICAL METHODS

CONTENTS: Potentiometry: Oxidation-Reduction Potentials—*S. Wawzonek.* Potentiometry: pH Measurements and Ion-Selective Electrodes—*R. P. Buck.* Conductometry—*T. Shedlovsky and L. Shedlovsky.* Determination of Transference Numbers—*M. Spiro.* Polarography—*O. H. Muller.* Cyclic Voltammetry, Ac Polarography, and Related Techniques—*E. R. Brown and R. F. Large.* Voltammetry with Stationary and Rotating Electrodes—*S. Piekarski and R. N. Adams.* Chronoamperometry, Chronocoulometry, and Chronopotentiometry—*R. W. Murray.* Controlled-Potential Electrolysis—*L. Meites.* Subject Index.

1971 752 pages 219 illus. $32.50

PART IIB: ELECTROCHEMICAL METHODS

CONTENTS: Electrochemical Synthesis—*J. Chang, R. F. Large, and G. Popp.* Organic Reactions in Electrical Discharges—*B. D. Blaustein and Y. C. Fu.* Photoconductivity of Organic Solids—*R. C. Nelson.* Organic Electroluminescence—*D. M. Hercules.* Zone Electrophoresis—*S. L. Kirschner.* Electrodialysis—*J. L. Eisenmann and F. B. Leitz.* Subject Index.

1971 448 pages 74 illus. $23.50

PART IIIC: POLARIMETRY

CONTENTS: Theory of Optical Rotation—*H. Eyring and D. J. Caldwell.* Optical Rotation—Experimental Techniques and Physical Optics—*W. Heller and H. G. Curme.* Optical Rotatory Dispersion and Circular Dichroism—*P. Crabbe and A. C. Parker.* Streaming Birefringence—*A. Peterlin and P. Munk.* Faraday Effect—*J. M. Thorne.* The Kerr Effect—*C. G. LeFevre and R. J. W. LeFevre.* Ellipsometry—*N. M. Bashara, A. C. Hall, and A. B. Buckman.* Subject Index.

1971 528 pages 222 illus. $24.95

PART V: DETERMINATION OF THERMODYNAMIC AND SURFACE PROPERTIES

CONTENTS: Temperature Measurement—*J. M. Sturtevant.* Determination of Pressure and Volume—*G. W. Thomson and D. R. Douslin.* Determination of Melting and Freezing Temperatures—*E. L. Skau and J. C. Arthur, Jr.* Determination of Boiling and Condensation Temperatures—*J. R. Anderson.* Determination of Solubility—*W. J. Mader and L. T. Grady.* Determination of Osmotic Pressure—*J. R. Overton.* Calorimetry—*J. M. Sturtevant.* Differential Thermal Analysis—*B. Wunderlich.* Determination of Surface and Interfacial Tension—*A. E. Alexander and J. B. Hayter.* Determination of Properties of Insoluble Monolayers at Mobile Interfaces—*A. E. Alexander and G. E. Hibberd.* Author Index. Subject Index.

1971 624 pages 205 illus. $27.50

PHYSICOCHEMICAL MEASUREMENTS IN METALS RESEARCH

Parts 1 and 2
Edited by Robert A. Rapp, *Ohio State University*
Volume 4 of Techniques of Metals Research, edited by R. F. Bunshah

Volume 4 serves as a ready reference to proven experimental methods and critically selected data. The twenty-four papers comprising Parts 1 and 2 were written by experienced, qualified scientists to provide an authoritative, accessible, and current guide for both researcher and engineer.

Part 1: 1970 562 pages 130 illus. $29.95
Part 2: 1970 705 pages 229 illus. $34.95

MEASUREMENT OF MECHANICAL PROPERTIES

Parts 1 and 2

Edited by R. F. Bunshah, *University of California, Los Angeles*

Volume 5, Parts 1 and 2 of Techniques of Metal Research, edited by R. F. Bunshah

Volume Five deals with the measurement of mechanical properties of materials. Part 1 provides a theoretical basis for such topics as quasi-static mechanical testing, high strain rate tests, and creep and stress rupture testing. Part 2 considers fracture testing, and discusses fracture toughness for both high and low strength materials. Other topics covered include measurement of elastic constants, hardness and residual tests, acoustic emission effects during mechanical deformation, and photoelastic test methods.

Part 1: 1971 474 pages 212 illus. $29.50
Part 2: 1971 404 pages 476 illus. $29.50

PHASE TRANSITIONS

Proceedings of the Fourteenth Conference on Chemistry at the University of Brussels, May 1969

The International Institute of Physics and Chemistry, founded by Ernest Solvay

This collection of reports, and the ensuing discussions of the conference members, offers the chemist concerned with phase transitions a concise, in-depth treatment of the most recent developments in seven highly specialized areas.

OUTLINE OF CONTENTS: Statistical Mechanics of Phase Change—*J. E. Mayer.* Models—*E. Lieb.* Melting and Crystal Structure—*A. R. Ubbelhode.* The Divergence of Transport Coefficients in Fluids from Measurements of the Spectrum of Light Scattered by Thermal Fluctuations Near Critical Points—*G. B. Benedek.* Electronic Structure of Liquid Metals—*G. Busch.* Author Index. Subject Index. And two more articles.

1971 256 pages $16.50

S. I. UNITS

By B. Chiswell and E. C. M. Grigg, *both at the University of Queensland*

The aim of this book is to present the units, symbols and rules relating to SI units in a concise, complete and readily comprehended manner. In addition, a number of conversion tables have been included to allow many terms used in everyday life and commonly used in scientific and engineering practice to be readily converted into SI units.

1971 116 pages $3.50

WILEY-INTERSCIENCE

a division of JOHN WILEY & SONS, Inc.
605 Third Avenue, New York, New York 10016
In Canada: 22 Worcester Road, Rexdale, Ontario

Molecular Sieve Zeolites

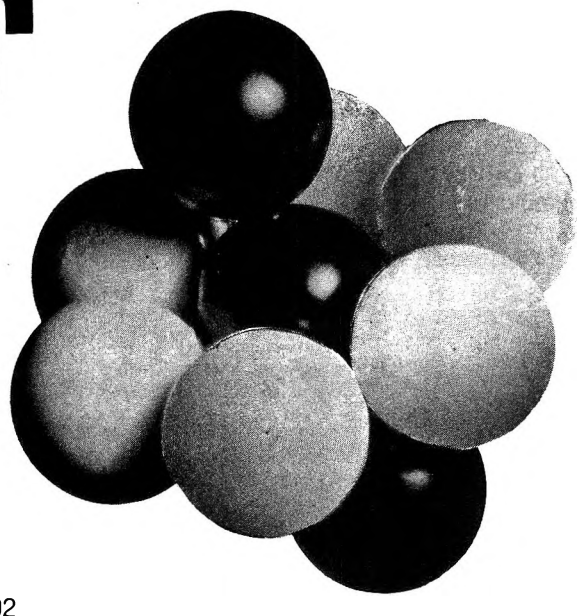

ADVANCES IN CHEMISTRY SERIES No. 101 and 102

Seventy-seven papers from a symposium co-sponsored by the Divisions of Colloid and Surface Chemistry, Petroleum Chemistry, and Physical Chemistry of the American Chemical Society and Worcester Polytechnic Institute, Edith M. Flanigen and Leonard B. Sand, co-chairmen.

Do you need a group of substances that can remove radioactive isotopes from nuclear wastes, remove ammonia from secondary sewage effluents, remove sulfur dioxide from waste gases, foster formation of actinides, or disrupt bacterial cells? These and many other possibilities are available through research on molecular sieve zeolites. For example, they are used for

- separating hydrogen isotopes
- solubilizing enzymes
- carrying active catalysts in curing of plastics
- transporting soil nutrients in fertilizers
- filtering tars from cigarette smoke

"Molecular Sieve Zeolites" reports recent advances in this rapidly developing field. Volume I offers 41 papers devoted to the synthesis, structure, mineralogy, and modification of sieve zeolites. These are followed in Volume II by 36 papers discussing sorption and catalysts.

Volume I: 526 pages with index. Cloth bound (1971) $16.00
Volume II: 459 pages with index. Cloth bound (1971) $16.00
No. 101 and 102 ordered together $30.00
Postpaid in U.S. and Canada; plus 35 cents elsewhere.
Set of L.C. cards with library orders upon request.

Other books in the ADVANCES IN CHEMISTRY SERIES of interest to colloid and surface, petroleum, and physical chemists include:

No. 97 Refining Petroleum for Chemicals
293 pages Cloth bound (1970) $11.50

No. 89 Isotope Effects in Chemical Processes
278 pages Cloth bound (1969) $13.00

No. 87 Interaction of Liquids at Solid Substrates
212 pages Cloth bound (1968) $9.50

No. 86 Pesticidal Formulations Research. Physical and Colloidal Chemical Aspects
212 pages Cloth bound (1969) $9.50

No. 79 Adsorption from Aqueous Solution
212 pages Cloth bound (1968) $10.00

No. 43 Contact Angle, Wettability, and Adhesion
389 pages Cloth bound (1964) $10.50

No. 31 Critical Solution Temperatures
246 pages Cloth bound (1961) $8.00

No. 29 Physical Properties of Chemical Compounds—III
489 pages Cloth bound (1961) $10.00

No. 22 Physical Properties of Chemical Compounds—II
491 pages Cloth bound (1959) $10.00

No. 20 Literature of the Combustion of Petroleum
295 pages Paper bound (1958) $8.00

No. 15 Physical Properties of Chemical Compounds
536 pages Cloth bound (1955) $10.00

Order from:
Special Issues Sales
American Chemical Society
1155 16th St., N.W.
Washington, D.C. 20036

THE JOURNAL OF

PHYSICAL CHEMISTRY

Volume 75, Number 19 September 16, 1971

Wall Effects on Concentrations of Reactive Intermediates in Gaseous Systems . . . **D. P. Jackson and D. A. Armstrong** 2883

Photoinduced Trapped Electrons in Rigid Polar Solution. I. A Study of the Recombination Luminescence . . . **Johan Moan and Harald B. Steen** 2887

Photoinduced Trapped Electrons in Rigid Polar Solution. II. Kinetics and Cross Section of Two-Quantum Ionization . . . **Johan Moan and Harald B. Steen** 2893

On the Photochemistry of the Ferrioxalate System . . . **G. D. Cooper and B. A. DeGraff** 2897

Photoelectron-Induced Decomposition of Ethane . . . **Robert R. Hutchins and Robert R. Kuntz** 2903

Kinetic Study of Species Formed during the Pulsed Radiolysis of Ammonia . . . **M. Clerc, M. Schmidt, J. Hagege-Temman, and J. Belloni** 2908

Catalytic Oxidation. IV. Ethylene and Propylene Oxidation over Gold . . . **Noel W. Cant and W. Keith Hall** 2914

Adsorption of Organic Gases on Clean Germanium Surfaces . . . **F. Meyer and J. M. Morabito** 2922

Infrared Spectra of Nitric Oxide Adsorbed on Evaporated Alkali Halide Films . . . **A. J. Woodward and Neville Jonathan** 2930

The Interaction of Halide Ions with Organic Cations Containing Charged Nitrogen, Phosphorus, or Sulfur in Aqueous Solutions Studied by Nuclear Quadrupole Relaxation . . . **Håkan Wennerström, Björn Lindman, and Sture Forsén** 2936

Far-Infrared Absorption of Some Organic Liquids . . . **S. R. Jain and S. Walker** 2942

Studies of Molten Lithium Chlorate and Its Aqueous Solutions with Laser Raman Spectroscopy . . . **B. G. Oliver and G. J. Janz** 2948

The Determination of the Number of Species Present in a System: a New Matrix Rank Treatment of Spectrophotometric Data . . . **Z Z. Hugus, Jr., and Abbas A. El-Awady** 2954

Electron Spin Resonance Studies of Short-Lived Radicals Generated by Fast Flow Techniques in Aqueous Solutions . . . **Gideon Czapski** 2957

The Effect of Coulombic Fields in the Vicinity of Metal Surfaces upon the Entropy and Absolute Rate of Reaction of Adsorbed Molecules . . . **Richard F. Copeland** 2967

Effect of Rapid Homogeneous Reaction on the Diffusion-Limited Lifetime of a Soluble Sphere of Arbitrary Density . . . **Daniel E. Rosner** 2969

A High-Yield Method for the Preparation of Anomalous Water . . . **S. B. Brummer, G. Entine, J. I. Bradspies, H. Lingertat, and C. Leung** 2976

Determination of Magnetic Moments of Paramagnetic Ions in Microgram Quantities Using Ion-Exchange Resins . . . **Toshio Ikeda, Sumio Ōe, and Kazuaki Yamanari** 2981

Photochemical Studies of Solid Potassium Trisoxalatoferrate(III) Trihydrate . . . **H. E. Spencer and M. W. Schmidt** 2986

Molar Absorptivity of Carbon Trioxide . . . **Patrick R. Jones and Henry Taube** 2991

Radiation Chemistry of Supercooled Water . . . **Inna Kules and Robert Schiller** 2997

Effect of Dissolved Paraffinic Gases on the Surface Tension and Critical Micelle Concentration (cmc) of Aqueous Solutions of Dodecylamine Hydrochloride (DACl) . . . **I. J. Lin and A. Metzer** 3000

The Reactions of Acetone and Hydrogen Peroxide. I. The Primary Adduct . . . **M. C. V. Sauer and John O. Edwards** 3004

Bonding Properties of Diatomic Molecular Orbitals . . . **Ricardo Ferreira** 3012

On the Validity of a Simple Theory for Transport in Ion-Exchange Membranes . . . **J. F. Osterle and M. J. Pechersky** 3015

NOTES

Reactivity of Hydrogen Atoms and Hydrated Electrons toward Aqueous Erythrosin. X-Radiolysis
. . . **John Chrysochoos and David S. Shihabi** 3020

Electron Spin Resonance Spectrum and Structure of the Radical Anion of Phosphorus Oxychloride
. . . **Carolyn M. L. Kerr and Ffrancon Williams** 3023

An Investigation of the Reaction $2COF_2 \rightarrow CO_2 + CF_4$ and the Heat of Formation of Carbonyl Fluoride
. . . **J. C. Amphlett, J. R. Dacey, and G. O. Pritchard** 3024

Specific Rates in the Acid Dissociation–Ion Recombination Equilibrium of Dilute Aqueous Hydrazoic Acid at 25°
. . . **James J. Auborn, Percy Warrick, Jr., and Edward M. Eyring** 3026

Molecular Complexes in the Vapor of Sodium Bromide and Zinc Bromide Mixtures
. . . **Douglas W. Schaaf and N. W. Gregory** 3028

COMMUNICATIONS TO THE EDITOR

Formation of Ozonide Ions in γ-Irradiated Aqueous Solutions of Alkali Hydroxides
. . . **K. V. S. Rao and M. C. R. Symons** 3030

Reply to "Formation of Ozonide Ions in γ-Irradiated Aqueous Solutions of Alkali Hydroxides"
. . . **N. B. Nazhat and J. J. Weiss** 3031

Extrapolation Procedures for Evaluation of Individual Partial Gram Ionic Volumes
. . . **B. E. Conway, J. E. Desnoyers, and R. E. Verrall** 3031

Reply to "Extrapolation Procedures for Evaluation of Individual Partial Gram Ionic Volumes"
. . . **M. H. Panckhurst** 3035

AUTHOR INDEX

Amphlett, J. C., 3024
Armstrong, D. A., 2883
Auborn, J. J., 3026

Belloni, J., 2908
Bradspies, J. I., 2976
Brummer, S. B., 2976

Cant, N. W., 2914
Chrysochoos, J., 3020
Clerc, M., 2908
Conway, B. E., 3031
Cooper, G. D., 2897
Copeland, R. F., 2967
Czapski, G., 2957

Dacey, J. R., 3024
DeGraff, B. A., 2897
Desnoyers, J. E., 3031

Edwards, J. O., 3004
El-Awady, A. A., 2954
Entine, G., 2976
Eyring, E. M., 3026

Ferreira, R., 3012
Forsén, S., 2936

Gregory, N. W., 3028

Hagege-Temman, J., 2908
Hall, W. K., 2914
Hugus, Z Z., Jr., 2954
Hutchins, R. R., 2903

Ikeda, T., 2981

Jackson, D. P., 2883
Jain, S. R., 2942
Janz, G. J., 2948
Jonathan, N., 2930
Jones, P. R., 2991

Kerr, C. M. L., 3023
Kules, I., 2997
Kuntz, R. R., 2903

Leung, C., 2976
Lin, I. J., 3000
Lindman, B., 2936
Lingertat, H., 2976

Metzer, A., 3000
Meyer, F., 2922
Moan, J., 2887, 2893
Morabito, J. M., 2922

Nazhat, N. B., 3031

Oe, S., 2981
Osterle, J. F., 3015
Oliver, B. G., 2948

Panckhurst, M. H., 3035
Pechersky, M. J., 3015
Pritchard, G. O., 3024

Rao, K. V. S., 3030
Rosner, D. E., 2969

Sauer, M. C. V., 3004
Schaaf, D. W., 3028
Schiller, R., 2997
Schmidt, M., 2908
Schmidt, M. W., 2986
Shihabi, D. S., 3020
Spencer, H. E., 2986
Steen, H. B., 2887, 2893
Symons, M. C. R., 3030

Taube, H., 2991

Verrall, R. E., 3031

Walker, S., 2942
Warrick, P., Jr., 3026
Weiss, J. J., 3031
Wennerström, H., 2936
Williams, F., 3023
Woodward, A. J., 2930

Yamanari, K., 2981

In papers with more than one author the name of the author to whom inquiries about the paper should be addressed is marked with an asterisk in the by-line.

THE JOURNAL OF
PHYSICAL CHEMISTRY

VOLUME 75, NUMBER 19 SEPTEMBER 16, 1971

Wall Effects on Concentrations of Reactive Intermediates in Gaseous Systems

by D. P. Jackson*

Chemistry and Materials Division, Atomic Energy of Canada Limited, Chalk River, Ontario, Canada

and D. A. Armstrong

Department of Chemistry, University of Calgary, Calgary, Alberta, Canada *(Received February 4, 1971)*

Publication costs assisted by Atomic Energy of Canada Limited

Previously we have published detailed tables of solutions for the problem of wall diffusion losses of radicals for the flat plate, cylindrical, and spherical cell geometries. The calculations assumed steady-state radical creation with competing losses due to first-order wall recombination and homogeneous second-order recombination. Effects of third bodies in the homogeneous recombination were considered. In the present paper these calculations are applied to experimental work. A method of deducing an effective γ, the probability of radical destruction during a collision at the wall, from experimental results is illustrated.

Introduction

Wall reactions of intermediates often compete with homogeneous recombination in gaseous systems.

$$\text{radical} + \text{radical} \xrightarrow{(+\,M)} \text{reaction products} \qquad (1)$$

$$\text{radical} \xrightarrow{\text{diffusion to wall}} \text{reaction products} \qquad (2)$$

The relative rates of these two reactions determine the lifetimes of the intermediates and, not infrequently, the nature of the products they form. Thus, in the design and interpretation of experiments the kineticist is often placed in the position of having to estimate the fraction, F_w, of intermediates which will react at the wall under a given set of conditions. Also of interest is $\bar{y}$, the mean concentration of intermediates throughout the cell.

A model situation can be represented by the equation

$$D\Delta^{(g)}y - \alpha y^2 + \varphi = 0 \qquad (3)$$

where φ is rate of formation of intermediates, α is the second-order recombination rate constant, y is concentration of intermediates, D is the diffusion constant of the intermediate relative to other species in vessel, and g on the Laplacian, Δ, represents three standard geometries ($g = 1$, infinite plates; $g = 2$, infinite cylinder; $g = 3$, sphere). In treating this we shall assume φ is uniform throughout the reaction cell. Therefore the concentration will be symmetric about the center and will be a maximum at the center, *i.e.*, $(dy/dr)_{r=0} = 0$ where r is distance from center. The most extreme boundary condition is where $y = 0$ at the wall but a more general boundary condition can be obtained by combining Fick's first law of diffusion with the well known Maxwellian expression for the rate of impingement of particles on a wall. This gives

$$\left(\frac{dy}{dr}\right)_{\text{wall}} = \beta y$$

where

$$\beta = \gamma \frac{\bar{c}}{4D} \qquad (4)$$

and $\bar{c}$ is the average speed of intermediates and γ the wall termination probability.

The problem of wall recombination has been treated previously[1-4] but the detailed results are somewhat limited and no treatment of cylindrical cells is given. The purpose of the present treatment is to remedy the large gaps in the existing data and to compare our results with experimental data to demonstrate their applicability. A description of our calculations and detailed results have already been published in comprehensive tables.[5] Our equations can be summarized by defining $x = r/\rho$, $y^* = y(D/\varphi\rho^2)$, and $A = \alpha\varphi\rho^4/D^2$, where ρ is distance from center to wall, eq 3 becomes

$$\Delta^{(g)}y^*(x) - Ay^{*2} + 1 = 0 \tag{5}$$

The boundary condition can be rewritten

$$B = \beta\rho = \gamma\bar{c}\rho/4D \tag{6}$$

Hence

$$\bar{y}^* = \bar{y}(D/\varphi\rho^2) = g\int_0^1 y^* x^{(g-1)}\,dx \tag{7}$$

and

$$F_\omega = 1 - gA\int_0^1 y^{*2}x^{(g-1)}\,dx \tag{8}$$

In general terms, A is an indication of the degree of recombination—when it is high recombination is dominant, when it is low diffusion effects are dominant. B refers to the situation at the wall—when it is high large numbers of intermediates are lost to the wall and inversely.

Figure 1 shows the general variation of the concentration profile with distance from the central axis of a cylinder for the case where $B = \infty$. $B = \infty$ means that $y^* = 0$ at $x = 1$; this boundary condition is the result given by eq 4 when dy^*/dx is finite at the wall but $y^* = 0$. Since $0 \leq \gamma \leq 1$, the maximum B is $\bar{c}\rho/4D$. However, this quantity may be made as large as one wishes. Two extreme cases are evident here. For the limit of pure diffusion

$$y^* \longrightarrow \frac{1}{2g}(1 - x^2) \tag{9}$$

which is a parabola; this trend is observed for the low A profiles. At the opposite extreme of pure recombination

$$y^* \longrightarrow A^{-1/2} \tag{10}$$

and therefore in the high A cases the curves are equal to this value for much of their lengths, but they decrease due to the boundary condition, close to the wall. Examples of the variation $\bar{y}^*$ with A and B will be shown below in connection with comparison of theory and experimental data.[6,7]

Figure 2 shows the variation of F_w with A and B for the cylindrical geometry. Reference can be made to

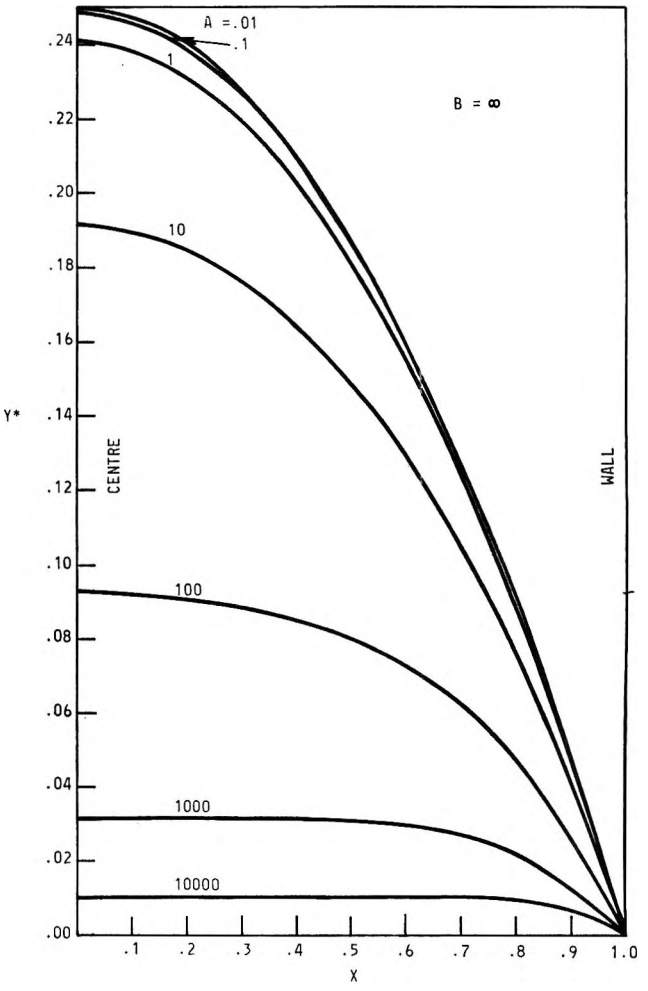

Figure 1. Scaled concentration (y^*) as a function of distance from the central axis of the vessel (x) for various A values: $B = \infty$, cylindrical geometry.

tables[5] for the detailed results for this and the other geometries considered. It should perhaps be mentioned that in general wall effects are greatest for spherical geometry and least for flat plates.

Comparison with Experiment

There are no experimental data giving reliable values of F_w. Our comparisons with experiment are therefore based on $\bar{y}$ values. In an experimental situation one of the fundamental properties of the system is the variation of this parameter with total gas pressure. Assuming an atom or a small radical, recombination is a three-body process and α increases linearly with the pressure of the third body. D varies inversely with

(1) R. Gomer, *J. Chem. Phys.*, 19, 284 (1951).
(2) R. M. Noyes, *J. Amer. Chem. Soc.*, 73, 3039 (1951).
(3) C. E. Klots and V. E. Anderson, *J. Phys. Chem.*, 71, 265 (1967).
(4) R. M. Marshall and C. P. Quinn, *Trans. Faraday Soc.*, 61, 2671 (1965).
(5) D. P. Jackson, AECL Report 3726, 1970.
(6) W. Jost, *Z. Phys. Chem., Abt. B*, 3, 95 (1929).
(7) M. I. Christie, R. S. Roy, and B. A. Thrush, *Trans. Faraday Soc.*, 55, 1139 (1959).

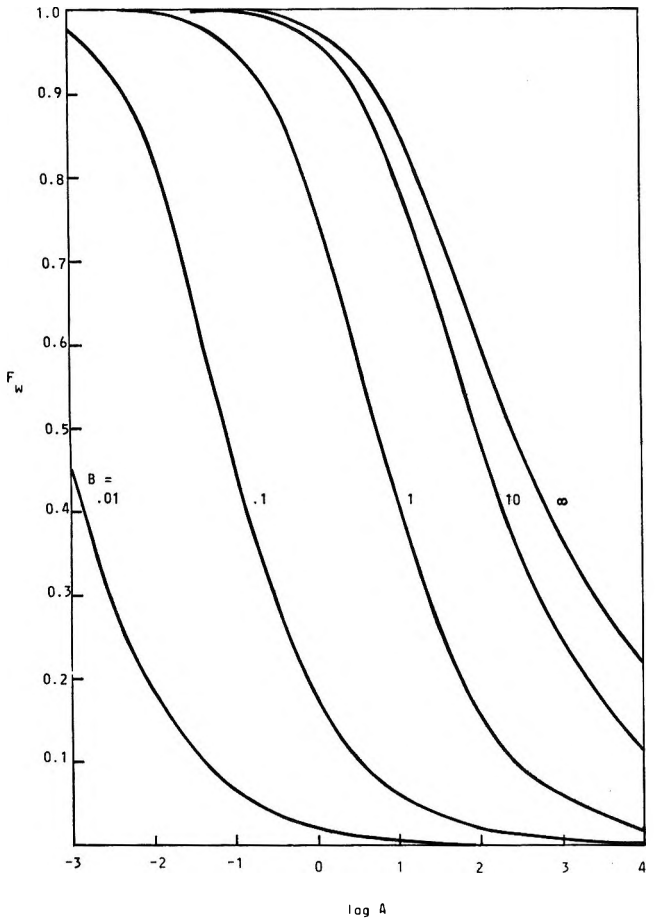

Figure 2. Fraction of intermediates reacting at the wall (F_w) as a function of A and B, cylindrical geometry.

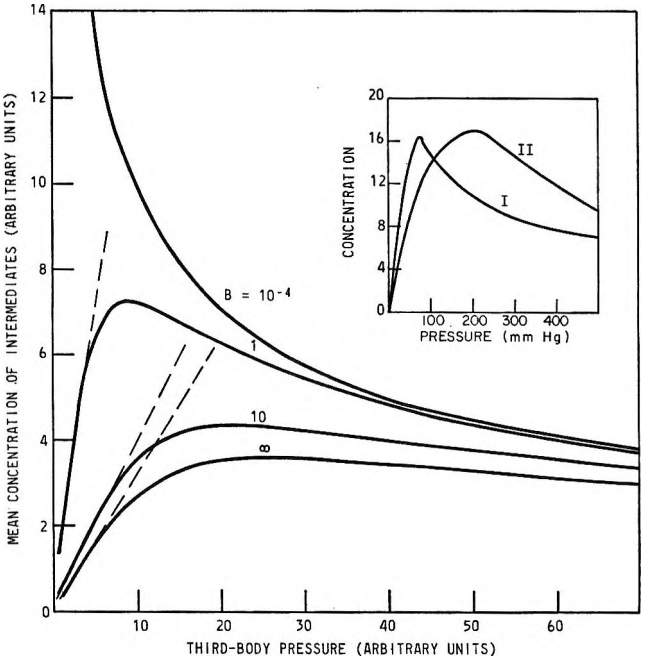

Figure 3. Curves of $\bar{y}$ *vs.* third-body gas pressure for an arbitrary case. The dashed lines indicate the almost linear dependence seen at low pressures. Inset experimental curves: (I) from ref 8; (II) from ref 9.

pressure; therefore A is in general a third-degree polynomial in pressure. B is also dependent on pressure through D and hence the relationship between $\bar{y}$ and pressure is complex. Figure 3 gives curves of $\bar{y}$ *vs.* third-body gas pressure for various B values calculated in a cylindrical cell, where typical values of α and other basic parameters have been chosen for illustrative purposes. Many of the features of these curves are explained by the foregoing discussions of the variation of y^* and $\bar{y}^*$ with A and B. For instance for the $B = 1$ curve we see a region of low pressure where the curve is linear corresponding to a pure diffusion situation, passing through a region of mixed diffusion and recombination to a region of total homogeneous recombination (*i.e.*, $\bar{y}^* = 1/\sqrt{A}$). There are many examples of this type of behavior in the literature.[8-11] The inset to Figure 3 illustrates the form of two such experimental curves for Br atoms obtained by Rabinowitch and Wood[8] (I) and by Schmitz, Schumacher, and Jäger[9] (II). For curve I the mean Br atom concentration (here of Br atoms) was determined by measuring the decrease in the light absorption of Br_2 molecules. Curve II was obtained by a kinetic method. In both cases we see qualitatively the features predicted by the calculated curves for moderate B values.

The behavior of the above curves at the extremes of high and low pressures was understood by Jost[6] and by Rabinowitch and Wood.[8] However, they were not able to reproduce theoretically the complete curves. In addition to doing this the present treatment[5] allows one to predict the effects of changing the α and B values for the three types of geometry. The results of variation in B are illustrated by the four curves in Figure 3.

Quantitative predictions of $\bar{y}$ values are at present difficult, since γ, which is required for the calculation of B, depends on the condition of the cell surface and its temperature and few reliable values are available. Therefore, the following approach was adopted for comparisons with experimental data.[6,7] We calculate *ab initio* values of the effective α from rate constants given in the recent literature and D from theoretical considerations; φ is taken from the experimental situation. Next the best approximation is taken for the experimental cell geometry. Values of A can be calculated for the data points. Applying the first part of eq 7 (which depends on D, φ, and ρ) to the experimental $\bar{y}$ data, $\bar{y}^*$ values can then be calculated and plotted against the A values. Comparison of the positions of these $\bar{y}^*$ points with theoretical curves based on our

(8) E. Rabinowitch and W. C. Wood, *Trans. Faraday Soc.*, **32**, 907 (1936).

(9) H. Schmitz, H. J. Schumacher, and A. Jäger, *Z. Phys. Chem., Abt. B*, **51**, 281 (1942).

(10) For example: E. Buckley and E. Whittle, *Trans. Faraday Soc.*, **58**, 529 (1962).

(11) E. Rabinowitch and W. C. Wood, *J. Chem. Phys.*, **4**, 497 (1936).

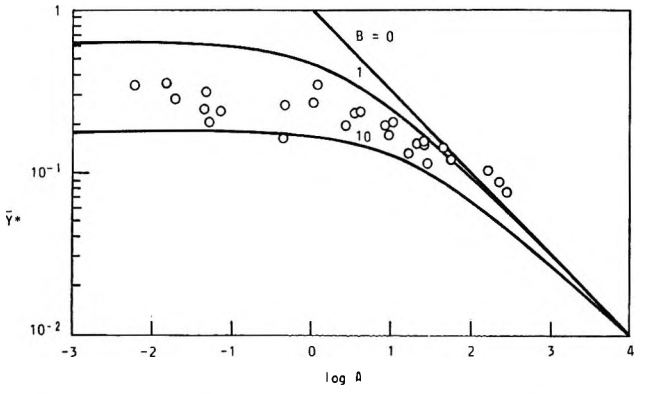

Figure 4. Experimental points of Jost[6] plotted on the $\bar{\gamma}^*$ *vs.* log A diagram for the cylinder.

tables in ref 5 leads to an estimate of B. The values of γ derived from this are then compared with data in the available literature.[12,13]

Jost[6] investigated the photochemical production of HBr. The reaction cell used (4 × 2 × 20 cm) was sufficiently long to justify neglect of end effects and the geometry was approximated by an infinite cylinder with a radius such that the cross-sectional area of the cylinder and reaction cell were equal. Evaluation of the diffusion coefficient D required an estimate of the Lennard-Jones (LJ) potential parameters for atomic bromine. Hill[14] gave self-interaction potential parameters for Br using a potential slightly different from the LJ. We used a technique of comparing potentials due to Hirschfelder, Curtiss and Bird[15] on Hill's parameters to obtain values of $\sigma = 3.90$ and $(\epsilon/k) = 157°K$ (in the usual LJ notation) for the self-interaction of Br atoms. In addition to Br atoms, Br_2 and H_2 were also present and acted as third bodies. The diffusion coefficient for a given experimental case was obtained by combining the binary diffusion coefficients for Br in Br_2 and Br in H_2 in proportion to their partial pressures. The formulas used (and the LJ parameters for Br_2 and H_2) were taken from Bird, Stewart, and Lightfoot.[16] Similarly, the effective rate of second-order homogeneous recombination α consisted of pressure-dependent contributions from the rates of the Br third-body reactions with Br_2 and H_2 (at $\sim$ 500°K). The former rate was obtained from Ip and Burns,[17] the latter from Rabinowitch and Wood.[11] The rate of radical production φ, was a function of Br_2 pressure which was calculated from the energy absorption data given in the paper.[6]

$\bar{\gamma}^*$ was evaluated from Jost's observed reaction rates ($d[HBr]/dt$) using standard kinetic expressions and Fettis and Knox's value[18] of $k_{Br + H_2 \rightarrow HBr + H}$. Some 27 of the data points given in this work were treated and the results are plotted in Figure 4.

There is scatter in the results partly experimental and partly due to the differing D values for each point which gave slightly different B values (eq 6). However,

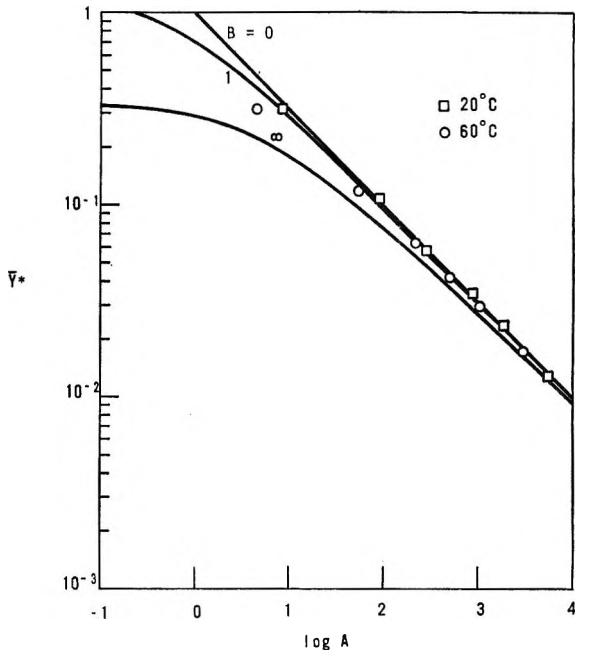

Figure 5. Experimental points of Christie, Roy, and Thrush[7] plotted on the $\bar{\gamma}^*$ *vs.* log A diagram for the flat plate geometry.

it is clear that $1 < B < 10$; therefore assuming a mean $D \sim 5$, which was typical in the calculations, $3 \times 10^{-4} \lesssim \gamma \lesssim 3 \times 10^{-3}$ from eq 4. A numerical search for γ can be made using the precisely correct $\bar{\gamma}^*$ and taking into account the role of D in eq 4. This gives a mean γ of 1.75×10^{-3} but the scatter in γ was a large as the above limits. This order of magnitude of γ agrees with literature values of similar experimental conditions.[13,19,20] This demonstrates a convenient method of deriving γ from experimental data.

Christie, Roy, and Thrush[7] studied the photochemical reaction between bromine and chlorine. The experimental reaction vessel was a cylinder of diameter 7.5 cm and length 2 cm. This is difficult to reconcile with one of the standard geometries, but since the surface area of the ends is slightly less than twice that of the side (or cylindrical portion) the approximation used was the flat plate geometry. We calculated the pressure-dependent parameters α, D, and φ by methods similar to those used for the Jost[6] work discussed above;

(12) M. A. A. Clyne and D. H. Stedman, *J. Phys. Chem.*, **71**, 3071 (1967).

(13) J. T. Herron, *ibid.*, **67**, 2864 (1963).

(14) T. L. Hill, *J. Chem. Phys.*, **16**, 399 (1948).

(15) J. O. Hirschfelder, C. F. Curtiss, and R. B. Bird, "Molecular Theory of Gases and Liquids," Wiley, New York, N. Y., 1954.

(16) R. B. Bird, W. E. Stewart, and E. N. Lightfoot, "Transport Phenomena," Wiley, New York, N. Y., 1960.

(17) J. K. K. Ip and G. Burns, *J. Chem. Phys.*, **51**, 3414 (1969).

(18) G. C. Fettis and J. H. Knox, *Progr. React. Kinet.*, **2**, 1 (1964).

(19) M. A. A. Clyne and D. W. Stedman, *Trans. Faraday Soc.*, **64**, 2698 (1968).

(20) K. M. Evenson and D. S. Burch, *J. Chem. Phys.*, **45**, 2450 (1966).

in this case Br_2, Cl_2, and CO_2 can act as third bodies. Again the experimental $\bar{y}^*$ values were plotted as a function of A; the results are shown in Figure 5 for two temperatures. According to the tables F_w for these cases is between about 0.05 to 0.15 for CO_2 concentrations between 4×10^{-3} and 0 M^{-1}. Therefore the effect of the walls is relatively small as is clear from Figure 5. Fitting a γ to each point indicated that $10^{-4} \lesssim \gamma \lesssim 10^{-5}$ for both temperatures. Again this is a reasonable order of magnitude for γ under these conditions since one would expect it to be somewhat lower than that found by Jost at lower temperatures.[13]

Both of the above comparisons have been with experiments involving Br atoms in photolysis. However, the treatment can be applied to other radicals in other reaction systems. This is illustrated by Marshall and Quinn's[4] earlier treatment of H atoms in the pyrolysis of ethane and by Klots and Anderson's[3] application of their calculation to the ambipolar wall diffusion of ions in radiolysis. The tables of ref 5 represent a far more general treatment than these earlier ones. They should provide a ready means for the estimation of F_w and $\bar{y}$ in gaseous systems undergoing reaction in cells of spherical, cylindrical, or flat plate geometry.

Photoinduced Trapped Electrons in Rigid Polar Solution. I.

A Study of the Recombination Luminescence

by Johan Moan* and Harald B. Steen

Norsk Hydro's Institute for Cancer Research, Montebello, Norway *(Received November 24, 1970)*

Publication costs assisted by Norsk Hydro's Institute for Cancer Research

The afterglow (A) and thermoluminescence (TL) of tryptophan in ethylene glycol–water glass exposed to intense 250-nm uv light at 77°K have been studied. Both A and TL are attributed to recombination between tryptophan cations and electrons formed by ionization of tryptophan by triplet absorption. The spectra of both A and TL are identical with the phosphorescence spectrum of tryptophan, demonstrating that the only radiative transition of both processes is the $T_1 \rightarrow S_0$ transition in this solute. The intensity, I, of A decays according to I = constant $t^{-1.09}$. The TL glow curve has two peaks at about 90 and 135°K, respectively. From the effects of three electron scavengers, HCl, CCl_3COOH, and $NaNO_3$, we conclude that A and the first glow peak are both associated with a small fraction of the trapped electrons which are trapped fairly close to the cations and which are guided by the Coulomb field of the cation when they recombine. The second glow peak represents the release of the majority of the trapped electrons, which are trapped at somewhat larger distances and which probably recombine "accidentally" by random diffusion.

Introduction

It is known that when rigid solutions of aromatic molecules are exposed to intense uv light, ionization of the solute may result although the quantum energy of the light is well below the ionization potential,[1-3] and it has been shown that the ionization is brought about by the two-photon process called triplet absorption.[2,4,5] Provided the solvent used is transparent to the appropriate wavelength of uv light, this type of irradiation offers an efficient means for studying the direct effect of radiation on the solute. This is very difficult when conventional types of ionizing radiation, such as X- or γ-rays, are being used because of the dominating number of radiolytic products of the solvent, which usually completely conceals those originating from the solute.

The products formed in such solutions by exposure to uv light may become trapped in the rigid solvent and can be readily studied by various methods such as esr spectroscopy[5,6] and optical absorption measurements.[7,8] Indole derivatives are well suited to this

(1) W. A. Gibbons, G. Porter, and M. I. Savadatti, *Nature*, **206**, 1355 (1965).

(2) R. Guermonprez, C. Hélène, and M. Ptak, *J. Chim. Phys.*, **64**, 1376 (1967).

(3) Yu. A. Vladimirov and E. E. Fesenko, *Photochem. Photobiol.*, **8**, 209 (1968).

(4) K. D. Cadogan and A. C. Albrecht, *J. Chem. Phys.*, **43**, 2550 (1965).

(5) H. B. Steen, *Photochem. Photobiol.*, **9**, 479 (1969).

(6) O. A. Azizova, Z. P. Gribova, L. P. Kayushin, and M. K. Pulatova, *ibid.*, **5**, 763 (1966).

(7) H. Hase, *J. Phys. Soc. Jap.*, **24**, 589 (1968).

purpose, and several authors have studied tryptophan in a solvent consisting of ethylene glycol and water.[3,5-7] There is unanimous agreement that a certain fraction of the electrons produced by the ionization of this solute become permanently trapped in the glassy solvent at temperatures below 100°K, while the fate of the positive solute ions seems to be less certain.[5,6] It is known also that this solution, as well as other similar ones, exhibits thermoluminescence and afterglow when irradiated below 100°K, and it is commonly assumed that this luminescence is due to recombination between the electrons and the positive solute ions.[1,2,9,10] The study of these luminescence phenomena may therefore give further information on the nature of these ions and on the mechanisms of their subsequent reactions.

In the present work the characteristics of the thermoluminescence and afterglow of tryptophan in ethylene glycol–water glass irradiated with uv light have been studied. It is concluded that both types of luminescence are due to the deexcitation of the lowest triplet state of tryptophan, which is formed by geminate recombination between positive tryptophan ions and electrons. The addition of electron scavengers gives some information about the distribution of the electrons associated with the afterglow and with the various parts of the thermoluminescence glow curve.

Materials and Methods

Sample Preparation. L-Tryptophan was obtained from Sigma Chemical Co. and used without further purification. HCl, CCl_3COOH, and $NaNO_3$ were Merck p.a. Ethylene glycol was chromatographic grade from Fluka and H_2O was triple distilled. Tryptophan was dissolved to a concentration of 5×10^{-4} mol/l. in a mixture of ethylene glycol and water 1:1 by volume (EG–H_2O). The sample holder was a circular vessel made of 0.05-mm aluminum foil. The vessel was 1 mm deep, 8 mm in diameter, and contained 50 μl of sample solution. The sample was placed in the irradiation chamber, degassed by controlled evacuation, and cooled down to 77°K. At this temperature the sample had the appearance of a completely transparent glass without cracks or bubbles. The vacuum in the irradiation chamber was better than 10^{-5} Torr during the experiments.

Irradiation and Luminescence Measurements. The uv source was a 200-W high-pressure mercury lamp fitted to two Bausch & Lomb grating monochromators in series. The monochromators were operated at 254 nm, thus utilizing an intense line in the spectrum of the lamp. The intensity of uv light at the sample was about 10^{-8} einstein/cm^2 sec and the exposure time was usually 10 sec. The luminescence was registered by the use of an EMI 9558 QB photomultiplier tube. Spectra of the luminescence were obtained by means of a 0.25-m Jarrel–Ash grating monochromator which scanned the spectra at a rate of 400 nm/min. The thermoluminescence glow curves were recorded while the temperature of the sample was raised at a rate of 14 deg/min. The temperature could be kept constant anywhere between 77°K and room temperature. Further details of the apparatus can be found elsewhere.[11] The optical density of the sample could be measured immediately after irradiation. The details of this method will be described elsewhere.[12]

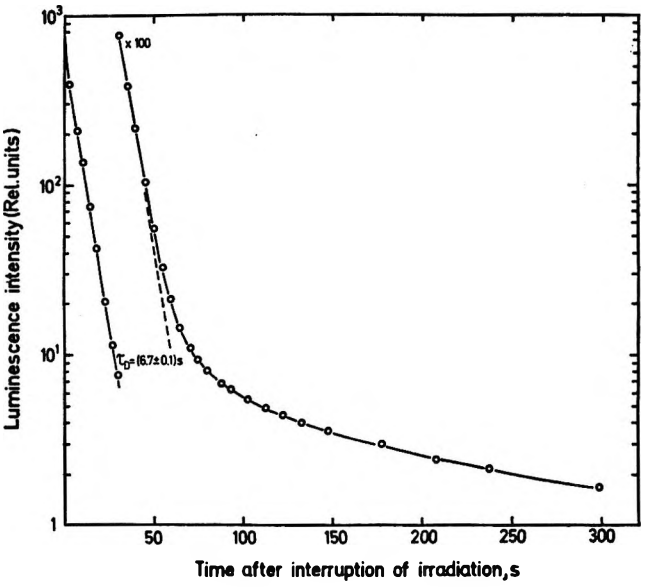

Figure 1. Semilogarithmic plot of the luminescence decay of a uv-irradiated sample of tryptophan in EG–H_2O at 77°K.

Results and Discussion

Luminescence Decay. The luminescence observed subsequent to the irradiation consisted of two components (Figures 1 and 2). One component of high intensity decayed exponentially with a decay time of 6.7 ± 0.1 sec. This is obviously the ordinary phosphorescence of tryptophan caused by de-excitation of its lowest triplet level (T_1).[11] The other component (which is denoted here as afterglow) became noticeable after some 30 sec and decayed so as to produce a straight line when traced on a double-logarithmic scale (Figure 2). Thus, the intensity of the afterglow, I, follows the relationship $I = At^{-m}$, where t is the time after irradiation and A is a constant which depends on the intensity of the uv light and the time of the exposure. At 77°K we found $m = 1.09 \pm 0.02$, from measurements on different samples.

This type of decay kinetics is the same as that ob-

(8) Ye. Ye. Fesenko, E. A. Burstein, and Yu. A. Vladimirov, *Biofizika*, **12**, 616 (1967).

(9) D. I. Roshchupkin and Yu. A. Vladimirov, *ibid.*, **10**, 48 (1965).

(10) B. Brocklehurst, R. D. Russell, and M. I. Savadatti, *Trans. Faraday Soc.*, **62**, 1129 (1966).

(11) H. B. Steen, *Photochem. Photobiol.*, **6**, 805 (1967).

(12) H. B. Steen, *J. Phys. Chem.*, in press.

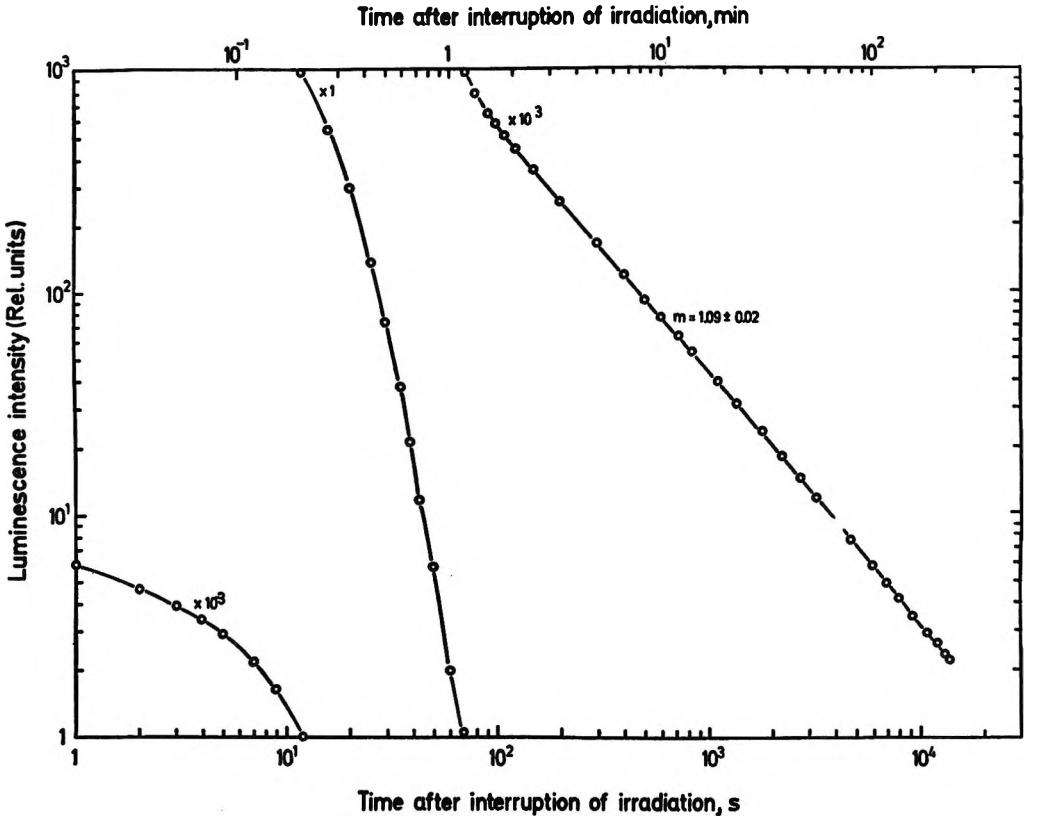

Figure 2. Double-logarithmic plot of the luminescence decay of a uv-irradiated sample of tryptophan in EG–H_2O at 77°K.

served by Debye and Edwards[13] and by Guermonprez, *et al.*[2] Debye and Edwards found that these kinetics are consistent with the assumption that the afterglow is produced by the recombination between trapped positive ions and electrons which move by random diffusion. As noted below, this conclusion does not seem to be consistent with the present results.

The intensity of the afterglow and the thermoluminescence relative to that of the ordinary phosphorescence, *i.e.*, the magnitude of A, increased with increasing intensity of the uv light and with increasing exposure time in a manner which is consistent with the assumption that the afterglow and the thermoluminescence are both initiated by a two-photon ionization having the T_1 level of tryptophan as the intermediate.[14]

Luminescence Spectra. From the results presented in Figure 3 it can be seen that the spectra of the afterglow as well as all parts of the thermoluminescence glow curve are identical with the spectrum of the ordinary phosphorescence observed during irradiation. This is in correspondence with the findings of Guermonprez, *et al.*[2] No component similar to the fluorescence spectrum of tryptophan could be detected in the recombination luminescence. Hence, the only radiative step of the afterglow and thermoluminescence is the $T_1 \rightarrow S_0$ transition in tryptophan.

This result indicates that the energy of the recombining ion–electron pair is less than that of the fluorescent singlet level of tryptophan, *i.e.*, <4.0 eV, while it is larger than the energy of the T_1 level, *i.e.*, >3.0 eV. The difference between the ionization energy of tryptophan, which is 7.8 eV in the gas phase,[15] and the recombination energy can probably be attributed to the trapping energy of the ions.

Glow Curves. The thermoluminescence glow curve has two peaks, as shown in Figure 4. In this figure is shown also the optical density of the sample at two different wavelengths as a function of temperature. The initial concentration of trapped electrons varied from approximately 3×10^{-5} M in most of the TL experiments to about 1.5×10^{-4} M in the measurement of optical density. The light absorption at both 580 and 710 nm is supposedly due almost entirely to trapped electrons. Thus, according to the work of Hase[7] the optical extinction of the tryptophan cation at 710 nm is negligible while at 580 nm it is less than 10% of that of the trapped electrons. It can be seen that the low-temperature peak in the glow curve (TL_1) is accompanied by a decrease in optical density at 710 nm, while there is no noticeable change at 580 nm. The glow peak at the higher temperature (TL_2) is accompanied by a complete elimination of the light absorption at both wavelengths. This is in accordance

(13) P. Debye and J. O. Edwards, *J. Chem. Phys.*, 20, 236 (1952).
(14) J. Moan and H. B. Steen, *J. Phys. Chem.*, 75, 2893 (1971).
(15) I. Fischer-Hjalmars and M. Sundhom, *Acta Chem. Scand.*, 22, 607 (1968).

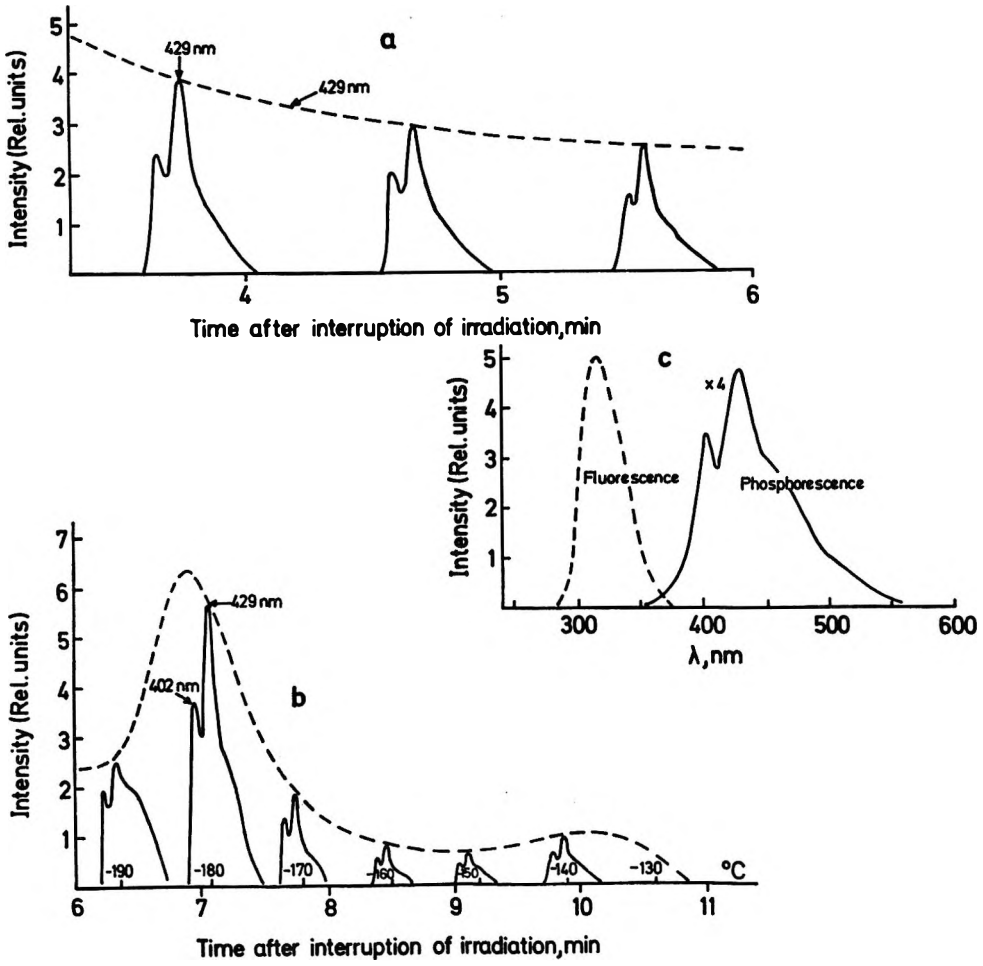

Figure 3. Luminescence spectra of tryptophan in EG–H_2O at 77°K: a, spectra of the afterglow of a uv-irradiated sample; b, spectra of the thermoluminescence of the same sample; c, the luminescence spectrum observed during excitation with 250-nm uv light.

with the experiments of Hase,[7] who found that there are two different types of electron traps in EG–H_2O at 77°K having absorption maxima at 565 and 660 nm, respectively.

In Figure 5 are shown the glow curves obtained when the sample was stored for various periods of time before heating was started. It can be seen that the TL_1 peak decreases significantly with increasing time of storage, indicating that the electrons associated with this peak disappear. The fact that at the same time the peak is shifted toward higher temperatures demonstrates that this glow peak represents a distribution of trap depths rather than a discrete one.

It appears that the type of electron trap associated with TL_1 is the same as that causing the afterglow. Figure 6 shows that the combined yield of afterglow and TL_1 increases with increasing time of storage, which means that radiationless reactions of the trapped electrons become increasingly favored when the temperature is raised. This seems a reasonable result, both because the rate of the chemical reactions, which presumably compete with trapping and recombination, is likely to increase with temperature and because the critical radius, *i.e.*, the distance at which the Coulomb energy of the pair of ions equals their thermal energy,[16] will decrease.

The TL_2 peak is not noticeably affected by storing the sample at 77°K for 30 min (Figure 5 and 6). This is in accordance with our esr measurements,[5] which showed that the total number of trapped electrons was unaltered to within 10% after several hours storage at 77°K. Similarly, both esr and optical absorption measurements show that the total number of trapped electrons does not decrease noticeably (<10%) upon heating the sample to 120°K, *i.e.*, to a temperature well above the TL_1 and just below TL_2. These results demonstrate that the afterglow and that part of the glow curve which is below 120°K, and which represents more than 95% of the recombination luminescence, represents a very small fraction of the total number of trapped electrons. Indeed, our esr measurements indicate that only of the order of 0.1% of the trapped electrons recombine with subsequent emission of luminescence. This is consistent

(16) L. Onsager, *Phys. Rev.*, **54**, 554 (1938).

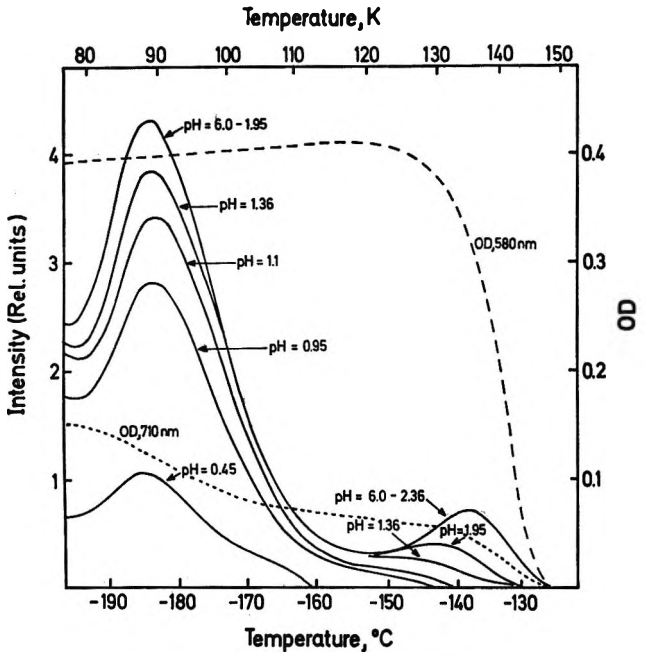

Figure 4. Glow curves of uv-irradiated samples of tryptophan in EG–H_2O at different pH values and the optical density of a sample (pH 6.0) at 580 and 710 nm as a function of the temperature. Heating rate: 14 deg/min.

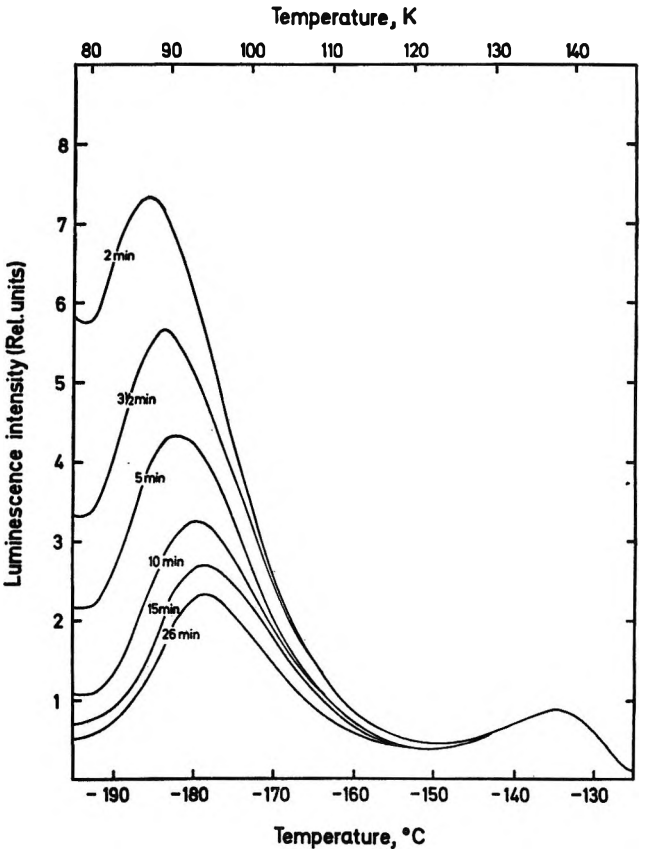

Figure 5. Glow curves obtained after storing the irradiated sample for various times at 77°K. The time of storage at 77°K is measured from interruption of the irradiation till starting of the heating.

with the previous conclusion that the great majority of the trapped electrons eventually react with ethylene glycol.[5]

Scavenger Effects. In order to find out if there is any correspondence between the trap depth and the initial distance between the recombining ions, we studied the effect of three electron scavengers, HCl, CCl_3COOH, and $NaNO_3$, on the recombination luminescence. Figure 4 shows the glow curves obtained with samples of different pH. Qualitatively similar results were obtained with CCl_3COOH and $NaNO_3$. The scavenger concentrations needed to halve TL_1 and TL_2 are given in Table I. These results demonstrate that TL_2 was quenched by considerably smaller concentrations of scavenger than was TL_1. Moreover, it was found that TL_1 was more susceptible to quenching than was the afterglow. A closer inspection of the glow curves in Figure 4 also shows that the electrons representing the high-temperature side of each glow peak are quenched more easily than those associated with the low-temperature side of the same peak. Hence, if it is assumed that there is a competition for the ejected electrons between trapping and reaction with scavenger and/or a competition for the trapped electrons between recombination and reaction with scavenger, the glow curve can be interpreted in terms of the distance between the tryptophan ions and the trapped electrons. Thus, the distance between two ions increases with the temperature at which they recombine. A similar conclusion was reached by Brocklehurst and Russell,[17] who studied the thermoluminescence of γ-irradiated naphthalene solutions.

Table I: The Electron Scavenger Concentrations Needed to Halve the Yields of TL_1, TL_2, and Trapped Electrons

Scavenger	$C_{1/2}$, mol/l. TL_1[a]	TL_2[a]	e_t^-[b]
HCl	~0.20	0.020	>0.20
$NaNO_3$	0.03	0.018	~0.025
CCl_3COOH	0.02	0.009	~0.012

[a] Values are believed to be correct to within ±20%. [b] Yields of e_t^- were determined by measurements of optical absorption at 585 nm.

By measuring the rate of discharge of a simple EG–H_2O filled capacitor at various temperatures at very low frequencies (~ 1 Hz) we found that the dielectric constant remained constant at approximately $\epsilon = 3.5$ up to about 140°K. This corresponds to a critical radius[16] of about 600 Å at 77°K. In accordance with the results of others[18] we find that the concentrations of efficient electron scavengers needed to halve the yield of trapped electrons (Table I), as observed by

(17) B. Brocklehurst and R. D. Russell, *Trans. Faraday Soc.*, 65, 2159 (1969).

(18) H. Hase and L. Kevan, *J. Phys. Chem.*, 74, 3358 (1970).

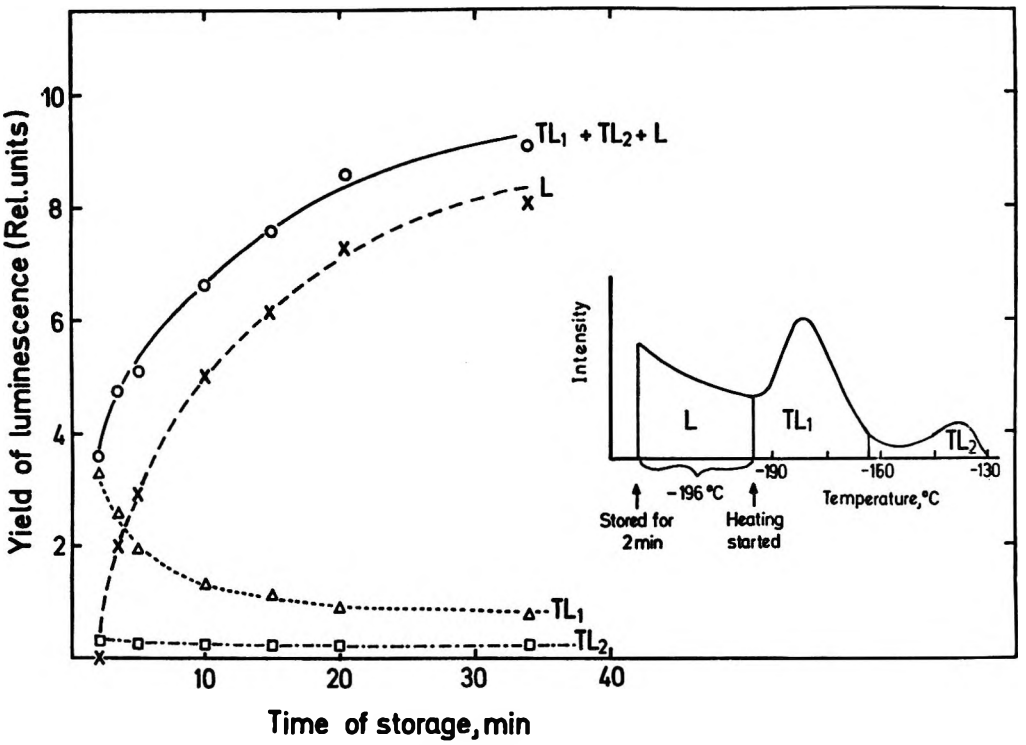

Figure 6. Yield of luminescence as a function of the time of storage of the sample at 77°K. L is the yield of afterglow measured from 2 min after interruption of the irradiation till the time when the heating was started, TL_1 is the yield of thermoluminescence between 77 and 110°K, and TL_2 is the yield of thermoluminescence between 110 and 150°K.

optical absorption measurements,[12] correspond to a mean distance between tryptophan cations and scavenger molecules of the order of 30 Å. Hence, although this estimate is, admittedly, the lower limit of the average distance between tryptophan cations and trapped electrons,[19] it seems likely that the majority of the electrons become trapped within the critical radius (*i.e.*, within 600 Å). Thus, when released from their traps at temperatures below 140°K the electrons will diffuse in the Coulomb field of the positive ions and their probability of geminate recombination will be relatively large. This conclusion is at variance with that of Debye and Edwards,[13] who assumed the Coulomb interaction to be negligible.

Above 140°K the dielectric constant was found to increase rapidly to about $\epsilon = 60$ at 160°K. This increase was associated with a marked softening of the solvent as measured by a simple viscosimeter as well as by a significant increase in the specific heat of the solvent, indicating that a phase transition takes place. The increase of the dielectric constant leads to a reduction of the critical radius to about 35 Å. Hence, the trapped electrons which are released above 140°K are likely to move randomly and their chances for geminate recombination will be greatly reduced. This may explain why TL_2 is much smaller than TL_1 in spite of the fact that TL_2 seems to be associated with the release of by far the greatest fraction of the trapped electrons.

According to Table I the efficiency of H^+ in reducing the yield of trapped electrons is at least one order of magnitude smaller than that of NO_3^- in spite of the fact that the reactivity of H^+ toward solvated electrons is larger than that of NO_3^-.[20] This is in accordance with the observation that the reactivity of H^+ toward "mobile electrons," *i.e.*, electrons in the pre-trapped state, is much smaller than that of many other efficient electron scavengers.[21] On the other hand, it appears from Table I that H^+ and NO_3^- are of equal efficiency in reducing TL_2 which is associated with the release of the trapped electrons. Hence, we conclude that H^+ reacts mainly with the electrons after they have been released from their traps, and furthermore, that these released electrons seem to be comparable to solvated rather than to mobile electrons with regard to reactivity.

(19) P. S. Dyne and O. A. Miller, *Can. J. Chem.*, 43, 2696 (1965).

(20) M. Anbar and P. Neta, *Int. J. Appl. Radiat. Isotopes*, 18, 493 (1967).

(21) L. Kevan in "Radiation Chemistry of Aqueous Systems," G. Stein, Ed., Interscience, London, 1968, pp 21–71.

Photoinduced Trapped Electrons in Rigid Polar Solution. II. Kinetics and Cross Section of Two-Quantum Ionization

by Johan Moan* and Harald B. Steen

Norsk Hydro's Institute for Cancer Research, Montebello, Norway (Received November 24, 1970)

Publication costs assisted by Norsk Hydro's Institute for Cancer Research

The kinetics of the ionization of tryptophan in an ethylene glycol–water glass at 77°K induced by 250-nm uv exposure have been studied. The dependence on exposure intensity and exposure time of (1) the yield of ionization (measured by the yield of thermoluminescence), (2) the kinetics of the buildup and decay of the phosphorescence observed upon onset and interruption of the exposure, and (3) the phosphorescence intensity with extended exposure are all in accordance with a theoretical scheme which implies that the ionization occurs exclusively by triplet absorption in the T_1 level of tryptophan. The ionization cross section of this level determined from these three types of experiment are, respectively: 5300 ± 2000, 4100 ± 600, and 3800 ± 800 l./mol cm.

Introduction

It is well known that uv exposure of certain solutes may cause ionization by triplet absorption, *i.e.*, when a molecule, excited to its lowest triplet level (T_1) absorbs a light quantum, and ionization may occur if the quantum energy is sufficiently high.[1-3] If the solvent is transparent to the uv light, it will be left unaffected during the primary action of the irradiation. All the uv-induced species in such solutions, therefore, have their origin in excited solute molecules. This is a favorable situation for studying ionic processes, and it is of interest to find methods to determine the absorption cross section of T_1 with regard to permanent ionization.

In the present work we have studied the kinetics of this type of photoionization, and three different methods to determine the ionization cross section of T_1 are described.

Kinetic Model

Figure 1 illustrates the various steps in the two-quantum ionization. A solute molecule absorbs a light quantum, giving rise to a transient intermediate, *e.g.*, T_1. This intermediate may absorb a second quantum and ionization may result. The following symbols are used: N_0, initial number of solute molecules; N_M, number of molecules in the intermediate state M; N_S, number of permanently ionized molecules; ϵ_0, extinction coefficient of the ground state; C_M, probability that light absorption by the ground state will give rise to the intermediate state; ϵ_M, extinction coefficient of the intermediate state; C_S, probability that light absorption by the intermediate leads to permanent ionization; k, rate of depopulation of the intermediate by other processes, *e.g.*, phosphorescence; I, intensity of uv exposure; I_P, phosphorescence intensity.

Referring to Figure 1 we have

$$\frac{d}{dt}N_M = C_M\epsilon_0 I[N_0 - N_M - N_S] - kN_M - C_S\epsilon_M I N_M \quad (1)$$

$$\frac{d}{dt}N_S = C_S\epsilon_M I N_M \quad (2)$$

The solution of these equations is

$$N_M = \frac{N_0 A}{R}[e^{-t/2(B-R)} - e^{-t/2(B+R)}] \quad (3)$$

$$N_S = \frac{N_0}{2R}[2R + (B - R)e^{-t/2(B+R)} - (B + R)e^{-t/2(B-R)}] \quad (4)$$

where t = time after onset of irradiation.

$$A = C_M\epsilon_0 I \quad (5)$$

$$B = k + aI \quad (6)$$

$$a = C_S\epsilon_M + C_M\epsilon_0 \quad (7)$$

$$C = C_S\epsilon_M I \quad (8)$$

$$R = \sqrt{B^2 - 4AC} \quad (9)$$

Provided that $4AC/B^2 \ll 1$, which turns out to be a valid assumption for our experimental conditions, and that we choose $t < B/AC$, we find from eq 4

(1) W. A. Gibbons, G. Porter, and M. I. Savadatti, *Nature*, **206**, 1355 (1965).

(2) Yu. A. Vladimirov and E. E. Fesenko, *Photochem. Photobiol.*, **8**, 209 (1968).

(3) H. B. Steen, *ibid.*, **9**, 479 (1969).

$$N_S \approx \frac{N_0 A C}{B}\left[t - \frac{1}{B}(1 - e^{-Bt})\right] =$$

$$\frac{N_0 C_M \epsilon_0 C_S \epsilon_M I^2}{k + aI}\left[t - \frac{1}{k + aI}(1 - e^{-(k+aI)t})\right] \quad (10)$$

Knowing N_S in relative units as a function of t for various values of the exposure intensity one can find the value of a and the apparent lifetime $\tau_D = 1/k$ of the intermediate as follows.[3]

For large values of t, N_S is seen to approach asymptotically a straight line which intercepts the t axis in $1/B = 1/(k + aI)$. Hence, by plotting B *vs.* I one should obtain a straight line which intercepts the B axis in k. If I is known in absolute units, a can be found from the slope of this line.

Provided a relatively high concentration of molecules in T_1 is obtained by the uv exposure, triplet absorption will compete noticeably with phosphorescence and radiationless modes of depopulation of T_1. As a result the kinetics of the buildup of the phosphorescence intensity following the onset of the uv exposure will be different from the kinetics of the phosphorescence decay as observed when the exposure is interrupted. We define the phosphorescence rise time, τ_R, by the equation

$$I_P = I_P^0(1 - e^{-t/\tau_R}) \quad (11)$$

where t is measured from the onset of the irradiation. The phosphorescence decay time, τ_D, is obtained from $I_P = I_P^0 e^{-t/\tau_D}$ where t is the time after interruption of the irradiation. Under the same assumptions as above we find from eq 3

$$N_M = \frac{N_0 A}{B}(1 - e^{-Bt}) = \frac{N_0 C_M \epsilon_0 I}{k + aI}(1 - e^{-(k+aI)t}) \quad (12)$$

If we assume that M is a phosphorescent triplet state, we can find relative values for N_M by measuring the phosphorescence intensity, *i.e.*, N_M = constant I_P. Comparing eq 6 and 7 we find

$$1/\tau_R = B = k + aI = 1/\tau_D + aI \quad (13)$$

Hence, by plotting $1/\tau_R$ *vs.* I, one should obtain a straight line from which k and a can be determined.

The difference between τ_R and τ_D described by eq 13 was first pointed out by Srinivasan, *et al.*[4] As noted by Jones,[5] however, these authors neglected the depletion of the ground state resulting from the light absorption. This effect is taken into account in the present treatment.

The third method to find the quantity a is to measure the maximum phosphorescence intensity I_P^0 for various uv intensities. For two values, I and I', of the exposure intensity we have according to eq 12

$$\frac{I_P^{0\prime}}{I_P^0} = \frac{I'}{B'}a + \frac{k}{B'}\left(\frac{I'}{I}\right) = I'\tau_R' a + k\tau_R'\left(\frac{I'}{I}\right) \quad (14)$$

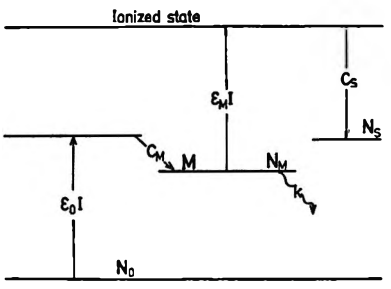

Figure 1. Scheme of the model for the two-quantum ionization.

Hence, a plot of $I^{0\prime}/I_P^0$ *vs.* I'/I should give a straight line which intercepts the $I_P^{0\prime}/I_P^0$ axes in $I'\tau_R' a$. If τ_R' has been determined as described above, a can be found. It should be noted that it is sufficient to measure N_S and I_P in relative units in order to determine a by the above three methods.

Having determined a, the value of $C_M \epsilon_0$ must be known in order to find the ionization cross section $C_S \epsilon_M$ (eq 7); ϵ_0 can be found from the absorption spectrum of the solute. Provided M is the T_1 state, C_M can be found from the phosphorescence to fluorescence ratio, Q, of the solute for the case that the combined quantum yield of fluorescence and phosphorescence at low-exposure intensity is unity. Thus

$$C_M = Q/(1 + Q) \quad (15)$$

Materials and Methods

L-Tryptophan was obtained from Sigma Chemical Co. and chromatographic grade ethylene glycol from Fluka. Both were used without further purification. Tryptophan was dissolved to a concentration of 5×10^{-4} M in a mixture of ethylene glycol and water 1:1 by volume. The sample containers were vessels of aluminum foil, 1 mm deep and 8 mm in diameter, containing 50 μl. The samples were cooled to 77°K, where they had the appearance of transparent, rigid glasses without visible cracks. The light source was a 200-W high-pressure mercury lamp fitted to two Bausch & Lomb grating monochromators in series. The surface of the sample was irradiated with 254-nm uv light. The light was focused on the sample by a quartz lens and the intensity was varied either by the use of a light chopper[3] or by varying the entrance slit of the monochromator nearest the lamp. The uv intensity was measured by actinometry[6] as well as by the use of a calibrated thermopile. The EMI 9558 BQ photomultiplier tube used to detect the phosphorescence and afterglow was protected by a Kodak 2A gelatin filter to exclude fluorescence. Thermoluminescence glow curves

(4) B. N. Srinivasan, M. Kinoshita, J. W. Rabalais, and S. P. McGlynn, *J. Chem. Phys.*, **48**, 1924 (1968).

(5) P. F. Jones, *ibid.*, **49**, 3730 (1968).

(6) C. A. Parker, "Photoluminescence of Solutions," Elsevier, London, 1968, p 208.

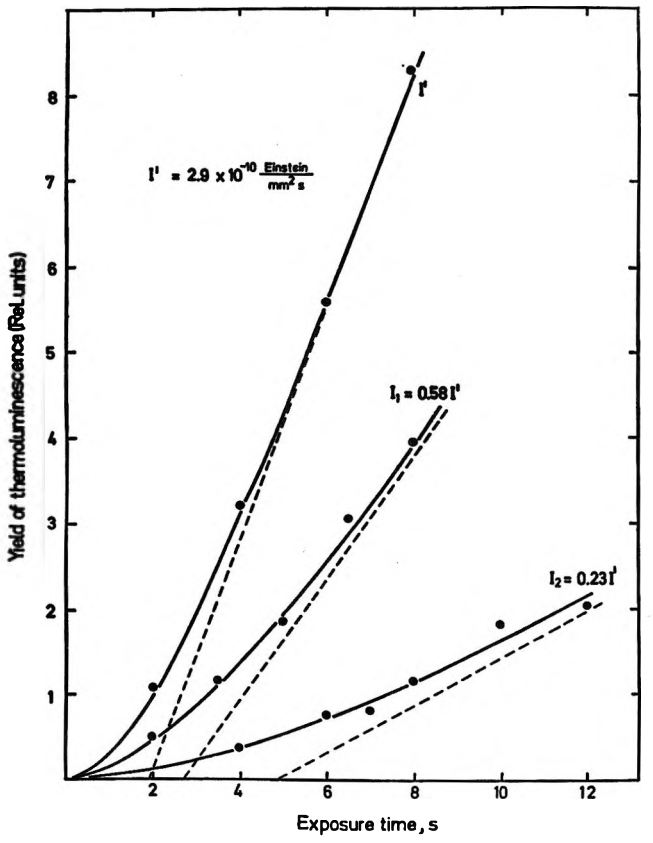

Figure 2. The yield of thermoluminescence as a function of the exposure time observed with three different intensities. The full curves represent eq 10 fitted to the experimental points (after correction for optical bleaching) by the method of least squares. The broken lines are the asymptotes of these curves.

were recorded while the sample was heated at 14 deg/min. The apparatus and the experimental procedure are described in more detail elsewhere.[7,8]

Results and Discussion

Thermoluminescence Yields. It is commonly assumed that the thermoluminescence (TL) of rigid solutions of aromatic compounds arises from thermally activated charge recombination.[1,9,10] In the following, therefore, we assume that the yield of thermoluminescence is proportional to the yield of ionization. The shape of the TL glow curves was independent of the yield of TL. The TL of the solvent was negligible. The characteristics of the TL are described elsewhere.[8]

Figure 2 shows the yield of TL as a function of the exposure time for three different intensities. It was found that the uv light used for excitation caused a noticeable bleaching, *i.e.*, reduction of the TL. The magnitude of this effect, which was usually of the order of a few per cent, was determined separately and has been corrected for in Figure 2. As demonstrated in Figure 2, curves described by eq 10 can be fitted to these corrected values to within the limits of experimental uncertainty. Furthermore, by plotting the interception of the asymptotes of these curves with the t axis *vs.* I, a

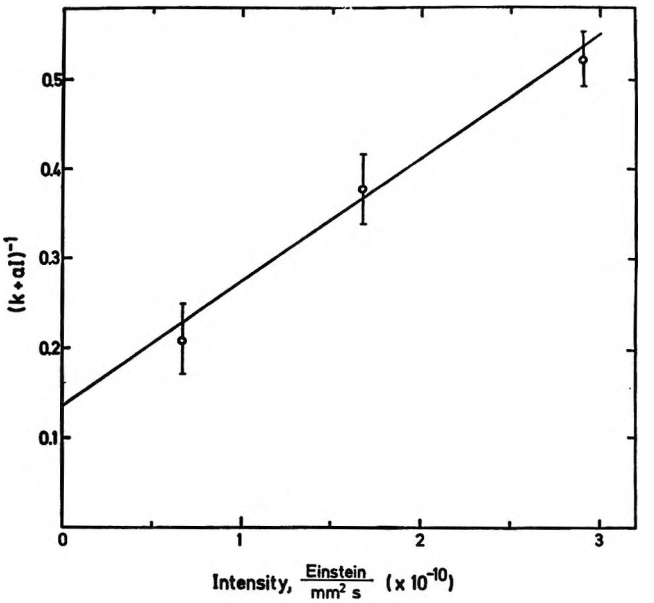

Figure 3. The interception with the t axis of the asymptotes of the curves in Figure 2 *vs.* intensity (eq 6).

straight line is obtained (Figure 3) as predicted by eq 6 and 10. From Figure 3 we obtain $a = 6000 \pm 2000$ l./mol cm and $k = 0.14 \pm 0.04$ sec^{-1}. The latter value is in good agreement with the decay constant of the T_1 level of tryptophan, which is 0.15 sec^{-1} under the present conditions (Figure 4). This value also agrees with the findings of Rabinovitch.[11] Hence, it appears that the T_1 level is indeed the intermediate involved in the ionization observed here.

Another test of the model is to compare the measured relative exposure intensities with those which can be determined from the slopes of the asymptotes of the curves in Figure 2 by the use of eq 10. The results listed in Table I demonstrate that reasonable agreement is found.

The large uncertainties in the values of k and a determined from the TL measurements are due to poor

Table I

Measured intensity, rel units	Intensity calculated from model, rel units
I	1
0.58	0.62
0.23	0.29

(7) H. B. Steen, *Photochem. Photobiol.*, 6, 805 (1967).
(8) J. Moan and H. B. Steen, *J. Phys. Chem.*, 75, 2887 (1971).
(9) D. I. Roshschupkin and Yu. A. Vladimirov, *Biofizika*, 10, 48 (1965).
(10) B. Brocklehurst, R. D. Russell, and M. I. Savadatti, *Trans. Faraday Soc.*, 62, 1129 (1966).
(11) B. Rabinovitch, *Arch. Biochem. Biophys.*, 128, 252 (1968).

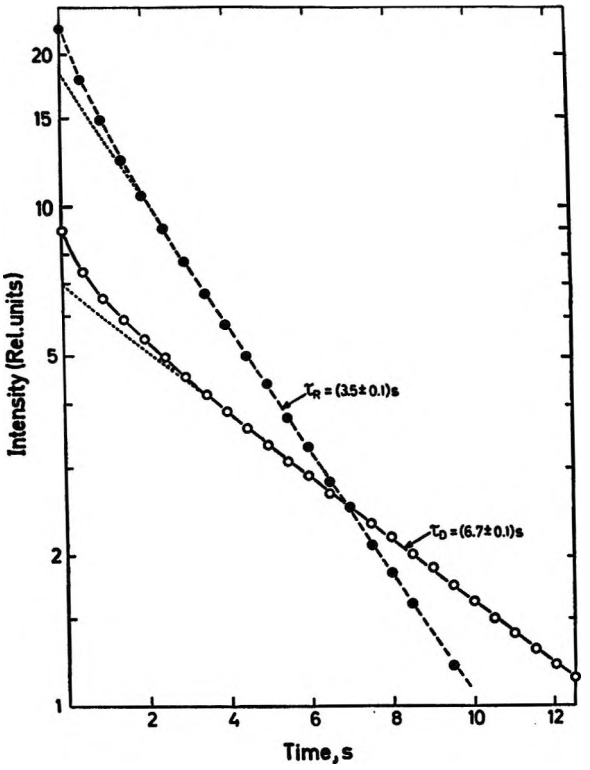

Figure 4. Rise and decay of phosphorescence intensity, I_P. For the rise period $I_P^0 - I_P$ is plotted *vs.* time, and for the decay period I_P is plotted *vs.* time; I_P^0 is the maximum intensity of phosphorescence.

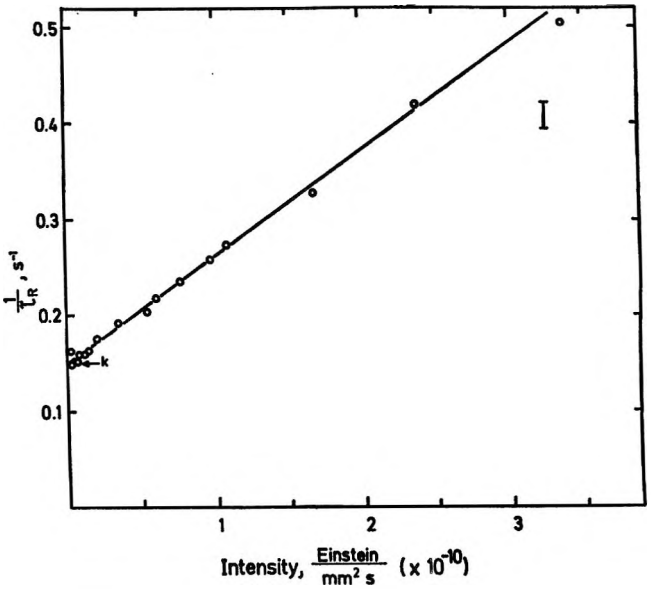

Figure 5. The reciprocal value of the rise lifetime as a function of the intensity of the uv exposure.

Table II

Results obtained by	k, sec^{-1}	a, l./mol cm	C_S, ϵ_M, l./mol cm
Thermoluminescence (eq 10, Figure 3)	0.14 ± 0.04	6000 ± 2000	5300 ± 2000
Phosphorescence (eq 13, Figure 5)	0.15 ± 0.01	4800 ± 600	4100 ± 600
Phosphorescence (eq 14, Figure 6)	0.16 ± 0.02	4500 ± 800	3800 ± 800

reproducibility of these data. The reason for this is not clearly understood, but our impression is that the yield of TL depends somewhat on the exact procedure of the cooling of the sample and on the time of storage prior to irradiation.

Phosphorescence Rise and Decay. In the following it is assumed that the intermediate M is the T_1 level of tryptophan. Figure 4 shows that the rise and decay of the phosphorescence follow first-order kinetics except for a small deviation in the first few seconds which is probably due to luminescence from the solvent. It appears also that τ_R is markedly shorter than τ_D. In Figure 5 τ_R is plotted as a function of the exposure intensity in accordance with eq 13. The points conform to a straight line, thus supporting the above model. The values of a and k found from this graph are given in Table II.

In contrast to the present conclusion that the difference between τ_R and τ_D is caused by triplet absorption, Rabinovitch[11] suggests that the bimolecular quenching process $T_1 + S_0 \rightarrow 2S_0$ is responsible for this difference as observed for tryptophan in 6 *N* HCl at 77°K. However, he used a tryptophan concentration which corresponds to a mean distance between solute molecules of about 120 Å. To us this process seems very unlikely at such distances. Another consequence of the Rabinovitch hypothesis is that τ_D should depend on the intensity of exposure. No such dependence is observed in the present work.

Phosphorescence Intensity. Figure 6 shows $I_P^{0\prime}/I_P^0$ plotted *vs.* I'/I according to eq 14, and again the data conform to the model to within experimental uncertainty. The values of a and k found from Figure 6 are given in Table II.

The values of a and k obtained by the three different methods (Table II) are seen to agree to within the limits of uncertainty. It should be noted that there is a small systematic error in all these experiments which has not been taken into account, namely the absorption of phosphorescence and TL which is caused by the trapped electrons. From the data of Table II, however, we calculate that the maximum error in N_S caused by this effect does not exceed a few per cent in these experiments.

The value of $C_M\epsilon_0$ needed to calculate $C_S\epsilon_M$ has been found by using the phosphorescence to fluorescence ratio of tryptophan under the present conditions[12] and

(12) H. B. Steen, *Radiat. Res.*, **41**, 268 (1970).

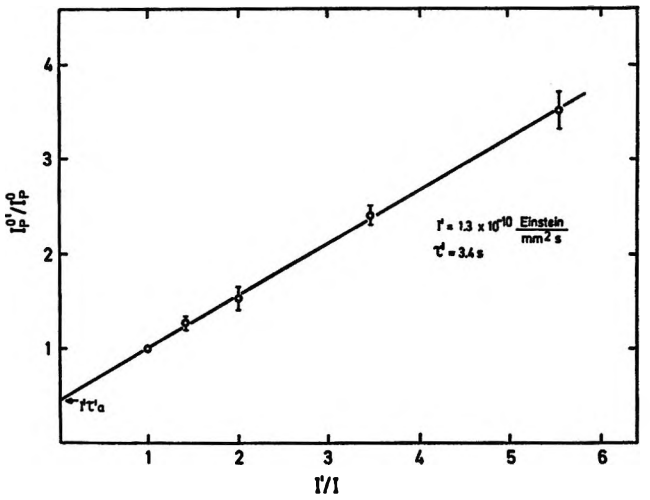

Figure 6. Phosphorescence data plotted in accordance with eq 8.

the extinction of tryptophan at 250 nm in H_2O at room temperature. The values for $C_S\epsilon_M$ are given in Table II. These values are considerably smaller than triplet extinction coefficients of various aromatic molecules,[13] indicating that C_S is considerably smaller than unity, *i.e.*, that spontaneous electron–ion recombination has a relatively high probability. This is in accordance with our previous finding[14] that the yield of the X-ray induced ionization of tryptophan which is followed by spontaneous recombination is very high, *i.e.*, $G \approx 4$. The measurement of ϵ_M of tryptophan which will allow a direct determination of C_S is now being prepared.

Conclusion

It appears that all the present data are in accordance with the above model, implying that triplet absorption is the only mode of ionization in this case. The cross section of the triplet state with regard to permanent ionization can be determined from measurements of the yield of TL as well as from the kinetics of the phosphorescence buildup and decay and from the maximum phosphorescence intensity. However, the two latter methods give more accurate results and are both much easier and less laborious to employ experimentally than the measurement of TL.

(13) R. A. Keller and S. G. Hadley, *J. Chem. Phys.*, 12, 2382 (1965).
(14) H. B. Steen, *Israel J. Chem.*, 8, 227 (1970).

On the Photochemistry of the Ferrioxalate System[1]

by G. D. Cooper and B. A. DeGraff*

Department of Chemistry, University of Virginia, Charlottesville, Virginia 22901 *(Received April 26, 1971)*

Publication costs assisted by the Department of Chemistry, University of Virginia

The photochemistry of the ferrioxalate system has been investigated under neutral and acid conditions with excess oxalate using kinetic spectroscopy. While the earlier results are qualitatively confirmed, the system is somewhat more complex than previously thought. A new short-lived transient was detected at $\lambda \leq 300$ nm in both acid and neutral solutions and assigned as either the $\cdot CO_2^-$ or $C_2O_4\cdot^-$ radical. This radical is responsible for the secondary reduction of Fe(III). Evidence suggests that photoaquation competes effectively with photoredox as a primary process. The slower absorbance changes which occur at $t > 200$ μsec after the flash in the 310–500-nm region are due to the decomposition of the Fe(II) oxalato complexes and the anation of $Fe(C_2O_4)_n(H_2O)_m^{+3-2n}$. Observed kinetic parameters are presented and a mechanism is discussed.

Introduction

The photoredox of aqueous ferrioxalate solutions has been investigated extensively.[2-5] The absolute quantum yields for Fe(II) production at a number of wavelengths have been determined and when the experimental conditions are within the limits suggested by Parker and Hatchard,[6] this photoredox system forms the basis of one of the more popular chemical actinometers. While there is general agreement on the quantum yields at the common mercury lines,[7-9] the actual detailed mechanism of the photoredox and secondary redox reactions is still incomplete. Examination of the

(1) Presented in part at the 9th Informal Conference on Photochemistry, Columbus, Ohio, Sept 1970.
(2) (a) A. J. Allmand and W. W. Webb, *J. Chem. Soc.*, 1518 (1929); (b) R. Livingston, *J. Phys. Chem.*, 44, 601 (1940).
(3) C. A. Parker, *Proc. Roy. Soc., Ser. A*, 220, 104 (1953).
(4) C. A. Parker, *Trans. Faraday Soc.*, 50, 1213 (1954).
(5) K. Yamashita and H. Imai, *Bull. Chem. Soc. Jap.*, 41, 1339 (1968).

system by kinetic spectroscopy under conditions in which the trisoxalato complex predominated indicated that a reactive intermediate was formed but its decay rate did not appear to depend on the concentration of the complex.[10] This finding prompted the suggestion that the intermediate was not a fragment ($\cdot CO_2^-$, $C_2O_4\cdot^-$, or $HC_2O_4\cdot$) from the photoredox of the complex as originally thought, but was some excited form of the complex itself and that the observed decay was likely the unimolecular decomposition of the "metastable complex." The effect of light dosage on the amount of intermediate generated and its decay rate was also studied with results which seemed to point to a second-order decay component at high light dosage. Earlier experiments on the photolysis of frozen ferrioxalate solutions using esr showed that free radicals were generated and that the solution also turned brown.[11] However, the intensity of coloration did not seem to correlate with the apparent population of free radicals. Thus, there is evidence to support each of the various detailed mechanisms that have been suggested, but no conclusive case could be made for a particular mechanism. We therefore undertook a reexamination of the aqueous ferrioxalate system under experimental conditions such that the tris complex is the only significant complex and also under acid conditions such that the dioxalato complex is the predominant species.

Experimental Section

The basic flash photolysis apparatus used in this work has been described previously.[12] The monitoring light source for kinetic experiments was a Hanovia 200-W Hg–Xe lamp while a Hanovia 150-W Xe lamp was used for obtaining spectra *via* the point by point method.

Solutions were prepared using distilled and deionized water. The ionic strength was adjusted for kinetic experiments with $LiClO_4$. Reagent grade chemicals were used as supplied. A recrystallized sample of $K_3Fe(C_2O_4)_3$ was kindly supplied by Professor R. A. Rousseau. Solutions were purged with either Ar, O_2, or N_2O (depending on the experiment) for at least 45 min and transferred to the photolysis cell without contact with air. Photolysis cells used in this study included 2-, 10-, and 20-cm single wall and a 20-cm double wall type, all of fused quartz. The outer chamber of the latter could be filled with various filter solutions to delimit the range of wavelengths incident on the sample.

The temperature dependence of the rate constants was obtained using the 20-cm double wall cell. The cell, charged with sample and with water in the outer jacket, was brought to the desired temperature in a small thermostated box and held at that temperature for at least 1 hr. The cell was then quickly placed in the photolysis apparatus and flashed within 2 min of its removal from the thermostat. Immediately following the flash, the temperature of the sample was obtained using a calibrated copper–constantan thermocouple. From blank experiments the rate of warming (or cooling) of the filled cell was known, and thus the sample temperature at flash time could be estimated to within $\pm 0.2°$.

Rate constants were derived from Polaroid pictures of the oscilloscope traces. Points on the voltage–time curve obtained from the scope were read with calipers and converted to absorbancy with the aid of a Hewlett-Packard Model 9100B computer. The usual least-squares first- or second-order plots were then constructed to obtain the rate constant.

Unless otherwise noted, the cell was filled with fresh solution for each experiment and all solutions deaerated by argon purging.

Except as noted, the total percentage decomposition for all kinetic experiments was limited to under 10%. This was accomplished by either wrapping the cell with a translucent paper or by using a Plexiglas filter. Both materials effectively limited the light absorbed by the sample to the 340–500-nm region. Using these filters, pseudo-first-order kinetics were observed for all absorbance changes occurring at $t > 200$ μsec after the flash.

Results

Experiments at pH 6.7 with Excess Oxalate. As the oxalate/Fe(III) ratio was always at least 10:1 and usually 25:1, the only significant iron species is the trisoxalato complex. The cell filters provide that only the complex absorbs the flash light. Qualitatively, the absorbance–time behavior of these solutions upon flashing is in agreement with that reported previously.[10] A transient(s) is produced that absorbs more strongly than the starting complex in the 370–500-nm region. A "spectrum" of the intermediate obtained by taking the difference in sample optical density at 1 and 20 msec after the flash is shown in Figure 1 and is also similar to that previously reported.[10] Further, we confirm the first-order decay of the "transient(s)" absorbing in the 370–500-nm region. However, the results of experiments to determine the kinetic dependence of the transient decay on iron and excess oxalate shown in Figure 2 indicate that the situation is somewhat more complicated than previously thought. These experiments were done at constant ionic strength ($I = 0.1$) and monitored at 420 nm, an isosbestic point for the initial and final complexes. For the determination of the Fe(III) dependence, solutions containing from 2.1

(6) C. G. Hatchard and C. A. Parker, *Proc. Roy. Soc., Ser. A*, **235**, 518 (1956).

(7) G. B. Porter, J. G. W. Doering, and S. Karanka, *J. Amer. Chem. Soc.*, **84**, 4027 (1962).

(8) J. Lee and H. H. Seliger, *J. Chem. Phys.*, **40**, 519 (1964).

(9) J. Baxendale and N. K. Bridge, *J. Phys. Chem.*, **59**, 783 (1955).

(10) C. A. Parker and C. H. Hatchard, *ibid.*, **63**, 22 (1959).

(11) D. J. E. Ingram, W. G. Hodgson, C. A. Parker, and W. T. Rees, *Nature*, **176**, 1227 (1955).

(12) B. A. DeGraff and K. J. Lang, *J. Phys. Chem.*, **74**, 4181 (1970).

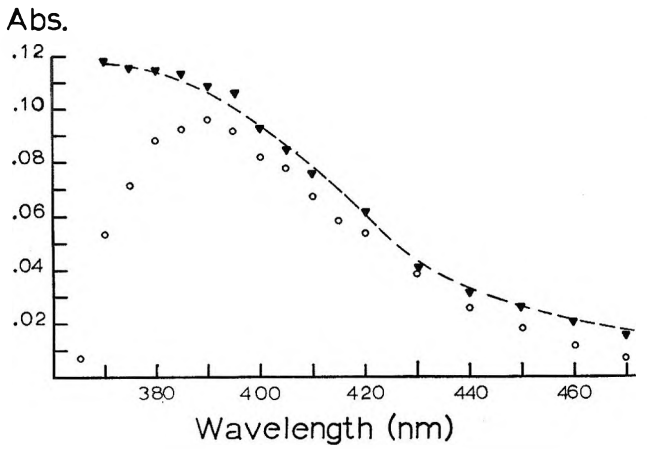

Figure 1. Absorption spectrum of the transient observed at pH 6.7 with excess oxalate: ▼, observed values calculated as the difference between sample absorbance at 1 msec and 20 msec after the flash; ●, calculated spectrum based on reaction 4.

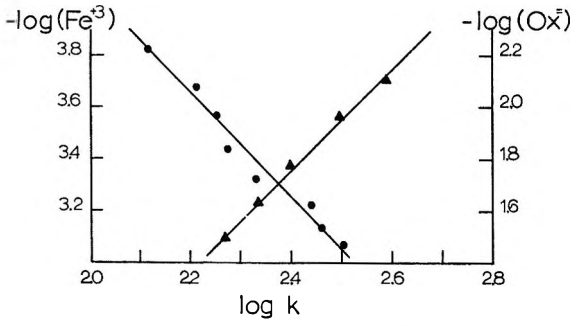

Figure 2. Kinetic dependence of slow transient decay at pH 6.7 with excess oxalate: ●, for Fe(III); ▲, for $C_2O_4^{2-}$, monitored at 420 nm.

to 8.4×10^{-4} M Fe(III), 1.5×10^{-2} M oxalate, and the appropriate amount of $LiClO_4$ were flashed and the pseudo-first-order rate constant was computed. For the oxalate dependence, the Fe(III) was held at 6×10^{-4} M and the total oxalate varied from 6×10^{-3} to 3×10^{-2} M. Again, $LiClO_4$ was used to maintain the ionic strength. The slopes of the appropriate log–log plot indicated a half-order dependence on Fe(III) and a minus half-order dependence on oxalate ion. A small reduction in the quantum yield of Fe(II) with added oxalate was noted by Allmand and Webb.[2a]

Starting at about 300 nm and continuing to 265 nm, the practical wavelength limit for this study, the absorbance changes on flashing showed a new feature. A species was observed which was formed during the flash and which decayed very rapidly (*i.e.*, $t_{1/2} < 50$ μsec). Plots of the decay fitted to various orders showed the intermediate was disappearing by a first-order process. However, as the flash intensity decay constant, also "first order" at $t > 40$ μsec, was of comparable magnitude to that of the species decay, its apparent order and decay constant are of doubtful quantitative significance. An additional problem was encountered in that

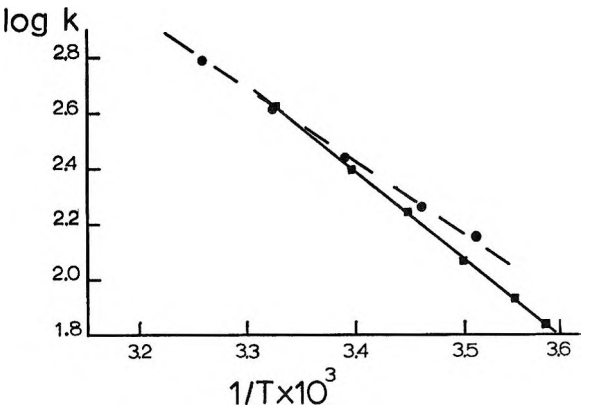

Figure 3. Arrhenius plots for slow transient decay at pH 6.7 with excess oxalate: ●, monitored at 366 nm; ■, monitored at 420 nm.

the high extinction coefficients of ferrioxalate at these wavelengths necessitates the use of rather dilute solutions. Under these circumstances, local depletion by the analysis lamp beam makes the exact ferrioxalate concentration at the time of the flash subject to some uncertainty. Although a complete spectrum of the transient was not obtained, a comparison, based on the mechanism discussed later, of the observed transient absorbance at several wavelengths with the observed reduction of Fe(III) gave molar extinction values comparable to those reported for $CO_2\cdot^-$ or $C_2O_4\cdot^-$.[13,14] The preceding observation lead us to further examine the "transients" which were observed in the near-ultraviolet and visible spectral regions.

To ascertain whether more than one intermediate was responsible for the absorbance changes in the 310–500-nm region, the oxalate dependence and the "apparent" activation energy were determined at various monitoring wavelengths. The Arrhenius plots are shown in Figure 3 while the oxalate dependence is shown in Table I. Although the variation with wavelength is not dramatic, it appears to lie outside the limits of experimental error.

Table I: Dependence of Kinetic Parameters on Monitoring Wavelength for Transient Decay at pH 6.7 with Excess Oxalate

λ, nm	E_A, kcal/mol	k,[a] sec^{-1}	$[Ox]^n$	$[Fe(III)]^n$
420	14.2	$2.4 \pm 0.3 \times 10^2$	$n = -1/2$	$n = 1/2$
405		$2.4 \pm 0.3 \times 10^2$	$n = -1/2$	
366	11.8	$3.1 \pm 0.3 \times 10^2$	$n = -1/2$	

[a] Average of two experiments with $[FeOx_3^{3-}] = 6 \times 10^{-4}$ M and added $[Ox^{2-}] = 1.5 \times 10^{-2}$ M.

(13) P. Neta, M. Simie, and E. Hayon, *J. Phys. Chem.*, **73**, 4207 (1969).

(14) N. Getoff, F. Schworer, V. M. Markovic, K. Sehested, and S. O. Nielsen, *ibid.*, **75**, 749 (1971).

Experiments at pH 1.4 with Added Excess Oxalate. As the pH is lowered to ~1.4 (sulfuric acid being used to adjust pH) the predominant iron species changes from the tris to the dioxalato complex. Concomitant with the change in composition, the temporal behavior of the absorbance after the flash changes markedly from that observed at higher pH. While the absorbance still decays by a first-order process in the 310–500-nm region, the observed decay rate constants are a factor of at least 10 greater than was observed at pH 6.7.

A search of the spectral region below 310 nm revealed a fast decaying intermediate with spectral and kinetic properties identical, within the large experimental error, with those observed at the higher pH. In the region 320–500 nm, there are three principal features to the absorbance changes. These are (1) a sharp drop complete within about 200 μsec, (2) a rapid decay which is complete within 2–4 msec, and (3) finally a slow increase in absorbance which is not yet complete at the end of 20 msec. A "spectrum" of the intermediate responsible for the rapid decay, computed as the difference between the sample absorbance at 300 μsec after the flash and that at the end of the rapid decay (*i.e.*, ~4 msec), is shown in Figure 4.

To determine the kinetic dependence of the rapid decay on total Fe(III) and excess oxalate, experiments similar to those described for pH 6.7 were performed. In this series, the Fe(III) dependence was obtained by varying the total iron over the range 3×10^{-4} to 1.08×10^{-3} M while the oxalate dependence was determined over the range 1.8×10^{-3} to 1.6×10^{-2} M. The results for Fe(III), Figure 5, indicate a first-order dependence while the oxalate results, not shown, give an order of 0.08 with scatter and hence is taken as effectively zero.

Since changing the pH of a solution of fixed total iron and oxalate concentration also changes the relative percentage of the three oxalate complexes, experiments were carried out in which the $[H^+]$ was varied from 4.46×10^{-2} to 11.8×10^{-2} M with only minor changes in the relative amounts of the three complexes. The results, shown in Table II, indicate that the reaction responsible for the decay is not particularly sensitive to the pH.

To confirm that changes in the relative amounts of the three oxalate complexes are responsible for the observed changes in the absorbance decay rates, a series of experiments was done to determine the Fe(III) dependence of the absorbance decay at 436 nm for several different pH values. The initial composition of the solutions was calculated from the measured pH and published stability constants.[15] Although the value given by Lambling for the $Fe(C_2O_4)^+$ ion has been questioned,[16] the more recent values[17] are lower and confirm that this species is unimportant under our conditions. The results of the series are shown in Table III. The calculation of solution composition is not corrected for

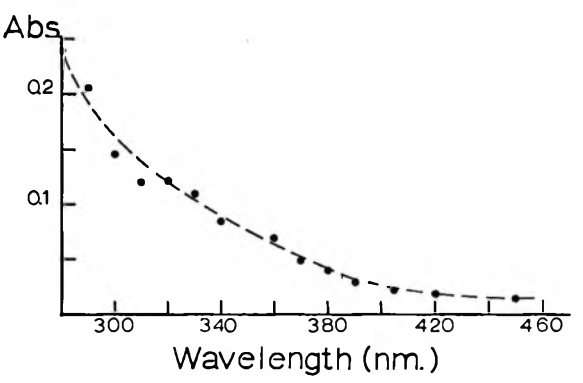

Figure 4. Absorption spectrum of the transient observed at pH 1.4 with excess oxalate. Calculated as the difference between sample absorbance at 300 μsec and 4 msec after the flash.

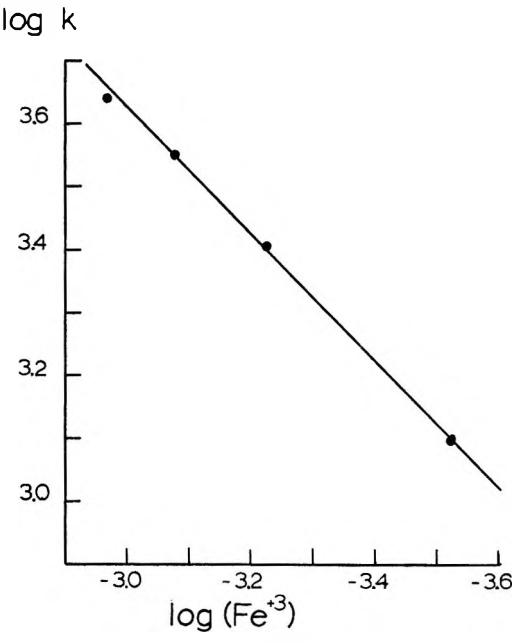

Figure 5. Kinetic dependence of rapid transient decay at pH 1.4 with excess oxalate on Fe(III), monitored at 436 nm.

Table II: Effect of $[H^+]$ on the Observed Rate Constant for the Absorbance Decay at 436 nm

$[H^+] \times 10^2$	$Fe(C_2O_4)_2^-$,[a] %	k, sec^{-1}
4.46	86.7	$2.5 \pm 0.3 \times 10^3$
8.93	92.7	$2.9 \pm 0.3 \times 10^3$
11.8	92.3	$2.7 \pm 0.3 \times 10^3$

[a] The total Fe(III) was 6×10^{-4} M with 1.68×10^{-2} M total oxalate.

(15) M. J. Lambling, *Bull. Soc. Chim. Fr.*, 495 (1949).

(16) A. K. Babko and L. I. Dubovenko, *J. Gen. Chem. USSR*, 26, 757 (1956).

(17) E. G. Moorhead and N. Sutin, *J. Inorg. Chem.*, 5, 1866 (1966).

Table III: Kinetic Parameters for the Absorbance Decay at 4360 Å for Solutions of Various Complex Compositions

pH	Fe-$(C_2O_4)_3^{3-}$,[a] %	Fe-$(C_2O_4)_2^{2-}$, %	k_{obsd},[b] (sec^{-1})	[Fe(III)][a]	Abs[c] at λ = 400 nm
6.7	100		2.3×10^2	$n = 0.51$	0.623
5.0	99.2	0.8	2.2×10^2	$n = 0.53$	0.628
3.35	94.3	5.5	4.9×10^2	$n = 0.51$	0.640
1.4	12.6	86.5	2.6×10^3	$n = 0.98$	0.901

[a] The percentage of $Fe(C_2O_4)^+$ was always negligible. [b] The values quoted are for a solution containing 6×10^{-4} *M* Fe(III) and 1.68×10^{-2} *M* oxalate. [c] Absorbance values for solution noted in *b* with 10-cm cell.

ionic strength. Though the calculations must be regarded as approximate, the absorbance values at 400 nm clearly indicate a marked change in solution composition in going from pH 3.35 to 1.40.

Finally, the apparent activation energy for the fast absorbance decay at 436 nm at pH 1.4 was found to be 8.6 kcal/mol.

The slow increase in absorbance which followed the two fast decays was investigated briefly. The increase followed first-order kinetics at $t \geq 10$ msec after the flash and was independent of the Fe(III) concentration. In a typical experiment with 6×10^{-4} *M* Fe(III), 1.68×10^{-2} *M* oxalate, and pH 1.35, the observed rate constant was $k = 4.5 \pm 1$ sec^{-1}.

Discussion

The several previous steady illumination studies on the ferrioxalate system dictate several rather stringent conditions which an acceptable mechanism must meet. Because the quantum yield of Fe(II) exceeds 1.0 at $\lambda \leq 436$ nm, the primary photochemical process must generate fragments capable of further reduction of the ferrioxalate molecule. Further, the insensitivity of the quantum yield to temperature and intensity variation strongly suggests that the reaction of the reducing photofragment with the ferrioxalate has a high specific rate constant and low activation energy.

With the above boundary conditions in mind, the results of this study can be discussed in terms of a general mechanism shown below using the trisoxalate ion as the example.

$$Fe(C_2O_4)_3^{3-} + h\nu \longrightarrow Fe(C_2O_4)_2^{2-} + C_2O_4^-/CO_2,CO_2^- \quad (1a)$$

$$Fe(C_2O_4)_3^{3-} + h\nu \longrightarrow Fe(C_2O_4)_2^{1-} + 2CO_2^- \quad (1b)$$

$$Fe(C_2O_4)_3^{3-} + h\nu \xrightarrow{H_2O} [Fe(C_2O_4)_2(H_2O)_2]^{-1} + C_2O_4^{2-} \quad (1c)$$

$$C_2O_4^-/CO_2^- + Fe(C_2O_4)_3^{3-} \longrightarrow 2CO_2/CO_2 + Fe(C_2O_4)_3^{4-} \quad (2)$$

$$Fe(C_2O_4)_3^{4-} \rightleftharpoons Fe(C_2O_4)_2^{2-} + C_2O_4^{2-} \quad (3)$$

$$[Fe(C_2O_4)_2(H_2O)_2]^{1-} + C_2O_4^{2-} \rightleftharpoons Fe(C_2O_4)_3^{3-} \quad (4)$$

$$2C_2O_4^-/2CO_2^- \longrightarrow \text{products } (C_2O_4^{2-}, CO_2, \text{other}) \quad (5)$$

In the above, the $C_2O_4^{2-}$, $C_2O_4^-$, or CO_2^- may be protonated depending on the pH.

A clear choice between (1a) and (1b) as a primary process is difficult with the present data. The reported spectra for CO_2^- [13] and $C_2O_4^-$ [14] are very similar and there appears to be some question as to the separate existence of $C_2O_4^-$. Further, even if (1b) were the sole primary process, the newly formed CO_2^- would be expected to react at least part of the time with its parent complex thus rendering (1b), on our time scale, indistinguishable from (1a). However, the detection of reaction 4 in our system means that reaction 1b must be considered as a possible primary process. A more likely explanation for the origin of reaction 4 is that photoaquation, reaction 1c, is competitive with the photoredox. Since the quantum yield of Fe(II) does not equal 2 and is rather intensity insensitive, the implication would seem to be that the photoredox process does not have a quantum efficiency of 1.0. Hence other primary processes must be competing with the redox step.

A series of experiments were performed using steady illumination (λ 313 nm) with added isopropyl alcohol in an attempt to scavenge all the free $CO_2^-/C_2O_4^-$ and from the observed quantum yield allow a choice between (1a) and (1b). The solutions were oxygen saturated to prevent the $CH_3\dot{C}HOHCH_3$ radical from reacting with the complex. As previously reported, oxygenation had little effect on the observed quantum yield for the acid solution in the absence of the alcohol. Though a reduction in the quantum yield of Fe(II) on addition of isopropyl alcohol was observed, the effect was small (*i.e.*, a 10% reduction at 0.87 *M* isopropyl alcohol) and unacceptably high alcohol concentrations would have been required to ensure complete scavenging.

The rapid decay of the species detected at $\lambda \leq 300$ nm in both neutral and acid solution is assigned to reactions 2 and 5. Under the conditions used for the experiments, reaction 5 predominates for $t \leq 100$ μsec. As previously noted, quantitative kinetic study of this intermediate's reaction with ferrioxalate is precluded with the present system. Based on the extinction coefficients and recombination rate constants for either CO_2^- or $C_2O_4^-$, we can estimate a lower limit for $k_2 \geq 5 \times 10^7$ M^{-1} sec^{-1}. This estimate is of the same magnitude as found for the reaction of ·OH with various metal ions.[18] In any case, it appears that a primary process for both the tris- and dioxalato ferrate ions results in generation of either $C_2O_4^-$ or CO_2^- and that this radical reacts with ferrioxalate or itself, depending on experimental conditions, very rapidly. This implies

(18) M. Anbar and P. Neta, *Int. J. Appl. Radiat. Isotop.*, **16**, 227 (1965).

that the "slower" absorbancy changes seen in the region $\lambda > 300$ nm are a result of various ligand substitution reactions involving the Fe(II) and Fe(III) complexes resulting from the primary process and subsequent reactions of $C_2O_4^-/CO_2^-$ with the ferrioxalate.

Reaction 5 is competitive with reaction 2 only under conditions of dilute Fe(III) and high light intensity such as found in flash experiments. Pulse radiolysis studies suggest rate constants, $2k_5$, of 1.5×10^9 M^{-1} sec^{-1} and 9.6×10^8 M^{-1} sec^{-1} for CO_2^- and $C_2O_4^-$, respectively.[13,14] However, the latter value was derived rather indirectly and must be regarded with some skepticism at present.

At pH 6.7 and at our oxalate/Fe(III) ratios, the predominant final product of the photolysis is $Fe(C_2O_4)_2^{2-}$ while the $Fe(C_2O_4)_3^{3-}$ ion is essentially the only initial Fe(III) complex. If reaction 1a were the sole primary process, the only "slow" absorbance change expected after the fast reduction steps would be that due to reaction 3. If, however, either reaction 1b or 1c are primary processes, then two "slow" absorbance changes due to (3) and (4) might be expected. However, the release of one oxalate by $Fe(C_2O_4)_3^{4-}$ might be expected to be a rather rapid process and hence the slow decay seen at pH 6.7 might be due primarily to reaction 4. To test this, the expected absorbance changes were calculated from spectra of $Fe(C_2O_4)_3^{3-}$, $Fe(C_2O_4)_2^{1-}$,[19] and $Fe(C_2O_4)_2^{2-}$ [20] assuming reaction 4 was responsible for the observed changes. This calculated spectrum is compared with the observed in Figure 1. While the fit is reasonably good at $\lambda \geq 400$ nm, the two diverge markedly in the near-ultraviolet. Thus, while reaction 4 may contribute to the absorbance changes at $\lambda \geq 310$ nm, it is not the only contributor. Further, since reaction 4 is an anation reaction, a kinetic order between zero- and first order with respect to oxalate is expected rather than the minus half-order observed.

It is possible to eliminate the contribution from reaction 4 to the observed absorbance changes by monitoring at ~366 nm, an isosbestic point for $Fe(C_2O_4)_3^{3-}$ and $Fe(C_2O_4)_2^-$. As shown in Table I, a reaction other than (4) is occurring and appears to be the origin of the minus half-power oxalate dependence. It seems likely that reaction 3 is responsible and that the reverse reaction accounts for the negative oxalate dependence. Experiments done using 334 and 313 nm as monitoring wavelengths showed that after the initial drop in absorbance, complete within 200 μsec, a slow decay followed by a slow absorbance increase occurred. While spectral data for $Fe(C_2O_4)_3^{4-}$ are not available, comparison of the spectra of the other ferrous and ferrioxalates indicate that the observed decay should be attributed to reaction 3 and the absorption increase to reaction 4.

Because an independent spectrum of $Fe(C_2O_4)_3^{4-}$ is not available, it was not possible to eliminate the contribution of reaction 3 from the observed absorbance changes and obtain some measure of and kinetic parameters for reaction 4. Because of this difficulty, we refrain from further detailed speculation on the mechanistic implications of the observed half-order dependences. We are presently examining the monooxalatoferrate system in order to gain some additional understanding of these labile systems.

Around pH 1.4 the situation appears somewhat more tractable. The absorbance changes suggest that both reactions 3 and 4 are occurring, but under these conditions the rates of the two processes are sufficiently different that they can be effectively separated. At this pH the principal Fe(III) species is the dioxalato complex while the products are a mixture of aquo and monoxalatoferrous complexes. Based on the spectra of the various complexes, the absorbance decay which is observed immediately after the $CO_2^-/C_2O_4^-$ has disappeared is assigned to the decomposition of the unstable ferrous complex(s) while the much slower absorbance increase is attributed to the anation reaction 4.

The apparent first-order dependence of the ferrous complex decomposition on Fe(III) suggests that an electron-transfer mechanism is involved. Indeed, the observed activation energy is quite similar to that found for the Fe^{2+}–$Fe(C_2O_4)^+$ system.[21] However, if the apparent first-order dependence on Fe(III) is real, then $k_3 = 1.1 \times 10^{13} \exp(8600/RT)$ and the A factor seems rather high. Further, the rate constant is such as to require an outer sphere transfer mechanism. Thus, we regard this interpretation as tentative.

The slow absorbance increase is reasonably attributed to reaction 4. The fact that an increase in absorbance is observed in the 300–400-nm region agrees with the observed independent spectra of $Fe(C_2O_4)^+$ and $Fe(C_2O_4)_2^-$.

Finally, it appears that flash photolysis may provide a means not only of studying photoredox reactions, but also of obtaining rate constants for processes such as $ML_n^{+m} \rightarrow ML_{n-1}(H_2O)_r^{+m+r} + L^{-r}$. Such kinetic data for unstable species is, at present, difficult to obtain.

Acknowledgments. This work was supported in part by the Petroleum Research Fund and by the Cottrell Fund of the Research Corp. It is a pleasure to acknowledge helpful conversations with Professor M. Z. Hoffman.

(19) Data obtained in this laboratory.

(20) V. Babaera and M. A. Mosyagina, *Dokl. Akad. Nauk SSSR*, **64**, 823 (1949).

(21) R. A. Horne, *J. Phys. Chem.*, **64**, 1512 (1960).

Photoelectron-Induced Decomposition of Ethane[1]

by Robert R. Hutchins and Robert R. Kuntz*

Department of Chemistry, University of Missouri, Columbia, Missouri 65201 *(Received December 31, 1970)*

Publication costs assisted by The National Science Foundation

The decomposition of ethane by low-energy electrons has been investigated using photoelectrons accelerated by electric fields. The mechanism of this decomposition is characterized by formation of neutral excited states and the absence of major ionic processes. Isotope and inhibition experiments establish the similarity between this decomposition and that which accompanies vacuum-uv and applied field radiolysis studies. Evidence is presented suggesting that superexcited states contribute significantly to the decomposition. Apparent differences between the electron energy degradation spectrum caused by ionizing radiation and the energy distribution resulting from acceleration of electrons in an electric field do not substantially alter the neutral processes.

Introduction

When ionizing radiation interacts with matter, a complex spectrum of ionic and neutral chemical processes results. The importance and nature of each of these mechanisms has not been easy to establish because many of the products and intermediates are formed both from neutral electronically excited states (excitation mechanism) and from ionic intermediates (ionic mechanism). Studies of the excitation mechanism have been made using electrical discharges, applied fields during radiolysis, vacuum uv photolysis, and accelerated photoelectrons.[2] The present investigation is an extension of the earlier studies by Williams[3] and was designed to determine the extent to which accelerated photoelectrons could duplicate the excitation mechanism in radiation chemistry. Ethane was chosen as the subject of this investigation primarily because sufficient knowledge about its decomposition in the vacuum uv is available[4-7] for a mechanism comparison and evaluation.

Experimental Section

Apparatus and Procedures. The reaction vessel consisted of a set of cylindrical coaxial electrodes, 7 mm apart, surrounded by a Vycor 7910 jacket and was similar in design to one described by Williams.[3] Electrons were generated photoelectrically at the inner silver electrode by light from a Hanovia SC-2537 low-pressure mercury coil lamp which passed first through the Vycor jacket and copper screen anode. It was possible to maintain a relatively high photoelectric efficiency in a vacuum system capable of maintaining pressure of less than 10^{-4} mm after a short cleaning process involving an electrical discharge in hydrogen.

Potentials of 0–400 V were applied to the reaction vessel electrodes by an external dc power supply. A microammeter in series with the power supply permitted the measurement of photocurrent which was usually maintained between 4 and 10 μA. Constant photocurrents were maintained during irradiation by adjustment of the lamp intensity. Photocurrent was directly proportional to lamp intensity in all cases.

The preparation of reactants and reaction mixtures and filling of the reaction vessel was carried out on a mercury-free vacuum line. The reaction vessel was filled by allowing the reactant to expand into it and an adjacent oil manometer. After irradiation, the reaction vessel was connected to a Toepler pump through a liquid air trap. Considerable care was exercised at this point in order to prevent the entrance of mercury into the reaction vessel. Frequent checks for mercury sensitized reactions were made by performing experiments with no electrical field applied.

The product mixture was transferred to collection vessels of known volume by the Toepler pump. The collection vessels were fitted with a silicone rubber septum and attached to the vacuum line by means of a syringe barrel permanently sealed onto the vacuum line. This made it possible to inject known fractions of the reaction mixture directly into a gas chromatograph with a gas syringe. This collection procedure was tested for product recovery by filling the reaction vessel with a synthetic product mixture containing quantities corresponding to the small yields in actual irradiations. Recovery was always quantitative within analysis error.

(1) Based on the Ph.D. Thesis of R. R. Hutchins, University of Missouri, Columbia, Mo., 1970.

(2) See L. Wayne Sieck, "Fundamental Processes in Radiation Chemistry," P. Ausloos, Ed., Interscience, New York, N. Y., 1968, p 119.

(3) R. R. Williams, Jr., *J. Phys. Chem.*, **63**, 776 (1959); **66**, 372 (1962).

(4) (a) H. H. Carmichael, R. Gordon, Jr., and P. Ausloos, *J. Chem. Phys.*, **42**, 343 (1965); (b) R. F. Hampson, Jr., J. R. McNesby, H. Akimoto, and I. Tanaka, *ibid.*, **40**, 1099 (1964).

(5) R. F. Hampson, Jr., and J. R. McNesby, *ibid.*, **42**, 2200 (1965).

(6) A. H. Laufer and J. R. McNesby, *ibid.*, **42**, 3329 (1965).

(7) S. G. Lias, G. J. Collin, R. E. Rebbert, and P. Ausloos, *ibid.*, **52**, 1841 (1970).

Analyses of the hydrocarbon products were made on a chromatograph with hydrogen flame detectors, while hydrogen was analyzed with a thermal conductivity gas chromatograph. A 9-ft column 1/4 in. in diameter and containing a mixture of 95% Porapak-Q and 5% Porapak-T was used to separate and measure CH_4, C_2H_2, C_2H_4, C_3H_6, and C_3H_8. A second fraction of the reaction mixture was injected onto a 2-ft Porapak-T column for measurement of *n*-butane. A third fraction was injected onto a molecular sieve column, 5 ft × 1/4 in., for measurement of hydrogen. Much of the gas injected into the chromatograph was laboratory air which contained traces of methane. A correction (<20%) was made on the methane yields by injecting the corresponding quantity of air before each sample injection. Material balances of $C_{2.00}H_{6.15}$ were typical for the products at low conversions, which indicates a satisfactory recovery and measurement of all major products.

The hydrogen and methane resulting from irradiation of deuterium labeled ethane were separated from ethane by means of a liquid nitrogen trap, collected, and then analyzed by mass spectrometer.

Reagents. Ethane purchased from Matheson was passed through a column of bromine adsorbed on charcoal to remove the unsaturates. Methane was removed by a combination of trap-to-trap distillation and prolonged pumping at liquid air temperatures. All impurities except C_2H_4 were always reduced to less than 10^{-3} mol %. The C_2H_4 impurity was never greater than 1.6×10^{-3} mol %. Nitric oxide, obtained from Matheson, was used without further purification. Mass spectrometric analysis of C_2D_6, purchased from Merck Sharp and Dohme revealed the C_2D_6, contained 4.4% C_2D_5H.

Results and Discussion

It was presumed at the beginning of this investigation that a range of applied voltage and pressure (V/P) could be established in which ionic processes would play a chemically insignificant role. Few assumptions regarding the nature or energy of the excited species may be made, however, as can be surmized from the experimental data from ionizing radiation and discharge studies. Electrons in radiation chemistry are degraded from high initial energies by inelastic collisions. The electron energy distribution in these cases favors the production of superexcited states.[8] In discharge studies, electrons have low initial energies and are accelerated by electrical fields. The electron energy distribution in discharges favors excitation to levels below the ionization potential and the probability of spin-forbidden excitation becomes large. In addition, the discharge studies are complicated by electron densities such that successive excitation of free radical intermediates by low-energy electrons is possible[9] and by the unknown influence of vibrationally hot molecules.[10]

These photoelectron experiments resemble more closely the applied field radiolysis studies than discharge or radiation experiments. A comparison of the product yields from this study with those assigned to the excitation part of the radiolysis is shown in Table I.

Table I: Products from the Decomposition of Ethane by Low-Energy Electrons

	Applied field radiolysis,[a] $X/P \sim 20$ V/cm-mm	Accelerated photoelectrons,[b] $V/P = 29$ V/mm
	C_2H_6–NO (1:0.02)	
H_2	1.50	1.44
CH_4	0.19	0.19
C_2H_4	(1.00)	(1.00)
C_2H_2	0.26	0.24
C_3H_8	0.043	0.019
	C_2H_6–C_2D_6–NO (1:1:0.04)	
H_2	47	48.2
HD	22	20.0
D_2	31	31.9

[a] See ref 4a, $P = 30$ mm. [b] $P = 10$ mm.

Electron impact spectra of ethane[11] suggest that the excited triplet state is comparable in importance to the excited singlet under conditions of low-energy electron radiolysis, but a dependence of the decomposition mechanism for excited states of saturated hydrocarbons on multiplicity has not been demonstrated.[2] In applied field radiolysis studies it has been possible to explain the decomposition mechanism of excited neutrals by involving only those excited singlet states characteristic in the vacuum-uv photolysis of ethane. Therefore, it is convenient to also compare this mechanism with the photolysis mechanism. A recent paper[7] reports quantum yields for four primary processes at photolysis energies of 8.4, 10.0, and 11.6–11.8 eV. The following is a list of the primary processes reported in decreasing order of relative importance in the 11.6–11.8-eV photolysis

$$C_2H_6^* \longrightarrow C_2H_5^{\ddagger} + H \quad (1)$$

$$C_2H_6^* \longrightarrow C_2H_4^{\ddagger} + H_2 \quad (2)$$

$$C_2H_6^* \longrightarrow CH_4 + CH_2 \quad (3)$$

$$C_2H_6^* \longrightarrow CH_3 + CH_3 \quad (4)$$

(8) R. L. Platzman, *Radiat. Res.*, **17**, 419 (1962).

(9) J. L. Magee and M. Burton, *J. Chem. Phys.*, **23**, 2194, 2195 (1955).

(10) For a summary of differences in radiation chemistry and discharge chemistry, see M. Burton and K. Funabashi, *Advan. Chem. Ser.*, **No. 80**, 140 (1969).

(11) H. H. Brongersma and L. J. Oosterhoff, *Chem. Phys. Lett.*, **3**, 437 (1969).

Some of the fast secondary processes observed photolytically are

$$C_2H_5^{\ddagger} \longrightarrow C_2H_4 + H \quad (5)$$

$$C_2H_4^{\ddagger} + M \longrightarrow C_2H_4 \quad (6)$$

$$C_2H_4^{\ddagger} \longrightarrow C_2H_2 + H_2 \quad (7)$$

$$CH_2 + C_2H_6 \longrightarrow C_3H_8^{\ddagger} \quad (8)$$

$$C_3H_8^{\ddagger} + M \longrightarrow C_3H_8 \quad (9)$$

$$C_3H_8^{\ddagger} \longrightarrow CH_3 + C_2H_5 \quad (10)$$

Ionic Contribution. In order to study neutral chemical processes, it is necessary to find a range of V/P (volts/millimeter) where ionization is not chemically significant. On the other hand, if one is to try to approximate the excitation mechanism of ionizing radiation, it is necessary that the electronically excited states be produced with relatively high energy.[8] Consequently, it was considered desirable to work in regions of V/P where the excitation mechanism dominated the observed chemistry rather than excluded ionic processes completely.

A typical study of product yield and cell current as a function of V/P is shown in Figure 1 for an ethane pressure of 4 mm. The vacuum photocurrent was established in a completely evacuated cell. The cell current at all pressures approached the vacuum photocurrent limit as V/P was increased, but only at a pressure of 1 mm or less did the two coincide prior to the onset of ionization. It is assumed that this decrease in electron collection efficiency at low accelerating voltages is due to back scattering of electrons from collisions near the cathode. The threshold for product formation is well within the vacuum photocurrent limit and yields vary smoothly through the onset of ionization indicating no major change in decomposition mechanism as ionization becomes important. Product yields were found to be directly proportional to cell current over a 1–7 μA range.

Ion pair yields for the decomposition of ethane may be calculated from the data used in Figure 1 assuming complete collection of ions and photoelectron production equivalent to the vacuum photocurrent after the onset of ionization.[12] These yields appear as a function of V/P in Figure 2. If ionization plays a major role in the decomposition, then ion pair yields should be near 1.0. The observed decrease in yields with increasing V/P may be an indication of increased ion collection efficiency at the electrodes in addition to increased ionization since homogeneous neutralization cannot be ruled out. The apparent ion pair yields, however, appear to approach a plateau region near a value $M/N \sim 12$ at $V/P > 50$.[13] Thus it appears that the major decomposition path is by excitation rather than ionization. Another indication that homogeneous neutralization is of minor importance in these studies

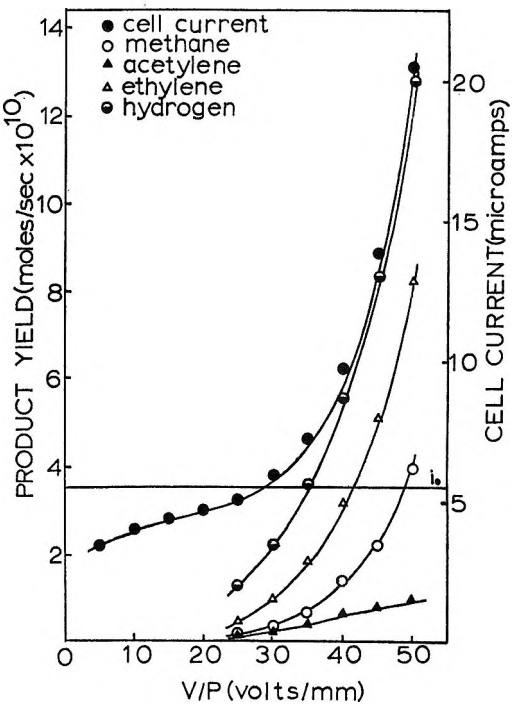

Figure 1. Cell current and product yield as a function of V/P in volts/millimeter. Vacuum photocurrent is designated by line labeled i_0, P = 4 mm.

comes from the excellent agreement of product yields in this study with those from the excitation part of applied field radiolysis studies (Table I). In the latter studies, all products were collected in regions of V/P such that the cell current never exceeded the saturation current level. These results are consistent with those of Williams,[3] who argues that a similar region of V/P existed for CH_4 and C_2H_6 where excitation was the major path to decomposition. Subsequent studies in this series were conducted at V/P = 29 and 10 mm pressure where less than one ion pair was collected per six primary photoelectrons, which corresponded to an apparent ion-pair yield of 63.

Time Studies. Product yields were measured as a function of time in order to obtain the initial product distribution. From Figures 3 and 4, which contain yields measured in the absence of NO, initial rates of formation can be observed for all of the indicated products. At conversions above 0.07% (t = 5 min in Figure 4) a secondary mechanism, characterized primarily by

(12) This assumption, in effect, neglects electron back scattering to the cathode at values of V/P at which ionization starts to occur. Extrapolations of ion current calculated with the assumption *vs.* V/P give consistent values of ionization thresholds at various pressures, however, considering the nonparallel plate electrode assembly.[17]

(13) Small deviations of photoelectron production from that predicted from the vacuum photocurrent (<40% in the pressure range investigated here) would lower the apparent values of M/N at low values of V/P, but would not greatly affect the plateau region where cell current exceeds vacuum photocurrent by an order of magnitude. The conclusions of this argument are, then, independent of the back scattering problem.[12]

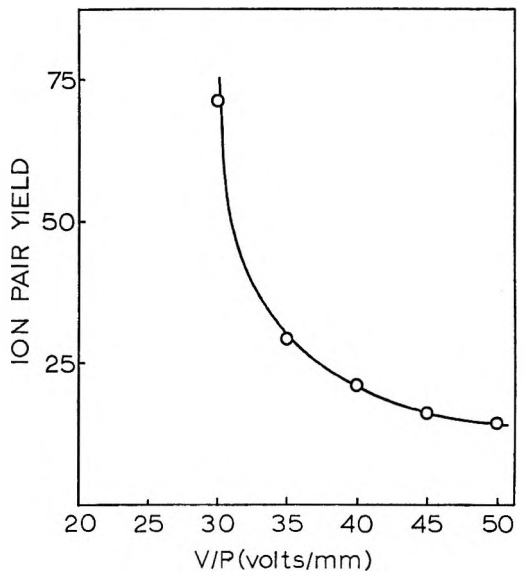

Figure 2. Ion-pair yields for the decomposition of ethane. Ethane decomposition yield is based on product material balance and yields are calculated on the basis of complete ion collection, P = 4 mm.

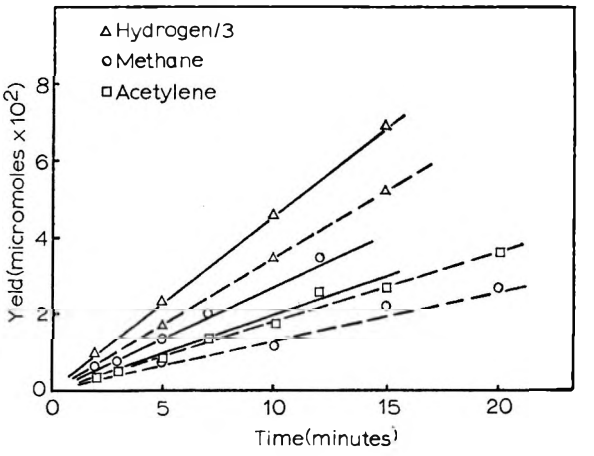

Figure 3. Time studies of yields of hydrogen, methane, and acetylene: △, $H_2/3$; ○, CH_4; □, C_2H_2. Solid lines are yields in absence of NO, broken lines indicate presence of 2% NO. Reactant P = 10 mm, V/P = 29 V/mm.

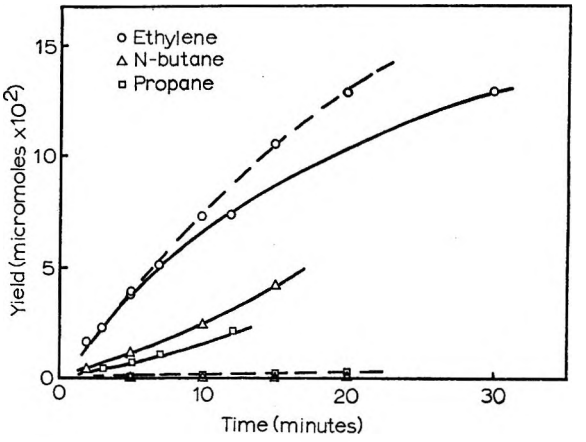

Figure 4. Time studies of yields of ethylene, propane, and n-butane: ○, ethylene; □, propane; △, n-butane. Solid lines are yields in the absence of NO, broken lines indicate presence of 2% NO. Reactant P = 10 mm, V/P = 29 V/mm.

decreasing $R_{C_2H_4}$ (rate of C_2H_4 production) and increasing $R_{n\text{-}C_4H_{10}}$ begins. The importance of thermal H-atom scavenging by C_2H_4 could not be ascertained from these experiments, since the lowest conversions measured here would correspond to nearly complete scavenging of thermal H atoms.[14] It was discovered that the decrease in ethylene yield is related to the increase in butane yields by adding ethylene to the system prior to irradiation in an amount equal to its concentration at 0.07% conversion. In this experiment the butane was formed at an initial rate equal to the rate of the secondary step in Figure 4.

Nitric Oxide Inhibition. In a number of experiments, NO was added to the reaction mixture to inhibit free radical processes. A concentration of 2 mol % was used since it has been shown that the concentration is sufficient for maximum inhibition in the γ radiolysis of ethane.[15] The effect, also shown in Figures 3 and 4, may be explained in terms of the photolysis mechanism.

The C_2H_2 yields and the initial yields of C_2H_4 are unaffected by the presence of NO, suggesting "molecular" formation of these products. This observation is compatible with reactions 1, 2, 5, 6, and 7. At higher conversions, $R_{C_2H_4}$ decreases significantly faster in the absence of NO which suggests that C_2H_4 is removed as the result of a secondary reaction involving C_2H_4 and a free radical.

The rate of formation of methane was reduced by a factor of 2.1 when NO was added. The substantial fraction not scavenged indicates the importance of "molecular" formation of CH_4 which, if truly molecular as in reaction 3, would require production of an equivalent quantity of CH_2. A subsequent reaction of CH_2 (reaction 8) provides an explanation for the small but significant yields of unscavenged C_3H_8. Propane formed by CH_2 insertion is excited and will decompose unless stabilized by collision. A value of 0.14 was found for the ratio $R_{C_3H_8}/R_{CH_4}$ in the presence of NO at a total pressure of 10 mm, indicating that most of the propane formed by reaction 8 decomposes before stabilization at this pressure. This interpretation is consistent with the mechanism proposed by Carmichael, *et al.*,[4a] in the 1236-Å photolysis of ethane in which the $R_{C_3H_8}/R_{CH_4}$ value was found to be 0.117 at 10.1 mm pressure and 2% NO.

The H_2 yields are reduced by about 25% upon the addition of NO which is strong evidence for the formation of H_2 from atomic hydrogen. The "molecular" hydrogen may result partially from hot H atoms or hetero-

(14) R. A. Back, *Can. J. Chem.*, **37**, 1834 (1959).

(15) K. Yang and P. J. Manno, *J. Amer. Chem. Soc.*, **81**, 3507 (1959).

geneous reactions which are competitive with NO inhibition.

Isotope Studies. Isotope studies can distinguish unambiguously between molecular and "hot" atomic process if the isotopic distributions of the molecular products are unique. The results of irradiation of equimolar mixtures of C_2H_6 and C_2D_6 in the presence and absence of NO are shown in Table II. It can be seen that both molecular H_2 and H_2 formation through atomic processes are important. Also, these atomic processes are not completely quenched by 2% NO indicating that "hot" H atoms are involved in the process. An increase in V/P, which should favor the formation of atomic hydrogens shows only a small increase over the small range of V/P studies. This change is not large enough to argue that reaction 1 is increasing in importance, as indicated by the photolysis studies,[7] but it cannot be certain that a small change in V/P will significantly alter the high energy tail of the electron energy distribution.

Table II: Irradiation of Isotopically Labeled Ethanes[a]

V/P	%NO	H_2	HD	D_2	CD_3H/CD_4
25	0	48.3	25.7	25.9	
29	0	46.8	26.4	26.7	0.896
34	0	44.0	27.3	28.6	
29	2	48.2	20.0	31.9	0.171

[a] 50% C_2H_6 + 50% C_2D_6.

If methane is formed exclusively by methyl radical abstraction, CD_3H/CD_4 should be greater than unity due to isotope effects. The value here of 0.9 indicates that much of the CD_4 formed in the absence of NO is molecular as in reaction 3. Removal of free radicals by added NO further decreases this ratio to 0.171 in qualitative support of a molecular formation of methane. The molecular yield of CD_3H from C_2D_5H would constitute $^2/_3$ of the total molecular methane produced from this isotopic impurity assuming no isotope effect. The expected CD_3H/CD_4 ratio should be (0.67) (0.044) = 0.029 from purely molecular reactions. It would appear, since excess CD_3H in the observed ratio must arise from CD_3 radical abstraction, that a substantial part of the methyl radicals are not scavenged by NO and may have excess energy.

Energy of Excitation. Interpretation of the data observed here by a mechanism based on thermal decomposition or electronic excitation of intermediates[10] cannot be ruled out. It does seem unlikely, however, that a mechanism resulting from such processes would be explained as well be the photolysis mechanism as this one is. The occurrence of reactions 1, 2, and 3 is strongly indicated in this study. Reaction 4, observed photolytically, cannot be evaluated here since other sources of CH_3, such as reactions 10 and 11, occur to an unknown extent.

$$H + C_2H_5 \longrightarrow C_2H_6^{\ddagger} \longrightarrow 2CH_3 \qquad (11)$$

Comparison of the HD measured here with amounts produced in photolytic studies[7] (Table III) suggests that the average energy of excitation in this work was greater than 11.6 eV. This assumes that the increase in HD, interpreted here as an increase in the importance of reaction 1 compared with reaction 2, continues to increase with excitation energy as observed in the photolytic work. The HD yields reported here should be somewhat smaller since the C_2D_5H (4.4% of C_2D_6) present could yield some HD *via* reactions 2 and 7. However, a correction based on the maximum HD obtainable from this source does not change the HD yields significantly.[16] Two other reactions, 12 and 13, could also affect these yields.

Table III: Effect of Excitation Energy on Decomposition Modes

	Photolysis			Accelerated photoelectrons		
	8.4 eV	10.0 eV	11.6 eV	V/P 25	V/P 29	V/P 34
	C_2H_6–C_2D_6 (1:1)[a]					
H_2	65	53	43	48		44
HD	3	12	19	26		27
D_2	32	35	38	26		29
	C_2H_6–C_2D_6–NO (1:1:0.04)[b]					
H_2	66.5	51.5			48	
HD	3.5	10.5			20	
D_2	30.0	38.0			32	

[a] See ref 6. [b] See ref 4a.

$$C_2H_4^{\ddagger} \longrightarrow C_2H_3 + H \qquad (12)$$

$$C_2H_5^{\ddagger} \longrightarrow C_2H_3 + H_2 \qquad (13)$$

Neither of these reactions is significant below 11.6 eV[7] and should not affect the estimate of 11.6 eV as the lower limit of the effective excitation energy. It is possible that ionic processes could have contributed to the HD yields, especially if homogeneous neutralization is important. This does not appear likely, however, when one considers that the relative amount of HD obtained at a V/P of 25 (where $i < i_0$) is larger than the corresponding photolysis yields.

It could well be that the HD yields reported here are actually lower limits since conversions were too high to exclude scavenging of thermal H atoms by C_2H_4. The

(16) Assuming no isotope effects and equal excitation cross sections for C_2D_6 and C_2D_5H, the H_2–HD–D_2 ratio may be corrected for HD produced in reactions 2 and 7 from the 4.4% C_2D_5H impurity. This correction leads to H_2:HD:D_2 = 48:25:27 instead of the value reported in Table III.

possibility of heterogeneous H-atom abstractions and combinations should also be noted since diffusion times to the wall based on a rigid sphere collision model and thermal kinetics are about 2 orders of magnitude smaller than the H-atom lifetime in nonscavenged systems.

Further qualitative estimates of the effective electron energies may be made by reference to the magnitude of the V/P parameter at which ionization starts to occur. Appearance potential-like plots of ion current *vs.* V/P at 4 mm pressure extrapolates to a value of V/P = 28.5 for the onset of ionization. Assuming the ionization potential of C_2H_6 in 11.6 eV leads to a scale adjustment factor of 0.102 for the 4 mm data. The onset of product formation from a similar yield *vs.* V/P plot is 17.5, which corresponds to a product appearance potential of 7.1 ± 0.8 eV where the error is based on estimates of the uncertainty of extrapolations. This value is in good agreement with the 7.1 eV threshold for electron impact excitation[11] considering the questionable validity of using a scaling factor under conditions of multiple electron–molecule collisions.[17] Use of the equivalent scale factor at 10 mm predicts a maximum electron energy of 12.3 eV under conditions of the studies here (V/P = 29, 10 mm). Photoionization studies by Schoen[18] have shown that excitation cross sections are larger than ionization cross sections below 12.0 eV. Assuming the cross sections for electron impact excitations are similar in behavior to photon absorption cross sections near the ionization region as in the case of CH_4,[11] the present data should be interpreted in terms of a predominant excitation mechanism with effective excitation energies in the vicinity of the ionization potential.

The similarity of these studies to the applied field radiolysis experiments leads us to conclude that both techniques should yield similar information. They differ essentially in the initial electron energy distribution and in the production of ions as a source of electrons in the latter. Although the products resulting from the excitation mechanism in the applied field radiolysis studies were established rather convincingly, the complication of ionic processes is a potential disadvantage to the use of this technique. The accelerated photoelectron technique, on the other hand, does not involve initial ionization, and ionization by the accelerated photoelectrons does not appear to be a serious problem.

Acknowledgment. This research was supported in part by Grants GP5912 and GP8684 from the National Science Foundation. The authors are grateful to Professor R. Kent Murmann for his help in the determination of product distributions in the isotope studies.

(17) Additional evidence for the consistency of this approach, even with the nonparallel electrode system used here, is indicated by the ion appearance values of V/P = 33.0, 32.5, 28.5, and 27.5 at pressures of 1, 2, 4, and 10 mm, respectively. Uncertainty in the extrapolation is estimated at ±1.0 V/mm.

(18) I. Schoen, *J. Chem. Phys.*, **37**, 2032 (1962).

Kinetic Study of Species Formed during the Pulsed Radiolysis of Ammonia

by M. Clerc,* M. Schmidt,* J. Hagege-Temman,[1a] and J. Belloni[1b]

Centre d'Etudes Nucléaires de Saclay, DRA SRIRMA, B.P. N°2, 91, Gif s/Yvette, France
(Received February 1, 1971)

Publication costs assisted by Commissariat à l'Énergie Atomique, France

Pulsed radiolysis of NH_3 by 560-keV electrons at pressures ranging from 0.1 to 760 Torr was used to study the reactions of the excited species NH($c^1\Pi$) and NH($A^3\Pi_i$) and the ground state NH($X^3\Sigma^-$). The radiative lifetimes of the excited species were measured and the values τ = 500 ± 100 and 500 ± 60 nsec found for NH($c^1\Pi$) and NH($A^3\Pi_i$), respectively. The radical NH_2 was also observed in absorption but could not be studied quantitatively. The radiolytic yield of hydrazine formation was measured at different ammonia pressures and the influence of N_2H_4 in the NH($X^3\Sigma^-$) disappearance kinetics was demonstrated. The reactions of the radical NH($X^3\Sigma$) are more complex than would appear from previous studies; the addition of rare gases has shown its disappearance kinetics to be a function of its rotational and vibrational temperature.

Introduction

The reaction kinetics of the fragments produced by decomposition of NH_3 have been studied by most fast kinetic spectroscopy methods.[2-4] The NH radical has been detected in the ground state and in the singlet and triplet excited states.

Figure 1 shows the correlation diagram of this radical and the transitions observed either in absorption or in emission.

(1) (a) CNRS, Equipe de recherche N°57, ESPCI, Paris 5è, France. (b) CNRS, Faculté des Sciences, 91, Orsay, France, Laboratoire de Physico-chimie des Rayonnements.

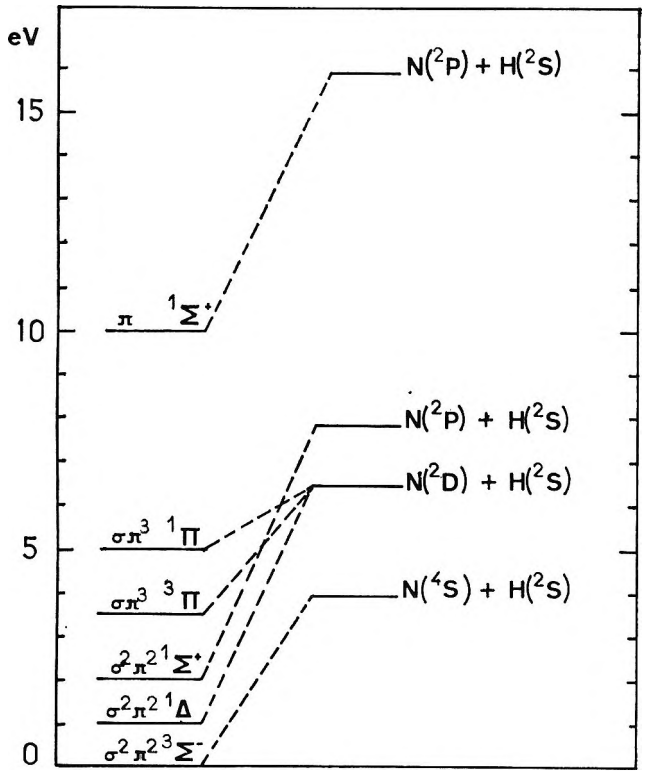

Figure 1. Diagram showing the energy of the electronic states of NH and their mode of dissociation.

Bennett and Dalby[2a] measured a radiative lifetime of 425 ± 60 nsec for NH($A^3\Pi \rightarrow X^3\Sigma^-$), in good agreement with that obtained by Fink and Welge[2b] (460 ± 80 nsec). The latter authors determined a lifetime of 430 ± 40 nsec for NH($c^1\Pi \rightarrow a^1\Delta$).

Many studies have been devoted to the disappearance kinetics of these radicals. To quote only the most recent, Mantei and Bair[3] observed the disappearance of the NH radical in its ground state ($X^3\Sigma^-$) according to a pseudo-first-order law during the flash photolysis of NH_3 at low pressure. On the other hand at pressures around 1 atm, using pulsed radiolysis, Meaburn and Gordon[4] found a second-order reaction for the disappearance of this species, which implies a much lower reactivity of NH($X^3\Sigma$) toward NH_3 than that found by Mantei and Bair.[3]

In addition, Belloni[5] has interpreted results obtained from the radiolysis of liquid ammonia on the similar assumption that the rate constant of the reaction between NH($X^3\Sigma$) and NH_3 is low enough for this reaction to be strongly inhibited in the presence of the ammoniated electron or of N_2H_4.

We have investigated the pulsed radiolysis of ammonia at pressures ranging from 0.1 to 760 Torr, thus covering in a single study all the pressure ranges examined by other authors in an attempt to solve the apparent contradiction between the different results.

Owing to recent technical improvements it is possible to measure a lifetime of *ca.* 20 nsec in emission and 1 μsec in absorption. Knowing that the average time interval between collisions is equal to $10^{-9}p^{-1}$ sec, with p in Torr, by varying p we can thus observe species, which on the average have not yet undergone a collision.

Experimental Methods

The pulsed electron source is a Febetron 706 gun, giving a triangular 560-keV electron pulse of 3.10^{-9} sec duration at half-height. The experimental device has already been described;[6] the monochromator spectrograph used is a Huet M65 apparatus with a dispersion of 0.8 nm mm^{-1} in the first order.

The NH absorption in the transition NH($A^3\Pi_i \leftarrow X^3\Sigma^-$) is measured by microdensitometry at 336.0 nm (Q(0,0) band); the length of the optical absorption path in the multiple reflection cell is fixed at 7.2 m in order to obtain a continuous absorption background of optical density equal to 1 on Ilford HP 3 plates.

The ammonia first used was supplied by Air Liquide Co. and its purity (99.99%) was checked by mass spectrometry. Later we used Matheson compressed ammonia of purity 99.95%, redistilled. The diluent rare gases (He, Ar) were purified by passage at 77°K through a spiral tube, of length 1 m, filled with molecular sieve, and the absence of N_2, O_2, and OH emission spectra, which would indicate the presence of impurities, was verified.

Hydrazine was prepared by dehydration of its hydrate by calcium hydride under a nitrogen atmosphere at −20°.[7] Low pressures (10^{-4} to 1 Torr) were measured with a McLeod gauge preceded by a solid CO_2-cooled trap, to avoid the presence of mercury vapor in the radiolysis cell. Intermediate pressures (1–10 Torr) were measured with a manometer containing Apiezon L oil, and those above 100 Torr, with a metallic manometer.

Hydrazine was determined by absorption spectrometry of *p*-dimethylaminobenzaldehyde hydrazone at 458 nm (ϵ 6.10^4 cm^{-1} M^{-1}).

The dosimetry of the gun was carried out taking N_2O irradiated at 500 Torr of pressure as standard of reference and assuming a yield $G(N_2) = 10$. It was also assumed that the dose absorbed by NH_3 was proportional to its electron density and hence to its pressure.

(2) (a) R. G. Bennett and F. W. Dalby, *J. Chem. Phys.*, **32**, 1716 (1960); (b) E. Fink and K. H. Welge, *Z. Naturforsch. A*, **19**, 1193 (1964).

(3) K. A. Mantei and E. J. Bair, *J. Chem. Phys.*, **49**, 3248 (1968).

(4) G. M. Meaburn and S. Gordon, *J. Phys. Chem.*, **72**, 1592 (1968).

(5) J. Belloni, IVth International Congress of Radiation Research, Evian, France, 1970.

(6) M. Clerc and B. Lesigne, *J. Chim. Phys.*, **67**, 701 (1969); J. Le Calve, M. Bourene, M. Schmidt, and M. Clerc, *J. Phys. (Paris)*, **30**, 807 (1969).

(7) J. Blais, B. Gitton, and M. Cottin, submitted for publication in *Int. J. Radiat. Phys. Chem.*

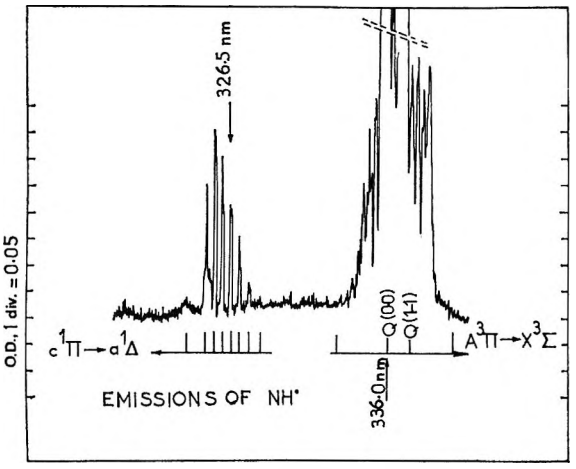

Figure 2. Emission spectra of $NH(A^3\Pi_i)$ and $NH(c^1\Pi)$.

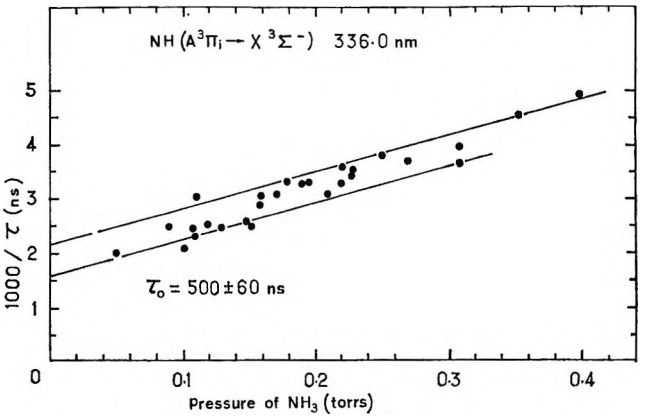

Figure 3. Stern–Volmer diagram for the measurement of the radiative lifetime of $NH(A^3\Pi_i)$ at 336.0 nm.

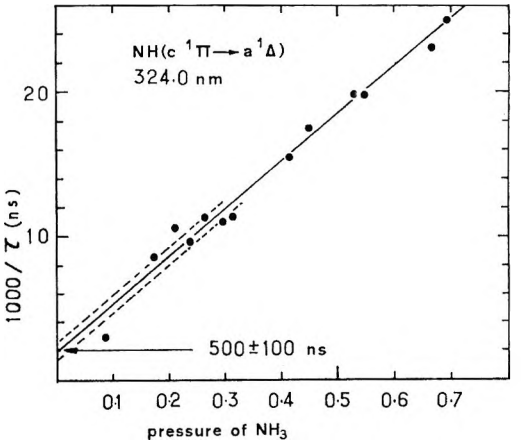

Figure 4. Stern–Volmer diagram for the measurement of the radiative lifetime of $NH(c^1\Pi)$ at 324.0 nm.

Experimental Results

The reactions of the excited species $NH(A^3\Pi_i)$ and $NH(c^1\Pi)$, their disappearance kinetics, and lifetimes will be discussed first. This will be followed by an examination of the ground state of $NH(X^3\Sigma^-)$ and of the formation of hydrazine and its influence on the disappearance kinetics of $NH(X^3\Sigma^-)$ and finally a review of the species which have merely been observed, showing why it was impossible to study their reactions in more detail.

(*a*) *Fluorescence and Disappearance of the Excited Species Formed.* Figure 2 shows the emission spectra of $NH(c^1\Pi \rightarrow a^1\Delta)$ (0–0) and $NH(A^3\Pi_i \rightarrow X^3\Sigma)$ (0–0 and 1–1). The emission intensity of the state $c^1\Pi$ at 324.0 nm is 5 times as weak as that of the strong branches Q(0–0) at 336.0 nm and Q(1–1) at 337.0 nm of the transition $(A^3\Pi \rightarrow X^3\Sigma^-)$. The light emission from $NH(c^1\Pi)$ and $NH(A^3\Pi_i)$ reaches a maximum intensity 100 ± 10 nsec after the electron pulse, when the NH_3 pressure is 2 Torr.

Figure 3 shows the Stern–Volmer plot of which the intersection with the ordinate axis gave the radiative lifetime of $NH(A^3\Pi_i)$, *i.e.*, $\tau = 500 \pm 60$ nsec. Its slope gives the rate constant of the deexcitation reaction of this species by collision with NH_3

$$k = (3.1 \pm 0.2) \times 10^{11} \text{ l. mol}^{-1} \text{ sec}^{-1}$$

i.e.

$$5.1 \times 10^{-10} \text{ cm}^3 \text{ molecule}^{-1} \text{ sec}^{-1}$$

Figure 4 shows the Stern–Volmer diagram used to determine the radiative lifetime $\tau_0 = 500 \pm 100$ nsec of the radical $NH(c^1\Pi)$, and a rate constant $k = 5.7 \times 10^{11}$ l. mol^{-1} sec^{-1}, *i.e.*, 9.5×10^{-10} cm^3 $molecule^{-1}$ sec^{-1}, for its deexcitation by NH_3.

The oscillator strength can be calculated from the transition probability $A_{nm} = 1/\tau_0$, by the formula $f_{nm} = (\mu c/8\pi^2\gamma^2\epsilon^2)((dn/(dm))A_{nm}$: with μ, electron mass; c, speed of light, γ, frequency in cm^{-1}; ϵ, electron charge; and dn/dm, degeneracy ratio. The value $f = 1.0 \times 10^{-2}$ is found for the transitions $NH(^3\Pi_i \rightarrow X^3\Sigma)$ and 1.9×10^{-3} for $NH(c^1\Pi \rightarrow a^1\Delta)$. The linearity of the optical density with the number of paths across the cell has been checked; for this parameter Beer's law is verified, but the concentration along the axis is certainly not uniform.

(*b*) *Reactions of the NH Radical in Its Ground State. 1. Aspect of the Absorption Spectrum.* The $NH(X^3\Sigma)$ absorption spectrum is also different at high and low pressure. Examining the R branches of the $NH(A^3\Pi_i \rightarrow X^3\Sigma^-)$ (0–0) transition it is observed (Figure 5) that the distribution in intensity and wavelength of the rotation lines is quite different at 0.67 Torr and at 760 Torr; these lines extend in the former case to $k = 10$, and in addition the vibrationally excited (1–1) bands only appear at low pressure. Whereas the observation of these rotational lines in the R branch represents good evidence for the existence of hot NH radicals, their intensities are far too low to enable kinetic measurements to be made at the corresponding wavelengths. For kinetic studies it was necessary to make observations on the strongest Q(0–0) band at

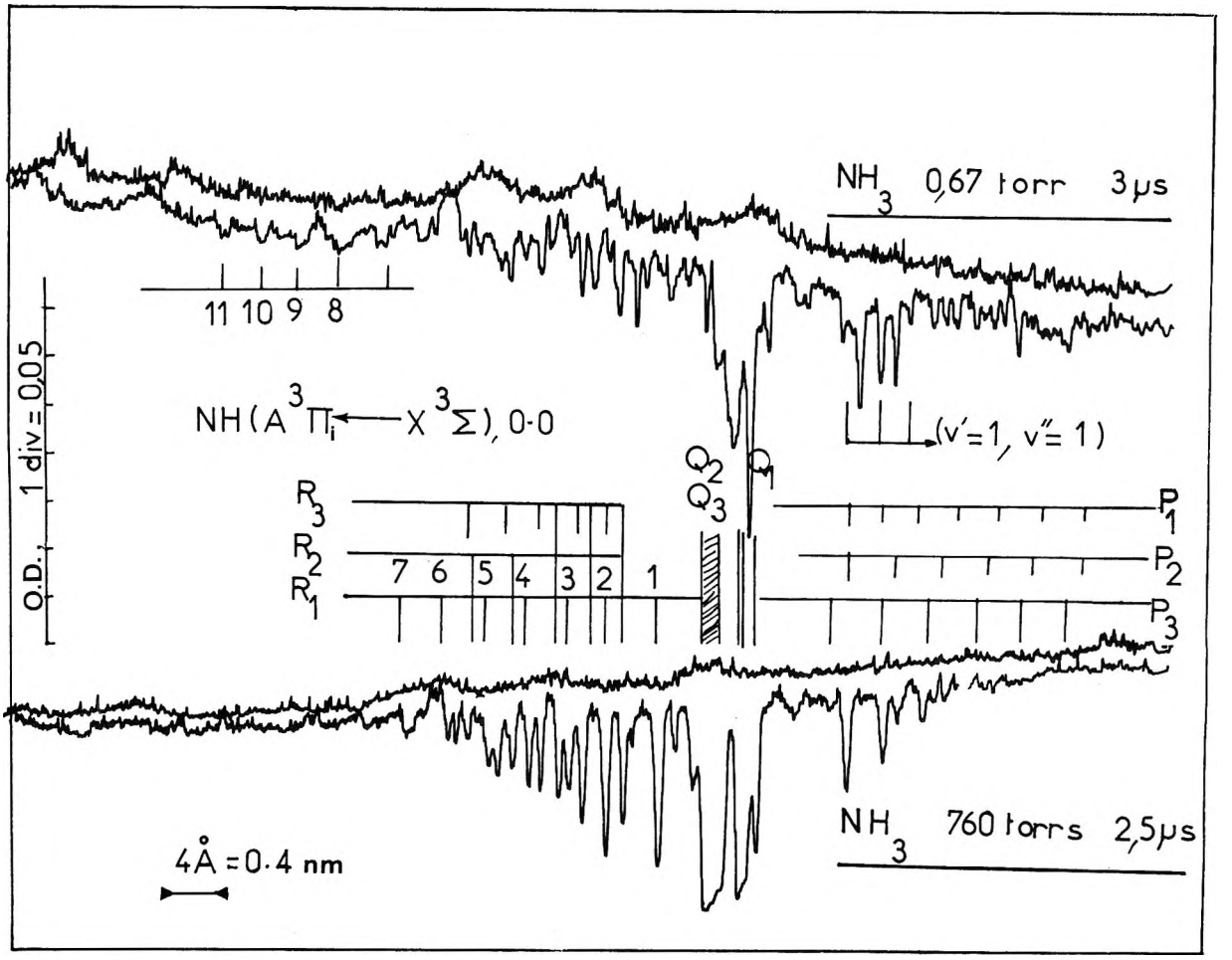

Figure 5. NH($A^3\Pi \leftarrow X^3\Sigma$) absorption spectrum.

336 nm where the spectroscopic resolution did not allow separation at the thermal and hot NH lines but where a difference in the kinetic behavior of the thermal and hot radicals became apparent.

2. Kinetic Behavior. Figure 6 shows that NH($X^3\Sigma$) disappears according to an apparent second-order law independent, within the limits of experimental error, of the NH_3 pressure when this lies between 300 and 760 Torr (curves 5–7). However, at NH_3 pressures between 55 and 300 Torr the NH disappearance rate ceases to be independent of pressure (curves 1 and 2), and below 55 Torr the results no longer correspond at all to a second-order diagram.

In the low-pressure range (~1 Torr) the kinetic variation of NH($X^3\Sigma$) absorption is fairly complex. Figure 7 (curve 1) shows that after a rapid decay ($\tau_{1/2} \simeq 10$ μsec) continuing to 20 μsec, the NH concentration increases once more, to reach a maximum around 50 μsec then finally disappears very slowly. Curve 2 represents the kinetics observed after a preirradiation of NH_3 in a preliminary pulse; it is found that at first $\tau_{1/2}$ is greater, up to 50 μsec the NH concentration is higher, and the maximum appears sooner than previously.

(c) *Formation of N_2H_4.* Each pulse produces hydrazine in quantities measurable at equilibrium, for example about 2.3×10^{-8} mol $l.^{-1}$ at 3 Torr pressure of NH_3 (1.4×10^{-2}%). The yield $G(N_2H_4)$ increases as the NH_3 pressure decreases (Figure 8), and the curve obtained agrees with that of Willis, Boyd, and Miller[8] in the common range between 200 and 760 Torr.

(d) *Formation of NH_2.* The NH_2 radical was observed in absorption at 597.7 and 630.2 nm, but in this wavelength region the photographic plates used are not sensitive enough and quantitative measurements were impossible. NH_2 appears 3 μsec after excitation of a mixture NH_3 (0.67 Torr) + He (500 Torr); to produce an adequate image on the photographic plate it was necessary to accumulate 30 successive pulses. It was not possible to follow the decay of NH_2 and say whether it is a primary product of NH_3 dissociation or is produced by the decomposition of N_2H_4. Recently Gordon, Mulac, and Nangia[9] observed the disappearance of NH_2 according to an apparent second-order law during the pulsed radiolysis of NH_3, using a photoelectric measurement method.

(8) C. Willis, A. W. Boyd, and O. A. Miller, *Can. J. Chem.*, **47**, 3007 (1969).

(9) S. Gordon, W. A. Mulac, and P. Nangia, IVth International Congress of Radiation Research, Evian, France, 1970.

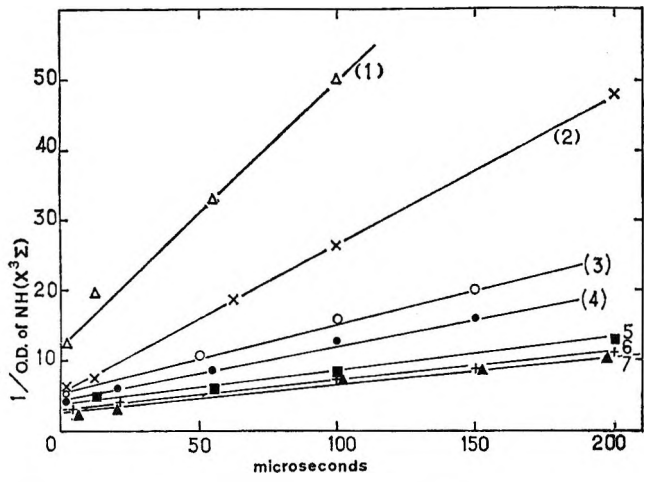

Figure 6. Second-order diagram (1/optical density of NH as a function of time) for different pressures: 1, NH_3 (55 Torr); 2, NH_3 (100 Torr); 3, NH_3 (0.77 Torr) + Ar (500 Torr); 4, NH_3 (0.77 Torr) + He (500 Torr); 5, NH_3 (760 Torr); 6, NH_3 (300 Torr); 7, NH_3 (500 Torr).

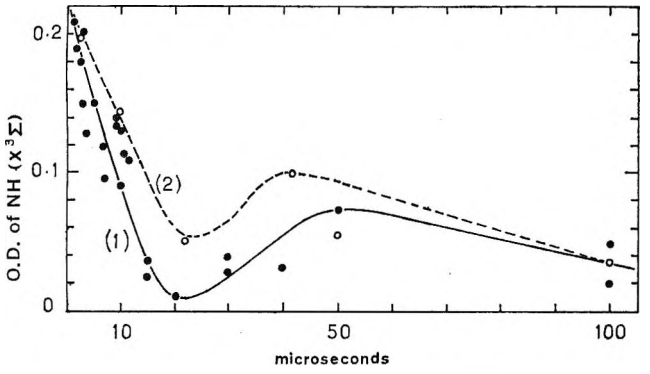

Figure 7. Rapid disappearance of NH at low NH_3 pressure (0.67 Torr): 1, NH_3 renewed at each pulse; 2, NH_3 (0.67 Torr) + decomposition products of a preliminary pulse.

Reactions of the Radical NH($a^1\Delta$). Whereas the transition $NH(A^3\Pi \leftrightarrow X^3\Sigma^-)$ was observed in absorption as well as in emission, the transition $NH(c^1\Pi \rightarrow a^1\Delta)$ was only detected in emission; it was impossible to observe it in absorption in spite of the very short minimum delays of the spectroscopic flash (Δt = 1 μsec) and the photoelectric recording (Δt = 10 nsec). In view of the briefness of these delays and the relatively high value of the oscillator strength this absorption should have been detectable at an ammonia pressure of 1 Torr, immediately after the fluorescence and before the collisions with NH_3 occurred. It is difficult therefore to explain why it was not observed, unless $NH(a^1\Delta)$ reacts with NH_3 at each collision. $O(^1D)$ atoms isoelectronic with $NH(a^1\Delta)$ are known to react very rapidly; the rate constants of these addition reactions are of the order of 10^{-10} cm^3 $molecule^{-1}$ sec^{-1} and the activation energies are very low or even zero.

Discussion

In the course of this work the formation of excited species $NH(A^3\Pi_i)$ and -$(c^1\Pi)$ during the pulsed radiolysis of gaseous ammonia was observed and their radiative lifetimes were measured. The values obtained are in good agreement with published data.[2] The deexcitation constants of these excited species were also determined.

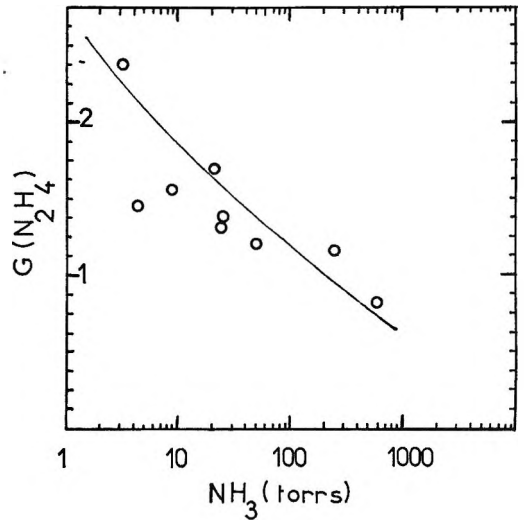

Figure 8. N_2H_4 formation yield as a function of NH_3 pressure.

After 1 μsec the excited states have returned to the ground state, and only $NH(a^1\Delta)$ and $NH(X^3\Sigma^-)$ remain. Although as mentioned above the absorption of the $NH(a^1\Delta)$ radical could not be studied, probably because of its rapid disappearance by insertion reactions with NH_3, it was possible to examine the reactions of the $NH(X^3\Sigma^-)$ radical.

The kinetic behavior and absorption spectra of $NH(X^3\Sigma^-)$ suggest that at low pressure it is produced with a much higher rotational and vibrational temperature and reacts much more quickly with ammonia than at high pressure, whether this high pressure is obtained by increasing the ammonia pressure or by adding helium or argon (Figure 6, curves 3 and 4). The conclusion is that at high pressure NH loses its vibrational and rotational energy by collisions with the other molecules present, this thermalization taking place all the more rapidly as the total pressure of the mixture is high. After thermalization, NH stops reacting rapidly with NH_3 since it disappears according to apparent second-order law.

At low pressure the radiolysis products appear to affect the NH disappearance kinetics because the quantities formed in a single pulse can change the kinetic curve and promote in particular the secondary formation of NH beyond 20 μsec. Hydrogen and nitrogen, which with hydrazine are the only stable radiolysis products, could only cause this secondary formation by an indirect mechanism requiring longer delays than those used.

On the other hand hydrazine is known to decompose thermally[10] or under the action of electrical discharges, giving the radical $NH(X^3\Sigma)$.[11]

The following kinetic mechanism attempts to account for all these experimental results. If we represent by NH* the rotationally and vibrationally excited NH($X^3\Sigma$) radical, we can write

$$NH^* + NH_3 \xrightarrow{k_1} N_2H_4^* \quad (1)$$

With NH($X^3\Sigma$) and singlet NH_3, this reaction is only rapid in the case where $N_2H_4^*$ is formed in a triplet state.

We also have the deexcitation reaction

$$NH^* + M \xrightarrow{k_2} NH + M \quad (2)$$

which occurs by collision with any molecule M of the medium. Similarly we should have

$$N_2H_4^* + M \xrightarrow{k_3} N_2H_4 + M \quad (3)$$

$$N_2H_4^* \xrightarrow{k_4} NH + NH_3 \quad (4)$$

To this reaction of excited hydrazine dissociation to form NH we add a reaction of excited hydrazine formation from N_2H_4 in the ground state, since the initial presence of N_2H_4 accelerates secondary NH formation (Figure 7, curve 2). Direct excitation by electrons not yet thermalized is the most probable reaction in this time range, and at this pressure.

$$e^- + N_2H_4 \xrightarrow{k_5} N_2H_4^* + e^- \quad (5)$$

Finally, the NH radicals having lost their energy can disappear either by reaction 6 with NH_3 or by reaction 7 with any one of the species R formed.

$$NH + NH_3 \xrightarrow{k_6} Y \quad (6)$$

$$NH + R \xrightarrow{k_7} X \quad (7)$$

High-Pressure Region (300–760 Torr of NH_3 or 0.7 Torr of NH_3 Diluted with Ar or He at 500 Torr). In this region the NH($X^3\Sigma^-$) absorption decay obeys a second-order law independent of pressure, and its half-life at the origin is $\tau_{1/2} = 150$ μsec. At high pressure the role of M is important, the result being that reaction 2 takes precedence over (1) and similarly (4) is negligible with respect to (3). The NH* radical is very rapidly thermalized, in times less than the shortest observation time (1 μsec) and only the thermalized NH spectrum is recorded (Figure 5). The NH disappearance reaction is not first order, which implies that k_6 is extremely weak. This agrees with the Wigner–Witmer law because reaction 6 between NH($X^3\Sigma$) and NH_3(singlet), to give N_2H_4(singlet), is forbidden.

Low-Pressure Region (0.5–1 Torr of NH_3). Conversely, reactions 2 and 3 have lost their importance in favor of (1) and (4). As shown above, NH being measured on the Q(0–0) branch, the optical absorption density plotted on Figure 6 concerns both NH* and NH. We know, however, that for a 3-μsec delay the spectrum of the radical NH has a hot rotational distribution

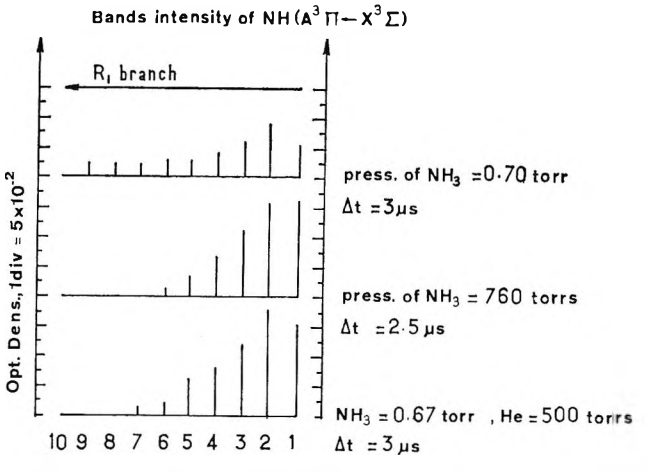

Figure 9. Diagram of the intensities and wavelength distributions of the rotation lines of NH absorption bands at different NH_3 pressures (0.67 and 760 Torr) and in the presence of argon (500 Torr).

(Figures 5 and 9), which we have called NH*. This species has a half-life of 10 μsec which could correspond, for a pseudo-first-order decay, to a $k_1[NH_3]$ value equal to 6.9×10^4 sec^{-1} and, accounting for the NH_3 pressure, to an approximate k_1 value of 1.4×10^9 l. mol^{-1} sec^{-1}. This latter value is close to that calculated by Mantei and Bair for reaction 1 when NH($v'' = 0$) reacts with NH_3.

On the other hand the absorption decay after 50 μsec concerns a species less reactive toward NH_3 than that observed at short periods, which points to NH formed in reaction 4 or NH* deexcited by reaction 2. It should be observed however that this disappearance takes place in times when diffusion phenomena out of the observation zone are involved.

The secondary formation of NH by reaction 4 would be responsible for the increase in absorption beyond 20 μsec. This delayed NH formation can be explained either by an $N_2H_4^*$ lifetime of around 20 μsec or by the fact that this excited state of hydrazine, to be formed by reaction 5, requires a previous accumulation of N_2H_4, possibly resulting from other reactions not considered here. If hydrazine is already present before the pulse (Figure 7, curve 2), reaction 5 plays a greater part and the delay after which the NH concentration passes through a maximum due to reactions 4 and 6 is shorter.

Conclusion

The radiative lifetimes of the states NH($A^3\Pi_i$) and NH($c^1\Pi$) are short, and the oscillator strengths of these transitions are high. The maximum fluorescence emission intensity lies at 100 nsec, which means that NH($A^3\Pi$) and NH($c^1\Pi$) are not primary products of ammonia decomposition by electrons but have as precursor an ion or an excited state of NH_3.

(10) H. E. Avery and J. N. Bradley, *Trans. Faraday Soc.*, 60, 857 (1964).

(11) E. F. Logan and J. M. Marchello, *J. Chem. Phys.*, 49, 3929 (1968).

The radical $NH(X^3\Sigma)$ can be found in more or less energetic vibrational or rotational states. The "hottest" NH* is observed at low pressure and reacts quickly according to reaction 1. At high pressure the kinetic behavior of $NH(X^3\Sigma)$ shows that it disappears slowly. The reactivities of $NH(X^3\Sigma)$ differ according to its energy and explain the fact that at high pressure, in common with Meaburn and Gordon, we observe a slow disappearance according to an apparent second-order reaction, while at low pressure we find a fast reaction with NH_3, in agreement with the findings of Mantei and Bair. However at high pressure (300–760 Torr) we find an initial NH half-life $\tau_{1/2} \simeq 150$ μsec, 10 times as long as that observed by Meaburn and Gordon, which may be due to a better purification of NH_3, or to a different extinction coefficient for NH, resulting from a higher spectral resolution in our case, or to the nonuniform distribution of the radicals along the light path.

Acknowledgments. The authors wish to thank Drs. C. Vermeil and S. Leach, for their assistance in the interpretation of various points.

Catalytic Oxidation. IV. Ethylene and Propylene Oxidation over Gold

by Noel W. Cant and W. Keith Hall[1]

Mellon Institute, Carnegie-Mellon University, Pittsburgh, Pennsylvania 15213 *(Received February 19, 1971)*

Publication costs assisted by the Gulf Research & Development Company

The heterogeneous oxidation of C_2H_4 and C_3H_6 was studied over several gold catalysts. The principal products from C_2H_4 were CO_2 and H_2O, but small amounts of acetic acid and acetaldehyde were also found. In addition to these products, up to 3% acetone and 50% acrolein were obtained from C_3H_6. Gold sponge and Au/SiO_2 were much more selective for acrolein formation than $Au/\alpha\text{-}Al_2O_3$. For both olefins, the rate of total oxidation was first order in oxygen pressure and zero order in olefin pressure at low pressures. The apparent activation energies (except for C_2H_4 over Au sponge) ranged from 17 to 22 kcal mol^{-1}. Acrolein formation had a much lower apparent activation energy (9–12 kcal mol^{-1}), was also first order in O_2, but showed a maximum rate for C_3H_6 pressures near 30 Torr. Oxidation of propylene-*1*-^{13}C produced acrolein molecules in which the ^{13}C was equally distributed between the end positions. Similarly, CD_3CHCH_2 and CH_3CHCD_2 both yielded CH_2CHCDO and CD_2CHCHO in about equal amounts, although the rate of the reaction with the former olefin was only about 40% that of the latter or that of CH_3CHCH_2. These results indicated that the rate-determining step in acrolein formation was abstraction of a methyl hydrogen (or deuterium) to yield a symmetrical allylic intermediate. The modes of fragmentation of acrolein during mass spectral analysis are discussed on the basis of high-resolution measurements of the labeled acroleins formed in the present work.

Introduction

The low activity of Au for most catalytic reactions generally has been attributed to its lack of a partially filled d band at the usual experimental temperature, and its consequent inability to chemisorb simple molecules. Thus, Trapnell[2a] reported that Au was the only metal which did not chemisorb O_2 or H_2. CO and C_2H_4 were weakly chemisorbed, however, with heats of adsorption of 8.7 and 20.8 kcal/mol.[2a] More recently, a small chemisorption of O_2 on very pure Au has been reported by a couple of groups.[2b] It amounted to at most about 1% of a monolayer; the isobars had maxima above 200°. Moreover, Au catalyzed the $H_2 + O_2$ reaction, but at a much lower rate than does Ag,[3] and has been briefly studied as the end member of the Pd–Au alloy system in the catalysis of the oxidation of CO,[4] CH_4,[5] and C_2H_4.[6] Recently, Cha and Parravano[7] reported rate constants for the transfer of O from $^{14}CO_2$ to CO which were from two to three orders of magnitude higher for Au supported on MgO, than for Pt on alumina. Also, Boudart and Ptak[8] found that Au catalyzed the isomerization

(1) Address correspondence to this author at Gulf Research & Development Co., P. O. Box 2038, Pittsburgh, Pa. 15230.

(2) (a) B. M. W. Trapnell, *Proc. Roy. Soc., Ser. A*, **218**, 566 (1953); (b) N. Endow, B. J. Wood, and H. Wise, *J. Catal.*, **15**, 316 (1969); W. R. MacDonald and K. E. Hayes, *ibid.*, **18**, 115 (1970).

(3) A. F. Benton and J. C. Elgin, *J. Amer. Chem. Soc.*, **48**, 3027 (1926); (b) *ibid.*, **49**, 2426 (1927).

(4) A. G. Daglish and D. D. Eley, *Proc. Int. Congr. Catal., 2nd, Paris, 1960*, **2**, 1615 (1961).

(5) J. G. Firth, *Trans. Faraday Soc.*, **62**, 2566 (1966).

(6) H. R. Gerberich, N. W. Cant, and W. K. Hall, *J. Catal.*, **16**, 204 (1970).

(7) D. Y. Cha and G. Parravano, *ibid.*, **18**, 200 (1970).

and hydrogenolysis of neopentane. Patterson and Kemball[9] detected only CO_2 and H_2O as products from C_2H_4 and C_3H_6 oxidation over Au films. However, Inami, *et al.*,[10] found that Au had a selectivity for the oxidative dehydrogenation of butenes to butadiene which was increased by alloying with Pd. According to patent claims,[11] other group VIII noble metals functioned in the same way.

We have now employed a flow system to study the oxidation of C_2H_4 and C_3H_6 over both supported and unsupported Au. Traces of acetic acid and acetaldehyde were detected in the products from the former and substantial amounts of acrolein from the latter. The mechanism of acrolein formation was investigated using ^2H- and ^{13}C-labeled propylenes. The results differed significantly from our findings for the same reaction over Rh[12] but provided added support for the conclusions reached for that system. The mechanism over these metals is not identical with that operative with oxide catalysts,[13] even though allylic intermediates appear to function in both cases.

Experimental Section

Detailed studies were made over Au catalysts in the following three forms: a high-purity gold sponge (>99.9%) obtained from Englehard Industries (Lot R-32-53), having a surface area (BET, Kr) of 0.091 m^2 g^{-1}; Au/α-Al_2O_3 was also prepared for us by Engelhard Industries (Lot C-5093); it was 1.5% Au supported on the exterior of fused α-alumina (Alcoa T-61, 14–28 mesh, surface area <0.3 m^2 g^{-1}; and Au/SiO_2. The latter was prepared by impregnation of Cab-O-Sil (HS-5, surface area 330 m^2 g^{-1}) with an aqueous solution containing sufficient $HAuCl_4 \cdot 3H_2O$ (Fisher reagent ACS) to produce a material containing 5% Au.

The nominal volume of the tubular Pyrex reactor was 2.0 cc, requiring 6.80 g of Au sponge, 1.18 g of Au/SiO_2, and 8.67 g of Au/α-Al_2O_3, respectively, to fill. Each catalyst sample was initially pretreated *in situ* with H_2 flowing at 50 cc min^{-1} as the temperature was slowly raised to 300° where it was maintained for several hours. The reactor was then purged overnight with helium at 300° and cooled to the temperature chosen for starting the reaction.

All catalytic experiments were carried out in the single-pass flow system employed in studies of the same reactions over silica-supported group VIII noble metals.[14] The analysis method was also identical, with the selectivity being defined as the number of moles of a given compound produced per 100 mol of olefin converted into all products. Olefin and oxygen pressures ranged from 5 to 60 Torr and from 10 to 130 Torr, respectively, with the balance to atmospheric pressure being made up with helium. Standard conditions were olefin pressure 20 Torr, oxygen pressure 65 Torr, and an overall flow rate of 45 cc (NTP) min^{-1}. The system was operated as a differential reactor using conversions of less than 10% for the determinations of apparent activation energies and pressure dependencies. However, efficient use of labeled propylenes dictated higher conversions and an overall flow rate of 20 cc min^{-1} was sometimes used for this purpose.

The techniques employed in the oxidation of the deuterium and ^{13}C-labeled propylenes were identical with those described elsewhere for the same reactions over Rh.[12] Mass spectral analyses were routinely carried out using a Nuclide 6-in. magnetic sector instrument under conditions of both extensive fragmentation (70 eV) and minimal fragmentation (10 eV). To determine the modes of fragmentation of acrolein, measurements made in the above way were complimented with results from spectra of authentic samples of acrolein-d_4 and acrolein-2-d_1 which were recorded with an AEI MS-9 instrument operating at 70 eV with a resolution of about 14,000. This was sufficient to resolve peaks fully due to N_2^+, $C_2H_4^+$, and CO^+ ions, all with nominal m/e 28. Infrared spectra were recorded with a Beckman IR-12 spectrometer from gaseous samples contained in a small-volume cell having a path length of 5 cm.

Results

Selectivity to Partial Oxidation Products. Total oxidation of both olefins invariably produced H_2O and CO_2; CO was not detected. The partial oxidation products and their selectivities are listed in Table I. None of the three gold catalysts was very selective in the oxidation of ethylene; each produced acetic acid and acetaldehyde in only trace amounts. However, Au sponge and particularly Au/SiO_2 produced relatively large amounts of acrolein from propylene, although Au/α-Al_2O_3 yielded much smaller quantities. Acetone, acetic acid, and acetaldehyde were formed in still smaller amounts over each catalyst. Brief investigations with other gold catalysts confirmed that these were general phenomena; thus, the use of silica (preferably nonporous) as a support for gold led to catalysts with considerable selectivity for acrolein formation, whereas preparations supported on alumina having both low and high area showed little or no selectivity. Blank experiments with the catalyst chamber empty produced no products.

Apparent Activation Energies. Figure 1 shows the effect of temperature on the rates of total oxidation of C_3H_6 and of acrolein formation over Au/SiO_2 under standard conditions. The numbers refer to per cent

(8) M. Boudart and L. D. Ptak, *J. Catal.*, 16, 90 (1970).
(9) W. R. Patterson and C. Kemball, *ibid.*, 2, 465 (1963).
(10) S. H. Inami, B. J. Wood, and H. Wise, *ibid.*, 13, 397 (1969).
(11) W. E. Armstrong, U. S. Patent No. 3,156,735, assigned to the Shell Oil Co.
(12) Part III: N. W. Cant and W. K. Hall, *J. Catal* in press.
(13) H. H. Voge and C. R. Adams, *Advan. Catal.*, 17, 151 (1967).
(14) N. W. Cant and W. K. Hall, *J. Catal.*, 16, 220 (1970).

Table I: Selectivities and Kinetic Parameters for Olefin Oxidation over Gold

Catalyst	Olefin	Selectivity,[a] % Acet-aldehyde	Acetic acid	Acrolein	Acetone	Activation energy[b] Total oxidation	Oxidation to acrolein	Temp for std rate,[c] °C	Apparent reaction order[d] Olefin	Oxygen
6.8 g Au sponge	C_2H_4	<2	<2	...	...	8.0 ± 0.6	...	289	~0.5	~0.3
6.8 g Au sponge	C_3H_6	<1	<2	18	0.5	21 ± 3	9 ± 1	269	≤0	1
8.67 g Au/α-Al_2O_3	C_2H_4	<2	<2	...	...	18 ± 1	...	287	0	≤1
8.67 g Au/α-Al_2O_3	C_3H_6	<1	<2	3	3	22 ± 1	...	294	Slightly negative	1
1.18 g Au/SiO_2	C_2H_4	1.5	1.7	...	...	19.4 ± 0.8	...	275	Negative	1
1.18 g Au/SiO_2	C_3H_6	0.5	2.5	33	3.5	17.6 ± 0.2	11.6 ± 0.4	262	≥0	1

[a] Under standard conditions at temperatures shown in column 9. [b] In kilocalories per mole with standard deviations as shown. [c] Temperature required to achieve overall oxidation rate of 2.7 μM (olefin) min^{-1} (equivalent to conversion of about 5%). [d] For total oxidation to CO_2 and water.

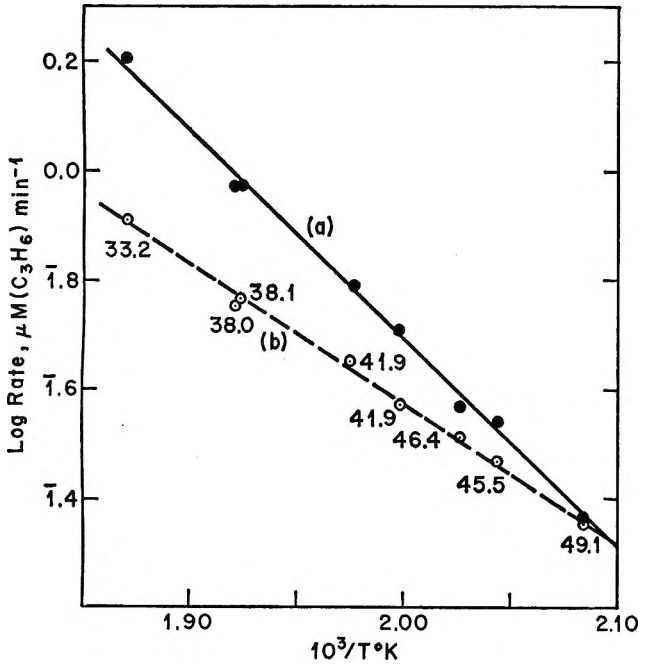

Figure 1. Effect of temperature on rate of propylene oxidation over Au/SiO_2 under standard conditions: (a) total oxidation; (b) acrolein formation.

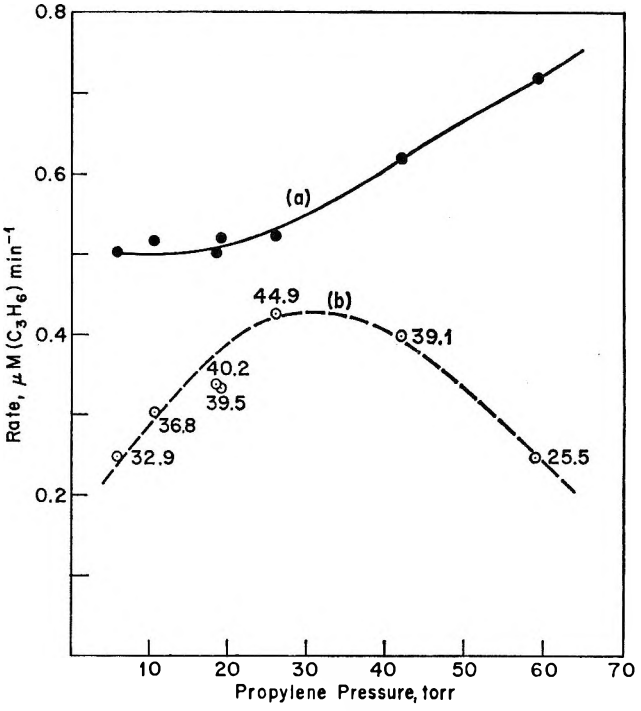

Figure 2. Effect of propylene pressure on oxidation rate over Au/SiO_2 at 229° with P_{O_2} of 63 Torr: (a) total oxidation; (b) acrolein formation.

selectivity to acrolein, which decreased with temperature because of the lower activation energy for partial, as compared with total, oxidation. Apparent activation energies were calculated from the slopes of the straight lines shown in Figure 1, and these results are listed in Table I together with the corresponding values for the other systems studied. The reactions over the Au sponge were quite sluggish in responding to temperature changes so that it was difficult to obtain very accurate results with this catalyst. The anomolously low activation energy for C_2H_4 (line 1) may be a reflection of this fact. Except for this case, the activation energies for total oxidation were all very similar. Because of the low selectivity, the rate of acrolein formation during C_3H_6 oxidation over Au/α-Al_2O_3 could not be measured accurately, but it appeared to be nearly temperature independent. Column 9 of Table I gives the experimental temperature required to achieve an overall oxidation rate of 2.7 μM (olefin) min^{-1} under standard conditions. These data allow the two reactions to be compared over a given catalyst. The relative effectiveness of the three catalysts for a given reaction cannot be judged, except very approximately. Both of the selective catalysts oxidized propylene slightly faster than ethylene while the nonselective catalyst, Au/α-Al_2O_3, had a similar activity for the two reactions.

Pressure Dependencies. Figure 2 shows the effect

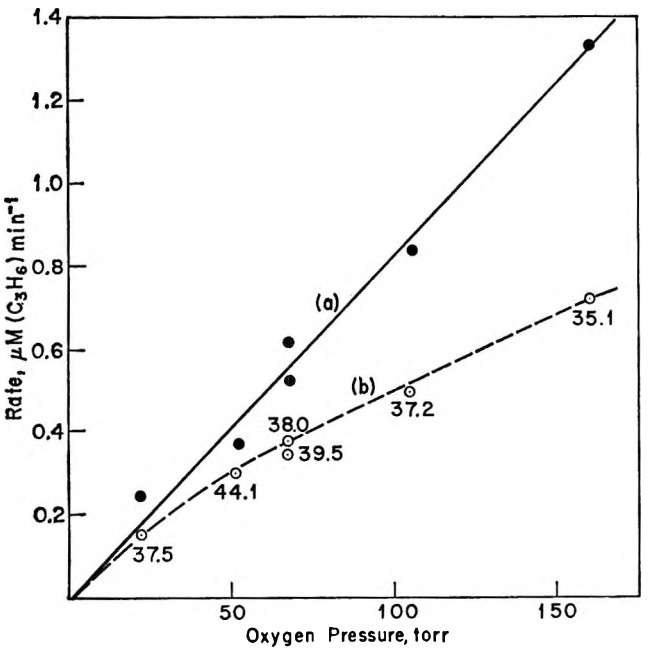

Figure 3. Effect of oxygen pressure on rate of propylene oxidation over Au/SiO_2 at 229° with $P_{C_3H_6}$ of 19 Torr: (a) total oxidation; (b) acrolein formation.

of C_3H_6 pressure on the rates of acrolein formation and of total oxidation over Au/SiO_2. Acrolein formation went through a maximum near 30 Torr; while total oxidation was near zero order at low pressures, the order increased at high propylene pressures. Thus, the selectivity to acrolein went through a maximum, as can be seen from the numbers labeled on Figure 2. The corresponding effects of oxygen pressure on both modes of propylene oxidation over Au/SiO_2 are shown in Figure 3. Total oxidation was first order in oxygen while the order for acrolein formation was somewhat lower. Thus, the selectivity was only weakly dependent on oxygen pressure.

The effects of propylene and oxygen pressures on acrolein formation over Au sponge were almost identical with those shown in Figures 2 and 3. The observed reaction orders for total oxidation of both olefins over the three gold catalysts studied are given in the final two columns of Tabel I. Except for ethylene oxidation over Au sponge, which again gave anomolous results, all data conformed to the same pattern, *i.e.*, first order or nearly first order in oxygen pressure and near zero order in olefin for H_2O formation. The rate of acrolein formation was sensitive to the olefin pressure.

Kinetic Isotope Effects in Propylene Oxidation. For the purpose of tracer studies of oxidation, Au sponge was preferable to Au/SiO_2 because the absence of a support reduced product retention by the catalyst bed. The relative rates of total and partial oxidation of deuterated propylenes over Au sponge are compared in Table II, relative to the rates for the unlabeled olefin. Rates of acrolein formation from the propylenes labeled in the methyl group were less than half that of C_3H_6; rates of *total* oxidation were significantly greater. Labeling at the center carbon atom was without effect. Oxidation of CH_3CHCD_2 to acrolein was slightly faster than for C_3H_6 while total oxidation was much slower. The present results for acrolein formation are similar to our findings for the same reaction over Rh,[12] but the pattern for relative rates of oxidation to CO_2 and water are quite different, *vide infra*.

Table II: Relative Rates of Oxidation of Labeled Propylenes over Gold Sponge[a]

Propylene	Acrolein formation	Total oxidation[b]
C_3H_6	1.0	1.0
C_3D_6	0.4 ± 0.05	1.3 ± 0.1
CH_3CDCH_2	1.0	1.0
CH_3CHCD_2	1.2 ± 0.15	0.55 ± 0.1
CD_3CHCH_2	0.4 ± 0.05	1.1 ± 0.1

[a] Temperature, 265–285°; propylene pressure, 12–22 Torr; oxygen pressure, 60–110 Torr. [b] To CO_2 and water.

Experiments were made to determine the extent to which exchange processes might affect the compositions of the labeled acroleins produced on oxidation of labeled propylenes; these results are given in Table III. (The data have been corrected for acrolein produced from impurity propylenes, *i.e.*, the 4.9% C_3H_6 in the CH_3CDCH_2 and 3.5% C_3HD_5 in the C_3H_6–C_3D_6 mixture.) In each case, the oxidations were very clean, exchange amounting to a few per cent at most. This can be contrasted with the corresponding reactions over Rh where up to 40% of the acrolein molecules underwent exchange at the 2 position. The kinetic isotope effect (k_D/k_H) for acrolein formation, as calculated from the relative amounts of d_0 and d_4 acroleins formed from the 1:1 C_3H_6–C_3D_6 mixture was 0.44, in good agreement with the values given in Table II where the results were obtained by comparing the rates.

Table III: Composition of Acroleins Formed from Labeled Propylenes by Oxidation over Gold Sponge[a]

	Deuterium content, %[b]				
Propylene	d_0	d_1	d_2	d_3	d_4
CH_3CDCH_2	0.7	99.3	...	...	...
C_3H_6–D_2O[c]	98.0	2.0	...	...	...
C_3H_6–C_3D_6[d]	69.3	0.7	...	...	30.0

[a] At 265°; propylene pressure, 12–22 Torr; oxygen pressure, 60 Torr. [b] Corrected for ^{13}C, fragmentation, and starting impurities with lesser deuterium contents. [c] Reactant stream saturated with D_2O at 18°. [d] Composition of mixture: C_3H_6, 48.7%; C_3HD_5, 3.5%; C_3D_6, 47.8%.

Table IV: Composition of Acroleins from Oxidation of CH_3CHCD_2 or CD_3CHCH_2 over Gold Sponge

Temp, °C	Overall flow rate, cc min^{-1}	Propylene pressure, Torr	Oxygen pressure, Torr	Propylene conversion, %	Selectivity to acrolein, %	Propylene oxidized	Deuterium content,[a] % d_0	d_1	d_2	d_3
265	47	11	60	10	17	CH_3CHCD_2	1.1	47.9	51.0	...
						CD_3CHCH_2	1.1	54.1	44.1	0.7
285	24	22	110	25	15	CH_3CHCD_2	0.7	51.0	48.3	...
						CD_3CHCH_2	1.5	48.3	49.1	1.6

[a] Corrected for ^{13}C, fragmentation, and starting impurities.

Stereospecificity of Acrolein Formation. The deuterium contents of the acroleins produced by oxidation of CH_3CHCD_2 or CD_3CHCH_2 over Au sponge under several conditions are given in Table IV. The infrared spectra of the unreacted propylenes were indistinguishable from the starting olefins, *i.e.*, no isomerization took place. However, the mixture of acroleins formed from each olefin was nearly the same; both contained about equal quantities of monodeuterio- and dideuterioacrolein. Furthermore, the mass spectra of each mixture established that these major components were exclusively CH_2CHCDO and CD_2CHCHO, respectively (see Appendix). This could not have happened if any step in reaction involved transfer of atoms from one end carbon to the other. Thus, the results indicated that acrolein formation proceeded *via* an intermediate in which the two end carbons were equivalent.

Further confirmation of this conclusion was provided by the oxidation of propylene-*1*-^{13}C. The distribution of ^{13}C in the acrolein formed during this reaction over Au sponge was determined by mass spectral means following the procedure outlined in the Appendix. Values based on the relative intensities of four mass spectral peaks, with respect to the parent molecular ion, with *m/e* 57, are given in Table V. The agreement was excellent and established beyond doubt that ^{13}C in labeled acrolein molecules was distributed equally between the two end positions.

Table V: Location of ^{13}C in Acrolein Formed by Oxidation of $CH_3CH^{13}CH_2$ over Gold Sponge[a]

Calculated from intensity of peak with *m/e* of[b]	% retention of label in 1 position
25	50 ± 5
26	47 ± 3
27	52 ± 2
30	49.5 ± 1

[a] At 283°; propylene pressure, 22 Torr; oxygen pressure, 100 Torr; overall flow rate, 20 cc min^{-1}. [b] See Appendix.

Discussion

In agreement with an earlier study,[6] selectivities (Table I) for partial oxidation products from oxidation of C_2H_4 over Au catalysts approached zero. Selectivities for acrolein production from propylene, on the other hand, approached 50% under optimum conditions, and the mechanism of this reaction is the chief concern of the present paper.

The most significant observations were the large normal isotope effect stemming from substitution of deuterium for hydrogen in the methyl group of propylene and the evidence that acrolein is formed *via* a symmetrical intermediate (Tables II, IV, and V); the latter was unambiguously established by the mass spectrographic identification of nearly equal quantities of CH_2CHCDO and CD_2CHCHO formed from both CH_3CHCD_2 and CD_3CHCH_2. The kinetic isotope effect ($k_H/k_D \approx 2.5$) was close to the theoretical maximum for the temperature employed,[15] indicating that the primary attack was on the methyl group and that breaking of a C–H or a C–D bond thereon was involved in the rate-determining step. The resulting symmetrical intermediate has been previously tentatively identified[13,16,17] as the allylic radical when this reaction was catalyzed by oxide systems. However, the details of the mechanism beyond this point were evidently different. Adams and Jennings[16] found that the isotope effect for the removal of the second H or D over oxides was about equal to that for the first abstraction. In this case, a mixture of about 70% CD_2CHCHO and 30% CH_2CHCDO would be predicted for the kinetic isotope effect which we observed. Since we found nearly equal amounts of these two acroleins, the discrimination isotope effect for the second abstraction over Au cannot be appreciable. This points out one advantage of using deuterium, rather than carbon, labeling in studies of this reaction. Our results for ^{13}C-labeled propylene (Table V) showed no significant difference from those of Voge, Wagner, and Stevenson[17] (for the reaction over CuO), while the data for the deuterated hydrocarbon differed significantly from those of Adams and Jennings.

(15) L. Melander, "Isotope Effects on Reaction Rates," Ronald Press, New York, N. Y., 1960.

(16) (a) C. R. Adams and T. J. Jennings, *J. Catal.*, **2**, 63 (1963); (b) *ibid.*, **3**, 549 (1964).

(17) H. H. Voge, C. D. Wagner, and D. P. Stevenson, *ibid.*, **2**, 58 (1963).

The present results compliment and extend a similar study made over Rh catalysts,[12] the chief difference being that over Rh about 15% of the acrolein was formed with retention of double-bond position; *i.e.*, 15% of the time the methyl group was oxidized directly to the aldehyde linkage. Another, perhaps related, difference was the nearly complete absence over Au of exchange of the H for D on the center carbon atom as compared with the extensive exchange at this position over Rh. These factors made the Au data more tractable. Consequently, the new data established beyond doubt the validity of our experimental procedures, thus strengthening the conclusions derived from the Rh data.[12]

To explain the minor pathway proceeding with retention of double-bond position over Rh, it was suggested that peroxide formation[18] competed with formation of the allylic radical. The latter was supposed to be formed in the initiation step of a chain reaction, the propagation steps of which were

$$\dot{C}H_2CH\dot{C}D_2 + O_2 \longrightarrow CH_2CHCD_2\dot{O}_2 + CD_2CHCH_2\dot{O}_2 \quad (1)$$

and

$$\left.\begin{matrix}CH_2CHCD_2\dot{O}_2\\ CD_2CHCH_2\dot{O}_2\end{matrix}\right\} + CD_3CHCH_2 \longrightarrow \left\{\begin{matrix}CH_2CHCD_2O_2D\\ CD_2CHCH_2O_2D\end{matrix}\right\} + \dot{C}H_2CH\dot{C}D_2 \quad (2)$$

with product formation by

$$\left.\begin{matrix}CH_2\dot{C}HCD_2O_2D\\ CD_2CHCH_2O_2D\end{matrix}\right\} \longrightarrow \left\{\begin{matrix}D_2O\\ DHO\end{matrix}\right\} + \left\{\begin{matrix}CH_2CHCDO\\ CD_2CHCHO\end{matrix}\right. \quad (3)$$

Over Au, the data indicated only a slight tendency for retention of double-bond position (first experiment, Table IV). This could be explained if the chain length were longer over Au (at the higher reaction temperature) relative to peroxide formation than over Rh. Alternatively, the minor pathway could be missing. Whatever the cause, it is certain that with both metals the major pathway involved the formation of the symmetric intermediate.

Equations 1–3 should be viewed as a working hypothesis. The scheme rests on three factors. Over Rh,[12] the reaction could be made immeasurably fast by adjusting the pressure of either reactant so that the pressure ratio fell into a critical region; it was shown that this was not a temperature effect. Such behavior is suggestive of radical chain processes. The lack of an isotope effect for the removal of the second H or D from the symmetric intermediate requires a step not involving a CH or CD bond, which fixes the configuration equally at both ends; eq 1 accomplishes this. The scheme affords a satsifactory explanation for the large primary isotope effect for the removal of the first H or D, and it is centered on the symmetric intermediate. It has many shortcomings. Admittedly, conclusive evidence for radical chains is lacking. It does not include an explanation for certain observations, *e.g.*, the loss in selectivity at the higher olefin pressures. It does suggest possible experiments and therein, we think, lies its usefulness.

The gross kinetics over the two metals were quite different. The apparent activation energies over Rh were about 35 and 30 kcal/mol for total oxidation and acrolein formation, respectively.[12] Over Au, the corresponding values were 21 and 10 kcal/mol. Moreover, over Rh the rate of total oxidation increased with olefin pressure and decreased with oxygen pressure, the latter order eventually approaching zero. Nearly, the reverse was found for Au (Figures 2 and 3). With both metals, however, the selectivity for acrolein went through a maximum with olefin pressure. If it is assumed that the same basic mechanism applies over both metals, as suggested by the tracer data, the question arises as to whether or not these differences can be explained by properties of the two metals.

Qualitatively, the lower apparent activation energy over Au could stem from a longer chain length. Au chemisorbs little O_2, but heats of adsorption up to 21 kcal/mol have been reported[2a] for C_2H_4 on this metal. Thus, either the adsorption of C_3H_6 modifies the Au surface so that it can chemisorb O_2 or the first-order dependence on this gas results from the collision frequency of O_2 molecules with the surface or species chemisorbed thereon. The latter interpretation would be in agreement with eq 1 but a similar first-order dependence on C_3H_6 pressure corresponding to eq 2 was not observed. Presumably this was because the rate-determining step involved chain initiation so that the rate was not limited by eq 2 or 3. This is consistent with the observed isotope effects.

Over Rh, O_2 is strongly chemisorbed[19] and C_3H_6 must compete for sites. Hence, the reaction was inhibited by O_2 and approached first order in olefin pressure at low pressures. Beyond this, little can be reliably inferred because the chemistry is still largely unknown. Acetone formation was an important side reaction. The effect of this drain on the kinetics cannot be evaluated from the presently available data. Moreover, the chemistry leading to total oxidation is not understood. The data of Figure 2 indicate a decrease in selectivity for acrolein formation over Au when the olefin pressure varied from about half the oxygen pressure. Similar behavior was found with Rh catalyst where the maximum selectivity was found near the critical conditions (where the rate rose as

(18) L. Ya. Margolis, *Advan. Catal.*, **14**, 429 (1963).

(19) G. C. Bond, "Catalysis by Metals," Academic Press, New York, N. Y., 1962, p 76 ff.

expected for a branching chain reaction). Thus, although the pressure dependencies differed for the two metals, there were decided similarities with respect to acrolein formation. In particular, both sets of data suggest a role for olefin in total oxidation which is not yet understood.

It would be helpful to distinguish whether acrolein formation and total oxidation are independent parallel paths or are consecutive reactions, or whether both contribute. The evidence favors the last possibility, although the relative importance of the two paths cannot presently be assessed. Acrolein is more easily oxidized to CO_2 and H_2O than propylene.[12] Moreover, the decrease in selectivity at higher reactant pressures (higher conversion rates) shown in Figures 2 and 3 is consistent with a consecutive scheme, because higher acrolein pressures would be present. The markedly different apparent activation energies for the two overall reactions is not inconsistent with this picture. On the other hand, the same kinetic data could be used to argue that parallel pathways exist. The key piece of information, whether or not the activation energy for the oxidation of acrolein is higher or lower than that for its formation, is missing. To acquire this knowledge would require a series of tracer experiments not yet performed. There are, however, other bits of evidence which suggest the presence of parallel pathways. Small amounts of acetaldehyde and acetic acid were produced from propylene, whereas the corresponding C_3 compounds were undetected. These compounds were probably formed by direct cleavage of the olefinic double bond,[20] *i.e.*, by initial attack on the olefinic end of the molecule rather than the methyl group. Moreover, on the basis of a clean consecutive scheme, it is not possible to offer a convincing explanation for the relative oxidation rates and peculiar isotope effects shown in Table II. True, deuterating the methyl group greatly inhibited the rate of acrolein formation, but at the same time it *increased* the rate of total oxidation. This was quite different from the behavior found for Rh catalysts where it was possible to postulate that most of the CO_2 resulted from chain-termination reactions. The fact that the rate of total oxidation over Au was lowered *only* when the olefin was CH_3CHCD_2 strongly suggests that attack on the olefinic linkage is a principal source of CO_2. It therefore seems likely that parallel reaction pathways exist but that acrolein formation is limited by further oxidation. The very much lower apparent activation energy for oxidation to acrolein than to CO_2 is a great deterrent to the achievement of high yields of this product over Au; high selectivity can only be accomplished at the expense of low yields.

The reasons for the large effect of the support on selectivity is not clear. Au supported on α-alumina was relatively nonselective; Rh on the same support was much more selective. Hence, decomposition of acrolein on the support was probably not a factor, but this is not certain because the reaction over Au required a temperature nearly 100° higher than that for Rh. Recently, Cha and Parravano[7] showed that the properties of the support had a controlling effect on the transfer of O from $^{14}CO_2$ to CO when catalyzed by Au. In particular, they found Au supported on alumina much less active for this reaction than when supported on more inert MgO. Their results emphasize the importance of metal particle size on the reaction kinetics. These interesting leads should provide the basis for future research.

Acknowledgment. This work was supported by the Gulf Research & Development Co. as part of its research program on the Fellowship on Petroleum. Thanks are due to Mr. J. R. Boal for assistance in the recording of high-resolution mass spectra.

Appendix

Measurements were made to determine the mass spectral modes of fragmentation of acrolein-d_0, acrolein-d_4, and acrolein-2-d_1 (prepared by oxidation of CH_3CDCH_2 over Au sponge). Both the Nuclide relatively low-resolution mass spectrometer and the high-resolution AEI MS-9 instrument were used. The latter instrument enabled positive identification of each component of each peak by accurate mass comparison with the known mass of the N_2^+ ion. The spectra were taken with an ionizing voltage of 70 eV, and the agreement of relative intensities was good wherever comparison was possible. The Nuclide values were favored whenever only one ion was contributing to a peak because its detector was intrinsically the more accurate.

The relative intensities and identification of the major peaks, assigning the molecular ion a value of 100, are given in Table VI. Minor peaks were located between 37 and 44 and between 12 and 17, but their origin will not be considered here. The major mode of fragmentation was scission of the bond between the aldehyde group and the rest of the molecule. With acrolein-d_0, this produced either a $C_2H_3^+$ (m/e 27) or a CHO^+ ion (m/e 29) with the charge preferring to lie in the two-carbon fragment by a factor of about 3. With acrolein-d_4 in the two fragments were $C_2D_3^+$ and CDO^+, both with m/e 30. However, the high-resolution measurements confirmed that their relative intensities were similar to the equivalent fragments in the unlabeled molecule. With CH_2CDCHO the corresponding fragments were $C_2H_2D^+$ and CHO^+, with m/e of 28 and 29, respectively. The very low intensity for CDO^+ showed that scrambling of hydrogens and deuterium prior to this major mode of fragmentation was at most 5%.

(20) Part IV: N. W. Cant and W. K. Hall, to be submitted for publication.

The spectra of the d_0 and d_4 materials showed peaks corresponding to $C_2H_2^+$ and $C_2D_2^+$ which were probably formed by loss of H or D from the $C_2H_3^+$ and $C_2D_3^+$ ions. With acrolein-*2*-d_1, there were two ions, $C_2H_2^+$ and C_2HD^+, with relative intensities approximately equal to 1:2. Thus, this mode of fragmentation involved random loss of H or D probably due to scrambling prior to the removal.

Table VI: Identification and Relative Intensities of Peaks in the Mass Spectrum of Acrolein-d_1, Acrolein-d_4, and Acrolein-2-d_1[a]

Acrolein *m/e*	$CH_2{=}CH{-}CHO$ Assignment	Intensity	$CD_2{=}CD{-}CDO$ Assignment	Intensity	$CH_2{=}CD{-}CHO$ Assignment	Intensity
25	C_2H	8			C_2H	5
26	C_2H_2	61	C_2D	12	C_2H_2	26
27	C_2H_3	127			C_2HD	53
28	CO	23	CO	25	CO	26
	C_2H_4	65	C_2D_2	79	C_2H_2D	130
29	CHO	44			CHO	41
					C_2H_3D	68
30			CDO	51	CDO	2
			C_2D_3	123		
32			C_2D_4	74		
55	C_3H_3O	70			C_3H_3O	2
56	C_3H_4O	100			C_3H_2DO	70
57					C_3HD_2O	100
58			C_3D_3O	57		
60			C_3D_4O	100		

[a] Measured with ionizing voltage of 70 eV.

Consideration of the spectra also indicated that during scission of the bond between carbons 1 and 2, the aldehydic H or D could be transferred to the two-carbon fragment. Thus, $C_2H_4^+$ and CO^+, again with relative intensity approximately equal to 3, were formed from normal acrolein. Since both these ions have the same unit mass, this fragmentation method was not immediately apparent in low-resolution measurements of the material but was obvious with acrolein-d_4 where the $C_2D_4^+$ fragment has *m/e* 32. High-resolution measurements of acrolein-*2*-d_1 enabled separation of the corresponding $C_2H_3D^+$ (*m/e* 29) and CO^+ (*m/e* 28) peaks from those of the major fragmentation producing CHO^+ and $C_2H_2D^+$ ions with the same unit masses.

Table VI shows that isotope effects in the modes of fragmentation described above are probably small and could be neglected, at least for the experimental accuracy available here. However, careful measurements in the range *m/e* 55–60 showed that a small effect (H/D = 1.23) did occur for loss of a single H or D from the parent molecular ions. One would expect that the atom lost would be from the aldehyde group, and this can be shown to be true since the ratio of loss of H to loss of D was greater than 30 for acrolein-*2*-d_1 The small isotope effect in loss of H or D from the aldehyde group agreed with observations by Brinton and Blacet[21] for deuterated acetaldehydes.

Information concerning mass spectral fragmentation modes was invaluable in two respects in the present work. Firstly, it was thought that the d_1 and d_2 acroleins, shown by conventional low-electronvolt measurements to be formed in nearly equal amounts during oxidation of both CD_3CHCH_2 and CH_3CHCD_2 over Au sponge, were CH_2CHCDO and CD_2CHCHO, respectively. The corresponding molecular ions have *m/e* 57 and 58 and fragmentation by loss of the aldehydic D or H, as described above, would give the ions CH_2CHCO^+ and CD_2CHCO^+ with *m/e* 55 and 57; *i.e.*, there was no way in which ions with *m/e* 56 could be produced in more than small amounts. Experimentally, the *m/e* 56 peak in the spectra of the d_1 and d_2 acroleins was of very low relative intensity and could be almost entirely accounted for on the basis of the small quantities of other acroleins produced from impurities in the propylenes. Thus, the expectations were confirmed. Knowledge with respect to fragmentation was also important in analysis of the overall mass spectrum of acroleins formed by oxidation of propylene-1-^{13}C (which contained 46.5% unlabeled propylene as an impurity). In the mixture so formed, the peak due to ions with *m/e* 55 could only be due to loss of H from *unlabeled* acrolein, and by a ratio method the contributions that this acrolein made to the peaks attributable to ions with *m/e* 25, 26, 27, 30, and 56 were subtracted out. The remaining intensities were thus due to labeled molecules, presumably $CH_2CH^{13}CHO$ and $^{13}CH_2CHCHO$. The relative amounts of each were calculated from the ratio of the corrected intensities due to ions with *m/e* 57, in comparison with ratios expected by fragmentation according to the ways described above. As mentioned, earlier results obtained by this method showed excellent internal agreement.

(21) R. K. Brinton and F. E. Blacet, *J. Chem. Phys.*, 17, 797 (1949).

Adsorption of Organic Gases on Clean Germanium Surfaces

by F. Meyer and J. M. Morabito

Philips Research Laboratories, N. V. Philips' Gloeilampenfabrieken, Eindhoven, The Netherlands *(Received December 29, 1970)*

Publication costs assisted by Philips Research Laboratories

The chemical adsorption of a number of organic compounds (CH_3OH, CH_3SH, CH_3Cl, CH_3Br, and CH_3OCH_3) on clean germanium surfaces has been investigated by means of gas volumetric measurements on powder samples and ellipsometric measurements on single-crystal faces. The reactions appear to be dissociative and plane-specific, compensating the so-called dangling bonds of the germanium surface atoms. Structures for the adsorption complexes have been proposed and evidence is presented for shifts in the positions of the surface atoms due to the bonding in the adsorption complex.

I. Introduction

The clean surfaces of germanium and silicon appear to be highly reactive to many gases, which can be ascribed to the presence of uncompensated (dangling) bonds at the surface atoms. This was demonstrated for a number of inorganic hydrides[1] (HCl, H_2S, NH_3, etc.) and for some organic molecules (methanol, ethanol, and others).[2] These adsorption reactions have been interpreted as being dissociative, compensating the dangling bonds of the surface atoms.[3]

It is the purpose of this paper to obtain information on the structure of adsorption complexes on germanium, since this is an essential step in the understanding of the chemical behavior of these clean surfaces and their catalytic properties.

We have combined several techniques for surface study in this investigation. Gas volumetric adsorption measurements on powders with a large surface area ($\sim$1 m^2) yield the amount adsorbed and subsequent desorption experiments as a function of temperature give decomposition products, which can be analyzed mass spectrometrically. The inherent difficulty of the powder measurements is the presence of more than one crystallographic orientation. The cleavage plane (111) will be the main but not the only constituent of the powder surface.

Ellipsometry ties in very well with the gas volumetric measurements. Ellipsometry is an accurate optical method, which measures, in principle, surface coverages on single-crystal surfaces with an accuracy of approximately 0.05 of a monolayer. A previously reported study, in which ellipsometric and gas volumetric data have been compared,[4] led to the conclusion that in the special case of silicon and germanium ellipsometry also gives information about the number of dangling bonds compensated by the adsorbed molecules. This gives direct information on the structure of the adsorption complexes.

Auger electron spectroscopy (aes) has been used to check surface cleanliness and to give further support to the ellipsometric measurements since both methods have approximately the same sensitivity and can be used to study single-crystal faces.

Low-energy electron diffraction has been tried, but no ordered structures for the organic adsorption complexes have been observed. The only structure which has been found, was a Ge(111) 2 × 1 after hydrogen sulfide adsorption at 250°.[5]

II. Experimental Section

The adsorption and desorption experiments on powders were performed in an all-glass apparatus. A low pressure of 10^{-7} Torr was obtained with a mercury diffusion pump provided with a liquid nitrogen cold trap. Pressure readings of the organic gases were taken with a McLeod manometer.

The germanium powder, obtained by crushing a high-ohmic single crystal in air, was cleaned by heating to 650° at 10^{-7} Torr for 15 hr.[1] After cooling to room temperature, the gas was admitted and the pressure decrease was recorded. The excess gas was pumped off at room temperature. Then the temperature was raised by using an electric furnace around the reaction tube. Temperature readings were taken with a Pt—Pt–10% Rd thermocouple imbedded in the powder. The decomposition products were analyzed with an Atlas M86 mass spectrometer connected to the reaction tube. The sensitivity of the mass spectrometer has been calibrated separately for the different gases in the appropriate pressure range. The total pressure calculated from the mass spectra agreed within 3% with

(1) A. H. Boonstra and J. van Ruler, *Surface Sci.*, **4**, 141 (1966); A. H. Boonstra, *Philips Res. Rep., Suppl.*, **No. 3** (1968).

(2) F. Meyer, *J. Phys. Chem.*, **73**, 3844 (1969).

(3) We will use the term "dangling" bond throughout this paper, without having any special electronic configuration in mind. Prior to adsorption the electrons in the nonbonding orbitals will probably form some type of bond at the surface, which may induce the shifts in atomic positions associated with the surface structures observed by LEED. In the adsorption reactions these bonds will dissociate again and react as uncompensated (radical-like) bonds with the adsorbate.

(4) G. A. Bootsma and F. Meyer, *Surface Sci.*, **14**, 52 (1969).

(5) A. J. van Bommel and F. Meyer, *ibid.*, **6**, 391 (1967).

the total pressure in the desorption system as measured with the McLeod manometer.

The total surface area of the germanium powder was obtained by the BET method,[6] utilizing krypton as the adsorbate at liquid nitrogen temperature. For the cross-sectional area of one krypton atom a value of 19.5 Å^2 was taken.[7] The total *clean* surface can be determined by the chemical adsorption of oxygen, which adsorbs at room temperature to an extent of one O atom per surface atom both on the (111) and (100) faces at an exposure of approximately 1 Torr-min.[1,8] The further reaction, *i.e.*, the adsorption on a covered surface, is much slower. The surface areas from BET calculations and from oxygen adsorption measurements agreed well for freshly prepared powders after the heat treatment at 650°. If the powder had been often exposed to carbon-containing gases and subsequently heated under vacuum, the clean surface area decreased, probably due to carbon contamination, which could not be removed by heating under vacuum nor by heating in oxygen. The determination of the clean surface area by oxygen adsorption can also be used if the surface contains some preadsorbed organic gas. This has been used in cases where no complete adsorption layers of the organic compound could be obtained. The specific surface area of the powder was 0.1 m^2/g and total surface areas of ~1 m^2 have been used.

The ellipsometric measurements were carried out on polished single-crystalline germanium samples which had been oriented within 0.5° of the desired crystallographic orientation. The crystals were clamped in tantalum strips and cleaned by resistive heating to 800° for several hours *in vacuo* (10^{-9} Torr). The surface cleanliness was checked by measurements of the ellipsometric effects upon chemical adsorption of a test gas (HCl), of which the effects can be predicted within certain assumptions (compare ref 3 and section IIIA of this paper). These measurements suggested that the samples could be cleaned to at least 80–90%. Aes measurements indicated that some carbon persists on the surface, which cannot be removed by heating under high vacuum or in oxygen. LEED measurements gave the diffraction patterns Ge (111)-8 and Ge (100)-2, which have been ascribed to the clean surfaces.[9]

The reaction chamber for the ellipsometric measurements is connected to a 50-l./sec Mullard Vac Ion pump, and the base pressure as measured by the pump current or by an ionization manometer directly connected to the reaction chamber is ~10^{-9} Torr.

The Vac Ion pump was turned off prior to the adsorption measurements. No adsorption on the sample from the residual gas could be detected ellipsometrically (<0.05 monolayer) for several hours, if no gas was admitted. To obtain the ellipsometric data as a function of surface coverage, small doses of gas (typically 1–10 cm^3 of 1 Torr) were admitted in the reaction chamber (total volume of the chamber including the Vac Ion pump is 1.5 l.).

The ellipsometric apparatus has been described elsewhere.[4]

III. Interpretation of the Experimental Data

A. Ellipsometric Measurements. Ellipsometry measures the change in the state of polarization of polarized light upon reflection at a surface. The amplitude reflection coefficients R_p and R_s are related to the ellipsometrically determined angles Δ and ψ as in

$$R_p/R_s = \tan \psi \exp i\Delta \quad (1)$$

where the subscripts p and s refer to the directions parallel with and perpendicular to the plane of incidence. The angles Δ and ψ, therefore, contain information on the optical constants of the reflecting substrate and the optical constants and thickness, d_a, of layers on the substrate surface. For thin layers ($d_a < 100$ Å) the changes in Δ and ψ are in first approximation linearly dependent on the layer thickness

$$\delta\Delta = \Delta_{clean} - \Delta_{ads} = \zeta d \quad (2)$$

$$\delta\psi = \psi_{clean} - \psi_{ads} = -\eta d \quad (3)$$

The sensitivity of $\delta\Delta$ in terms of average layer thickness is approximately 0.1–0.4 Å depending on the type of adsorbate. Comparison of ellipsometry with other methods such as radiotracer techniques[10] and gas volumetric measurements on powders[11] suggests that in many cases the macroscopic theory can be applied in the submonomolecular region using an effective index of refraction, n_a, and thickness. These macroscopic parameters are related to the microscopic parameters surface coverage, θ, and polarizability of the adsorbed molecule, α, which is described to a good approximation by the Lorentz–Lorenz equation

$$\frac{n_a^2 - 1}{n_a^2 + 2} = \frac{4\pi}{3}\frac{\alpha N\theta}{d} \quad (4)$$

where N is the number of germanium surface atoms per square centimeter, and θ and d are the surface coverage and diameter of the adsorbed molecules, respectively.[11] For α the sum of the atomic polarizabilities of the atoms in the adsorbed molecule has been taken and it appeared that one could use the literature values of these polarizabilities for the type of adsorbates studied here.

Chemical adsorption on the clean surfaces of silicon and germanium[4,12] appeared to give ellipsometric effects

(6) S. Brunauer, P. H. Emmett, and E. Teller, *J. Amer. Chem. Soc.*, **60**, 309 (1938).

(7) A. J. Rosenberg, *ibid.*, **78**, 2929 (1956).

(8) A. Liberman and M. Green, *Phys. Chem. Solids*, **23**, 1407 (1962).

(9) F. Jona, *IBM J. Res. Develop.*, **9**, 375 (1965).

(10) J. R. Miller and J. E. Berger, *J. Phys. Chem.*, **70**, 3070 (1966).

(11) G. A. Bootsma and F. Meyer, *Surface Sci.*, **13**, 110 (1969).

(12) F. Meyer, E. E. de Kluizenaar, and G. A. Bootsma, *ibid.*, **27**, 88 (1971).

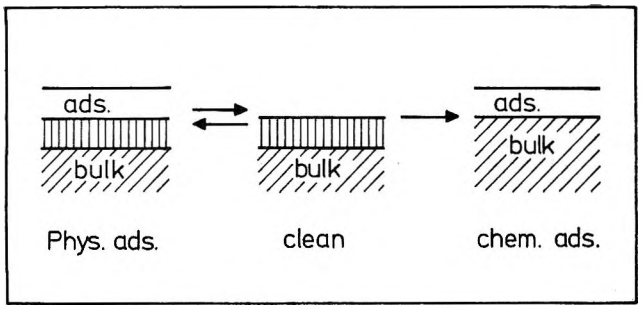

Figure 1. Schematic representation of physical and chemical adsorption on a clean germanium surface.

which can be divided in an adsorbate-dependent part, obeying the simple macroscopic theory outlined above, and an adsorbate-independent part, which is related to the substrate optical properties. The latter effect has been interpreted as a substrate change upon chemical adsorption. This change is probably related to the compensation of the dangling bonds, since this seems to be the process which all chemical adsorptions have in common. This model is supported by the observation that physical adsorption, which does not compensate the dangling bonds, gives only the adsorbate-dependent ellipsometric effects.

This adsorption behavior is schematically given in Figure 1. The surface atoms of the clean surface with their dangling bonds are depicted as a transition layer (thickness ~5 Å) with optical constants, n_t and k_t, different from those of the bulk material. Physical adsorption leaves this layer unchanged, but chemical adsorption compensates the dangling bonds and the optical constants of the transition layer return to the normal bulk values; *i.e.*, the transition layer is optically removed, giving the adsorbate-independent ellipsometric effects. This phenomenological description using dangling bonds has a physical interpretation in terms of bands of surface states. A more detailed study on this is in progress.

A study of the wavelength dependence[12] of the optical constants of the transition layers on clean silicon and germanium showed a remarkable resemblance with the dispersion of the optical constants of the corresponding amorphous materials. This has been explained by the assumption that the lattice-like amorphous material has dangling or distorted bonds throughout its bulk giving the same optical differences with the crystalline material as the surface atoms on a clean surface. An example of the wavelength dependence of $\delta\Delta$ and $\delta\psi$ upon chemical adsorption to the "monolayer" point on Ge (100) is given in Figure 2. One can calculate the ellipsometric effects due to the adsorbate layer ($\delta\Delta_a$ and $\delta\psi_a$) by assuming a surface coverage of one HCl molecule per germanium surface atom (from a comparison with the same adsorption on Si (100)). The difference between measured and calculated effect should result in the adsorbate-independent effect ($\delta\Delta_t$ and $\delta\psi_t$). It appears that the $\delta\psi_a$ values are negligibly small in all cases, which implies that the measured change in ψ is approximately

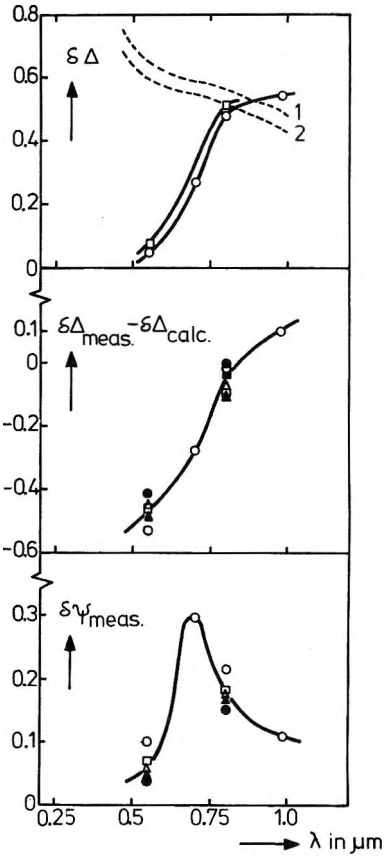

Figure 2. Wavelength dependence of the ellipsometric effects $\delta\Delta$ and $\delta\psi$ upon chemical adsorption on Ge (100); angle of incidence 70.0°: ○, HCl; ●, CH_3OCH_3; △, CH_3Br; ▲, CH_3Cl; □, CH_3SH; ■, CH_3OH. The dashed lines represent the calculated $\delta\Delta$ effects for the CH_3SH monolayer (curve 1) and the HCl monolayer (curve 2). For all gases the calculated effects in Δ have been obtained using the values of θ and α from Table I.

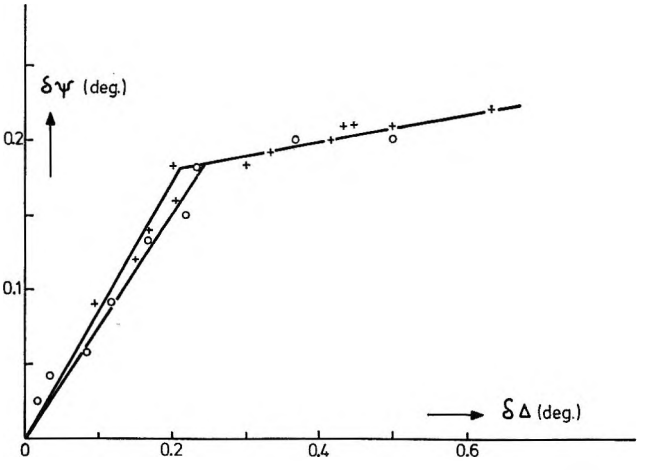

Figure 3. $\delta\psi$ *vs.* $\delta\Delta$ plots for CH_3OH and CH_3SH adsorption on Ge (111): +, CH_3OH; ○, CH_3SH. Angle of incidence 70.0° and wavelength 0.80 μm.

Table I: Ellipsometric Data for Gas Adsorption on Germanium (111) and (100); Wavelength 0.80 μm, Angle of Incidence 70°[a]

			Adsorption on Ge (111)				Adsorption on Ge (100)			
Adsorbate	α, Å³	d, Å	$\delta\psi$	$\delta\Delta$	θ, %	"Idealized" coverage in molecules/surface atom	$\delta\psi$	$\delta\Delta$	θ, %	"Idealized" coverage in molecules/surface atom
CH_3OH	3.23	4.1	0.19	0.21	0.24 ± 15	1:4	0.15	0.35	0.45 ± 15	1:2
CH_3SH	5.65	4.1	0.19	0.23	0.14	1:6	0.18	0.50	0.42	1:2
CH_3Cl	4.29	4.1	0	0	0	0	0.17	0.35	0.40	1:2
CH_3Br	5.28	4.1	0.15	0.27	0.17	1:6	0.17	0.47	0.44	1:2
CH_3OCH_3	4.86	4.1	0.12	0.12	...	...	0.15	0.48	0.47	1:2
HCl	2.65	3.6	0.18	0.41	0.52	1:2	0.21	0.47	0.92	1:1

[a] For α the sum of the atomic polarizabilities is given and d is for the organic components taken as the van der Waals diameter of the methyl group and for HCl as the van der Waals diameter of the Cl atom.

equal to $\delta\psi_t$. The $\delta\Delta$ *vs.* $\delta\psi$ plots, therefore, show a kink at the coverage where all dangling bonds are just compensated and further adsorption gives mainly an increase in Δ. The kinks for different adsorbates occur at the same value of $\delta\psi$. This is shown in Figure 3 for methanol and methyl mercaptide adsorption on Ge (111) measured at a wavelength of 0.80 μm.

At certain wavelengths, *i.e.*, 0.55 μm for silicon and 0.80 μm for germanium, the substrate change has only an effect on ψ and not on Δ, whereas the measured change in Δ corresponds to the effect of the adsorbate layer. These wavelengths are therefore very convenient for measuring the number of molecules adsorbed and the corresponding number of dangling bonds compensated.

The surface coverages on Ge (111) and Ge (100) for a number of organic gases calculated from the ellipsometric data at the "monolayer" are given in Table I. The indicated error of 15% contains both the experimental error in the determination of the ellipsometric data and the estimated error introduced by the use of literature values of atomic polarizabilities in the calculation. The data from Table I give valuable information on the structure of the adsorption complexes. We have made the following assumptions with regard to these structures.

1. The chemically adsorbed molecules dissociate and compensate the dangling bonds of the surface atoms, *i.e.*, one bond per surface atom on the (111) face and two bonds per surface atom on the (100) face.
2. The normal valency of the adsorbed atoms is preserved in the adsorption complex.
3. No bonds are formed between the adsorbed molecules themselves.

This implies that the adsorbing molecules can only compensate an even number of dangling bonds, giving surface coverages at the monolayer of 1:2, 1:4, 1:6, etc., molecules per surface atom on the (111) face and 1:1, 1:2, etc., on the (100) face. These "idealized" coverages are given in Table I along with the experimentally determined ones.

B. Gas Volumetric Measurements. The chemical adsorptions on clean powders usually show a "fast" reaction followed by a slower further adsorption, which might be reversible.[1] The amount of gas adsorbed in the fast reaction seems to be related with the compensation of the dangling bonds. As mentioned already in the Introduction, the main problem in the interpretation of adsorption on powders is the occurrence of more than one crystallographic orientation of the surface. Calculations based on bond energies[13] predicted relative areas of 75 and 25% for (111) and (100) in germanium, respectively. Previous work on methanol adsorption[2] suggested relative areas of 80 and 20% in good agreement with the calculated values. There is some indication that the particle size of the powder has an influence on this distribution. A powder with a specific surface area of 0.2 m^2/g, twice as large as normally employed, gave consistently lower adsorption in cases where adsorption on the (100) face is the main reaction (CH_3Cl, CH_3Br, CH_3OCH_3). The results would agree with ellipsometric data if a ratio of 85:15 for (111) and (100) in the powder is assumed.

IV. Results and Discussion

A. Methanol. The gas volumetric measurements of methanol adsorption on germanium powders have been described in detail in ref 2. From the relative amounts of decomposition products (H_2, CO, and CH_4) at temperatures between 150 and 500° the conclusion was drawn that there is a 1:4 coverage on the (111) and a 1:2 coverage on the (100) face. This is in good agreement with the ellipsometric data as shown in Table II. The proposed structures for the adsorption complexes are given in Figure 4.

B. Methyl Mercaptide. The amount of CH_3SH adsorbed on a germanium powder in the "fast" reaction (~1 Torr-min) corresponds to 0.23 ± 0.01 molecules per surface atom. This is in excellent agreement with the ellipsometrically determined 1:6 coverage

(13) A. J. Rosenberg, *Phys. Chem. Solids*, **14**, 175 (1960).

Table II: Comparison of Ellipsometrically Calculated and Gas Volumetrically Determined Coverages on Germanium Powders[a]

Adsorbate	Coverage (ellipsometrically)	Coverage (gas volumetrically)
CH_3OH	0.300	0.30 ± 0.01[b]
CH_3SH	0.233	0.23
CH_3Cl	0.100	0.10
CH_3Br	0.20–0.23	0.17
CH_3OCH_3	...	0.10

[a] The ellipsometric coverages have been calculated using the "idealized" coverages of Table I and assuming an 80:20% distribution of (111) and (100) planes in the powder.

on the (111) and 1:2 coverage on the (100) face assuming an 80:20% distribution of (111) and (100) planes in the powder. The gas volumetrically and ellipsometrically determined average coverages have been compared in Table II. An exposure of 1 Torr-min oxygen on the CH_3SH-covered powder gave no significant adsorption (<0.05 monolayer) indicating that the methyl mercaptide compensates all the dangling bonds.

The excess methyl mercaptide vapor was removed by pumping, and the decomposition of the adsorbed amount was followed as a function of temperature as shown in Figure 5. At each temperature the desorption was continued until the pressure stayed constant.

The decomposition products were hydrogen and methane. The formation of methane depended on the hydrogen pressure in the system. If the desorption was carried out at hydrogen pressures below 0.1 Torr, hardly any methane was formed, but hydrogen instead. The volume of the apparatus compared to the powder surface was such that the hydrogen pressure, which was built up during the desorption below 300°,

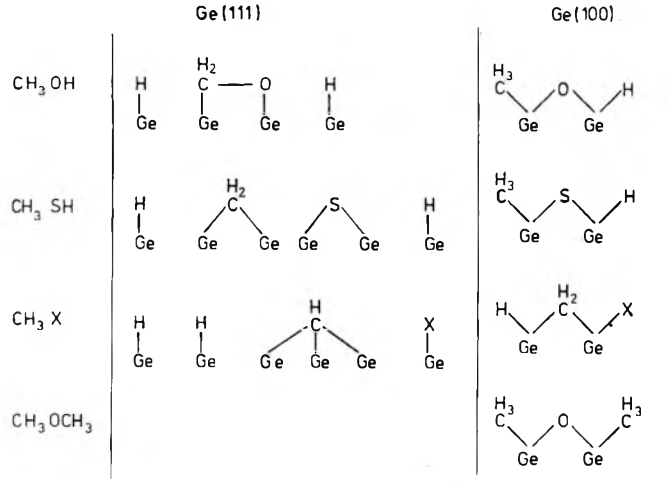

Figure 4. Structure models for the adsorption complexes on Ge (111) and Ge (100).

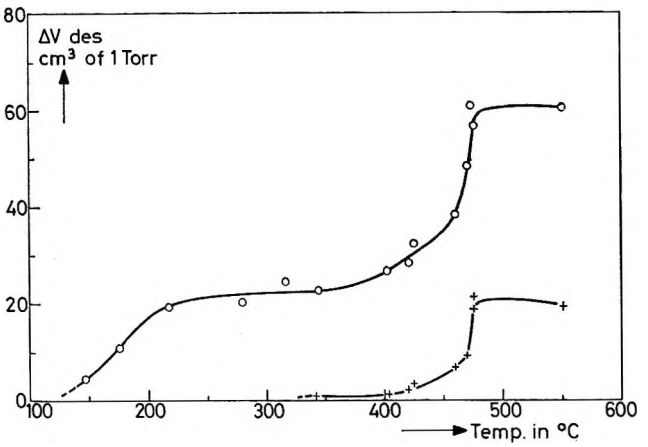

Figure 5. Decomposition of the CH_3SH adsorption complex as a function of temperature. The amount of CH_3SH adsorbed at room temperature was 53 cm³ of 1 Torr: O, H_2 desorption; +, CH_4 desorption.

exceeded 0.1 Torr. If this hydrogen was removed, however, before the methane formation would start, a total evolution of 4 cm³ of CH_4 and 87 cm³ of 1 Torr H_2 was observed (compare Figure 5). In all cases the total amount of hydrogen and methane desorbed corresponds closely to the total amount of hydrogen adsorbed in the form of methyl mercaptide.

Very similar behavior has been observed for methanol decomposition[2] where the critical hydrogen pressure for methane formation was 0.4 Torr. By volumetric measurements on (100) oriented slices it was shown that the reaction took place on the (100) face. Since the amount of methane desorbed corresponds closely to the calculated amount of CH_3SH adsorbed on the (100) face, it is very likely that these reactions are the same for CH_3OH and CH_3SH. There probably exists an equilibrium between two adsorption complexes with and without two hydrogen atoms, which give irreversibly either methane or hydrogen. This is shown schematically in Figure 6.

The data from Figure 5 show clearly that the hydrogen desorption occurs in two steps. If the (100) face gives only methane (under influence of the H_2 pressure in the system built up by the desorption from the (111) planes), the hydrogen will come from the (111) plane, suggesting two different binding states. The structure model for the adsorption complex as given in Figure 4 exhibits two types of hydrogen, one bonded directly to a germanium surface atom and the other bonded to carbon in a CH_2 group. Hydrogen bonded directly to germanium will desorb for at least 90% at 200° as shown by Tamaru[14] for adsorption and desorption of H_2 and also by the desorption experiments of methanol. It is therefore very likely that the first adsorption step corresponds to the hydrogen

(14) K. Tamaru, *J. Phys. Chem.*, 61, 647 (1957).

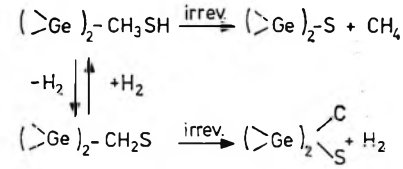

Figure 6. Decomposition of the CH_3SH adsorption complex on Ge (100).

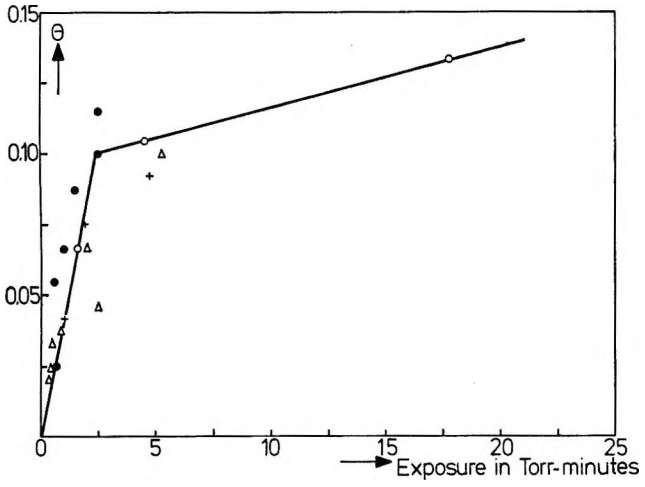

Figure 7. Adsorption of methyl chloride on a clean germanium powder as a function of exposure. θ is given in molecules adsorbed per surface atom: △, adsorption at 0.3 Torr CH_3Cl; ●, adsorption at 0.5 Torr CH_3Cl; +, adsorption at 0.9 Torr CH_3Cl; ○, adsorption at 1.5 Torr CH_3Cl.

bonded to germanium and the second step to hydrogen bonded to carbon.

C. Methyl Chloride. Gas volumetric measurements of CH_3Cl adsorption on a germanium powder showed a "fast" adsorption to an average coverage of 0.10 ± 0.01[5] molecule per surface atom, followed by a very slow further reaction. The results at different pressures given in Figure 7 suggest that the amount adsorbed in the "fast" reaction is independent of the CH_3Cl pressure during the adsorption.

Oxygen adsorption on the CH_3Cl-covered powder surface indicated that 70–80% of the surface was still clean. This is in good agreement with ellipsometric results which show a 1:2 coverage on the Ge (100) plane, whereas no adsorption was observed on the Ge (111) face with exposures up to 10 Torr-min.

Desorption was observed starting at 300° with hydrogen as main reaction product and some methane formation. The desorption was complete at 550° and the amount of hydrogen in the form of H_2 and CH_4 corresponded roughly (within 20%) to the amount adsorbed as methyl chloride.

D. Methyl Bromide. CH_3Br gave an average coverage on the germanium powder surface of 0.17 ± 0.02[5] molecules per surface atom as shown in Figure 8; 20–30% of the surface area did not react with CH_3Br as indicated by a subsequent O_2 adsorption. Compari-

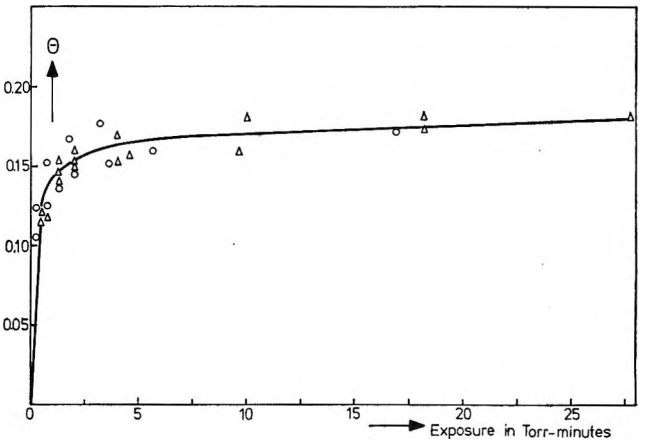

Figure 8. Adsorption of methyl bromide on a clean germanium powder as a function of exposure. θ is given in molecules adsorbed per surface atom: ○, adsorption at 0.16 Torr CH_3Br; △, adsorption at 0.4 Torr CH_3Br.

son with ellipsometric measurements (see Table II), suggests that the (100) face has a 1:2 coverage just as for CH_3Cl and that the (111) surface of the powder reacts to approximately 70% giving a 1:6 coverage. The ellipsometric measurements, however, did not show clearly the partial coverage on the single-crystalline (111) sample, the $\delta\psi$ value being not significantly lower than for the monolayer coverage of the other gases. It should be noted that an ellipsometric study of methyl halides on silicon gave also a 1:2 coverage on the (100) face and a 1:6 coverage on the (111) face. CH_3Cl reacted to a complete monolayer whereas CH_3Br compensated only 70% of the available dangling bonds.

If all normal valencies are preserved in the adsorption complex, it has to exhibit a carbon atom bonded to three germanium surface atoms either as a $(\geq Ge-)_3CH$ group or as a $(\geq Ge-)_3CBr$ group. The first possibility is given in Figure 4 since it is more probable that the first adsorption step involves an interaction of the Br atom and a Ge surface atom. The substituent in CH_3X (*e.g.*, H, Cl, Br) appears to have a great influence on the adsorption characteristics as demonstrated by the fact that CH_4 does not react chemically with germanium at room temperature and that CH_3Cl reacts only with the (100) face of germanium.

The highly strained $(\geq Ge-)_3CH$ unit might be compared with the equally strained $(\geq Ge-)_3N$ group proposed as the adsorption complex in NH_3 absorption on germanium.[1]

Desorption of CH_3Br gave the unexpected result that hydrogen evolution did not start below 350°, although the (111) face should exhibit Ge–H bonds which normally dissociate at 200°. A possible explanation involves a change in structure of the adsorption complex at a temperature where the hydrogen normally desorbs. This is depicted schematically in

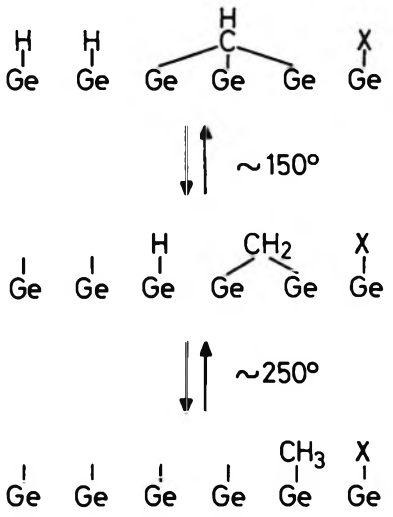

Figure 9. Rearrangements of the adsorption complex of CH_3Br on Ge (111).

Figure 9. The driving force for the transition is the entropy gained by going from a relatively rigid $(\geq Ge-)_3CH$ group to a $(>Ge<)_2CH_2$ group which has one low-frequency vibration mode. Thermodynamic calculations give a possible effect of 1–2 kcal/mol, which should be compared with adsorption enthalpies of 10–20 kcal/mol.

If the germanium powder is heated in the presence of CH_3Br, an additional adsorption is observed at temperatures between 100 and 200° to an average coverage of 0.3 ± 20%. Heating under vacuum, however, to 200° followed by room temperature adsorption of CH_3Br produced no appreciable effect. This supports the model of a *reversible* transition in which extra dangling bonds are formed in the temperature range of 100–200°.

It has been reported[15] that at temperatures of 300° and higher a reaction takes place between CH_3Br and germanium with the formation of mixed germanes, $Ge(CH_3)_xBr_{4-x}$. We found that the germanium surface was heavily contaminated after such a treatment and could not be completely cleaned again.

E. Dimethyl Ether. The average coverage from gas volumetric measurements is 0.10 ± 0.01[5] molecules per surface atom. Subsequent O_2 adsorption indicates that 80–90% of the surface-dangling bonds are still uncompensated. Ellipsometric results give a 1:2 coverage on the (100) face, which would agree very nicely with the gas volumetric data if no adsorption would have been observed on the (111) face. Significant adsorption, however, takes place on the (111). The reason for this discrepancy is not clear although contamination of the dimethyl ether with small amounts of another gas might be an explanation.

Cross experiments on powders with subsequent adsorption of CH_3Cl and CH_3OCH_3 showed that dimethyl ether did not adsorb to a measurable extent on a surface with preadsorbed CH_3Cl and *vice versa*. This suggests that both gases react with the same part of the powder surface, namely, the (100) planes.

F. Discussion of the Structure Models for the Adsorption Complexes. The structures given in Figure 4 have been constructed in such a way that all normal valencies have been preserved. The drawings are highly schematic and represent an oversimplified picture of the adsorption complexes. Infrared spectra could give additional information but, to our knowledge, there have been no spectra reported in the literature of this type of adsorption complexes on clean germanium or silicon. McManus, *et al.*,[16] gave infrared absorption spectra of methanol adsorbed on germanium oxide. They proposed a dissociative adsorption under formation of an –OH and an $-OCH_3$ group. The germanium oxide surface in this study was probably less reactive than the clean germanium surfaces used here, and therefore it is not surprising that the $-OCH_3$ group did not react further as seems to be the case for our adsorptions.

The tendency to compensate the surface-dangling bonds by further dissociation of the adsorbed molecule leads to strained configurations with an atom or group of atoms in a bridge position. The strain can possibly be lessened by shifts of the surface atoms from their original positions. The results for adsorption on the (100) plane can be explained by this effect. The structures on the (100) face have an oxygen or sulfur or methylene group in a bridge position. The formation of an oxygen or sulfur bridge is likely since water and hydrogen sulfide also adsorb to a 1:2 coverage on the (100) which implies the same type of bridge formation. It is interesting to note that probably no double-bridge formation occurs. The 1:2 coverages suggest that the methyl group from CH_3OH and CH_3SH attached to the O or S bridge does not react further with the next pair of dangling bonds, whereas the methyl group of CH_3Cl and CH_3Br forms a methylene bridge. This behavior can be possibly explained from geometrical considerations. Bridge formation may draw together the two surface atoms involved, widening the gap with the next nearest neighbors. This will certainly enhance the strain for double-bridge formation.[17]

This effect can be treated quantitatively within certain assumptions.

1. It is well known that bond stretching is energetically less favorable than bond bending. Only bond bending will therefore be considered in the calculation

(15) E. G. Rochow, *J. Amer. Chem. Soc.*, **69**, 1729 (1947).

(16) J. C. McManus, K. Matsushita, and M. J. D. Low, *Can. J. Chem.*, **47**, 1077 (1969).

(17) From these considerations it is more likely that the adsorption complex for ethanol on Ge (100) involves an ethylene bridge instead of a methylene bridge as proposed in ref 2. The structure can be presented as H–(Ge)–CH_2–CH_2–(Ge)–O–(Ge)–H.

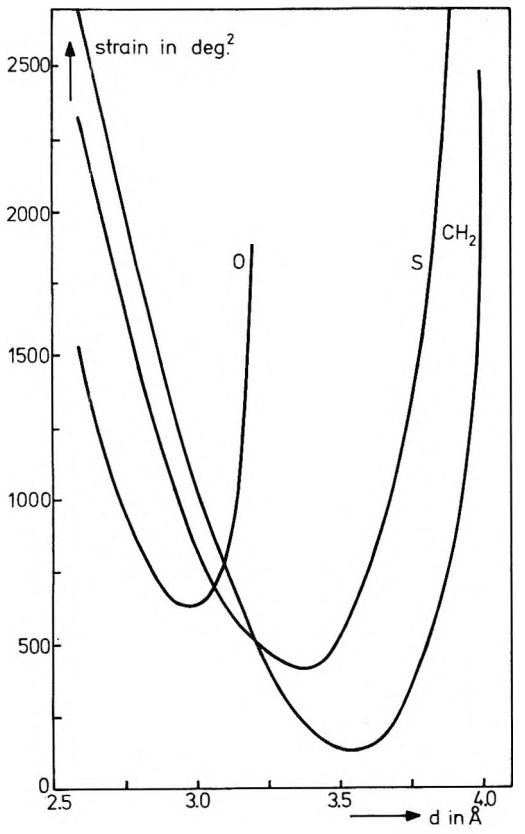

Figure 10. Strain in the adsorption complexes on Ge (100) due to bridge formation as a function of the distance between the germanium surface atoms involved. The strain is given as the sum of the squared angles of distortion of the bonds in the adsorption complex. Bond lengths and angles (undistorted) have been taken as follows: Ge-O, 1.6 Å; Ge-O-Ge, 130°; Ge-S, 1.9 Å; Ge-S-Ge, 92°; Ge-C, 2.0 Å; Ge-O-Ge, 110°.

of the strain in the adsorption complex on the (100) face (compare ref 18).

2. The strain energy will be taken proportional to the sum of the squared angles of distortion.

3. This strain energy due to bond distortion is assumed to be independent of the type of atom.

The strain energy of the O, S, and CH_2 bridges has been calculated as a function of the distance between the surface atoms. The normal distance between germanium atoms on the (100) face is 4.0 Å, and the calculations presented in Figure 10 show a minimum strain for the different type bridges at distances of 3.05–3.6 Å. The deviations from the normal directions of the bonds in the bridge-forming atom or group and of the germanium atoms in the first and second atomic layer have been taken into account.

On the (111) plane each surface atom is bonded by three bonds to the underlying layer and both bond distortion and bond stretching are necessary in the accommodation of the adsorbing molecule. No calculations have been carried out for this plane. It is very likely, however, that in general adsorption complexes are more easily formed on the (100) plane than on the (111) plane.

On the (111) plane there seems to be bridge formation with two bonds (for CH_3OH, CH_3SH, H_2S, etc.) and with three bonds (for CH_3Br, NH_3, etc.). The reason that the CH_2 bridge in the case of CH_3SH adsorption does not react further to a trivalent CH bridge might be that the presence of the divalent sulfur bridge gives slight displacements of the surface atoms, which makes a trivalent bridge formation even more strained then in the CH_3Br adsorption complex.

Conclusion

1. The chemical adsorption of gaseous adsorbates on a clean germanium surface seems to be governed by the uncompensated bonds at the surface and the presence of an active atom (or active bond) in the adsorbate. This implies that the adsorptions are dissociative and plane specific.

2. The experimental data presented in this paper can be interpreted in terms of adsorption complexes in which all participating atoms have their normal valencies.

3. Comparison of the proposed structures on Ge (100) leads to the assumption that the surface atoms can shift from their normal positions to accommodate the adsorbing molecule.

Acknowledgment. We wish to thank Dr. A. J. van Bommel and Mr. A. van Tooren for performing a number of Auger and LEED measurements and Mr. J. J. de Rooy for carrying out the ellipsometric part of this work.

(18) M. Green, *Ann. N. Y. Acad. Sci.*, **101**, 1001 (1963).

Infrared Spectra of Nitric Oxide Adsorbed on Evaporated Alkali Halide Films

by A. J. Woodward* and Neville Jonathan

Chemistry Department, The University, Southampton, SO9 5NH England *(Received January 11, 1971)*

Publication costs borne completely by The Journal of Physical Chemistry

Infrared spectra are reported for nitric oxide adsorbed at different surface coverages on high surface area films of evaporated NaCl, NaBr, NaI, KCl, and CsCl. The data are interpreted in terms of monomeric and dimeric species adsorbed on the surface planes and at the edges of the alkali halide crystallites. Possible adsorption sites and orientations of the adsorbate are discussed. The spectra provide support for the surface structures previously proposed for alkali halide films.

Introduction

Kozirovski and Folman have pioneered the production of alkali halide films in a form suitable for infrared spectroscopic studies of adsorption.[1] In the present work an apparatus of similar design has been used to study the adsorption of nitric oxide on films of NaCl, NaBr, NaI, KCl, and CsCl. The interest in these systems arises because of the possibility of determining the nature of the adsorption, particularly as there is some doubt as to whether or not nitric oxide exists in a dimerized form on these surfaces.

Adsorption isotherms have been reported for systems of this type and the data used to determine the extent of interaction of the NO quadrupole with the alkali halide surface and also to find whether or not dimerization accompanies the adsorption.[2] It was argued that in the absence of quadrupole interaction the heats of adsorption of argon and NO should be in a similar ratio to that of their equilibrium separation energies obtained from 9:6 intermolecular potential functions.[3] The agreement between heats of adsorption estimated on this basis and the experimental low-coverage heats for NO adsorption was good except for a LiCl surface. It was therefore concluded that the quadrupole moment of NO is not of sufficient magnitude to have any significant effect on the heats of adsorption of NO on NaCl, KCl, and CsCl but it does seem to have an appreciable effect where the much smaller cation of LiCl is concerned. No evidence was found for dimerization.

These conclusions are now considered open to question since the parameters used for the 9:6 potential of NO are known to relate to the double molecule.[4] The agreement between experimental and calculated heats of adsorption is therefore reinterpreted as being indicative of a significant contribution to the heat of adsorption from dimerization and/or quadrupole interaction.

Experimental Section

The adsorbent films were prepared *in situ* by evaporation from a small tantalum furnace onto a window cooled with liquid nitrogen at approximately −196°. The films were then annealed at −80° for 10–24 hr prior to adsorption studies. This treatment increases the homogeneity and stability of the films[1] and after it they are believed to have surface areas of *ca.* 200 m^2/g. Ron and Folman[5] have previously discussed the adsorptive and thermodynamic properties of alkali halide films prepared under similar conditions. A conventional high-vacuum system with a mercury diffusion pump and liquid nitrogen trap was used for evacuating the cell and admitting gas to the film. Adsorption studies were made in the temperature range −145 to −150°, the spectra being recorded with a Grubb-Parsons GS2A grating spectrometer. The salts used were of analytical grade. Nitric oxide supplied by Air Products Ltd. was purified by repeated fractional sublimations from liquid argon to liquid nitrogen.

Results

Figures 1–6 show spectra obtained from the various NO–alkali halide systems for different surface coverages, although the actual extent of the coverage could not be determined. In all cases the variations in band intensities on the desorption cycle were the exact reverse of the adsorption cycle data. The observed frequencies and their shifts with coverage are summarized in Table I. Changes in band shapes, widths, and frequencies with temperature were small and attempts to make systematic studies of these factors proved to be inconclusive. All spectra were accompanied by a very weak absorption in the region 2.9–3.0 μm. This problem which has been referred to previously[1] arises from traces of water which desorb slowly from the walls of the metal cell and become adsorbed on the alkali halide film. However, in view of the low

(1) Y. Kozirovski and M. Folman, *Trans. Faraday Soc.*, **62**, 808 (1966).

(2) A. Granville and P. G. Hall, *ibid.*, **63**, 701 (1967).

(3) E. A. Moelwyn-Hughes, "Physical Chemistry," Pergamon Press, London, 1961, p 335.

(4) E. A. Moelwyn-Hughes, private communication.

(5) I. Ron and M. Folman, *Isr. J. Chem.*, **3**, 18 (1965).

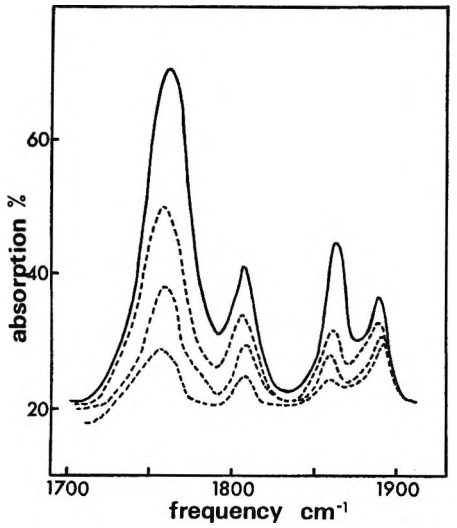

Figure 1. Spectra of NO adsorbed at different coverages on NaCl.

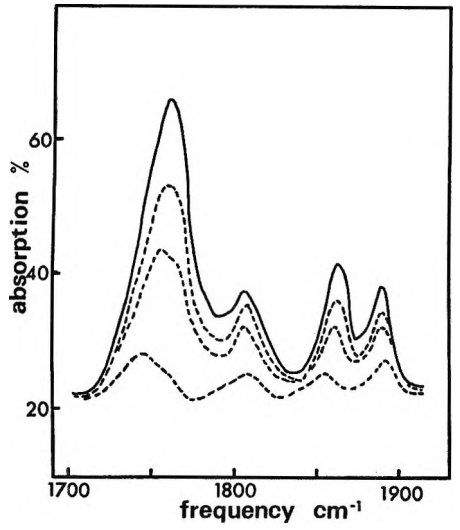

Figure 2. Spectra of NO adsorbed at different coverages on NaBr.

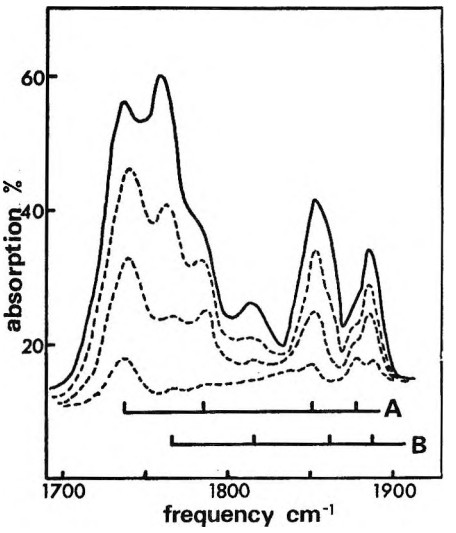

Figure 3. Spectra of NO adsorbed at different coverages on a NaI film annealed at −80° for 10 hr.

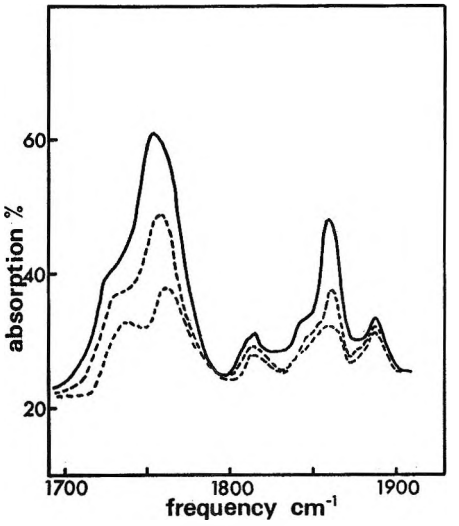

Figure 4. Spectra of NO adsorbed at different coverages on a NaI film annealed at −80° for 18 hr.

intensity of the band the usual assumption is made that only a small fraction of the surface is affected.

Discussion

The existence of the nitric oxide dimer in the low-temperature gas and in the condensed phase is now firmly established. A bent ONNO structure for the molecule was first suggested by Raman and infrared studies of NO in the solid and liquid states and in matrix isolation.[6,7] The infrared data for the low-temperature gas is consistent with an N–N bond distance of about 1.75 Å and an N–N–O angle of around 90°[8] while for the solid dimer the dimensions N···N = 2.16 Å, O···O = 2.62 Å, N–O = 1.12 Å have been determined by X-ray crystallography.[9] The heat of dissociation of the dimer in the gas phase has been found to be 2.7 kcal/mol.[10]

In addition to the normal cis dimer, monomeric and trans dimeric NO species have been isolated in a CO_2 matrix.[7] Table II gives relevant data from these studies.

A recent communication has reported an infrared spectroscopic study of NO physisorbed on lithium halide films.[11] On LiF, LiCl, and LiBr four absorp-

(6) A. L. Smith, W. H. Keeler, and H. L. Johnston, *J. Chem. Phys.*, 19, 189 (1951).

(7) W. G. Fateley, H. A. Bent, and B. Crawford, Jr., *ibid.*, 31, 204 (1959).

(8) C. E. Dinerman and G. E. Ewing, *ibid.*, 53, 626 (1970).

(9) W. J. Dulmage, *et al.*, *Acta Crystallogr.*, 14, 1100 (1961).

(10) C. E. Dinerman and G. E. Ewing, *J. Chem. Phys.*, 54, 3659 (1971).

(11) A. Lubezky and M. Folman, *Proc. Israel Chem. Soc., Suppl.*, 8, 99 (1970).

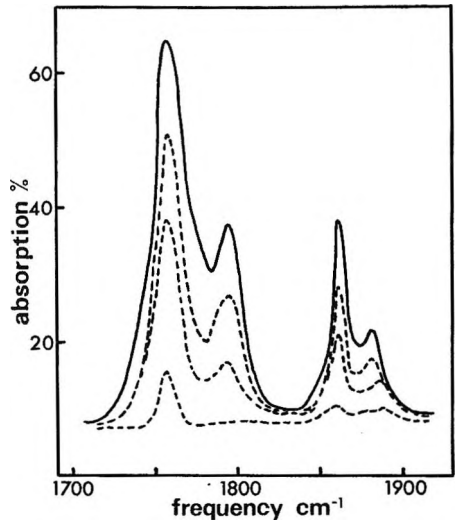

Figure 5. Spectra of NO adsorbed at different coverages on KCl.

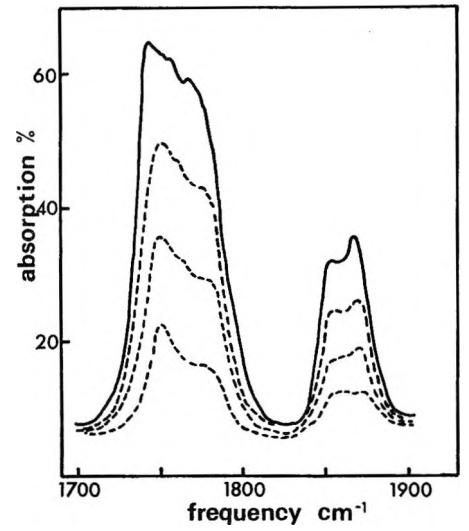

Figure 6. Spectra of NO adsorbed at different coverages on CsCl.

tion bands were observed, two in the region 1900–1830 cm^{-1}, the other two in the 1800–1760-cm^{-1} region. It was concluded that two different adsorption sites exist at these surfaces and that the nitric oxide is adsorbed as a dimer at both types of site. On LiI only two absorptions were obtained.

Adsorption on Sodium Salts. For the NO–NaCl system, four ir absorption bands were observed at each of the surface coverages studied. With increasing coverage the absorptions at 1893 and 1809 cm^{-1} showed markedly decreasing rates of growth compared with those of the 1860- and 1751-cm^{-1} absorptions. A similar effect has been noted previously in a study of N_2O adsorption on these surfaces,[12] although here some bands were actually found to cease growing from a certain coverage onward. Such bands were assigned to adsorbate at sites of limited number which were thought

Table I: Frequencies Observed for the NO–Alkali Halide Systems, cm^{-1}

Surface	ν_{obsd}		
NaCl	1893 → 1889		
	1860 → 1863		
	1809 → 1809		
	1751 → 1761		
NaBr	1893 → 1889		
	1857 → 1863		
	1807 → 1807		
	1746 → 1761		
NaI	1889 → 1886	~1876	set A[a]
	1861 → 1861	~1852	set A[a]
	1815 → 1817	~1785	set A[a]
	1764 → 1757	~1737	set A[a]
KCl	1889 → 1883		
	1860 → 1862		
	1790 → 1795		
	1757 → 1757		
CsCl	~1877 → ~1868		
	~1858 → ~1862		
	~1778 → ~1772		
	~1753 → ~1743		

[a] See text.

Table II: Infrared Spectral Data for NO, Cm^{-1}, Taken from Ref 6–8

	Matrix isolated[7]				Gas[8] at 123°K
	InNO	$InCO_2$	In argon	Liquid[8]	
NO (monomer)		1883	1875	1872 (in krypton)	1876
cis-$(NO)_2$ sym	1862	1862	1866	1865	1860
cis-$(NO)_2$ asym	1768	1768	1776	1770	1788
trans-$(NO)_2$ asym		1740			

to be located at the edges of the alkali halide crystallites. It seems reasonable to assume a similar assignment for the present spectra; *i.e.*, the bands at 1893 and 1809 cm^{-1} are attributed to adsorption at sites which are limited in number and possibly located at the crystallite edges, while the 1860- and 1757-cm^{-1} bands are attributed to adsorption on the surface planes of the crystallites.

A close correlation was observed between the optical density data for the 1860- and 1757-cm^{-1} bands. In view of this and of the close similarity of the frequencies to those previously reported for the stretching modes of the cis $(NO)_2$ dimer (Table II), these two bands are assigned to a cis dimeric species on the NaCl surface planes. The asymmetric stretching mode at 1751 cm^{-1} is shifted downward by 37 cm^{-1} with respect to the gas-phase frequency indicating that the interaction of

(12) Y. Kozirovski and M. Folman, *Trans. Faraday Soc.*, **65**, 244 (1969).

the dimer with the NaCl surface is greater than that occurring between dimer molecules in the solid for which the corresponding shift is 20 cm^{-1}. A dimer molecule could be adsorbed at the surface plane by interaction of either one or both of the NO structures with the surface. If the separation of adjacent adsorption sites is suitable, adsorption through both structures will be favored. Calculations of the heats of adsorption for N_2[13] and CO[14] on the (100) surface plane of NaCl have indicated that as a result of a large quadrupole interaction with the surface an adsorption perpendicular to the surface and above a cation is the most favorable. The same site is anticipated for NO adsorption on this plane since the quadrupole moments of NO and N_2 have been found to be similar.[15,16] This is supported by the recent calculations on the NO–LiCl system which found a normal orientation above the Li^+ ion to be most favorable. The separation of adjacent cations on the NaCl surface plane is about 4.0 Å and is suitable for the adsorption of a dimer by the interaction of each NO structure with a surface cation (taking into account the ionic radius for the oxygen of NO). The structure of the adsorbed molecule would be similar to that of the solid-state dimer and each NO molecule would be slightly displaced from the surface normal. This is believed to be the predominant mode of adsorption on the surface planes of the crystallites at the lower surface coverages. At high coverages there is probably a contribution from dimers adsorbed by the interaction of one NO structure with a surface cation. This could explain the shift in dimer frequencies with increasing coverage (see Table I), although this could also be due to energetic heterogeneity of the surface sites and adsorbate–adsorbate interactions.

The lack of correlation in the optical density data for the 1893- and 1809-cm^{-1} absorptions would seem to preclude a simple assignment of these bands to a second dimeric species, although in the study of NO adsorption on LiF, LiCl, and LiBr[11] bands at 1890 and 1800 cm^{-1} were assigned in this manner. The two alternative assignments are either (a) there is an overlap of absorptions due to monomeric and dimeric adsorbate molecules or (b) each band arises from a monomeric species at the NaCl surface. An assignment of the bands in part to a dimer is considered unsatisfactory since it requires that the symmetric and asymmetric stretching modes of the dimer are shifted upward by 33 and 21 cm^{-1}, respectively, from the corresponding gas-phase frequencies. A downward frequency shift would be anticipated as observed for the 1860- and 1757-cm^{-1} bands.

An assignment of the 1893-cm^{-1} absorption to a monomeric species is suggested by its similarity to the frequency reported for the NO monomer isolated in a CO_2 matrix.[7] Since the NO^+ ion absorbs at ~2210 cm^{-1} [17] the upward shift of the band by 17 cm^{-1} from the gas-phase frequency represents a slight increase in NO bond order on adsorption. Such a change can only occur as a result of close association with surface cations. Adsorption above a cation located at a crystallite edge would be even more favorable than above an in-plane cation due to the somewhat greater surface field at this point. A perpendicular orientation is indicated by the lack of any significant frequency shift with a change in anion from Cl^- to I^-, and although the dipole moment of NO is small (0.16 D[18]), an adsorption through oxygen would give a contribution to the interaction potential from dipole interaction with the surface field. Adsorption as a dimer at these sites in the manner proposed for the in-plane adsorptions is prevented by the large separation of cations in a crystallite edge (5.6 Å). Adsorption as a dimer by the interaction of one NO structure with an edge-located cation will be less favorable than adsorption as two monomers provided the heat of adsorption is significantly greater than the heat of dimerization.

The 1809-cm^{-1} frequency is shifted 67 cm^{-1} downward from the gas-phase monomer frequency indicating an increase in electron density in the π system of the NO and hence association with the anion. The shift is considerably larger than that which one normally associates with physisorption. However, such a shift only involves a small change in the NO bond order since the NO^- ion absorbs in the region 1100–1000 cm^{-1} [19] (gas-phase frequency NO monomer 1876 cm^{-1}). The change is of similar magnitude to that accompanying adsorption above a cation. A significant shift in the low-coverage frequency of this band with a change in cation indicates that the adsorption is not perpendicular to the crystallite edge. It therefore seems probable that the adsorption is such that the nitrogen atom is almost above the edge-located anion and that the oxygen is directed toward the cation. Such an adsorption would be expected to be accompanied by a far lower heat of adsorption than that due to monomeric adsorption above an edge-located cation. This would explain the somewhat lower intensity of the 1809-cm^{-1} band (relative to the 1893-cm^{-1} band intensity) at the lowest coverage studied. Furthermore, since the in-plane sites are far more numerous than edge sites, the fact that all four absorptions appear for the lowest coverage studied suggests that the edge sites are the more energetic. It should be noted that both argu-

(13) T. Hayakawa, *Bull. Chem. Soc. Jap.*, **30**, 236 (1957).

(14) R. Gevirzman, Y. Kozirovski, and M. Folman, *Trans. Faraday Soc.*, **65**, 2206 (1969).

(15) B. T. Berendts and A. Dymanus, *J. Chem. Phys.*, **49**, 2632 (1968).

(16) J. S. Murphy and J. E. Boggs, *ibid.*, **49**, 3338 (1968).

(17) D. W. Turner and D. P. May, *ibid.*, **45**, 471 (1966).

(18) H. E. Watson, G. G. Rao, and K. L. Ramanaswamy, *Proc. Roy. Soc., Ser. A*, **143**, 558 (1934).

(19) W. P. Griffith, J. Lewis, and G. Wilkinson, *J. Inorg. Nucl. Chem.*, **7**, 38 (1958).

ments make the reasonable assumption of a similarity in the extinction coefficients of the various absorptions.

The spectral data for NO–NaBr (Figure 2) were almost identical with the above and bands are assigned in a similar manner; *i.e.*, the low-coverage frequencies of 1893 and 1807 cm^{-1} are attributed to monomeric NO adsorbed at edge sites, while those at 1857 and 1746 cm^{-1} are attributed to dimeric adsorption on the surface planes. In a previous study of N_2O–NaBr,[12] absorptions were detected for adsorption at sites in a second surface plane. It is possible that the slight asymmetry in the 1746-cm^{-1} band at low coverage might be due to dimers adsorbed on such a plane, but it would appear that the films were either of slightly lower surface area or annealed to a somewhat greater extent than those of the previous study.

The data for the NO–NaI system were complicated by the fact that the spectra obtained were strongly dependent on the time for which the film was annealed at −80°. Figures 3 and 4 show examples of the spectra obtained from films annealed for 10 and 18 hr, respectively. Eight absorptions were distinguished for NO adsorbed on the 10-hr film and from their intensity variation with surface coverage these are readily divided into two sets of four, each set behaving in an analagous manner to the bands described for NO–NaCl. The bands are labeled A and B in Figure 3. The approximate low-coverage frequencies are: for set A, 1876, 1785 cm^{-1} and 1852, 1737 cm^{-1}; for set B, 1889, 1815 cm^{-1} and 1860, 1764 cm^{-1}. Only the bands of set A and the highest frequency of set B were observed at the lowest coverage studied. At the higher coverages the bands of set B increased in intensity at a much greater rate than did those of set A. The spectra from the 18-hr film showed a greater correspondence with those for NO–NaCl. Four main absorptions were observed with frequencies similar to those of set B described above, *i.e.*, 1889, 1815 cm^{-1} and 1861, 1757 cm^{-1}. Additional absorptions were present as shoulders on the low-frequency sides of the 1861- and 1757-cm^{-1} absorptions, their frequencies being similar to those of the strong absorptions of set A, namely, ~1739 and ~1853 cm^{-1}. Each set of bands is assigned to monomeric edge and dimeric in-plane adsorptions on a particular type of crystallite. Set A arises from adsorption on a high-energy form which is somewhat unstable at −80°. The number of these crystallites is dependent on the annealing time and in the 18-hr film is not sufficient to allow detection of edge adsorptions. Bands of set B arise from adsorption on a more stable crystallite type and in view of the similarity of frequencies with those recorded for the NO–NaCl–NaBr systems the crystallite type is probably the same as that existing in the other sodium halides. The difference in frequencies is attributed to the different arrangement of ions in the surface and underlying planes of the two crystallites. This different arrangement could also mean that for the less stable form the sites and orientations of the adsorptions are somewhat different from those of the more stable form. The latter are assumed to be similar to those discussed for NaCl, although it is probable that in view of the larger cation separation in NaI the mode of dimer adsorption may be somewhat different, *viz.*, adsorption by interaction of only one NO molecule of the dimer with a surface cation.

The above analysis supports the interpretation given by Kozirovski and Folman for the N_2O–NaI system.[12] This work indicated that two crystallite types were present in NaI films annealed for 24 hr at −80°. Absorptions were observed for edge and in-plane adsorptions on one crystallite, whereas only in-plane adsorptions could be detected for the other.

The slower rate of annealing for the NaI film is attributed to the size of the anion. Studies of the dielectric properties of alkali halide films formed in this manner have shown pronounced aging effects.[20] These occur as the result of high vacancy concentrations, the excess of which is steadily annealed out. In order to maintain electrical neutrality the cation vacancies can only condense as the less mobile anion vacancies condense. The annealing rate is therefore determined by the anion mobility which is highest for a small anion and/or a large cation and *vice versa*.

It must be pointed out that in view of the above data for NaI, care was taken to ensure that films of all the other alkali halides were fully annealed.

Adsorption on Potassium Chloride. Three of the four bands observed for NO–KCl, *viz.*, the high-frequency monomer absorption (1889 cm^{-1}) and the dimer absorptions (1860, 1757 cm^{-1}), followed a similar pattern to that described for NO–NaX. However, for all coverages the intensity of the monomer absorption relative to those of the dimer bands was weaker than the corresponding cases for the NaX surfaces. This effect is attributed to the somewhat larger cation which leads to a more extensive annealing in the KCl films than in the NaX films and hence larger crystallites with a higher ratio of in-plane to edge sites.

For all except the lowest coverage studied a fourth absorption was observed at 1790 cm^{-1}, its increase in intensity with coverage being more rapid than that of the other three absorptions. The band is again assigned to monomeric NO molecules associated with surface anions, but in view of the intensity variations of the band, these anions are considered to be located at both edge and in-plane sites. The calculations for N_2[21] have indicated that the difference in energy between anion and cation sites in a (100) surface plane decreases for a change from NaCl to KCl which fits in with this explanation.

Adsorption on Cesium Chloride. Two regions of

(20) C. Weaver and S. Lorenzoni, *J. Vac. Sci. Technol*, **6**, 597 (1969).
(21) T. Hayakawa, *Bull. Chem. Soc. Jap.*, **30**, 332 (1957).

absorption were observed for this system, *viz.*, 1850–1880 cm^{-1} and 1740–1780 cm^{-1}. The high-frequency region appeared to arise from two overlapping absorptions of similar intensity and approximate frequencies 1877 and 1858 cm^{-1}. Similarly the low-frequency region appeared to be due to two or perhaps three overlapping bands (~1778, ~1753 cm^{-1} and ~1760 cm^{-1}(?)). An assignment to monomeric species at edge and in-plane sites and dimeric species at in-plane sites is considered unsatisfactory. No frequency showed an upward shift from the gas-phase monomer frequency as would be expected for monomeric adsorption over an edge-located cation and the apparent similarity in intensity of the overlapping bands would not be expected for edge and in-plane adsorptions.

Kozirovski and Folman in previous studies of CsCl have considered the films to be a mixture of bcc crystallites exposing (110) faces and fcc crystallites exposing (100) faces.[1,22,23] Spectra of adsorbed HCN, CO_2, and N_2O were then interpreted in terms of adsorption on these two planes. The lack of adsorptions due to edge adsorptions (assuming the above assignment to be correct) was not discussed. Using such a structure for the present surfaces, our interpretation of the data for the NO–NaX and NO–KCl systems may now be extended to give a satisfactory explanation of the NO–CsCl data. It is reasonable that due to the large cation, the annealing in the CsCl films is even more extensive than for the KCl films. As a result the crystallites are relatively large and prevent detection of edge adsorptions. Absorption bands are observed for NO dimers adsorbed on the surface planes of the two crystallite types. In view of the similarity of the frequencies at ~1858 and ~1753 cm^{-1} to those recorded for the other surfaces these absorptions are assigned to dimeric adsorption on the fcc structure. The bands at ~1877 and ~1760 cm^{-1} are attributed to dimeric adsorption on the bcc structure. The spectra indicate that a third absorption overlaps in the low-frequency region (~1753 cm^{-1}) and this is probably due to adsorption above anions located in the surface planes of the two crystallite types.

In this paper we have considered the various possible assignments of the spectral data in relation to our present knowledge of the structures of the alkali halide films. We believe that our final assignments are the most coherent and logical since they satisfactorily explain the changes in spectra which accompany a change in the alkali halide surface.

Finally we note that the consistent detection of a dimer on all of these surfaces strongly supports the conclusions reached by reinterpretation of the heats of adsorption for low surface coverages of NO on alkali halide films.[2]

Acknowledgments. We wish to thank the Science Research Council for the award of a studentship to A. J. W.

(22) Y. Kozirovski and M. Folman, *Trans. Faraday Soc.*, **62**, 1431 (1966).

(23) Y. Kozirovski and M. Folman, *Isr. J. Chem.*, **7**, 595 (1969).

The Interaction of Halide Ions with Organic Cations Containing Charged Nitrogen, Phosphorus, or Sulfur in Aqueous Solutions Studied by Nuclear Quadrupole Relaxation

by Håkan Wennerström,* Björn Lindman, and Sture Forsén

Division of Physical Chemistry 2, The Lund Institute of Technology, Chemical Center, P.O.B. 740, S-220 07 Lund 7, Sweden *(Received February 1, 1971)*

Publication costs assisted by The Lund Institute of Technology

Measurements of the nuclear magnetic resonance line widths of ^{35}Cl, ^{79}Br, ^{81}Br, and ^{127}I in aqueous solutions of various substituted ammonium, phosphonium, and sulfonium salts are presented. All line widths are found to be considerably larger than those for aqueous solutions of alkali halides. The effects on the relaxation rate of varying the charged central atom in the cation, the halogen ion, and the nature of the organic substituents attached to the central atom in the cation have been investigated. The relative line broadening observed is somewhat greater for ^{79}Br and ^{127}I than for ^{35}Cl. The line-broadening effect of the cation is found to be roughly proportional to the number of carbon atoms in the ion. The introduction of polar groups in the cation reduces the line width. In mixtures of Et_4NCl–Et_4NI, no competitive effects are found between the anions; consequently the line width depends only on the concentration of the cation. Substitution of deuterium oxide for ordinary water increases the line width by about 20% over a wide concentration range. These findings lead to the conclusion that the observed line broadening arises from anion–solvent interactions. The hydrophobic parts of the cations give rise to a structure stabilization of the water in their vicinity, and the large line widths are due to an interaction of this modified water with the anions. Polar groups on the cation reduce the structure stabilization and thus the line width of the halogen nuclear magnetic resonance signal. The description of these solutions in terms of contact ion-pairing and micelle formation, as proposed by other workers, is not compatible with the present study.

Introduction

Measurements of the nuclear magnetic relaxation times of various halogen nuclei have become a valuable tool in studying ion binding to proteins and other biologically interesting compounds.[1-3] A natural first step in investigations of this type is to investigate certain model compounds to obtain information about the factors that predominantly influence the relaxation times. An obvious choice of such model substances is substituted ammonium salts and similar compounds. These salts have a charged atom surrounded by organic groups, an arrangement often found in water-soluble biological substances.

Aqueous solutions of tetraalkylammonium salts have been thoroughly studied during recent years by various physical methods.[4-8] Most authors in the field agree that the alkyl groups in the cations cause a certain structure stabilization of the water in the vicinity of the cations. The structure of this stabilized water may for example be similar to that of the water cages in the solid clathrates which some of these salts can form.[9] A more detailed discussion of the effects of nonpolar solutes on the water structure has been given by Hertz.[10] In two previous articles Lindman, *et al.*,[11,12] have shown that the interaction between the stabilized water and bromide ions in aqueous solutions of alkylammonium bromides causes a decrease in the nuclear magnetic relaxation time of ^{79}Br. The aim of the present work was to investigate the generality of the effects observed in ref 11 and 12 and also to provide experimental results leading to a deeper understanding of the cause of the decrease in relaxation times.

Experimental Section

Nmr Measurements. A Varian V-4200 nmr spectrom-

(1) M. Zeppezauer, B. Lindman, S. Forsén, and I. Lindqvist, *Biochem. Biophys. Res. Commun.*, **37**, 137 (1969).

(2) R. P. Haugland, L. Stryer, T. R. Stengle, and J. D. Baldeschwieler, *Biochemistry*, **6**, 498 (1967).

(3) A. G. Marshall, *ibid.*, **7**, 2450 (1968).

(4) H. G. Hertz and M. D. Zeidler, *Ber. Bunsenges. Phys. Chem.*, **68**, 821 (1964).

(5) F. Franks and H. T. Smith, *Trans. Faraday Soc.*, **63**, 2586 (1967).

(6) S. Lindenbaum and G. E. Boyd, *J. Phys. Chem.*, **68**, 911 (1964).

(7) W.-Y. Wen and K. J. Nara, *ibid.*, **71**, 3907 (1967).

(8) H. E. Wirth, *ibid.*, **71**, 2922 (1967).

(9) D. Feil and G. A. Jeffrey, *J. Chem. Phys.*, **35**, 1863 (1961).

(10) H. G. Hertz, *Ber. Bunsenges. Phys. Chem.*, **68**, 907 (1964).

(11) B. Lindman, S. Forsén, and E. Forslind, *J. Phys. Chem.*, **72**, 2805 (1968).

(12) B. Lindman, H. Wennerström, and S. Forsén, *ibid.*, **74**, 754 (1970).

eter equipped with a 12-in. V-3603 magnet was used in the measurements. The general experimental procedure for studying the ^{79}Br, ^{81}Br, and ^{127}I resonances was as described in ref 12. The frequencies employed were 14.98 MHz for ^{79}Br, 15.82 MHz for ^{81}Br, and 11.96 MHz for ^{127}I. The derivative of the absorption curve was recorded for these nuclei. The line width was taken as the distance between maximum and minimum slopes of the absorption curve. The modulation frequency was 80 Hz for line widths greater than 0.12 mT (T = tesla, 1 T = 10^4 G) and 40 Hz for more narrow signals. The peak-to-peak modulation field was kept at approximately one-fourth of the line width.

The ^{35}Cl measurements were made at 5.78 MHz with the side-band technique using a modulation frequency of 400 Hz. The line width was taken as the full width at half-height of the first side-band signal. We have no exact measure of the magnetic field inhomogeneity, but the line width of ^{35}Cl in a 1 *M* solution of NaCl was 7.7 ± 0.3 μT giving an inhomogeneity broadening of 4.1 ± 0.5 μT. The true line width was determined to be 3.6 ± 0.2 μT by a Varian HA-100 nmr spectrometer as described in ref 13. Comparison of data for some samples obtained with both the spectrometers showed that no significant error arises if the inhomogeneity is simply substracted from the observed line widths.

In all measurements the amplitude of the radiofrequency field was chosen to give a saturation broadening of at most 1% (*cf.* Pake[14]). The validity of Pake's equation was checked experimentally. Calibration of the sweep was performed with the conventional side-band technique. In all measurements the temperature was 29 ± 2°. The line widths given below have been corrected for inhomogeneity broadening, for saturation broadening, and, when appropriate, for modulation broadening.[15] To guarantee the absence of line broadening due to I_2 in the iodide solutions (*cf.* ref 16), the ^{127}I line widths were measured before and after adding a couple of $Na_2S_2O_3$ crystals to the solution. This had no detectable influence on the line widths. All line widths reported are the means of three to six measurements. The error in the reported line widths is normally about 5%.

Materials. The chemicals used were of Purum or Purissimum grade. The following abbreviations are used: Me = methyl; Et = ethyl; Pr = propyl; Bu = butyl; and Ph = phenyl. Et_4NCl, Me_4NCl, Bu_4NI, Pr_4NI, Et_4NI, and Me_4NI were obtained from Fluka AG, and Bu_4NCl and Pr_4NCl from Eastman Organic Chemicals. These salts were used without further purification. Bu_4PBr was synthetized by treating tributylphosphine with butyl bromide,[17] Me_3SBr by treating Me_3S with MeI[18] and then converting the Me_3SI thus obtained to Me_3SBr by means of an ion-exchange process, and Et_3SBr by treating Et_2S with EtBr.[18] The pyridinium and lutidinium salts and $(C_2H_4OH)_3NHBr$ were prepared by treating the organic base with an equivalent amount of aqueous hydrobromic acid. After evaporation the product was purified by recrystallization twice in an ethanol–diethyl ether mixture. The $(C_2H_4OH)_4NCl$ and Ph_4PCl were generously placed at our disposal by Dr. M. Zeppezauer, Uppsala, the *p*-diaminobenzene hydrochloride by Dr. U. Kölle, Lund, and the $(CH_2)_4N^+$-$(CH_2)_4Br^-$ by Docent B. Lüning, Stockholm.

Experimental Results

Nuclear magnetic resonance line widths of ^{35}Cl in 0.100 and 0.50 *M* aqueous solutions of four tetraalkylammonium chlorides are presented in Figure 1. The corresponding data for ^{127}I in aqueous tetraalkylammonium iodide solutions are given in Figure 2. (The solubility of Me_4NI, Pr_4NI, and Bu_4NI is less than 0.5 *M*.) In addition, measurements of ^{35}Cl and ^{127}I line widths were performed in aqueous solutions of Et_4NCl and Et_4NI in various proportions. As may be inferred from Table I, the replacement of one anion by the other does not influence the line widths in these solutions markedly.

Table I: Nmr Line Widths of ^{35}Cl and ^{127}I in Aqueous Solutions of Tetraethylammonium Chloride and Tetraethylammonium Iodide (Special Care Was Taken to Make All Runs at the Same Temperature)

Concn of Et_4NCl, *M*	Concn of Et_4NI, *M*	Line width of ^{35}Cl, μT	Line width of ^{127}I, mT
0.5	0	14.1	
0.4	0.1	13.2	0.73
0.1	0.4	13.8	0.75
0	0.5		0.77

In Table II the ^{79}Br line widths for aqueous solutions of some alkyl-substituted sulfonium and phosphonium bromides are given. For comparison, data for the corresponding ammonium salts are included.

To investigate the effect of varying the organic group in the cation, we measured the ^{79}Br and ^{35}Cl resonance line widths in 0.5 *M* aqueous solutions of several substituted phosphonium and ammonium halides. The results are given in Table III where the line widths for alkyl-substituted ammonium salts are also included for comparison when appropriate. We have investigated cations with polar groups, aromatic groups, and aliphatic rings and doubly charged cations.

(13) H. Csopak, B. Lindman, and H. Lilja, *FEBS (Fed. Eur. Biochem. Soc.)*, **9**, 189 (1970).

(14) G. E. Pake, *Amer. J. Phys.*, **18**, 437 (1950).

(15) G. W. Smith, *J. Appl. Phys.*, **35**, 1217 (1964).

(16) O. E. Myers, *J. Chem. Phys.*, **28**, 1027 (1958).

(17) A. J. Speziale and L. R. Smith, *J. Amer. Chem. Soc.*, **84**, 1868 (1962).

(18) D. F. Evans and T. L. Broadwater, *J. Phys. Chem.*, **72**, 1037 (1968).

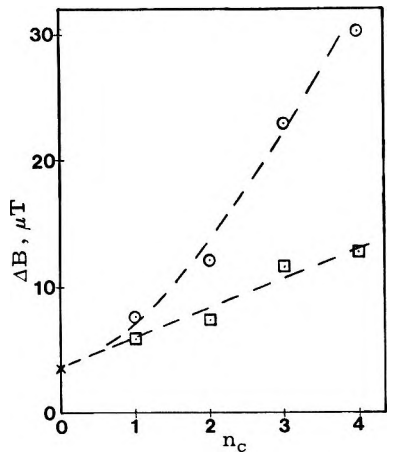

Figure 1. The nmr line width, ΔB, for ^{35}Cl in aqueous solutions of R_4NCl: ⊙, 0.50 M solutions; ⊡, 0.100 M solutions. The lines in this and the following figures are drawn as an aid to the eye. In Figures 1 and 2 × represents a 0.5 M NH_4Cl and a 0.5 M NH_4I solution, respectively. In Figures 1, 2, 4, and 5 n_c stands for the number of carbon atoms in the alkyl chain.

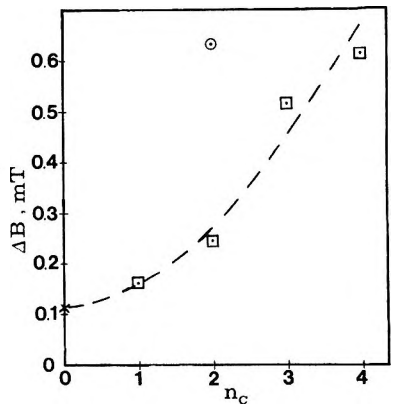

Figure 2. The nmr line width for ^{127}I in aqueous solutions of R_4NI: ⊙, 0.50 M solution; ⊡, 0.100 M solutions.

The importance of the cationic charge on the ^{79}Br line width was investigated. Data for an aqueous solution of Et_3N + NaBr were compared with those for solutions of Et_3NHBr and Et_3SBr. (See Table IV.) In a mixture of Et_4NBr (0.5 M)–NaOH (0.5 M), the ^{79}Br line width showed no dependence on pH or ionic strength.

The concentrations dependence of the ^{81}Br nmr line width for aqueous solutions of tetrabutylammonium bromide was investigated over an extended concentration range. (See Figure 3.) The very broad signals obtained for some of these solutions makes it advantageous to study the ^{81}Br instead of the ^{79}Br nmr signal. For comparison the ^{81}Br line width for some solutions in deuterium oxide was also measured. The ratio between the line widths in D_2O and H_2O is give in Table V.

Table II: The ^{79}Br Magnetic Resonance Line Width of Analogous Phosphonium, Sulfonium, and Ammonium Salts (Special Care Was Taken to Make All Runs at the Same Temperature; Solutions are 0.50 M)

Salt	Line width, μT
NaBr	37
Me_3SBr	82
Me_3NHBr	60
Et_3SBr	133
Et_3NHBr	112
Bu_4PBr	498
Bu_4NBr	483

Table III: ^{35}Cl and ^{79}Br Nmr Line Widths in 0.50 M Solutions of Salts Containing Various Organic Cations

Salt	Nucleus studied	Line width, μT
NaCl	^{35}Cl	3.6
$(C_2H_4OH)_4NCl$	^{35}Cl	9.0
Et_4NCl	^{35}Cl	12.0
Ph_4PCl	^{35}Cl	34
p-Diaminobenzene dihydrochloride	^{35}Cl	8.0
NaBr	^{79}Br	37
Pyridinium bromide	^{79}Br	88
Lutidinium bromide	^{79}Br	119
$(CH_2)_4N^+(CH_2)_4Br^-$	^{79}Br	159
$(C_2H_4OH)_3NHBr$	^{79}Br	96
Et_3NHBr	^{79}Br	112

Table IV: Investigation of the Influence of the Charge on the ^{79}Br Nmr Line Width (All Solute Concentrations Are 0.5 M)

Salt	Line width, μT
NaBr	37
Et_3N + NaBr	88
Et_3NHBr	118
Et_3SBr	133

Table V: The Ratio $\Delta B(D_2O)/\Delta B(H_2O)$ between the ^{79}Br Nmr Line Widths in Solutions of Tetrabutylammonium Bromide (TBAB), in D_2O and H_2O at Different Concentrations

Concn of TBAB, mol/l.	$\Delta B(D_2O)/\Delta B(H_2O)$
0.10	1.17
0.50	1.20
1.00	1.16
2.00	1.27
0.50[a]	1.16

[a] 0.5 M NaBr solution.

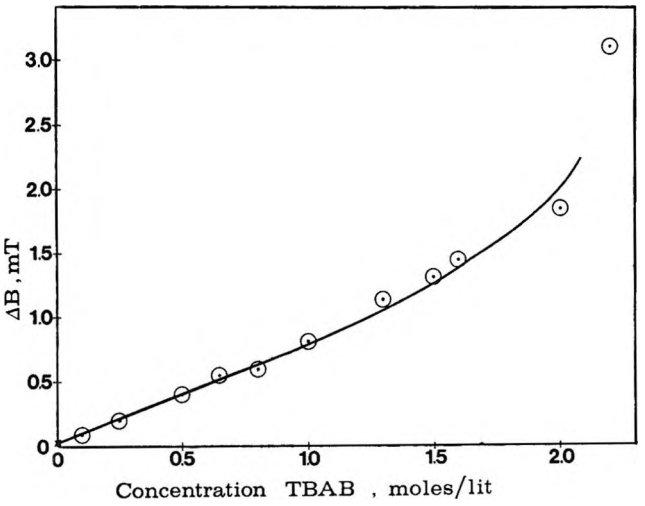

Figure 3. The ^{79}Br nmr line width for aqueous solutions of Bu_4NBr as a function of the salt concentration in moles per liter.

Discussion

1. General Considerations. The process which is mainly resonsible for the nuclear magnetic relaxation of ^{35}Cl, ^{79}Br, ^{81}Br, and ^{127}I is the interaction between the nuclear electric quadrupole and the electrical field gradients at the nucleus. It was shown in ref 11 and 12 that for alkylammonium bromide solutions the mean lifetimes of the bromide ions in different binding sites are much shorter than the relaxation times T_1 and T_2 ("fast exchange"). It was also shown that $\omega_0\tau_c \ll 1$ ("extreme narrowing"). Here ω_0 is the Larmor precession frequency and τ_c is the correlation time characterizing the molecular motion. It can certainly be assumed that these findings are also applicable in the present work. The observed line with ΔB_{obsd} may then be written

$$\Delta B_{obsd} = \sum_i p_i \Delta B_i \qquad (1)$$

where i stands for different binding sites of the anion, p_i is the fraction of the anions situated in site i, ΔB_i is the line width characterizing site i and is given by, neglecting the asymmetry parameter

$$\Delta B_i = K_1 \frac{1}{(T_2)_i} = K_1 \frac{1}{(T_1)_i} = K_2 \left(\frac{\partial^2 V}{\partial z^2}\right)_i^2 (\tau_c)_i \qquad (2)$$

where $(T_1)_i$ and $(T_2)_i$ are the longitudinal and transverse relaxation times, respectively, and K_1 and K_2 are constants. $(\partial^2 V/(\partial z^2)$ is the largest of the components of the electric field gradient tensor, taken in its principal axes system, at the nucleus. For complexes which are not extremely short-lived, the correlation time equals the rotational correlation time which characterizes the time change of the direction of the field gradients in the complex (*cf.* Marshall[19]). A large number of investigations,[4,20,21] mainly on tetraalkylammonium salts by various physical methods, have shown that the hydrophobic part of the cation is surrounded by structure-stabilized water. In ref 11 and 12 the remarkably low relaxation times, in comparison with alkali halide solutions, for ^{79}Br in aqueous solutions of alkylammonium bromides were interpreted as the result of an interaction between anion and structure-modified water. Other possibilities for explaining the observed relaxation rates, such as direct cation–anion interaction, were excluded by comparing the line widths obtained in different solvents and by investigating the dependence of the line widths on the number and length of the alkyl groups in the cation. The exact nature of the anion–solvent interaction is difficult to establish, but the present investigation casts some new light on this problem.

Since the anion nuclear magnetic relaxation in these solutions is due to anion–water interactions, the correlation time, τ_c, relevant for the halide ions should be intimately connected with the motion of the water molecules. From the fact that the changes in the water correlation times[22] are much smaller than the changes in halide ion nmr line widths we may conclude that the field gradients, $\partial^2 V/\partial z^2$, in the present case must be considerably greater than those in aqueous alkali halide solutions. There are two ways of explaining the high values of $\partial^2 V/\partial z^2$. Firstly, the large field gradients can arise from an enchanced anion–water binding as compared to aqueous alkali halide solutions. Secondly, the increased field gradients can be due to a lowered symmetry in the anion hydration near the cations. The latter effect will be important if the electronic distribution of the halide ion is strongly affected by hydration. In the case of symmetric hydration the net field gradient at the halogen nucleus will be small, whereas an unsymmetric hydration, due to for example the replacement of one water molecule in the hydration sphere for a solute, may give rise to large field gradients at the nucleus. From the known crystal structures of tetraalkylammonium halide hydrates[9] it is clear that the location of a halide ion in the first hydration sphere of the large cation gives an unsymmetrical anion water interaction. A combination of the two factors influencing the field gradient mentioned above is also possible. Even if it is not possible to give an exact explanation of the effects observed in the present work, the line-broadening effect can be correlated with the amount of structure-stabilized water near the cation in a semiquantitative way. In the Discussion we will use the simplest model possible, namely, that in which the halide ion has two possible sites, one as in an ordinary aqueous solution, here called X_{free}^- (X = Cl,

(19) A. G. Marshall, *J. Chem. Phys.*, **52**, 2527 (1970).

(20) H. S. Frank and W.-Y. Wen, *Discuss. Faraday Soc.*, **23**, 133 (1957).

(21) R. Pottel and O. Lossen, *Ber. Bunsenges. Phys. Chem.*, **71**, 135 (1967).

(22) H. G. Hertz, *Progr. Nucl. Magn. Resonance Spectrosc.*, **3**, 218 (1967).

Br, I), and one where it is in the vicinity of the cation, here called X_{cat}^-. This reduces eq 1 to

$$\Delta B_{obsd} = p_{free}\Delta B_{free} + p_{cat}\Delta B_{cat} \quad (3)$$

One factor influencing p_{cat} is the electrostatic attraction between the anion and cation (*cf.* below).

2. Comparison between Different Anions. As seen in Figures 1 and 2 very large widths are observed in solutions of tetraalkylammonium chlorides and iodides. This is an effect exactly parallel to the one reported in ref 11 for the corresponding bromides. The representation of the quotient $\Delta B_{obsd}/\Delta B_{free}$ for chlorides, bromides, and iodides seen in Figures 4 and 5 shows that the relative line-broadening effect is of the same order of magnitude for the different anions. This taken together with the dependence of the relaxation on cation size and solute concentration shows that the effect observed has the same origin for the three halogen nuclei studied. This observation also lends further support to the idea that direct cation–anion interaction is relatively insignfiicant. Thus it is to be expected that a direct anion–cation interaction should depend in the opposite way, than is observed, on the size of the anion. A cancellation of opposing effects in p_{cat} and in $\partial^2 V/\partial z^2$ could give the observed result but is less probable.

The data given in Table I show that the anions bind independently of each other, *i.e.*, no competitive effect has been observed. If contact ion pairing is important, the association constants are expected to depend on the size of the anion, and thus the anions should bind competitively.

3. The Role of the Charged Central Atom in the Cation. According to the data given in Table II there is no significant difference in ^{79}Br nmr line width between aqueous solutions of Bu_4NBr and Bu_4PBr; *i.e.*, the line width is independent of whether the central atom is nitrogen or phosphorus. This fact is in accordance with our exclusion of a direct cation–anion interaction as the cause of line broadening, since the interaction of the halide ion with the charged central atom in the cation is expected to depend on the size of the central atom. However, it is interesting to note that the sulfonium salts give larger line widths than the corresponding ammonium salts. This is explained by the smaller screening of the charge on sulfur, which leads to a somewhat higher p_{cat} (*cf.* eq 3) due to the electrostatic attraction between anion and cation. It should perhaps be pointed out here that, in the systems investigated, one has to distinguish between the effect of the cation on the distribution of the anions between different parts of the solution and the cation–anion interaction in a contact ion pair. That the electrostatic attraction is of importance for p_{cat} is shown by a comparison of the ^{79}Br line widths in solutions of Et_3N + NaBr, Et_3NHBr, and Et_3SBr (Table IV). It can be inferred from these data that the line width increases in going from a neutral solute to a solute with "screened" and

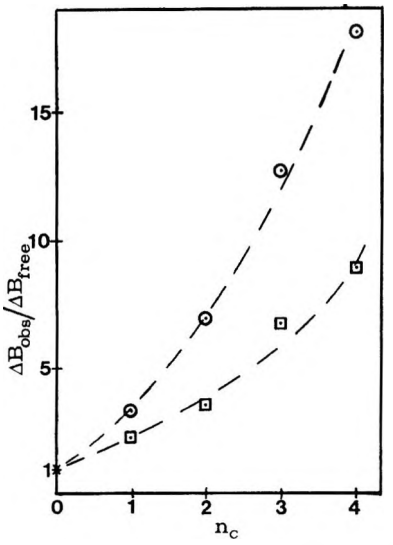

Figure 4. The quotient $\Delta B_{obsd}/\Delta B_{free}$ for ^{35}Cl and ^{79}Br in 0.50 *M* solutions of R_4NX (X = Cl, Br): ⊡, ^{35}Cl; ⊙, ^{79}Br. Data for ^{79}Br in this and the next figure are taken from ref 11. ΔB_{free} is taken as the line width for an alkali halide solution of corresponding concentration. The halogen nmr line widths for alkali halide solutions are essentially independent of concentration in this range.

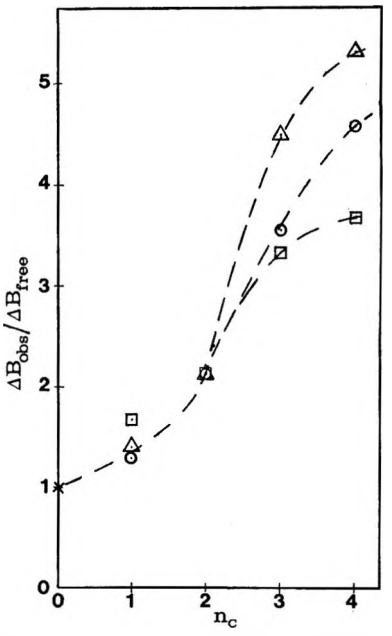

Figure 5. The quotient $\Delta B_{obsd}/\Delta B_{free}$ for 0.100 *M* solutions of R_4NX (X = Cl, Br, I): ⊡, ^{35}Cl; ⊙, ^{79}Br; △, ^{127}I.

less "screened" charge. In solutions containing negative organic ions the anion nuclear magnetic relaxation rates are much smaller.[23,24]

4. The Effect on the Line Widths of the Organic Groups in the Cation. We have investigated the ^{35}Cl and ^{79}Br nmr line widths in aqueous solutions of salts with different organic groups in the cation (Table III).

(23) B. Lindman and I. Danielsson, *J. Colloid Interface Sci.*, in press.
(24) B. Lindman and P. Kinell, unpublished measurements.

It is found that the line widths are roughly proportional to the number of carbon atoms per unit volume. As can be seen in Table I, the line widths are determined by the cation concentration and not by that of the partner anion.

The line widths in solutions containing ethanolammonium salts are much smaller than in the corresponding solutions of propylammonium salts and significantly smaller than in solutions of ethylammonium salts. In earlier work[7,25] the tetraethanolammonium salts have been compared with tetrapropylammonium salts on the basis of approximately equal size. In the discussions of structure stabilization effects we find it more to the point to compare them with the tetraethylammonium salts on the basis of the number of carbon atoms. The smaller line widths for the ethanolammonium salts have an apparent explanation in the tendency of the hydroxyl groups to form hydrogen bonds to water (*cf.* ref 20). This hydrogen bonding will tend to perturb the water structure normally formed in the vicinity of alkyl groups. In contrast to Wen and Nara[7] and Evans, *et al.*,[25] we find the ethanolammonium salts structure making. The discrepancy is most probably due to the fact that different methods are more or less sensitive to the two competing effects, structure stabilizing and structure breaking. Conway, *et al.*,[26] have reported that pyridinium bromide and lutidinium bromide have a structure-making effect on the water lattice and this is confirmed in the present work.

The ratio between the ^{81}Br nmr line widths in deuterium oxide and ordinary water solutions of Bu_4NBr is expected to be about 1.23 if the correlation time is determined by the motion of the water molecules (*cf.* ref 27). This is indeed found to be the case even at very high concentrations of Bu_4NBr (see Table V). This observation seems to rule out the explanation that the anion relaxation at these high concentrations is due to the motions of some large aggregates. Instead these findings indicate that the bromide ions are coupled to water even at high concentrations.

Comparison with Results Obtained by Other Methods. Some ions in aqueous solution are characterized as structure makers by some authors and as structure breakers by others. This is due to the different criteria for defining structure stabilization (see, *e.g.*, ref 28). The criterion for structure making by Hertz[10] as a slowing down of the solvent molecular motion seems reasonable. The influence of such a slowing down on different macroscopic quantities is difficult to determine unambiguously, but reasonable interpretations can of course be given. In the present work we are using the indirect method of measuring the line width of halogen nuclei to trace the structure-stabilized water. In this way the presence of stabilized water is given full weight and competing effects are disregarded. (As may be inferred from data on halogen nuclear magnetic relaxation in aqueous alkali halide solutions,[29] structure breaking has a very small effect on the relaxation rates.) This explains why we find Me_4N^+ and $(C_2H_4OH)_4N^+$ to be structure making while other authors regard them as structure breaking.[7,25,28] In accordance with our findings, however, is the fact that both the rotational[21,22] and the translational[30] motion of the water molecules in solutions containing Me_4N^+ has been found to occur at a lower rate than in pure water.

The species giving rise to the large line widths in the present work seem to conform closely to the concept of "structure-enforced ion pairs" proposed by Diamond.[31] It is clear from the evidence provided above that among the forces giving rise to such an ion pair, the ion–ion electrostatic interaction is of secondary importance, and consequently there is no direct contact between the charges of the anion and cation. The neglect of giving a detailed molecular picture of such an ion pair has given rise to some confusion in the past. Thus for example the arguments against ion pairing advocated by Evans and Broadwater[18] are not relevant for this structure-enforced type. One possible interpretation of the equilibrium constants found by Wirth,[8] Levien,[32] and Fernandez-Prini[33] is in terms of a structure-enforced ion pair. At present we have found it impossible to correlate their data with ours in a quantitative way. It should be noted that p_{cat} in eq 3 might be very small (*cf.* ref 12) and consequently difficult to detect by other methods.

Recently Larsen[34] has presented ^{14}N nuclear magnetic relaxation data which support our view that contact ion pairing is not important in aqueous solutions of tetraalkylammonium halides. Earlier Larsen[35] demonstrated that in aqueous solutions of tetraalkylammonium salts of some negative paramagnetic ions, solvent-separated ion pairs occur. No indication of contact ion pairing was found in these studies.

At high concentrations it has been proposed that symmetrical tetraalkylammonium salts form micelles.[6,8,36] We do not observe the characteristic abrupt increase in counterion nmr line width,[12,37,38] at the

(25) D. F. Evans, G. P. Cunningham, and R. L. Kay, *J. Phys. Chem.*, **70**, 2974 (1966).

(26) B. E. Conway and L. H. Laliberté in "Hydrogen-Bonded Solvent Systems," A. K. Covington and P. Jones, Ed., Taylor and Francis, London, 1968, p 139.

(27) M. Eisenstadt and H. Friedman, *J. Chem. Phys.*, **44**, 1407 (1966).

(28) R. L. Kay, *Advan. Chem. Ser.*, **No. 73**, 1 (1968).

(29) H. G. Hertz, G. Stalidis, and H. Versmold, *J. Chim. Phys., Physiochim. Biol.*, 177 (1969) (Numéro special, Oct 1969).

(30) H. G. Hertz, B. Lindman, and V. Siepe, *Ber. Bunsenges. Phys. Chem.*, **73**, 542 (1969).

(31) R. M. Diamond, *J. Phys. Chem.*, **67**, 2513 (1963).

(32) B. J. Levien, *Aust. J. Chem.*, **18**, 1161 (1965).

(33) R. Fernandez-Prini, *Trans. Faraday Soc.*, **64**, 2146 (1968).

(34) D. W. Larsen, *J. Phys. Chem.*, **74**, 3380 (1970).

(35) D. W. Larsen, *J. Amer. Chem. Soc.*, **91**, 2920 (1969).

(36) H. E. Wirth and A. LoSurdo, *J. Phys. Chem.*, **72**, 751 (1968).

critical micelle concentrations proposed by Wirth. The widely accepted picture of micelles (as well as the characteristic amphiphilic nature of compounds known to form micelles) indicates that micelles are highly improbable for symmetrical tetraalkylammonium salts on steric grounds. The evidence given in ref 6, 8, and 36 is not convincing. It is interesting to note, for example, that at the concentration where Wirth reported micelle formation (1 *m*) there is about the same number of water molecules per cation as the number of water molecules surrounding each cation in the crystalline hydrate.[9] The effect observed could thus probably be explained in terms of the changes in cation hydration which should apparently occur in this concentration range. For long-chain surfactants the solubilization of organic compounds is an established procedure for studying micelle formation. In the present case, however, in which the number of methyl and methylene groups is of the same order of magnitude as the number of water molecules at the reported critical micelle concentration, it seems to be doubtful whether the method is applicable. At sufficiently high concentrations of tetraalkylammonium salts cation–cation interaction will of course occur. However, it seems preferable to reserve the concept micelle formation for cases where cation–cation interaction occurs as a consequence of true aggregation and not to use it where the cation–cation association takes place largely for geometrical reasons.

From the present investigation no definite conclusion can be drawn regarding the nature of the anion–water coupling. It is interesting to note, however, that the cation ($^{23}Na^+$ and $^{85}Rb^+$) nuclear quadrupole relaxation[24,39] in aqueous solutions is only slightly altered by the presence of organic anions, such as alkanoate ions and alkyl-substituted BH_4^- ions. The difference between alkali cations and halogen anions in this respect may be due either to a specific anion–water interaction which is not operating in the case of cations or to the hydration of cations which may make an incorporation of these ions in the structure-modified water lattice less extensive. Another possibility to clarify the situation is to study ^{19}F magnetic relaxation. Since this nucleus does not possess a quadrupole moment, an estimate of the correlation time should be possible from such studies. Work along these lines is presently in progress in our laboratories.

Acknowledgments. Mrs. K. Sjölin is heartily thanked for synthetizing Me_3SBr and Et_3SBr and Mr. H. Lilja for running the spectra on the HA-100 spectrometer. We are indebted to Dr. Robert Carter for revising the English of the manuscript.

(37) J. C. Eriksson, Å. Johansson, and L.-O. Andersson, *Acta Chem. Scand.*, **20**, 2301 (1966).

(38) G. Lindblom and B. Lindman, manuscript in preparation.

(39) I. Danielsson, B. Lindman, and L. Ödberg, *Suom. Kemistilehti B*, **43**, 209 (1970).

Far-Infrared Absorption of Some Organic Liquids

by S. R. Jain and S. Walker*

Department of Chemistry, Lakehead University, Ontario, Canada *(Received November 19, 1970)*

Publication costs assisted by Lakehead University

Far-infrared absorption spectra of a number of simple polar and nonpolar organic liquids have been recorded in the region 5–70 cm^{-1} mainly by a Fourier transform spectrometer, and the maximum value of the absorption coefficient (α_{max}) has been determined. The α_{max} of the band obtained for each of the polar liquids has been found to be directly proportional to the square of the electric dipole moment and inversely to the mean moment of inertia of the molecule. The α_{max} of polar liquids shifts appreciably to higher frequency with decrease in temperature, whereas for the four nonpolar liquids examined over a similar temperature range, if there is any shift, then it is of the order of the experimental error.

Introduction

Far-infrared absorption of liquids in the frequency range 5–150 cm^{-1} has been a subject of increasing interest during the last few years. The absorption spectra of a number of organic liquids, polar as well as nonpolar, have been reported.[1–8] Polar liquids absorb more strongly than nonpolar. These absorption bands cannot normally be accounted for by intramolecular

(1) G. W. Chantry, H. A. Gebbie, B. Lassier, and G. Wyllie, *Nature*, **214**, 163 (1967).

(2) (a) M. Davies, G. W. F. Pardoe, J. E. Chamberlain, and H. E. Gebbie, *Trans. Faraday Soc.*, **64**, 847 (1968); (b) *Chem. Phys. Lett.*, **2**, 411 (1968); (c) *Trans. Faraday Soc.*, **66**, 273 (1970).

vibrations of the molecule but rather arise from the molecular environmental conditions. Absorption in this frequency range by polar liquids was first considered by Poley,[9] and his concept was examined quantitatively by Hill,[10] who considered this phenomenon as a librational motion of a polar molecule in a cage of neighboring molecules about temporary equilibrium positions. Though Hill's expression predicts the region of the absorption maxima in the frequency range below 150 cm^{-1}, the observed frequency maxima do not agree with those predicted by a simplified form of the expression,[2a] while the unabbreviated equation is difficult to test by experimental data. Attempts have been made to account for such bands by using the full Debye equation which includes the moment of inertia term.[2a] However, the far-infrared bands are of greater intensity than that predicted by such a treatment. Moreover, Leroy, *et al.*,[11] have indicated that such relaxation theories are inadequate for wavelengths smaller than a few millimeters.

In the gaseous state at normal pressures, the far-infrared absorption arises from rotation of the molecules, and in the solid state the absorption is usually ascribed to lattice vibrations. In the liquid state they have met various interpretations, including librational motion of the polar molecule in a cage[10] and rotational–translational motions[7] of the polar molecules. Further, since the absorption maxima, both in the liquid and the solid state, have been found to occur in the same spectral region, these absorptions have also been termed "liquid lattice" vibrations.[1] An additional type of absorption has been observed for aliphatic nitriles and dimethyl sulfoxide in this region and has been related to dimer formation in solution.[12,13]

The absorption in nonpolar liquids has been attributed to the presence of induced dipole moments of the molecules which do not cancel because of lack of long-range order, and this concept is borne out by the large variation in the spectral intensity with pressure for liquid carbon disulfide.[14] Recently Garg, *et al.*,[3] have accounted for the intensities of the absorption bands in nonpolar liquids on the basis of multipole-induced dipole absorption, and Davies, *et al.*,[2c] have also recently considered this problem.

The present investigation aimed to study a fairly wide variety of organic liquids with a view to determining any general features as to the nature of the absorption, since surprisingly few data are available for polar liquids. The liquids chosen were of simple rigid structure type. Hydrogen-bonded liquids such as alcohols, amines, phenols, etc., were avoided as several mechanisms could be involved in their absorption of far-infrared radiation.

Experimental Section

The spectra were recorded mainly from an RIIC LR-100 lamellar grating Fourier spectrometer in conjunction with an analog to digital converter. This instrument operates over the spectral region 5–70 cm^{-1}, although the results between 5 and 20 cm^{-1} can sometimes be unreliable. The operation of the instrument involves evacuation of the system to about 50 μ as water vapor absorbs strongly in this region. At a later stage in this work a Grubb–Parsons cube interferometer became available, and this was employed to check about half the spectra. A background or reference spectrum was punched on a tape for a definite optical path difference (± 5 mm), by using an empty cell with either high density polyethylene windows or Teflon spacers and evacuating the system, and the sample was then examined under similar conditions. A number of the spectra were checked using quartz windows. The spectra were usually run to provide a resolution of 2 cm^{-1} and the spectra, other than at room temperature ($\sim$22°), were recorded using an RIIC variable temperature cell unit, VLT-2, with automatic temperature controller, TEM-1.

The ratio computed from the intensities of the background and sample spectra was calculated and plotted against the frequency in reciprocal centimeters by the computer IBM 360-40. The absorption coefficient, α, is defined as

$$\alpha = \frac{1}{l} \ln \frac{I_0}{I_s} \qquad (1)$$

where l is the path length in centimeters, taken to be equal to the mean width of the spacer, and I_0 and I_s are the transmitted intensities of the background and the sample, respectively. A few spectra run at various path lengths yielded similar results. Our α_{max} results were in good agreement with literature data (see footnote in Table I) while the wave number (ν_{max}) corresponding to α_{max} was probably accurate to better than ± 5 cm^{-1}, although the accuracy of ν_{max} can diminish when there is a very broad maximum.

The compounds used in this investigation were com-

(3) S. K. Garg, J. E. Bertie, H. Kilp, and C. P. Smyth, *J. Chem. Phys.*, **49**, 2551 (1968).

(4) H. S. Gabelnick and H. L. Strauss, *ibid.*, **46**, 396 (1967).

(5) A. Hadni, *J. Phys.* (*Paris*), **28**, 978 (1967).

(6) Y. Leroy and E. Constant, *C. R. Acad. Sci., Ser. B*, **262**, 1391 (1966).

(7) S. G. Kroon and J. Van Der Elsken, *Chem. Phys. Lett.*, **1**, 285 (1967).

(8) J. W. Brasch, Y. Mikawa, and R. J. Jakobsen, *Appl. Spectrosc. Rev.*, **1**, 187 (1968).

(9) J. Ph. Poley, *J. Appl. Sci.*, **4B**, 337 (1955).

(10) N. E. Hill, *Proc. Phys. Soc.*, **82**, 723 (1963).

(11) Y. Leroy, E. Constant, C. Abbar, and P. Desplanques, *Advan. Mol. Relaxation Processes*, **1**, 273 (1967–1968).

(12) R. J. Jakobsen and J. W. Brasch, *J. Amer. Chem. Soc.*, **86**, 3571 (1964).

(13) B. J. Bulkin, *Helv. Chim. Acta*, **52**, 1348 (1969).

(14) C. C. Bradley, H. A. Gebbie, A. C. Gilby, V. V. Kechin, and J. H. King, *Nature*, **211**, 839 (1966).

mercially available, and the reagent grade liquids were suitably dried before use.

The principal moments of inertia I_x, I_y, I_z of the molecules were calculated, and the internuclear distances were taken from Sutton's[15] tables. In the substituted benzene compounds the resultant dipole moment of the molecule lies along the z axis, and, as the torques about this axis do not affect the dipole moment, then only the remaining two moments of inertia were used in averaging for I (Table I). Where available the calculated mean moments of inertia agreed well with those reported in the literature. The moments of inertia of symmetric top molecules were derived from the B_0 values obtained from microwave spectra.[16]

Table I: Molecular Parameters and Spectral Data at ~22°

Liquid	Dipole moment μ, D	Average moment of inertia, $I \times 10^{40}$, g cm²	Peak absorption, α_{max}, neper cm⁻¹	Absorption maximum, ν_{max}, cm⁻¹
C_6H_5F	1.40	404	25	32
C_6H_5Cl	1.58	616	16	44
C_6H_5Br	1.56	931	13	37
C_6H_5I	1.39	1155	14	39
$C_6H_5NO_2$	3.97	785	79	43
C_6H_5CN	3.97	619	94	53
$C_6H_5CH_3$	0.36	404	6	80
o-FC_6H_4F[a]	2.40	510	48	34[a]
o-ClC_6H_4Cl[a]	2.27	805	18	45[a]
o-BrC_6H_4Br[a]	1.90	1286	14	42[a]
o-IC_6H_4I	1.70	1851	10	38
m-FC_6H_4F[a]	1.58	516	19	53[a]
m-ClC_6H_4Cl[a]	1.49	798	14	58[a]
m-BrC_6H_4Br[a]	1.47	1529	9	~60[a]
p-FC_6H_4F	0	675	4	62
p-ClC_6H_4Cl[b]	0	1427	4	65
p-$FC_6H_4NO_2$	2.65	1194	21	37
CH_3I	1.67	112[c]	100	60
$CHCl_3$	1.11	254[c]	16	~35
$CHBr_3$[c]	1.0	660[c]	10	~35
CH_3CCl_3	1.66	345	32	26
$(CH_3)_3CCl$	2.14	279[c]	68	23
$(CH_3)_3CBr$	2.23	412[c]	51	19
1-$C_{10}H_7F$	1.42	...	10	63
1-$C_{10}H_7Cl$	1.60	...	7	>60
1-$C_{10}H_7Br$	1.59	...	7	40
1-$C_{10}H_7I$	1.44	...	6	31

[a] Mansingh[17] also reported the α_{max} values for these six liquids and obtained the following values for o-difluorobenzene, m-difluorobenzene, o-dichlorobenzene, m-dichlorobenzene, o-dibromobenzene, and m-dibromobenzene of 44, 22, 22, 14, 15, and 9 nepers cm⁻¹, respectively. Thus, the agreement is, on the whole, reasonable. [b] The spectrum of p-dichlorobenzene was recorded at 70° in the liquid state as given in Figure 2. [c] Moment of inertia values derived from B_0 values.[16]

Discussion

Some of the typical far-infrared absorption spectra of both polar and nonpolar liquids are presented in Figures 1–3. Though the absorption maxima of some

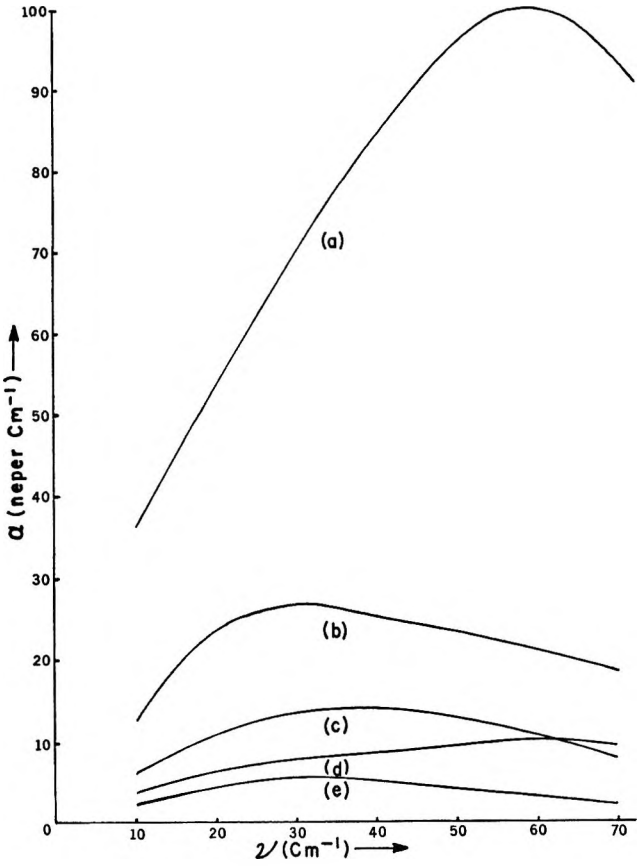

Figure 1. Far-infrared spectra of some polar liquids at room temperature (~22°): (a) methyl iodide, (b) fluorobenzene, (c) iodobenzene, (d) 1-fluoronaphthalene, and (e) 1-iodonaphthalene.

of the liquids lie above the frequency range covered by the lamellar grating instrument, range 5–70 cm⁻¹, both polar and nonpolar liquids exhibit a broad absorption band. In general, our studies confirm that the intensities of the absorption bands of polar liquids are considerably higher than those of nonpolar, indicating dependence of the absorption intensity on the polarity of the molecule. The dependence of the absorption intensity on the dipole moment of the molecule is qualitatively demonstrated by examining the absorption bands of ortho, meta, and para derivatives of dihalobenzenes. The dipole moments of these derivatives decrease in the order ortho > meta > para, and it can be seen in Table I that in all the cases examined an ortho-substituted derivative exhibits a higher absorption coefficient, α_{max}, than the corresponding meta derivative which in turn has a higher α_{max} than that of a para-substituted derivative. This was observed previously by Mansingh.[17] A typical example of the ab-

(15) L. E. Sutton, "Tables of Interatomic Distances," Special Publication No. 11, The Chemical Society, London, 1958.

(16) (a) E. W. Jones and H. W. Thompson, *Proc. Roy. Soc., Ser. A*, **228**, 50 (1965); (b) W. V. Smith and R. R. Undesberger, *J. Chem. Phys.*, **17**, 1348 (1949); (c) M. Mizushima and I. Ito, *ibid.*, **20**, 804 (1952); (d) J. Q. Williams and W. Gordy, *ibid.*, **18**, 994 (1950).

(17) A. Mansingh, *ibid.*, **52**, 5896 (1970).

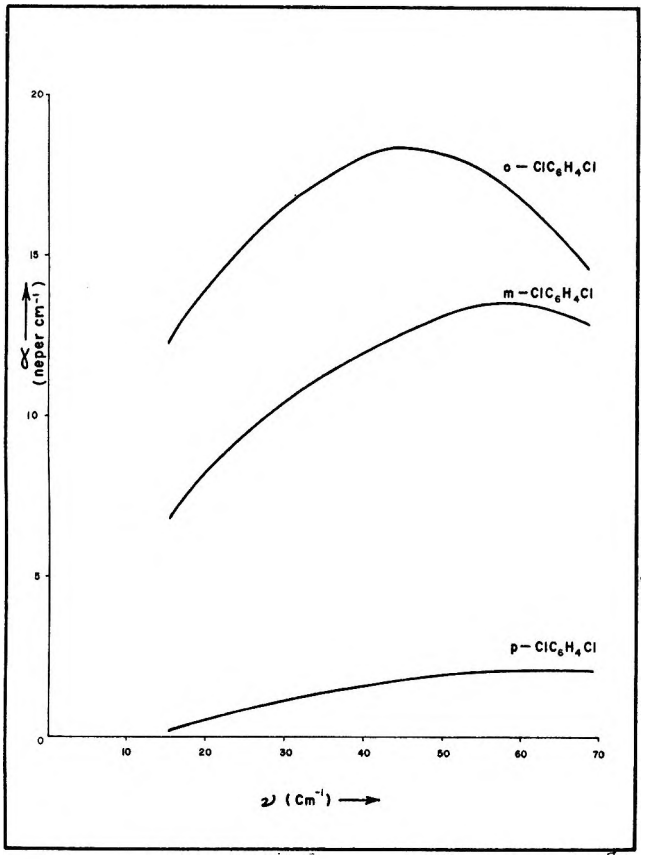

Figure 2. Far-infrared spectra of *o*- and *m*-dichlorobenzene at room temperature. The spectrum of *p*-dichlorobenzene was obtained at 70° in the liquid state.

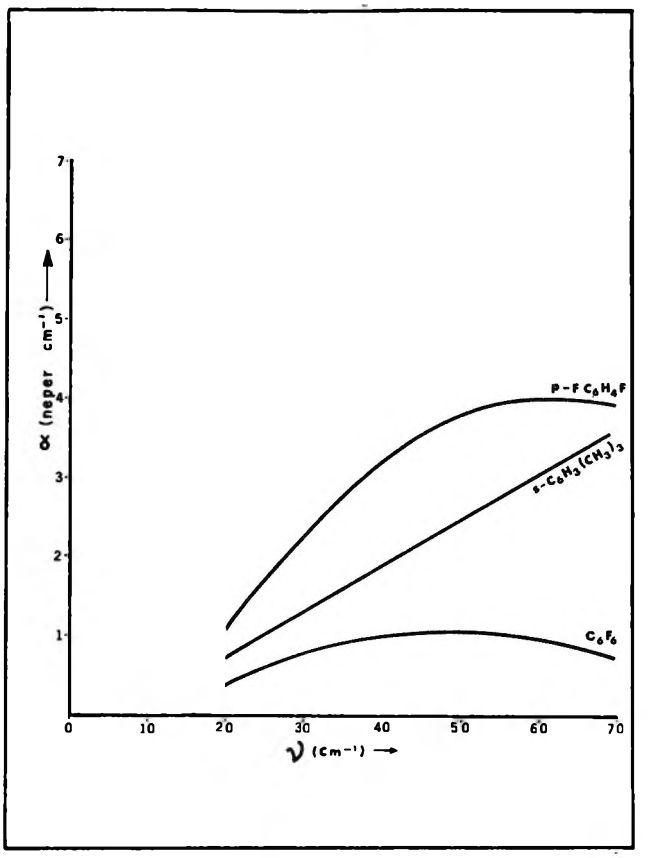

Figure 3. Far-infrared spectra of *p*-difluorobenzene, 1,3,5-trimethylbenzene, and hexafluorobenzene at room temperature.

sorption bands of dichlorobenzenes is given in Figure 2 which shows *o*-, *m*-, and *p*-dichlorobenzene having dipole moments 2.47, 1.49, and 0 D, respectively, exhibiting absorption bands with α_{max} 18, 14, and 4 nepers/cm, respectively.

In Figure 1, absorption bands of a number of liquids having dipole moments[18] (see Table I) of the same order are presented. There is considerable difference in the intensities of these absorption bands. Methyl iodide absorbs more strongly than iodobenzene which in turn absorbs more than 1-iodonaphthalene. Similarly, the absorption of fluorobenzene is more intense than 1-fluoronaphthalene though their dipole moments are of the same magnitude. These results are similar to those obtained by Kroon and Van Der Elsken,[7] who found that in two cases phenyl-substituted compounds have lower absorption than their methyl analogs. Hence, it appears necessary to involve factor(s) other than μ to account for the intensities of these absorption bands.

It is interesting to note in Figure 1 that the α_{max} values increase in the order iodonaphthalene < iodobenzene < methyl iodide while the moments of inertia of these molecules decrease in that order. This suggests a possible dependence of the α_{max} on the inverse value of the moment of inertia of the molecule. With the dependence of α_{max} on the magnitude of the permanent dipole moment (μ) of the molecule in mind, values of α_{max} were plotted against μ/I and μ^2/I, where I is the mean moment of inertia of the molecule. In Figure 4, a plot of α_{max} *vs.* μ^2/I is shown which is almost linear for a variety of polar compounds.

For a pure rotational spectrum Gordon has obtained a formula relating total intensity of absorption (A)[19a] to the reciprocal moment of inertia. In addition he has deduced another formula[19b] which relates the band width to the reciprocal moment of inertia. In the case of the total intensity of absorption when the axis of the resultant dipole moment lies along one of the principal axes of the moment of inertia, we have

$$A = \int_0^\infty \sigma(\nu)\mathrm{d}\nu = \frac{\pi}{3c^2}\sum\mu_z^2\left(\frac{1}{I_x} + \frac{1}{I_y}\right) \qquad (2)$$

where μ_z is the dipole moment along the molecular axis and I_x and I_y are the moments of inertia perpendicular to this axis. The sum is over all molecules. The absorption coefficient (in square centimeters), $\sigma(\nu)$, is taken to be equal to α (in nepers cm^{-1})/(number of absorbing molecules per cm^3). Thus, the band in-

(18) A. L. McClellan, "Tables of Experimental Dipole Moments," W. H. Freeman, San Francisco, Calif., 1963.

(19) (a) R. G. Gordon, *J. Chem. Phys.*, **38**, 1724 (1963); (b) *ibid.*, **41**, 1819 (1964).

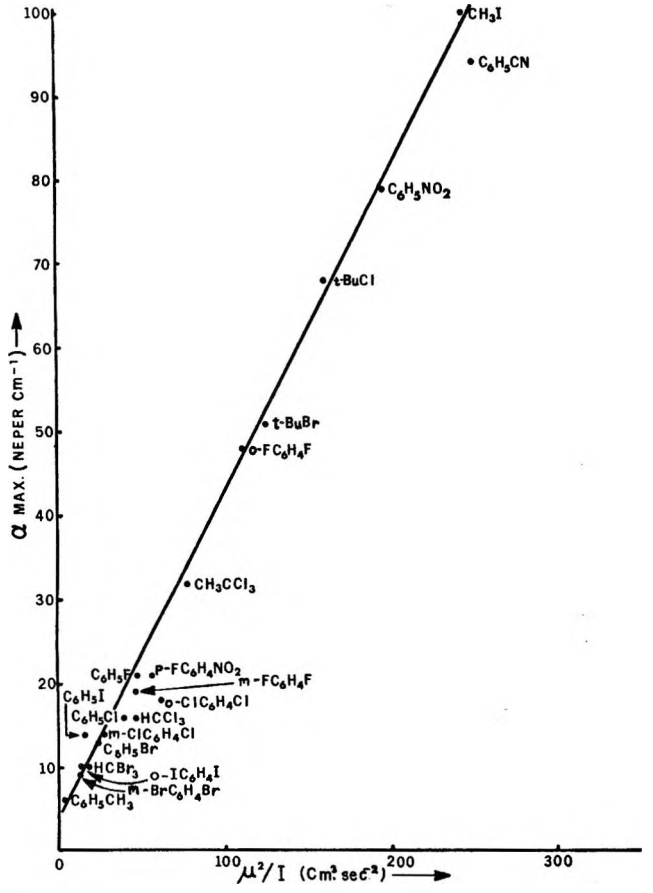

Figure 4. Variation of the absorption coefficient, α_{max} (which we have determined—see Table I), of various compounds with μ^2/I. Dipole moments were obtained from McClellan[18] and internuclear distances from Sutton.[15]

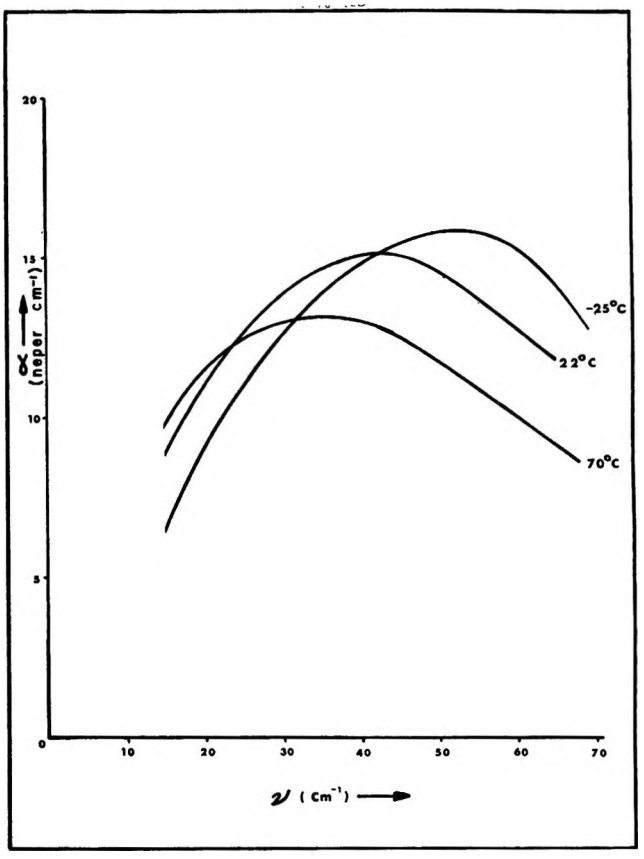

Figure 5. Effect of the variation of temperature on the far-infrared spectrum of chlorobenzene.

tensity of a pure rotational spectrum for such a molecule is proportional to the square of the permanent dipole moment of the molecule and has an inverse dependence on the moment of inertia. If I_x and I_y are of the same order, then a mean moment of inertia I, where I is taken as $(I_x + I_y)/2$, may be used as an approximation.

The linear plot of α_{max} *vs.* μ^2/I may at first sight seem to suggest, at least in part, the involvement of some sort of rotational motion of the molecules as the origin of the far-infrared absorption in these liquids in this frequency range. However, from the work by Davies, Pardoe, Chamberlain, and Gebbie[2c] and also Kroon and Van Der Elsken[7] and more recently by Mansingh[17] it is apparent that the observed integrated intensities cannot be fully accounted for on the basis of a pure rotational mechanism, and the calculated values are always significantly less than the observed intensities. Further, since for a rotational motion the band width is proportional to the reciprocal moment of inertia,[19b] then the peak height might be expected to be proportional to a higher power of $1/I$.

The effect of temperature on the far-infrared absorption of liquid chlorobenzene is given in Figure 5. The position of the absorption maximum shifts continuously to higher frequencies, from 35 cm^{-1} at 70° to 53 cm^{-1} at 25°, by decreasing the temperature with some sharpening in the absorption profile. The α_{max} decreases for chlorobenzene as the temperature is raised; this is in harmony with the work of Davies, Pardoe, Chamberlain, and Gebbie.[2a] Other polar liquids such as bromobenzene and *m*-difluorobenzene (Figure 6) also show a similar temperature effect on the absorption band. This type of spectral behavior on variation of the temperature cannot be explained on the basis of a pure rotational spectrum but is similar to a translational lattice mode absorption in solids. For example, the far-infrared spectral behavior of solid naphthalene[20] and benzene,[21] the frequency maxima of which are shifted to low frequencies with increase in temperature, has been accounted for on the basis of translational lattice vibrations in the crystalline state which involves an electric dipole moment change during the vibration.

The observed absorption bands in liquids having no permanent dipole moments cannot be accounted for as arising from a simple rotational mechanism, and mechanisms involving absorption arising from induced dipole

(20) A. Hadni, B. Wyncke, G. Morlot, and X. Gerbaux, *J. Chem. Phys.*, 51, 3514 (1969).

(21) I. Harada and T. Shimanouchi, *ibid.*, 46, 2708 (1967).

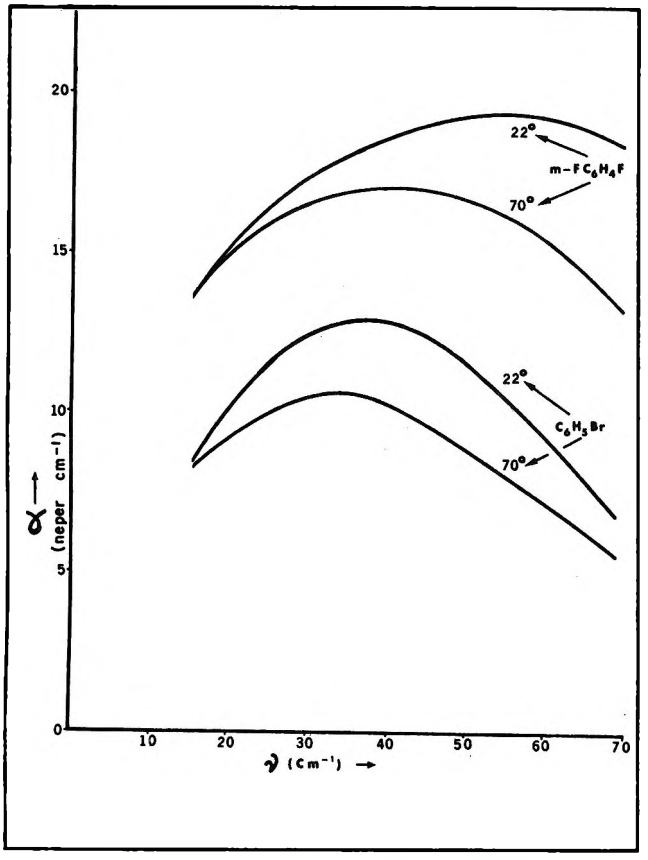

Figure 6. Far-infrared spectra of *m*-difluorobenzene and bromobenzene at different temperatures.

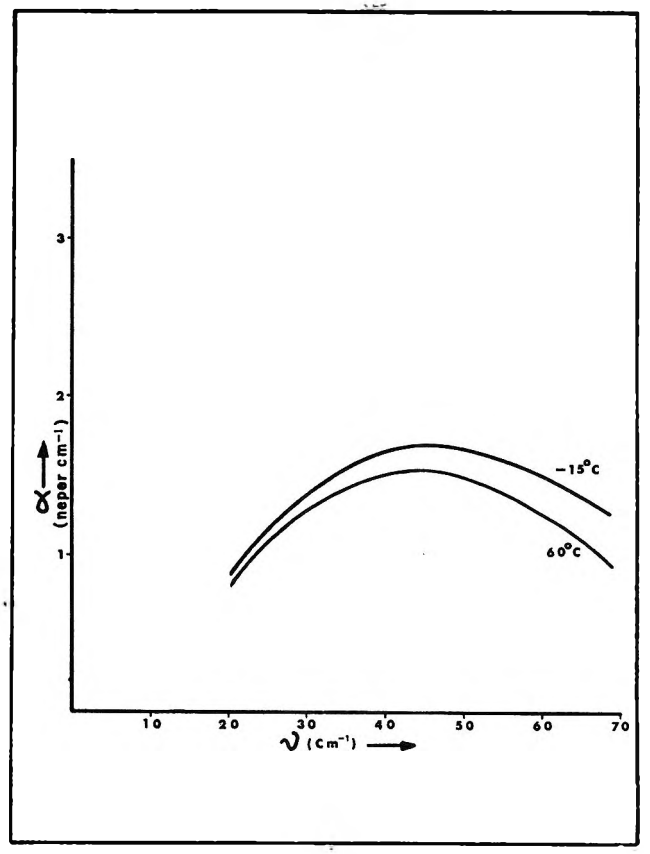

Figure 7. Far-infrared spectrum of carbon tetrachloride at −15 and 60°.

moments in the liquid state have been considered.[3,4] Since the possession of, or a change in, or a reorientation of the dipole moment is a prerequisite for the absorption of infrared radiation, this seems to be a reasonable assumption. Weak absorptions observed in the nonpolar compounds may be reasonably accounted for on the basis of small values, of the order of 0.1 D, of the induced dipole moments. In polar compounds an induced moment effect may also be a factor; however, the relative contribution of this effect may be small compared with that due to the effect involving the permanent dipole moment.

In the absorption band of carbon tetrachloride in Figure 7, there is only a small change in the position of the absorption maximum over the temperature range examined. In fact, the variation in ν_{max} is from 45 cm^{-1} at −15° to 44 cm^{-1} at 60°. These values are to be compared with those of Garg, *et al.*,[3] and Davies, *et al.*,[2c] who obtained values of 47 cm^{-1} (accuracy not quoted) and 49 ± 4 cm^{-1} at room temperature, respectively. Thus the change in ν_{max} between our two temperatures is not significant relative to the experimental error. The repeatability of our results in this case was better than ±4 cm^{-1}. Behavior of these nonpolar liquids is to be contrasted with that of the polar liquids in Figure 6 where over a similar temperature range the latter showed a significant variation in the frequency maximum value. In the solid state for the nonpolar organic substances, such as naphthalene and anthracene,[20] there is about 10% increase in frequency by lowering the temperature ~200°. Hence, if the shift in frequency for the polar liquids is to be attributed to a translational effect, then it is much more pronounced in the polar than in the nonpolar liquid examined here.

In conclusion, the present work indicates for polar molecules the existence of a mechanism in which the maximum value of the absorption coefficient is directly proportional to μ^2/I. The variation of the absorption band of a polar liquid over a temperature range cannot be explained solely by a rotational mechanism. Further a greater number of nonpolar liquids need to be examined—over as wide a temperature range as possible —to determine whether some yield significant shifts in ν_{max}. The next step in this work will be to examine the absorption of polar liquids over almost a complete frequency range of the band to determine its absolute intensity and any variation with temperature. In addition, further studies of the difference between the observed integrated band intensity and that calculated from Gordon's equation[19a] would seem worthwhile.

Acknowledgments. We wish to thank Mr. B. K. Morgan for invaluable assistance and the National Research Council of Canada for support.

Studies of Molten Lithium Chlorate and Its Aqueous Solutions with Laser Raman Spectroscopy

by B. G. Oliver and G. J. Janz*

Department of Chemistry, Rensselaer Polytechnic Institute, Troy, New York 12181 *(Received December 11, 1970)*

Publication costs assisted by the National Science Foundation

The laser Raman spectrum of molten $LiClO_3$ at 132° and of $LiClO_3$–H_2O solutions at 25 and 132° has been studied together with the infrared spectrum of the solutions at room temperature. Striking results are the removal of the degeneracy of the ν_3(E) and ν_4(E) modes of the chlorate ion in both the melt and the solutions and the changes in the 3000–3800 cm^{-1} region of the water band spectrum of the solutions. These results are examined from current viewpoints of ionic interactions and hydration in such salt solutions.

Introduction

Vibrational spectroscopy has been extensively used to explore interactions in molten electrolytes and in electrolyte solutions. Much of the work to date has been concentrated on molten and aqueous nitrate systems,[1,2] and it is of interest to extend these studies to systems containing other polyatomic anions. A study of molten $LiClO_3$ and $LiClO_3$–H_2O solutions by laser Raman and infrared techniques is reported in this article. The interest arises from earlier suggestions[3-7] that there is considerable association of ions in molten $LiClO_3$.

Experimental Section

Lithium chlorate was prepared by the method of Campbell and Griffiths.[8] The melting point of $LiClO_3$, 127.9°, was in agreement with the value reported by Campbell, *et al.*[5,7] Because of the extremely hygroscopic nature of $LiClO_3$, all weighings were performed in a drybox. Solutions were prepared by weight and filtered through medium porosity sintered glass filters.

For the Raman measurements, the solutions were transferred to Pyrex glass Raman tubes (0.7 cm o.d. and 10 cm long) with optical flats as windows. The spectra were recorded with a Jarrell–Ash Laser–Raman spectrometer (Model 25-300) using both He–Ne (6328 Å) and Ar^+ ion (4880 Å) lasers (55 and 125 mW, respectively) as excitation sources. Raman depolarization measurements were made using the polarizer, analyzer, scrambler arrangement recommended by Allemand.[9] Infrared spectra were obtained as smears between KRS-5 plates, using a Perkin–Elmer 457 grating infrared spectrometer.

All band contours were resolved with a Du Pont curve analog computer. Gaussian curve analysis was used owing to the appreciable band half-widths and since the tails were not exponential. The band intensities by this procedure are reported to an accuracy of ±10%.

Results

The Raman spectrum of molten $LiClO_3$ at 132° is illustrated in Figure 1, and the frequencies and polarization characteristics of the bands are tabulated in Table Ia. The infrared spectrum for molten $LiClO_3$, as reported elsewhere by Wilmshurst,[10] is quite similar to the Raman results; the splitting in the ν_4(E) region, however, is not revealed.

When water is added to $LiClO_3$ melt at 132°, the low frequency band at 140 cm^{-1} disappears. Also, striking changes occur in the 500 cm^{-1} region of the spectrum as the water content is increased. This is illustrated in Figure 2a, where the band is resolved into two nearly Gaussian components. The Raman frequencies for several solutions at 25° are shown in Table Ib and the changes in the spectrum in the 500 cm^{-1} region at this temperature are illustrated in Figure 2b. Although the intensity of the total band contour 500 cm^{-1} region is a linear function of concentration at both temperatures, large changes in the relative intensities of the two components with concentration are observed. These changes are shown graphically in Figure 3.

A comparison of the 3000–3800 cm^{-1} region, the OH stretching "water band region," at 25 and 132° for these solutions is illustrated in Figure 4, together with the

(1) G. J. Janz and S. C. Wait, Jr., in "Raman Spectroscopy Theory and Practice," H. A. Szymanski, Ed., Plenum Press, New York, N. Y., 1967.

(2) D. E. Irish, A. R. Davis, and R. A. Plane, *J. Chem. Phys.*, **50**, 2262 (1969).

(3) A. N. Campbell and W. G. Paterson, *Can. J. Chem.*, **36**, 1004 (1958).

(4) A. N. Campbell and M. K. Nagarajan, *ibid.*, **42**, 1137 (1964).

(5) A. N. Campbell and M. K. Nagarajan, *ibid.*, **42**, 1616 (1964).

(6) A. N. Campbell and D. F. Williams, *ibid.*, **42**, 1178 (1964).

(7) A. N. Campbell and D. F. Williams, *ibid.*, **42**, 1984 (1964).

(8) A. N. Campbell and J. E. Griffiths, *ibid.*, **34**, 1647 (1956).

(9) C. D. Allemand, *Appl. Spectrosc.*, **24**, 348 (1970).

(10) J. K. Wilmshurst, *J. Chem. Phys.*, **36**, 2415 (1962).

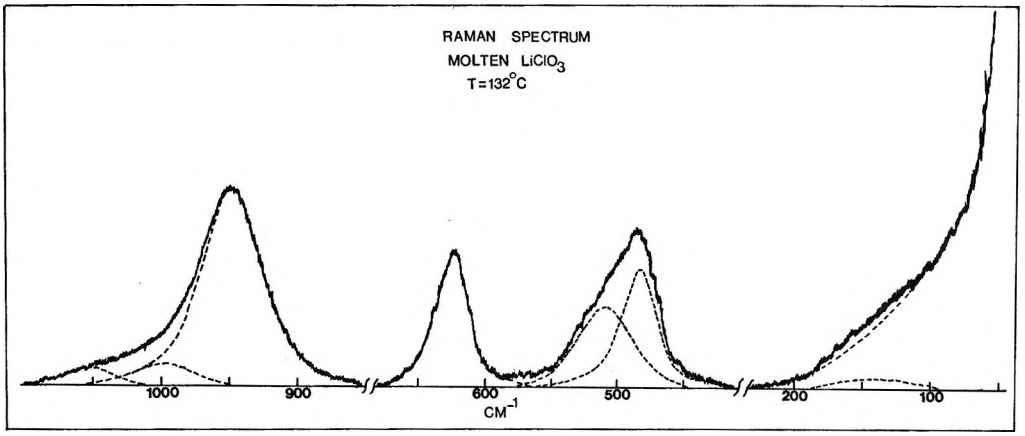

Figure 1. Raman spectrum of molten $LiClO_3$ at 132° with an amplification of 4 in the 450–650 cm^{-1} region.

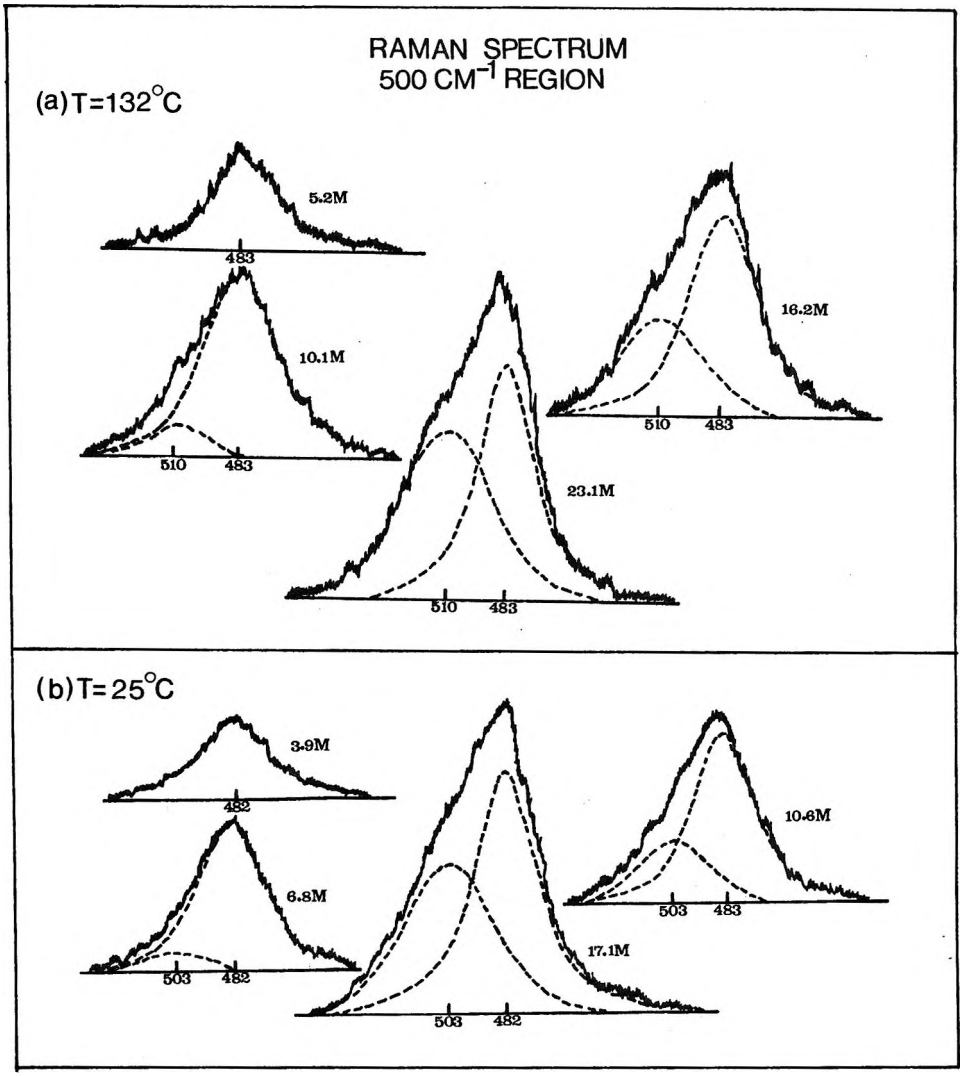

Figure 2. Raman spectrum of aqueous $LiClO_3$ in the 500 cm^{-1} region at 132 and 25°.

Raman spectrum of water alone. With increasing $LiClO_3$ concentration, the intensity of the higher frequency side of the band increases. The resolution of the band contours into four Gaussian components, based on the interpretation of Walrafen,[11] is shown in Figures 5a and b for water and two solutions of comparable concentrations at 25 and 132°. The percentage of each band in the total band contour at various con-

(11) G. E. Walrafen, *J. Chem. Phys.*, **47**, 114 (1967).

Table I: Raman Spectrum of ClO_3^- in Molten $LiClO_3$ (132°) and in Aqueous Solutions (25°)

	(a) Molten $LiClO_3$ (132°)[a]						
ν, cm^{-1}	1043	978	948	625	510	483	140
Polarization	(?)	(?)	P	P	dp	dp	(?)

(b) Aqueous $LiClO_3$ Solutions (25°)

Concn, mol/l.	Raman frequencies					
17.14	1030	975	943 (p)	623 (p)	505 (dp)	483 (dp)
13.12	1023	969	939 (p)	620 (p)	500 (dp)	480 (dp)
10.63	1021	968	938 (p)	620 (p)	501 (dp)	482 (dp)
8.92	1015	970	936 (p)	616 (p)	503 (dp)	481 (dp)
6.78	1013	971	935 (p)	616 (p)	503 (dp)	482 (dp)
5.46	1012	972	934 (p)	615 (p)		483 (dp)
3.92	1008	973	934 (p)	614 (p)		483 (dp)
2.00	1001	967	933 (p)	613 (p)		482 (dp)
	Infrared frequencies					
10.63	1021	968	920	610		470

[a] The resolution of the broad overlapping bands in the ν_3, ν_1 region (refer to Figure 1, 950–1050 cm^{-1} region) was possible by subtracting the remnants of the highly polarized component (ν_1) from the depolarized scattering (largely due to ν_3). The accuracy of the values thus gained is estimated to be ±10 cm^{-1}.

centrations is represented graphically in Figure 6. The H–O–H bending frequency, which is observed at ~1640 cm^{-1}, is relatively insensitive to concentration; it sharpens considerably as the concentration of $LiClO_3$ increases.

Some limited infrared measurements at 25° were undertaken in support of the preceding Raman investigations. The results for a concentrated $LiClO_3$ solution in H_2O and in D_2O are given in Figure 7, and the frequencies are tabulated in Table Ib. The expanded infrared spectrum of this region at several concentrations is shown in Figure 8. It is evident that the infrared spectrum in the low frequency region (<700 cm^{-1}) is much improved by using D_2O as the solvent. It is also apparent that an intensity reversal has occurred in the 900 cm^{-1} region of the infrared spectrum as compared to the Raman spectrum. The water bands in the solutions were also investigated and it is sufficient to note that the results also were closely similar to the Raman observations.

Discussion

The symmetry point group for an unperturbed and isolated ClO_3^- is C_{3v}, and the selection rules are: $2A_1$ (polarized) and 2E (depolarized), with the generalized assignment $\nu_1(A_1) \sim 950$ cm^{-1}; $\nu_2(A_1) \sim 620$ cm^{-1}; $\nu_3(E) \sim 1000$ cm^{-1} (doubly degenerate); and $\nu_4(E) \sim 480$ cm^{-1} (doubly degenerate). The Raman spectrum of $LiClO_3$ melt shows two bands in the $\nu_3(E)$ and in the $\nu_4(E)$ regions of the ClO_3^- spectrum. The splitting of the E modes into two components usually indicates a lowering of the point group symmetry of the ClO_3^-

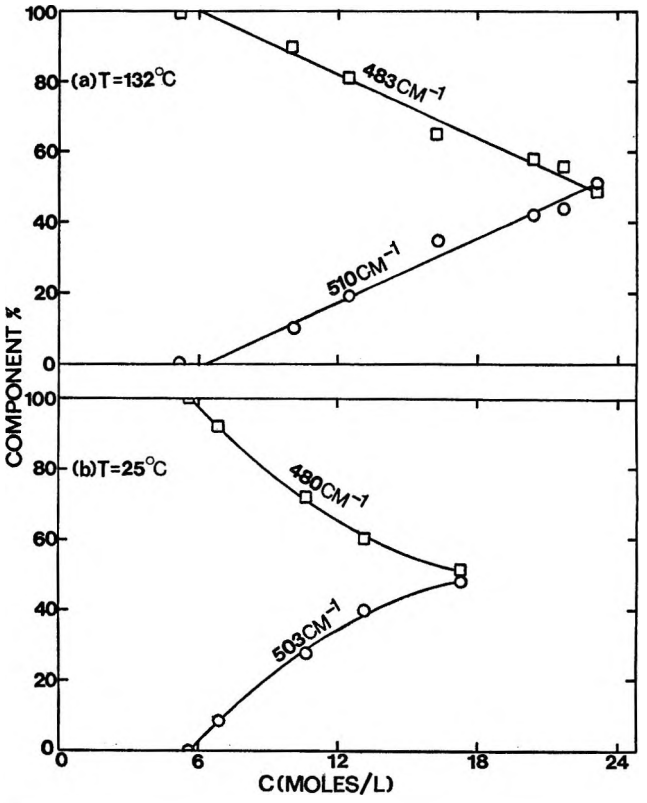

Figure 3. Component percentages *vs.* concentration in the 500 cm^{-1} region at 132 and 25°.

from C_{3v}. For C_s symmetry, apart from the bands in the ν_1 and ν_2 regions, one should observe two components, one polarized and one depolarized, in both the ν_3 and ν_4 regions.[12] Because of the limitations involved in the curve resolution of two closely spaced broad bands, it is not possible to decide uniquely whether both components are antisymmetric modes or whether one of the components is a symmetric mode and the other an antisymmetric mode. However, from the splitting of the spectral lines in the ν_3 and ν_4 regions (and assuming that one of the components in the ν_4 region is a symmetric mode), it is inferred that the symmetry of the ClO_3^- ion has been lowered from C_{3v}. The considerable association of ions in molten $LiClO_3$ inferred from the studies of the thermodynamic and transport properties[2–6] thus is sensed spectroscopically as the lowering of the symmetry point group from C_{3v}, most probably to C_s, through rather pronounced ion–ion interactions.

Further support for this viewpoint comes from the low frequency band at 140 cm^{-1}. This compares with the low frequencies found in molten nitrates and their mixtures[13–15] and has been assigned to the librational

(12) E. B. Wilson, J. C. Decius, and P. C. Cross, "Molecular Vibrations," McGraw-Hill, New York, N. Y., 1955, p 334.

(13) J. P. Devlin, P. C. Li, and G. Pollard, *J. Chem. Phys.*, 52, 2267 (1970).

(14) K. Balasubrahmanyam and G. J. Janz, *ibid.*, in press.

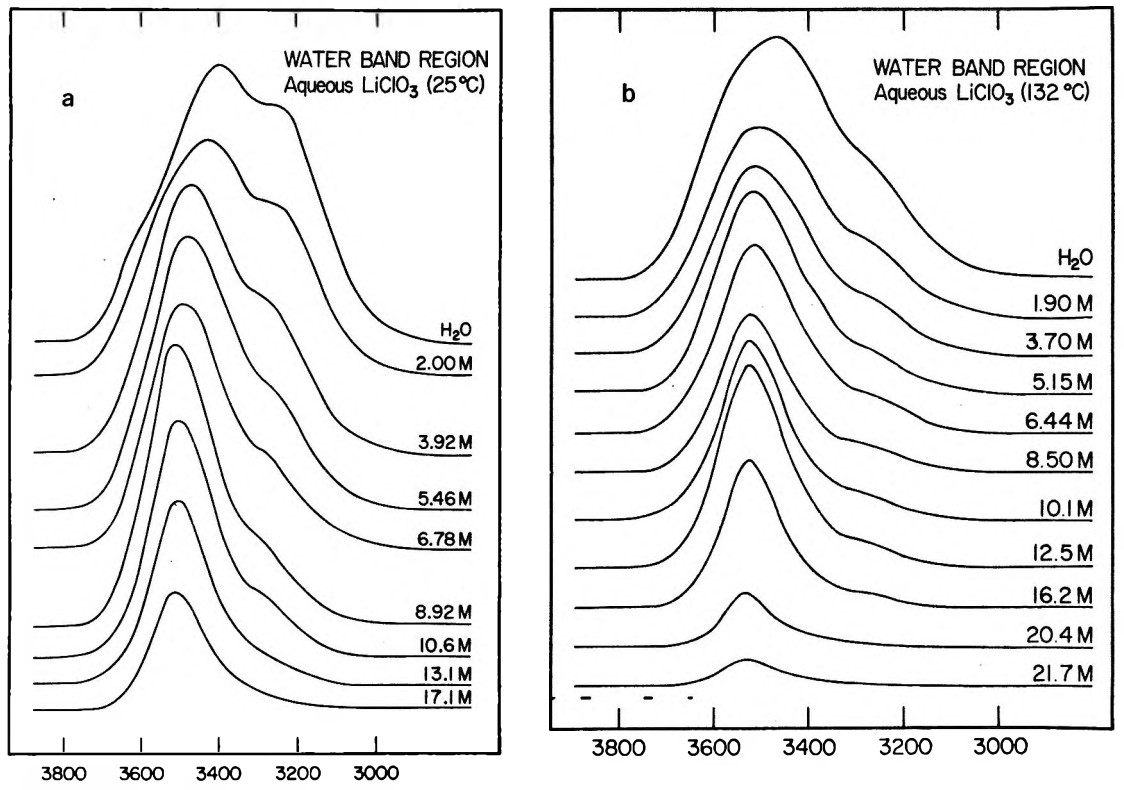

Figure 4. The Raman spectrum of the water band region of aqueous $LiClO_3$ at 25 and 132°.

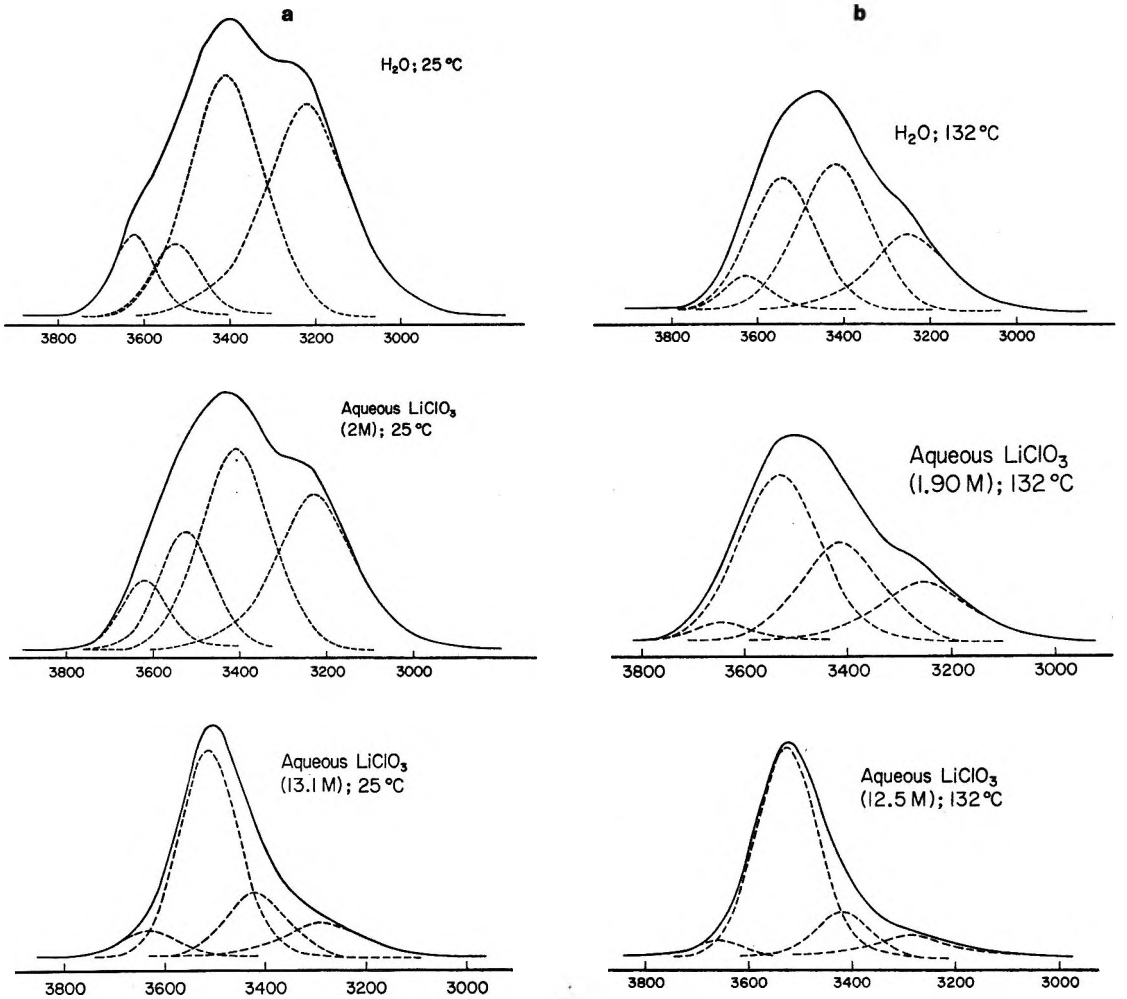

Figure 5. Resolution of Raman water band region into four Gaussian components in water and aqueous $LiClO_3$ at 25 and 132°.

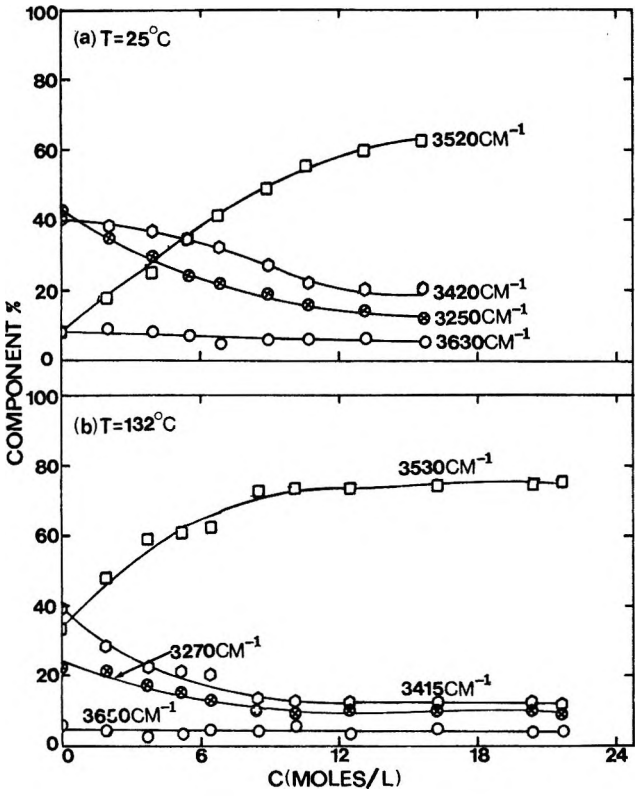

Figure 6. Component percentages *vs.* concentration for the four Gaussian component synthesis of the water band region in aqueous $LiClO_3$ at 25 and 132°.

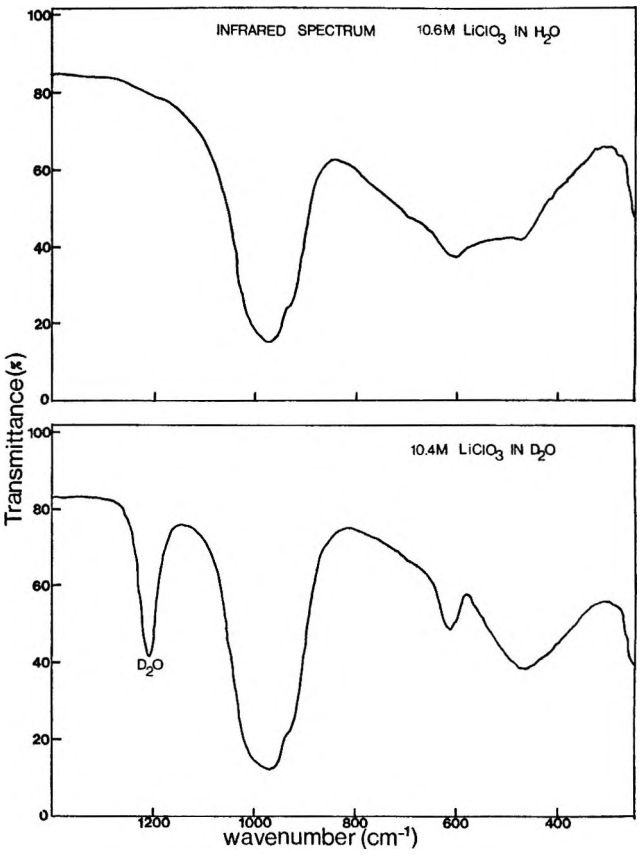

Figure 7. Infrared spectrum of 10.5 *M* $LiClO_3$ in H_2O and D_2O in the chlorate region.

lattice-like motions of anions. It is likely that the same assignment holds for molten $LiClO_3$.

The spectrum of $LiClO_3$ in concentrated aqueous solutions is very similar to that for the molten state, while in dilute solutions it is quite different. Below a concentration of about 5 *M* only one band at 483 cm^{-1} is present in the ν_4 region. As the concentration is increased beyond 5 *M*, a new band at 510 cm^{-1} appears and its relative intensity increases as the concentration increases until it reaches about the same intensity as the 483 cm^{-1} band in the molten salt (Figures 2 and 3). Also, the splitting of the bands in the 900 cm^{-1} region gradually changes from 34 cm^{-1} at concentrations less than 5 *M* to 65 cm^{-1} in the molten salt (Table I, Figure 8). At the higher concentrations, where there is insufficient water to complete the inner hydration shell of the ions, the ClO_3^- ions probably compete with the water for sites in the primary hydration shell of the Li^+ ions.

In this highly concentrated region, Campbell and Oliver[16] have shown that the vapor pressures of $LiClO_3$ solutions can be accounted for by the B.E.T. adsorption model first advanced by Stokes and Robinson in 1948.[17] The thermodynamic water activity is thus understood if the Li^+ ion has four sites available for H_2O and/or ClO_3^- competitive occupancy. A maximum in the specific conductance *vs.* concentration curve, at about 5 *M*, and a significant increase in viscosity of such concentrated $LiClO_3$ solutions have been noted by Campbell, *et al.*[3,5,6] These observations undoubtedly reflect the decreased mobility that would follow from the penetration of the primary solvation shells by the gegenion species.

It is also of interest to note that the degeneracy of the ν_3(E) mode has been lost in such aqueous solutions. Thus inspection of Table Ib and Figure 8 shows that the ν_3(E) band of ClO_3^- ion is split by 34 cm^{-1} in the dilute and moderate concentrations, and that at higher concentrations (>5 *M*) the split increases up to 55 cm^{-1} at 17.1 *M*. Below 5 *M*, however, the splitting of the ν_3(E) mode assumes a constant value, *i.e.*, this loss of degeneracy extends to high dilutions (*i.e.*, the Debye region, where ion pairing is negligible). The degeneracy of the ClO_3^- ν_3(E) mode in such dilute solutions is thus lifted through interaction of the ClO_3^- with the solvent, *i.e.*, hydration. This corresponds closely with the observations advanced by Irish, *et al.*,[2,18,19] elsewhere for aqueous nitrates.

(15) J. H. R. Clarke, *Chem. Phys. Lett.*, **4**, 39 (1969).

(16) A. N. Campbell and B. G. Oliver, *Can. J. Chem.*, **47**, 2671 (1969).

(17) R. H. Stokes and R. A. Robinson, *J. Amer. Chem. Soc.*, **70**, 1810 (1948).

(18) D. E. Irish and A. R. Davis, *Can. J. Chem.*, **46**, 943 (1968).

(19) A. R. Davis, J. W. Macklin, and R. A. Plane, *J. Chem. Phys.*, **50**, 1478 (1969).

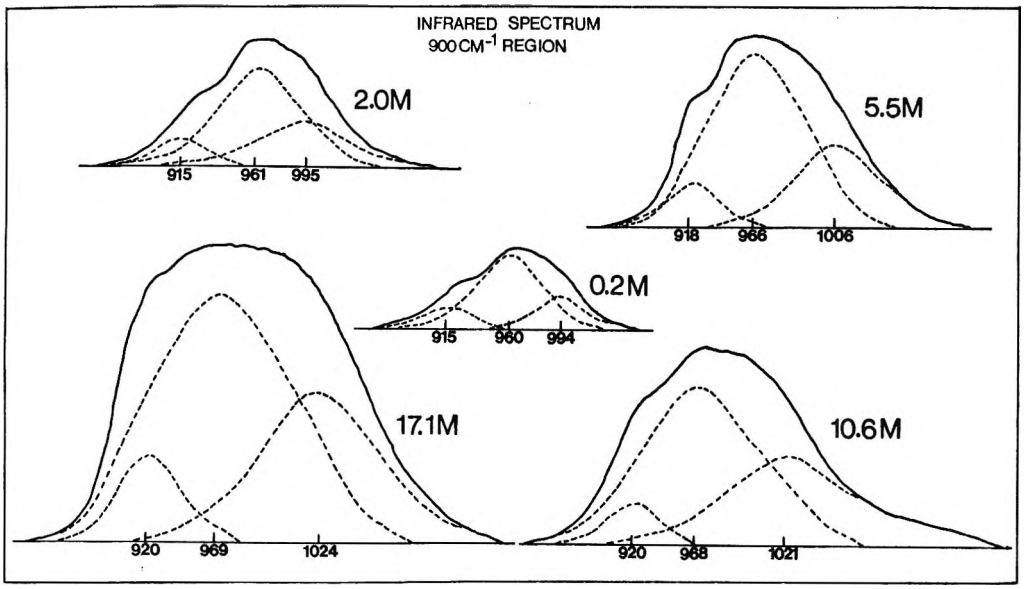

Figure 8. Expanded infrared spectrum of aqueous $LiClO_3$ in the 900 cm^{-1} region.

An examination of the water band region in these solutions was undertaken for additional information. The OH stretching region of the spectrum was resolved into four components, after Walrafen,[11] as already noted (see Figures 4 and 5), for self-consistency although it is recognized that this approach is not without its limitations, especially at higher concentrations. For example on the range of 8–22 M, the ratio of water/$LiClO_3$ varies from ~6 molecules of H_2O per $LiClO_3$ to about 1:1. The sharpening of the water band spectrum thus could be attributed equally well to trapping of water molecules in the $LiClO_3$ bulk structure, and thus to high electric field strengths. The water band structure (and width) in this region closely resemble those of crystal hydrates.

An analysis of the percent of each water band in the total contour, assuming the four-component structure for self consistency, was undertaken with due cognizance of the preceding limitations. The results are illustrated in Figure 6. For concentrations less than 8 M, it is found that the intensity of the 3520 cm^{-1} band relative to the intensities of the 3520 and 3420 cm^{-1} components increases with decreasing concentrations; this is comparable to the earlier Raman[20,21] and infrared[22,23] studies on aqueous electrolyte solutions. It is probable that this increase in intensity of the 3520 cm^{-1} band is at least in part due to an increasing concentration of H_2O bound to cations. The observed splitting of the $\nu_3(E)$ ClO_3^- mode in dilute aqueous solutions indicates that hydrogen bonding between water and ClO_3^- may also be a factor. At the highest concentrations, the sharpness of the water bands (compared to the spectral bands at lower concentrations) suggests that little or no bulk water structure remains in these ultraconcentrated solutions.

Acknowledgments. This work was undertaken during the tenure of a visiting appointment at Rensselaer by one of us (B. G. O.). We acknowledge, with pleasure, the discussions and continued interest of K. Balasubrahmanyam throughout this investigation. Constructive suggestions from A. R. Davis (Ottawa) are acknowledged. The studies at Rensselaer of the structure and vibrational spectroscopy of ionic solutions are made possible, in large part, by support received from the Chemistry Division, National Science Foundation, Washington, D. C.

(20) T. T. Wall and D. F. Hornig, *J. Chem. Phys.*, **47**, 784 (1967).
(21) G. E. Walrafen, *ibid.*, **52**, 4176 (1970).
(22) G. Zundel, *Angew. Chem., Int. Ed. Engl.*, **8**, 499 (1969).
(23) G. Brink and M. Falk, *Can. J. Chem.*, **48**, 3019 (1970).

The Determination of the Number of Species Present in a System: a New Matrix Rank Treatment of Spectrophotometric Data[1]

by Z Z. Hugus, Jr.,

Department of Chemistry, North Carolina State University, Raleigh, North Carolina 27607

and Abbas A. El-Awady*

Department of Chemistry, Western Illinois University, Macomb, Illinois 61455 *(Received March 8, 1971)*

Publication costs borne completely by The Journal of Physical Chemistry

A method is described for the determination of the number of independent variables (*e.g.*, number of different species) in a chemical system. For the application of the method one measures a set of properties P_{ij} (such as absorbances at different wavelengths) in several different mixtures, with the requirement that $P_{ij} = \Sigma_k P_{ik} C_{kj}$. These are then arranged in a rectangular matrix and the number of independent variables is determined from the rank of the matrix, obtained by finding the number of nonzero eigenvalues. In addition, a statistical criterion for the vanishing of an eigenvalue is proposed.

Introduction

In connection with a study of the hydrolytic depolymerization of certain binuclear cobalt(III) complexes[2] it became desirable to know the number of species present in the reacting solution in order to fit experimental spectrophotometric data to a detailed kinetic model.

Published methods given by Wallace,[3] Ainsworth,[4] and Wallace and Katz[5] and more recently by Katakis[6] and Coleman, Varga, and Mastin[7] involve excessive computation, even when high speed digital computing machinery is used. Consequently, we felt that a method of matrix rank analysis that could be used with large rectangular matrices would be of considerable advantage.

Although our intention was to apply the procedure only to the determination of the rank of a matrix of spectrophotometric absorbances, the method is of far wider applicability and may be found of utility by workers in the fields of ORD (optical rotatory dispersion), CD (circular dichroism), fluorescence spectroscopy, and so on.

For the application of this method, one measures a set of properties, the ith property being denoted by P_i, in several different mixtures, the subscript j denoting the jth mixture, and there is the requirement that the properties be constitutive, that is, that

$$P_{ij} = \sum_k P_{ik} \cdot c_{kj} \qquad (1)$$

In this equation, P_{ik} is the value that would be measured for P_i if only the kth species were present, and that at unit concentration; c_{kj} is the concentration of the kth species in the jth mixture. It is evident that Beer's law is an example of a relationship of the type of eq 1.

Method of Rank Determination

It is a theorem in the theory of matrices that the rank of a matrix which can be written as the product of two other matrices is equal to the smaller of the ranks of the two latter matrices.[8] Based on this theorem and on the assumption of Beer's law for each species present in a mixture, the following analysis results.

The absorbance per unit cell legnth, $D_{\lambda i}$, at the λth wavelength in the ith solution, is given by

$$D_{\lambda i} = \sum_1^m{}_k \epsilon_{\lambda k} c_{ki} \qquad (2)$$

where $\epsilon_{\lambda k}$ is the extinction coefficient of the kth species at the λth wavelength, and c_{ki} is the concentration of the kth species in the ith solution. m is the total number of species that contribute to the absorption of light at any wavelength. Evidently, eq 2 follows the definition of matrix multiplication and may be written in the form

$$D = EC \qquad (3)$$

Since the number of wavelengths at which measurements are made will not equal either the number of species present, nor the number of solutions measured,

(1) Abstracted in part from the Ph.D. dissertation of A. A. El-Awady, University of Minnesota, 1965.

(2) A. A. El-Awady and Z Z. Hugus, Jr., *Inorg. Chem.*, 10, 1415 (1971).

(3) R. M. Wallace, *J. Phys. Chem.*, 64, 899 (1960).

(4) S. Ainsworth, *ibid.*, 65, 1968 (1961).

(5) R. M. Wallace and S. M. Katz, *ibid.*, 68, 3890 (1964).

(6) D. Katakis, *Anal. Chem.*, 37, 876 (1965).

(7) J. S. Coleman, L. P. Varga, and S. H. Mastin, *Inorg. Chem.*, 9, 105 (1970).

(8) A. C. Aitken, "Determinants and Matrices," Oliver and Boyd, Edinburgh and London, 9th ed, 1956, p 96.

all three matrices are rectangular rather than square. Clearly, there should be more experiments than wavelengths, and more wavelengths than the suspected number of species.

Since the rank of D is equal to the rank of E or C, whichever is smaller, and since the rank of either C or E can be no larger than m, the rank of D can be no larger than m,[9] provided the number of wavelengths and the number of experiments are both greater than m.

Consider now the matrix, A, formed from the product of D with its transpose, $\tilde{D}$

$$A = D\tilde{D} \tag{4a}$$

$$A_{\lambda\lambda'} = \sum_t D_{\lambda t}\tilde{D}_{t\lambda'} \tag{4b}$$

$$= \sum_t D_{\lambda t}D_{\lambda' t} \tag{4c}$$

A is symmetric (square) matrix of order n, the number of wavelengths, of rank m. Now, since A is symmetric and real, it can be expressed in terms of its eigenvalues and eigenvectors as

$$A = \alpha_1 P_1{}^{**} P_1 + \alpha_2 P_2{}^{**} P_2 + \cdots \tag{5}$$

and this will contain as many terms as there are nonzero eigenvalues of A. Here $P_1{}^*$, $P_2{}^*, \cdots$ are the column eigenvectors of A, and ${}^*P_1$, ${}^*P_2$, $\cdots$ are the row eigenvectors (transposes of $P_1{}^*$, $P_2{}^*$, $\cdots$). The α_t are the corresponding eigenvalues, and by $P_1{}^{**}P_1$, etc., is meant the dyad or outer product.

Viewed in this way, the number of nonzero eigenvalues is the mathematical rank of the matrix A. Any nonsingular procedure that serves to diagonalize A would then provide an immediate indication of its rank. To obtain both the eigenvalues and eigenvectors of the matrix A, one needs to utilize the method of orthogonal transformation.[10]

When the absorbance matrix, D, is derived from experiment, however, each element in D, and therefore in A, is subject to error. In general, on this account one finds the mathematical rank of A to be the same as its order.

What is necessary, therefore, is a statistical criterion for the "vanishing" of an eigenvalue, and one can attack the problem in the following way.

The matrix A was defined in eq 4c as

$$A_{jk} = \sum_t D_{jt}D_{kt}$$

Regarding the standard deviation in A_{jk} as a vector quantity,[11-13] $\vec{\sigma}_{A_{jk}}$, based on the not necessarily orthogonal vectorial standard deviations in the elements of D, for examples, $\vec{\sigma}_{D_{ji}}$, we then have[14,15]

$$\vec{\sigma}_{A_{jk}} = \sum_i \left\{\left(\frac{\partial A_{jk}}{\partial D_{ji}}\right)\vec{\sigma}_{D_{ji}} + \left(\frac{\partial A_{jk}}{\partial D_{ki}}\right)\vec{\sigma}_{D_{ki}}\right\} \tag{6}$$

$$\vec{\sigma}_{A_{jk}} = \sum_i \left\{D_{kt}\vec{\sigma}_{D_{ji}} + D_{jt}\vec{\sigma}_{D_{ki}}\right\} \tag{7}$$

If we diagonalize the matrix A, we obtain the matrix, ν, whose elements are given by equations of the form

$$\nu_{ll} = \sum_{j,k} S_{lj}A_{jk}S_{kl} \tag{8}$$

$$\nu_{ll} = \sum_{j,k} S_{jl}S_{kl}A_{jk} \tag{9}$$

Here, the elements of the matrix, S, correspond to the principal axis transformation that diagonalizes A. Moreover, an element, S_{jl}, is the eigenvector of the matrix A corresponding to the lth eigenvalue, ν_{ll}. The matrix S could be obtained using a variety of standard procedures. In this work an iterative procedure based on the classical method of Jacobi was developed.[16]

The standard deviation of an element of the diagonal matrix, ν_{ll} say, is given by

$$\vec{\sigma}_{\nu_{ll}} = \sum_{j,k}\left(\frac{\partial \nu_{ll}}{\partial A_{jk}}\right)\vec{\sigma}_{A_{jk}} \tag{10}$$

Using eq 9, and then eq 7, it follows that

$$\vec{\sigma}_{\nu_{ll}} = \sum_{j,k} S_{jl}S_{kl}\vec{\sigma}_{A_{jk}}$$

$$\vec{\sigma}_{\nu_{ll}} = \sum_{t,j,k} S_{jl}S_{kl}(D_{kt}\vec{\sigma}_{D_{ji}} + D_{jt}\vec{\sigma}_{D_{ki}}) \tag{11}$$

The variance of an element in the diagonal matrix will then be given by

$$\sigma_{\nu_{ll}}{}^2 = \vec{\sigma}_{\nu_{ll}}\cdot\vec{\sigma}_{\nu_{ll}}$$

$$\sigma_{\nu_{ll}}{}^2 = \sum_{j,k}(S_{jl}S_{kl})^2\{\sum_t(D_{kt}{}^2\vec{\sigma}_{D_{ji}}{}^2 + D_{jt}{}^2\vec{\sigma}_{D_{ki}}{}^2 + 2\rho_{jk}D_{kt}D_{jt}|\vec{\sigma}_{D_{ki}}|\cdot|\vec{\sigma}_{D_{ji}}|)\} \tag{12}$$

The quantity ρ_{jk} is a correlation coefficient between the standard deviations in D_{kt} and in D_{jt}. We now make the assumption that $\rho_{jk} = 0$, unless $j = k$, and

(9) Wallace[3] pointed out that the rank of E or C will be less than m only if (a) the concentration of one or more species is zero in all experiments, (b) the concentrations of all species are zero in more than m experiments, and (c) the concentrations of one or more species can be expressed as a linear combination of the other species in all experiments. The first two of these conditions are trivial, while the third can be violated by choosing different concentration levels in some experiments.

(10) H. Margenau and G. M. Murphy, "The Mathematics of Physics and Chemistry," Van Nostrand, Princeton, N. J., 1956, p 324 ff.

(11) The standard deviation in A_{jk} is not viewed as a vector in the sense of the row or column vector interpretation of matrices as is generally accepted in matrix calculus. We are introducing geometrical concepts here on top of the usual matrix algebra. One may interpret the errors in the individual measurements as the length of the vectors from the mean of the observations in an N dimensional space. This description is useful when considering correlated errors where the correlations vary from one pair of measurements to the other.

(12) W. C. Hamilton, "Statistics in Physical Science," Ronald Press, New York, N. Y., 1964, pp 132–134, 174 ff.

(13) K. J. Holzinger and H. H. Harman, "Factor Analysis," The University of Chicago Press, Chicago, Ill., 1941, p 56 ff.

(14) E. R. Cohen and J. W. M. DuMond, *Rev. Mod. Phys.*, **37**, 546 (1965).

(15) E. R. Cohen, K. M. Crowe, and J. W. M. DuMond, "The Fundamental Constants of Physics," Interscience, New York, N. Y., 1957, p 222 ff.

(16) D. K. Faddeev and V. N. Faddeeva, "Computational Methods for Linear Algebra," W. H. Freeman and Co., San Francisco, Calif., 1963, p 482 ff.

$\rho_{jj} = 1$, which implies that there is no correlation between $\sigma_{D_{ji}}$ and $\vec{\sigma}_{D_{ki'}}$ for $i \neq i'$. This yields the result that for $j \neq k$ the quantity in brackets is

$$\{\sum_i (D_{ki}^2 \sigma_{D_{ji}}^2 + D_{ji}^2 \sigma_{D_{ki}}^2)\} \quad (13)$$

while for $j = k$, the quantity in brackets has the value

$$\{\sum_i A D_{ji}^2 \sigma_{D_{ji}}^2\} \quad (14)$$

Using the symbol $\sigma_{A_{jk}}^2$ for quantity 13 and the symbol $\sigma_{A_{jj}}^2$ for quantity 14, we then have for the variance in the lth eigenvalue, ν_{ll}

$$\sigma_{\nu_{ll}}^2 = \sum_{j,k} S_{jl}^2 S_{kl}^2 \sigma_{A_{jk}}^2 \quad (15)$$

Then by comparing each eigenvalue with the square root of its variance as computed from (15), we have a criterion for its differing from zero to a statistically significant extent.

However, because our assumptions concerning the correlations in D_{ji} and $D_{ki'}$ may be questionable, there is yet another method that we decided to use to establish whether m species are sufficient to fit the experimental data satisfactorily.

The matrix A was defined in eq 4a as the product of the optical density matrix D and its transpose $\tilde{D}$. Upon diagonalization of A we get

$$\tilde{S}AS = N \text{ (diagonal)} \quad (16)$$

where

$$\tilde{S}S = I \text{ (the identity or unit matrix)}$$

Substitution of (4a) into (16) gives

$$\tilde{S}\tilde{D}DS = N \quad (17)$$

$$\tilde{T}T = N \quad (18)$$

where

$$T \equiv DS \quad (19)$$

On multiplication of (19) by $\tilde{S}$ on the right we get

$$T\tilde{S} = DS\tilde{S} = D \quad (20)$$

$$D_{i\lambda} = \sum_j T_{ij} \tilde{S}_{j\lambda} \quad (21)$$

If we now arrange the eigenvalues in order of decreasing value—since the matrix A is real and symmetric, the eigenvalues are nonnegative definite—then an approximation to the measured absorbance at the lth wavelength in the ith experiment, D_{il}, using only the first m eigenvectors will be given by

$$B_{il}^{(m)} = \sum_j^m T_{ij} \tilde{S}_{jl} \quad (22)$$

where

$$T_{ij} = \sum_k \tilde{D}_{ik} S_{kj} \quad (23)$$

In these equations S_{kj} and $\tilde{S}_{jl}$ are the jth components of, respectively, the kth or lth eigenvector, and are represented by row and column matrices, respectively.

By comparing $|B_{il}^{(m)} - \tilde{D}_{il}|$ with $\sigma_{D_{il}}$ we then can find, for each value of m, how many residuals in absorbance compared to their estimated errors lie in various ranges. In addition, we can compute the value of χ^2 and use well-known statistical tests to determine whether the fit is satisfactory.

Here

$$\chi_m^2 = \sum_{i,l} \frac{(B_{il}^{(m)} - \tilde{D}_{il})^2}{\sigma_{D_{il}}^2}$$

A typical treatment of a set of our data, 38 experiments at nine wavelengths, led to the results summarized in Table I. It is evident that only the first three eigenvalues are larger than their standard errors, but perhaps more significantly, the other six eigenvalues are so much smaller than their standard errors that they should surely be regarded as being statistically equivalent to zero. Whether a third species should be assumed at any high level of confidence is open to some question on the first two columns of Table I. However, the results given in the last two columns leave no

Table I: Data from 38 Solutions[a] at Nine Wavelengths (342 Experimental Points)

Eigenvalue	Std error in eigenvalue	No. of residuals more than $3x\sigma_{est}$	χ_m^2
1637.301311	0.231	311	222227.0
2.642417	0.092	155	8741.9
0.140060	0.111	0	34.67
0.000091	0.057	0	21.04
0.000057	0.063	0	14.40
0.000035	0.071	0	9.88
0.000027	0.056	0	5.15
0.000022	0.073	0	2.83
0.000015	0.052	0	0.00

[a] The solutions contain $[(en)_2Co(OH)_2Co(en)_2]^{4+}$ and its hydrolysis products.

Table II: Data from Eight Solutions[a] at Eight Wavelengths (64 Experimental Points)

Eigenvalue	Std error in eigenvalue	No. of residuals more than $3x\sigma_{est}$	χ_m^2
11.579207	0.0173	53	130091.0
1.167141	0.0013	9	408.3
0.003276	0.0046	0	44.27
0.000323	0.0058	0	8.40
0.000053	0.0046	0	2.55
0.000016	0.0054	0	0.76
0.000005	0.0036	0	0.20
0.000002	0.0064	0	0.00

[a] The solutions contain methyl red at different pH values (see ref 5).

doubt that a third species must be present, since the fit with only two species (eigenvectors) is completely unsatisfactory.

Actually the expectation value[17,18] of χ_3^2 is 339, and our unduly pessimistic estimates of error—too large by a factor of about 3—cause the value, 34.67, to be as small as it is.

An additional set of data taken from the paper of Wallace and Katz[5] on methyl red solutions at varying pH's was treated using our program and gave the results summarized in Table II. These measurements were made at eight wavelengths on solutions at eight different pH's. The questionable fourth component mentioned by Wallace and Katz is not supported by the value of χ_3^2 which has an expectation value of 61. In addition, the probability of obtaining a value of χ_4^2 as low as 8.4 is much smaller than 0.001, although an overestimate of the measurement errors could cause such a low value of χ^2. In our treatment each error was set at 0.003, the same value used by Wallace and Katz, which seems reasonable.

The data were treated by means of a FORTRAN program, ØPTICØN, using a Control Data Corp. 1604 computer. The program as written could be used for up to 200 experiments at ten wavelengths, but adaptation to larger numbers of experiments or of wavelengths would entail only changes in DIMENSION statements.

(17) O. L. Davies, Ed., "Statistical Methods of Research and Production," Oliver and Boyd, London, 1961, p 283.

(18) L. G. Parratt, "Probability and Experimental Errors in Science, An Elementary Survey," Wiley, New York, N. Y., 1961, pp 188–191.

Electron Spin Resonance Studies of Short-Lived Radicals Generated by Fast Flow Techniques in Aqueous Solutions[1]

by Gideon Czapski

Radiation Research Laboratories and Department of Chemistry, Mellon Institute of Science, Carnegie-Mellon University, Pittsburgh, Pennsylvania 15213 *(Received April 16, 1971)*

Publication costs assisted by Carnegie-Mellon University and the U. S. Atomic Energy Commission

The application of fast reaction flow systems with esr detection to studies of free radicals in aqueous solution is analyzed in detail. It is shown that for short-lived radicals it is essential that the chemical reactions which produce the intermediates proceed within the cavity and that few radicals will be observed if the reactions responsible for the radical formation are complete immediately after mixing. The assumption frequently made in these studies, that this reaction is complete before the solution enters the cavity, is shown to be incorrect. It is believed that many of the controversies in the literature can be readily cleared up by analysis of the kinetics as is done here.

Introduction

In most cases the study of free radical intermediates in aqueous solutions demands fast detection techniques since these radicals normally have very short lifetimes. Most recent studies of the kinetics of free radical reactions in aqueous solutions have been carried out with flash photolysis or pulse radiolysis techniques using optical detection. With these techniques, the absorption spectra and decay of the radicals can be directly observed. The esr spectra of many radicals have been studied in aqueous systems in experiments which mainly employed flow techniques where the radicals were generated chemically. In most of these studies the emphasis was on the qualitative identification of the radicals and a determination of the esr parameters with little work being directed toward obtaining kinetic information. Until recently there were difficulties in fast recording of esr spectra. Fessenden,[2a] using the pulse radiolysis technique, developed a sampling device for esr measurements by which spectra and kinetics of radicals living longer than several milliseconds could be recorded. Even this method is rather slow for most radicals in aqueous solution. Recently Smaller, *et al.*,[2b,3] combined pulse radiolysis with esr detection to follow the decay of

(1) Supported in part by the U. S. Atomic Energy Commission.

(2) (a) R. W. Fessenden, *J. Phys. Chem.*, 68, 1508 (1964); (b) E. C. Avery, J. R. Remko, and B. Smaller, *J. Chem. Phys.*, 49, 951 (1968).

(3) B. Smaller, J. R. Remko, and E. C. Avery, *ibid.*, 48, 5174 (1968).

radicals with $\tau_{1/2}$ as short as 2–3 μsec. Atkins, *et al.*,[4-6] developed a combined esr–flash photolysis experiment which enabled them to follow radicals at times as short as 1 μsec. In some investigations the radicals were generated by photolysis or by irradiating solution inside an esr cavity with fast electrons from a Van de Graaff accelerator. This steady-state method was used extensively in radiolysis by Fessenden and Schuler[7,8] and in photolysis by Livingston and Zeldes,[9-11] but mostly in organic solutions.

The purpose of this study is to demonstrate that most of the kinetic studies performed with the flow techniques are based on incorrect assumptions which led the authors to invalid reaction mechanisms and rate constants. In one particular case, in the work of Sicilio, *et al.*,[12-14] a similar criticism to the assumptions made was very recently raised by Burchill.[15] In this work these problems and their applications to a number of studies will be discussed in a much more general way.

The Use of Flow Techniques in Esr Studies of Free Radicals. Bielski and Saito[16,17] were the first to use the reaction

$$Ce^{4+} + H_2O_2 \longrightarrow Ce^{3+} + H^+ + HO_2 \qquad (1)$$

in a flow system in order to study the esr spectra and decay kinetics of the HO_2 radical. (Soon afterward this method was similarly applied by Norman and Dixon[18] using the Ti^{3+}–H_2O_2 system.) The two solutions (Ce^{4+} and H_2O_2, both in acid solution) in containers A and B were forced through a mixing chamber and the mixed solution thereafter entered the esr cavity.

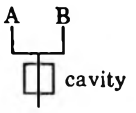

In Bielski and Saito's[16,17] experiment the esr signal was recorded while the solution was flowing and, by changing either flow rates or the dead volume between the mixing chamber and the cavity, the decay of the radical was recorded as the change in the intensity of the esr signal. In their experiments the time delay between the mixer and the cavity was of the order of 10 msec and this was also about the time required for the solution to pass through the cavity. The assumption in these experiments was that reaction 1 is completed immediately after mixing and that the esr signal recorded is that of the $HO_2\cdot$ radicals surviving to reach the cavity. In their case reaction 1 is fast ($k_1 \sim 10^6\ M^{-1}\ \text{sec}^{-1}$ and under their experimental conditions $\tau_{1/2} \leq 10$ μsec) and thier assumption is completely justified. The HO_2 radical decays through

$$2HO_2 \longrightarrow H_2O_2 + O_2 \qquad (2)$$

This reaction is relatively slow for free radical recombination ($k_2 \sim 10^6\ M^{-1}\ \text{sec}^{-1}$), hence concentrations of $HO_2 \sim 10^{-4}\ M$, which are measurable by esr techniques, reached the cavity. In most other cases radical combination takes place with a rate constant three to four orders of magnitude greater and the recombination lifetimes are correspondingly shorter.

Different Experimental Procedures Used with the Flow Technique. Radicals may be produced in esr flow experiments by several procedures.

(a) In the first method a radical R· is formed by mixing two solutions of A and B and flowing the mixture through an esr cavity

$$A + B \longrightarrow R\cdot + P \qquad (3)$$

By this procedure the radical R is formed in the primary reaction (3) and its properties may be investigated. This procedure was used to investigate the radicals shown in Table I.

(b) In a modification of procedure (a) radicals can be produced through two or more consecutive reactions. In reaction 3, R is formed from the reaction of A + B. This radical can react further to yield a radical R′. This can be a first-order reaction as in the case of the reduction of *tert*-butyl hydroperoxide, where $(CH_3)_3CO\cdot$ is initially formed but decomposes to $CH_3\cdot$ and acetone.[18] More often R′ is formed in a reaction of R with another molecule, S. In several cases S is either one of the reactants (A or B) or the product (P) of reaction 3. Examples for such reactions are given in Table II. Many organic radicals have been examined by using the reaction of Fe^{2+} or, more frequently, that of Ti^{3+} with H_2O_2 to generate OH radicals which react thereafter with S to produce a secondary radical R′ (where R = OH)

$$R + S \longrightarrow R' \qquad (4)$$

The solute is added either to the Ti^{3+} or to the H_2O_2 solutions or even to both of them. Results using this

(4) P. W. Atkins, K. A. McLauchlan, and A. F. Simpson, *Chem. Commun.*, 179 (1968).
(5) P. W. Atkins, I. C. Buchanan, R. C. Gurd, K. A. McLauchlan, and A. F. Simpson, *ibid.*, 513 (1970).
(6) P. W. Atkins, K. A. McLauchlan, and A. F. Simpson, *J. Sci. Instrum.*, 547 (1970).
(7) R. W. Fessenden and R. H. Schuler, *J. Chem. Phys.*, **39**, 2147 (1963).
(8) R. W. Fessenden and R. H. Schuler, *Advan. Radiat. Chem.*, **2**, 1 (1970).
(9) R. Livingston and H. Zeldes, *J. Chem. Phys.*, **44**, 1245 (1966).
(10) R. Livingston and H. Zeldes, *J. Amer. Chem. Soc.*, **88**, 4333 (1966).
(11) P. Smith and P. B. Wood, *Can. J. Chem.*, **45**, 649 (1967).
(12) F. Sicilio, R. E. Florin, and L. A. Wall, *J. Phys. Chem.*, **70**, 47 (1966).
(13) E. L. Lewis and F. Sicilio, *ibid.*, **73**, 2590 (1969).
(14) R. E. James and F. Sicilio, *ibid.*, **74**, 1166 (1970).
(15) C. E. Burchill, *ibid.*, **75**, 167 (1971).
(16) E. Saito and B. H. J. Bielski, *J. Amer. Chem. Soc.*, **83**, 4467 (1961).
(17) B. H. J. Bielski, *J. Phys. Chem.*, **66**, 2263 (1962).
(18) W. T. Dixon and R. O. C. Norman, *Nature*, **196**, 891 (1962).

Table I: Radicals Formed Directly by Various Chemical Reactions

Reaction	Radicals formed	Ref
$Ce^{4+} + H_2O_2$	$HO_2\cdot$	16, 17
$Ce^{4+} + (CH_3)_3COOH$	$(CH_3)_3CO_2\cdot$	18
$Ti^{3+} + (CH_3)_3COOH$	$CH_3\cdot$ and $(CH_3)_3CO\cdot$	18
$Ce^{4+} + RSH$	$RS\cdot$	19
$Ce^{4+} +$ phenols	Aryloxy radicals ($ArO\cdot$)	20
$Ce^{4+} +$ aryl sulfinic acids ($ArSO_2H$)	Arylsulfonyl radicals ($ArSO_2\cdot$)	21
$Ce^{4+} +$ hydroxylamines $Fe(CN)_6^{3-} +$ hydroxylamine } (RNHOH)	R-NHO·	22 22
Ce^{4+} $Fe(CN)_6^{3-} +$ hydroxamic acid (RCONHOH)	RCONHO· (cis and trans)	23 23
$ArNO_2 + S_2O_4^{2-}$	$ArNO_2\cdot^-$	24
$MnO_4^- +$ tyrosine	Tyrosyl radical	25
$Ti^{3+} + NH_2OH$	NH_2 (possibly $NH_2O\cdot$)	26
$Ce^{4+} +$ hydroxyquinone	Semiquinone	27
$Ti^{3+} + S_2O_8^{2-}$	SO_4^-	28

Table II

Initiation reaction	R	Secondary reaction	R′	Ref
$Ti^{3+} + H_2O_2$	OH	OH + H_2O_2	HO_2	29
$Fe^{2+} + H_2O_2$	OH	OH + H_2O_2	HO_2	29
$V^{4+} + H_2O_2$	OH	OH + H_2O_2	HO_2	30
$Ti^{3+} + H_2O_2$	OH	OH + (Ti^{4+}–H_2O_2)	TiO_3^{3+}	29
$V^{4} + H_2O_2$	OH	OH + (V^{5}–H_2O_2)	VO^{3+}	30

method have been reviewed by Norman and Gilbert.[31] This method is probably the most convenient method to record esr spectra of a large variety of organic radicals in solution. While this method is excellent for the qualitative identification of the radicals present in the reaction mixture on the millisecond time scale it is of doubtful value for kinetic measurements since in most cases studied the time involved in reaction 4 is ill-defined.

(c) The last procedure employs double mixing. In the first mixer (as in procedure a or b) R is produced through reaction 3 or 4. The solution of R· leaving the first mixer is in turn mixed with S in a second mixer. In the solution leaving the second mixer, reaction 4 yields R′ which enters the esr cavity. The last

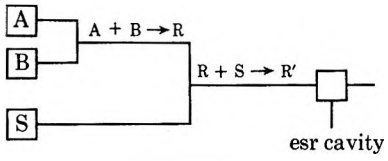

method has been used to study the formation and exchange reactions of peroxy complexes of different cations[32] as well as reactions between alcohols and alcoholic radicals[33] (Table III).

The Concentrations of the Radicals in the Cavity. In the different procedures described, reaction 3 generates the radical R after the solutions are mixed. There may be two extreme cases which will be considered. (A) Reaction 3 is very fast and is over immediately after the solutions are mixed. (B) The reaction proceeds slowly along the flow tube and in the cavity.

Generally the free radicals formed may recombine very efficiently through

$$2R \longrightarrow \text{products} \qquad (5a)$$

$$2R' \longrightarrow \text{products} \qquad (5b)$$

$$R + R' \longrightarrow \text{products} \qquad (5c)$$

In the first case (A) where either reaction 3 or 3 and 4 are instantaneous, R or R′ are formed immediately after mixing. Thereafter R or R′ decay through (5a) or (5b) or (5c), and the concentration will be given by

$$R = \frac{R_0}{1 + R_0 2k_5 t} \qquad (I)$$

(where t is the time it takes the solution to get from the

(19) W. Wolf, J. C. Kertesz, and W. C. Landgraf, *J. Magn. Resonance*, **11**, 618 (1969).
(20) T. J. Stone and W. A. Waters, *J. Chem. Soc.*, 213 (1964).
(21) M. McMillan and W. A. Waters, *ibid.*, *B*, 422 (1966).
(22) C. J. W. Gutch and W. A. Waters, *ibid.*, 752 (1965).
(23) J. V. Ramsbottom and W. A. Waters, *ibid.*, 132 (1966).
(24) P. L. Kolker and W. A. Waters, *ibid.*, 1136 (1964).
(25) D. C. Borg, "Rapid Mixing and Sampling Techniques in Biochemistry," Academic Press, New York, N. Y., 1964, p 135.
(26) P. B. Ayscough, "ESR in Chemistry," pp 296–298 (1962).
(27) I. Yamazaki and L. H. Piette, *J. Amer. Chem. Soc.*, **87**, 986 (1965).
(28) R. O. C. Norman, P. M. Storey, and P. R. West, *J. Chem. Soc. B*, 1087 (1970).
(29) G. Czapski, H. Levanon, and A. Samuni, *Isr. J. Chem.*, **7**, 375 (1969).
(30) A. Samuni and G. Czapski, *ibid.*, **8**, 563 (1970).
(31) R. O. C. Norman and B. C. Gilbert, *Advan. Phys. Org. Chem.*, **5**, 53 (1967).
(32) A. Samuni and G. Czapski, *J. Phys. Chem.*, **74**, 4592 (1970).
(33) R. O. C. Norman and P. R. West, *J. Chem. Soc. B*, 389 (1969).

Table III

Initial reaction A + B + S_1 → R			Secondary reaction R + S_2 → R′			
A	B	S_1	R	S_2	R′	Ref
Ce^{4+}	H_2O_2		HO_2	M_1^{n+} [a]	$(HO_2\text{–}M_1)^{n+}$	29, 30
Ce^{4+}	H_2O_2	M_1^{n+}	$(HO_2\text{–}M_1^{n+})$	M_2^{m+}	$(HO_2\text{–}M_2)^{m+}$	32
Ti^{3+}	H_2O_2	R_1R_2>CHOH	R_1R_2>$\dot{C}$OH	$R_3'R_4$>CHOH	R_3R_4>$\dot{C}$OH	33

[a] M_2^{m+} and M_1^{n+} = Th^{4+}, V^{5+}, U^{6+}, Ti^{4+}, Ce^{3+}.

mixer to the cavity, and R_0' is the concentration of R′ at the end of mixing which equals B_0). For radical recombination reactions the rate constants are generally $\sim 10^9$ to 10^{10} M^{-1} sec^{-1}. Typically $B_0 = 10^{-3}$ to 10^{-2} M and flow times are $\sim 10^{-2}$ sec or longer; hence $R \sim 10^{-7}$ to 10^{-8} M. For aqueous solutions where cell volumes are about 0.1 cm^3 or less only 10^{12} to 10^{13} spins would reach the cell which is the detection limit of most esr spectrometers, while most signals observed correspond to concentrations which are higher by about two orders of magnitude.

In the second case (B), when the reaction is slow and is still proceeding in the cavity, the steady state for R′ for $A_0 \gg B_0$ is given as

$$R_{ss} = \left(\frac{k_3(A_0)(B_0)e^{-k_3A_0t}}{2k_5}\right)^{1/2} \qquad \text{(II)}$$

Under most experimental conditions, where the Ti^{3+}–H_2O_2 reagent was used, $k_3 \sim 10^3$ M^{-1} sec^{-1}, $A_0 \sim 10^{-2}$ M, $B_0 \sim 10^{-3}$ M, $2k_5 \sim 4 \times 10^9$ M^{-1} sec^{-1}, and $t \sim 10^{-2}$ sec. With these values we obtain from eq II $R_{ss}' \sim 1$ μM. (If we were to calculate R' under the above-mentioned conditions, but assume that reactions 3 and 4 are complete immediately after mixing, the concentration of R_{ss}' in the cavity would be $\sim 2.5 \times 10^{-8}$ M.) Equations I and II are valid only if the radical disappears through reactions 5a–c. In case other decay pathways for R· occur, eq I and II give only the upper limit for the concentrations of the radical. One may, however, alter the signal by changing the concentrations of A_0 and B_0 or the observation time, t. The dependence of R as a function of A_0, B_0, and t is given in Figure 1 for the reaction of Ti^{3+} with H_2O_2 in the presence of ROH with $k_3 = 500$ M^{-1} sec^{-1}, $2k_5 = 4 \times 10^9$ M^{-1} sec^{-1}. It is demonstrated in this figure that R has a maximum, and too high or too low $[H_2O_2]$ both decrease the signal. (At too high $[H_2O_2]$ the reaction is over long before the solutions reach the cavity, while at very low $[H_2O_2]$ the reaction is proceeding in the cavity, but with a very low rate of radical production.) The maximal value of R_{ss} increases with $[Ti^{3+}]_0^{1/2}$ but R_{ss} reaches its maximum for various $[Ti^{3+}]_0$ at the same $[H_2O_2]$. At shorter observation times, t_1, the maximal value of R_{ss} increases but is obtained at higher H_2O_2 concentrations.

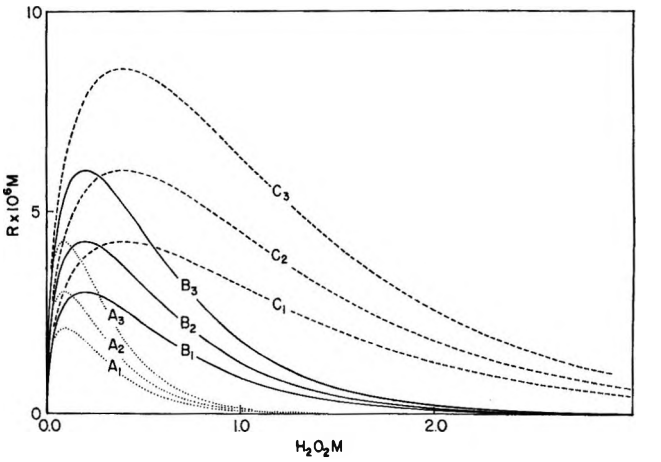

Figure 1. The concentration of R_{ss} as a function of $[H_2O_2]$. The curves are calculated from eq II taking $k_3 = 500$, $k_5 = 2 \times 10^9$ M^{-1} sec^{-1}. In curves A, B, and C, the observation time equals 20, 10, and 5 msec, respectively. The indexes 1–3 represent $[Ti^{3+}]_0$ as 1, 2, and 4 mM, respectively.

Limitations and Optimal Conditions for Esr Studies of Radical Intermediates. In principle the best methods for studying the kinetics and mechanisms of reactions involving free radicals are the pulse methods. The advantage of these methods lies in the fact that the initial radicals can usually be observed on a time scale of microseconds or even shorter, so that their reactions can be followed directly. As applied to esr detection, measurements in the microsecond time scale demand more sophisticated and expensive experimental setups than the steady-state methods and as a result pulse esr experiments are currently being carried out in only a few laboratories.

Pulse radiolysis and flash photolysis experiments can be reasonably readily carried out on the millisecond time scale but most esr studies of radical intermediates have been carried out by steady-state radiolysis, photolysis, or more conventional flow methods. In these cases one is limited by the radical production rates attainable. In the steady-state radiolysis experiments, for example, Eiben and Fessenden[34] obtained radical concentrations at the micromolar level with continuous electron beam currents of ~ 10 μA. At this level the

(34) K. Eiben and R. W. Fessenden, *J. Phys. Chem.*, **75**, 1186 (1971).

mean radical lifetime is of the order of milliseconds. Somewhat higher concentrations, and consequently shorter lifetimes, can be obtained in flow experiments. The principal disadvantages of the steady-state methods are, in certain cases, the uncertainty as to whether or not the radicals observed are those initially formed and the relatively long time scale over which the observation is made. This time scale permits secondary reactions.

In steady-state *in situ* electron radiolysis for any given system, the higher the electron beam current the higher the concentration of R that will be observed.

In the case of photolysis R increases similarly with increasing light intensity, but depends as well on the concentration of the absorbing species. Increasing the OD of the solution does not necessarily increase the signal as the radicals are then formed near the cell walls only and recombine faster. One can show that in the *in situ* photolysis the maximum signal is obtained when the optical density of the irradiated solution is about unity.

In both of the *in situ* methods the irradiated solutions flow through the cavity in order to avoid depletion of solutes or complications arising from accumulation of products. The flow rate has to be such that the flow time of the solution through the cavity is longer than the radical lifetime, otherwise the signals will decrease.

Optimal Conditions for Detecting R in Flow Experiments. In order to find the optimal conditions for the detection of R we will analyze eq II (assuming R decays only through reaction 5a). There are several parameters which can be adjusted experimentally, A_0, B_0, and k_3 (either by changing the pH of the solutions or by using different ligands, or even by replacing B (Fe^{2+}, Ti^{3+}, V^{4+}, Cr^{2+}, etc.)). In addition there are two other parameters, t_1 and t_2 (t_1 is the time it takes for the solution to enter the cavity and t_2 is the time the solution leaves the cavity). The times t_1 and t_2 can be adjusted by changing the flow rate, the time delay, and the cell volume, but in any given experimental arrangement these times are not independent parameters.

For a given cell and flow time the average concentration is given by

$$\bar{R} = \frac{\int_{t_1}^{t_2} R_{ss}\,dt}{\int_{t_1}^{t_2} dt} = \frac{1}{t_2 t_1}\int_{t_1}^{t_2} R_{ss}\,dt \qquad \text{(III)}$$

where

$$R_{ss} = \left(\frac{k_3(A_0)(B_0)e^{-k_3 A_0 t}}{2k_5}\right)^{1/2} \qquad \text{(II)}$$

$$\bar{R} = \frac{1}{t_2 - t_1}\left(\frac{2B_0}{k_3 k_5 A_0}\right)^{1/2} e^{-k_3 A_0 t_1/2} - e^{-k_3 A_0 t_2/2} \qquad \text{(IV)}$$

for given flow conditions (t_1 and t_2) R_{ss} has a maximum for $A_0 = 1/k_3 t$. $\bar{R}$ has a maximum at similar conditions. The dependence of $\bar{R}$ and R_{ss} as a function of $[H_2O_2]$ is given in Figures 2–4. If we define $\bar{t} = (t_1 + t_2)/2$ it is seen in Figures 2–4 that both $\bar{R}$ and R_{ss} reach their maximum at the same $[H_2O_2]$ for any given value of $\bar{t}$. For low values of $\bar{t}$ (Figure 2) the values of $\bar{R}$ and R_{ss} are approximately equal over the entire range of $[H_2O_2]$; this is quite obvious, as under these conditions $\bar{t}$ should be a good average as $\bar{t}$ is small in comparison to the half-life of reaction 3.

At higher values of $\bar{t}$, $\bar{R}$ and R_{ss} differ. This difference is enhanced at higher $[H_2O_2]$, although $\bar{R}$ and R_{ss} are almost equal at their maximum values (Figures 3–4).

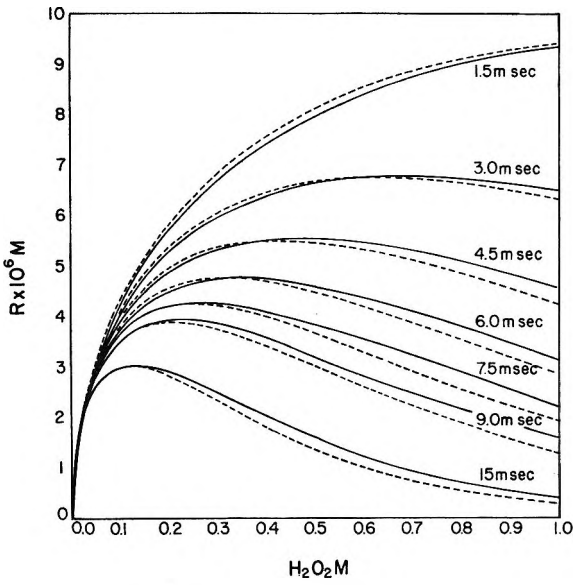

Figure 2. R_{ss} and $\bar{R}$ as a function of H_2O_2. R_{ss} is calculated from eq II (broken lines). $\bar{R}$ is calculated from eq IV (solid lines). Times correspond to t for eq II and $(t_2 + t_1)/2$ for eq IV.

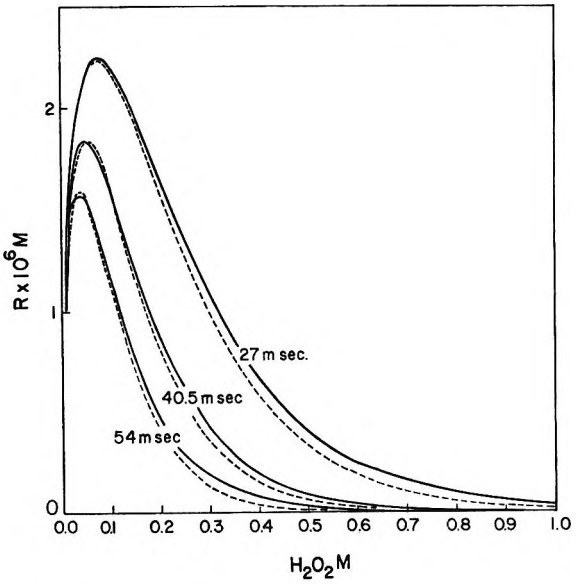

Figure 3. Same as in Figure 2.

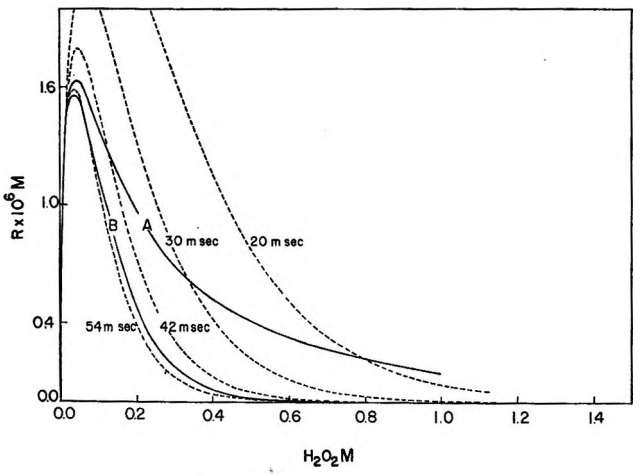

Figure 4. R_{ss} and $\bar{R}$ as a function of H_2O_2. Broken lines are that of R_{ss} for different values of t. The solid lines are for $(t_1 + t_2)/2 = 54$ msec. In curve A, $t_2 = 11t_1 = 99$ msec, and curve B, $t_2 = 2t_1 = 72$ msec.

Figure 4 demonstrates that for a given value of $\bar{t} = 54$ msec, the dependence of $\bar{R}$ on $[H_2O_2]$ depends on t_2/t_1. As long as $t_2/t_1 \leq 2$ (curve A, Figure 4), $\bar{R}$ and R_{ss} have a very similar dependence on $[H_2O_2]$ over the entire range. When $t_2/t_1 = 11$ (curve B, Figure 4) $\bar{R}$ and R_{ss} differ for $[H_2O_2]$ which exceeds that of $\bar{R}_{max}$, and in this case at a high ratio of t_2/t_1 and high $[H_2O_2]$, $\bar{R}$ is very much greater than the values of R_{ss}. It is obvious from eq II and IV that a knowledge of the rate constant, k_3, of the reaction initiating the production of R is essential to plan for the optimal concentration of the radical.

Complications Encountered in Studies with Flow Methods. As indicated above the concentration of radicals one can obtain by the use of flow methods is generally somewhat higher than that obtained through the other methods. This makes it easier to measure accurately the esr spectra of radicals, and therefore for this purpose the flow method is excellent. The only danger in obtaining spectra of radicals in the flow method as well as in the *in situ* photolysis and radiolysis methods lies in the possibility of line broadening due to interactions with the solutes. The line broadening may occur in these methods due to the presence of rather high concentrations of solutes. This is particularly true for the flow methods where rather high concentrations of H_2O_2, Ti^{3+}, and organic solutes are used.

The complications are mainly in the kinetics and mechanisms of the formation and decay of the radicals. The radicals R or R′ are formed either directly by the reaction

$$A + B \longrightarrow R \qquad (3)$$

or in some cases by a secondary reaction (4) of S with the primary radical (R) which is formed in reaction 3. (There are cases where R′ is formed from several fast consecutive steps from the initial radical R.) In order to study the esr spectra of R or R′ one should aim for a maximum value of the concentration of the radical in the cavity. In the case that the lifetime of the radical is long compared with t_1 and t_2 the concentrations A_0 and B_0 should be as high as possible and chosen so that the reaction of A + B is practically complete at times shorter than t_1. If the radical's lifetime is long as compared with t_1 the radical concentration in the cavity will depend on A_0 and B_0 and by varying these concentrations k_3 can be obtained. But generally t_1 is much longer than the lifetimes of free radicals, and therefore no appreciable amount of the radical will reach the cavity provided reaction 3 or 4 is complete immediately after the solutions are mixed. In these cases, in order to observe R, the concentration of A and B should be chosen such that the reaction will still occur in the cavity and the radical will be at a steady state along the flow tube and in the cavity. From eq II, by differentiating R_{ss} with respect to A_0, for a given value of t_1, B_0, k_3, and k_5, it can be shown that the optimal signal will be observed if

$$t_1 = \frac{1}{k_3[A]_0} \text{ (for } [A]_0 > [B]_0) \qquad (V)$$

Recently, we verified this relationship experimentally using different reagents (Ti^{3+}, V^{5+}, Fe^{2+}, Cr^{2+} with H_2O_2) for which k_3 differed.[35,36]

From the above discussion it seems obvious that in order to study reactions of these types under optimal conditions the value of k_3 has to be measured first.

In most of the studies performed using the flow methods, the value of k_3 was unknown and in many cases it is obvious that very small signals were observed due to the poor choice of the concentrations of the reactants. One such example was the failure to observe the HO_2 radical in the Fenton reagent where $H_2O_2 > Fe^{2+}$.[37,38] The reaction of H_2O_2 with Fe^{2+} is very slow ($k_3 \sim 50\ M^{-1}$ sec^{-1}) and as $[H_2O_2]$ and $[Fe^{2+}]$ used were too low $(HO_2)_{ss}$ was below the detection limit. When in this system higher concentrations were used, it was shown that HO_2 is formed from this reagent as expected.[29] The resulting esr spectrum was shown to be identical with that of HO_2 formed by other methods.[16,17,29]

Decay Kinetics of the Radical. If the radical R has a lifetime comparable to t_1 and its formation is complete before the solution reaches the cavity, the decay kinetics of R can be studied. This was done in the case of HO_2[16,17] by the use of the continuous flow method and with HO_2–metal ion complexes with a stopped flow technique.[30,32]

If the mean lifetime of R is much shorter than t_1 the

(35) G. Czapski, A. Samuni, and D. Meisel, submitted for publication in *J. Phys. Chem.*

(36) G. Czapski, A. Samuni, and D. Meisel, unpublished data.

(37) M. S. Bains, J. C. Arthur, and O. Hinojosa, *J. Phys. Chem.*, 72, 2250 (1968).

(38) K. Tabakura and B. Ranby, *ibid.*, 72, 164 (1968).

decay rate cannot be measured by the above-mentioned methods since R reaching the cavity at time t_1 would be too small to be detected. If on the other hand the initial concentrations of A and B are chosen so that reaction 3 is still proceeding in the cavity, then changing t_1 and measuring R as a function of t_1 will not yield the rate of either reaction 4 or 5.

As discussed earlier, for radicals where $k_5 \sim 10^9$ to 10^{10} M^{-1} sec^{-1}, R can be observed only if reactions 3 and 4 are still proceeding in the cavity. In the majority of studies of radicals formed by the $Ti^{3+} + H_2O_2$ or $Fe^{2+} + H_2O_2$ reagents, the radicals were observed as a result of the fact that reactions 3 and 4 were proceeding in the cavity, although generally it was incorrectly assumed in discussing the kinetics that the formation of the radical was complete prior to the entry of the solution into the cavity. In almost all studies with the Ti^{3+}–H_2O_2 system $(Ti^{3+})_0 < (H_2O_2)_0$ and $(H_2O_2)_0 \leq 5 \times 10^{-2}$ M. Observation times (t_1) were of the order of 10^{-2} sec, and concentrations of R observed were generally of the order of 10^{-6} M. Since $k_{Ti^{3+}+H_2O_2} = 500$ M^{-1} sec^{-1} [36] we can calculate $\tau_{1/2}$ of the reaction $Ti^{3+} + H_2O_2$ being not less than 10 msec or roughly equal to t_1. In the case of the Fenton reagent $\tau_{1/2}$ is much longer than t_1. Therefore, it is clear that the assumption of completion of (3) and (4) is incorrect in all of these studies.

It is worthwhile to note that, for the Ti^{3+}–H_2O_2 system generally, the gross rate of formation of R inside the cavity exceeds $\bar{R}_{ss}$ in the cavity.

R_{ss} is given in eq II and we will define $\bar{R}_{ss}$ as R_{ss} at $(t_1 + t_2)/2$. ΔR, the gross rate of formation of R in the cavity between t_1 and t_2, is given by

$$\Delta R = (t_2 - t_1)k_3(Ti^{3+})_0(H_2O_2)_0 e^{-k_3(H_2O_2)_0(t_2-t_1)} \quad \text{(VI)}$$

therefore

$$\frac{\Delta R}{R_{ss}} \sim (t_2 - t_1)2k_5k_3(Ti^{3+})_0(H_2O_2)_0 e^{-k_3(H_2O_2)_0(t_2+t_1)/2} \quad \text{(VII)}$$

or under Sicilio's and Norman and West's experimental conditions where $t_2 \sim 2t_1 \sim 10^{-2}$ sec, $k_5 \sim 2 \times 10^9$, $k_3 = 500$ M^{-1} sec^{-1},[36] and $(Ti^{3+})_0 = 5$–8×10^{-3} M, one finds that as long as $(H_2O_2)_0 < 1.5$ M $\Delta R > \bar{R}_{ss}$. Therefore, most of the radicals observed in the cavity are formed in the cavity.

There are several cases where decay studies of radicals were undertaken and erroneous results obtained.

In early work on the Ti^{3+}–H_2O_2 system the esr spectrum was incorrectly assigned to the OH radical and the resultant apparent decay rate was orders of magnitude too low.[12] In this case the main error lay in the wrong identification of the radical. In more recent studies the recombination rate constants of alcohol radicals were studied.[14,39] In these cases the radical assignment was correct but the apparent rate constants were much too low as compared with previous direct determinations, as well as in one case where the decay appeared to follow an unexpected order.[13] Shiga[39] studied the decay of the alcohol radical where R was generated by the Fenton reagent. The reaction of Fe^{2+} is even slower than that of Ti^{3+} with H_2O_2 and in these experiments less than 5% of the reaction occurred before the solutions reached the cavity. It was found that R decays in the second-order process with $2k_5 = 1.4 \times 10^7$ M^{-1} sec^{-1} [39] (a value which is lower by at least a factor of 100 from values measured directly). In this system R is described by eq II but as $k_3A_0t \ll 1$ eq II can be expanded as a series and $1/R$ will be given by

$$\frac{1}{R} = \frac{1}{R_0} + \left(\frac{k_3k_5(H_2O_2)_0}{2(Fe^{2+})_0}\right)^{1/2} t \quad \text{(VIII)}$$

Thus, under Shiga's experimental conditions an apparent second-order decay is expected. Nevertheless, using various initial $[H_2O_2]$ the decay extrapolates at $t \to 0$ to different initial concentrations of the radical (R_0) in contrast to his own mechanism, as R_0 should in all cases be equal to $(Fe^{2+})_0$.[39] The values of R_0 found[39] depend on $(H_2O_2)_0$ and are lower by at least a factor of 500 from the expected concentration according to his mechanism.

The second-order rate constant, if calculated from eq VIII, is lower by about one order of magnitude than Shiga's measurements. This fact, the apparent dependence of R_0 on $[H_2O_2]$, and the apparent lack of dependence of the decay rate of R on H_2O_2 all could be due to an additional decay mode of R such as in the reaction

$$R\cdot + Fe^{3+} \longrightarrow Fe^{2+} + P \quad (6)$$

Limitations of These Methods in Reaction Mechanism Assignments. It was already mentioned earlier that in this technique, as in the steady-state *in situ* radiation techniques, one may be misled about the mechanism by which the radical is formed. As with all these techniques one may observe secondary radicals only, if the radical primarily formed has a lifetime shorter than $\sim 10^{-4}$ sec. For example, the photolysis of H_2O_2 in solutions of allyl alcohol gave rise only to the two stereo isomers of the $CH_2{=}\dot{C}HCHOH$ radical.[9-11] In other studies in a flow system only the OH adducts $\dot{C}H_2$-$CHOHCH_2OH$ or $CH_2OH\dot{C}HCH_2OH$ were observed.[11] As it turns out the initial reaction of OH with allyl alcohol yields the adduct which then may react with allyl alcohol to abstract an H atom. This mechanism has

$$\begin{matrix} CH_2OH\dot{C}HCH_2OH \\ \text{or} \\ \dot{C}H_2CHOHCH_2OH \end{matrix} + CH_2{=}CHCH_2OH \longrightarrow \begin{matrix} CH_2OHCH_2CH_2OH \\ \text{or} \\ CH_3CHOHCH_2OH \end{matrix} + CH_2{=}\dot{C}HOH$$

(39) T. Shiga, *J. Phys. Chem.*, 69, 3805 (1965).

been proved by the study of the effect of allyl alcohol concentrations on the relative yields of the OH adduct and the radical from which an H atom is abstracted.[11] A similar mechanism may affect the ratio of α and β radicals formed by OH abstraction from alcohols initiated by the Fe^{2+}– or Ti^{3+}–H_2O_2 systems. The β radical may react with the alcohol

$$RCHOH\dot{C}H_2 + RCHOHCH_3 \longrightarrow RCHOHCH_3 + R\dot{C}OHCH_3 \quad (7)$$

and the α radical primarily may react with H_2O_2 initiating a chain reaction by

$$R\dot{C}OHCH_3 + H_2O_2 \longrightarrow RC(=O)CH_3 + H_2O + OH\cdot \quad (8)$$

In flow experiments $\tau_{1/2}$ of the radicals is generally less than 10^{-4} sec. Burchill measured k_7 for ethanol and 2-propanol as 16 and 53 M^{-1} sec^{-1}, respectively, and k_8 for methanol was found to be $\sim 4 \times 10^4$ M^{-1} sec^{-1}. k_8 for 2-propanol may exceed this value by one order of magnitude.[40,41] From these values it can be shown that reaction 7 as well as reaction 8 for very low $[H_2O_2]$ can be ignored. Both of these reactions ((7) and (8)) were shown to occur in the γ radiolysis of solutions of H_2O_2 and alcohols.[40,41] These reactions are less important in flow experiments where the radical concentration is higher by more than two orders of magnitude than in the γ radiolysis studies.

Indirect evidence for a reaction of H_2O_2 with a radical was given by Paul and Fischer in the case of propionic acid radicals.[42] Other examples of how the study of a radical by the flow method may yield incorrect conclusions are the studies on the nature of the Fenton reagent. Shiga[39] observed that the reactivity of ethanol with either the Ti^{3+}–H_2O_2 or Fenton reagent appears to give qualitatively two different radicals. In the first case α abstraction is dominant while β abstraction is the main product observed in the reaction with the Fenton reagent. This led Shiga to assume that the Fenton reagent does not yield OH radical but some "active reagent" (Fe^{4+}?).[39] It is known that Fe^{3+} is reduced very efficiently by α radicals ($CH_3\dot{C}HOH$) but much more slowly by β radicals ($CH_2\dot{C}H_2OH$).[35,43] Ti^{4+} is much slower in its reactions with both the α and β radicals.[35] Norman and West showed that α radicals react faster than β radicals with Ti^{4+} and Fe^{3+}.[33] In solutions of either ethanol or allyl alcohol which were reacting with $H_2O_2Ti^{3+}$, the ratio of CH_2CH_2OH/CH_3CHOH and that of $CH_2CHOHCH_2OH/CH_2OHCHCH_2OH$ increased with increasing concentration of Ti^{4+} or Fe^{3+} ions.[33] Shiga's results are, therefore, interpreted by assuming that in both systems OH is formed which in the reaction with ethanol yields α and β radicals at a ratio of about 6:1 as observed in the Ti^{3+}–H_2O_2 system. In the Fe^{2+}–H_2O_2 system the Fe^{3+} formed reacts preferentially with the α radical and, therefore, apparently it seems that only β radicals are formed.

An extreme example of an improbable mechanism that one can derive by the use of the esr–flow technique is given in the study of Ti^{3+}–H_2O_2 with isopropyl alcohol.[14] In these studies the authors found that the decay of R can be described by a decay order of $^3/_2$, which seems meaningless.[14] A first-order decay of R also gave a satisfactory fit with their experimental results, where the first-order rate constant was, however, found to be proportional to the initial H_2O_2 concentration.[14] This behavior is consistent with the assumption that R is determined by a steady state as given in eq II where k_I, the pseudo-first-order decay rate constant, is given by

$$k_I = \frac{k_3(H_2O_2)}{2} \quad (IX)$$

In these experiments much less than 90% of the reaction occurred prior to the cavity; thus the assumption made by the authors that the reaction is complete is not justified as pointed out by Burchill.[15] Using eq IX, we recalculated k_3 from their results and found $k_3 \sim 700$ M^{-1} sec^{-1} in very good agreement with the measured values of k_3 (500 M^{-1} sec^{-1}).[36]

A further misinterpretation of the mechanism of this system resulted in values of k_{R+R} and $k_{R+H_2O_2}$ which are too low by at least two orders of magnitude; the authors[14] suggested that in the reaction

$$R + H_2O_2 \longrightarrow ROH + \text{"OH"} \quad (8)$$

an unreactive form of OH was produced. This suggestion makes no apparent chemical sense.

James and Sicilio in a very recent publication[44] tried to defend their interpretation and attacked Burchill's criticism[15] of their mechanism. In this publication[14] these authors showed a complete misunderstanding of the kinetic scheme proposed by Burchill.[15] They also ignore the main point. That it was proven that their assumption that the reaction of Ti^{3+} with H_2O_2 is completed long before the solution reaches the cavity is wrong. Their other comment on the difference in the decay rate of R and R′ is in agreement with a mechanism including reactions 6 and 8 followed by reaction 4.

$$R + Ti^{4+} \longrightarrow Ti^{3+} \quad (6)$$

$$R + H_2O_2 \longrightarrow OH + ROH \quad (8)$$

Figures 5 and 6 show the time dependence of R and R' under the experimental conditions of James and Sicilio

(40) C. E. Burchill and I. S. Ginns, *Can. J. Chem.*, **48**, 2628 (1970).
(41) C. E. Burchill and I. S. Ginns, *ibid.*, **48**, 1232 (1970).
(42) H. Paul and H. Fischer, *Z. Naturforsch. A*, **25**, 443 (1970).
(43) G. E. Adams and R. L. Wilson, *Trans. Faraday Soc.*, **65**, 2981 (1969).
(44) R. E. James and F. Sicilio, *J. Phys. Chem.*, **75**, 1326 (1971).

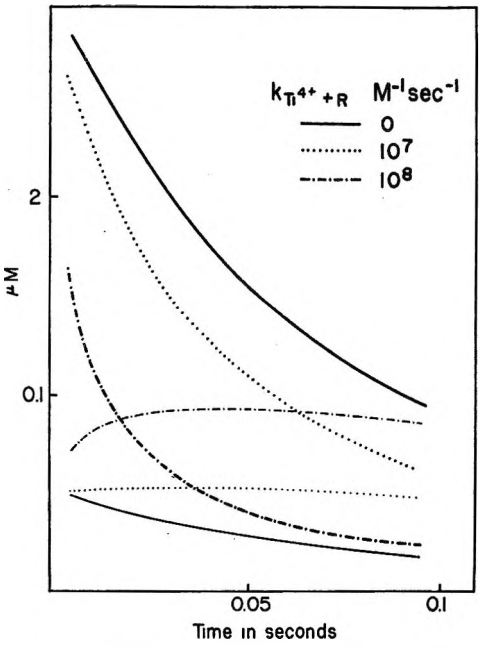

Figure 5. R and R' as a function of time. Heavy lines represent R, light lines R' calculated assuming reactions 3–6 with $k_3 = 500$, $k_{5a} = k_{5b}/2 = k_{5c} = 2 \times 10^9\ M^{-1}\ sec^{-1}$, $k_\alpha/k_\beta = 6$, $[H_2O_2]_0 = 0.05\ M$, $[Ti^{3+}]_0 = 2\ mM$, and $t = 10^{-2}$ sec and various values of k_6: $k_6 = 0.0\ M^{-1}\ sec^{-1}$, ————————; $k_6 = 10^7\ M^{-1}\ sec^{-1}$, ·····; $k_6 = 10^8\ M^{-1}\ sec^{-1}$, —·—·—·—·—.

as calculated from a mechanism including reactions 3–6 and 8 on a σ-5 computer.

As shown in these figures, this mechanism predicts a different decay rate of R and R′ as found in the experiment of James and Sicilio. Both reactions 6 and 8 cause R′ to decay slower than R does and to increase the ratio R'/R.

Norman and West studied the Ti^{3+}–H_2O_2 reaction with various alcohols.[33] In some of their experiments they used a double mixing technique. In a first mixer Ti^{3+} was mixed with an H_2O_2–alcohol solution which was thereafter mixed with a solution of a different alcohol with or without excess of peroxide. The principal advantage of the double mixing technique lies in the possibility of forming a radical and then studying its reactions. In these experiments they observed radicals originating from both alcohols and considered the mechanism of their formation.

Several mechanisms may explain their results. (a) The radical R formed in the first mixer from the first alcohol (RH) is reacting after the second mixer with the second alcohol R′H according to

$$R + R'H \longrightarrow RH + R' \qquad (7)$$

(b) OH radicals are still produced in mixer (2) as some Ti^{3+} escaped reaction with H_2O_2 at this point. If both alcohols are present, OH will compete with RH and R′H forming R and R′. (c) No OH is formed in the cavity from the reaction of residual Ti^{3+} with H_2O_2; but OH is perpetually reformed by the reaction

$$R + H_2O_2 \longrightarrow OH + ROH \qquad (8)$$

and the OH, therefore, in the cavity competes with RH and R′H.

Norman and West conclude from various experiments that R′ is formed only partially through mechanism c, mainly through a and none through b.[33] It is believed that their interpretation is inconsistent with their experiments and we believe that the main source of R′ is mechanism b.

As to mechanism a, k_7 was determined to be $\sim 50\ M^{-1}\ sec^{-1}$; therefore, $\tau_{1/2}$ of reaction 7 in their experiments is about 30 msec and the radicals will disappear in reactions 5a and 5b whose half-life is very much shorter (less than 0.3 msec).

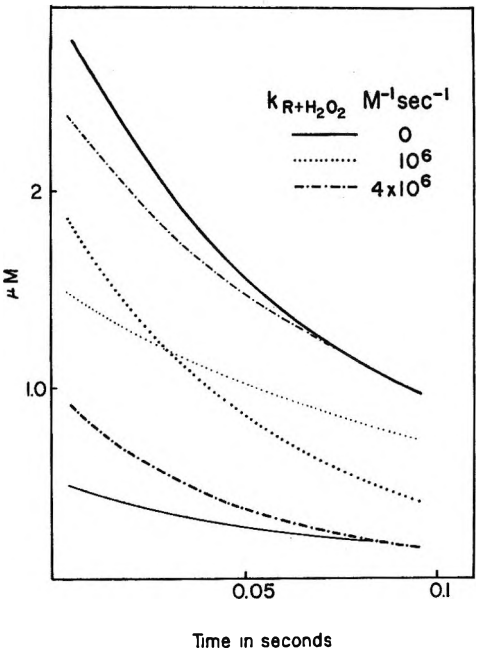

Figure 6. R and R' as a function of time. Heavy lines represent R, light lines R' calculated assuming reactions 3–5 and 8 with $k_3 = 500$, $k_{5a} = k_{5b}/2 = k_{5c} = 2 \times 10^9\ M^{-1}\ sec^{-1}$, $k_\alpha/k_\beta = 6$, $[H_2O_2]_0 = 0.05\ M$, $[Ti^{3+}]_0 = 2\ mM$, and $t = 10^{-2}$ sec and various values of k_8: $k_8 = 0.0\ M^{-1}\ sec^{-1}$; ————————; $k_8 = 10^6\ M^{-1}\ sec^{-1}$, ·····; $k_8 = 4 \times 10^6\ M^{-1}\ sec^{-1}$, —·—·—·—·—.

As to mechanism c we believe that reaction 8 may possibly compete to some extent with (5a) and (5b) at a very high H_2O_2 concentration, but this reaction will not perpetuate the OH in the sense proposed. No R will reach the cavity if the reaction of Ti^{3+} with H_2O_2 is complete at either of the mixers. Therefore, mechanism c is wrong even if reaction 8 plays a role. R· and R′ are found due to the fact that in all the experiments with double mixing the radicals observed in the cavity are formed there. We calculated before and have shown that even at the highest H_2O_2 concentration ($H_2O_2 \sim 0.25\ M$ and $Ti^{3+} = 8 \times 10^{-3}\ M$) in the cavity ($\sim$20 msec after the last mixing) the gross rate of production

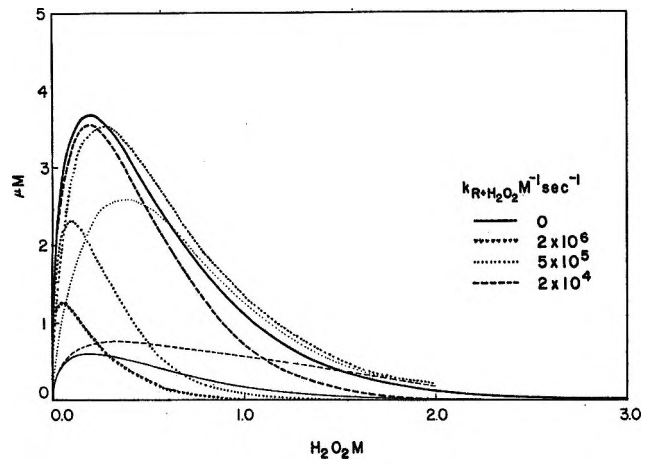

Figure 7. R and R' as a function of H_2O_2. Heavy lines represent R, light lines R' calculated assuming reactions 3–5 and 8 with $k_3 = 500$, $k_{5a} = k_{5b}/2 = k_{5c} = 2 \times 10^9\ M^{-1}\ \text{sec}^{-1}$, $k_\alpha/k_\beta = 6$, $[Ti^{3+}]_0 = 2\ \text{m}M$, and $t = 10^{-2}$ sec and various values of k_8:
$k_8 = 0.0\ M^{-1}\ \text{sec}^{-1}$, ————;
$k_8 = 2 \times 10^4\ M^{-1}\ \text{sec}^{-1}$, – – – – –;
$k_8 = 5 \times 10^5\ M^{-1}\ \text{sec}^{-1}$, · · · · · · · · ·;
$k_8 = 2 \times 10^6\ M^{-1}\ \text{sec}^{-1}$, √ √ √ √ √.

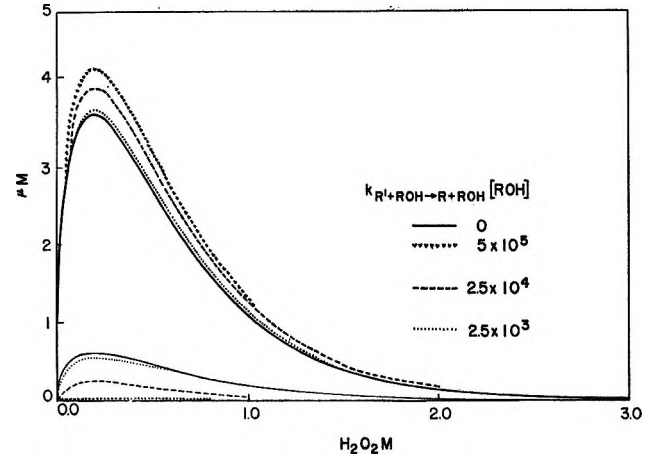

Figure 8. R and R' as a function of H_2O_2. Heavy lines represent R, light lines R' calculated assuming reactions 3–5 and 7 with $k_3 = 500$, $k_{5a} = k_{5b}/2 = k_{5c} = 2 \times 10^9\ M^{-1}\ \text{sec}^{-1}$, $k_\alpha/k_\beta = 6$, $[Ti^{3+}]_0 = 2\ \text{m}M$, and $t = 10^{-2}$ sec and various values of k_7 with ROH = 0.5 M:
$k_7 = 0.0\ M^{-1}\ \text{sec}^{-1}$, ————;
$k_7 = 2.5 \times 10^3\ M^{-1}\ \text{sec}^{-1}$, · · · · · · · · ·;
$k_7 = 2.5 \times 10^4\ M^{-1}\ \text{sec}^{-1}$, – – – – – –;
$k_7 = 5 \times 10^5\ M^{-1}\ \text{sec}^{-1}$, √ √ √ √ √.

of OH through the cavity exceeds the radical concentration.

The effect of H_2O_2 through reaction 8 is only on the ratio of the different radicals. Norman and West pointed out that α radicals react faster with H_2O_2 in reaction 8 than β radicals, therefore the ratio α/β decreases with increasing H_2O_2.[33]

To demonstrate the possible contribution of the different reactions in the 2-propanol–Ti^{3+}–H_2O_2 system

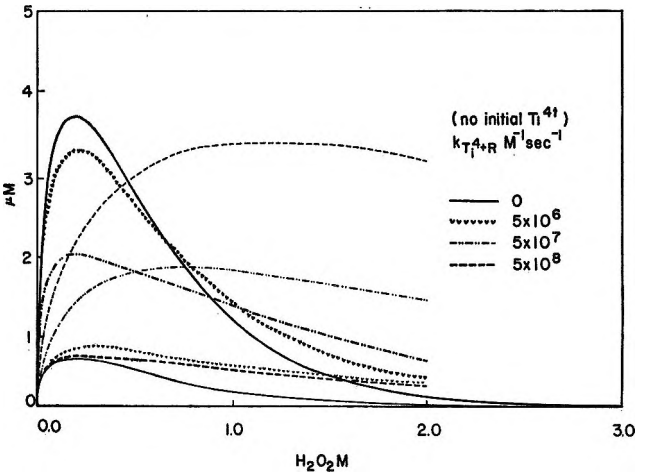

Figure 9. R and R' as a function of H_2O_2. Heavy lines represent R, light lines R' calculated assuming reactions 3-6 with $k_3 = 500$, $k_{5a} = k_{5b}/2 = k_{5c} = 2 \times 10^9\ M^{-1}\ \text{sec}^{-1}$, $k_\alpha/k_\beta = 6$, $[Ti^{3+}]_0 = 2\ \text{m}M$, and $t = 10^{-2}$ sec and various values of k_6 with $[Ti^{4+}]_0 = 0$:
$k_6 = 0.0\ M^{-1}\ \text{sec}^{-1}$, ————;
$k_6 = 5 \times 10^6\ M^{-1}\ \text{sec}^{-1}$, √ √ √ √ √;
$k_6 = 5 \times 10^7\ M^{-1}\ \text{sec}^{-1}$, —· · —· · —· · —;
$k_6 = 5 \times 10^8\ M^{-1}\ \text{sec}^{-1}$, – – – – – –.

we calculated the dependence of R and R' on the different parameters.

The reaction scheme used is

$$Ti^{3+} + H_2O_2 \longrightarrow Ti^{4+} + OH^- + OH \qquad (3)$$

$$OH + RH \xrightarrow{k\alpha} R \qquad OH + RH \xrightarrow{k\beta} R' \qquad (4)$$

Figures 6–8 show the plot of R and R' as a function of H_2O_2 for different values of k_4, k_7, k_8, and $(Ti^{4+})_0$ with $k_1 = 500\ M^{-1}\ \text{sec}^{-1}$, $(Ti^{3+})_0 = 2\text{m}M$, $k_\alpha/k_\beta = 6$, $k_{5a} = 2 \times 10^9$, $k_{5b} = 2 \times 10^9$, and $k_{5c} = 4 \times 10^9\ M^{-1}\ \text{sec}^{-1}$, assuming the time from mixing to the cavity is 10 msec.

$$R + R \longrightarrow \text{products} \qquad (5a)$$

$$R' + R' \longrightarrow \text{products} \qquad (5b)$$

$$R + R' \longrightarrow \text{products} \qquad (5c)$$

$$R + Ti^{4+} \longrightarrow Ti^{3+} \qquad (6)$$

$$R' + RH \longrightarrow RH + R \qquad (7)$$

$$R + H_2O_2 \longrightarrow OH + ROH \qquad (8)$$

These figures were calculated by numerical integration on a σ-5-computer. The figures indicate the following features.

(1) As long as reactions 6–8 are ignored $R/R' = 6$ and both R and R' reach their maxima at $H_2O_2 = 1/k_1t$.

(2) The contribution of reaction 7 is negligible as long as $k_7 < 10^3\ M^{-1}\ \text{sec}^{-1}$, which is 20-fold the experimental

value. When k_7 exceeds $10^4\ M^{-1}\ \sec^{-1}$ the ratio R/R' decreases while [R] + [R'] and the $[H_2O_2]$ where they reach their maximum concentration is not affected.

(3) The effect of reaction 8 is noticeable when $k_8 > 10^4\ M^{-1}\ \sec^{-1}$. As k_8 is increased R/R' decreases and this ratio is dependent on the observation time and on $[H_2O_2]$. For $[H_2O_2] > 0.3\ M$ and $k_8 > 5 \times 10^5$ $[R'] \gg [R]$. Under such conditions R reaches its maximum value at lower $[H_2O_2]$ while R' at higher $[H_2O_2]$. [R] + [R'] is increased as well. The ratio R/R' decreases at longer reaction times.

(4) The reaction of R + Ti^{4+} (Figure 9) has a very similar effect to that of R + H_2O_2. The contribution of this reaction depends on k_4 and $[Ti^{4+}]_0$. In cases where $[Ti^{4+}]_0 = 0$ or $[Ti^{4+}]_0 \ll [Ti^{3+}]_0$ the effect will depend on the observation time, as $[Ti^{4+}]$ is time dependent.

From these calculations it is clear that R' will predominate at high $k_8[H_2O_2]$ and/or at high $k_4[Ti^{4+}]$ values (or $k_4[Fe^{3+}]$ in the case of the Fenton reagent). In Figure 5 under these last conditions R/R' depends also on the observation time.

Conclusions

(1) The flow method seems to have the principal advantage of obtaining high radical concentrations, and therefore it is an excellent method for recording esr spectra of radicals. The method is also capable of producing a large variety of free radicals. (2) In order to obtain optimal esr signals of free radicals produced chemically in a flow system, the rate constant of the chemical reaction producing the radical should be studied first. (3) In these flow experiments in aqueous solutions of short-lived radicals (where recombination constants are of the order of $10^9\ M^{-1}\ \sec^{-1}$) the radical can be observed only if the reaction causing its formation occurs inside the cavity. Therefore, the use of double mixing in such cases is meaningless. (4) Kinetic decay studies of such radicals can easily be misinterpreted and may lead to incorrect results in rate constant values and reaction orders. (5) The method is often unable to determine the exact mechanism of the radical formation, and sometimes only secondary radicals will be observed.

Acknowledgment. We gratefully acknowledge the support of this research by the U. S. Atomic Energy Commission under contracts AT(30-1)-3753 and AT(30-1)-2310 and NIH Contract RR 00292 for the use of the σ-5 computer. I am very grateful to Dr. C. E. Burchill for reading the manuscript and for his comments and suggestions.

The Effect of Coulombic Fields in the Vicinity of Metal Surfaces upon the Entropy and Absolute Rate of Reaction of Absorbed Molecules

by Richard F. Copeland*

Department of Chemistry, The University of Michigan, Ann Arbor, Michigan 48104 *(Received October 27, 1970)*

Publication costs borne completely by The Journal of Physical Chemistry

A statistical-mechanical model of the effect of Coulombic interactions between a metal surface and adsorbed dipolar molecules indicates a significant, and heretofore neglected, change in the entropy and predicted rate of reaction of the adsorbed molecules. Decreases in entropy of 1.38 to 3.32 cal/(mol deg) and increases in the predicted rate of reaction of from two to four orders of magnitude are calculated for a 1 D dipole.

The effect of polarization of molecules in an electric field, treated by Debye as early as 1912,[1] is usually considered to be negligible.[2,3] In most cases the assumption is entirely valid, for the field strength is ordinarily much less than 10^6 V/cm. In some special cases, primarily in heterogeneous catalysis, the Coulombic field strength in the immediate vicinity of the metal surface may be sufficient to have a significant effect upon the entropy and rate of reaction of molecules adsorbed on the surface. Bewig and Zisman[4] have

* Address correspondence to Box 346, Bethune-Cookman College, Daytona Beach, Fla. 32015.

(1) P. Debye, *Phys. Z.*, 13, 97 (1912).

(2) T. L. Hill, "An Introduction to Statistical Thermodynamics," Addison-Wesley, Reading, Mass., 1960, p 209.

(3) G. S. Rushbrooke, "Introduction to Statistical Mechanics," Oxford University Press, London, 1962, p 167.

measured approximate electric field strengths of the order of 9×10^7 V/cm at 2 Å from the surface by studying the polarizability of monomolecular layers of nonpolar organic molecules on tungsten, and Gundry and Tompkins[5] have, through quantum-mechanical models, calculated fields of 1.2×10^8 V/cm in their study of the heat of adsorption of the noble gases on copper surfaces. Both of these approaches lead to reasonably consistent values for the short-range Coulombic field strength, D. Surface fields of the strength reported can, by orientation of adsorbed molecules, lead to a significant change in the entropy and predicted rate of reaction of the adsorbed species.

By using Debye's approach to the effect upon a dipole of an electrostatic field, it can be shown[6] that for one molecule of an ideal gas with a permanent dipole moment μ and polarizability α in an electrostatic field of strength D, the partition function may be written as

$$Q_1(D) = Q_1(0) \frac{\sinh (\mu D/kT)}{\mu D/kT} \exp\left(\frac{\alpha D^2}{2kT}\right) \quad (1)$$

where $Q_1(D)$ and $Q_1(0)$ are the partition functions for one molecule in a field of strength D and in a zero field, respectively. In the immediate vicinity of a surface, the Coulombic field–dipole interaction of an adsorbed molecule may be treated as an electrostatic field–dipole interaction. It follows from this that

$$\ln Q_1(D) = \ln Q_1(0) + \frac{\alpha D^2}{2kT} - \ln\left(\frac{\mu D}{kT}\right) + \ln\left(\sinh \frac{\mu D}{kT}\right) \quad (2)$$

$$\left(\frac{\partial \ln Q_1(D)}{\partial T}\right)_{D,V,N} = \left(\frac{\partial \ln Q_1(0)}{\partial T}\right)_{D,V,N} - \frac{\alpha D^2}{2kT} + \frac{1}{T} - \frac{\mu D}{kT^2} \coth\left(\frac{\mu D}{kT}\right) \quad (3)$$

Nonlocalized Model

If it is assumed that the system can be approximated by an independent, nonlocalized model of N adsorbed dipoles on the surface (a two-dimensional gas or free-layer model), then the partition function of the system can be related to the partition function of one molecule by

$$Q_N = \frac{Q_1{}^N}{N!} \quad (4)$$

and the entropy of the system is given by

$$S = kT\left(\frac{\partial \ln Q_N}{\partial T}\right)_{D,V,N} + k \ln Q_N \quad (5)$$

and, applying Stirling's approximation

$$S = NkT\left(\frac{\partial \ln Q_1}{\partial T}\right)_{D,V,N} + Nk \ln Q_1 - N^2k \ln N + N^2k \quad (6)$$

The difference in entropy ΔS due solely to the effect of the Coulombic field interacting with the dipole will be

$$\Delta S = S(D) - S(0) = Nk\left[1 - \ln\left(\frac{\mu D}{kT}\right) - \frac{\mu D}{kT} \coth\left(\frac{\mu D}{kT}\right) + \ln \sinh\left(\frac{\mu D}{kT}\right)\right] \quad (7)$$

Localized Model

If it is assumed that the system can be approximated by an independent, localized model of N adsorbed dipoles on the surface, then $Q_N = Q_1{}^N$, and

$$\Delta S = Nk\left[-\frac{\mu D}{kT} \coth\left(\frac{\mu D}{kT}\right) - \ln \sinh\left(\frac{\mu D}{kT}\right)\right] \quad (8)$$

The derivation of various thermodynamic functions by Fröhlich,[7] from dielectric theory, is a classical approach to this problem.

Application to Absolute Rate Theory

Application to the theory of absolute rates of reaction can be made through Eyring's equation[8]

$$k' = \varkappa(kT/h)K_c{}^{\ddagger} \quad (9)$$

Assuming a bimolecular reaction of the type $A + A \rightleftharpoons [AA]^{\ddagger} \rightarrow$ products

$$K_c{}^{\ddagger} = \frac{F_{AA}{}^{\ddagger}}{(F_A)^2} \exp(-E_0/RT) \quad (10)$$

where F is the partition function for unit volume for the molecule or activated complex under consideration, and E_0 is the energy of activation for the reaction. Since the deviation under consideration can be described in terms of a reduction in the rotational contribution to the partition function, any effect will be found predominantly in the denominator of the expression for the equilibrium constant $K_c{}^{\ddagger}$. The effect of the Coulombic field is to reduce the entropy of the adsorbed dipoles by orienting them in the direction of the field, thus reducing the rotational part of the partition function, increasing the equilibrium constant for the activated complex, and, thereby, increasing the rate constant of the reaction. This will be offset to some degree by the normally larger dipole moment of the activated complex, but, because of the limited rotational freedom of the activated complex, the contribution of the rotational partition function to $F_{AA}{}^{\ddagger}$ will, most frequently, approach unity.

(4) K. W. Bewig and W. A. Zisman, *J. Phys. Chem.*, **68**, 1804 (1964).

(5) P. M. Gundry and F. C. Tompkins, *Trans. Faraday Soc.*, **56**, 846 (1960).

(6) Reference 3, pp 155–168.

(7) H. Fröhlich, "Theory of Dielectrics: Dielectric Constant and Dielectric Loss," 2nd ed, Clarendon Press, Oxford, 1958, p 9 ff.

(8) S. Glasstone, K. J. Laidler, and H. Eyring, "The Theory of Rate Processes," McGraw-Hill, New York, N. Y., 1941.

Application of this effect toward explanation of some catalytic phenomena is readily apparent. Consider, as an example, an adsorbed gas with a total moment of 1 D = 3.33×10^{-28} C cm at 27° and in a surface field of 9×10^7 V/cm. $(\mu D/KT) = 7.24$, and $Q_1(D) = Q_1(0)(\sinh 7.24/7.24) = 96.4Q_1(0)$, corresponding to a change in entropy of −3.32 cal/(mol deg) for the nonlocalized model, −1.38 cal/(mol deg) for the localized model, and a change of two orders of magnitude in the partition function. This leads to an increase of from 10^2 to 10^4 in the value calculated for the rate constant, provided that the dipole moment of the activated complex is also 1 D and depending on the assumptions made concerning the rotational mobility of the activated complex. Because of residual, though weakened, attractive forces between the surface and the original reacting dipoles, the activated complex will be restricted in its rotational freedom to a substantial degree, and the values expected for the rate constant should be toward the higher end of this range. It may be noted that attempts to apply absolute rate theory to surface reactions[9] have been fairly successful in several cases, but that the rate constants calculated for some, primarily polar, molecules have proved to be lower than the experimental rate constants by several orders of magnitude.[10,11] It is possible that this discrepancy could be accounted for by making a correction for the effect postulated here.

It should be emphasized that the model used for this calculation is grossly oversimplified with respect to the actual situation in heterogeneous catalysis. Further, the magnitude of the surface field D can only be determined indirectly and approximately. This or some equivalent effect should exist to a significant degree, however, in the case of surface reactions of polar molecules.

Acknowledgments. I am indebted to Dr. V. K. Wong of the Department of Physics and to many of my colleagues in the Department of Chemistry at The University of Michigan for their assistance in the formulation of this work.

(9) K. J. Laidler in "Catalysis," P. H. Emmett, Ed., Reinhold, New York, N. Y., 1954, Chapter 5.

(10) A. B. J. Robertson, *J. Colloid Sci.*, 11, 308 (1956).

(11) K. J. Laidler, "Chemical Kinetics," McGraw-Hill, New York, N. Y., 1965, p 292.

Effect of Rapid Homogeneous Reaction on the Diffusion-Limited Lifetime of a Soluble Sphere of Arbitrary Density[1]

by Daniel E. Rosner[2]

Department of Engineering and Applied Science, Yale University, New Haven, Connecticut 06520
(Received November 16, 1970)

Publication costs assisted by the U. S. Air Force Office of Scientific Research

The time required to completely dissolve a stationary sphere can be shortened by deliberate addition of a reactive solute to the solvent. It is shown that if the homogeneous reaction is rapid and the reactants have nearly equal diffusion coefficients with respect to the solvent, then the shortened sphere lifetime is readily obtained analytically from the corresponding sphere lifetime in the absence of homogeneous chemical reaction. This interrelation, valid for spheres of arbitrary density (dense particles, droplets, or bubbles), follows from a fully transient analysis of the resulting nonlinear boundary value problem for constant physical properties. Results are shown to be related to, but more general than, previously obtained lifetime ratios based on quasi-steady and/or sparing solubility approximations. Quantitative criteria are derived to define when the "rapid" reaction condition is satisfied for any particular finite second-order reaction rate constant, and illustrative calculations are included to demonstrate the computational algorithm and its expected domain of validity.

I. Introduction

Knowledge of the total time required to dissolve a motionless sphere (gas bubble, droplet, or particle) in a liquid solvent is necessary in the design of mass transfer equipment and in understanding geophysical and even pharmaceutical phenomena. In ref 3 and 4 the author showed that useful correlation formulas

(1) Supported by the Propulsion and Energy Conversion Division of the U. S. Air Force Office of Scientific Research under Contract F44620-70C-0026.

and lifetime predictions can be obtained for systems in which interfacial solute detachment kinetics and/or long-range solute diffusion limit the rate of dissolution,[5] regardless of the magnitude of the mutual solubility or solute/solvent density ratio. While these and previous[6-8] authors assumed that no further chemical reaction occurs in the solvent enveloping the sphere, it is well known from work in related fields[9-14] that *homogeneous* chemical reactions (acting as a local solute sink) can accelerate diffusion-limited mass transfer rates by steepening the concentration gradient of the dissolving substance in the vicinity of the solute/solvent interface. This raises the important but hitherto unanswered question of how much the total dissolution lifetime t_{life} of a sphere $\mathfrak{A}$ can be shortened by taking advantage of homogeneous chemical reaction with a reactant $\mathfrak{B}$ deliberately added to the surrounding solvent.[15] The purposes of this paper are to (i) show, mathematically, that for the commonly encountered case of nearly equal Fick diffusion coefficients ($D_A \approx D_B = D$) the effect on t_{life} of rapid irreversible homogeneous reaction between $\mathfrak{A}$ and $\mathfrak{B}$ can be predicted exactly in terms of results for the dimensionless nonreactive ("physical" dissolution) lifetime τ_{life} recently given in ref 4 and 5, (ii) present the graphical correlation and construction illustrating the resulting computational algorithm, (iii) briefly discuss the relation between this dissolution problem and analogous problems involving the reactive augmentation of mass transfer rates in the fields of metallurgy,[11] chemical engineering[9,10] and combustion,[12-14] and (iv) clarify the simultaneous conditions required to adequately satisfy the "rapid" homogeneous reaction assumption.

II. Physicochemical Model

With the exception that we now allow homogeneous chemical reaction in solution, our continuum model and nomenclature are identical with those of ref 3 and 4, *viz.* we consider an isolated sphere of pure solute $\mathfrak{A}$, having an initial radius R_0 dissolving into an isothermal, constant property, otherwise quiescent solvent containing reactant $\mathfrak{B}$ but (initially) no $\mathfrak{A}$ (see Figure 1 and the Appendix). The only fluid motion considered is the spherically symmetric *radial* motion induced by the interfacial mass transfer process itself (when the solvent and solute densities are not equal). In the fluid, components $\mathfrak{A}$ and $\mathfrak{B}$ react irreversibly in accord with the effective stoichiometry

$$\mathfrak{A} + \nu'\mathfrak{B} \longrightarrow \text{soluble products} \qquad (1)$$

The reaction is assumed to proceed rapidly enough so that both c_B and $\partial c_B/\partial r$ at the sphere surface ($r = R(t)$) are negligible (see section IV-D below), although, as discussed in section IV, it is not really necessary that the reaction be "instantaneous" (*i.e.*, confined to a sharp reaction "front" of thickness negligible compared to R). Solution properties, including density and temperature, are considered constant, and the presence of reaction products in solution is assumed to have a negligible effect on the equilibrium (saturation) mass fraction $c_{A,sat}$, which therefore remains constant during the dissolution process. Both components are assumed to diffuse in accord with a Fick-type flux law, with the resulting effective diffusion coefficients D_A, D_B being approximately equal[16] to some common value, hereafter written as D. At time $t = 0$ the sphere of pure $\mathfrak{A}$ is confronted with an unbounded constant density solution of

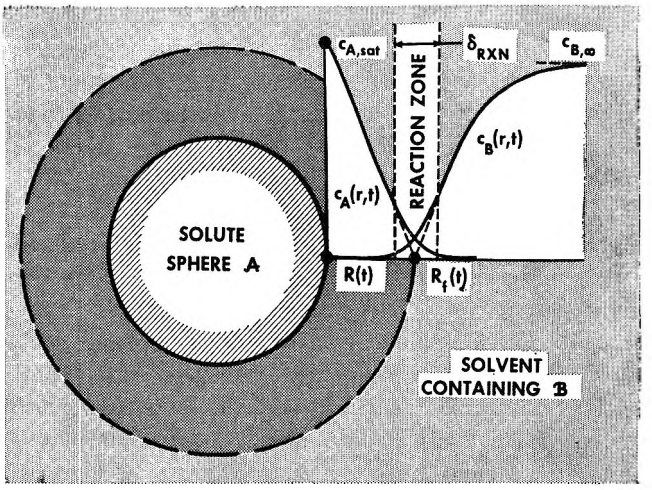

Figure 1. Configuration and notation; diffusion-controlled dissolution of an isolated sphere in the presence of rapid homogeneous chemical reaction.

(2) Associate Professor, Chemical Engineering Group.

(3) D. E. Rosner, *J. Phys. Chem.*, **73**, 382 (1969).

(4) D. E. Rosner and M. Epstein, *ibid.*, **74**, 4001 (1970).

(5) In the latter case, accurate numerical lifetime predictions (using finite difference methods) have just been reported by D. L. Duda and J. S. Vrentas [*Int. J. Heat Mass Transfer*, **14**, 395 (1971)]. To convert their notation into that used in the present work and ref 3 and 4, simply make the replacements $N_a \rightarrow (\rho/\rho_A)\cdot B$, $N_b \rightarrow B$.

(6) P. S. Epstein and M. S. Plesset, *J. Chem. Phys.*, **18**, 1505 (1950).

(7) M. Cable and D. J. Evans, *J. Appl. Phys.*, **38**, 2899 (1967).

(8) See, *e.g.*, (a) E. A. Moelwyn-Hughes, "Physical Chemistry," 2nd rev. ed, Pergamon Press, Oxford, 1964; (b) E. A. Moelwyn-Hughes, "The Kinetics of Reactions in Solutions," 2nd ed, Oxford University Press, London, 1947, p 374 ff.

(9) (a) H. J. Den Hartog and W. J. Beek, *Appl. Sci. Res.*, **19**, 311 (1968); (b) S. K. Friedlander and M. Litt, *ibid., Sect. A*, **8**, 403 (1959); (c) S. K. Friedlander and M. Litt, *Chem. Eng. Sci.*, **7**, 229 (1958).

(10) See, *e.g.*, (a) G. Astarita, "Mass Transfer with Chemical Reaction," Elsevier, Amsterdam, 1967; (b) T. K. Sherwood and R. L. Pigford, "Absorption and Extraction," McGraw-Hill, New York, N. Y., 1952; (c) P. V. Danckwerts, "Gas Liquid Reactions" McGraw-Hill, New York, N. Y., 1970.

(11) E. T. Turkdogan, P. Grieveson, and L. S. Darken, *J. Phys. Chem.*, **67**, 1647 (1963).

(12) D. B. Spalding, *Fuel*, **29**, 25 (1950); *ibid.*, **30**, 121 (1951).

(13) F. A. Williams, in "Combustion Theory," Addison-Wesley, Reading, Mass., 1965.

(14) D. E. Rosner in "Liquid Propellant Rocket Motor Combustion Instability," D. T. Harrje, Ed., NASA Publication, in press, available from the U. S. Government Printing Office, Section 2.4.

(15) Familiar examples would be the accelerated dissolution of (i) solid benzoic acid or cinnamic acid in aqueous solutions containing KOH or NaOH, or (ii) gaseous bubbles of H_2S, HF, CO_2, or NO_2 in aqueous solutions of NaOH, or (iii) gaseous bubbles of Cl_2 in aqueous solutions containing ferrous chloride and hydrogen chloride.

uniform concentration $c_{B,\infty}$. We then consider the fully transient diffusion–convection problem of predicting the elapsed time, t_{life}, at which the sphere radius vanishes. Corresponding quantities in the absence of additive ℬ (purely physical dissolution) will be denoted hereafter by the superscript 0 (*e.g.*, t_{life}^0).

III. Analysis

According to our model, the concentration fields of species 𝒜 and ℬ each satisfy the partial differential equation

$$\frac{\partial c_i}{\partial t} + \frac{R^2}{r^2}\left(1 - \frac{\rho_A}{\rho}\right)\dot{R}\frac{\partial c_i}{\partial r} = \frac{D_i}{r^2}\frac{\partial}{\partial r}\left(r^2\frac{\partial c_i}{\partial r}\right) + \frac{\dot{w}_i'''}{\rho} \tag{2}$$

where i = A or B, and the volumetric "source" terms are locally related (*via* stoichiometry) by the mass ratio condition

$$\nu\dot{w}_A''' = \dot{w}_B''' \tag{3a}$$

where

$$\nu = (m_B/m_A)\nu' \tag{3b}$$

Therefore, regardless of the kinetic dependence of $\dot{w}_A'''$, $\dot{w}_B'''$ on the concentrations c_A, c_B, it follows from eq 2 and 3 that, if $D_A = D_B = D$, the new concentration variable

$$c_E \equiv c_A - \frac{1}{\nu}c_B \tag{4}$$

will satisfy the same "homogeneous" (nonreactive) conservation equation as treated in ref 4 and 5, *viz.*

$$\frac{\partial c_E}{\partial t} + \frac{R^2}{r^2}\left(1 - \frac{\rho_A}{\rho}\right)\dot{R}\frac{\partial c_E}{\partial r} = \frac{D}{r^2}\frac{\partial}{\partial r}\left(r^2\frac{\partial c_E}{\partial r}\right) \tag{5}$$

Moreover, if $c_B(R,t) \approx 0$ and $(\partial c_B/\partial r)_{r=R} \approx 0$ (as would be the case over most of the time interval t_{life} for sufficiently rapid homogeneous kinetics; see section IV-D), then the solute boundary condition (continuity of 𝒜 flux across the interface)

$$\rho_A\dot{R} = \frac{D\rho}{(1 - c_{A,sat})}\cdot\left(\frac{\partial c_A}{\partial r}\right)_{r=R} \tag{6}$$

transforms to

$$\rho_A\dot{R} = \frac{D\rho}{(1 - c_{E,w})}\cdot\left(\frac{\partial c_E}{\partial r}\right)_{r=R} \tag{7}$$

Thus, the new normalized independent variable, Θ_E, defined by

$$\Theta_E \equiv \frac{c_E - c_{E,\infty}}{c_{E,w} - c_{E,\infty}} \tag{8}$$

satisfies the same boundary value problem as already solved in ref 4 and 5, where the quantity

$$B_E \equiv \frac{c_{E,w} - c_{E,\infty}}{1 - c_{E,w}} = \frac{c_{A,sat}}{1 - c_{A,sat}}\cdot\left[1 + \frac{1}{\nu}\frac{c_{B,\infty}}{c_{A,sat}}\right] \tag{9}$$

plays the same role here that the mass transfer driving force parameter

$$B^0 \equiv \frac{c_{A,sat} - c_{A,\infty}}{1 - c_{A,sat}} \tag{10}$$

played in the nonreactive sphere dissolution problem. It follows that *the dimensionless sphere lifetime, τ_{life}, with rapid homogeneous chemical reaction is the same function of B_E and ρ/ρ_A* as $\tau_{life}(B,\rho/\rho_s)$ reported in ref 4 (hereafter rewritten as $\tau_{life}^0(B^0,\rho/\rho_A)$) and $\tau_{life}(N_b,N_a/N_b)$ in ref 5. Using the definition of the dimensionless sphere lifetime, the real time equivalent of this conclusion constitutes one of our desired results, *viz.*

$$\frac{t_{life}}{t_{life}^0} = \frac{\ln(1 + B^0)}{\ln(1 + B_E)}\cdot\frac{\tau_{life}^0(B_E,\rho/\rho_A)}{\tau_{life}^0(B^0,\rho/\rho_A)} \tag{11}$$

which relates the physical and actual lifetimes for a sphere of any initial size R_0 and density ρ_A. Here (since $c_{A,\infty} = 0$) eq 9 reveals

$$B_E = B^0\left[1 + \frac{1}{\nu}\left(\frac{c_{B,\infty}}{c_{A,sat}}\right)\right] \tag{12}$$

and, as indicated above, the function $\tau_{life}^0(B,\rho/\rho_A)$ is identical with that first calculated by Rosner and Epstein [using a moment method (ref 4)] and, more recently by Duda and Vrentas [using a finite difference method (ref 5)]. Alternately, the anticipated sphere lifetime in the presence of homogeneous chemical reaction can be calculated directly from

$$t_{life} = \frac{1}{2}\cdot\frac{R_0^2}{D}\cdot\frac{\rho_A}{\rho}\cdot\frac{1}{\ln(1 + B_E)}\cdot\tau_{life}^0(B_E,\rho/\rho_A) \tag{13}$$

which is seen to approach t_{life}^0 in the limit $c_{B,\infty} \to 0$ (since $B_E \to B^0$ in that limit).

IV. Discussion of Results

A. Magnitude of the Reaction-Induced Reduction in Dissolution Lifetime. Using the notation of ref 3 and 4 but numerical values from ref 5, we have constructed the τ_{life} cross-plot shown in Figure 2 to facilitate calculations of t_{life} using the algorithm 11. Since $B_E \geqslant B^0$ and $(\partial \log \tau_{life}^0/\partial \log B^0)_{\rho/\rho_A=\text{const}} \leqslant 0$ one notes that in general the effect of homogeneous chemical reaction is to shorten the time necessary to completely dissolve the sphere by an amount greater than that anticipated simply from the ratio $\ln(1 + B^0)/\ln(1 + B_E)$. This is readily appreciated by considering the illustrative construction shown in Figure 2, for $\rho/\rho_A = 10^3$. It is clear that the reaction-augmented

(16) Especially for dilute solutions of nondissociating solutes, it is well known that molecules of widely disparate molecular weights and sizes have remarkably similar diffusion coefficients (*cf.* J. H. Perry, Ed., "Chemical Engineers Handbook," McGraw-Hill, New York, N. Y., 4th ed, 1963, pp 14-25, 14-26; and R. C. Reid and T. K. Sherwood, "Properties of Gases and Liquids," McGraw-Hill, New York, N. Y., 1958. An example would be ammonia (M = 17.03) and bromine (M = 159.83) in water, for which the respective values of 10^5D at 25° are 2.0 and 1.3 cm²/sec.

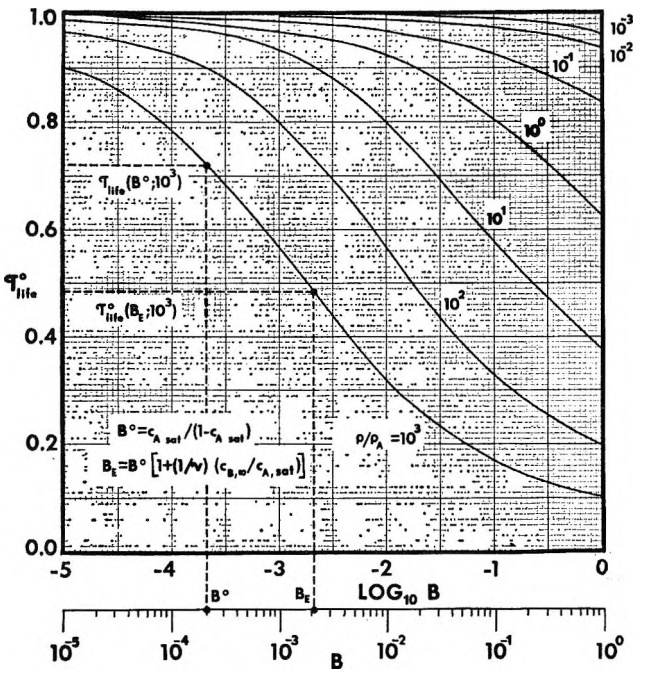

Figure 2. Dimensionless sphere lifetime as a function of solubility parameter and density ratio; effect of homogeneous chemical reaction on the effective value of B.

value of B corresponds to a lower $\tau_{life}^0(B^0,\rho/\rho_A)$, hence t_{life}/t_{life}^0 (eq 11) is smaller than the logarithmic ratio $\ln(1 + B^0)/\ln(1 + B_E)$. Only in the dense sphere limit ($\rho/\rho_A \to 0$) and/or the sparingly soluble limit ($B \to 0$) does t_{life}/t_{life}^0 approach $\ln(1 + B^0)/\ln(1 + B_E)$, and only in the sparingly soluble limit does the inverse lifetime ratio t_{life}^0/t_{life} approximate the familiar[9,10,17] "reaction factor," B_E/B^0, given by

$$F_{RXN} \equiv 1 + \frac{1}{\nu}\cdot\frac{c_{B,\infty}}{c_{A,sat}} \qquad (\text{for } D_A = D_B) \qquad (14)$$

These observations are made to emphasize the fact that eq 11, which results from a fully *transient* analysis of the relevant *nonlinear* boundary value problem for arbitrary B and ρ/ρ_A, is more general than quasi-steady estimates previously found in the droplet mass transfer literature.[9,10,17] As will be illustrated below, the error incurred by simply assuming that the inverse lifetime ratio t_{life}^0/t_{life} is approximately equal to F_{RXN} (eq 14) (*i.e.*, the error of the "quasi-steady" or "invariant field" approximation for a dense sphere and/or a dilute system, with $D_A = D_B$) will depend on the system considered, and will be particularly serious for combinations of density ratio ρ/ρ_A and solubility parameter B^0 such that both τ_{life}^0 and $[\ln(1 + B^0)]/B^0$ are noticeably less than unity.

B. A Numerical Example. To illustrate (i) how the present results are to be applied and (ii) some of their practical implications, we briefly consider a solid–liquid system with properties approximating those of benzoic acid–water.[18] Then, according to the present physicochemical model, the diffusion-controlled dissolution lifetime t_{life}^0 will be reduced by a calculable amount by the deliberate addition of a reactive solute (*e.g.*, sodium hydroxide) to water at, say, 25°. For this case we make the mnemonic identifications $\mathfrak{A} \equiv$ acid and $\mathfrak{B} \equiv$ base, and note that[19,20] $\rho_A \approx 1.266$ g cm^{-3}, $\rho \approx 1$ g cm^{-3}, $B^0 \approx 3.4 \times 10^{-3}$, $D_A \approx 0.94 \times 10^{-5}$ cm^2 sec^{-1} and, from Figure 2[18], $\tau_{life}^0(B^0,\rho/\rho_A) \approx 0.96$. Therefore, in the absence of $\mathfrak{B}$ the limiting form of eq 13 leads to the predicted "physical" lifetimes given in Table I. Now if enough $\mathfrak{B}$ is added to the water to cause $F_{RXN} = 10$, then $B_E = 3.4 \times 10^{-2}$ and, again from Figure 2, $\tau_{life}^0(B_E,\rho/\rho_A) \approx 0.88$. Therefore, applying eq 11, we find that in this case the quasi-steady/dilute system approximation: $t_{life}^0/t_{life} \approx F_{RXN}$ would *underestimate* the effect of adding reactant $\mathfrak{B}$ by some 6.5%. For the present system parameters this systematic error would increase if a more concentrated solution of $\mathfrak{B}$ in water were considered. Moreover, it is clear from inspection of eq 11 and Figure 2 that larger differences between the actual t_{life}^0/t_{life} ratio and F_{RXN} will occur for spheres which (i) are not sparingly soluble, and/or (ii) have densities lower than the surrounding solvent.[21] Thus, for soluble spheres which are not dense compared to the surrounding solvent, eq 11–13 (which take full account of the transient nature of sphere dissolution in systems exhibiting appreciable solubility) must be used to obtain reasonable lifetime predictions in the presence of a reactive additive $\mathfrak{B}$. However, the mathematical and physicochemical approximations underlying eq 11–13 must not be contravened, and in section IV-D we show

(17) In linear, fixed boundary problems with sparing solubility, rapid homogeneous reaction is found to augment local or instantaneous mass transfer rates by the factor F_{RXN} (eq 14) when $D_A = D_B$, a result independent of the nature of the boundary layer hydrodynamics.[9] Most previous analyses of the "reaction factor" deal (implicitly or explicitly) with a hydrodynamic steady flow which is externally imposed, and independent of the mass transfer process itself [see, *e.g.*, R. J. Bronson and R. Wellek, *Chem. Eng. Sci.*, 25, 904 (1970)]. This is not the case in the present sphere dissolution problem, in which the radial convective flow is entirely *caused* by the interfacial mass transfer rate (the latter being itself influenced by homogeneous chemical reaction).

(18) These estimates are not strictly accurate for the benzoic acid–water–sodium hydroxide system since, in the latter case, D_B/D_A is expected to be somewhat greater than unity (Friedlander and Litt[9c] estimate $D_B/D_A \approx 1.8$). Moreover, as will be seen below, the need to graphically interpolate between available exact solutions for $\tau_{life}^0(B,\rho/\rho_A)$ introduces an additional inaccuracy (*cf.* Figure 2) which would be less severe for systems with larger values of ρ/ρ_A and/or larger solubility. However, since our main purpose here is to illustrate the *procedure*, this numerical example should suffice.

(19) C. D. Hodgman and R. C. Weast, Ed., "Handbook of Chemistry and Physics," Chemical Rubber Publishing Co., Cleveland, Ohio; H. Stephen and T. Stephen, Ed., "Solubilities of Inorganic and Organic Compounds," Vol. 1, Part 1, Macmillan, New York, N. Y., 1963, Tables 1447–1449.

(20) E. S. Emanuel and D. R. Olander, *Int. J. Heat Mass Transfer*, 7, 539 (1964).

(21) It can be seen from Figure 2, which summarizes available numerical calculations of τ_{life}, that additional calculations will be required to provide a complete picture of the "bubble" regime, $\rho/\rho_A \gg 1$. Moreover, in the latter regime a logarithmic scale for τ_{life} (Figure 2) would be preferable, or a more suitable lifetime variable should be adopted for the "bubble limit."

Table I: Estimated Physical Dissolution Lifetimes for a Stationary Benzoic Acid Sphere in 25° Water

Initial radius, R_0, cm	Lifetime, t^0_{life}, sec
10^0	1.9×10^7
10^{-1}	1.9×10^6
10^{-2}	1.9×10^3
10^{-3}	1.9×10^1
10^{-4}	1.9×10^{-1}

that for any particular solute–solvent system the required inequalities can be satisfied, provided (i) the relative concentration of ℬ (and, hence, F_{RXN} and t_{life}^{-1}) is not too large, and (ii) the initial sphere size R_0 (and, hence, t_{life}) is not too small.

C. Relation to Droplet Combustion Theory. While the problems of fuel droplet vaporization and "envelope flame" droplet *combustion* are usually discussed in terms of *energy* transport limitations,[12-14] there is a close similarity between these problems and the isothermal dissolution problem treated herein and in ref 4. Indeed, using a quasi-steady model applicable when the droplet density far exceeds that of the surrounding vapor, Spalding[12] and others have shown that the ratio of the "combustion time" to the (physical) "vaporization time" is expressible in terms of a ln $(1 + B)$ ratio, where combustion merely modifies the effective mass transfer driving force parameter B. We now observe that, in the limiting conditions considered by Spalding, $\tau_{life} = 1$ (*cf.* Figure 2) since, as pointed out in ref 3 and 4, regardless of B, $\tau_{life} \to 1$ for $\rho/\rho_A \to 0$. Our present work would therefore indicate that when the droplet and vapor densities became *comparable* (as they do when the prevailing pressure level becomes comparable to the thermodynamic critical pressure of the fuel)[22a] combustion should have a greater effect on the droplet lifetime than that expected from a simple ln $(1 + B)$ ratio[23] since $\tau_{life} < 1$ for systems with appreciable $(\rho/\rho_A)B$.

D. Instantaneous Location of the Reaction Zone and Validity of the Rapid Homogeneous Reaction Assumption. While similar mathematical and physicochemical approximations have been used in treating simpler mass transfer problems in the literature, unfortunately, few authors have discussed the limitations of the rapid homogeneous reaction model in any detail, much less offer convenient quantitative criteria for the expected domain of validity. Yet, despite the complexity of this highly nonlinear boundary value problem, a combination of physical reasoning and relevant results derived from simpler configurations can be invoked, as done below, to derive sufficient conditions for the validity of the present mathematical and physicochemical approximations. As in all problems, it is prudent to keep such conditions in mind to avoid applying the principal results [here given by eq 11–13] outside of their expected domain of validity.

It is interesting to observe that while we are dealing with an important effect of homogeneous chemical reaction on a rate (phase change) process, our results are *independent* of chemical kinetic parameters. However, in obtaining eq 11–13 we have assumed that the homogeneous reaction is sufficiently rapid to prevent ℬ from "penetrating" to the sphere surface over most of the sphere's lifetime. More explicitly, the analysis of section III requires satisfaction of the following three inequalities over most of the time interval t_{life}

$$\frac{1}{\nu}\frac{c_{B,w}}{c_{A,sat}} \ll 1 \tag{15}$$

$$-\frac{1}{\nu}\left(\frac{\partial c_B}{\partial r}\right)_{r=R} \Big/ \left(\frac{\partial c_A}{\partial r}\right)_{r=R} \ll 1 \tag{16}$$

$$1 - (c_{A,w}/c_{A,sat}) \ll 1 \tag{17}$$

together with the implicit assumption that the initial contact of ℬ with the sphere 𝒜 does not irreversibly alter the subsequent solubility of 𝒜. The condition 17 is closely related to that already discussed[24] in ref 3; however, condition 15, and, especially, condition 16 cannot be discussed without reference to the rate of the homogeneous reaction between 𝒜 and ℬ in solution[25] (*i.e.*, for any particular physicochemical problem how rapid is "sufficiently" rapid?). We outline below two distinct approaches to the problem of defining the circumstances under which conditions 15 and 16 are simultaneously valid. The first approach, based on the general asymptotic theory of homogeneous reaction zone structure,[26-28] provides insight into the validity of these inequalities at all times; however, the resulting equations and inequalities are found to be inconvenient to apply. Accordingly, a second approach is introduced and exploited, based instead on the similarity (for small times) between the present problem and the problem of enhanced gas absorption in one-di-

(22) (a) D. E. Rosner, *AIAA J.*, 5, 163 (1967); (b) D. E. Rosner, in preparation.

(23) A quantitative account of the effects of departures from the quasi-steady approximation in the high pressure vaporization and combustion of liquid fuels is beyond the scope of the present paper (see D. E. Rosner and W. S. Chang, in preparation, and ref 22).

(24) An interesting corollary of the finiteness of the interfacial dissolution ("detachment") rate constant is that under no circumstance could t_{life} be reduced to values smaller than the chemically controlled dissolution lifetime $t_{life,chem}$ (see ref 3). Thus, condition 17 would be violated when enough ℬ was added to the solvent to cause t_{life} predicted from eq 11–13 to become of the same order of magnitude as $t_{life,chem}$ (see also section IV-D).

(25) For this reason alone, Danckwerts' criterion for the validity of the "instantaneous" reaction rate limit in gas–liquid absorption (eq 3-33, p 41 in ref 10c) appears to be groundless.

(26) A. Liñan, "On the Structure of Laminar Diffusion Flames," Ph.D. Dissertation, California Institute of Technology, Pasadena, Calif., 1962: available through the Defense Documentation Center as AD 432 882 (June 1963).

(27) S. K. Friedlander and K. H. Keller, *Chem. Eng. Sci.*, 18, 365 (1963).

(28) F. E. Fendell, *ibid.*, 22, 1829 (1967).

mensional semi-infinite liquids, treated earlier by van Krevelen and Hoftijer, and Hikita and Asai (for accounts of this and related work see, *e.g.*, ref 10b and c). While somewhat more restrictive, this second approach leads to explicit, *sufficient* conditions for the accuracy of eq 11–13 which are more straightforward to apply. In either case, for a quantitatively useful definition of what constitutes a "sufficiently rapid" reaction, one must assign to the chemical "source" terms in eq 2 a specific functional form. For the present we choose the second-order, irreversible form

$$\dot{w}_A''' = -m_A k n_A n_B \tag{18}$$

although the arguments below can be readily extended to include other important possibilities.

In pursuing the first approach, we investigate the relative order of magnitude of the terms in eq 2 when the homogeneous reaction rate constant k in eq 18 becomes large, but remains finite. In this asymptotic limit one expects a "reaction zone" (of some nominal thickness δ_{RXN}) to develop within which species $\mathfrak{A}$ and $\mathfrak{B}$ will co-exist (see Figure 1). This zone should be nominally centered around the instantaneous location $R_f(t)$ a sharp "front" would have (in the limit $k \to \infty$).[29] Owing to the definition of Θ_E, the front location would be obtainable from the implicit equation

$$\Theta_E(R_f,t) = \frac{1}{\nu}\left(\frac{c_{B,\infty}}{c_{A,sat}}\right)\left[1 + \frac{1}{\nu}\cdot\frac{c_{B,\infty}}{c_{A,sat}}\right]^{-1} \tag{19}$$

which simply reexpresses the conditions $c_A \to 0$, $c_B \to 0$ applicable at the front in this asymptotic ($k \to \infty$) limit. Following Liñan,[26] and subsequent investigators[27,28] of diffusion flame "structure," an estimate of δ_{RXN} can be obtained by inquiring into the conditions for which the diffusion and reaction terms in eq 2 can be locally in balance, with c_A and c_B approaching the reaction front ($k \to \infty$) concentration distributions only "far" from the front. In this way we estimate

$$\delta_{RXN} = \left\{\left(\frac{\nu' k n_{A,sat}}{4D}\right) \times \left(1 + \frac{1}{\nu}\cdot\frac{c_{B,\infty}}{c_{A,sat}}\right)\left|\frac{\partial\Theta_E}{\partial r}\right|_{r=R_f}\right\}^{-1/3} \tag{20}$$

Accordingly, we conclude that our present solution is self-consistent only when δ_{RXN} calculated from eq 20 satisfies the condition

$$\delta_{RXN} \ll 2(R_f - R) \tag{21}$$

over most of the sphere lifetime, where R_f and R are, respectively, the instantaneous "front" and sphere radii. However, because of the implicit nature of criterion 21, and its dependence on a detailed knowledge of the exact nonreactive solution function $\Theta_E(r,t)$, we turn now to the second approach mentioned above.

In the theory of transient gas absorption into a solvent containing a reactant, numerical methods and analytical approximations (for the case of second-order irreversible reactions in one-dimensional dilute systems with $D_A = D_B$) show that the instantaneous absorption rates approach those for $k \to \infty$ to within a few per cent when (see, *e.g.*, ref 10c)

$$(kn_{B,\infty}t)^{1/2} > 10\left(1 + \frac{1}{\nu}\frac{c_{B,\infty}}{c_{A,sat}}\right) \tag{22}$$

If we define the characteristic reaction time, t_{RXN}, by

$$t_{RXN} \equiv (kn_{B,\infty})^{-1} \tag{23}$$

and demand that the inequality 22 be satisfied for times much less than our predicted sphere lifetime, t_{life}, then, in the present notation, condition 22 will be satisfied if

$$t_{life} \gg 10^2 F_{RXN}{}^2 t_{RXN} \tag{24}$$

However, as applied to the problem of transient *sphere* dissolution, this estimate [based on a planar (one-dimensional) absorption analysis] will be self-consistent in dilute systems only if, when viewed on the scale of R_0, the reaction "front" has not moved far from the initial sphere surface in the time necessary to satisfy condition 22. Since the instantaneous "front" location in the one-dimensional absorption problem[10c] is given by $2\beta t^{1/2}$, where (for $D_A = D_B$) β satisfies the transcendental equation

$$\mathrm{erf}(\beta D^{-1/2}) = F_{RXN}{}^{-1} \tag{25}$$

then, for the sphere dissolution problem, we simultaneously impose the condition

$$R_0 \gg 2\beta t_{RXN}{}^{1/2}(10F_{RXN}) \tag{26}$$

Thus, for systems of limited solubility the explicit conditions 24 and 26 should be *sufficient* to ensure the accuracy of the results of section III.

The implications of these restrictions can be readily demonstrated for a system with parameters comparable to those considered in section IV-B. Suppose $F_{RXN} \approx 10$, $D \approx 10^{-5}$ cm^2 sec^{-1}, and the characteristic reaction time t_{RXN}, defined by eq 23, were of the order of 1 msec. Then condition 24 could only be met for systems with lifetimes in excess of 10 sec. Condition 26 could only be met for spheres with initial radii much larger than about 2×10^{-3} cm. Turning to Table I, and recalling that (for this particular choice of parameters) the reactively reduced lifetimes would be smaller than those tabulated by a factor of about 10, we conclude that, when $t_{RXN} \approx 1$ msec, both criteria would be satisfied for the "NaOH"-induced dissolution of "benzoic acid" spheres of initial radii equal to, or larger than,

(29) The sharp reaction front ("sheet") limit is sometimes known as the Burke–Schumann limit,[14,26] since this asymptotic extreme was first considered by these authors in their now-classical treatment of the shape of atmospheric diffusion flames in cylindrical ducts [see S. P. Burke and T. E. W. Schumann, *Ind. Eng. Chem.*, **20**, No. 10, 998 (1928)].

about 10^{-2} cm. While reliable rate constants are not yet known for many important systems, it is clear that conditions 24 and 26 would be even more readily satisfied for homogeneous bimolecular reactions which were (intrinsically) sufficiently rapid to be more nearly "diffusion-controlled" in the Smoluchowski sense.[8] In that (limiting) case

$$k \longrightarrow 4\pi(r_A + r_B)(D_A + D_B) \qquad (27)$$

where r_A and r_B are the effective molecular radii of species 𝔄 and 𝔅, respectively, and D_A, and D_B are the corresponding Fick diffusion coefficients in the prevailing solvent. For molecular sizes of the order of 10 Å, and diffusion coefficients of the order of 10^{-5} cm^2 sec^{-1}, eq 27 predicts maximum rate constants between 10^{-11} and 10^{-10} $(molecule)^{-1}$ cm^3 sec^{-1}. For a system with parameters similar to those considered in section IV-B, this would correspond to a characteristic reaction time of the order of only 10^{-9} sec (*i.e.*, 1 nsec!). While observed homogeneous rate constants are rarely so large as that given by eq 27 in aqueous solutions, this diffusion-controlled k estimate should be relevant for reactive systems in more viscous solvents.

We conclude this discussion with the observation that for any particular chemical system inequalities 21, 24, 26 become increasingly difficult to satisfy for small initial sphere radius R_0 and/or large F_{RXN} (*i.e.*, large concentrations of reactive additive 𝔅, despite the fact that t_{RXN} decreases as $n_{B,\infty}^{-1}$). Moreover, as pointed out in footnote 24, under no circumstance could t_{life} be reduced to values below the chemically controlled sphere lifetime, $t_{life,chem}$, given by[3]

$$t_{life,chem} = \frac{\rho_A R_0}{k_A'' \rho c_{A,sat}} \qquad (28)$$

where k_A'' is the interfacial (detachment) rate constant for the dissolution of species 𝔄 (see ref 3).

V. Conclusions

We have shown that recently computed dimensionless sphere lifetimes for the "nonreactive" sphere dissolution problem[4,5] can be successfully applied to more complex physicochemical circumstances than those for which they were originally intended, provided the explicit conditions of section IV-D are satisfied. While those cases for which $D_A \neq D_B$ and/or conditions 15–17 are violated over most of the dissolution lifetime will, of course, require further analysis, the present solution to the problem of reaction-enhanced dissolution of soluble spheres with arbitrary density provides a simple, useful, and rather instructive limiting case—and one which is formally *exact* within the confines of the presently adopted physicochemical model (*i.e., free of the restrictive quasi-steady, quasi-stationary, and/or diluteness assumptions*). In subsequent publications[22b,23] we will show that a similar transformation approach can be used to include the effects of nonzero heat of phase change and/or heat of homogeneous reaction on the lifetime of dissolving or evaporating spheres.

Acknowledgment. The writer wishes to thank Dr. J. L. Duda and Dr. J. S. Vrentas (Dow Chemical Co.) for making available their numerical results (ref 5) prior to their publication.

Appendix

Glossary of Symbols

𝔄	Symbol for chemical species from dissolving sphere
𝔅	Symbol for chemical species added to solvent
B^0	Solubility parameter for physical dissolution,[3] eq 10
B_E	Effective driving force parameter for reactive dissolution; eq 9
c_i	Mass fraction of species i (i = A, B)
c_E	Composite mass fraction, eq 4
D	Effective Fick diffusion coefficient in prevailing solvent
F_{RXN}	Reaction factor; eq 14
k	Second-order homogeneous rate constant; eq 18
k_A''	Interfacial dissolution ("detachment") rate constant; eq 28
m_i	Molecular mass (per molecule) of species i, i = A, B
M	Molecular weight (per mole)
n_i	Number density of species i (i = A, B); eq 18
r	Radial coordinate reckoned from sphere center
r_A, r_B	Molecular radii of species 𝔄, 𝔅 in solution; eq 27
R	Instantaneous radius of dissolving sphere
$\dot{R}$	dR/dt
R_f	Reaction "front" radius defined by eq 19
$\dot{w}_i'''$	Mass of species i produced per unit volume and time due to homogeneous chemical reaction; eq 2
t	Time (measured from commencement of dissolution)
t_{RXN}	Characteristic reaction time; eq 23
t_{life}	Total time required to dissolve sphere of initial size R_0
δ_{RXN}	Nominal thickness of homogeneous reaction zone; eq 20
Θ_E	Dimensionless, normalized concentration variable; eq 8
ν	Mass of species 𝔅 combining with unit mass of species 𝔄; eq 3
ν'	Molecules of species 𝔅 combining with one molecule of species 𝔄; eq 1
ρ	Mass density
ρ_A	Mass density of dissolving sphere of solute 𝔄
τ_{life}	Dimensionless sphere lifetime; $2(\rho/\rho_A)(Dt_{life}/R_0^2)$ ln $(1 + B)$ (see ref 3 and 4)
β	Constant satisfying the implicit eq 25

Subscripts

A Pertaining to solute 𝔄
B Pertaining to solute 𝔅
E Pertaining to the reactive combination of 𝔄 and 𝔅
sat Saturated (equilibrium at solute–solution interface)
S Pertaining to pure solute (prior to dissolution; (ref 3 and 4)
0 Evaluated at $t = 0$
∞ Far from sphere surface

Superscripts

0 Pertaining to the absence of homogeneous chemical reaction (*i.e.*, purely "physical" dissolution)

A High-Yield Method for the Preparation of Anomalous Water

by S. B. Brummer,* G. Entine, J. I. Bradspies, H. Lingertat, and C. Leung

Tyco Laboratories, Inc., Bear Hill, Waltham, Massachusetts 02154 *(Received May 13, 1971)*

Publication costs borne completely by The Journal of Physical Chemistry

An experimental method for the preparation of anomalous water and its involatile residue "polywater" in large glass tubes is described. This technique involves the use of flame-tapered Pyrex and quartz tubes. In contrast to previously reported results, *every tube*, up to the largest explored (23-mm i.d.), *successfully produces material*. The material thus prepared has an infrared spectrum similar to that reported for "polywater" and its molecular weight is similar to that reported in the Russian literature. Although the yields are still small (about 0.08 $\mu g/cm^2$ on quartz), the elimination of previously reported erratic behavior suggests that it will be possible to resolve the chemical nature of "polywater" by suitably scaling up the procedure to produce macroscopic quantities of material.

Introduction

Anomalous water is the name given by Fedyakin[1] to the fluid which condenses inside fine capillaries in the presence of undersaturated H_2O vapor. This material has been extensively investigated by Deryagin and his coworkers (see for example ref 2 and 3). From this work it has been shown that anomalous water is a solution of a residue in H_2O. The residue solidifies at $-40°$, distils under vacuum at 300°,[2] has a density of 1.4,[4] and a refractive index of 1.48,[5] and mol wt 180 ± 50,[6] and raises the surface tension of water when dissolved.[7] It decomposes back to water on excessive heating.[2,3,8] Some of these properties have been explored by Western workers and, specifically, the freezing behavior[9-11] and the refractive index,[12,13] have been verified.

In addition, the residue has been chemically analyzed[13-15] and its infrared spectrum has been determined.[13,14,16] In their work on the ir spectrum and the chemical analysis of the residue, Lippincott, *et al.*,[13] found the virtual absence of all significant impurities except for variable amounts of Na (< 0.5%) and obtained a "unique" infrared spectrum. They also reported on the Raman spectrum. From these data they concluded that the residue is a polymer of water, in agreement with conclusions in the Russian literature;[3] they called the material "polywater."

Rousseau and Porto[14] undertook studies similar to

(1) N. N. Fedyakin, *Kolloid Zh.*, 24, 497 (1962).

(2) B. V. Deryagin and N. V. Churaev, paper presented at Lehigh University Conference on "Anomalous Water," June 1970, submitted for publication in *J. Colloid Interface Sci.*

(3) B. V. Deryagin, N. V. Churaev, N. N. Fedyakin, M. V. Talaev, and I. G. Ershova, *Izv. Akad. Nauk SSSR, Ser. Khim.*, 1278 (1967).

(4) B. V. Deryagin, D. S. Lychnikov, K. M. Merzhanov, Ya. I. Rabinovich, and N. V. Churaev, *Dokl. Akad. Nauk SSSR*, 181, 823 (1968).

(5) B. V. Deryagin, Z. M. Zorin, and N. V. Churaev, *ibid.*, 182, 811 (1968).

(6) B. V. Deryagin, B. V. Zhelezny, Ya. I. Rabinovich, V. K. Simonova, M. V. Talaev, and N. V. Churaev, *ibid.*, 190, 372 (1970).

(7) B. V. Deryagin, Z. M. Zorin, V. V. Karasev, V. D. Sobolev, E. N. Khromova, and N. V. Churaev, *ibid.*, 187, 605 (1969).

(8) B. V. Deryagin, Z. M. Zorin, Ya. I. Rabinovich, M. V. Talaev, and N. V. Churaev, *ibid.*, 191, 859 (1970).

(9) E. Willis, G. K. Rennie, C. Smart, and B. A. Pethica, *Nature (London)*, 222, 159 (1969).

(10) S. B. Brummer, F. H. Cocks, G. Entine, and J. I. Bradspies, paper presented at Lehigh University Conference on "Anomalous Water," June 1970, submitted for publication in *J. Colloid Interface Sci.*

(11) B. Fabuss, paper presented at Lehigh University Conference on "Anomalous Water," June 1970, submitted for publication in *J. Colloid Interface Sci.* See also, report on Contract 14-01-0001-2096, R and D Progress Report No. 558, Published by the Office of Saline Water, Department of the Interior.

those of Lippincott, *et al.* They confirmed the infrared spectrum, concluded that the Raman spectrum was in error, and found relatively large concentrations of inorganic salts in their samples. While the latter could not account for the infrared spectrum, it was inferred that "polywater" was unlikely to be a polymer of water. Subsequently,[17] it was suggested that the "unique" infrared spectrum of "polywater" could be duplicated by trivalent formates and acetates. This model was not satisfactory, however, because trivalent ions are not found in the samples[13,14] and because of the difficulty of understanding how these unusual materials could have been introduced into the product. In further work[18,19] it was suggested that the infrared-active component of "polywater" derives from a human sweat aerosol present in laboratory air which deposits on the surface of the glass. The infrared-active component was claimed to be sodium lactate.[18] In support of this hypothesis were analytical data involving electronic spectra and mass spectra.[20] The former showed the presence of carboxylic acid groupings in U. S. prepared material; the latter indicated the presence of phospholipids in USSR prepared material.

This conclusion that "polywater" is a conglomeration of inorganic and infrared-active organic compounds cannot account for all the reported properties of the material, however. For example, the surface tension of anomalous water,[7] its decomposition properties,[8] its volatility,[2,3] and the reported absence of organic material, in some samples,[20] pose problems. In addition, some workers[2,20-22] reported forming the material under organic-free conditions.

It is clear then that a considerable controversy exists over the possible identity of "polywater." The recent report[17] that "poly(heavy water)" has a similar spectrum to "polywater," argues strongly against a polymerized water model. However, positive identification of what appears to be an interesting fluid has not been made. The difficulty in this regard relates to the very low and erratic yields of material which have been reported by the various workers. For example, Willis, *et al.*,[9] reported that 5–10% of their capillaries contained product. Others[14,15] have also reported poor and irreproducible material preparation. The only prior report of substantial material production was by Page, *et al.*,[23] who claimed that milligram-size quantities of "polywater" had been produced in large quartz tubing. Preliminary results with this material indicated, however, that it was highly contaminated, containing up to 12% carbon.

The purpose of the present paper is to describe a preparative method for "polywater" which is successful with large glass tubing (at least up to 23-mm i.d.) and which shows product in 100% of the tubes used. The similarity of this product to previously prepared "polywater" has been demonstrated by infrared spectroscopy and molecular weight determinations. With this preparative method, we believe it will be possible to produce enough material to carry out unequivocal determination of its chemical identity.

Preparation Method

Our previously reported work[10] indicated that two factors are important in stimulating the yield of anomalous water in quartz tubes. On the one hand, a high surface concentration of OH groups is helpful. This probably results from the role of these groups in adsorbing H_2O on quartz (see, for example, ref 24). A more important effect related to the instability of the glass–vapor system. It was shown that the fractional number of capillaries, both quartz and Pyrex, which are productive increases dramatically as temperature instability in the system is increased. More recently,[25] we have shown that the important step is a period of supersaturation during the cycle.

Taking account of these factors, there is a general decrease in erraticism of yield, but the *actual amounts* of material produced are very unsatisfactory (typically, $\ll 0.1$ μg/successful capillary). Correspondingly, we were stimulated to seek alternative methods to enhance the reactivity of the glass surface. The early observation by Fedyakin of "daughter columns" in fine sealed capillaries[1] suggested an approach. Quartz and Pyrex capillaries containing water columns and sealed at both ends were carefully thermostated at 20 ± 0.02°. Daughter columns that grew at the expense of the original columns were found in the Pyrex capillaries but not in the quartz. All Pyrex tubes were successful and the product appeared to originate at the apex of the cone where the capillary had been tapered and sealed. Annealing of these tubes dramatically decreased their effectiveness and this suggested the possible

(12) G. A. Castellion, D. G. Grabar, J. Hession, and H. Burkhard, *Science*, **167**, 865 (1970).

(13) E. R. Lippincott, R. R. Stromberg, W. H. Grant, and G. L. Cessac, *ibid.*, **164**, 1482 (1969).

(14) D. L. Rousseau and S. P. S. Porto, *ibid.*, **167**, 1715 (1970).

(15) S. W. Rabideau and A. E. Florin, *ibid.*, **169**, 48 (1970).

(16) T. F. Page, R. J. Jakobsen, and E. R. Lippincott, *ibid.*, **167**, 51 (1970).

(17) D. L. Rousseau, paper presented at Lehigh University Conference on "Anomalous Water," June 1970, submitted for publication in *J. Colloid Interface Sci.*

(18) R. E. Davis, D. L. Rousseau, and R. O. Board, *Science*, **171**, 167 (1971).

(19) D. L. Rousseau, *ibid.*, **171**, 170 (1971).

(20) A report on the data of V. L. Tal'roz' is given by V. Zhvirblis, *Zhizn Zemli*, **5**, 37 (1969).

(21) V. V. Karasev and Yu. M. Luzhnov, *J. Phys. Chem. (USSR)*, **42**, 2366 (1968).

(22) L. J. Bellamy, private communication.

(23) T. F. Page and R. J. Jakobsen, paper presented at Lehigh University Conference on "Anomalous Water," June 1970, submitted for publication in *J. Colloid Interface Sci.*

(24) M. L. Hair, "Infrared Spectroscopy in Surface Chemistry," Marcel Dekker, New York, N. Y., 1967.

(25) S. B. Brummer and G. Entine, First Semi-Annual Report on Contract DAAHO1-70-C-1006, Nov 1970.

role of strain in the glass in determining its reactivity. Since thicker walled tubes should have more strain, we were encouraged to examine the reactivity of larger tubing, *e.g.*, with 5-mm i.d. Once again all Pyrex tubes were found to give a product. Subsequent experiments with large quartz tubes showed that they too almost invariably yield a product.

The following are experimental procedures used in subsequent preparative work. Glassware was washed in chromic acid and then in quadruply distilled water (once from alkaline permanganate). A small amount of high-vacuum Apiezon grease was used on stopcocks, etc., but, where possible, gaskets (*e.g.*, of silicone rubber) were employed. Preparative tubes were maintained out of contact with the surfaces of the containing glassware. Reduced pressure was applied to the preparative systems with a "roughing" oil pump *via* cold traps. Other procedures were as described earlier.[10]

The glass tubing used for material production was treated as follows. The tubing was boiled in concentrated HNO_3 (electronic grade from Lehigh Valley Chemical Co.) for 4 hr. Then, care being taken to avoid handling, it was boiled six times in aliquots of distilled water. The tubing was vacuum dried at room temperature and then sealed at one end using an oxidizing propane–air flame. The inside of the tubing was not exposed to the flame. As a result of this procedure, glass tubes with a tapered sealed cone at one end were produced. Typically they were 7–12 cm long with a tapered region of ~1.5 cm.

For sample preparation, the tubes were exposed to water vapor in an evacuated desiccator for 2 days. It was found necessary occasionally to stimulate the process by causing the temperature of the room to fluctuate. Mostly, though, the normal diurnal day–night fluctuation in room temperature (±3°) was sufficient for the process to occur. The production of material is much less sensitive to ambient conditions than in capillaries;[10,25] a single supersaturation appears to be adequate to stimulate it.

Figure 1 shows a typical tube (6-mm i.d.) containing "wet" product, *i.e.*, at high humidity. It is to be noticed that material forms in the region of the cone but not on the body of the tube.[26] The tube was covered with plastic (parafilm) and the liquid centrifuged to the bottom of the cone. The liquid was removed from the cones with a micropipet and, typically, the product was collected in one cone for storage before use.

Yields of residue were estimated by collecting the liquid in a fine capillary and desiccating it. The latter was accomplished by storage over P_2O_5 for from 2 to 4 days, followed by evacuation for 4 hr. A density of 1.4 was used to estimate the mass of product.[4]

Typically ~0.08 $\mu g/cm^2$ of residue was formed in a quartz cone with 5-mm i.d. Using a molecular weight of 200 (see below), this corresponds to ~4 × 10^{-10} mol/cm^2, *i.e.*, ~1 molecule of product per 5 surface sites. With a large molecule, this could correspond to a monolayer, although it is not likely in the present case since, as Figure 1 shows, the product was not uniformly distributed over the surface. It may be then that there are local centers of activity rather than general surface reactivity. Yields were somewhat lower with larger tubing (~0.02 $\mu g/cm^2$ with 15-mm and 23-mm tubing).

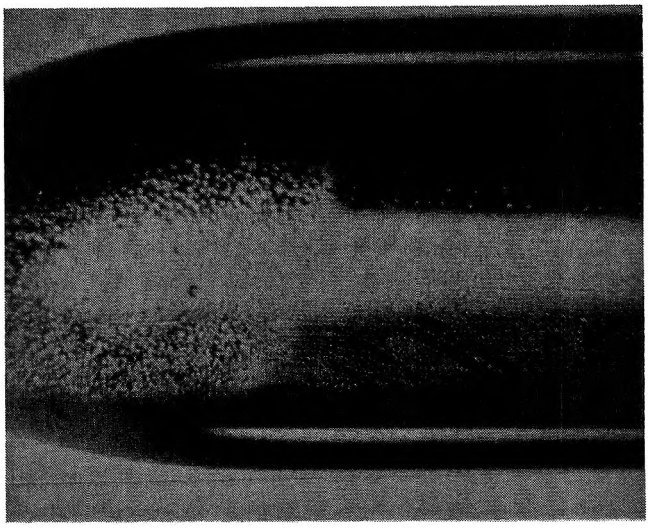

Figure 1. A 6-mm Pyrex cone after exposure to 100% relative humidity. Note patterned condensation.

Heating the tubes after preparation decreased their subsequent reactivity. For example, in one experiment with sets of five 10-mm quartz cones, the yields were 0.39, 0.11, 0.05, and 0.005 μg/cone of residue in the as-pulled and in the as-pulled plus heating to 700, 900 and 1100°, respectively. Interestingly, flaming the body of the tube to near-melting temperatures led to condensation in the flamed region on exposure to high humidity. However, the yield was very low, at least an order of magnitude worse than on the cone region itself. This result seems to suggest that some of the positive effect of the cone formation on yield relates to melting and *pulling* the glass.

Yields were systematically better in Pyrex cones than in quartz cones. For example, in one experiment with 15-mm cones, about five times the amount of material was extracted from Pyrex than from quartz. Typically, 0.3 μg of product was obtained per 1 cm^2 of Pyrex cone. Again, the active area was substantially located around the tapered flame-worked region. On successive exposures of Pyrex cones to water vapor, the yield was invariably lower than on the first exposure. For example in one experiment with 15-mm cones the yield decreased from 0.30 $\mu g/cm^2$ on the first

(26) The previous report of polywater production in large tubes[23] did not contain enough experimental detail to ascertain the relation of the technique to the present method. Our results indicate that the tapered cone of a tube is to be preferred to the body of the tube, whose use was indicated in ref 23.

exposure to 0.10, 0.09, 0.06, and 0.10 $\mu g/cm^2$ on subsequent exposures. These results indicate that after the first exposure there is a lower activity of the surface, but thereafter it seems to remain fairly constant. As will appear, the infrared spectrum of the Pyrex product is somewhat different from that of the quartz product and it may be that the higher yields in Pyrex, to some extent, reflect leaching of material from the glass. The clarity of the spectra indicates that we do have more product with Pyrex than quartz, however.

When the tip of the Pyrex cone was reflamed, product yield was intermediate between the as-drawn condition and the multiple exposure situation, *i.e.*, about 0.2 $\mu g/cm^2$. Annealing Pyrex was highly deleterious to its activity. For example, as we have previously reported,[10] very high percentage yields of material can be obtained in fine Pyrex capillaries under fluctuating environment conditions. These same capillaries give no yield after they have been subjected to a normal glassblower's anneal cycle. Pyrex cones still retain some activity after annealing, but it is grossly attenuated. These observations suggest the possible role of flame-induced strain or compositional changes in determining the activity of the glass.

With quartz tubes, successive exposures indicated some condensation of water on the cones, but after about four exposures the quantity of condensation was quite small. Our conclusion is that quartz is not indefinitely active. Reflaming the quartz, as with the Pyrex, somewhat restored its activity.

Verification of Identity of Product

Overtly, the material appears similar to that described elsewhere. It is a viscous fluid, usually colorless but some desiccated samples are pale yellow under reflected light. Two experiments have been performed to verify that the material is similar to that described elsewhere. These involve determination of its infrared spectrum and of its molecular weight.

The infrared spectrum was determined on a Perkin-Elmer spectrometer, Type 457. Two experimental techniques were employed. In early work, efforts were made to use internal reflectance spectrometer methods following Harrick.[27,28] For this purpose a wet sample was spread on the surfaces of a germanium multireflectance crystal covered with alumina powder.[28] The latter was used to assist spreading; in practice a glass cover slip on top of the sample was found to be more helpful. The technique for our rather viscous samples was difficult to employ and led to poor quality spectra. An example of the infrared spectrum of a quartz-grown sample is shown in Figure 2. The significant features are the singlet band at about 1600 cm^{-1} and the weaker doublet just below 1400 cm^{-1}. These agree very well with the previously reported spectrum of "polywater."[13,14,16] The large band at around 1000 cm^{-1} resulted from a reaction of the germanium with water vapor.

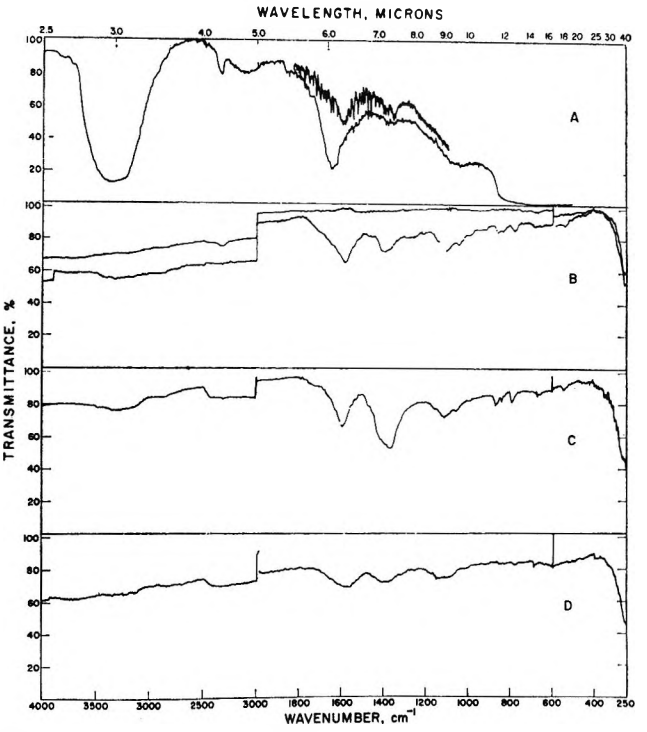

Figure 2. Infrared spectra: A, spectrum obtained using internal reflection for "polywater" in presence of water (lower curve) and in absence of water (upper curve); B, quartz-grown "polywater" and background using 4X beam condenser; C, Pyrex-grown "polywater"; D, quartz-grown "polywater" after being heated at 300° for 23 hr in air.

Because of the difficulty of spreading the sample and the poor quality of the resulting spectrum, further studies were carried out using transmission. For this purpose a 4X beam condenser was employed, and the sample, on a AgBr plate, was masked to increase sensitivity. Typical spectra for dried Pyrex- and quartz-grown samples are shown in Figure 2 (curves B and C). The spectrum of the quartz-grown material is similar to curve A, obtained by internal reflectance, and to that reported elsewhere. There is an additional peak at around 1100 cm^{-1} which has also been reported previously but variously attributed to a SO_4^{2-} impurity. The Pyrex sample shows the same peaks but the heights of the higher frequency bands are inverted. The substantial similarity of this material is evident, however. These spectra decreased somewhat on heating for 24 hr in air at 350° (see for example, curve D of Figure 2). The indication was that the 1100-cm^{-1} band was relatively more stable than the other bands. The general high thermal stability of the material, as evidenced here, is in good agreement with previous reports.[2,3,8,13]

(27) N. J. Harrick, "Internal Reflection Spectroscopy," Interscience, New York, N. Y., 1967.

(28) N. J. Harrick, *Anal. Chem.*, **40**, 1755 (1968).

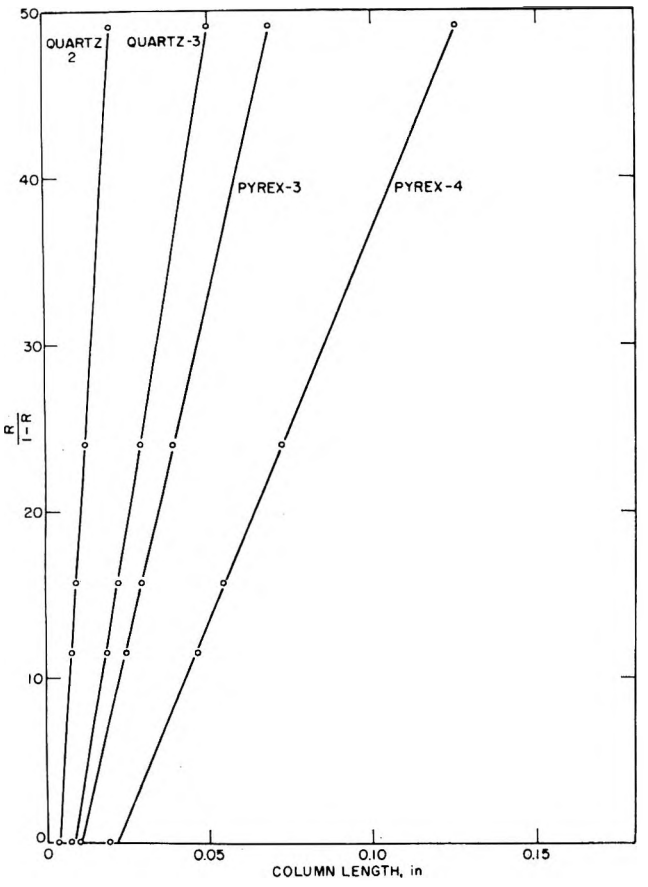

Figure 3. Relationship between column length and relative humidity, used for Raoult's law determination of molecular weight.

The above spectra indicate fairly clearly that the material of interest is similar to the "polywater" of workers in this country. However, the Russian material has not been infrared-analyzed and some experimental point of contact with their work seemed appropriate. Correspondingly, the molecular weight of the material was determined. For this purpose samples were drawn into fine capillaries, typically about 80 μm in diameter, and, after desiccation, they were exposed to the vapors of aqueous salt solutions of known activity.[29] Then, after appropriate equilibration, the volume concentration of anomalous water with the same water activity as the standard salt solution could be determined. Evacuated samples were typically 0.006 in. long and, on exposure to salt solutions, they were typically 0.018 in. and 0.050 in. at 92 and 98% relative humidity (R). The precision of measurement was 2×10^{-4} in. Reproducibility of the evacuated length l_0 and of the exposed length l at any humidity was within this limit.

Molecular weights were determined from the formula

$$\text{molecular weight} = 25.2\left(\frac{R}{1-R}\right)\left(\frac{l_0}{l-l_0}\right)$$

This equation, based on Raoult's law, assumes that the density of the residue is 1.4[4] and that the density of the solution varies linearly with volume fraction. A plot of Raoult's law is shown in Figure 3 for two quartz-grown and two Pyrex-grown samples. Excellent linearity is obtained, indicating the validity of the assumptions. In all, four quartz-grown samples and four Pyrex-grown samples were studied. The molecular weights found from the slopes of the Raoult's law plot were 205, 235, 257, and 227 for the quartz-grown samples and 149, 165, 190, and 228 for Pyrex-grown material. The mean values were 231 ± 21 and 183 ± 35.

The l_0 values extrapolated from eq 1 were typically ~10% greater than the values observed directly. This difference is substantially contributed by meniscus errors. Using the observed values of l_0, the molecular weight appears to increase by ~10% over the range 92–98% humidity. At 96% humidity, which is suitable for comparison with previous work,[6] we obtain 193 ± 25 and 166 ± 45 for quartz- and Pyrex-grown material, respectively. These are in excellent agreement with the Russian data (180 ± 50),[6,30] indicating that we are dealing with the same material.

Summary and Conclusions

The present data indicate that the erratic nature of the "polywater" phenomenon may be overcome by use of large flamed and sealed glass tubes. Both Pyrex and quartz appear to yield products which, on the basis of both their infrared spectra and their molecular weights, appear to be similar to material elsewhere identified as "polywater." It is anticipated that using this technique it will be possible to resolve the chemical nature of the material.

Acknowledgments. We are pleased to acknowledge support of this work by the Advanced Research Agency of the Department of Defense (ARPA) and by the Office of Saline Water, Department of the Interior (OSW). The preparative work and some of the exploratory infrared work was carried out under ARPA support (Contract DAAH01-70-C-1006). The bulk of the infrared studies and the molecular weight determinations were carried out under OSW support (Contract 14-01-0001-2259). We are also pleased to acknowledge the contribution of Dr. F. H. Cocks, who suggested the "daughter column" experiment. We thank Dr. James N. Butler for a number of helpful discussions concerning the molecular weight determinations.

(29) R. A. Robinson and R. H. Stokes, "Electrolyte Solutions," 3rd ed, Butterworths, London, 1965.

(30) M. V. Talaev and N. V. Churaev, *Dokl. Akad. Nauk SSSR*, **189**, 1282 (1969).

Determination of Magnetic Moments of Paramagnetic Ions in Microgram Quantities Using Ion-Exchange Resins

by Toshio Ikeda,* Sumio Ōe, and Kazuaki Yamanari

Department of Chemistry, Shizuoka University, Shizuoka, Japan *(Received September 9, 1970)*

Publication costs borne completely by The Journal of Physical Chemistry

A modified Faraday method which makes use of ion-exchange resins is reported for determining the magnetic moments of very small quantities of paramagnetic ions. The critical strength of the magnetic attraction required to suspend a resin bead in a liquid in a magnetic field was measured and was found, as expected from the theory, to be directly related to the magnetic susceptibility of the resin, characteristic of the nature of the ions adsorbed but independent of the size of the resin beads. The susceptibilities of the paramagnetic ions adsorbed on the resin beads were estimated from the measured susceptibilities of the resin beads by the aid of Wiedemann's additivity law, taking nickel(II) ions as a reference. The direct experimental test of the present method using the first-row transition group elements has proved that the method is useful for determining magnetic moments even when these ions are available only in microgram quantities.

Principle

When a bead of an ion-exchange resin, saturated with paramagnetic cations in order to display paramagnetism, is placed in an inhomogeneous magnetic field in an appropriate liquid having a density slightly lower than that of the resin, the resin bead is expected to be suspended at a position corresponding to maximum attraction of the field. In this case, there is a certain critical magnetic force which just balances the gravitational force acting on the resin bead. This condition may be expressed by

$$(\rho - \rho_0)gv = \int_v (\kappa - \kappa_0)H\left(\frac{dH}{dx}\right)dv \qquad (1)$$

where ρ and κ are the density and the volume magnetic susceptibility, respectively, of the bead of paramagnetic resin; ρ_0 and κ_0 are the similar quantities for the liquid, for example, water, in which the resin bead is suspended; g is the gravitational constant; dv is the volume element of the resin bead; H and (dH/dx) are, respectively, the strength of the magnetic field and its gradient at a point on the x axis, where the x axis is assigned to the vertical line passing through the center of the pole gap of the magnet, perpendicular to the axis of the pole pieces (Figure 1). Here, integration is restricted within v, the space occupied by the resin bead in the critical region of the field. When the resin bead is so small that both H and (dH/dx) can be taken as constants within the space v, then integration of eq 1 gives

$$\kappa = \kappa_0 + (\rho - \rho_0)g/\left(H\frac{dH}{dx}\right)_c \qquad (2)$$

where $[H(dH/dx)]_c$ is the critical strength of the maximum magnetic attraction for suspending a resin bead in a liquid medium in the field. Since ρ, ρ_0, and $[H(dH/dx)]_c$ are measurable, the mass magnetic susceptibility, χ, of the paramagnetic resin bead can be calculated from eq 2, taking water or some other convenient solvent with known susceptibility as a standard substance and using the defined relation $\kappa = \rho\chi$.

When Wiedemann's additivity law is applied, the paramagnetic susceptibility of an ion-exchange resin in the form MR may be expressed as

$$\left.\begin{aligned} \chi &= f_M\chi_M + f_R\chi_R \\ f_M &+ f_R = 1 \end{aligned}\right\} \qquad (3)$$

where f_M is the weight fraction of a paramagnetic ion species M with the mass magnetic susceptibility χ_M, and f_R is that of the resin residue R (including water of swelling) with the mass magnetic susceptibility χ_R.

When the exchange capacity of the fully swollen, ion-exchange resin in the H form is Q equivalents per gram, the masses of the hydrogen ions and the resin residue R (including water of swelling) may be assigned at QH and $(1 - QH)$ grams per gram of resin, respectively, where H denotes the atomic weight of hydrogen. If the change in the water content of the resin due to ion exchange is negligible, one may write

$$\left.\begin{aligned} f_M &= \frac{QM/z}{1 - QH + QM/z} \\ f_R &= \frac{1 - QH}{1 - QH + QM/z} \end{aligned}\right\} \qquad (4)^1$$

for a resin of the type MR, where z and M are the ionic valency and the atomic weight of an ion species M, respectively. When χ_R in eq 3 is once determined,

(1) Since Q is usually insignificant compared with unity, QH may be omitted from eq 4 for the first approximation.

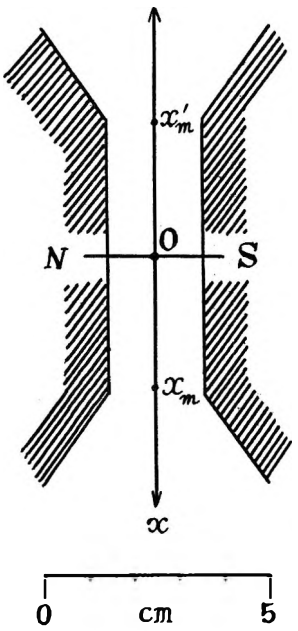

Figure 1.

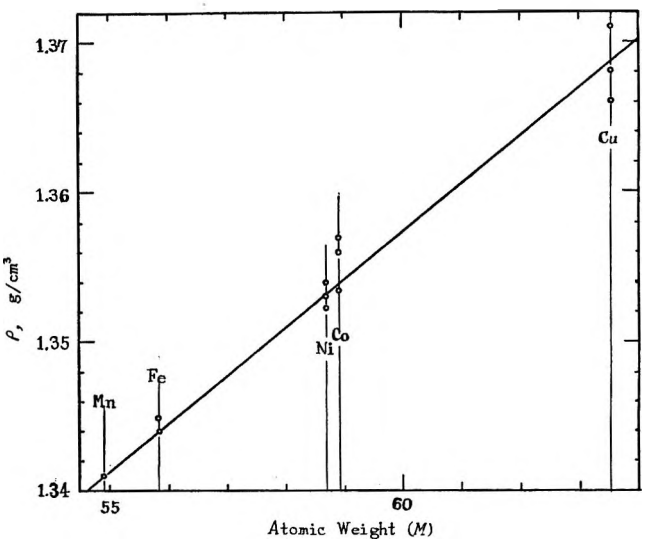

Figure 2. Relation between the densities of fully swollen resin beads and the atomic weights of cations adsorbed.

χ_M can be calculated from the observed susceptibility of the resin in the form MR.

Experimental Section

Material. All chemicals used were Guaranteed reagent grade obtained from Wakō Pure Chemical Industries, Ltd. Oxygen-free distilled water was used throughout the experiments. A new type of Amberlite IR-120B cation-exchange resin (polystyrenesulfonate) in the Na form was graded with sieves roughly into three sizes: L (~1 mm), M (~0.7 mm), and S (~0.4 mm) in diameter. The bead diameter was measured with a micrometer gauge if necessary. The resin was conditioned by several cycles of exchange between the Na and H forms, accompanied by washes with distilled water. It was then stored in the H form in water for ready use. The H-form resin was converted into the paramagnetic form by ion-exchanging paramagnetic cations to saturation from aqueous 0.1 *M* solutions of salts (chlorides or sulfates) of the transition group elements, using the column process. In the case of ferrous ion exchange, a 0.1 *M* solution of ferrous sulfate in 0.01 *N* sulfuric acid with 0.05% glucose added was used in order that the ferrous ions were not oxidized or hydrolyzed.

Measurements of the Physicochemical Properties of Fully Swollen Resin Beads. In the present method, the density of the fully swollen ion-exchange resin in equilibrium with water must be known; it is very difficult to measure this quantity, however, when the resin is in water. To approach the true value as closely as possible, the weight of the resin was measured under such conditions that the resin beads, removed from the bulk of water, were dry on their surface while being fully swollen inside as they were in water. In practice, external water was removed from the surface of the fully swollen resin beads by mopping with filter papers for about 1 min. The resin beads were then weighed in the open for about 20 min at appropriate intervals. A linear relation was found between the weight of resin and the time, and the weight extrapolated to time zero was taken as representing the true weight of the fully swollen resin beads in a state of equilibrium with water. This is the standard weighing of the fully swollen resins adopted in the present study.

Densities of the fully swollen resin beads in the form MR (M = Mn^{2+}, Fe^{2+}, Co^{2+}, Ni^{2+}, and Cu^{2+}) were measured by the pycnometric method, using about 1 g of resin (Table II). They were found to be expressed roughly in a linear relation with regard to the atomic weights of cations adsorbed, namely, $\rho = 1.165 + 0.00321M$ (Figure 2). Of course, the relation may be different for other resins having different exchange capacities. A rough value of the density of a resin may be estimated by this linear relation when direct measurement of the density of the resin beads is difficult for some technical reasons, particularly in such a case when only a very small quantity of ion sample is available for ion exchange and hence only a few beads are available for measuring the density.

The ion-exchange capacity of a resin in the H form was determined by titration of the acid eluted from the resin by a 1 *M* aqueous solution of calcium chloride. The exchange capacity of the Amberlite IR-120B used in the present study was found to be 2.596 mequiv g^{-1} of fully swollen H form resin.

Apparatus. The experimental apparatus used is shown in Figure 3. A glass capillary C having an inner diameter of 1.5–2.0 mm is dipped vertically (along the *x* axis) into a convenient liquid (usually water) contained in test tube B so that its lower end nearly reaches the bottom of B. A rubber bulb was attached

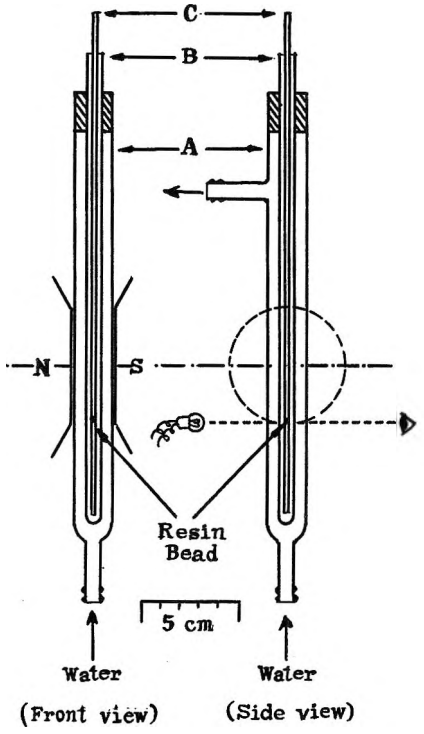

Figure 3. Apparatus for measuring the critical magnetic suspension of a resin bead in liquids.

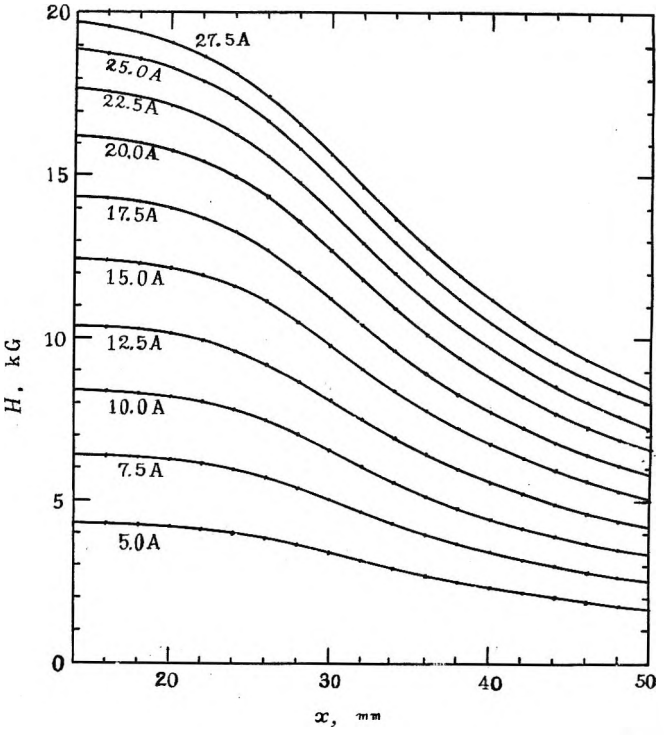

Figure 4. Radial distribution of the magnetic field strength H along the x axis below the center of the electromagnet at various magnetizing current intensities.

to the upper end of the capillary C. This serves to suck up a resin bead, together with solvent (water), from the bottom of the test tube to a position in the capillary C where the magnetic attraction is maximum and sufficient to suspend the paramagnetic resin bead in the liquid. The rubber bulb can be used as well to withdraw and insert resin beads. The test tube B is equipped with a thermostated water jacket A. The apparatus was mounted in the pole gap of an electromagnet so that capillary C passes through the midpoint of the pole gap and extends vertically by about 30 mm below the lowest level of the periphery of the pole pieces of the magnet, where the maximum attraction is expected.

A miniature light bulb provided rear illumination for monitoring the movement of the bead suspended in the liquid medium.

Determination of the Maximum Strength of the Magnetic Attraction of the Field, $(H\mathrm{d}H/\mathrm{d}x)_{max}$. A 500-kg electromagnet (water-cooling type) made by Tokyo Denki Seiki Co., Ltd., was used to produce a steady field, continuously variable up to 20 kG with a fluctuation as low as $\pm 0.01\%$. The pole pieces have a diameter of 60 mm and are fixed at a distance 21 mm apart. The strength of the magnetic field was measured with a Toshiba HM-3 Hall element magnetic field meter along the vertical line (x axis, Figure 1), covering a range of about 60 mm below the center of the pole gap of the electromagnet at intervals of 2 mm, and the results were smoothed carefully on a graph (Figure 4). The gradient of the magnetic field, $(\mathrm{d}H/\mathrm{d}x)$, was determined at intervals of 1 mm along the x axis by the interpolation method, and the product of H and $(\mathrm{d}H/\mathrm{d}x)$, or $[H(\mathrm{d}H/\mathrm{d}x)]$, named the strength of magnetic attraction, was plotted against x (Figure 5). Finally, the maxima of $[H(\mathrm{d}H/\mathrm{d}x)]$ were read graphically for different magnetizing current intensities, and a calibration curve (Figure 6) was drawn up so that one may find at once the value of the maximum strength of magnetic attraction corresponding to the observed magnetizing current intensity for the critical suspension of a resin bead. The position at which $[H(\mathrm{d}H/\mathrm{d}x)]$ is a maximum along the vertical x axis was found to be invariably fixed at a certain point x_{max}, entirely independent of the magnetizing current intensity but depending on the geometry of the magnet used (Figure 5). Accordingly, as a matter of course, any particle which is paramagnetic has to be suspended, insofar as the strength of the field is sufficiently large, invariably at the same fixed level x_{max}, independent of the magnetizing current intensity.

Measurement. A bead of a paramagnetic resin saturated with paramagnetic cations by ion exchange was placed in the test tube B. The resin bead, lying at the bottom of the test tube, was sucked, under the action of a sufficiently high magnetic field, into the capillary C by using the rubber bulb and was suspended at a position corresponding to the maximum attraction of the field. The resin bead is seen in the illumination as a bright point suspended in the solvent, usually clinging to either side of the capillary wall nearest to the

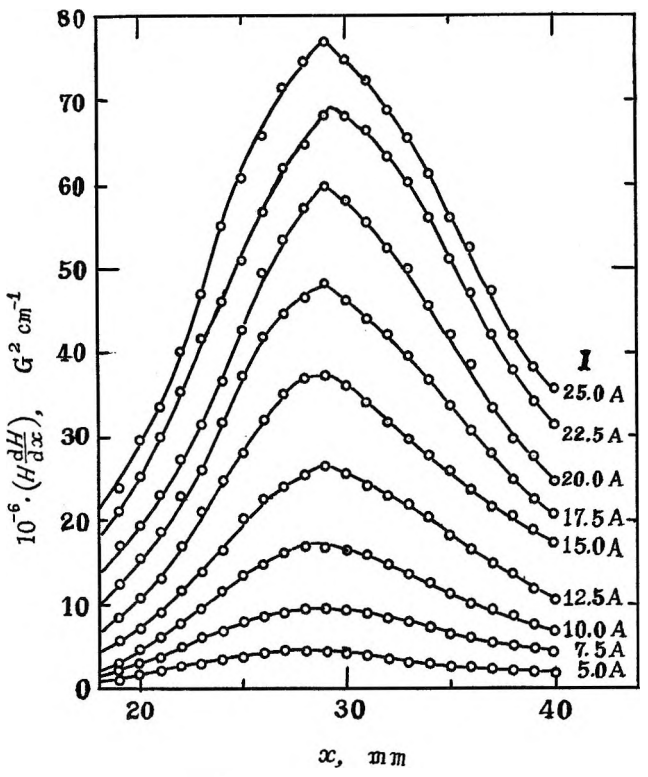

Figure 5. Relations between the strengths of magnetic attraction, $(H\mathrm{d}H/\mathrm{d}x)$, and x at different magnetizing current intensity, I.

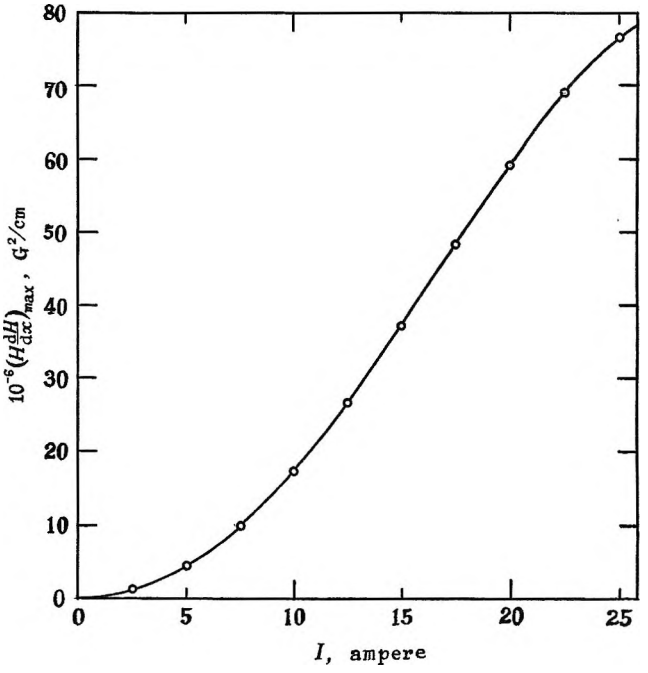

Figure 6. Relation between the maximum strength of magnetic attraction, $(H\mathrm{d}H/\mathrm{d}x)_{max}$, and magnetizing current intensity, I.

pole pieces of the magnet. By shifting the capillary C with care in the direction opposite to the side the resin bead is on, one may then find the resin bead transversing abruptly to the opposite side of the capillary wall and likely locating at a level, if possible, below the original. When this procedure has been repeated two or three times, one may confirm that the resin bead settles down ultimately at a fixed position corresponding to the maximum attraction of the field and no longer changes level. When the magnetizing current is reduced to just below the critical value, the balance is broken between the gravitational and magnetic forces acting on the resin bead, and the bead begins to fall. In practice, this turning point was determined as follows. The magnetizing current is reduced very gradually from a sufficiently high value while the light reflected from the surface of the resin bead is closely watched. The current is read just at the moment when any sign of the slightest displacement of the bead has been perceived. The critical strength of magnetic attraction, $(H\mathrm{d}H/\mathrm{d}x)_c$, for suspending the resin bead in the solvent in the field is read from the observed critical magnetizing current intensity using the calibration curve in Figure 6.

In the case of copper resin, the strength of the field of the electromagnet in our laboratory was insufficient to succeed in measurements with water as the solvent. Consequently, it was necessary to use another solvent having an appropriate density higher than that of water but lower than that of the resin bead. In the present study, a mixture of 70.26% carbon tetrachloride and 29.74% ethanol by weight was used, the density of which was 1.232 at 20°. The magnetic susceptibility of the mixed solvent was estimated by the Pascal rule[2] to be -0.576×10^{-6} emu/g or -0.708×10^{-6} emu/cm³.

Results and Discussion

Magnetizing Current Intensity for the Critical Suspension and the Size of Resin Beads. As is clear in eq 3, the force balance must be independent of the size of the resin beads, so long as the beads are not too large. This was proved to be true by the fact that the magnetizing current intensities for the critical suspension of resin beads of different sizes were found to be identical (Table I).

In the case of copper resin, however, the critical current intensity for magnetic suspension of the resin bead was found to increase gradually in a mixed solvent as time goes on. This must be due, according to eq 2, to (i) the increase in ρ or (ii) the decrease in κ. The possibility i is very likely to occur. Ion-exchange resins are known to swell considerably in various kinds of organic solvents, changing in volume and density. The density of copper resin in a mixed solvent such as ethanol and carbon tetrachloride as used here will increase gradually by uptake of the heavy component, carbon tetrachloride. An increase in volume due to swelling of the resin bead may accompany a decrease in the concentration of cupric ions, hence causing the

(2) I. Prigogine, Ed., *Advan. Chem. Phys.*, **3**, 209 (1961).

Table I: Critical Magnetizing Current Intensities I_c for Magnetic Suspension of Resin Beads of Different Sizes (in Diameter) in Water or a Mixed Solvent[a] at 20°

Mn^{2+}		Fe^{2+}		Co^{2+}		Ni^{2+}		Cu^{2+}	
Size, mm	I_c, A	Size, mm	I_c, A	Size, mm	I_c, A	Size, mm	I_c, A	Size, LMS	I_c, A
1.07	9.0	1.00	10.0	1.05	11.0	1.24	17.5	L	18.4[a]
0.55	9.0	0.62	10.0	0.69	11.0	0.91	17.4	M	18.5[a]
0.30	9.0	0.33	10.0	0.39	11.0	0.68	17.4	S	18.6[a]
						0.50	17.4		
						0.28	17.4		

[a] Mixed solvent: 29.74% ethanol + 70.26% carbon tetrachloride.

Table II: Magnetic Moments of Paramagnetic Ions Obtained from Data on the Critical Magnetic Suspension of Some Resin Beads in Water or a Mixed Solvent[a] at 20° (Q = 2.596 mequiv/g of Resin)

Ion	I_c, A	$(HdH/dx)_c$, G^2/cm	ρ, g/cm^3	ρ_0, g/cm^3	$10^6\kappa_0$, emu/cm^3	$10^6\chi$, emu/g	μ_{eff}, BM: This work	μ_{eff}, BM: Reference[b]
Mn^{2+}	9.00	13.8×10^6	1.341	0.998	−0.720	17.62	5.93	5.90–5.92
Fe^{2+}	10.00	17.0×10^6	1.344	0.998	−0.720	14.30	5.37	5.44
Co^{2+}	11.00	20.6×10^6	1.356	0.998	−0.720	12.03	4.95	5.02
Ni^{2+}	17.42	48.0×10^6	1.353	0.998	−0.720	4.822	3.24	3.22
Cu^{2+}	18.5	52.7×10^6	1.368	1.232[a]	−0.708[a]	1.331	1.94	1.91–1.96

[a] Mixed solvent: 29.74% ethanol + 70.26% carbon tetrachloride. [b] Landolt-Börnstein, "Zahlenwerte und Funktionen aus Naturwissenschaften und Technik," New Series, Group II, Vol. 2, Springer-Verlag, Berlin, 1966.

decrease in κ of the resin bead. When copper resin was allowed to stand in the mixed solvent, the solvent, which was originally colorless, became greenish in time. This indicates that dissolution of copper resin is occurring but does not always necessitate a decrease in the concentration of Cu^{2+} in the resin beads. The possibility of a decrease in κ due to dissolution of the resin beads seems to be rather unlikely, but since the dissolution of copper resin will increase the susceptibility of the liquid medium at the same time, the results may be in error.

Calculations. In principle, χ_M can be determined from eq 3 if χ_R is known. For an approximation, it may be permissible to use χ_{HR}, the susceptibility of the resin in the H form, in place of χ_R. In practice, however, it was difficult to determine χ_{HR} directly by the present method, because the strength of the maximum magnetic attraction, $[H(dH/dx)]_{max}$, available in our laboratory was limited to a value up to about 85 × 10^6 G^2/cm, which is insufficient to perform measurements of χ_{HR} with resins in the form HR to a tolerable degree of accuracy. To avoid this difficulty, χ_R was estimated, with the aid of eq 3, from an observed susceptibility value of a resin MR involving an appropriate paramagnetic ion species whose susceptibility χ_M is known accurately. For this purpose, nickel(II) ion was adopted as a reference in the present study. The atomic susceptibility of Ni^{2+} was estimated as 4489 × 10^{-6} emu from the molar susceptibility, (4433 ± 12) × 10^{-6} emu, of nickel(II) chloride in aqueous solutions,[3] making correction for the diamagnetic contribution from the chloride ions.[4] When this value is used, $\chi_R = -0.652 \times 10^{-6}$ emu/g, which is of a reasonable order of magnitude for a swollen resin residue and was used in the present calculation. The effective magnetic moment, μ_{eff}, in Bohr magnetons was calculated by using the Curie equation

$$\mu_{eff} = 2.828\sqrt{M\chi_M T}\ \text{BM}$$

where T is the absolute temperature. The results are shown in Table II. The magnetic moments determined by the present method are in good agreement with those reported in literature, the deviations being within 1–2%.

The present method is characterized by the following aspects. (i) The ion-exchange resin acts as a constant capacity ion measure, and so we do not need to weigh samples directly. This makes a remarkable contrast with the Faraday method. (ii) The method, in principle, must be applicable to resin beads of any small size, as long as the Brownian movement does not disturb the balancing of the magnetic suspension of the resin beads in liquids. Accordingly, one may carry out the measurements with samples of any small quantities of ions, so long as they meet the ion-exchange capacity of a single resin bead; for example, in the case

(3) P. W. Selwood, "Magnetochemistry," Interscience, New York. N. Y., 1943, p 29.

(4) Landolt-Börnstein, "Zahlenwerte und Funktionen aus Physik, Chemie, Astrophysik, Geophysik und Technik," Vol. I, 6th ed, Section 1, Springer-Verlag, Berlin, 1950, pp 396, 397.

of iron group elements, ions must be available in quantities of, for instance, about 0.01, 0.1, 0.35, 0.8, and 1.6 μequiv (or 0.4, 3, 10, 25, and 50 μg) for bead diameters of 0.2, 0.4, 0.6, 0.8, and 1.0 mm, respectively.

(iii) However, the method is inapplicable to ion species, such as polyelectrolytes, which may not be adsorbed by the resin in sufficient quantity to saturate the exchange capacity of the resin.

Photochemical Studies of Solid Potassium Trisoxalatoferrate(III) Trihydrate

by H. E. Spencer* and M. W. Schmidt

Research Laboratories, Eastman Kodak Company, Rochester, New York 14650 *(Received April 19, 1971)*

Publication costs assisted by the Research Laboratories, Eastman Kodak Company

To investigate some of the principles of solid-state photochemistry, three kinds of crystals of $K_3[Fe(C_2O_4)_3]\cdot 3H_2O$, large crystals, powdered large crystals, and microcrystalline coatings, have been studied. A correction for the optical filtering by solid photoproducts is applied to obtain the quantum yield for production of Fe(II), ϕ. The value of ϕ increases appreciably upon evacuation. Addition of water vapor reverses the effect of evacuation, whereas the addition of O_2, air, CO_2, or H_2 causes only slight change. Heating immediately before exposure increases ϕ. The value of ϕ for the large crystals is lower than that for the smaller crystals. Carbon dioxide is a photoproduct for all crystals, and carbon monoxide is also for the coatings. A mechanism with electron–hole pairs and radical ions as intermediates is suggested. Comparison is made to the photochemical mechanism of acidic solutions of the compound.

There are two major reasons for studying the solid-state photochemistry of potassium trisoxalatoferrate(III) trihydrate, $K_3[Fe(C_2O_4)_3]\cdot 3H_2O$. First, an acidic solution of the compound is a widely used actinometer for the blue, violet, and ultraviolet wavelength regions. Extensive studies of the solution mechanism have been made; it is worthwhile to study the mechanism in the solid state and compare it with the better understood solution mechanism. Second, the compound serves as a model for studying the principles of solid-state photochemistry. Effects of crystal size, optical filtering by accumulated solid photoproducts, and consequences of electronic band structure, for example, are unique to the solid phase. Also, the general interest in solid-state photochemistry of coordination compounds is increasing, as is shown by a number of recent papers dealing with $K_3[Fe(C_2O_4)_3]\cdot 3H_2O$,[1-4] as well as with related cobalt and manganese compounds.[3,5]

Here we report studies concerned mostly with the effects of evacuation and of crystal size upon the photochemistry of $K_3[Fe(C_2O_4)_3]\cdot 3H_2O$. The composition of both gaseous and solid photoproducts is studied, also.

Experimental Section

Three types of crystals were used in this study: coatings, large crystals, and powdered large crystals. The coatings, prepared by pouring a water solution of $K_3[Fe(C_2O_4)_3]\cdot 3H_2O$ into an organic solvent, miscible with water but in which the compound is insoluble (*e.g.*, ethanol, isopropyl alcohol, or acetone), have been described previously.[3]

Large crystals were grown from aqueous solution by imbedding a seed crystal in a piece of paraffin and floating the combination upon the surface of a saturated aqueous solution of $K_3[Fe(C_2O_4)_3]\cdot 3H_2O$. After several hours or days of evaporation, large crystals with edges 1 or 2 cm long were formed.[6] Seed crystals were made by evaporation of water from a beaker containing an aqueous saturated solution. To form the ground crystals, large crystals were ground first in a ball mill with

(1) J. N. Pitts, Jr., J. K. S. Wan, and E. A. Schuck, *J. Amer. Chem. Soc.*, **86**, 3606 (1964).

(2) W. W. Wendlandt and E. L. Simmons, *J. Inorg. Nucl. Chem.*, **28**, 2429 (1966).

(3) H. E. Spencer, *J. Phys. Chem.*, **73**, 2316 (1969).

(4) R. Ballardini and M. T. Gandolfi, *Ann. Chim. (Rome)*, **60**, 272 (1970).

(5) (a) D. Klein, C. W. Moeller, and R. Ward, *J. Amer. Chem. Soc.*, **80**, 265 (1958); (b) W. W. Wendlandt and J. H. Wooklock, *J. Inorg. Nucl. Chem.*, **27**, 259 (1965); (c) W. W. Wendlandt and E. L. Simmons, *ibid.*, **27**, 2317 (1965); (d) E. L. Simmons and W. W. Wendlandt, *ibid.*, **27**, 2325 (1965); (e) V. Balzani, R. Ballardini, N. Sabbatini, and L. Moggi, *Inorg. Chem.*, **7**, 1398 (1968); (f) D. A. Johnson and J. E. Martin, *ibid.*, **8**, 2509 (1969); (g) H. E. Spencer, *Photogr. Sci. Eng.*, **13**, 147 (1969); (h) H. E. Spencer and M. W. Schmidt, *J. Phys. Chem.*, **74**, 3472 (1970); (i) G. Lohmiller and W. W. Wendlandt, *Anal. Chim. Acta*, **51**, 117 (1970); (j) G. D'Ascenzo and W. W. Wendlandt, *J. Inorg. Nucl. Chem.*, **32**, 3109 (1970); (k) S. T. Spees, Jr., and P. Z. Petrak, *ibid.*, **32**, 1229 (1970); (l) A. C. Sarma, A. Fenerty, and S. T. Spees, *J. Phys. Chem.*, **74**, 4598 (1970).

(6) A. J. Fishinger, *J. Chem. Educ.*, **46**, 486 (1969).

Burumdum media for several hours; the resulting compact mass was then forced through an 88-μ sieve with a pestle.

The 200-W superhigh-pressure mercury source and monochromator used to carry out the irradiations were described previously.[7] The vacuum system consisted of a forepump, a mercury diffusion pump, and an all-glass line with a McLeod gauge and manometer. A liquid nitrogen trap was always used between the diffusion and forepumps. The glass vacuum cell was provided with a flat quartz window.

Large crystals were mounted with paraffin with the large (110) faces perpendicular to the radiation beam. Ground crystals were evacuated and irradiated by placing the material in a 1.0 mm thick spectrophotometer cell covered by a plastic cap through which small holes were bored to allow gas to escape. Slow initial evacuation was necessary to prevent scattering of the powdered sample.

After irradiation of an evacuated coating, air was admitted to the cell, the slide was removed immediately, and the coating was washed into a weighed glass beaker. Added to this were 5 ml of an acetate buffer solution (0.6 mol of sodium acetate and 360 ml of 1 N H_2SO_4 diluted to 1 l.) and 10 ml of a 0.1% 1,10-phenanthroline solution. Enough water was added to bring the weight of the solution to a given value, usually 20 g. After the solution had stood for 30 min, its optical density at 5100 Å was measured against a reference solution which was identical except that an unirradiated coating was used in its preparation. The concentration of Fe(II) was calculated using a value of 1.11×10^4 l./mol cm as the molar extinction coefficient.[8] Ground crystals were analyzed in much the same manner as the coatings. For irradiation of large crystals, a fresh crystal was used for each exposure. Before exposure, the crystal was soaked for 5 min in water. After removal of the crystal, the solution was analyzed for Fe(II) in the same way described for coatings. The crystal was rinsed in acetone, dried, mounted, evacuated, exposed, removed from the cell, soaked in water for 5 min, rinsed again in acetone, and dried. Again the aqueous solution was analyzed for Fe(II). Finally the dried crystal was soaked a third time in water for 5 min, and the solution was analyzed for Fe(II). This elaborate procedure was used to ensure that all the Fe(II) produced by irradiation was removed during the second soak. The criterion used to judge this was the agreement between the amounts of Fe(II) found in the first and third soak.

The pressure of the gas produced by irradiation was measured with a McLeod gauge, often with a Dry Ice cooled trap between the irradiation cell and the gauge. After mass spectrometric determination indicated that only CO and CO_2 were present, the composition was found by determining the pressure with and without a liquid nitrogen trap in the line. Such a trap condenses CO_2 but not CO.

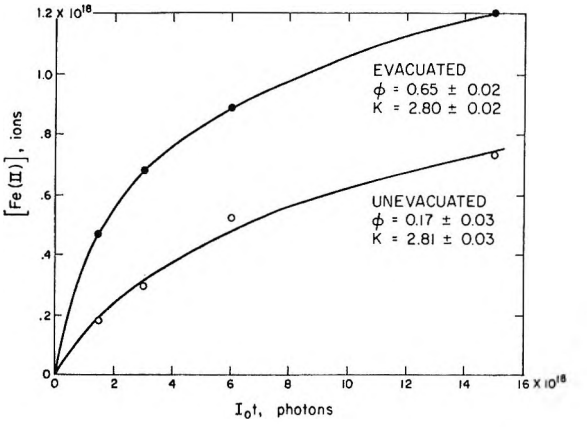

Figure 1. Effect of evacuation of coatings, wavelength 366 nm.

Results and Discussion

I. Evacuation and Determination of ϕ. Whereas evacuation of the coatings after exposure but before dissolution stops the slight decay of Fe(II) which occurs upon holding for a period of hours, evacuation before exposure greatly increases the efficiency of Fe(II) production. In contrast, we find that coatings of the corresponding cobalt compound, $K_3[Co(C_2O_4)_3]\cdot 3H_2O$, are unaffected by evacuation, either before or after irradiation.

Figure 1 illustrates the effect for coatings of $K_3[Fe(C_2O_4)_3]\cdot 3H_2O$. Plotted is the amount of Fe(II) produced as a function of number of incident photons, I_0t, where I_0 is the incident intensity and t is the time of exposure. The curves drawn are those calculated by computer; they obey the two-parameter equation

$$[\text{Fe(II)}] = \frac{1}{\kappa} \ln (1 + \kappa\phi I_0 t) \qquad (1)$$

where [Fe(II)] is the number of Fe(II) ions, ϕ is the quantum efficiency for Fe(II) production, and κ is an attenuation factor characteristic of the solid photoproducts. This equation is identical in form with one derived previously for the photolysis of $K_3[Co(C_2O_4)_3]\cdot 3H_2O$.[5h] It differs only in that Fe(II) replaces Co(II) and in that [Fe(II)], I_0, and κ are not normalized to unit area. Because the irradiated area varies with experimental conditions, it is convenient not to have to correct the raw data, values of [Fe(II)] and I_0t, to unit area. From the raw data, values of ϕ and κ are calculated by computer, as discussed previously.[5h] For the definition made here, the parameter of most interest, ϕ, does not depend on the size of the irradiated spot, whereas the other parameter, κ, is inversely proportional to the area.

The agreement of eq 1 with the data in Figure 1 is additional justification for the simple model used to derive the equation comparable to eq 1 in a previous publica-

(7) H. E. Spencer and J. O. Darlak, *J. Phys. Chem.*, **72**, 2384 (1968).

(8) J. G. Calvert and J. N. Pitts, Jr., "Photochemistry," Wiley, New York, N. Y., 1966, p 785.

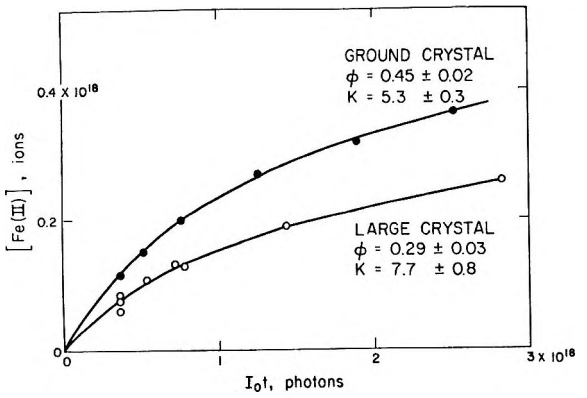

Figure 2. Effect of crystal size upon Fe(II) yield, wavelength 366 nm.

tion.[5h] Essentially, eq 1 provides a means of extrapolating back to obtain the initial value of ϕ at zero exposure time, or, in other words, to correct for radiation lost by photoproduct attenuation. Also, eq 1 fits data for both large and ground crystals (Figure 2) and has proved to provide a useful and convenient method for obtaining ϕ.

For coatings of Figure 1 evacuation increases ϕ by almost 400% but changes the attenuation factor, κ, almost not at all. For a given area of irradiation, κ depends only upon the optical properties of the solid photoproducts and thus should not be affected by evacuation.

Another result of evacuation is that the Fe(II) yield for all three crystal types is independent of intensity, in contrast to the slight intensity dependence reported previously for unevacuated coatings.[3] Because of this latter intensity dependence, we were surprised to find that the data for unevacuated coatings obey eq 1. However, although the lower curve in Figure 1 fits the points fairly well, these points from the unevacuated coating do not fit so well as the upper curve fits the data for evacuated coatings.

The yield does depend upon pumping time and rate of pumping, however. For a given rate of pumping, there is an optimum time of pumping for each type of crystal (see Figure 3). Experiments made with a smaller roughing pump indicate that the optimum time increases with a lower rate of pumping. Our technique has been to determine the optimum time for a given rate of evacuation of each crystal type before performing subsequent experiments.

Probably the initial increase in Fe(II) yield for short evacuation times is caused by water removal from the crystal–air interfaces, because adding water vapor, after evacuation but before exposure, decreases the yield below that for the unevacuated crystals. Addition of O_2, air, CO_2, or H_2 under the same conditions only slightly lowers ϕ.

The drop in yield for longer pumping times may be caused by loss of water of hydration. Thus two kinds of water need be considered, molecules which are an integral part of the crystal structure, water of hydration, and another kind which is adsorbed to the interfaces.

II. Crystal Size. Figure 2 clearly shows that the magnitude of ϕ increases with decreasing crystal size. This indicates a dependence upon surface-to-volume ratios, commonly found for solid-state reactions.

Yet there must be other important unknown factors because ϕ for coatings always exceeds ϕ for ground crystals, although microscopic examination indicates that the microcrystals in the coatings are larger. For instance, localized surface topography and the way the crystals are packed together may be very important.

III. Stoichiometry. Wendlandt and Simmons originally reported the products of photolysis to be oxalate, FeC_2O_4, and CO_2.[2] Unfortunately, the stoichiometry is not that simple. Two unpublished theses[9,10] reported that CO as well as CO_2 is produced. We have confirmed that CO comprises 20–30% of the gaseous photoproducts from the coatings, but little or none is found for the large and the ground crystals. These facts suggest that at least some of the organic solvents used for precipitation of the microcrystals are retained in the coatings and that this organic material leads to CO. Although for coatings we have always found CO among the photoproducts, we have also found that the CO/CO_2 ratio increases with increasing amount of photolysis. Perhaps the initially formed solid photoproduct, which absorbs some of the radiation,[3,5h] reacts with the adsorbed organic solvents.

We find equal amounts of Fe(II) and CO_2 produced by photolyzed large crystals. For coatings, not as much CO_2 as Fe(II) is detected, presumably because some of the gas is trapped inside the microcrystals. For the coatings in which CO is a photoproduct, there must be another product; we have been unable to identify it.

We have attempted unsuccessfully to identify the solid Fe(II) photoproduct from its X-ray diffraction spectrum. An unidentified product, not FeC_2O_4, along with $K_2C_2O_4$, was found. Presumably the unknown compound is $K_6Fe_2(C_2O_4)_5$, identified by Bancroft, Dharmawardena, and Maddock[11] in Mossbauer studies of the thermal and γ-ray decomposition of $K_3[Fe(C_2O_4)_3]\cdot 3H_2O$. However, there has to be some other product; the simplest stoichiometry is the formation of 1 mol of $K_6Fe_2(C_2O_4)_5$, 2 mol of CO_2, and 6 mol of H_2O from 2 mol of $K_3[Fe(C_2O_4)_3]\cdot 3H_2O$. Neither $K_2C_2O_4$ nor CO is accounted for this way.

IV. Mechanism. First, we consider the essential features of the generally accepted mechanism for photol-

(9) J. B. Holden, Jr., Thesis, Princeton University, 1961.

(10) W. M. Riggs, Thesis, University of Kansas, 1967.

(11) G. M. Bancroft, K. G. Dharmawardena, and A. G. Maddock, *Inorg. Chem.*, 9, 223 (1970); *J. Chem. Soc. A*, 2914 (1969).

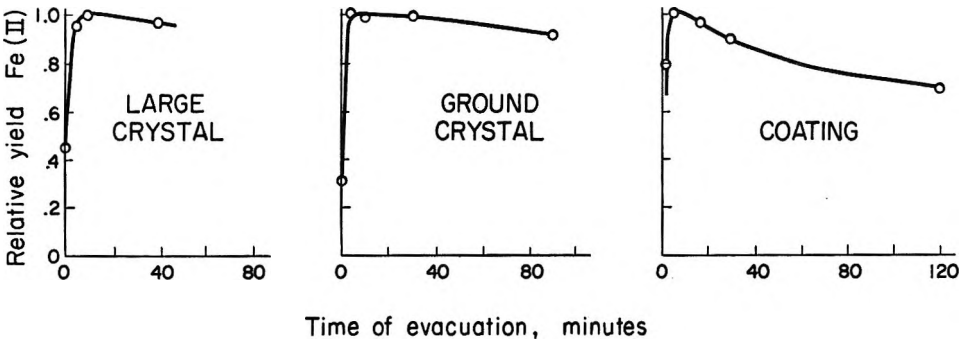

Figure 3. Variation of Fe(II) yield with evacuation time.

ysis of $Fe(C_2O_4)_3$ in acid solution.[12,13] For each photon absorbed, two Fe(II) ions and two CO_2 molecules

$$h\nu + Fe(C_2O_4)_3^{3-} \longrightarrow Fe(C_2O_4)_2^{2-} + \cdot C_2O_4^- \quad (2)$$

$$\cdot C_2O_4^- + Fe(C_2O_4)_3^{3-} \longrightarrow Fe(C_2O_4)_2^{2-} + 2CO_2 + C_2O_4^{2-} \quad (3)$$

are produced. Over a considerable range of wavelengths, the experimental quantum yields are not 2, however, but are about 1.2, indicating some deactivation not included in the above reaction scheme. The important point is that quantum yields greater than unity dictate a reaction sequence such as given by eq 2 and 3, in which radicals formed in the first step produce additional products in the second.

For the solids studied here, ϕ never exceeds unity; the highest values, for evacuated coatings at 313, 335, 366, and 405 nm, are 0.56 ± 0.01, 0.67 ± 0.02, 0.68 ± 0.03, and 0.52 ± 0.02, respectively. For solid $K_3[Fe(C_2O_4)_3]\cdot 3H_2O$ irradiated in KBr matrices, Ballardini and Gandolfi also found ϕ to be less than but almost unity,[4] although for the same type of matrix system a preliminary value of 1.3 was reported by Pitts, Wan, and Schuck.[1] If we presume that the more recent and extensive work of Ballardini and Gandolfi is correct, there is no need for the reaction sequence represented by eq 2 and 3 in the solid-state mechanism.

It is appropriate to digress at this point and discuss the almost unity quantum yield values for KBr matrices.[1,4] The technique of forming the KBr disks requires the use of relatively high pressure. Ballardini and Gandolfi state that this high pressure leads to a high enough temperature to cause an 8% thermal decomposition of the iron compound. Presumably, this heat must also dry the crystals and increase the value of ϕ. We have found that heating the coatings immediately before exposure appreciably increases ϕ. If the heated coatings remain in room air at room temperature for more than 15–20 min the value of ϕ begins to decrease and eventually approaches that found with no heating. Ballardini and Gandolfi find that higher pressures, presumably with concurrent higher temperatures, decrease the value of ϕ. Although this decrease could be a direct result of the pressure, we wonder if the greater heat is removing some of the water of hydration in the same way that long times of evacuation (Figure 3) remove water of hydration and produce lower values of ϕ.

Returning now to the mechanistic discussion, we must explain additional experimental facts. These are photoconductivity,[3] the large effect of evacuation, and the intensity dependence of ϕ for unevacuated coatings.[3]

The photoconductivity indicates hole–electron pair production in the electronic bands of the solid

$$h\nu \longrightarrow h + e \quad (4)$$

where h and e represent holes and electrons, respectively. The fates of these electrons and holes occupy much of the subsequent mechanistic considerations. We write $C_2O_4^{2-}$, Fe(III), and Fe(II) to represent species which are oxidized or reduced, although, in general, these species are coordinated to other species. Our designation is merely a shorthand notation. Also, the radicals written as $C_2O_4\cdot^-$ and $CO_2\cdot^-$ possibly are coordinated to Fe(III).

The holes cause oxidation of oxalate

$$h + C_2O_4^{2-} \longrightarrow \cdot C_2O_4^- \quad (5)$$

This oxalate radical may react by two alternative paths

$$h + \cdot C_2O_4^- \longrightarrow 2CO_2 \quad (6)$$

or

$$\cdot C_2O_4^- \longrightarrow \cdot CO_2^- + CO_2 \quad (7)$$

$$h + \cdot CO_2^- \longrightarrow CO_2 \quad (8)$$

each producing two CO_2 molecules.

There is esr evidence that free radicals such as $\cdot C_2O_4^-$ and $\cdot CO_2^-$ are produced at low temperatures[5k,14] and we assume here that radicals are important as intermediates at room temperature (reactions 5–8). In

(12) C. A. Parker, *Trans. Faraday Soc.*, **50**, 1213 (1954).

(13) C. A. Parker and C. G. Hatchard, *J. Phys. Chem.*, **63**, 22 (1959). This paper contains much more detail about the mechanism than given by eq 1 and 2 which give only the features essential for our argument.

(14) D. J. E. Ingram, W. G. Hodgson, C. A. Parker, and W. T. Rees, *Nature (London)*, **176**, 1227 (1955).

fact, Gross reported flash photolysis studies of $K_3[Co(C_2O_4)]$ solutions in which he detected $\cdot C_2O_4^-$ at room temperature.[15]

The primary effect of the other half of the electron–hole pair, the electron, is to induce reduction of Fe(III) to Fe(II)

$$e + Fe(III) \longrightarrow Fe(II) \quad (9)$$

The increase in ϕ caused by evacuation and the subsequent decrease caused by admitting water vapor to the system indicates that adsorbed water somehow induces a recombination reaction.[16] We list two possibilities. The first is that adsorbed water molecules create electron-trapping centers which we designate as X_{H_2O}. The X indicates that we do not know if the center is water itself or is some hydrated ion at the interface. The reaction which competes with reaction 9 is

$$e + X_{H_2O} \longrightarrow X_{H_2O}^- \quad (10)$$

Upon evacuation, this adsorbed water is removed and reaction 10 becomes unimportant. We emphasize that we are discussing adsorbed water and not water which is an integral component of the crystal.

Recombination occurs when X_{H_2O} reacts with a hole

$$h + X_{H_2O}^- \longrightarrow X_{H_2O} \quad (11)$$

The other possibility is that the adsorbed water promotes the surface mobility of the oxalato radicals such that the radicals have increased probability of oxidizing Fe(II)

$$\cdot C_2O_4^- + Fe(II) \longrightarrow C_2O_4^{2-} + Fe(III) \quad (12)$$

This explanation has the attractive capability of explaining the lack of effect when $K_3[Co(C_2O_4)_3]\cdot 3H_2O$ is evacuated. The photoproduct Co(II) is more stable than Fe(II), and we presume that oxalato radicals would react little with Co(II). However, in dilute solid solution, Sarma, Fenerty, and Spees[51] gave conclusive evidence for back-reaction of photoproducts of $K_3[Co(C_2O_4)_3]\cdot 3H_2O$. Of course, our conditions are different, and it is not surprising to find different results. At present there is no contradiction between this second explanation and the experimental findings.

Other recombination steps undoubtedly are important; several may be written, but two will suffice for this discussion

$$e + \cdot C_2O_4^- \longrightarrow C_2O_4^{2-} \quad (13)$$

$$h + Fe(II) \longrightarrow Fe(III) \quad (14)$$

High values of ϕ for evacuated crystals and for KBr matrices[4] indicate that these recombination steps can be minimized, especially for small crystals.

For the unevacuated coatings, the intensity dependence of ϕ reported earlier[3] could arise from recombination reactions such as (11) or (12) competing with reaction 6. Evacuation removes adsorbed water, eliminates either reaction 11 or 12, and eliminates the intensity dependence.

Conclusions

Some comment is warranted about the several techniques for measuring ϕ with seemingly discordant results. The interesting situation of greater-than-unity values for solution experiments *vs.* less-than-unity values for solids has already been discussed. Additional attempts should be made with solids to find values of ϕ greater than unity. It is clear that experimental conditions such as crystal size, solvent history, pressure, and ambient conditions are important.

The dilute-solid-solution technique has not been reported for $K_3[Fe(C_2O_4)_3]\cdot 3H_2O$ yet, but low values of ϕ presumably would be found, analogous to the low values of quantum yields for production of Co(II) found for dilute solid solutions of $K_3[Co(C_2O_4)_3]\cdot 3H_2O$.[51] Apparently, back-reaction between photoproducts, which was actually demonstrated,[51] is of overriding importance for this type of materials. The complexes are molecularly dispersed; the cage of the surrounding solid greatly retards separation of photoproducts and greatly enhances back-reaction. In solution, on the other hand, the cage is far less rigid, photoproducts can separate, and high values of ϕ result. In the solids reported here, separation of photoproducts is achieved by the electronic carriers. If this were not so, photoconductivity would not be detected. Thus high values of ϕ are found.

The mechanism proposed here is greatly expanded over the brief discussion given earlier.[3] It is stated mostly in chemical terms. Physical factors such as sites of reaction, atomic arrangements, trapping probabilities, lifetimes of various entities, and mobilities through the bulk and along interfaces are highly significant. At the present time, practically nothing is known about these factors; future research will deal with them, undoubtedly.

Acknowledgments. We appreciate the X-ray analysis made by Mr. S. Donley and the mass spectrometric analysis by Mr. G. P. Happ.

(15) R. C. Gross, Abstracts, 156th National Meeting of the American Chemical Society, Atlantic City, N. J., Sept 1968, No. PHYS 50.

(16) Recombination induced by water adsorbed to semiconductors is discussed in A. Many, Y. Goldstein, and N. B. Grover, "Semiconductor Surfaces," North-Holland Publishing Co., Amsterdam, 1965, Chapter 9.

Molar Absorptivity of Carbon Trioxide

by Patrick R. Jones and Henry Taube*

Department of Chemistry, Stanford University, Stanford, California 94305 *(Received April 2, 1971)*

Publication costs assisted by the National Science Foundation

The photolysis of ozone in a matrix of CO_2 at 60–80°K produces the infrared spectrum assigned to CO_3 and a broad, weak absorption at 406 nm with molar absorptivity of 10.8 ± 2.7 l. mol^{-1} cm^{-1} and oscillator strength of 3×10^{-4}. Infrared measurements reveal that at the photosteady state in a CO_2 matrix in which O_2 has been produced, CO_3 and O_3 can be interconverted photolytically with virtually no loss per cycle. Band strengths are given relative to the 1040-cm^{-1} band of ozone for four of the infrared bands of CO_3.

Introduction

The carbon trioxide molecule was postulated to explain isotopic oxygen atom exchange in the gas phase.[1] Since that time it has been invoked as an intermediate in a number of other gas-phase reactions and thus has been frequently discussed.[2] There remains some uncertainty in the interpretation of results reported concerning the behavior and/or existence of carbon trioxide in the gas phase. For instance, work by Arvis indicates that the CO_3 molecule has an appreciable lifetime in a stream of CO_2 at 1 Torr.[3] Recent work by DeMore and Dede, however, indicates that the formation of a deactivated, ground-state carbon trioxide molecule is very inefficient at low gas pressures, with the dominant process being the rapid predissociation of an excited CO_3 intermediate to give CO_2 and $O(^3P)$.[4] The molecular structure of CO_3 is believed from matrix infrared studies to be analogous to that for cyclopropanone.[5-7] There also exist theoretical calculations favoring the C_{2v} assignment for the structure.[8,9] As such, the CO_3 molecule can be expected to have an $n \rightarrow \pi^*$ absorption in the near-uv characteristic of the carbonyl moiety and, in fact, the observations made by Moll, *et al.*,[5,6] on the photodecomposition of CO_3 show that the substance does absorb at wavelengths longer than 300 nm. Previous efforts to observe the electronic absorption spectrum of CO_3 have failed.[3,5,7,10] Presumably the difficulties in observing the CO_3 spectrum are ascribable both to the extinction coefficient being small and to the absorption band being close to the very intense uv band of ozone.

Experimental Section

The low-temperature studies were conducted in an Andonian Associates helium dewar, which has been described previously,[6] and in a small glass dewar designed for use with liquid nitrogen coolant. The helium dewar was used at solid nitrogen temperatures near 60°K with liquid oxygen as the heat-exchange medium. The problem of color center formation in the KBr windows and sample support which we normally use made it necessary to perform most of the study with alternative BaF_2 optics. The use of the BaF_2 and the use of a Perkin-Elmer Model 21 infrared spectrophotometer with a NaCl prism restricted the study to the four strongest bands of CO_3 which occur at wavelengths less than 13 μ, namely, those at 2053, 1890, 1072, and 972 cm^{-1}. A Cary 14 spectrophotometer was used to record the ultraviolet and visible spectral features.

The ozone was prepared in a silent electric discharge using Matheson research grade oxygen in a closed system cooled with liquid nitrogen. The ozone–oxygen mixture was then distilled from trap to trap at liquid nitrogen temperatures and pumped to remove as much of the remaining oxygen as possible. Airco research grade carbon dioxide was used without further treatment. The gas mixtures were prepared by distilling a given amount of each component gas (measured in a quartz spiral manometer) into a Pyrex flask which could be removed from the vacuum line. Glass beads in the sample flask could then be shaken to achieve a homogeneous mixture of the gases.

Throughout most of this work a Hanovia 450-W medium-pressure mercury lamp was used with appropriate filters to isolate either the 260- or the 400-nm region. A PEK 200-W high-pressure mercury arc was used as an intense visible light source to find the long-wavelength limit for photodecomposition of CO_3.

(1) D. Katakis and H. Taube, *J. Chem. Phys.*, **36**, 416 (1962).

(2) D. L. Baulch and W. H. Breckenridge, *Trans. Faraday Soc.*, **62**, 2768 (1966); M. Clerc and A. Rieffsteck, *J. Chem. Phys.*, **48**, 2799 (1968); E. C. Zipf, *Can. J. Chem.*, **47**, 1863 (1969), and the discussion following; J. F. Noxon, *J. Chem. Phys.*, **52**, 1852 (1970); P. M. Scott and R. J. Cvetanovic, *ibid.*, **54**, 1440 (1971); T. G. Slanger and G. Black, *ibid.*, **54**, 1889 (1971).

(3) M. Arvis, *J. Chim. Phys. Physicochim. Biol.*, **66**, 517 (1969).

(4) W. B. DeMore and C. Dede, *J. Phys. Chem.*, **74**, 2621 (1970).

(5) N. G. Moll, D. R. Clutter, and W. E. Thompson, *J. Chem. Phys.*, **45**, 4469 (1966).

(6) E. Weissberger, W. H. Breckenridge, and H. Taube, *ibid.*, **47**, 1764 (1967).

(7) M. E. Jacox and D. E. Milligan, *ibid.*, **54**, 919 (1971).

(8) B. M. Gimarc and T. S. Chou, *ibid.*, **49**, 4043 (1968).

(9) J. F. Olsen and L. Burnelle, *J. Amer. Chem. Soc.*, **91**, 7286 (1969).

(10) W. B. DeMore and C. W. Jacobsen, *J. Phys. Chem.*, **73**, 2935 (1969).

Since it was not feasible to use filters with sharp cutoff regions, only an approximate upper limit was found by the filter technique. As a further check, the CO_3 was irradiated with the 514-nm line of an argon laser and with the 632.8-nm line of a helium–neon laser, using appropriate interference filters in each case.

Results

The carbon trioxide was generated by photolysis at 254 nm of various mixtures of CO_2 and O_3 frozen on the sample support at temperatures between 60 and 80°K. Usually, the mixtures were about 9 mol % in ozone. Increasing the ozone concentration gave no appreciable increase in the total concentration of CO_3 obtained. The sample quantity was limited by the light scattering of the matrix deposit. Attempts to produce a more transparent matrix using SF_6 as a host material were not successful.

We found that irradiation of CO_3 with a filter that transmitted less than 1% below 500 nm using a high-pressure mercury arc gave little decomposition. However, the 514-nm line of an argon laser did photolyze the CO_3, leaving the CO_2 unchanged and regenerating O_3 in the matrix. Irradiation with the 632.8-nm line of a helium–neon laser produced no observable change in CO_3 concentration. For the photolysis of CO_3 with the medium-pressure mercury lamp, either a chemical filter which transmitted only the 310- to 450-nm region or a 10-mm thick Pyrex filter which transmitted wavelengths greater than 301 nm was used. The wavelength limits given for each filter correspond to a transmittance of less than 0.5%.

Molecular oxygen was trapped most efficiently in the matrix at the lowest temperature used, 60°K. During ozone photolysis at 80°K, there was a pressure increase in the dewar. The noncondensable gas produced is believed to be oxygen. Because at the lower temperature, 60°K, the pressure in a closed dewar increased relatively slowly, we believe that the mobility of O_2 is much less. A study of the interdependence of the infrared spectra during the photolysis of O_3 or of CO_3 in matrix mixtures at 60°K revealed that oxygen atom transfer could be followed. Photolysis of the ozone at 254 nm, and then of the carbon trioxide, using wavelengths greater than 300 nm, repeated many times for a given matrix deposit, resulted in a net decrease in the sum of these two observable oxygen atom carriers until a steady-state situation was attained—steady state in the sense that the total concentration of oxygen atom carriers (CO_3 + O_3) does not change rapidly. The decrease in the total concentration of the observable oxygen atom carriers is accompanied by an increase in molecular oxygen concentration. Continued repetition of the photolysis of ozone, then carbon trioxide, at the steady-state situation resulted in a cycling of oxygen atoms between the CO_3 and the O_3 with very little net diminution per cycle. The diffusion of molecular oxygen from the matrix presumably accounts for the slow continued diminution of the total observable oxygen carrier. The oxygen loss was significant only at higher temperatures or with a delay of several hours between scans of the spectrum (*cf.* Figure 1). Thus in the steady-state situation at 60°K, a photolytic decrease or increase in the ozone concentration resulted in an equivalent change in the carbon trioxide concentration.

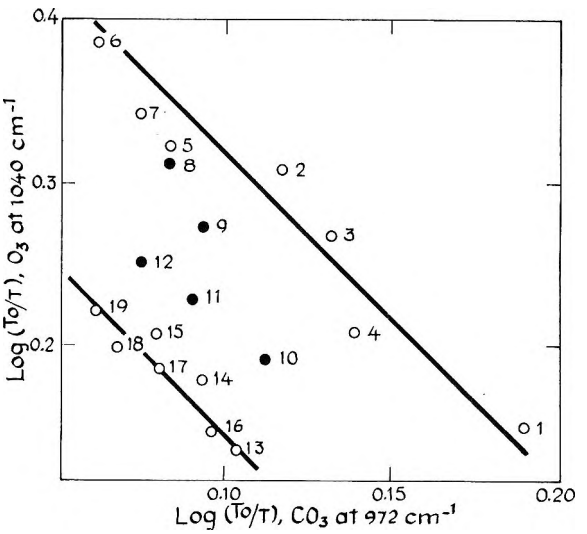

Figure 1. Plot of log (T_0/T) for CO_3 at 972 cm^{-1} *vs.* log (T_0/T) for O_3 at 1040 cm^{-1}. (a) The data points are numbered in the order in which they were recorded, each representing the photolysis of either ozone, by uv, or carbon trioxide, by visible light. The approach to the "steady state" suggested by the interrelationship of points 1–7 is not shown. (b) The succession of points 1–7 as well as 13–19 fall along the arbitrarily drawn lines of slope 2 showing that there exists a photolytic correlation between the CO_3 and O_3 concentrations in the matrix. (c) There was a 12-hr delay after point 7. Points 8–12 indicate the lack of correlation between CO_3 and O_3 while the concentration of O_2 in the matrix increases until the photosteady-state amount is attained.

Measurement of concentration changes using infrared spectra can be made either by determining the intensity as the absorbance (log (T_0/T)) or by measuring the integrated absorption intensity defined as the area under the absorption curve for frequency (cm^{-1}) plotted *vs.* absorbance. Since the band shape and height are less reliable parameters than the band area, the latter method was used. The definitions which we have used are those given by Ramsay[11] and adopted by Jones and Sandorfy.[12] The term "apparent" is used to denote a parameter measured from infrared data which is not the "true" parameter since the necessity of using finite slit widths perturbs the band shape and thus alters the observed parameters.

The photolytic interdependence of the ozone and carbon trioxide concentrations made it possible to

(11) D. A. Ramsay, *J. Amer. Chem. Soc.*, **74**, 72 (1952).

(12) R. N. Jones and C. Sandorfy in "Techniques of Organic Chemistry," Vol. IX, W. West, Ed., Interscience, New York, N. Y., 1956, pp 247–580.

determine both the extinction coefficients and the integrated absorption intensities for each of the infrared bands of carbon trioxide relative to the ozone absorption at 1040 cm^{-1}. Although the apparent extinction coefficient of an infrared band may vary among different instruments, using a single instrument we found it sufficiently reproducible to make feasible a semiquantitative treatment of the data. The relative band strengths were determined to provide a more nearly absolute parameter for use with other instruments and for use in comparison with other moleculer species.

Since the electronic spectrum of a matrix deposit as well as the infrared spectrum could be observed, it was possible to make reasonably quantitative comparisons of the intensities of the infrared bands with the intensities of bands in the uv or visible. The known molar extinction coefficients for the electronic absorption spectrum of ozone were used to determine the apparent molar extinction coefficient for the 1040-cm^{-1} band of ozone in the matrix. It was found most convenient to measure the ozone absorbance at 302 nm. Hearn's value of 81.68 l. mol^{-1} cm^{-1} was used for the ozone extinction coefficient at 302.15 nm.[13] The absorbance of the less intense band at 600 nm was measured, but the experimental errors were somewhat larger than those using the absorbance at 302 nm. The resulting value for the apparent extinction coefficient, E^a, for ozone at 1040 cm^{-1} in the matrix is 132 ± 6 l. mol^{-1} cm^{-1}. This result is in agreement with the value of 134 l. mol^{-1} cm^{-1} by Wilson and Badger,[14] but for which none of the instrumental conditions is given.

The apparent extinction coefficients of the infrared bands of CO_3 were determined using the value at 1040 cm^{-1} for ozone by making a plot of the absorbance of a given CO_3 infrared band *vs.* the corresponding absorbance for ozone at 1040 cm^{-1}, while the relative concentrations were changed by photolysis in the steady-state condition. The slope of such a plot is the negative ratio of the apparent extinction coefficient of CO_3 and O_3 (*cf.* Figure 2). The resulting apparent molar extinction coefficients for CO_3 using 132 l. mol^{-1} cm^{-1} for the 1040-cm^{-1} ozone band are given in Table I for the average of three different matrix experiments.

Observation of the electronic absorption spectrum in conjunction with the infrared measurements also made it possible to measure the extinction coefficient (*cf.* Table II) of the CO_3 absorption at 406 nm (*cf.* Figure 3). That is, the absorbance of ozone at 302 nm was measured to determine the apparent extinction coefficient of ozone at 1040 cm^{-1}. Then the extinction coefficients of the CO_3 infrared bands were determined from the photolytic interdependence of O_3 and CO_3 in the matrix at the photosteady state using the apparent extinction coefficient for ozone at 1040 cm^{-1}. Once the apparent extinction coefficients of the CO_3 bands were known in the infrared, the extinction coefficient at 406 nm was readily determined (*cf.* Table II). It should be noted that this technique circumvents the problem of determining the optical path length, which is the thickness

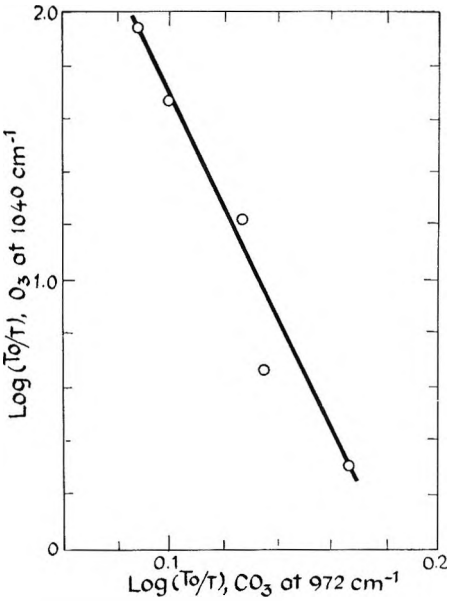

Figure 2. Plot of log (T_0/T) for the 972-cm^{-1} CO_3 band *vs.* log (T_0/T) for the 1040-cm^{-1} O_3 band recorded in the matrix photosteady-state condition illustrating that there exists a linear correlation, which is consistent with the interpretation that oxygen atoms are transferred reversibly by selective photolysis of either carbon trioxide or ozone.

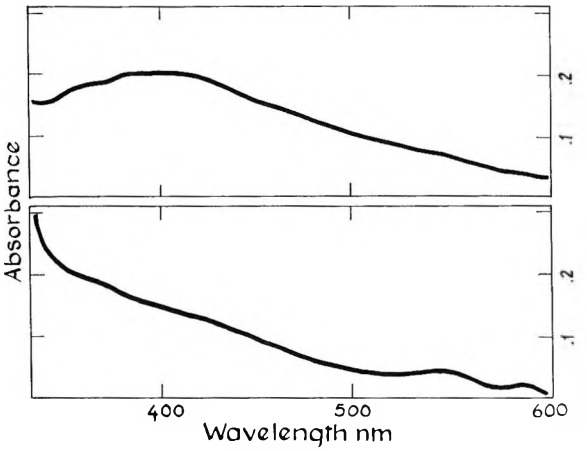

Figure 3. Absorption spectra for a matrix of carbon dioxide (absorbance log base 10) at 60°K containing either ozone or carbon trioxide and ozone. The lower spectrum is of the sample of ozone and carbon dioxide prior to photolysis. The ozone absorptions in the Hartley band (200–300 nm) are off-scale, but absorptions are seen for the Chappius band (450–850 nm). The upper spectrum is of the same CO_2 matrix after uv photolysis at 260 nm. The corresponding infrared spectrum of this sample indicated that very little ozone remained and that CO_3 was the only new species detected. Thus the broad weak absorption with a maximum near 406 nm correlates with infrared observations of carbon trioxide.

(13) A. G. Hearn, *Proc. Phys. Soc., London*, **78**, 932 (1961).

(14) M. K. Wilson and R. M. Badger, *J. Chem. Phys.*, **16**, 741 (1948).

Table I: Infrared Absorption Characteristics of Carbon Trioxide[a]

CO_3 bands, cm^{-1}	2053	1890	1072	972
Apparent extinction coefficient, l. mol^{-1} cm^{-1}	112 ± 15	96 ± 19	26 ± 5	63 ± 7
Apparent band half-width, $\nu_{1/2}^a$, cm^{-1}	15	22	6	10.5
Integrated absorption intensity, A, atm^{-1} cm^{-2}	590	480	140	185
Experimental ratio[b] of integrated absorption intensities, ozone at 1040 cm^{-1}/carbon trioxide	0.59 ± 0.19	0.73 ± 0.07	2.4 ± 1.9	1.9 ± 0.4

[a] Based on comparison with the infrared band for O_3 at 1040 cm^{-1}, using 132 l. mol^{-1} cm^{-1} for the extinction coefficient and 3.5×10^2 atm^{-1} cm^{-2} for the integrated absorption intensity. [b] Determined from the slope of $K \log (T_0/T)\Delta\nu_{1/2}^a$ for carbon trioxide *vs.* that for ozone.

Table II: Results and Data Used for the Determination of the Molar Absorptivity and the Integrated Absorption Intensities

	$\left[\frac{\text{Absorbance at } \lambda}{\log (T_0/T) \text{ at } \nu}\right]^n$	Molar absorptivity, l. mol^{-1} cm^{-1}, at λ	Integrated absorption intensity, at ν, atm^{-1} cm^{-2}
CO_3: ν = 972 cm^{-1}, λ = 400 nm, n = 1	$16.7 \times 2.4 \times 10^{-2}$ [a]	10.5 ± 2.7[b]	185
O_3: ν = 1040 cm^{-1}, λ = 302 nm, n = −1	1.45 ± 0.34[c,d]	81.68[e]	200[f,g]

[a] Average of 11 experiments. [b] Calculated using also the apparent extinction coefficient for CO_3 from Table I. Note that the value of 406 nm is 10.8 ± 2.7. [c] Average of 12 experiments. [d] From these data, E^a is 120 ± 50 l. mol^{-1} cm^{-1} for ozone at 1040 cm^{-1}. [e] From ref 13. [f] *Cf.* value of 350 atm^{-1} cm^{-2} from ref 15. [g] The value used for $\Delta\nu_{1/2}^a$ is 11.1 cm^{-1} for ozone at 1040 cm^{-1}.

of the matrix deposit, but it also means that only relative concentrations have been determined.

To provide a measure of the quantities involved using this technique, an estimate of the matrix thickness has been made. The method used for the estimation of the thickness involved the measurement of the total number of moles of sample deposited, an estimation of the area, and the use of the density of solid carbon dioxide. A typical result is $\sim 1 \times 10^{-2}$ cm for the matrix thickness. Although this method is very crude, it is reasonably consistent with the estimate on the basis of absorbance. Using the absorbance at 400 nm, the amount of carbon trioxide formed in a typical experiment was estimated to be about 0.5×10^{-5} mol cm^{-2}. If, from the initial O_3 content, the CO_3 is taken to be 1% of the material, the matrix thickness is calculated as 2×10^{-2} cm.

The integrated absorption intensity $A_{1040}{}^{O_3}$ of the 1040-cm^{-1} ozone band was estimated by measuring the absorbance at 302 nm, as well as the bandwidth at half-maximal intensity and log (T_0/T) for the infrared absorption. Ramsay's tables were used to correct for finite instrumental slit widths.[11] Ramsay's technique was adopted in which it is assumed that the true absorption band in a liquid (or as in this case a matrix) may be represented by a Lorentz curve. Then the true integrated absorption intensity, A, is given by

$$A = \left(\frac{K}{cl}\right) 2.3 \log (T_0/T) \Delta\nu_{1/2}^a$$

where c is the molar concentration, l is the path length in centimeters, $\Delta\nu_{1/2}^a$ is the measured bandwidth for half-maximal intensity, and K is a correction factor for finite slit width assuming a Lorentz curve. The factor K is related to the spectral slit width used for the particular infrared spectrophotometer.[11] For our Perkin-Elmer Model 21 with NaCl prism, the slit width was estimated for these purposes from tables supplied by the Perkin-Elmer Corp. In the region of the 1040-cm^{-1} ozone band and the CO_3 bands at 1072 and 972 cm^{-1} the NaCl prism gives sufficient resolution such that K was $\pi/2$, or very nearly $\pi/2$, for those bands. Spectral data for the 302-nm absorption and the 1040-cm^{-1} band of ozone for a given matrix deposit made it possible to estimate the integrated absorption intensity of ozone as a means of checking the technique. Since there was considerable error in the direct measurement of the area under the absorption curve, the method chosen was that attributed to Ramsay above

$$A_{1040}{}^{O_3} = \left(\frac{81.68}{A_{302}}\right) 2.3K \log (T_0/T) \Delta\nu_{1/2}^a$$

where A_{302} is the absorbance measured for ozone at 302 nm. The resulting experimental value for the integrated absorption intensity of ozone at 1040 cm^{-1} was 2×10^2 atm^{-1} cm^{-2} (*cf.* Table II). The agreement with the corresponding literature value, 3.5×10^2 atm^{-1} cm^{-2},[15] is by no means quantitative, but it can be seen

(15) D. J. McCaa and J. H. Shaw, *J. Mol. Spectrosc.*, 25, 374 (1968).

that our measurements are of the proper order of magnitude. Furthermore, the change in the observed integrated absorption intensities from the gas phase to a condensed phase have been shown to fit the Polo–Wilson equation $A_c/A_g = (n^2 + 2)/9n$, where A_c and A_g are the intensities in the condensed and gas phases, respectively, and n is the refractive index of the medium.[16] The equation was found by Schatz to be valid both for liquids and for symmetrical solids.[17] Since the measured band intensities are a function only of n for the medium, it is useful to determine the relative intensities of carbon trioxide bands with respect to the ozone band at 1040 cm^{-1} in the matrix and to compare the relative results with the absolute intensity for ozone in the gas phase. Furthermore, since the integrated absorption intensities for the CO_3 bands are determined relative to that of ozone, the experimental and systematic errors of the method should be constant. Thus the validity of the relative results, making due allowance for our experimental uncertainties, rests on the accuracy of the literature value for ozone. Table I gives the integrated absorption intensities for four infrared bands of CO_3 determined relative to that of ozone and using an absolute value for ozone of 3.5×10^2 atm^{-1} cm^{-2} as determined by McCaa and Shaw.[15]

In all cases the slope for each linear plot was found by a least-squares fit using the appropriate t value for a 50% confidence limit.

Discussion

It has been observed that after O_2 has accumulated in a matrix containing CO_2, CO_3, and O_3, selective photolysis of either CO_3 or O_3 produces a corresponding increase in the concentration of the other. In the approach to the steady-state situation, however, the formation of CO_3 by the ultraviolet photolysis of ozone is considerably less efficient than the one-to-one relationship seen in the steady state. This observation indicates that $O(^1D)$ formed by ozone photolysis is deactivated to $O(^3P)$ in the matrix, and rather than only regenerating O_3, $O(^3P)$ also produces molecular oxygen by recombination. Until some molecular O_2 accumulates, there is net loss of oxygen carrier, corresponding to the net conversion of O_3 into O_2. When sufficient O_2 accumulates so that $O(^3P)$ reacts with it rather than reacting with itself, oxygen carrier is conserved since under these conditions any $O(^3P)$ formed reappears quantitatively as O_3. To explain the efficient photochemical conversion of CO_3 into O_3, we must conclude that light at 400 nm leads to the net production of some $O(^3P)$ from CO_3. It is not possible from our studies to rule out the production of $O(^1D)$ by CO_3 photolysis, since $O(^1D)$ would lead either to more CO_3 resulting in no observed change or (by deactivation) to $O(^3P)$ and hence to ozone as is observed. To estimate the percentage of $O(^1D)$, if any, produced by CO_3 photolysis at these energies, quantum yield studies need to be made.

A further observation on the formation of CO_3 in a CO_2 matrix is that increasing the initial percentage of O_3 in the mixture will increase the total amount of CO_3 obtained up to a point. Thereafter, an increase in the initial amount of ozone does not produce a significant increase in the total amount of CO_3. This implies that at a given concentration of CO_3, the destruction of CO_3 by some active species, presumably $O(^1D)$, becomes competitive with its formation. Thus, the maximum CO_3 is obtained by the use of large matrix deposits and is limited by the transparency of the deposit.

The 2053-cm^{-1} band for CO_3 has been assigned by Moll[5] to the carbonyl stretch perturbed by Fermi resonance. Comparison of our intensity results with various carbonyl bands in steroids studied by Jones, *et al.*,[18] indicates that the intensity of the 2053-cm^{-1} band is somewhat less than that for steroid carbonyls, as is expected for a band perturbed by Fermi resonance. Whereas the observed intensity for the 2053-cm^{-1} band is 1.4×10^4 l. mol^{-1} cm^{-2}, the integrated absorption intensities for steroid carbonyls range from about 1.8×10^4 for α-brominated ketones to about 4.1×10^4 mol^{-1} cm^{-2} l. for conjugated ring ketones and about 1.8×10^4 to 2.9×10^4 for simple saturated steroid ketones.[18]

We turn now to a consideration of the near-ultraviolet absorption spectrum of CO_3 (*cf.* Figure 3). While both the extinction coefficient (11 mol^{-1} cm^{-1} l.) and the oscillator strength ($f = 3 \times 10^{-4}$) suggest an $n \rightarrow \pi^*$ transition in a carbonyl species with planar ground state, the energy of the maximum intensity at 406 nm is considerably lower than for simple aldehyde and ketone carbonyls. Two factors favor the shift to lower energy, however. One is the effect of ring strain. For alicyclic ketones, λ_{max} of the $n \rightarrow \pi^*$ transition is at lower energies for cyclopropanone and for cyclopentanone than it is for cyclobutanone and cyclohexanone. Furthermore, Moll[5] argued for an O–C–O angle of less than 120°, as did Gimarc and Chou.[8] Recent work by Jacox and Milligan indicates that the angle may be 65°.[7] Second, one can make the argument converse to that normally given for the shift to higher energy seen on substitution of electron-donating groups adjacent to the carbonyl carbon. Although it is by no means clear what the effect of two oxygens adjacent to the carbonyl carbon might be, it is possible that the shift in electron density from the carbonyl oxygen to the carbon atom that occurs in an $n \rightarrow \pi^*$ transition is made somewhat more facile energetically by the presence of electron-withdrawing groups. That is, the π^* level is lowered with respect to the ground state.

(16) A. S. Wexler, *Appl. Spectrosc. Rev.*, **1**, 29 (1967).

(17) P. N. Schatz, *Spectrochim. Acta*, **21**, 617 (1965).

(18) R. N. Jones, D. A. Ramsay, D. S. Keiv, and K. Dobriner, *J. Amer. Chem. Soc.*, **74**, 80 (1952).

We considered the possibility that the presence of significant amounts of molecular oxygen in the presence of CO_3 might be enhancing the intensity of a singlet–triplet transition and thus might be giving an observed extinction coefficient which would be deceptively like that expected for an $n \rightarrow \pi^*$ singlet–singlet transition. Therefore, we compared the observations for the CO_3 absorption at 400 nm at both 60 and 80°K. In the latter case molecular oxygen was not readily trapped in the matrix. No differences were detected. Thus we have concluded that the observed CO_3 extinction coefficient at 400 nm has not been perturbed by the presence of of molecular oxygen and may be described as having the characteristic intensity for a singlet–singlet $n \rightarrow \pi^*$ transition.

Another interesting aspect of the near-ultraviolet absorption spectrum of CO_3 is that it is sufficiently low in energy to extend into the visible region so that CO_3 can exhibit a yellow color. For some time there has been speculation concerning the possible role of CO_3 as an explanation for the observed oxygen deficit in the planetary atmosphere of Venus[19] and Mars.[20] Moreover, recent evidence by Plummer and Carson[21] rules out the possibility of carbon suboxide producing the yellow stain in the clouds of Venus. It is tempting to suggest that CO_3 provides that coloration. However, recent work by DeMore and Dede[4] indicates that the formation of ground state CO_3 at the low pressures in question in the planetary atmosphere is very inefficient.

A striking observation concerning the formation of CO_3 in a matrix of CO_2 by photolysis of ozone is that the amount of CO_3 produced is remarkably enhanced by the use of a filter which transmits only in the 260-nm region. Even a low-pressure mercury lamp (for which most of the output is at 253.7 nm) is not efficient for the formation of CO_3. The comparison of results for the two cases suggests that the net quantum yield for ozone decomposition is small. Only in this way can the cophotolysis of the weakly absorbing CO_3 by the relatively weak Hg lines in the near-ultraviolet be significant in limiting the total amount of CO_3 which is obtained when the unfiltered light from the low-pressure arc is used.

The work of DeMore and Jacobsen[10] has called into question the spontaneous reaction of CO_3 with O_2, which was reported from this laboratory.[6] The early work[6] involved photolyzing isotopically normal ozone in ^{18}O-enriched carbon dioxide at liquid helium temperatures forming partially labeled CO_3. Warming the sample deposit resulted in the apparent regeneration of ozone, some of which was of normal isotopic composition and some which, as judged by the infrared absorption, was of the composition of one ^{18}O and two ^{16}O. The formation of some labeled ozone was interpreted as evidence for the reaction of the partially labeled CO_3 with normal O_2 which had been trapped in the matrix. A considerable effort has since been made to reproduce the results of the earlier warming experiments, but without success. Between the two sets of experiments the helium dewar was returned to the factory for repair and modifications. We are at a loss to explain the discrepancy between the earlier results and our present ones, but we are inclined to dismiss the earlier effect as an artifact resulting from the use of an imperfect dewar. The important conclusion is that we can no longer support the suggestion[6] that CO_3 reacts readily with O_2.

Acknowledgment. Financial support for this research, both for Grant No. GP5322 and for P. J.'s traineeship, 1967–1970, by the National Science Foundation, is gratefully acknowledged.

(19) M. B. McElroy, *J. Geophys. Res.*, **73**, 1513 (1968).

(20) M. B. McElroy and D. M. Hunten, *ibid.*, **75**, 1188 (1970).

(21) W. T. Plummer and R. K. Carson. *Astrophys. J.*, **159**, 159 (1970).

Radiation Chemistry of Supercooled Water[1]

by Inna Kules and Robert Schiller*

Central Research Institute for Physics, Budapest, Hungary *(Received September 25, 1970)*

Publication costs assisted by the Central Research Institute for Physics

Dilute aqueous solutions were irradiated between room temperature and −8° in the liquid phase to determine the primary radiation chemical yields of the decomposition products of water. The application of normal scavenger methods showed a linear decrease in G_H and G_{OH} and an increase in $G_{e_{aq}^-}$ with decreasing temperature below 0°, although these yields were temperature independent above the equilibrium melting point. This seems to be the first observation of an abrupt discontinuity due to supercooling in any property of water. $G_{H_2O_2}$ was not affected by supercooling, which suggests that the mechanism of H_2O_2 formation is probably not the combination of two OH radicals.

Introduction

Apart from their genuine theoretical interest, the properties of supercooled liquids are of great importance for the understanding of crystallization from melts. In theories of crystallization[2] supercooled melts are considered to be liquid phases containing a certain amount of embryos, *i.e.*, small clusters of molecules which have the structure of the solid phase. An embryo can increase spontaneously in size only if its radius attains a certain value. An embryo of this critical radius is called a nucleus. The critical radius decreases with decreasing temperature of the melt. It can be shown[2b] that the nucleation rate is perceptible only when the nucleus diameter is not larger than the order of ten molecular diameters. Thus, although any supercooled liquid contains embryos and some of them are large enough to act as nuclei, a certain degree of supercooling is required for a phase change to proceed with an observable rate.

The presence of a highly dispersed solid phase in supercooled liquids has already been deduced from the abrupt changes in properties like viscosity,[3-5] electric conductance,[3] dielectric constant,[6] ultrasonic absorption,[7] ultrasonic velocity,[8] thermal expansion,[4] refractive index,[4] and X-ray diffraction[9] of polar organic substances during supercooling. On the other hand, no such breaks could be detected in the temperature functions of the density,[3,5] surface tension, specific heat, and vapor pressure[3] of these substances.

The conditions and phenomenology of the supercooling of water[10-12] and aqueous solutions[13-15] have been fairly well described. The properties so far investigated, such as vapor pressure,[16] thermal conductivity,[17] refractive index,[18] dielectric constant, and relaxation time,[19] exhibit no break or discontinuity at the thermodynamic melting point. Koefoed,[20] Kavanau,[21] and Kuhns and Mason[22] are of the opinion that the structure of supercooled water does not differ from that of ordinary water.

The aim of the present work was to determine whether the radiation chemical behavior of supercooled aqueous solutions differs in any way from that of ordinary water. Radiation chemical yields were thought to be useful evidence of any structural transformation because of their appreciable difference in water and ice near the melting point. The yield of chemically scavengeable[23] or physically trapped[24] electrons is several

(1) Partly presented at the Fourth Congress of Radiation Research, Evian, June–July 1970.

(2) (a) D. Turnbull and J. I. Fisher, *J. Chem. Phys.*, **17**, 71 (1949); (b) J. H. Holomon and D. Turnbull, *Progr. Metal Phys.*, **4**, 333 (1953); (c) Ya. I. Frenkel, *Izv. Akad. Nauk SSSR*, 336 (1945).

(3) N. N. Greenwood and R. L. Martin, *Proc. Roy. Soc., Ser. A*, **215** 46 (1952).

(4) F. T. Nechai, *Uch. Zap. Beloruss. Gos. Univ. Ser. Fiz.*, **41**, 231 (1958).

(5) A. J. Barlow, J. Lamb, and A. J. Matheson, *Proc. Roy. Soc., Ser. A*, **292**, 322 (1966).

(6) C. Dodd and G. N. Roberts, *Proc. Phys. Soc. London, Sect. B*, **63**, 814 (1950).

(7) A. N. Hunter, *ibid., Sect. B*, **64**, 1086 (1951).

(8) S. Parthasarathy and V. N. Bindal, *Indian J. Phys.*, **34**, 272 (1960).

(9) M. A. Levashevich, N. N. Podosinnikov, and I. Kh. Varivoda, *Tr. Dnepropetrovsk. Khim.-Tekhnol. Inst.*, **4**, 84 (1955).

(10) B. J. Mason, *Advan. Phys.*, **7**, 221 (1958).

(11) R. S. Chanal and R. D. Miller, *Brit. J. Appl. Phys.*, **16**, 231 (1965).

(12) I. Yannas, *Science*, **160**, 298 (1968).

(13) K. A. Cooper and J. G. Watkinson, *Trans. Faraday Soc.*, **53**, 635 (1957).

(14) C. Lafargue, *C. R. Acad. Sci.*, **246**, 1894 (1958).

(15) H. R. Pruppacher, *J. Chem. Phys.*, **39**, 1586 (1963).

(16) D. Eisenberg and W. Kauzman, "The Structure and Properties of Water," Clarendon, Oxford, 1969, p 60.

(17) R. W. Powell, *Advan. Phys.*, **7**, 276 (1958).

(18) N. Dass and N. K. Gilra, *J. Phys. Soc. Jap.*, **21**, 2039 (1966).

(19) (a) J. A. Saxton, *Proc. Roy. Soc., Ser. A*, **213**, 473 (1952); (b) S. A. M. El-Sabeh, *Proc. Colloq. AMPERE (At. Mol. Etud. Radio Elec.)*, **11**, 351 (1963).

(20) J. Koefoed, *Discuss. Faraday Soc.*, **24**, 216 (1957).

(21) J. L. Kavanau, "Water and Solute-Water Interaction," Holden-Day, San Francisco, Calif., 1964, p 12.

(22) I. E. Kuhns and B. J. Mason, *Proc. Roy. Soc., Ser. A*, **302**, 437 (1968).

orders of magnitude lower in ice than in liquid water. Hart[25] stated that "in pure crystalline ice where very few traps exist, the yield of trapped electrons is vanishingly small at low temperatures." The high transient yield of e_{aq}^- observed in pulse radiolysis of ice does not contradict this finding since, in our view,[26] the main mode of e_{aq}^- disappearance in ice is geminate ion–electron recombination, in agreement with the much shorter lifetime of e_{aq}^- in single crystals of ice than in water.[27]

Experimental Section

Distilled water was twice redistilled from alkaline permanganate and acid dichromate and used, as a rule, within 2 days. All chemicals were of AR or GR grade, used without further purification, except for tetranitromethane, which was shaken repeatedly with triply distilled water before preparing the sample.

The sample solutions were deaerated on a vacuum line by freeze pumping or by argon bubbling. The same line was used for N_2O saturation. Owing to the volatility of tetranitromethane, its solutions had to be analyzed after deaeration or gas saturation, the method of Baillie, *et al.*,[28] being used. Samples were kept at each temperature for 0.5 hr prior to irradiation. No precautions were needed for keeping the solutions perfectly still.

The irradiations were carried out on a 2.000-Ci ^{60}Co γ source and on an 80.000-Ci facility, with doses varying from 4.5×10^{17} to 1.25×10^{19} eV/ml and dose rates of either 4.5×10^{16} or 1.8×10^{18} eV/ml min. Temperature stability of the samples during irradiation was maintained by constant-temperature baths or cooling thermostat and was measured as $\pm 0.5°$.

Analyses were made at room temperature. Nitroform was measured at 350 nm and ferricyanide at 420 nm on a Beckman DU spectrophotometer. Hydrogen peroxide was analyzed by the methods of Ghormley.[29]

Results and Discussion

The hydrated electron and H atom yields were determined directly from the measured nitroform products[30] on irradiation of nearly neutral solutions of 3×10^{-4} M tetranitromethane. [The total reducing agent yield exhibits only a negligible change when temperature decreases from 24 to $-7°$, in contradiction with our earlier finding[23] of a decrease of about 50% in the nitroform yield in the same temperature range. The cause of this discrepancy was probably the presence of an OH scavenging impurity, RH, in the batch of tetranitromethane, TNM, used in the earlier experiments. A reaction sequence of the form RH + OH → ·R; ·R + TNM → NF^- (a); ·R + NF^- → product (b), a difference of about 13 kcal between the activation energies of reactions a and b, and an amount of impurity which scavenges some half of the OH radicals can account quantitatively for the erroneous values. This numerical error has, however, absolutely no bearing on the statements and inferences made in ref 23.] The nitroform yield $G_I(NF^-)$ was found to be the same either in the presence or absence of air at any temperature. The addition of N_2O to a concentration of about 2×10^{-2} M reduced the yield to $G_{II}(NF^-)$. The primary yields G_H and $G_{e_{aq}^-}$ were evaluated from the equations

$$G_I(NF^-) = G_H + G_{e_{aq}^-} = G_{red} \quad (1)$$

$$G_{II}(NF^-) = G_H \quad (2)$$

The primary OH and H_2O_2 yields were calculated from the H_2O_2 yields measured in aerated 10^{-5} M KBr solutions and from the ferricyanide yield measured in a deaerated system containing 10^{-3} M $K_4Fe(CN)_6$ and 10^{-4} M $K_3Fe(CN)_6$,[31,32] using the equations

$$G_{OH} = 0.5G(Fe(CN)_6^{3-}) - G(H_2O_2) + G_{red} \quad (3)$$

$$G_{H_2O_2} = 0.5G(H_2O_2) + 0.25G(Fe(CN)_6^{3-}) \quad (4)$$

The primary yields are plotted as a function of temperature in Figure 1. It can be seen that the values

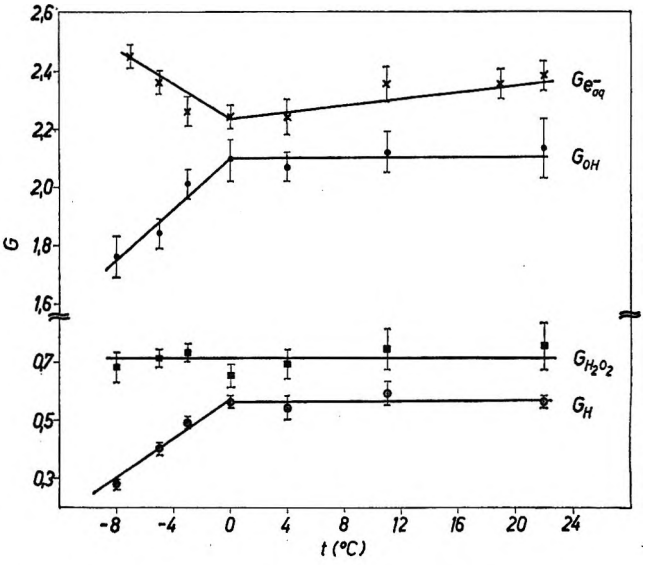

Figure 1. The primary yields as a function of temperature.

(23) R. Schiller, *J. Chem. Phys.*, **47**, 2281 (1967).
(24) K. Eiben and I. A. Taub, *Nature (London)*, **216**, 782 (1967).
(25) E. J. Hart, *Accounts Chem. Res.*, **2**, 161 (1969).
(26) R. Schiller, *Curr. Top. Radiat. Res.*, **6**, 1 (1970).
(27) G. Nilsson, A. C. Christensen, J. Fenger, P. Pagsberg, and S. O. Nielsen in *Advan. Chem. Ser.*, **No. 81**, 71 (1968).
(28) A. Baillie, A. K. Macbeth, and N. I. Maxwell, *J. Chem. Soc.*, 880 (1920).
(29) A. O. Allen, C. J. Hochanadel, J. A. Ghormley, and T. W. Davis, *J. Phys. Chem.*, **56**, 575 (1952).
(30) K. D. Asmus and A. Henglein, *Ber. Bunsenges. Phys. Chem.*, **68**, 348 (1964).
(31) T. J. Sworski, *J. Amer. Chem. Soc.*, **76**, 4687 (1954).
(32) (a) J. Rabani and G. Stein, *Trans. Faraday Soc.*, **58**, 2150 (1962); (b) F. S. Dainton and W. S. Watt, *Proc. Roy. Soc., Ser. A*, **275**, 447 (1963).

of G_H and G_{OH} do not show any appreciable variation from room temperature down to 0°.

A break is observed in the G_H *vs.* T curve at the thermodynamic melting point; below this point G_H decreases approximately linearly with decreasing temperature. The break in the temperature curve of the OH yield at 0° is not so unequivocal. However, if an approximation to the curve is made by constructing two straight lines intersecting at 0°, the quasilinear decrease of G_{OH} is commensurate with that of G_H in the supercooled region. A least-squares fit shows the slopes of the decreases to be about the same within the experimental error, namely, $dG_{OH}/dT = (4.4 \pm 0.8) \times 10^{-2}$ and $dG_H/dT = (3.6 \pm 0.5) \times 10^{-2}$ in radical/100 eV deg units. Approximating to the temperature curve of the solvated electron yield in the same way, above 0° the yield seems to decrease somewhat with decreasing temperature. Since the slope evaluated by the least-squares fit is only $(6 \pm 6) \times 10^{-3}$, no definite conclusion can be drawn on the temperature dependence. Below 0°, $G_{e_{aq}^-}$ increases with decreasing temperatures, exhibiting a slope $dG_{e_{aq}^-}/dT = (3 \pm 1) \times 10^{-2}$. The H_2O_2 yield was constant over the whole range of temperature.

Separate experiments showed that changes in total dose or dose rate had no noticeable effect on the yield *vs.* temperature curves. This insensitivity to dose and dose rate suggests that our results reflect some genuine property of the supercooled water that is independent of the interaction between radiation and metastable matter. This is far from being an obvious result in view of the observation[33] and theoretical explanation[34] of the nucleation of supercooled melts under radiation.

Supercooling reduces the net yield of water decomposition, $G(-H_2O)$, decreasing G_H and G_{OH} by about an equal amount, while it increases $G_{e_{aq}^-}$.

These radiation chemical yields seem to be the first measured properties which point to some discontinuous change in the structure of liquid water during supercooling.

Irradiated crystalline ice is known to be characterized by a high probability of geminate H + OH recombination[35] and by a very low yield of scavengeable or trapped e_{aq}^-.[23,24] In its radiation chemical behavior supercooled water shows an enhancement of geminate recombination similar to that of ice, but it differs considerably so far as $G_{e_{aq}^-}$ is concerned. Geminate radical recombination is most probably influenced by the nearest neighbors of the radical pair, while electron escape is governed by the average macroscopic properties of the system.[26,36] If it is justifiable at all to assume any similarity between the structure of ice and supercooled water, one could conclude that supercooling affects only the short-range order prevailing in water and leaves the long-range conditions unchanged.

A further observation of interest is the constant value of $G_{H_2O_2}$ and the large decrease of G_{OH} with decreasing temperature. If H_2O_2 is formed by the combination of two OH radicals, the peroxide yield could reasonably be expected to decrease with the decreasing number of available OH radicals. The measured yields of OH and H_2O_2 below the melting point, however, furnish a further confirmation of the view[37] that H_2O_2 must be formed by some other mechanism.

Acknowledgments. The authors are indebted to Prof. G. Földiák and Dr. V. Stenger for their advice and their kind permission to use the 80.000-Ci facility of the Institute of Isotopes, to Dr. G. Jancsó, Dr. L. Matus, and Dr. I. Opauszky for stimulating discussions, to an unknown reviewer for helpful comments, and to Mrs. A. Horváth and Mr. J. Mándics for their technical assistance.

(33) (a) D. E. Ovsienko, *Kristallografiya*, **5**, 779 (1960); (b) N. C. Varshneya, *Univ. Roorkee, Res. J.*, **8**, 3 (1965); (c) N. C. Varshneya, *Nature (London)*, **223**, 826 (1969).

(34) A. F. Pisaryev, *Zh. Eksp. Teor. Fiz.*, **54**, 463 (1968).

(35) (a) S. Siegel, J. M. Flournoy, and L. H. Baum, *J. Chem. Phys.*, **34**, 1782 (1961); (b) L. Kevan, P. N. Moorthy, and J. J. Weiss, *J. Amer. Chem. Soc.*, **86**, 771 (1964); (c) B. G. Ershov, *Him. Vys. Energ.*, in press.

(36) (a) R. Schiller, *J. Chem. Phys.*, **43**, 2760 (1965); (b) R. Schiller, *ibid.*, **47**, 2278 (1967); (c) A. Mozumder, *ibid.*, **50**, 3153 (1969).

(37) M. Anbar in "Fundamental Processes in Radiation Chemistry," P. Ausloos, Ed., Interscience, New York, N. Y., 1968, p 666.

Effect of Dissolved Paraffinic Gases on the Surface Tension and Critical Micelle Concentration (cmc) of Aqueous Solutions of Dodecylamine Hydrochloride (DACl)

by I. J. Lin

Technion, Israel Institute of Technology, Haifa, Israel

and A. Metzer*

Israel Mining Industries, Institute for Research and Development, Haifa, Israel *(Received December 29, 1970)*

Publication costs borne completely by The Journal of Physical Chemistry

The solubilities of ethane and propane in aqueous solutions of DACl have been measured at 25° and atmospheric pressure. Their solubility reaches a minimum for a concentration of DACl of 2×10^{-6} mol/l. For air, the lowest solubility was determined at a concentration of 5×10^{-5} mol/l. DACl. The decrease in surface tensions and in the cmc of solutions of DACl saturated with ethane and propane have been determined by two independent methods as equivalent to a lengthening of the hydrocarbon chain of the DACl of approximately 0.35–0.46 unit of $-CH_2-$ for ethane and 0.72–0.80 unit of $-CH_2-$ for propane.

Introduction

The solubilities in water of the homologous series of paraffinic gases from methane to butane have been reported in the literature, and a number of hypotheses on the mechanism of solubilization have been advanced, but practically no data are available on the surface and bulk properties of these solutions. Moreover, although there are many publications on the solubilization by surface-active agents, nothing has been reported on the effect of these agents on the solubility of paraffinic gases in water.

The effect of some paraffinic gases on the froth flotation of quartz with dodecylamine hydrochloride (DACl) was studied by Gratch,[1] who showed that these gases greatly enhanced the floatability as a result of increased contact angles as compared with those obtained when using air as the flotation gas. As a first step of a more detailed study, the effect of ethane and propane on the surface tension and cmc of solutions of DACl was investigated. In addition, the solubilities of these gases in aqueous solutions of DACl as a function of concentration were determined.

The solubility of inert gases in water is closely dependent on the structure of water. Ben Naim and Baer[2] have shown that the solubility of argon in water–ethanol mixtures shows a minimum at about 0.10 mol fraction ethanol. This anomaly was attributed to the influence of alcohol on the structure of water, a small amount of alcohol probably increasing the degree of crystallinity of water. Likewise, ionic salts decrease the solubility of gases in water by a partial disruption of the structure of water similar to an increase in temperature, which also decreases the gas solubility. This effect can also be explained by the fact that part of the water molecules become associated to the ions in the solvated layer, being unavailable for dissolving gas.

Frank and Evans[3] proposed a theory of solubility of inert gases in water, which assumes that the introduction of the gas causes the ordering of the water molecules to a state having lower energy and entropy (iceberg). They assumed that the water structure contains vacancies or holes, which are filled with the gas molecules.

The solubilities of the homolog series of normal paraffinic gases in water as determined by various authors are given in Table I.[4–7]

Experimental Section and Results

Solubilities. The solubilities of ethane, propane, and air in aqueous solutions of DACl were determined with the apparatus developed by Ben Naim and Baer.[2] The method is quite simple, rapid, and accurate to 0.2%. The solutions of DACl were prepared with bidistilled, deaerated water and introduced into the apparatus under vacuum. All the determinations were carried out at 25°. The results are shown in Figure 1 as cubic centimeters of gas absorbed in 1000 cm^3 of solution at 750 mm and 25 ± 0.1°.

(1) E. Gratch, M.Sc. Thesis, Israel Institute of Technology, Haifa, Israel, 1966.

(2) A. Ben Naim and S. Baer, *Trans. Faraday Soc.*, 59, 2735 (1963).

(3) H. S. Frank and M. M. Evans, *J. Chem. Phys.*, 13, 509 (1954).

(4) C. McAuliffe, *J. Amer. Chem. Soc.*, 86, 275 (1964).

(5) W. Y. Wen and J. H. Hung, *J. Phys. Chem.*, 74, 170 (1970).

(6) W. F. Claussen and M. F. Polglase, *J. Amer. Chem. Soc.*, 74, 4817 (1952).

(7) T. J. Morrison and F. Billett, *J. Chem. Soc.*, 3819 (1952).

Table I: Solubilities of Paraffinic Gases in Water

Gas	Mol wt	Molar vol at 20°, ml	Solubility, ml of gas/1000 g of water, at 25°, 760 mm		
CH_4	16	39[a]	31.35[b]	31.80[c]	30.14[d]
C_2H_6	30	55[a]	41.20[b]	43.00[c]	41.18[d]
C_3H_8	44	88.1[a]	32.31[b]	32.71[c]	33.30[d]
n-C_4H_{10}	58	100.4[a]	26.34[b]	23.40[c] (30°)	25.88[d]

[a] Reference 4. [b] Reference 5. [c] Reference 6. [d] Reference 7.

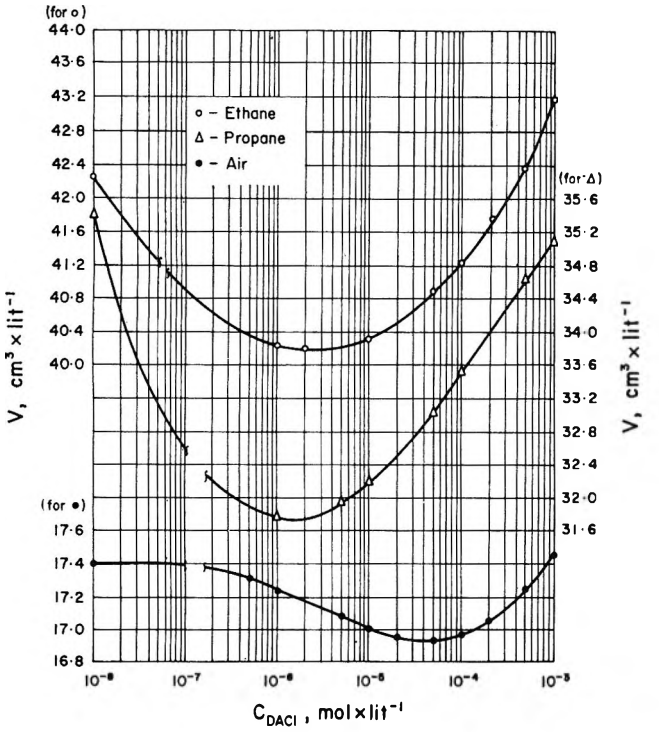

Figure 1. Solubility of gas in cubic centimeters per liter of DACl solution at 25°.

Surface Tensions. Measurements were performed by the ring method with a De Noüy tensiometer with an accuracy of ±0.1 dyn/cm. The DACl solutions were saturated with the respective gas and maintained in a thermostatic bath at 25° under an atmosphere of circulating gas. The results are shown in Figure 2.

Critical Micelle Concentration. Lawrence[8] determined the cmc of dodecylamine hydrochloride by measurements of pH values *vs.* concentration and confirmed the results of this method with conductivity measurements. He found that the cmc corresponded to a solution with 0.275 g of DACl per 100 g of solution (1.25×10^{-2} mol/l.) at 25°. This value is in quite good agreement with the previous determinations of Hoyer and Greenfield,[9] who found 1.38×10^{-2} mol/l., Corrin and Harkins,[10] 1.31×10^{-2} mol/l., and Ralston and Hoerr,[11] 1.3×10^{-2} mol/l. (All these values are at 25°.)

The method used in this work was that of Lawrence,[8]

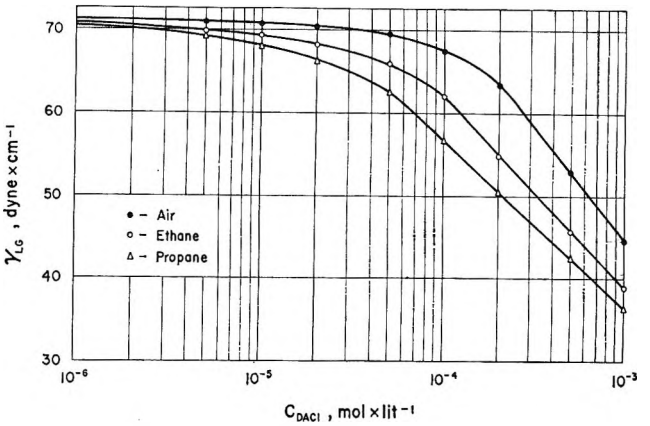

Figure 2. Surface tensions of DACl saturated with air, ethane, and propane at 25°.

based on the change of pH with concentration of solutions of DACl. Solutions of high-purity DACl in distilled, degassed water were prepared, and the pH's were measured after saturation with air, ethane, or propane. The results are given in Figure 3. The points of inflection of the curves indicate the cmc: for air, 1.3×10^{-2}; for ethane, 1.0×10^{-2}; for propane, 7.5×10^{-3}.

Discussion

The results show that the bulk as well as the surface properties of solutions of DACl are strongly affected by the presence of paraffinic gases.

With reference to Figure 1, the solubilities of ethane and propane decrease up to a concentration of DACl of 2×10^{-6} *M* and that of air decreases up to 5×10^{-5} *M* DACl. These decreases in solubility are followed by an increase for higher concentrations of DACl. A simple interpretation of this phenomenon is that for very dilute solutions of DACl this compound acts as an electrolyte, salting out the gas from solution. For higher concentrations the electrolyte character of DACl is balanced by the effect of the hydrocarbon chain, to which the gas molecules become attached by van der Waals forces, and therefore the solubility curve passes through a minimum. For still higher concentrations of DACl, but below the cmc, the heteropolar ions may associate progressively to form dimers, as suggested by Mukerjee,[12] on which the gas may become absorbed. It is interesting to note that the concentration of DACl at which the gas solubility is a minimum is lower for the paraffinic gases than for air. This should be connected with the lowering of the cmc of DACl in the presence of the gases, which will be discussed later.

(8) A. S. C. Lawrence, *et al.*, *Proc. Int. Congr. Surface Activ., 2nd*, 1, 385 (1957).

(9) H. W. Hoyer and A. Greenfield, *J. Phys. Chem.*, 61, 818 (1957).

(10) M. L. Corrin and W. C. Harkins, *J. Amer. Chem. Soc.*, 69, 638 (1947).

(11) A. W. Ralston and C. W. Hoerr, *ibid.*, 64, 772 (1942).

(12) P. Mukerjee, *Advan. Colloid Interface Sci.*, 1, 241 (1967).

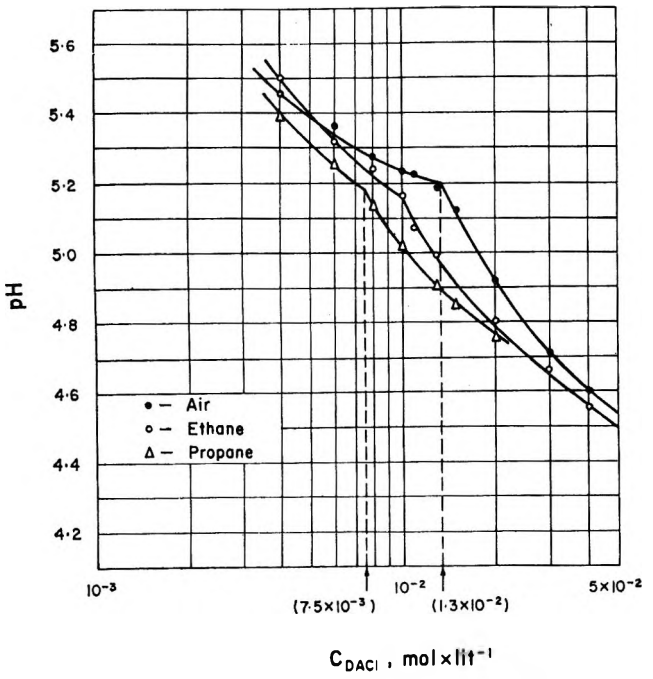

Figure 3. Cmc of solutions of DACl saturated with air, ethane, and propane at 25°.

With reference to Figure 2 the paraffinic gases appear to have a definite effect on the surface tension of DACl solutions. Since ethane and propane dissolved in pure water do not change appreciably the surface tension, it must be concluded that they do not concentrate at the surface. This is also true for very dilute solutions of DACl (10^{-6} mol/l.), for which it has been shown that the gas solubility reaches a minimum. However, the effect of ethane and propane begins to show at concentrations of 10^{-5} mol/l. DACl, for which a small decrease in surface tension is noted. For still higher concentrations of DACl the decrease in surface tension reaches more than 10 dyn/cm for propane and about 7 dyn/cm for ethane as compared with air. This behavior of the solution in the presence of the paraffinic gases indicates that these are adsorbed on the surface in the presence of the DACl.

Surface adsorption is represented by the Gibbs equation

$$\Gamma = -\frac{1}{RT}\frac{\partial\gamma}{\partial \ln c_{\mathrm{DACl}}} \qquad (1)$$

where Γ is the surface excess in mol/cm^2, γ is the surface tension in dyn/cm, and c_{DACl} is the molar concentration, which in dilute solution can be used instead of the more rigorous activity. The concentration of gas is considered constant, since the relative change in gas solubility is less than 10% in the range of concentration of DACl studied here. Equation 1 states that the slope of the surface tension γ *vs.* ln c is a measure of the surface adsorption of the solute.

Referring to the linear part of the curves of Figure 2, it can be seen that the maximum surface excess (calculated as DACl) decreases from air to propane, since the absolute value of the slope of the lines decreases in that order. Therefore, the effect of the gases is manifested as an absolute decrease in the magnitude of the surface tension—evidence of their adsorption on the surface—and also in decreasing the adsorption of DACl. Calculations based on eq 1 and results from Figure 2 (for the linear part of the curves) give the following values of adsorption of DACl on the surface: for air, 4.7×10^{-10} mol/cm^2; for ethane, 4.0×10^{-10} mol/cm^2; for propane, 3.5×10^{-10} mol/cm^2.

For the purpose of this discussion it has been assumed that only the amine ion or the undissociated amine salt (or hydroxide) is adsorbed on the surface layer. A rigorous treatment of the Gibbs equation would require the introduction of a coefficient 2 in the denominator of eq 1 to take care of the fact that the DACl is an electrolyte which dissociates into DA^+ and Cl^- ions.[13,14] However, the question of whether both cation and anion contribute to the lowering of the surface tension has been the subject of considerable controversy. Substantial experimental evidence available[15] indicates that eq 1 as it stands is applicable to dilute solutions of ionic surface-active reagents. This is also supported by the fact that the area per adsorbed molecule in the presence of air calculated from the value of $\Gamma_{\max}$ given above is 35.4 Å^2 per molecule, which is what might be expected, instead of double this value if the coefficient 2 is introduced.[15]

The contribution of the adsorbed gas to the decrease in surface tension can be calculated in terms of equivalent lengthening of the hydrocarbon chain of DACl. For homologous series of aliphatic substances in water, Traube observed that the surface activity increased by a factor of 3 for each additional methylene group in the alkyl chain. This relationship is known as Traube's rule. According to Langmuir's interpretation of this rule,[16] the work W to transfer 1 mol of solute from the bulk to the surface is

$$W = RT \ln (c^s/c) = RT \ln (\Gamma/\tau c) \qquad (2)$$

where $c^s = \Gamma/\tau$ is the surface concentration, Γ is the surface excess in mol/cm^2, and τ is the thickness of the surface region. For a difference in chain length of one $-CH_2-$ group, the difference in work is

$$W_n - W_{n-1} = RT \ln \frac{\Gamma_n/\tau c_n}{\Gamma_{n-1}/\tau c_{n-1}} \qquad (3)$$

(13) P. L. de Bruyn and G. E. Agar, "Froth Flotation," 50th Anniversary Vol., D. W. Fuerstenau, Ed., AIME, 1962, pp 91–138.

(14) K. Durham, "Surface Activity and Detergency," Macmillan, London, 1961.

(15) J. K. Dixon, C. M. Judson, and D. J. Salley, "Monomolecular Layers," American Association for the Advancement of Science, Washington, D. C., 1954, p 63.

(16) A. W. Adamson, "The Physical Chemistry of Surfaces," 2nd ed, Wiley, New York, N. Y., 1967.

Table II[a]

γ, dyn cm^{-1}	$\Gamma \times 10^{10}$, mol/cm^2			c_n, mol l.$^{-1}$	c_m, mol l.$^{-1}$		$\Gamma_m c_n / \Gamma_n c_m$	
	Air	Ethane	Propane	Air	Ethane	Propane	Ethane	Propane
45				9.5×10^{-4}	5.5×10^{-4}	3.8×10^{-4}	1.5	1.9
50	4.7	4.0	3.5	6.2×10^{-4}	3.3×10^{-4}	2.2×10^{-4}	1.6	2.1
55				2.0×10^{-4}	1.3×10^{-4}	1.3×10^{-4}	1.7	2.3
						Av	1.6	2.1

[a] From these values the effect of the two paraffinic gases in terms of $-CH_2-$ units can be calculated: for ethane, $m - n = \ln 1.6/\ln 2.8 = 0.46$; for propane, $m - n = \ln 2.1/\ln 2.8 = 0.72$.

where n is the number of $-CH_2-$ groups in the hydrocarbon chain. By Traube's rule, for values of $\gamma_n = \gamma_{n-1}$, $c_{n-1}/c_n = 3$, and if we assume Γ_n/Γ_{n-1} as approximately constant, then, at 25°

$$W_n - W_{n-1} = RT \ln 3 = 640 \text{ cal/mol} \quad (4)$$

This 640 cal/mol should be regarded as the work necessary to bring one $-CH_2-$ group from the bulk to the surface. Fuerstenau[17] determined experimentally this value as $1.0kT$, which is equivalent to 600 cal/mol, very close to the values derived from Traube's rule.

If this value is introduced in eq 4

$$W_n - W_{n-1} = RT \ln 2.76 \quad (5)$$

Indicating with subscript m the *apparent* hydrocarbon chain length of DACl in the presence of the paraffinic gases ($n = 12$), we have

$$W_m - W_n = RT \ln x \quad (6)$$

and eq 5. From eq 2 and 3 we obtain, on the assumption that τ is constant

$$m - n = \frac{W_m - W_n}{600} = \frac{\ln \left(\frac{\Gamma_m c_n}{\Gamma_n c_m}\right)}{\ln 2.76} \quad (7)$$

where Γ_m and c_m are the surface excess and the concentration of DACl, respectively, in the presence of paraffinic gases.

Calculation of $m - n$ for the system studied can be only approximate, since it varies with the concentration of DACl. Therefore, three values of the concentration of DACl were determined from Figure 2 for three values of the surface tension in the linear region of the curves, and an average value for the last term of eq 7 was calculated. The results are given in Table II.

In other words, the effect of ethane on surface tension in presence of DACl is equivalent to a lengthening of the hydrocarbon chain of 0.46 unit of $-CH_2-$ and for propane 0.72 of $-CH_2-$. Expressed in another form, it appears as if approximately 1 mol of gas is adsorbed on the surface for every 4 mol of DACl.

This apparent lengthening of the hydrocarbon chain of DACl in presence of ethane and propane also results in a corresponding decrease of the critical micelle concentration, as shown in Figure 4. It has been shown[18] that for each homologous series of normal hydrocarbon chain surface-active reagents the value of the cmc is doubled for each decrease in a $-CH_2-$ group. For long-chain amine salts the following relation was proposed[19]

$$\log \text{cmc} = A - Bn \quad (8)$$

where n is the number of $-CH_2-$ groups in the alkyl chain and A and B are constants. The results of the cmc of

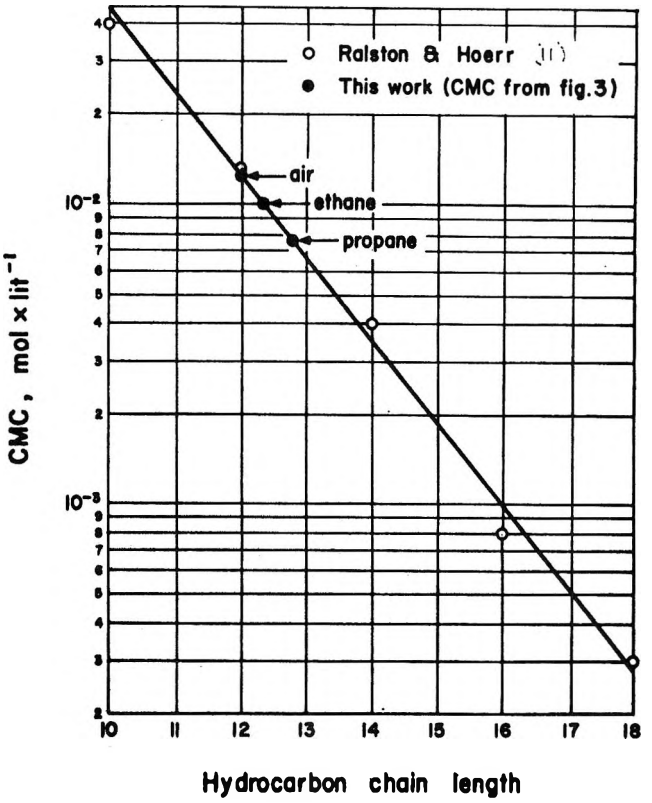

Figure 4. Cmc *vs.* hydrocarbon chain length of homologous amine hydrochlorides at 25°.

(17) D. W. Fuerstenau, T. W. Healy, and P. Somasundaran, *Trans. AIME*, 229, 321 (1964).

(18) A. B. Scott and H. V. Tartar, *J. Amer. Chem. Soc.*, 65, 692 (1943).

(19) L. I. Osipow, "Surface Chemistry," Chapman and Hall, London, 1963, p 473.

the homologous series of straight-chain amine hydrochlorides, as determined by conductivity measurements by Ralston and Hoerr,[11] are plotted in Figure 4, and a straight-line relationship, in accordance with eq 8, was obtained

$$\log \text{cmc} = 1.252 - 0.265n \quad (9)$$

If the values obtained for the cmc of dodecylamine hydrochloride from Figure 3 are introduced in eq 9, the values of n calculated for the paraffinic gases result: ethane, $n = 12.35$; propane, $n = 12.80$. *I.e.*, this is 0.35 unit of $-CH_2-$ for ethane and 0.80 for propane, in close agreement with the values calculated previously from surface tension considerations.

Acknowledgment. This work is part of I. J. Lin's D. Sc. (Tech) Thesis to the Technion, Israel Institute of Technology, Haifa.

The Reactions of Acetone and Hydrogen Peroxide. I. The Primary Adduct[1]

by M. C. V. Sauer and John O. Edwards*

Metcalf Chemical Laboratories, Brown University, Providence, Rhode Island 02912 *(Received May 6, 1971)*

Publication costs assisted by the U. S. Air Force Office of Scientific Research

The reaction between acetone and hydrogen peroxide leads to 2-hydroxy-2-hydroperoxypropane as a first product. The equilibrium constant of formation of this compound was found to be $K = 0.086\ M^{-1}$ at 25°. Thermodynamic parameters of the reaction are $\Delta H = -7.0$ kcal mol^{-1} and $\Delta S = -28$ cal mol^{-1} deg^{-1}. The kinetics of formation and dissociation of 2-hydroxy-2-hydroperoxypropane were studied by both uv spectroscopy and nmr line-broadening techniques. The reaction exhibits general acid and base catalysis. Values of the Brønsted parameters α and β were obtained. The variation of the base-catalyzed rate constants k_{OH} with temperature were studied by the nmr line-broadening technique. Values of activation enthalpy (1.7 kcal mol^{-1}) and entropy of activation (-18 cal mol^{-1} deg^{-1}) were obtained for the forward reaction; corresponding values for the reverse reaction were found to be 8.7 kcal mol^{-1} and $+10$ cal mol^{-1} deg^{-1}.

Introduction

The reaction between acetone and hydrogen peroxide in aqueous solution was studied by several investigators and different products were isolated and identified.[2] However, the product that results from the addition of 1 mol of hydrogen peroxide to acetone, that is 2-hydroxy-2-hydroperoxypropane (compound I), was not detected until recently.[1,3] This compound has, however, been isolated from the photosensitized oxidation of isopropyl alcohol.[4]

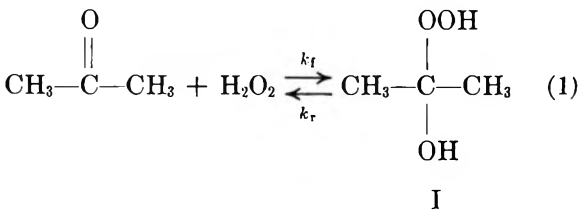

(1)

I

We have found considerable evidence for the existence of this compound in solutions of acetone and hydrogen peroxide. Studies of the thermodynamics and kinetics of its formation determine the experimental conditions under which detection and isolation of this compound may be possible. The quantitative solution data are presented in this article.

Experimental Section

Materials. Reagent grade acetone was used without further purification. Hydrogen peroxide [50% (w/w) and 90% (w/w) donated by the FMC Corp. and 30% (w/w) from Allied Chemical] was used in making peroxide solutions. Reagent grade inorganic salts were used as obtained. Organic acids and their salts were either distilled or recrystallized before use.

Analytical. The total peroxide was determined. A known volume of dilute sample was added to 10 ml of water, 1 ml of sulfuric acid (1/1), and 2 g of KI. In the analysis of acetone–hydrogen peroxide mixtures, acetic acid was used instead of water. Ammonium molybdate was added as a catalyst. The solution was allowed to

(1) Abstracted from part of the Ph.D. Thesis of M. C. V. Sauer at Brown University, June 1970.

(2) A. Rieche, *Angew. Chem., Int. Ed. Engl.*, **70**, 251 (1958); (b) N. A. Milas and A. Golubovic, *J. Amer. Chem. Soc.*, **81**, 6461 (1959).

(3) J. Hine and R. W. Redding, *J. Org. Chem.*, **35**, 2769 (1970).

(4) G. O. Schenk and H. D. Becker, *Angew. Chem., Int. Ed. Engl.*, **70**, 504 (1958).

stand for a few minutes and then the resultant iodine was titrated with standard sodium thiosulfate. The concentration of hydrogen peroxide in the mixtures with acetone was also checked using the same method. No appreciable difference in concentration was found between the value obtained from the titration and the value calculated from dilution with a known volume of acetone.

Equipment. A Varian A-60A nmr spectrometer was used. The temperature of the probe was set using the variable-temperature accessory attached to the spectrometer and was checked using the calibration determined from the separation of the two resonances of methanol.[5]

A Cary 14 recording spectrometer with chart speeds up to 8 in. min^{-1} was used for kinetic determinations. Measurements of pH were made with a Leeds and Northrup pH meter using glass electrodes standardized with commercial buffers. The pH values were corrected for effect of the H_2O_2 on the glass electrode readings.[6]

Equilibrium Constants by Nmr. All of the mixtures were prepared in a test tube and then a small volume was transferred to an nmr tube. This two-stage procedure was found to be optimum for complete mixing of the reactants. The samples were thermostated before the spectra were recorded.

Kinetic Measurements. In the uv spectroscopy runs, the rate was followed by measuring the decrease in carbonyl absorption at 275 nm. The reactions were initiated by the addition with a syringe of 1 ml of the thermostated acetone solution to 2 ml of the hydrogen peroxide solution previously placed in a cell and equilibrated at fixed temperature in the cell compartment of the spectrometer. A minimum of 4 sec was required before absorbance recordings could be obtained with this technique. The effect of hydrogen peroxide concentration on the glass electrode pH readings was very small in the range of concentrations of the uv kinetic runs,[6] so no corrections were applied unless noted otherwise. The ionic strength was maintained at 1 M by addition of KCl. The concentration of the acidic component of each buffer was calculated from the relationships

$$\frac{K_a}{[H^+]} = \frac{[B]}{[AH]}$$

and

$$[B] + [AH] = C_0$$

so

$$[AH] = \frac{C_0[H^+]}{K_a + [H^+]}$$

where C_0 is the buffer concentration, AH is the free buffer acid, B is the conjugate base of the buffer, K_a is the ionization constant of the buffer acid, and brackets are employed to denote concentration.

Nmr Line-broadening. The nmr lines were recorded on slow passage, and the width was measured from the recording. The effective T_2 obtained was then used to correct the measured line width of the samples with appreciable chemical exchange. The difference was attributed to exchange broadening. Before and after every measurement, a sample at the same concentration but on conditions of negligible chemical exchange (that is, lower pH) was recorded and the line width measured.

Results

Thermodynamics. The proton magentic resonance (nmr) spectra of aqueous mixtures of acetone and hydrogen peroxide were studied in the ranges of acetone concentration from 3.8 to 10 M and hydrogen peroxide concentration from 5 to 13 M. From the proton nmr spectra of aqueous acetone the chemical shifts of the methyl resonance of acetone and the proton resonance of water were found to be δ 2.23 and 5.48 with respect to the internal reference tetramethylsilane. The chemical shifts vary slightly with the acetone concentration.

The nmr spectrum of a freshly prepared mixture of acetone and hydrogen peroxide consists of two low-field signals at δ 2.23 and 1.43 and a very broad high-field signal at about δ 5. The high-field resonance corresponds to the protons of H_2O, H_2O_2, and –OH and –OOH groups exchanging very rapidly to produce a single resonance line which has a position established by the natures and relative concentrations of the involved species. The δ 1.43 resonance was assigned to the methyl protons of the addition product; this assignment is consistent with the line positions for known acetal-like species.[1,3]

In order to confirm the assumed stoichiometry the equilibrium position of the reaction was studied at several reactant ratios. Concentrations of acetone and 2-hydroxy-2-hydroperoxypropane (adduct) at equilibrium were found by integrating both resonances and are given by the following equations

$$[\text{acetone}]_e = \frac{I_{Ac}}{I_{Ac} + I_{AP}}[\text{acetone}]_0$$

$$[\text{adduct}]_e = \frac{I_{AP}}{I_{Ac} + I_{AP}}[\text{acetone}]_0$$

where I_{Ac} and I_{AP} are the integrated areas representing acetone and adduct and the subscripts 0 and e represent initial state and equilibrium state, respectively. The hydrogen peroxide concentration at equilibrium was found by the mass relation

$$[H_2O_2]_e = [H_2O_2]_0 - [\text{adduct}]_e$$

The equilibrium constants were found using the relation

(5) "Varian A-60A NMR Spectrometer System Manual," pp 4–12.

(6) J. R. Kolczinski, E. M. Roth, and E. S. Shanley, *J. Amer. Chem. Soc.*, 79, 531 (1957).

$$K = \frac{[\text{adduct}]_e}{[\text{acetone}]_e[H_2O_2]_e}$$

Each value of K reported in Table I is an average of at least four determinations. The thermodynamic parameters at 25° of the reaction are $\Delta G = 1.47$ kcal mol^{-1}, $\Delta H = -7.0$ kcal mol^{-1}, $\Delta S = -28$ cal mol^{-1} deg^{-1}, and $T\Delta S = -8.5$ kcal mol^{-1}.

Table I: Equilibrium Constants for the Primary Addition Reaction of Acetone and Hydrogen Peroxide at Different Temperatures

Temp, °C	K, M^{-1}
0.0 ± 0.5	0.23 ± 0.02
6.0	0.19 ± 0.02
12.0	0.14 ± 0.02
22.0	0.093 ± 0.02
27.0	0.078 ± 0.02
32.0	0.064 ± 0.03
42.0	0.042 ± 0.03

Kinetics by Uv Spectroscopy. The kinetics of reaction 1 were studied spectrophotometrically by following the decrease in carbonyl absorption at 275 nm in a range of acetone concentration from 0.09 to 0.13 M and hydrogen peroxide concentration from 0.31 to 0.62 M. Although the equilibrium constant of the reaction is small, it was found that by using an excess of hydrogen peroxide, the change in the absorbance was significant and the reaction proceeds at a measurable rate.

It was expected that the rate law would, at least insofar as the reactants were concerned, reflect the stoichiometry

$$\frac{-\mathrm{d}[\text{acetone}]}{\mathrm{d}t} = k_f[\text{acetone}][H_2O_2] - k_r[\text{adduct}]$$

When hydrogen peroxide is in considerable excess, the rate should follow pseudo-first-order kinetics. Using a to represent acetone absorption and the a_0, a_t, and a_e to denote initial absorption, absorption at time t, and absorption at equilibrium, respectively, the data can be treated by the equation[7]

$$-\log\left(\frac{a_t - a_e}{a_0 - a_e}\right) = k_{obsd}t$$

If k_f and k_r represent the forward and reverse rate constants, we know that

$$2.303k_{obsd} = k_f[H_2O_2] + k_r$$

Using the principle of microscopic reversibility

$$K = \frac{k_f}{k_r}$$

then

$$k_r = \frac{2.303k_{obsd}}{K[H_2O_2] + 1}$$

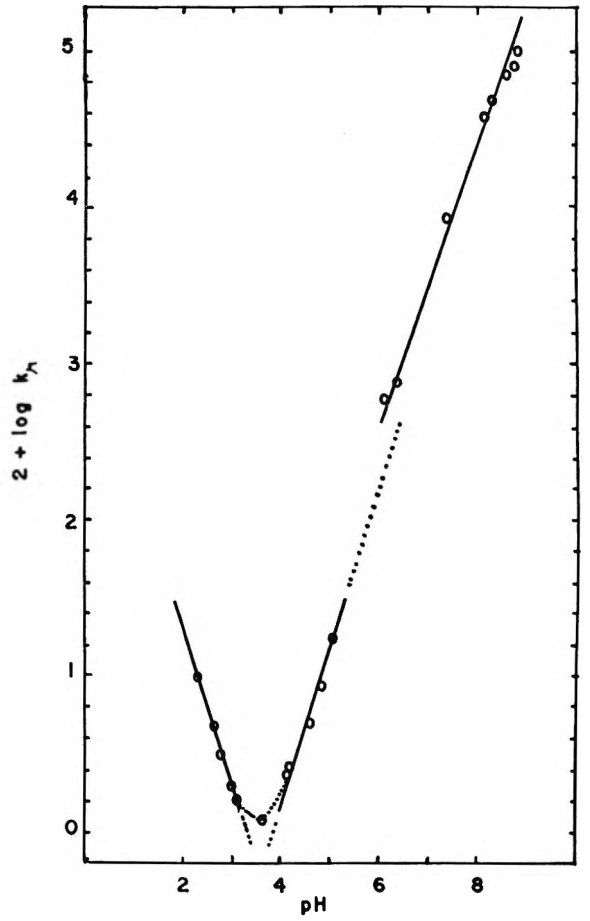

Figure 1. The dependence of rate of dissociation of 2-hydroxy-2-hydroperoxypropane on pH at 25°: pH 2–5, uv spectroscopy, [acetone] = 0.09–0.13 M, [H_2O_2] = 0.31–0.62 M; pH 6–9, nmr line-broadening technique, [acetone] = 0.62–1.42 M, [H_2O_2] = 8–20 M.

Values of K obtained by nmr were used in calculation of k_r and the k_f.

In the absence of any undissociated acid or base, the rate constant in either direction can be expressed as a sum of terms

$$k = k_0 + k_H[H^+] + k_{OH}[OH^-]$$

The pH dependence of the observed rate of adduct dissociation in the absence of general acids and bases is shown in Figure 1. At low pH, the appropriate expression is

$$\log k = \log k_H - \text{pH}$$

and a plot of log k *vs.* pH is a straight line with slope −1. From this line a value of k_H can be calculated. In the same way, the expression for basic solutions is

$$\log k = \log k_{OH} + \log [OH^-]$$

and a value of k_{OH} can now be calculated from the right-hand line of the plot.

(7) A. A. Frost and R. G. Pearson, "Kinetics and Mechanism," 2nd ed, Wiley, New York, N. Y. 1965, p 218.

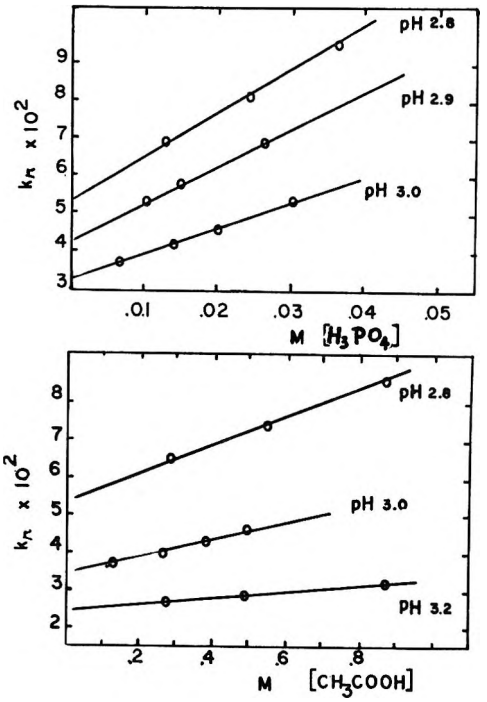

Figure 2. Dependence of rate of dissociation on concentration of buffer acid at 25°.

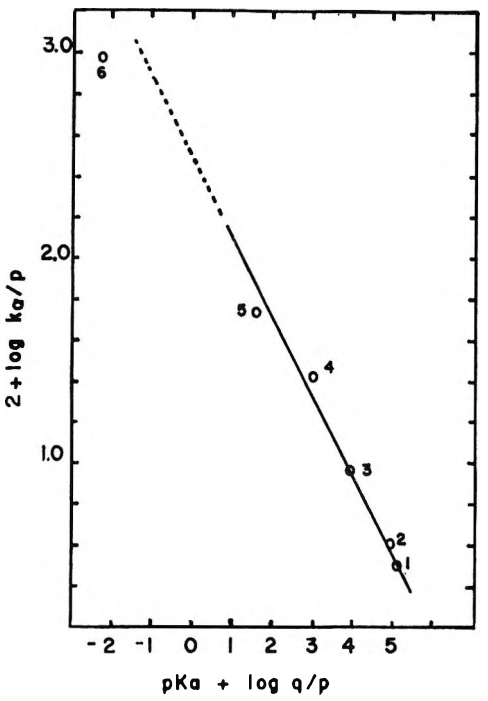

Figure 3. Brønsted plot for acid catalysis of dissociation at 25°. Buffer acids are designated: 1, propionic acid; 2, acetic acid; 3, formic acid; 4, chloroacetic acid; 5, phosphoric acid; and 6, hydronium ion.

These data give second-order rate constants (based on the hydrogen and hydroxide ion concentrations of the figure) of $k_{H,r} = 33.8\ M^{-1}\ \text{sec}^{-1}$ and $k_{OH,r} = 1.88 \times 10^8\ M^{-1}\ \text{sec}^{-1}$ for the dissociation of 2-hydroxy-2-hydroperoxypropane and third-order rate constants of $k_{H,f} = 2.9\ M^{-2}\ \text{sec}^{-1}$ and $k_{OH,f} = 1.6 \times 10^7\ M^{-2}\ \text{sec}^{-1}$ for the formation of the adduct.

The difference between the observed rate and that calculated for the sum of the acid- and base-catalyzed reactions at the pH rate minimum indicates that there is a water-catalyzed path for this reaction with a second-order rate constant $k_{H_2O,r} = 3 \times 10^{-5}\ M^{-1}\ \text{sec}^{-1}$ for adduct dissociation.

The general acid–base catalysis was studied with five different acids and their conjugate bases at increasing buffer concentrations and several buffer ratios. The rate data can be treated using the equation

$$k = k_0 + k_H[H^+] + k_{OH}[OH^-] + k_a[AH] + k_b[B]$$

At a given pH

$$\frac{[AH]}{[B]} = \frac{[H^+]}{K_a} = \theta$$

is a constant; then

$$[B] = \frac{[AH]}{\theta}$$

and the rate constant expression becomes

$$k = k_0 + k_H[H^+] + k_{OH}[OH^-] + (k_a + k_b/\theta)[AH]$$

A plot of k against [AH] at a given pH should be a straight line with slope $k_a + k_b/\theta$. It is clear that at several ratios [AH]/[B], in buffers at different pH, we should have different slopes when k is plotted against free acid concentration.

Figure 2 shows a plot of k_r against conjugate acid concentration for phosphoric acid buffers and acetic acid buffers. In Table II are shown the catalytic constants $k_{a,r}$, and $k_{b,r}$ for the reverse reaction and $k_{a,f}$ and $k_{b,f}$ for the forward reaction. The rate constants for the general acid and base catalysis followed the Brønsted law as can be seen in Figures 3 and 4. The parameters α and β were obtained from the figures and they are $\alpha = 0.43$ and $\beta = 0.50$ for the reverse reaction and $\alpha = 0.53$ and $\beta = 0.55$ for the forward reaction.

Line-Broadening Kinetics. It was observed that, due to the magnitude of the base catalysis, a study of the kinetics of the addition reaction by the nmr line-broadening technique would be possible at pH values higher than 6 and in concentrated solutions of hydrogen peroxide. The chemical exchange was studied in a range of acetone concentration from 0.62 to 1.42 M and hydrogen peroxide concentration from 8 to 20 M. Figure 5 shows the broadening of the methyl proton resonances for acetone and for the addition product as the pH is increased. The half-widths of the lines and the theory developed by Gutowsky, McCall, and Schlichter[8] were used to evaluate the exchange rates.

(8) J. A. Pople, W. G. Schneider, and J. H. Bernstein, "High-Resolution Nuclear Magnetic Resonance," McGraw-Hill, New York, N. Y., 1959, Chapter 10.

Table II: Catalytic Rate Constants for Dissociation and Formation of Adduct with General Acids and Their Conjugate Bases at 25° and $\mu = 1$

Acid	$k_{a,r}$, M^{-1} sec^{-1}	$k_{b,r}$, M^{-1} sec^{-1}	$k_{a,f}$, M^{-2} sec^{-1}	$k_{b,f}$, M^{-2} sec^{-1}
H_3O^+	33.8	$(1.5 \times 10^{-5})^a$	2.90	$(1.3 \times 10^{-6})^b$
H_3PO_4	1.63	2.7×10^{-2}	0.14	2.3×10^{-3}
$ClCH_2COOH$	0.27	5.7×10^{-2}	2.3×10^{-2}	4.9×10^{-3}
$HCOOH$	9.4×10^{-2}	0.13	8×10^{-3}	1.1×10^{-2}
CH_3COOH	4.3×10^{-2}	0.50	4×10^{-3}	4.3×10^{-2}
CH_3CH_2COOH	3.3×10^{-2}	0.58	3×10^{-3}	4.9×10^{-2}
H_2O	$(1.5 \times 10^{-5})^a$	1.88×10^8	$(1.3 \times 10^{6-})^b$	1.08×10^7

[a] Assignment is presently ambiguous since H_2O can act as an acid, as a base, or as both. [b] Also an ambiguous assignment.

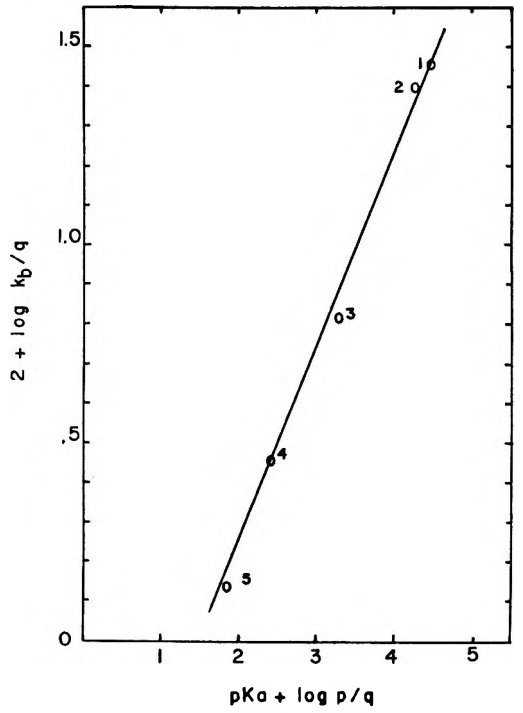

Figure 4. Brønsted plot for base catalysis of dissociation at 25°. Numbers designate conjugate bases of acids listed in Figure 3.

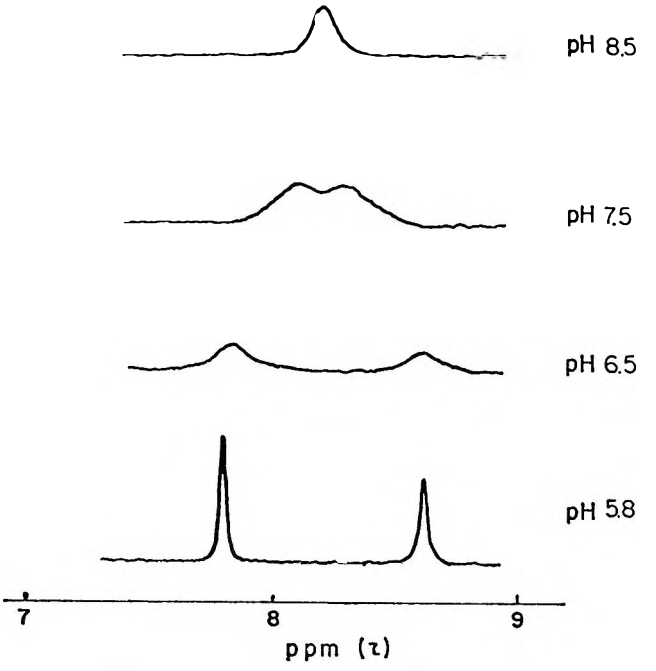

Figure 5. Effect of pH on nmr line width of proton resonances for acetone and 3-hydroxy-2-hydroperoxypropane; sweep time 250 Hz, sweep width 500 Hz, and probe temperature −40°.

When the spectrum consists of two isolated lines of acetone and adduct ("slow exchange"), it can be shown[8] that the individual line widths $\Delta\nu$ (full line width at half-height) are related to the rate constants by the equations

$$\tau_{Ac} = 1/\pi(\Delta\nu'_{Ac} - \Delta\nu_{Ac}) = 1/k_f[H_2O_2]$$

and

$$\tau_{AP} = 1/\pi(\Delta\nu'_{AP} - \Delta\nu_{AP}) = 1/k_r$$

where the $[H_2O_2]$, because it is present in considerable excess with respect to acetone, remains constant. In these equations, τ_{Ac} and τ_{AP} represent the mean lifetimes of the protons of acetone and 2-hydroxy-2-hydroperoxypropane, $\Delta\nu'_{Ac}$ and $\Delta\nu'_{AP}$ the line widths of the acetone and adduct resonances in the presence of exchange, and $\Delta\nu_{Ac}$ and $\Delta\nu_{AP}$ line widths of the acetone and adduct resonances in the absence of exchange.

At the point where both resonances coalesce ("intermediate exchange") calculations can be made using the equation

$$\tau = \left[\frac{1}{1 - \left(\frac{\Delta\nu_{Ac} - \nu_{AP}}{\nu_{Ac} - \nu_{AP}}\right)^2 2\pi^2(\nu_{Ac} - \nu_{AP})^2}\right]^{1/2}$$

along with the definition

$$\tau = \frac{\tau_{Ac}\tau_{AP}}{\tau_{Ac} + \tau_{AP}} = p_{Ac}\tau_{AP}$$

and from this we can calculate $1/\tau_{Ac}$ and $1/\tau_{AP}$.

When the rate of exchange is relatively rapid, the two lines overlap and a single resonance line is observed ("fast exchange"), centered on a weighted-mean frequency ω(mean). If we define

$$p_{Ac} = \tau_{Ac}/(\tau_{Ac} + \tau_{AP}) \text{ and } p_{AP} = \tau_{AP}/(\tau_{Ac} + \tau_{AP})$$

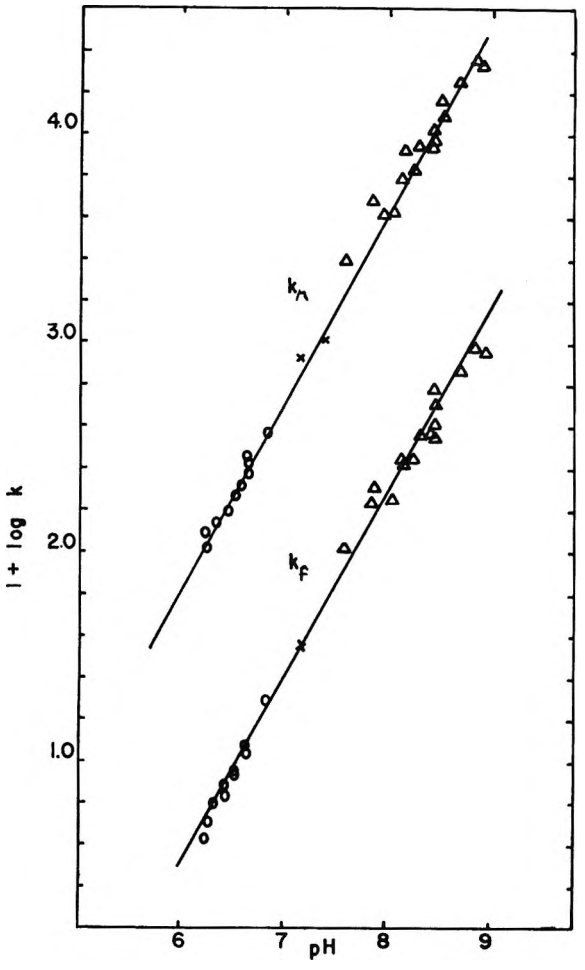

Figure 6. Rate data for dissociation (k_r) and formation (k_f) of 2-hydroxy-2-hydroperoxypropane taken by nmr line-broadening technique at 40°. Lines are drawn with a slope of 1. Circles are for slow exchange region, crosses for intermediate exchange region, and triangles are for fast exchange region.

then, $\omega(\text{mean}) = p_{Ac}\omega_{Ac} + p_{AP}\omega_{AP}$ where $\omega_{Ac}/2\pi$ and $\omega_{AP}/2\pi$ represent the Larmor frequencies of protons Ac and AP in cycles/sec. The half-width of the single line $\Delta\nu'$ now is related to the lifetimes of the protons of acetone and the adduct as follows

$$\pi\Delta\nu' = p_{Ac}\Delta\nu_{Ac} + p_{AP}\Delta\nu_{AP} + p_{Ac}^2p_{AP}^2(\omega_{Ac} - \omega_{AP})^2(\tau_{Ac} + \tau_{AP})$$

From this it can be shown that

$$\frac{1}{\tau_{Ac}} = \frac{p_{Ac}(1 - p_{Ac})^2(\nu_{Ac} - \nu_{AP})4}{\pi\Delta\nu' - \pi p_{Ac}\Delta\nu_{Ac} - \pi\Delta\nu_{AP}(1 - p_{Ac})} = k_f[H_2O_2]$$

with $1/\tau_{AP} = p_{Ac}/(1 - p_{Ac})$ and $1/\tau_{Ac} = k_r$.

The chemical exchange between acetone and adduct was studied at four different temperatures in the range of pH 6–9. Figure 6 shows the dependence of log k_f and log k_r on pH; as can be seen, the variation is represented by a straight line of slope equal to unity.

Values of $k_{OH,f} = k_f/[OH^-]$ and $k_{OH,r} = k_r/[OH^-]$ were found at each temperature, and they are listed in Table III. Relevant activation parameters are given in Table IV.

Table III: Base-Catalyzed Rate Constants of Adduct Formation and Dissociation at Four Temperatures

Temp, °C	$k_{OH,f} \times 10^{-7}$, M^{-2} sec^{-1}	$k_{OH,r} \times 10^{-8}$, M^{-1} sec^{-1}
0	0.90	0.41
12	1.11	0.86
25	1.50	1.81
40	1.61	3.62

Table IV: Activation Parameters for Base-Catayzed Reactions

	E_a, kcal mol^{-1}	$\Delta H^{\ddagger}$, kcal mol^{-1}	$\Delta S^{\ddagger}$, cal mol^{-1} deg^{-1}
Forward reaction	2.4	1.8	−18
Reverse reaction	9.2	8.6	10

Discussion

The small equilibrium constants for formation of 2-hydroxy-2-hydroperoxypropane ($K = 0.23$ at 0°) as compared with the equilibrium constant for formation of the analogous adduct from acetaldehyde and hydrogen peroxide ($K = 48$)[9] can be attributed to the additional methyl group of acetone. The electron deficiency at the carbonyl carbon is partially compensated by the electron-releasing nature of the methyl group (as compared with hydrogen). Consequently, the stability of acetone adducts with nucleophilic reagents is expected to be lower than the stability of acetaldehyde adducts. A small steric effect (methyl *vs.* hydrogen) would work in the same direction as the electronic effect.

The thermodynamic parameters for formation of this adduct are reasonable for an addition reaction similar to the hydration of a carbonyl carbon.[10] For example, formation of a single particle from two reactants would be expected to show a negative entropy, and this is observed ($\Delta S = -28$ cal mol^{-1} deg^{-1}).

The equilibrium constants for formation of the adduct describe the system quite precisely in certain ranges of concentration studied; nevertheless other equilibria must be considered. An influence of the secondary reaction

(9) P. L. Kooijman and W. L. Shijsen, *Recl. Trav. Chim. Pays-Bas*, 66, 205 (1947).

(10) R. P. Bell, *Advan. Phys. Org. Chem.*, 4, 1 (1966).

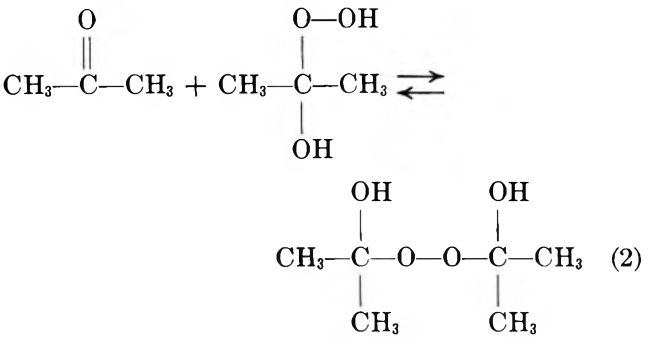

would be expected in solutions rich in acetone. However, there was no apparent effect of the variation in acetone concentration on the equilibrium constants in the range of concentrations studied.

At the pH (about 5) of the solutions without additives (catalysts, buffers, etc.) the formation of 2,2-bis(hydroperoxy)propane is negligible during the first hour after mixing of the reactants

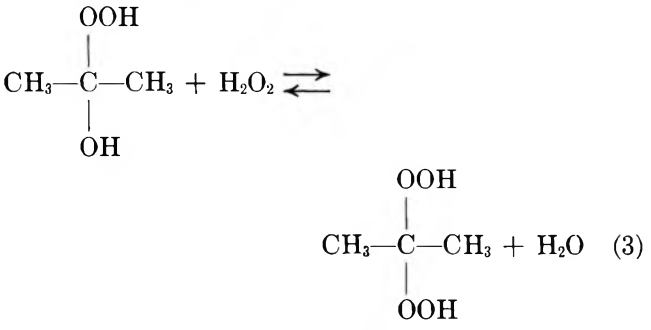

An independent check of the equilibrium constant (K) of the primary addition reaction between acetone and hydrogen peroxide can be obtained from the line-broadening data. Applying the principle of microscopic reversibility to the forward and reverse rate constants obtained separately under conditions of slow exchange, the equilibrium constant for the reaction can be calculated at each temperature. Further, under conditions of rapid exchange, the following equation can be applied

$$\omega_{mean} = \omega_{Ac}p_{Ac} + \omega_{AP}p_{AP}$$

where

$$p_{Ac} = \frac{1}{1 + K[H_2O_2]}$$

and

$$p_{AP} + \frac{K[H_2O_2]}{1 + K[H_2O_2]}$$

and a new value for K can be found. Table V shows the constants obtained in each case. As can be seen, the K values found by the mean frequency equation agree with the ones previously determined, considering the much lower concentrations in acetone used in the line-broadening technique. The values k_f/k_r are in agreement with the others at temperatures equal to and above 12°. However, the value at 0° seems to be lower than the K determined by the two other techniques. Given that this number is based on only two runs under slow exchange conditions, a low K value could be explained if the reaction 2 is considered. The formation of this new compound might cause an additional broadening of the 2-hydroxy-2-hydroperoxypropane resonance, and this would be reflected in a higher k_r value. This effect is more noticeable at low temperature where the 2-hydroxy-2-hydroperoxypropane concentration is higher and the equilibrium constant for this secondary stage becomes more important as happens with all the hydroperoxide additions to carbonyl compounds. In the hydration of acetaldehyde, the adduct

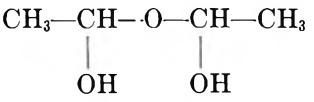

was detected by nmr line-broadening at high concentrations of acetadehyde.[11] It is concluded that a study of the chemical exchange at high acetone concentrations might lead to the detection of the adduct formed from one hydrogen peroxide and two acetone molecules.

Table V: Equilibrium Constants of Adduct Formation Obtained by Different Methods

Temp, °C	K, M^{-1} [a]	k_f/k_r, M^{-1} [b]	K, M^{-1} [c]
40	0.046	0.046	0.044
25	0.077	0.075	0.086
12	0.13	0.11	0.14
0	0.21	0.18	0.23

[a] Fast exchange data (ω_{mean}). [b] Slow exchange data. [c] Values interpolated from Table I.

The kinetics of formation and dissociation of 2-hydroxy-2-hydroperoxypropane present similar characteristics to those of other hydrogen peroxide additions to carbonyl compounds.[12,13] The mechanisms for concerted general acid and base catalysis proposed by Jencks[12,13] seem to fit our kinetic results without modification.

The kinetic results obtained by both uv and nmr line-broadening techniques are summarized in Figure 1. As can be seen the agreement among the data is quite good considering the variable reactant concentrations in the two types of experiments. From the rate profile of Figure 1, it would seem possible to study the kinetics of the reaction by the nmr line-broadening technique at pH values lower than 2, since the reaction

(11) G. Socrates, *J. Org. Chem.*, **34**, 2958 (1969).

(12) E. G. Sander and W. P. Jencks, *J. Amer. Chem. Soc.*, **90**, 4377 (1968).

(13) W. P. Jencks, *Progr. Phys. Org. Chem.*, **2**, 63 (1964).

is also fast in this region. However, this is not possible since the formation of 2,2-bis(hydroperoxy)propane (reaction 3) is acid-catalyzed and becomes very important in acid solutions. In the range of concentrations used in the uv technique (dilute solutions) this secondary reaction is not significant due to the high water concentrations involved in this type of experiment. Further, it was observed that there is no important reaction at basic pH other than the formation of 2-hydroxy-2-hydroperoxypropane. This fact immediately suggests one of the conditions under which isolation of this compound might be possible, that is, in the basic solutions of acetone and hydrogen peroxide.

The activation parameters obtained for the base-catalyzed reaction between acetone and hydrogen peroxide support the proposed mechanism. The similarity of the entropy of activation of the forward reaction $\Delta S_f^{\pm}$ with the entropy of the reaction ΔS ($\Delta S_f^{\pm} = -18$ cal mol^{-1} deg^{-1} and $\Delta S = -28$ cal mol^{-1} deg^{-1}) suggests that the transition state closely resembles the products and that a termolecular interaction among the hydrogen peroxide, the general base (OH^- in this case), and acetone is fundamental to the transition state

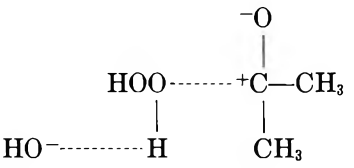

The reaction is accompanied by a substantial loss in entropy owing to the loss in translational freedom of hydrogen peroxide. Further, the small value in activation energy agrees with the fact that the carbonyl group of acetone is highly polarized which facilitates an attack on the carbonyl carbon by a hydrogen peroxide anion.

In the reverse reaction a higher value of the activation energy would be expected since bond breaking is in process, and the positive change in entropy agrees with the dissociation process of 2-hydroxy-2-hydroperoxypropane to form two particles.

The formation of 2-hydroxy-2-hydroperoxypropane as an intermediate has been postulated in the oxidation of ketones by the Baeyer–Villiger reaction.[14,15] Under the mild conditions employed in this study, this oxidation is at most a minor side reaction. Formation of methyl acetate was detected by nmr; however, this was seen only in the more concentrated solutions that were kept at 40° for several days.

The lack of stability of adduct I in aqueous solution is a thermodynamic as well as kinetic phenomenon. This can be seen from the equilibrium constants involved in the different processes. Constants for the processes represented by eq 1 and 3 can be combined to give the disproportionation reaction

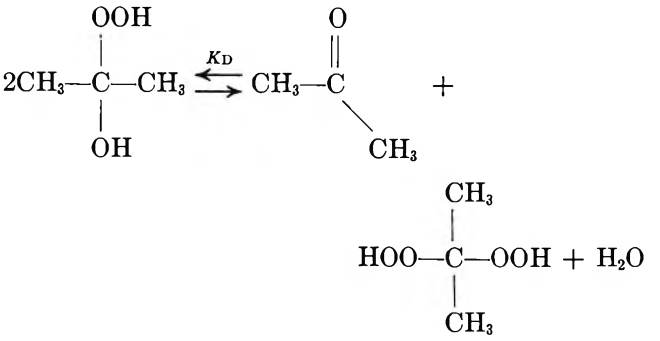

where

$$K_D = \frac{[CH_3COCH_3][(CH_3)_2C(OOH)_2][H_2O]}{[(CH_3)_2C(OH)(OOH)]^2}$$

From these equations, it can be seen that $K_D = K_3/K$, where K_3 is the equilibrium constant for reaction 3. The value of constant K is 0.08 M^{-1} at 25°; the value of K_3 is 170.[1a] Therefore K_D equals 2×10^3 which indicates that adduct 1 has a significant tendency to undergo disproportionation.

Acknowledgments. We thank the U. S. A. F. Office of Scientific Research (Grant 70-1839) for financial aid, Professor J. Hine for information concerning his work prior to publication, and Dr. H. J. Brass for his unfailing interest and cooperation.

(14) A. Baeyer and V. Villiger, *Chem. Ber.*, **32**, 3625 (1899).
(15) R. Criegee, *Justus Liebigs Ann. Chem.*, **560**, 127 (1948).

Bonding Properties of Diatomic Molecular Orbitals[1]

by Ricardo Ferreira

Chemistry Department, Earlham College, Richmond, Indiana 47374 *(Received January 6, 1971)*

Publication costs assisted by Earlham College

In the LCAO-MO approximations, atomic orbital energy matching is a necessary criterion of bond strength for half-filled molecular orbitals. Filled molecular orbitals built from atomic orbitals of differing energies may be strongly bonding due to the interatomic Coulomb energy. Implications of these principles are discussed in relation to the bonding properties of some molecules and free radicals.

Introduction

The differences in bonding properties between one-electron and electron-pair bonds have been discussed from the very beginnings of the valence bond (VB) theory by Heitler and London, Pauling, and others.[2] In VB theory, a necessary condition for the formation of a strong one-electron bond is a large value for the resonance integral between structures $\chi_A(1)\chi_B(0)$ and $\chi_A(0)\chi_B(1)$. This condition obtains only if the two structures have comparable energies, that is, if the energies of the valence orbitals χ_A and χ_B are very close. No such restrictive condition exists for the formation of strong electron-pair bonds, which are consequently of much more widespread occurrence. We have recently[3] returned to this problem from the molecular orbital viewpoint, stressing the differences in bonding properties between half-filled and filled MO's in the case of large differences in the diagonal elements. The purpose of the present paper is to discuss this problem in more detail and to analyze its implications to the rationalization of chemical phenomena.

In a two-center MO described by $\Psi = c_A\chi_A + c_B\chi_B$, if the diagonal matrix elements H_{AA} and H_{BB} are such that $|H_{AA} - H_{BB}| \gg |H_{AB} - H_{AA}S_{AB}|$ and $|H_{AA}| > |H_{BB}|$, the solutions of the secular equation can be approximated to

$$\epsilon_b = H_{AA} + \frac{(H_{AB} - H_{AA}S_{AB})^2}{H_{AA} - H_{BB}} \quad (1)$$

$$\epsilon_a^* = H_{BB} - \frac{(H_{AB} - H_{BB}S_{AB})^2}{H_{AA} - H_{BB}} \quad (2)$$

ϵ_b and ϵ_a^* are the bonding and the antibonding orbital energies and do not include the internuclear repulsion.[4] Further approximation gives

$$\epsilon_b = H_{AA} \quad (3)$$

$$\epsilon_a^* = H_{BB} \quad (4)$$

which corresponds to diagonalization of the determinantal equation. The orbital energies of the bonding and antibonding states become equal to, respectively, the lower (H_{AA}) and the higher (H_{BB}) diagonal elements. We shall now consider the implications of a large value for $(H_{AA} - H_{BB})$ in two distinct situations.

General Formulation. Case 1. Half-Occupied Bonding MO's. Included in this case are mainly molecule ions (H_2^+, LiH^+, HCl^+, CO^+, etc.) but also radicals (CN, BO, etc.) and metals. Mulliken[5] has shown that for a half-filled MO we can write

$$H_{AA} = \epsilon_A + \int \bar{u}_B\chi_A^*\chi_A d\tau \quad (5)$$

$$H_{BB} = \epsilon_B + \int \bar{u}_A\chi_B^*\chi_B d\tau \quad (6)$$

where ϵ_A and ϵ_B are the atomic orbital energies, and $\bar{u}_B$ and $\bar{u}_A$ are the potential energy operators for one electron in the field of the cores B^+ and A^+. The dissociation energy for the process $AB^+(g) \rightarrow A(g) + B^+(g)$ is

$$D_e = -\epsilon_b + \epsilon_A - V_{cc} \quad (7)$$

where V_{cc} is the nuclear (or core) repulsion energy. From (3) and (5)

$$D_e = -\epsilon_A - \int \bar{u}_B\chi_A^*\chi_A d\tau + \epsilon_A - V_{cc} \quad (8)$$

In the perfect screening approximation[6] $\int \bar{u}_B\chi_A^*\chi_A d\tau = -e^2/r_{AB}$. The core repulsion term may be represented by

$$V_{cc} = \frac{e^2}{r_{AB}} + R \quad (9)$$

where R is a noncoulombic term that vanishes rapidly

(1) Work supported by the Research Corp.

(2) For a lucid presentation see L. Pauling, "The Nature of the Chemical Bond," 3rd ed, Cornell University Press, Ithaca, N. Y., 1960, pp 21–23.

(3) R. Ferreira, *Chem. Phys. Lett.*, **2**, 233 (1968).

(4) As pointed out by G. Doggett [*Mol. Phys.*, **10**, 225 (1965)], F. E. Harris [*J. Chem. Phys.*, **51**, 2779 (1968)], and ourselves [R. Ferreira and J. K. Bates, *Theor. Chim. Acta*, **16**, 111 (1970)], in Hückel-type calculations in which the matrix elements are dependent on the net charges, the H matrix elements of eq 1 and 2 are not identical with the F matrix elements of the SCF eigenvalue equation $(F - \epsilon_i S)c_i = 0$. The corresponding operators are related by the expression $H = F - {}^1/_2G$, where G is the electronic interaction operator.

(5) R. S. Mulliken, eq 97 and 98 of *J. Chim. Phys. Physicochem. Biol.*, **49**, 497 (1949).

(6) J. A. Pople, *Trans. Faraday Soc.*, **49**, 1375 (1953).

Table I: Bonding in Half-Filled and Filled MO's

$\epsilon_A/\epsilon_B > 1$				$\epsilon_A/\epsilon_B = 1$			
Molecule	D_e, eV	Molecule ion	D_e, eV	Molecule	D_e, eV	Molecule ion	D_e, eV
LiH	2.5[a]	$LiH^+(^2\Sigma^+)$	<0.1[b]	H_2	4.75[a]	$H_2^+(^2\Sigma_g^+)$	2.79[a]
LiF	<6.6[a]	$LiF^+(^2\Sigma^+)$	<0.7[b]	Li_2	1.12[d]	$Li_2^+(^2\Sigma_g^+)$	1.55[d]
LiI	3.5[a]	$LiI^+(^2\Sigma^+)$	<0.6[c]	Na_2	0.73[d]	$Na_2^+(^2\Sigma_g^+)$	1.01[d]
NaCl	<4.2[a]	$NaCl^+(^2\Sigma^+)$	<0.3[c]	K_2	0.5121[d]	$K_2^+(^2\Sigma_g^+)$	0.75[d]
NaI	3.16[a]	$NaI^+(^2\Sigma^+)$	<−0.4[c]	Rb_2	0.49[d]	$Rb_2^+(^2\Sigma_g^+)$	0.73[d]
KF	<5.9[a]	$KF^+(^2\Sigma^+)$	<−0.6[c]	Cs_2	0.45[d]	$Cs_2^+(^2\Sigma_g^+)$	0.70[d]
KI	3.33[a]	$KI^+(^2\Sigma^+)$	<0.7[c]				

[a] G. Herzberg, "Molecular Spectra and Molecular Structure. I. Spectra of Diatomic Molecules," 2nd ed, Van Nostrand, New York, N. Y., 1950. [b] J. L. Franklin, J. G. Dilland, H. M. Rosenstock, J. T. Herron, K. Drance, and F. H. Field, "Ionization Potentials, Appearance Potentials, and Heats of Formation of Gaseous Positive Ions," NSRDS-NBS 26, Washington, D. C., 1969. Dissociation energies calculated from: $D(AB^+, {}^2\Sigma_g^+) = D(AB, {}^1\Sigma_g^+) + I(B) - I(AB)$. [c] F. H. Field and J. L. Franklin, "Electron Impact Phenomena," Academic Press, New York, N. Y., 1957. [d] Y. T. Lee and B. H. Mahan, *J. Chem. Phys.*, **42**, 2893 (1965).

as r_{AB} increases. If $R = 0$, D_e according to (8) is zero. We can say that within the limits of the perfect screening approximation, half-filled bonding[7] MO's for which $|H_{AA} - H_{BB}| \gg |H_{AB} - H_{AA}S_{AB}|$ correspond to $D_e = 0$. In other words, for half-filled MO's, strong bonding can only occur if $H_{AA} \cong H_{BB}$, or, since $\int \bar{u}_B \chi_A^* \chi_A d\tau = \int \bar{u}_A \chi_B^* \chi_B d\tau$, if $\epsilon_A \cong \epsilon_B$. This is the atomic orbital energy matching criterion for strong bonds.[8a] It should be emphasized that this is only a *necessary* condition: one-electron bonds between atomic orbitals of the same energy may be quite weak (see the discussion on the halogen molecules).

Case 2. Doubly Occupied Bonding MO's. This case includes mainly neutral molecules and some states of molecule ions (HCl^+, $^2\Pi$; Cl_2^+, $^2\Pi$; etc.).

Equations 3 and 4 are again valid if $|H_{AA} - H_{BB}| \gg |H_{AB} - H_{AA}S_{AB}|$, but now the same approximations that led to expressions 5 and 6 give[8b]

$$H_{AA} = \epsilon_A + c_A^2/2(I_A - A_A) - \frac{(1 + c_A^2)}{2}\int \bar{u}_B \chi_A^* \chi_A d\tau \quad (10)$$

$$H_{BB} = \epsilon_B + c_B^2/2(I_B - A_B) - \frac{(1 + c_B^2)}{2}\int \bar{u}_A \chi_B^* \chi_B d\tau \quad (11)$$

I_A, I_B and A_A, A_B are the ionization energies and the electron affinities of orbitals χ_A and χ_B, and $\epsilon_A = -I_A$, $\epsilon_B = -I_B$. In this case the dissociation energy for the process $AB(g) \rightarrow A(g) + B(g)$ is

$$D_e = -2\epsilon_b + \epsilon_A + \epsilon_B - V_{cc} \quad (12)$$

Since $|H_{AA} - H_{BB}| \gg |H_{AB} - H_{AA}S_{AB}|$, the coefficient c_A is close to unity and from (3) and (10) we may write

$$D_e = -I_B + A_A + 2\int \bar{u}_B \chi_A^* \chi_A d\tau - V_{cc} \quad (13)$$

Again, if we assume that $\int \bar{u}_B \chi_A^* \chi_A d\tau = -e^2/r_{AB}$ and recall eq 9, eq 13 goes to

$$D_e = -I_B + A_A + e^2/r_{AB} - R \quad (14)$$

which is the correct expression for the bond energy of an *ionic bond.* It is seen that in the case of filled MO's, even when $|H_{AA} - H_{BB}|$ is large, the bond A–B may be strong on account of the interatomic coulomb energy. Atomic orbital energy matching in these cases is not essential for strong bonding.

Discussion

We have collected in Table I some data that show the difference between singly and doubly occupied bonding MO's and its relation to the value of $\epsilon_A - \epsilon_B$. It is seen that strong one-electron bonds occur only in systems for which $\epsilon_A - \epsilon_B \cong 0$.

The halogen molecules represent an interesting case: Cornford, Frost, McDowell, Ragle, and Stenhouse[9] have recently reexamined the photoelectron spectra of the halogens and confirmed earlier results[10] for Cl_2^+, Br_2^+, and I_2^+ showing that the $^2\Sigma_g^+$ states are unstable and higher than both the $^2\Pi_u$ and $^2\Pi_g$ states. They have also shown that the $^2\Sigma_g^+$ state of F_2^+ cannot be observed up to 21.2 eV (their cutoff energy) and that the previously reported[10] state of F_2^+ at 17.35 eV should be attributed to nitrogen impurities. It seems therefore that the orbital sequence of the outer electrons of all halogen molecules is $(ns\sigma_g)^2(ns\sigma_u)^2(np\sigma_g)^2(np\pi_u)^4(np\pi_g)^4$, $^1\Sigma_g^+$. It should be pointed out that Wahl's SCF calculations of the F_2 system[11] put the $3\sigma_g$ orbital of $F_2(^1\Sigma_g^+)$ between the $^1\Pi_u$ and the $^1\Pi_g$ orbitals, and application of Koopmans' theorem, with its assumption

(7) There may be some question as to whether we should call these orbitals "bonding." However, we will continue to do so throughout this paper, since the orbital ϵ_a* is definitely antibonding. There is no consistent definition of what constitutes a bonding orbital. For example, the doubly occupied $2\sigma_g$ orbital in Li_2 is formally bonding, but removal of one electron strengthens the bond.

(8) (a) C. A. Coulson, "Valence," Oxford University Press, 1952, pp 71–73; (b) R. S. Mulliken, ref 5, eq 107 and 108.

(9) A. B. Cornford, D. C. Frost, C. A. McDowell, J. L. Ragle, and I. A. Stenhouse, *J. Chem. Phys.*, **54**, 265 (1971).

(10) D. C. Frost, C. A. McDowell, and D. A. Vroom, *ibid.*, **46**, 4255 (1967).

(11) A. C. Wahl, *ibid.*, **41**, 2600 (1964); unpublished results, 1970.

that the orbitals of the ion are the same as those of the neutral molecule, would lead to an inversion of the ionization energy assignments.

Recently Bertoncini, Das, and Wahl[12] made a SCF calculation of the NaLi molecule, arriving at the values $D_e(\text{NaLi}, {}^1\Sigma_g^+) = 0.852$ eV and $D_e(\text{NaLi}^+, {}^2\Sigma_g^+) = 0.919$ eV. This result is compatible with our arguments, since $\epsilon_{Li} \cong \epsilon_{Na}$.

Table II compares the dissociation energies of the $^2\Sigma^+$ states of the hydrogen halide ions, HX^+, with those of the neutral molecules, HX, $^1\Sigma^+$. The values of $D_e(HX^+, {}^2\Sigma^+)$ refer to the dissociation to $H^+(^1S) + X(^2P)$.[13] It is seen that for the $^2\Sigma^+$ state of the HX^+ ions the bond energies are in the reverse order of that of the molecules HX, $^1\Sigma^+$. The bond energy trend for the molecule ions correlates well with the differences in the diagonal elements. For the ionic species these are identified with the VSIE's.[14] For the neutral molecules $|H_{AA} - H_{BB}|$ corresponds to the differences in the valence-state electronegativities.[14] These results show how remarkably large the interatomic coulomb energy is in the HF molecule.

Table II: Dissociation Energy of the Hydrogen Halides

Molecule	D_e, eV	$\lvert H_{AA} - H_{BB}\rvert$, eV	Molecule ion	D_e, eV	$\lvert H_{AA} - H_{BB}\rvert$, eV
HF	5.87[a]	5.06	$HF^+(^2\Sigma^+)$	0.87[a] (0.72)[a]	7.38
HCl	4.43[a]	2.19	$HCl^+(^2\Sigma^+)$	1.80[a]	1.49
HBr	3.75[a]	1.38	$HBr^+(^2\Sigma^+)$	2.06[a]	0.12
HI	3.08[a]	0.69	$HI^+(^2\Sigma^+)$	2.81[a]	0.93

[a] H. J. Lempka, T. R. Passmore, and W. C. Price, *Proc. Roy. Soc., Ser. A*, **304**, 53 (1968).

It should be pointed out that, except for HF^+, the lowest possible dissociation limit for the $^2\Sigma^+$ states of the HX^+ species is $H(^2S) + X^+(^3P)$. However, the only bonding state arising from $H(^2S) + X^+(^3P)$ is the $^2\Pi$ state. The bonding state $^2\Sigma^+$ arises either from $H^+(^1S) + X(^2P)$ or from $H(^2S) + X^+(^1D)$, the former combination being the more stable one for HF^+ and HCl^+, the latter more stable for HBr^+ and HI^+. In order to make a meaningful comparison, the dissociation energies shown in Table II refer, as stated before, to $H^+(^1S) + X(^2P)$.

The case of the CH radical and the CH^+ molecule ion, discussed by Mulliken,[15] is of considerable interest. If $CH(\sigma^2\pi)$ is excited to $CH(\sigma\pi^2)$, both r_e and ω_e remain essentially the same. Again, if $CH(\sigma^2\pi, {}^2\Pi)$ is ionized to $CH^+(\sigma^2, {}^1\Sigma^+)$, $\Delta r_e \cong 0$ and $\Delta\omega_e \cong 0$. On the other hand, if $CH^+(\sigma^2, {}^1\Sigma^+)$ is excited to $CH^+(\sigma\pi, {}^2\Pi)$, r_e increases and ω_e decreases sharply. Also, the dissociation energy of the process $CH^+(\sigma^2, {}^1\Sigma^+) \rightarrow H(^2S) + C^+(^2P)$ is 3.6 eV, whereas for the process $CH^+(\sigma\pi, {}^2\Pi) \rightarrow H(^2S) + C^+(^2P)$ it is only 0.7 eV. These facts can be rationalized from the assumption that the 3σ and the 1π MO's are bonding when doubly occupied but nonbonding when singly occupied. This is expected from the large difference in the diagonal elements of hydrogen and carbon, indicating a large coulomb stabilization. This seems to remove the contradiction discussed by Mulliken.[15]

The importance of these considerations for the rationalization of chemical behavior can be seen in some further examples. Although the dissociation energy of CO is higher[16] (11.11 eV) than that of N_2 (9.76 eV), the reverse is true for the dissociation energies[16,17] of $CO^+(^2\Sigma^+)$ (8.36 eV) and $N_2^+(^2\Sigma^+)$ (8.69 eV).

The dimerization of $CN(g)(^2\Sigma)$ to cyanogen, and the polymerization of $BO(g)(^2\Sigma)$ to solid $(BO)_x$ can be rationalized in terms of the weakly bonding half-occupied $3\sigma_b$ MO in these radicals. The dissociation energy[18] of CN(g) is the same as that[19] of BO(g), 7.5 eV. Since the $3\sigma_b$ MO should be less bonding in BO(g) than in CN(g), we predict that $D(BO^+)$ is greater than $D(CN^+)$. From the ionization energy[17] of CN(g) to $CN^+(^1\Sigma)$, 14.5 eV, we obtain $D(CN^+) = 4.25$ eV. We predict that $D(BO^+) > 4.25$ eV and that $I(BO) < 12.54$ eV. The only values found in the literature[20] are those estimated by W. A. Chupka (3.9 eV for $D(BO^+)$ and 12.8 eV for I(BO)) and it is possible that they should be revised.

In our previous note[3] we pointed out that the stability of the HF_2^- ion is due to the large interatomic coulomb term of the doubly occupied bonding $\sigma_g = c_1\,1s + c_2(2p_{z_a} - 2p_{z_b})$ orbital. We also indicated that HeF_2 cannot be stable since $X_{He} \gg X_F$ and therefore no significant interatomic coulomb term occurs in the latter molecule. We can also predict that the $^2\Sigma_g$ state of HF_2 is unstable. However, from the data of Lempka, Passmore, and Price[13] on the HX^+ ions, the $^2\Pi$ state of HF_2 could be weakly bonding. These qualitative predictions have now been confirmed by the calculations of Noble and Kortzeborn.[21]

Acknowledgments. We thank Drs. C. A. McDowell and A. C. Wahl for sending their recent results prior to publication and for the benefit of correspondence. We are grateful to the referees for valuable comments.

(12) P. J. Bertoncini, G. Das, and A. C. Wahl, *J. Chem. Phys.*, **52**, 5112 (1970).

(13) H. J. Lempka, T. R. Passmore, and W. C. Price, ref *a* in Table II.

(14) J. Hinze and H. H. Jaffe, *J. Amer. Chem. Soc.*, **84**, 540 (1962); *J. Chem. Phys.*, **38**, 1834 (1963); *J. Phys. Chem.*, **67**, 1501 (1963).

(15) R. S. Mulliken in "Quantum Theory of Atoms, Molecules, and the Solid State," P.-O. Lowdin, Ed., Academic Press, New York, N. Y., 1966, p 231.

(16) G. Herzberg, ref *a* of Table I.

(17) J. L. Franklin, *et al.*, ref *b* of Table I.

(18) J. Berkowitz, *J. Chem. Phys.*, **36**, 2533 (1962).

(19) A. A. Mal'tsev, D. I. Kataev, and V. M. Tatevski, *Fiz. Probl. Spektrosk., Akad. Nauk SSR*, **1**, 194 (1960).

(20) J. Berkowitz, *J. Chem. Phys.*, **30**, 858 (1959).

(21) P. N. Noble and R. N. Kortzeborn, *ibid.*, **52**, 5375 (1970).

On the Validity of a Simple Theory for Transport in Ion-Exchange Membranes

by J. F. Osterle* and M. J. Pechersky

Carnegie-Mellon University, Pittsburgh, Pennsylvania *(Received November 19, 1970)*

Publication costs assisted by the National Science Foundation

The simple theory for transport in ion-exchange membranes based on the assumptions of local electroneutrality and uniform lateral distributions of ions and potential is reviewed and applied to the capillary model. Results are obtained for the efficiency of electrodialysis and compared with the exact theory. Indications are that the simple theory is a reasonable approximation provided the mean distance between fixed charges does not substantially exceed the Debye length.

Introduction

Certain solid ion-exchange membranes are modeled as tangles of fibers carrying fixed electrical charges at various points along their length. Schlögl[1] and others have presented theories for the operation of such membranes when separating aqueous electrolytes. The theory assumes that the permeant ions are dissociated from the fixed charges on the fibers and that local electroneutrality obtains within the membrane. Local electroneutrality means that in any volume within the membrane, provided only that it is large enough to contain at least a few fixed charges, the fixed charges are electrically balanced by the opposite charges on the ions in the surrounding fluid. It is further assumed that the ion concentrations and electrical potential are uniformly distributed laterally within the permeant fluid. They vary only with distance through the membrane. This latter assumption clearly violates Gauss' law (through the Poisson equation) and it is in this respect that the simple theory compromises the exact theory. We would expect this assumption to be less valid for loosely packed membranes than for tightly packed ones, since the charge counter to the fixed charge is contained within a thin sheath surrounding the fibers (with a thickness on the order of the Debye length), and the more loosely packed the membrane, the smaller the fraction of the permeant fluid contained in these sheaths.

Other theories have been presented which make certain simplifying assumptions so that a solution to Poisson's equation may be obtained. These assumptions include complete coion exclusion as by Dresner.[2] Kobatake[3] and others have modeled the membrane pores as parallel plates to obtain solutions of the Poisson–Boltzman equation. The Debye–Hückel approximation to the Poisson–Boltzman equation has also been used by Kobatake.[4] The simple theory differs from these theories in that the lateral electrical potential and concentration distributions are assumed to be uniform, thus eliminating the need for Poisson's equation in the analysis.

This paper addresses itself to the question of the validity of this assumption of uniform lateral distribution of ion concentrations and electrical potential. Since the theory described above applies equally well to membranes modeled as pores with their walls lined with charge and since this case permits us to be explicit about the permeability of the membrane to the solution flow (even with the exact theory), we will confine our attention to this model in the analysis to follow. Our membrane will consist of straight-through cylindrical pores of uniform bore carrying a uniformly distributed fixed charge on their walls. We will stipulate a trans-membrane concentration difference small enough to qualify as "near equilibrium" in the thermodynamics sense. The electrodialysis mode of operation (*i.e.*, zero trans-membrane solvent partial pressure difference) as defined in ref 5 will be considered and the electrolyte will be an ideal solution of a single equivalent binary salt.

The simple theory based on uniform lateral distribution of ion concentrations and electrical potential will be established and used to predict the conversion efficiency of the membrane in electrodialysis as a function of tube radius to Debye length ratio for several salts and an assumed constant wall charge. The results of this analysis will then be compared with the exact solution to the problem as reported earlier by Fair.[5]

The Simple Theory. The membrane consists of a bank of straight-through cylindrical capillary tubes

(1) R. Schlögl, "Stofftransport durch Membranen," Dr. Dietrich Steinkopff, Verlag, Darmstadt, Germany, 1964.

(2) L. Dresner, *J. Phys. Chem.*, **67**, 1635 (1963).

(3) Y. Kobatake, Y. Toyoshima, and N. Takeguchi, *ibid.*, **70**, 1187 (1966).

(4) Y. Kobatake, *J. Chem. Phys.*, **28**, 442 (1958).

(5) J. C. Fair and J. F. Osterle, *ibid.*, in press.

of length l and radius a. The separated phases will temporarily be taken to be identical, *i.e.*, at the same temperature T, hydrostatic pressure p, solute concentration c, and electrical potential ϕ. The fluid everywhere inside the membrane pores will also be at this temperature, but at a different pressure $\bar{p}$, cation concentration $\bar{c}_1$, anion concentration $\bar{c}_2$, and potential $\bar{\phi}$. We will assume electrochemical equilibrium between the solute ions inside and outside the membrane and between the solvent inside and outside the membrane and on this basis calculate the relationships between the intra- and extramembrane properties.

Charge neutrality inside the membrane requires that

$$\bar{c}_1 - \bar{c}_2 + \hat{c} = 0 \tag{1}$$

where for cylindrical capillaries

$$\hat{c} = \frac{2\sigma}{zFa} \tag{2}$$

with σ the density of the fixed charge on the capillary walls. $\hat{c}$ may be positive or negative depending on the sign of the wall charge density. Electrochemical equilibrium for the solute ions requires that

$$RT \ln \frac{\bar{c}_i}{c} + z_i F(\bar{\phi} - \phi) = 0 \tag{3}$$

In these equations R is the gas constant, F the Faraday constant, z_i the valence of the ith solute species (positive for the cation and negative for the anion), and z the absolute value of the valence. From eq 3 we can write

$$\bar{c}_1 = c \exp(-\delta\Phi) \tag{4}$$

$$\bar{c}_2 = c \exp(\delta\Phi) \tag{5}$$

where

$$\Phi = \frac{zF\phi}{RT} \tag{6}$$

and as a general notation

$$\delta(\ ) = (^-) - (\ ) \tag{7}$$

Substituting eq 4 and 5 into eq 1 there results

$$\hat{c} = 2c \sinh \delta\Phi \tag{8}$$

which can also be written

$$\exp(\delta\Phi) = \frac{\hat{c} + \sqrt{\hat{c}^2 + 4c^2}}{2c} \tag{9}$$

If we define $\bar{c}$ as the total ion concentration inside the membrane, *i.e.*

$$\bar{c} = \bar{c}_1 + \bar{c}_2 \tag{10}$$

then from eq 4 and 5

$$\bar{c} = 2c \cosh \delta\Phi \tag{11}$$

which can also be written

$$\exp(\delta\Phi) = \frac{\bar{c} + \sqrt{\bar{c}^2 - 4c^2}}{2c} \tag{12}$$

Equating eq 9 and 12 we obtain

$$\bar{c}^2 = \hat{c}^2 + 4c^2 \tag{13}$$

In terms of these three quantities ($\bar{c}$, $\hat{c}$, and c) we can write

$$\delta c_1 = \frac{\bar{c} - \hat{c}}{2} - c \tag{14}$$

$$\delta c_2 = \frac{\bar{c} + \hat{c}}{2} - c \tag{15}$$

$$\delta\Phi = \ln\left(\frac{\hat{c} + \bar{c}}{2c}\right) \tag{16}$$

Electrochemical equilibrium for the solvent requires that

$$\delta p_0 = 0 \tag{17}$$

where p_0 is the solvent partial pressure given by

$$p_0 = p - \pi \tag{18}$$

with π the solute partial pressure (osmotic pressure) given by

$$\pi = 2cRT \tag{19}$$

Thus

$$\delta p = RT(\bar{c} - 2c) \tag{20}$$

and the desired relationships have been obtained.

If now the properties p, c, and ϕ on one side (say the right side) of the membrane are allowed to differ from those on the other (the left) side by the arbitrary infinitesimals Δp, Δc, and $\Delta\phi$, we can write for any one of them

$$\Delta(^-) = \Delta(\ ) + \frac{\mathrm{d}\delta(\ )}{\mathrm{d}c}\Delta c \tag{21}$$

as the change in the intramembrane value of the property from the left side to the right side in terms of the change in its extramembrane value. Observing from eq 13 that

$$\frac{\mathrm{d}\bar{c}}{\mathrm{d}c} = \frac{4c}{\bar{c}} \tag{22}$$

it follows that

$$\Delta\bar{c}_1 = \Delta\bar{c}_2 = \frac{2c\Delta c}{\bar{c}} \tag{23}$$

$$\Delta\bar{\phi} = \Delta\phi - \frac{RT}{zF}\frac{\hat{c}\Delta c}{c\bar{c}} \tag{24}$$

$$\Delta\bar{p} = \Delta p + 2RT\left(\frac{2c - \bar{c}}{\bar{c}}\right)\Delta c \tag{25}$$

If we now stipulate that $\Delta p_0 = 0$, eq 25 reduces to

$$\Delta\bar{p} = 4RT\frac{c\Delta c}{\hat{c}} \tag{26}$$

The ion flux densities across the membrane from left to right are given by the Nernst–Planck equations

$$J_i = \bar{c}_i u - K_i z_i \bar{c}_i F\frac{\Delta\bar{\phi}}{l} - D_i\frac{\Delta\bar{c}_i}{l} \tag{27}$$

where J_i is the molar flux density of the ith species, u is the mean fluid velocity in the membrane, K_i is the mobility, and D_i is the diffusivity of the ith species related by the Einstein relation

$$K_i = \frac{D_i}{RT} \tag{28}$$

The mean velocity u is given by the Poiseuille law modified to account for the electrical body force

$$u = \frac{b}{l}(-\Delta\bar{p} + zF\hat{c}\Delta\bar{\phi}) \tag{29}$$

with

$$b = \frac{a^2}{8\mu} \tag{30}$$

the hydraulic permeability. Substituting eq 24 and 25 into eq 29 we obtain

$$u = \frac{b}{l}\left\{\bar{c}\left(\frac{\Delta\pi}{2c}\right) - zF\hat{c}(\Delta\phi)\right\} \tag{31}$$

for the mean velocity in terms of the appropriate[6] extra-membrane property differences, namely, $\Delta\pi/2c$, and $\Delta\phi$.

Substituting eq 31, 23, and 24 into eq 27 there results after some manipulation

$$J_i l = \bar{c}_1(b\bar{c} + K_i)\left(-\frac{\Delta\pi}{2c}\right) + zF\bar{c}_1(-b\hat{c} + nK_i)(-\Delta\phi) \tag{32}$$

where

$$n = \frac{z_i}{z} \tag{33}$$

having the value $+1$ for cations and -1 for anions.

From eq 32 the solute flux density J_s, defined by

$$J_s = J_1 + J_2 \tag{34}$$

and the electrical current density I, defined by

$$I = zF(J_1 - J_2) \tag{35}$$

can be formed. After considerable manipulation there results

$$J_s l = k_{22}\left(-\frac{\Delta\pi}{2c}\right) + k_{23}(-\Delta\phi) \tag{36}$$

$$Il = k_{32}\left(-\frac{\Delta\pi}{2c}\right) + k_{33}(-\Delta\phi) \tag{37}$$

where

$$k_{22} = \bar{c}\left\{b\bar{c} + K_2 + (r-1)K_2\frac{\bar{c}_1}{\bar{c}}\right\} \tag{38}$$

$$k_{23} = k_{32} = -zF\hat{c}\left\{b\bar{c} + K_2 - (r-1)K_2\frac{\bar{c}_1}{\hat{c}}\right\} \tag{39}$$

$$k_{33} = zF^2\{b\hat{c}^2 + K_2\bar{c} + (r-1)K_2\bar{c}_1\} \tag{40}$$

with

$$r = \frac{K_1}{K_2} \tag{41}$$

the ratio of cation to ion mobility. Equations 36 and 37 have been shown[5,6] to be in the proper form for the result that the cross-coupling coefficients k_{23} and k_{32} are equal. This is no surprise since Onsager's reciprocal theorem would demand this.

The Conversion Efficiency. The conversion efficiency of electrodialysis in the "forward" mode of operation, *i.e.*, conversion of electrical energy into "concentration" energy, is defined by

$$\eta_{23} = -\frac{J_s\left(\frac{\Delta\pi}{2c}\right)}{I\Delta\phi} \tag{42}$$

whereas the conversion efficiency in the "reverse" mode of operation, *i.e.*, conversion of "concentration" energy into electrical energy, is defined by

$$\eta_{32} = -\frac{I\Delta\phi}{J_s\left(\frac{\Delta\pi}{2c}\right)} \tag{43}$$

It has been shown[6] that the maximum values of these two efficiencies are equal and given by

$$\eta_{max} = \frac{1 - \sqrt{1-\gamma}}{1 + \sqrt{1-\gamma}} \tag{44}$$

where γ is the degree of coupling defined by

$$\gamma = \frac{k_{23}^2}{k_{22}k_{33}} \tag{45}$$

Substituting from eq 38, 39, and 40 into eq 45 we obtain

$$\gamma = \frac{\left\{\frac{\bar{c}}{\hat{c}} + \frac{K_2}{b\hat{c}}\left[1 + (1-r)\frac{\bar{c}_1}{\hat{c}}\right]\right\}^2}{\left(\frac{\bar{c}}{\hat{c}}\right)^2\left\{\frac{\bar{c}}{\hat{c}} + \frac{K_2}{b\hat{c}}\left[1 + (1-r)\frac{\bar{c}_1}{\bar{c}}\right]\right\} \times \left\{\frac{\hat{c}}{\bar{c}} + \frac{K_2}{b\hat{c}}\left[1 - (1-r)\frac{\bar{c}_1}{\bar{c}}\right]\right\}} \tag{46}$$

Now according to eq 13

(6) R. J. Gross and J. F. Osterle, *J. Chem. Phys.*, **49**, 228 (1968).

$$\bar{c} = |\hat{c}|\sqrt{1 + \left(\frac{2c}{\hat{c}}\right)^2} \tag{47}$$

where from eq 2

$$\hat{c} = \frac{2\sigma}{zF\delta A} \tag{48}$$

with

$$A = \frac{a}{\delta} \tag{49}$$

where δ is the Debye length defined by

$$\delta = \frac{1}{zF}\sqrt{\frac{\epsilon RT}{2c}} \tag{50}$$

In this equation, ϵ is the permittivity of the solution. For a salt concentration of 10^{-5} mol/l., δ works out to be 9.5×10^{-8} m.

The Chapman–Gouy equation

$$\sigma = 2\sqrt{2c\epsilon RT}\sinh\zeta \tag{51}$$

relates the charge density on a flat plate to the corresponding ζ potential in a solution of concentration c. The ζ potential is the potential at the plate less the potential in the solution far from the plate. A typical value for ζ in dilute salt solutions is about 70 mV, corresponding to a σ of 7×10^{-4} C/m^2 for the stipulated concentration of 10^{-5} mol/l. For this σ and the Debye length corresponding to this concentration

$$\frac{2c}{\hat{c}} = 0.131(zA) \tag{52}$$

The largest value of A to be considered in this paper is of order unity, and we will confine our attention to NaCl and KCl for which $z = 1$; therefore eq 47 can be adequately approximated by

$$\bar{c} = |\hat{c}|\left\{1 + 2\left(\frac{c}{\hat{c}}\right)^2\right\} \tag{53}$$

Substituting this value of $\bar{c}$ into eq 46 and after considerable manipulation, we obtain

$$\gamma = 1 - 8\beta(A\Omega)^2 \times \frac{1 - (1 - r)\left[\frac{1 + m}{2} - m(A\Omega)^2\right]}{\frac{mA}{\Omega} + 2\beta - \beta(1 - r)[(1 - m) + 2m(A\Omega)^2]} \tag{54}$$

with

$$m = \frac{|\sigma|}{\sigma} \tag{55}$$

having the value $+1$ for positively charged walls and -1 for negatively charged walls. Also

$$\Omega = \frac{1}{2\sigma}\sqrt{\frac{\epsilon cRT}{2}} \tag{56}$$

which has the value ± 0.0657, and

$$\beta = \frac{4\mu K_2}{c\delta^2} \tag{57}$$

which upon substitution from eq 28 and 50 becomes

$$\beta = \frac{8\mu D_2}{\epsilon}\left(\frac{zF}{RT}\right)^2 \tag{58}$$

For the common anion (Cl^-) in NaCl and KCl, $D_2 = 2.01 \times 10^{-9}$ m^2/sec; therefore β can be evaluated and is found to equal 36.6.

Upon substitution of the numerical values established above for Ω and β, eq 54 reduces to an expression for γ in terms of A with m and r as parameters, for the

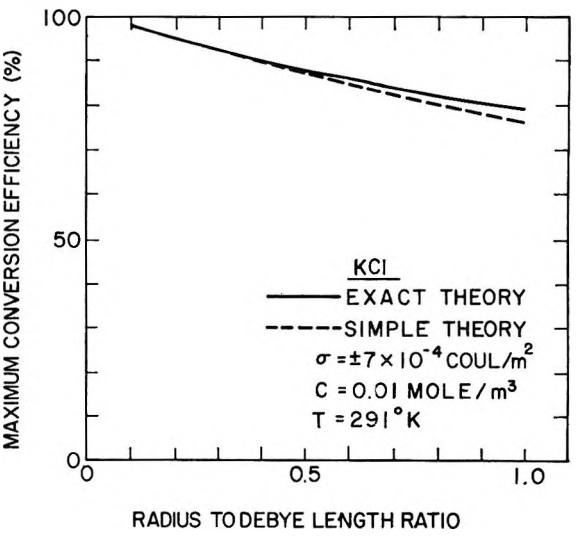

Figure 1. The maximum conversion efficiency is plotted against the radius to Debye length ratio for KCl and either a positive or negative constant wall charge. There is seen to be no effect of the sign of the wall charge since for KCl, the anion and cation mobilities are the same.

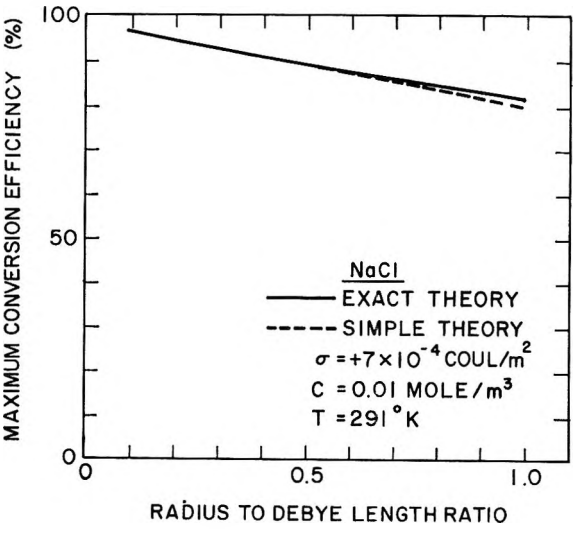

Figure 2. The same plot for NaCl and a positive constant wall charge.

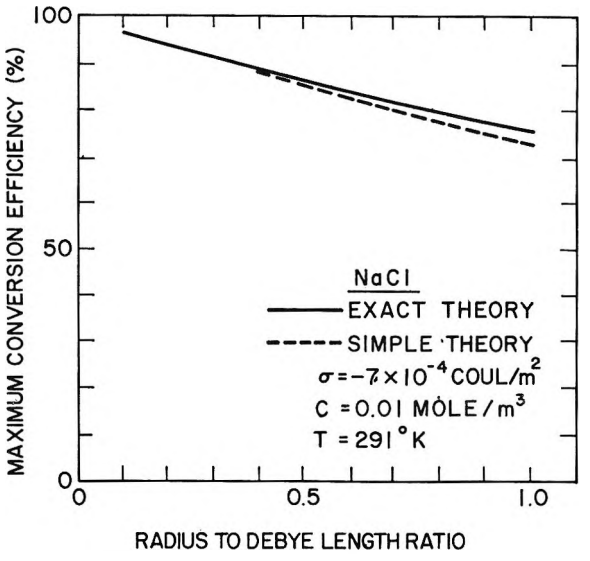

Figure 3. The same plot for NaCl and a negative constant wall charge.

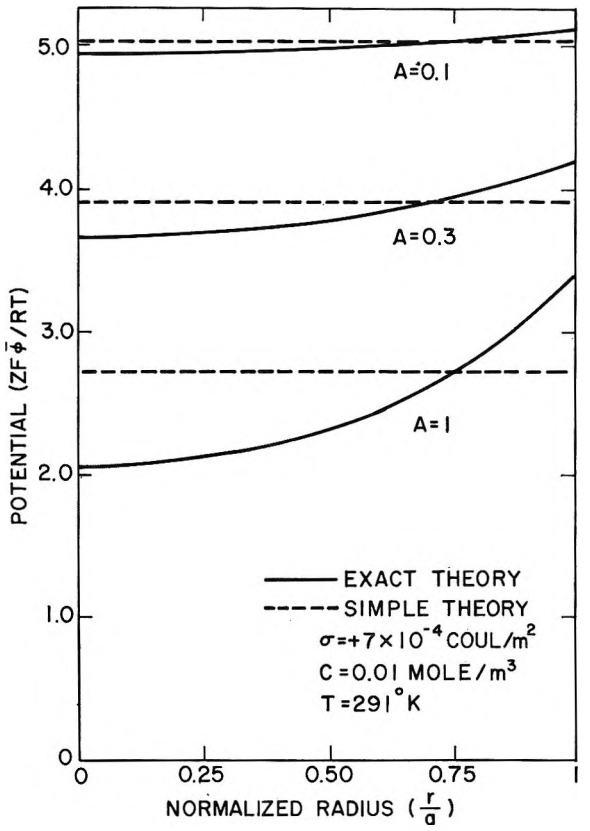

Figure 4. The potential distribution across the width of the pores for several values of A.

stipulated concentration and pore wall charge density. For KCl, $r = 1$, and for NaCl, $r = 0.657$.

The exact theory with which the results obtained from these equations will be compared, as developed in ref 5 and 6, differs from the simple theory presented here in that the exact theory does not assume uniform lateral distributions of concentrations and potential but rather insists that they obey Poisson's equation. We would expect the simple theory to approach the exact theory as the radius to Debye length ratio approaches zero.

Results

Results are obtained for the following values of the parameters governing this case of electrodialysis: $T = 291°K$, $c = 10^{-5}$ mol/l. (10^{-2} mol/m³), Cl^- the anion with either Na^+ or K^+ the cation, a pore wall charge density of either + or -7×10^{-4} C/m². The results of this simple theory are compared with the exact theory, presented elsewhere, in Figures 1–4.

Conclusions

Inspection of these graphs indicates that the simple theory is a reasonable approximation to the exact theory for values of the radius to Debye length ratio up to about 1. This suggests that in the tangled-fiber model one might well expect validity of the simple theory as long as the mean distance between fibers is not substantially greater than the Debye length.

Nomenclature

Frequently used symbols are listed in the table below. All symbols are defined when first used in the text. Units are included in parentheses after the symbol definition.

a	capillary radius (m)
A	radius to Debye length ratio
c	extramembrane solute concentration (mol/m³)
$\bar{c}_i$	intramembrane ion concentration (mol/m³)
$\bar{c}$	total intramembrane concentration (mol/m³)
$\hat{c}$	membrane concentration of fixed ions (mol/m³)
D_i	ion diffusivity (m²/sec)
F	Faraday's constant (C/mol)
i	subscript denoting species
	0 solvent
	1 cation
	2 anion
I	electrical current (A)
J_i	flux of component i (mol/sec)
J_s	solute flux (mol/sec)
K_i	ion mobility of ith species (m²/sec V)
k_{kj}	phenomenological coefficients
l	membrane thickness (m)
m	sign of wall charge (± 1)
p	hydrostatic pressure (N/m²)
p_0	solvent partial pressure (N/m²)
R	gas constant (N m/mol deg)
r	mobility ratio, radial coordinate in Figure 4
T	temperature (°K)
u	solvent velocity (m/sec)
z_i	valence at ith component
z	absolute value of ionic valence
β	defined by eq 57
γ	degree of coupling
δ	Debye length (m) (defined by eq 50)
η	conversion efficiency
μ	fluid viscosity (N sec/m²)

π osmotic pressure (N/m^2)
σ wall charge density (C/m^2)
ϕ electrical potential (V)
Ω defined by eq 56

Acknowledgment. The work underlying this paper was supported in part by a grant from the National Science Foundation.

NOTES

Reactivity of Hydrogen Atoms and Hydrated Electrons toward Aqueous Erythrosin. X-Radiolysis

by John Chrysochoos* and David S. Shihabi

Department of Chemistry, University of Toledo, Toledo, Ohio 43606 *(Received December 24, 1970)*

Publication costs assisted by the University of Toledo

The radiolysis of organic dyes in aqueous solutions involves a variety of transient species which relate to both the reducing and the oxidizing intermediates of the radiolysis of water. Furthermore, organic dyes exhibit strong characteristic absorption bands in the visible which may be markedly suppressed or completely disappear upon slight perturbation of the conjugation. In many cases, the dye bleaching, given in terms of $G(-S)$, can be used very effectively to study the mechanism of the radiolysis of an organic dye S. In addition, pulse radiolysis studies furnish more information regarding the transient intermediates.

Pulse radiolysis studies of eosin (tetrabromofluorescein)[1] and fluorescein[2] have shown that the following mechanism takes place

$$H_2O \rightsquigarrow e_{aq}^-, OH, H, H_2, H_2O_2$$

$$S + e_{aq}^- (H) \xrightarrow{H^+} R$$

$$S + OH \longrightarrow SOH$$

$$S + OH \longrightarrow X + OH^-$$

$$SOH \longrightarrow X + OH^-$$

$$R + X \longrightarrow 2S$$

$$R + R \longrightarrow L + S$$

$$X + X \longrightarrow \text{products}$$

where the free radicals R, X, and SOH stand for the semireduced dye, the semioxidized dye, and an OH adduct, respectively, and L denotes the leuco base (dihydro dye). The semioxidized dye X is a phenoxyl type free radical. This mechanism was partly verified by cobalt-60 radiolysis of fluorescein.[3] However, very little, if any, information is available regarding the reactions of H atoms with fluorescein dyes and no consistent data are available as far as the radiolysis of erythrosin (2′,4′,5′,7′-tetraiodofluorescein) is concerned.

The irradiation source used was a General Electric (Model XRO-3) X-ray diffraction unit with a copper target and a CA-7 Coolidge gun at 40 kV and 14 mA. The dose was 57.6 rads/min as determined by the Fricke dosimeter.[4] Pyrex cells were used which could be evacuated to 5×10^{-6} Torr. Absorption spectra were obtained with the Cary 14 recording spectrophotometer. Triply distilled water was used. Erythrosin was purified chromatographically to give ϵ_{max} (526 mμ) $9.4 \times 10^4\ M^{-1}\ cm^{-1}$. The other chemicals used were reagent grade.

Radiolysis under Reducing Conditions. Aqueous erythrosin (10 μM) was irradiated in the presence of 1 mM isopropyl alcohol at pH 8.3. The reactivity of OH radicals with isopropyl alcohol is $3.9 \times 10^9\ M^{-1}\ sec^{-1}$,[5] whereas the reactivity toward fluorescein was found to be $(1.6 \pm 0.3) \times 10^9\ M^{-1}\ sec^{-1}$.[2] Thus, OH radicals are scavenged by isopropyl alcohol almost completely. The reactivity of e_{aq}^- toward isopropyl alcohol is very low, *i.e.*, $k < 10^6\ M^{-1}\ sec^{-1}$, and therefore the reaction of e_{aq}^- with isopropyl alcohol can be neglected. On the other hand, the reactivity of H atoms with isopropyl alcohol has an intermediate value, $1.5 \times 10^8\ M^{-1}\ sec^{-1}$,[6] and a competition for H atoms can be set up between isopropyl alcohol and erythrosin. At lower concentrations of isopropyl alcohol, partial scavenging of OH radicals and partial formation of X leads to rather complex spectra.

(1) J. Chrysochoos, J. Ovadia, and L. I. Grossweiner, *J. Phys. Chem.*, **71**, 1629 (1967).

(2) P. Cordier and L. I. Grossweiner, *ibid.*, **72**, 2018 (1968).

(3) L. I. Grossweiner and A. F. Rodde, Jr., *ibid.*, **72**, 3337 (1968).

(4) L. M. Dorfman and M. S. Matheson, *Progr. React. Kinet.*, **3**, 239 (1965).

(5) G. E. Adams, J. W. Boag, J. Currant, and B. D. Michael, "Pulse Radiolysis," M. Ebert, J. P. Keene, A. J. Swallow, and J. H. Baxendale, Ed., Academic Press, London, 1965, p 131.

(6) J. Rabani, *Advan. Chem. Ser.*, **No. 50**, 242 (1965).

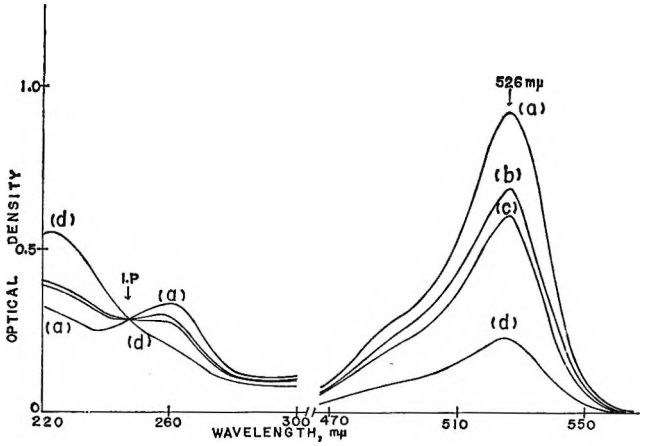

Figure 1. Absorption spectra of deaerated aqueous erythrosin (10 μM) in the presence of 1 mM isopropyl alcohol before and after irradiation: pH 8.3; optical path 1 cm; (a) unirradiated; (b) after 45 min of X-irradiation; (c) after 1 hr of X-irradiation; and (d) after 3 hr of X-irradiation.

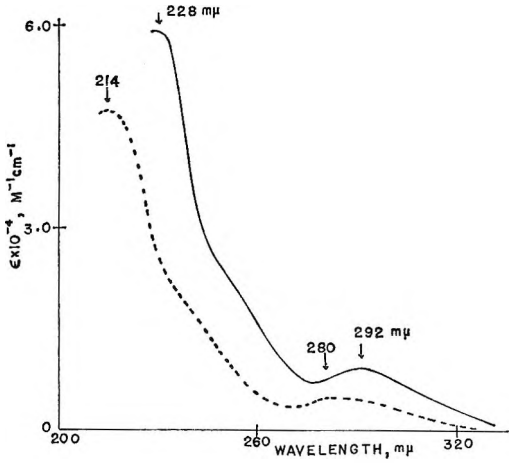

Figure 2. Absorption spectra of leucoerythrosin (L), solid line, and leucofluorescein,[8] broken line.

On the other hand, at much higher concentrations of isopropyl alcohol complete scavenging of H atoms and partial scavenging of e_{aq}^- leads to low dye bleaching. Therefore, the optimum concentration of isopropyl alcohol was used (1 mM) and the results are the averages of 20 determinations obtained at five different irradiation times from 30 min to 2 hr. In the presence of 1 mM isopropyl alcohol, the absorption spectra of the irradiated erythrosin exhibit uniform dye bleaching (reduction of the optical density in the visible region) which was found to be linear with the irradiation time up to 3 hr. At the same time, a uniform buildup of an absorption band is observed in the uv region with an apparent isosbestic point at 245 mμ, which indicates a 1:1 ratio between the dye and the product.[7] Some of these results are depicted in Figure 1. The absorption spectra of the irradiated erythrosin in the visible become identical, if normalized with respect to their maximum (*i.e*, 526 mμ) which indicates that no other species than erythrosin absorbs in this region. Therefore, from the amount of erythrosin destroyed and the dose used, the G value of bleaching, $G(-S)$ can be determined. The average value of $G(-S)$ was found to be equal to 1.02 ± 0.01. Actual values of $G(-S)$ for irradiation times up to 2 hr were found in the range of 0.97 up to 1.03 with the lower values obtained at irradiation times of 10–15 min. They are attributed to possible traces of residual O_2 in the samples. At much longer irradiation times the value of $G(-S)$ was slightly decreased possibly due to the gradual buildup of acetone and subsequent reactions with e_{aq}^-.

At prolonged irradiation times (3 hr), both the bleaching and the buildup of the absorption of the product in the uv region were considerable. The latter was corrected for the absorption of the residual erythrosin, and from the amount of erythrosin destroyed, the absorption spectrum of the product was reconstructed assuming a 1:1 relationship. The absorption spectrum is given in Figure 2. The spectrum of leucofluorescein determined in other studies[8] is also drawn for comparison. The two spectra are very similar, and exhibit the same red-shift which is observed in the absorption spectra of fluorescein and erythrosin. Therefore the uv absorption band is assigned to leucoerythrosin (L). These results can be accounted for

$$S + e_{aq}^- \xrightarrow{H^+} R$$

$$(CH_3)_2CHOH + OH \longrightarrow (CH_3)_2COH \qquad k = 3.9 \times 10^9\ M^{-1}\ sec^{-1}$$

$$(CH_3)_2CHOH + H \longrightarrow (CH_3)_2COH \qquad k_1 = 1.5 \times 10^8\ M^{-1}\ sec^{-1} \quad (1)$$

$$S + H \longrightarrow SH \quad (2)$$

$$R + R \longrightarrow L + S$$

$$R + H_2O_2 \longrightarrow S + OH + OH^- + H^+$$

$$SH + SH \longrightarrow SH_2(L) + S$$

$$2(CH_3)_2COH \longrightarrow (CH_3)_2C{=}O + (CH_3)_2CHOH$$

It was assumed that neither R nor SH reacts with isopropyl alcohol. In such an event, due to the high concentration of isopropyl alcohol, the low concentrations of R and SH, and the very low bimolecular reaction rate constants including R and SH, one should expect a large $G(-S)$ value, *i.e.*, $G(-S) = G(R) + G(SH)$. That is, $G(-S) \geq 2.65$ which is not the case. Furthermore, pulse radiolysis studies of eosin[1] have shown that the decay of R is not affected by the presence of 10 mM ethanol.

(7) M. Gouterman and P. Stevens, *J. Chem. Phys.*, **37**, 2268 (1962).
(8) K. Uchida, S. Kato, and M. Koizumi, *Bull. Chem. Soc. Jap.*, **35**, 16 (1962).

The reaction of H_2O_2 with SH was not considered. The formation of the latter in esosin was studied in the presence of 5 mM H_2O_2. Its decay was rather slow,[1] *i.e.*, $k = (3.6 \pm 2.0) \times 10^3$ sec^{-1}. If this decay is due to reactions with H_2O_2, one would expect a reaction rate constant of about 7.2×10^5 M^{-1} sec^{-1}. Under these conditions, the effect of H_2O_2 formed would be negligible.

The value of $G(-S)$ can be determined from this mechanism

$$G(-S) = {}^1/_2\{G(R) - G_{H_2O_2}\} + {}^1/_2G(SH\cdot)$$

or

$$2G(-S) = G_{e_{aq}^-} - G_{H_2O_2} + G_H\{k_2[S]/(k_2[S] + k_1[\text{isopropyl alcohol}])\} \quad (I)$$

From eq I we obtain $k_2 = 3.4 \times 10^9$ M^{-1} sec^{-1} based[4] on $G_{e_{aq}^-} = 2.65$, $G_{H_2O_2} = 0.7$, and $G_H = 0.55$. The value of k_2 is based on only one concentration of isopropyl alcohol and it is associated with a considerable error; *i.e.*, $k_2 = (3.4 \pm 0.6) \times 10^9$ M^{-1} sec^{-1}.

Irradiation of air-saturated aqueous erythrosin (10 and 0.25 mM O_2) under conditions of complete scavenging of the OH radicals ($[Br^-] \geq 5.0$ mM) at pH 8.0 leads to an estimate of the reactivity of e_{aq}^- toward erythrosin since H atoms will be scavenged by O_2 to within 99.5%. The absorption spectra of the irradiated erythrosin exhibit all the characteristics of the spectra in Figure 1, except that the changes are extremely small. The value of $G(-S)$ was found to be equal to 0.02. Some of the absorption spectra are shown in Figure 3. At low concentrations of Br^- the OH radicals are partly scavenged and the spectra are more complex due to the formation of X. The dye bleaching can be accounted for

$$Br^- + OH \longrightarrow Br + OH^- \qquad (k = 1.6 \times 10^9\ M^{-1}\ \text{sec}^{-1})^9$$

$$O_2 + H \longrightarrow HO_2 \qquad (k = 1.9 \times 10^{10}\ M^{-1}\ \text{sec}^{-1})^{10}$$

$$HO_2 \rightleftharpoons O_2^- + H^+ \qquad (pK = 4.5)$$

$$O_2 + e_{aq}^- \longrightarrow O_2^- \qquad (k_3 = 1.88 \times 10^{10}\ M^{-1}\ \text{sec}^{-1})^{11} \quad (3)$$

$$e_{aq}^- + S \xrightarrow{H^+} R \quad (4)$$

$$O_2^- + O_2^- \xrightarrow{2H^+} H_2O_2 + O_2 \qquad (k = 3 \times 10^7\ M^{-1}\ \text{sec}^{-1})^{12}$$

$$Br + Br^- \rightleftharpoons Br_2^-$$

$$Br_2^- + Br_2^- \longrightarrow Br_3^- + Br^- \qquad (k = 1.8 \times 10^9\ M^{-1}\ \text{sec}^{-1})^{13}$$

$$R + R \longrightarrow L + S \quad (5)$$

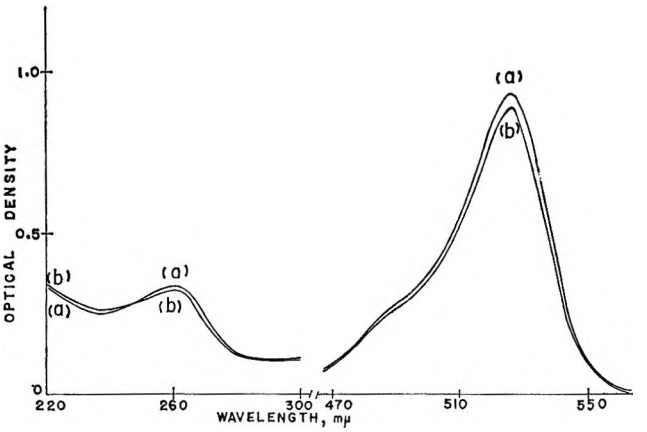

Figure 3. Absorption spectra of air-saturated (0.25 mM O_2) aqueous erythrosin in the presence of 5.0 mM bromide before and after irradiation: pH 8.0; optical path 1 cm; (a) unirradiated; (b) after 1 hr of X-irradiation.

Therefore

$$G(-S) = {}^1/_2G(R) = {}^1/_2G_{e_{aq}^-}\{k_4[S]/(k_4[S] + k_3[O_2])\} \quad (II)$$

From eq II we obtain

$$k_4 = 8 \times 10^9\ M^{-1}\ \text{sec}^{-1}$$

However, R reacts slowly with O_2[1]

$$R + O_2 \longrightarrow S + O_2^- + H^+ \quad (6)$$

Therefore, the observed value of $G(-S)$ is the result of a competition between reactions 5 and 6. The value of k_4 determined represents a lower limit. Thus, $k_4 \geq 8 \times 10^9$ M^{-1} sec^{-1}. The role of H_2O_2, both primary and secondary, is not clear, since both H_2O_2 and HO_2 are destroyed *via* the reactions[14]

$$Br + H_2O_2 \longrightarrow H^+ + Br^- + HO_2 \qquad (k > 2.5 \times 10^9\ M^{-1}\ \text{sec}^{-1})$$

$$Br^- + HO_2 \xrightarrow{H^+} Br_2 + H_2O_2 \qquad (k = 3.5 \times 10^9\ M^{-1}\ \text{sec}^{-1})$$

Reaction of H_2O_2 with R, generating S, will lead to a higher value for k_4.

(9) T. W. Woodward and H. C. Sutton, *Trans. Faraday Soc.*, **62**, 70 (1966).

(10) J. P. Sweet and J. K. Thomas, *J. Phys. Chem.*, **68**, 1363 (1964).

(11) E. J. Hart and E. M. Fielden, *Advan. Chem. Ser.*, **No. 50**, 253 (1965).

(12) G. Czapski and B. H. Bielski, *J. Phys. Chem.*, **67**, 2180 (1963).

(13) M. S. Matheson, W. A. Mulac, J. L. Weeks, and J. Rabani, *ibid.*, **70**, 2092 (1966).

(14) H. C. Sutton, G. E. Adams, J. W. Boag, and B. D. Michael, "Pulse Radiolysis," M. Ebert, J. P. Keene, A. J. Swallow, and J. H. Baxendale, Ed., Academic Press, London, 1965, p 61.

Electron Spin Resonance Spectrum and Structure of the Radical Anion of Phosphorus Oxychloride[1]

by Carolyn M. L. Kerr and Ffrancon Williams*

Department of Chemistry, University of Tennessee, Knoxville, Tennessee 37916 *(Received April 14, 1971)*

Publication costs assisted by the U. S. Atomic Energy Commission

Electron capture by molecules possessing unoccupied orbitals of low energy is generally recognized as an important primary process in radiation chemistry.[2] Among inorganic compounds,[3] there seem to be fewer recorded examples of electron capture by neutral molecules than by ions. In this note we present esr evidence for the formation of $POCl_3 \cdot^-$ in γ-irradiated $POCl_3$. We find that the magnetic resonance parameters of this species are entirely consistent with the structures advanced for other 33 valence electron radicals[3a] such as $PF_4 \cdot$,[4] $SF_4 \cdot^+$,[4c] and $PCl_4 \cdot$.[5]

Experimental Section

Phosphorus oxychloride was obtained from two suppliers, Baker and Adamson and Matheson Coleman and Bell, essentially the same results being obtained from both samples. Phosphorus trichloride was supplied by Alfa Inorganics. These materials were all used as received. Samples were degassed *in vacuo* by several freeze–pump–thaw cycles and transferred into Suprasil esr tubes. Irradiations were carried out at 77°K in a cobalt-60 γ source (Gammacell 200), the total dose in each case being 3–5 Mrads. Esr spectra were recorded at 77°K with the sample tubes contained in a liquid nitrogen dewar which fitted into the cavity of the Varian (V-4502) spectrometer. The instrumental arrangement has been described previously.[6]

Results and Discussion

Figure 1 shows the spectrum of γ-irradiated polycrystalline $POCl_3$ obtained at 77°K. In addition to the hydrogen atom doublet and unidentified resonances in the center region, there is an almost isotropic spectrum consisting prominently of a doublet of septets which can be ascribed to hyperfine interaction with one phosphorus and two equivalent chlorine nuclei. All the components of the septets show considerable substructure, and while this must be due in part to second-order effects and the different nuclear magnetic moments of ^{35}Cl and ^{37}Cl, analysis of the outermost components reveals more lines than would be expected for interaction with only two chlorines. This additional structure can be interpreted in terms of a third chlorine nucleus. The spectrum can therefore be assigned to $POCl_3 \cdot^-$, and the splittings are given in Table I.

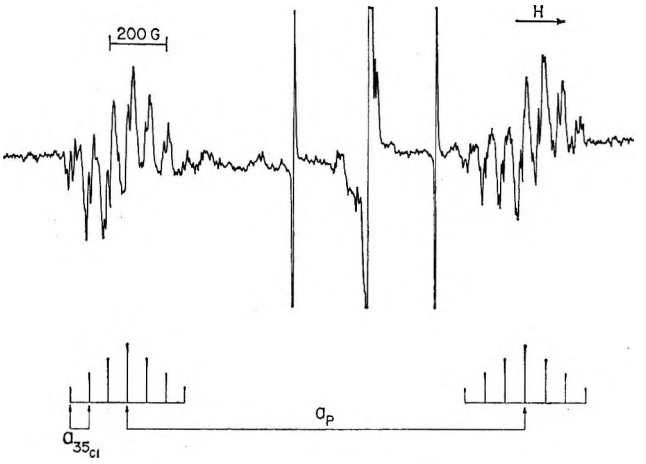

Figure 1. Esr spectrum of γ-irradiated polycrystalline phosphorus oxychloride at 77°K. Irradiation dose, 4 Mrads.

Further support for this assignment comes from the similarity in the esr spectra of $POCl_3 \cdot^-$ and $PCl_4 \cdot$.

Table I: Magnetic Resonance Parameters[a] for $POCl_3 \cdot^-$ and $PCl_4 \cdot$

Radical	a_P	a_{Cl}^1	a_{Cl}^2	g
$POCl_3 \cdot^-$ [b]	1367[c]	67[d]	14	2.014[c]
$PCl_4 \cdot$ [b,e]	1217[c]	60[d]		2.013[c]
$PCl_4 \cdot$ [f]	1206	62[d]	7.5[d]	2.013

[a] Hyperfine splittings in G. [b] This work; chlorine hfs for ^{35}Cl. [c] Value has been corrected for second-order effects using Breit–Rabi formula. [d] Two equivalent chlorines. [e] a_{Cl}^2 not resolved. [f] Reference 5; original values given in MHz; type of second-order correction used not known.

The spectrum of $PCl_4 \cdot$ obtained in γ-irradiated phosphorus trichloride is not reproduced here as it is virtually identical with the one reported by Kokoszka and Brinckman[5] in their study of the uv photolysis of phosphorus trichloride. Not only are the magnetic resonance parameters of $POCl_3 \cdot^-$ and $PCl_4 \cdot$ similar, as shown in Table I, but the overall shapes of the spectra are much alike. The individual septets appear to be

(1) This research was supported by the U. S. Atomic Energy Commission under Contract No. AT-(40-1)-2968 and this is AEC Document No. ORO-2968-63.

(2) D. J. Whelan, *Chem. Rev.*, **69**, 179 (1969).

(3) (a) P. W. Atkins and M. C. R. Symons, "The Structure of Inorganic Radicals," Elsevier, Amsterdam, 1967; (b) M. C. R. Symons, *Advan. Chem. Ser.*, **No. 88**, 1 (1968).

(4) (a) J. R. Morton, *Can. J. Phys.*, **41**, 706 (1963); (b) P. W. Atkins and M. C. R. Symons, *J. Chem. Soc.*, 4363 (1964); (c) R. W. Fessenden and R. H. Schuler, *J. Chem. Phys.*, **45**, 1845 (1966); (d) J. Higuchi, *ibid.*, **50**, 1001 (1969); (e) W. Nelson, G. Jackel, and W. Gordy, *ibid.*, **52**, 4572 (1970).

(5) G. F. Kokoszka and F. E. Brinckman, *J. Amer. Chem. Soc.*, **92**, 1199 (1970).

(6) J. Lin, K. Tsuji, and F. Williams, *ibid.*, **90**, 2766 (1968).

slightly asymmetric although the overall spectrum retains a center of symmetry in each case. This suggests that the asymmetry could be the result of an axially symmetric phosphorus hfs tensor. However, the anisotropy is small and implies that the radicals must be tumbling almost freely in both matrices.

From the magnitude of the phosphorus splitting the orbital of the unpaired electron in the valence shell is deduced to have *ca.* 37% s character. This lies within the range found for other 33 valence electron radicals, as shown in Table II. It is therefore logical to conclude that the structure of $POCl_3\cdot^-$ is similar to that of these other radicals. The structure is most easily visualized as a distorted trigonal bipyramid, and in this representation,[5] it is probable that the unpaired electron, the oxygen, and the chlorine giving the smaller splitting are in equatorial positions and the two remaining chlorines are axially placed.

Table II: Central Atom Parameters for 33 Valence Electron Radicals

	$POCl_3\cdot^-$ [a]	$PCl_4\cdot$ [a]	$PF_4\cdot$ [b]	$PO_4\cdot^{4-}$ [c]	$SF_4\cdot^+$ [d]	$AsO_4\cdot^{4-}$ [e] or $As(OH)_4\cdot$
a_{iso}, G	1367	1217	1330	1156	310	1084
c_s^2 [f]	0.37	0.33	0.37	0.32	0.32	0.32

[a] This work. [b] Reference 4a. [c] References 7 and 8. [d] Reference 4c. [e] M. Hampton, F. G. Herring, W. C. Lin, and C. A. McDowell, *Mol. Phys.*, **10**, 565 (1966). [f] Refers to 3s orbital for phosphorus and sulfur radicals and to 4s orbital for the arsenic radical.

The formation of $POCl_3\cdot^-$ by simple electron capture is in accord with the very recent suggestion by Symons[7] that $PO_4\cdot^{4-}$ is produced from PO_4^{3-} in phenacite crystals[8] and in inorganic phosphate glasses[9] by γ irradiation. Since there is no esr evidence for the production of $POCl_2\cdot$, it seems likely that radiation chemical mechanisms of P–Cl bond breakage by homolysis and dissociative electron capture are relatively unimportant in $POCl_3$. On the other hand, in the radiolysis of phosphorus trichloride, we observed only $PCl_2\cdot$ and $PCl_4\cdot$ with $PCl_2\cdot$ present in large excess ($\sim$10:1). These latter findings are qualitatively similar to those obtained by uv photolysis[5] which indicates that in PCl_3 the predominant mechanism is the rupture of a P–Cl bond to give $PCl_2\cdot$ and chlorine atoms.

(7) M. C. R. Symons, *J. Chem. Phys.*, **53**, 857 (1970); *cf.* G. O. Karapetyan and D. M. Yudlin, *Sov. Phys. Solid State*, **3**, 2063 (1962).

(8) (a) H. Lozykowski, R. G. Wilson, and F. Holuj, *J. Chem. Phys.*, 51, 2309 (1969); (b) F. Holuj, *ibid.*, **54**, 1430 (1971).

(9) R. A. Weeks and P. J. Bray, *ibid.*, **48**, 5 (1968).

An Investigation of the Reaction $2COF_2 \rightarrow CO_2 + CF_4$ and the Heat of Formation of Carbonyl Fluoride

by J. C. Amphlett, J. R. Dacey,

Department of Chemistry, Royal Military College, Kingston, Ontario, Canada

and G. O. Pritchard*

Department of Chemistry, University of California, Santa Barbara, California 93106 *(Received April 26, 1971)*

Publication costs assisted by the Defense Research Board of Canada

A study of the thermal decomposition of carbonyl fluoride, reaction 1, was originally reported by Ruff and

$$2COF_2 \rightleftharpoons CF_4 + CO_2 \qquad (1,-1)$$

Li.[1] The reaction was carried out in a flow system over a nickel catalyst between 300 and 650° and a platinum catalyst between 1000 and 1200°. An attempt was also made to approach the equilibrium position from the right-hand side with mixtures of CF_4 and CO_2 at 1000 and 1100°. In a subsequent paper Li[2] assumed that equilibrium had been established at 650° and reported $\Delta H_1 = +26$ kcal mol^{-1} over the temperature range 650–1200° from a conventional second-law plot; see the dashed line in Figure 1. This heat of reaction has been used to derive a value[3] for $\Delta H_f°(COF_2)$ in considerable excess to the value obtained from the heat of hydrolysis of COF_2.[4,5] The use of the second-law method in the interpretation of the data of RL[1] on reaction 1,−1 has recently been severely criticized and it is concluded[6] that a third-law treatment of the high-temperature data (obtained over the Pt catalyst) leads to the only valid thermodynamic interpretation of the system, with $\Delta H_1 = -12 \pm 3$ kcal mol^{-1}. We report a reinvestigation of the reaction in a static system over a Pt catalyst.

The reaction vessel was a 1150-ml Pyrex glass cylinder, with a platinum wire running axially down the center, located *via* two Kovar seals at the ends. The reaction temperature was taken to be the temperature of the Pt wire, measured by means of its resistance. The exterior of the glass reactor was cooled with a stream of air to reduce any attack by COF_2.

(1) O. Ruff and S-C. Li, *Z. Anorg. Allg. Chem.*, **242**, 272 (1939) (RL).

(2) S-C. Li, *J. Chin. Chem. Soc. (Peiping)*, **11**, 14 (1944).

(3) H. C. Duus, *Ind. Eng. Chem.*, **47**, 1445 (1955).

(4) H. von Wartenberg, *Z. Anorg. Chem.*, **258**, 356 (1949).

(5) "JANAF Thermochemical Tables," Dow Chemical Co., Midland, Mich., 1965.

(6) (a) D. R. Stull, E. F. Westrum, Jr., and G. C. Sinke, "The Chemical Thermodynamics of Organic Compounds," Wiley, New York, N. Y., 1969, pp 78–86 (SWS). (b) See also C. R. Patrick, *Advan. Fluorine Chem.*, **2**, 1 (1961).

Table I: Data on COF_2 Decomposition

Run	ΔP, %[a]	Initial and final pressures, mm: COF_2		CF_4		CO_2		T, °K	$-\log K_{eq}$	$\Delta H_1°$(298°K), kcal mol^{-1}
6	2.9	33.1	29.6		1.23		1.26	545	2.754	+1.40
16	2.8	33.1	28.4		1.92		1.86	784	2.353	+0.735
15	2.6	33.1	28.2		2.05		2.03	854	2.280	+0.561
12	3.2	35.5	29.4		2.53		2.50	873	2.134	+0.004
14	3.7	32.9	26.5		2.60		2.56	905	2.025	−0.426
13	3.3	32.7	26.5		2.61		2.56	956	2.021	−0.433
11	2.6	28.2	27.4	4.03	3.94	3.91	3.84	992	1.697	−1.90
10	4.3	33.3	25.5		3.18		3.23	1017	1.802	−1.43
3	3.3	28.1	19.8		3.64		3.68	1053	1.467	−3.07
9	4.3	16.0	14.6	4.75	4.93	4.86	5.01	1066	0.935	−5.69
1	4.3	20.6	16.1		1.85		1.75	1075	1.904	−0.968
2	5.5	23.3	18.0		1.97		2.06	1126	1.901	−0.990
18	4.6	32.7	18.8		6.16		6.21	1168	0.967	−5.99
17	4.5	28.6	19.4	2.96	6.77	2.93	6.74	1202	0.918	−6.41
19	5.4	35.1	16.5		8.47		8.26	1215	0.589	−8.29
5	11	16.0	7.58	4.40	7.29	3.87	6.75	1314	−0.068	−12.8
4	9.3	24.6	6.24		7.55		7.53	1448	−0.166	−14.7
7	9.0			14.6	13.2	13.8	12.6	1036		
8	8.7			14.4	13.1	15.5	14.2	1173		

[a] ΔP is the percentage discrepancy in pressure between the initial and final total pressures. The run numbers indicate the sequence in which the experiments were carried out.

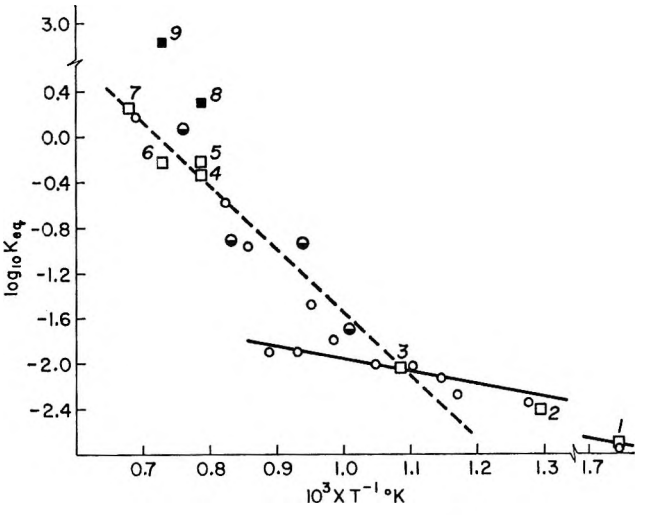

Figure 1. Log K_{eq} *vs.* $10^3/T$ °K for $2COF_2 \rightleftharpoons CO_2 + CF_4$: ○, our data; ◒, our data when CO_2 and CF_4 were also present initially; □, Ruff and Li's data, numbered as in ref 1. Runs 1–3, Ni catalyst, CO carrier gas. Runs 4–7, Pt catalyst. In all cases CO_2 was initially present. ■, runs 8 and 9, attempt to approach equilibrium from the reverse direction with $CO_2 + CF_4$ mixture. Run 9 was rejected.[1,2] The dashed line corresponds to $\Delta H_1 = +26$ kcal mol^{-1}, and the solid line to $\Delta H_1 = +5$ kcal mol^{-1}.

COF_2, CF_4, and CO_2 were Matheson Co. research grade. Their purity was checked mass spectrometrically, and in the case of COF_2 by the infrared spectrum;[7] any CO_2 impurity in it was <1%. Products were analyzed by gas chromatography on a 125-cm silica gel column at 100°. COF_2 and CO_2 showed identical retention times and sensitivities due to the quantitative conversion of COF_2 to CO_2 on a silica gel column.[8] The decrease in the number of moles of $(COF_2 + CO_2)$ because of reaction was equivalent to the number of moles of CF_4 formed, as required by the reaction stoichiometry. SiF_4 was detected as a minor product (<1%) mass spectrometrically.

There was reaction in 3 weeks at 545°K. At higher temperatures reaction was completed in about 1 week, and at the highest temperatures in about 1 day. Completion of reaction was established when there was no further change in the system with lapsed time. No apparent reaction was observed between CO_2 and CF_4 in 3 weeks. Our data are presented in Table I where K_{eq} is given by $[CO_2][CF_4]/[COF_2]^2$. All of the data are presented in Figure 1. The slope of the solid line corresponds to $\Delta H_1 = +5$ kcal mol^{-1}. The values of $\Delta H_1°$ given in Table I are obtained by the third-law method using the Gibbs energy functions.[5,6] The corresponding values obtained from the RL data[1] are tabulated by SWS.[6]

There was a small loss in total pressure during reaction which increased at very high temperatures. A 3% discrepancy is within the range of our analytical procedures. RL[1] suggested that there is a significant reaction between COF_2 and Pt at high temperatures, which could account for the increasing loss in total pressure.

SWS[6] concluded that true equilibrium may not have been reached at low temperatures, and our observations substantiate this. In high-temperature experiments

(7) A. H. Nielsen, T. G. Burke, P. J. H. Woltz, and E. A. Jones, *J. Chem. Phys.*, **20**, 596 (1952).

(8) J. Heicklen, V. Knight, and S. A. Greene, *ibid.*, **42**, 221 (1965).

Table II: The Thermochemical Data of Duus[3]

ΔH,[a] kcal mol^{-1}	Fraction to COF_2	$\Delta H_f°$(fluorocarbon),[b] kcal mol^{-1}	$\Delta H_f°(COF_2)$, kcal mol^{-1}
-160.3 ± 2.9	0.1178	C_2F_4, -155 ± 2[g]	-151 ± 23[f]
-116.5 ± 4.6	0.202	$(1/n)(C_2F_4)_n$, -199.16 ± 1.07[c]	-155 ± 15
-209.9 ± 4.6	0.1163	C_3F_6, -263.4 ± 12.0[d]	-152 ± 49[f]
-271.8 ± 7.8	0.1156	c-C_4F_8, -360.3 ± 4(?)[e]	-154 ± 27(?)[f]

[a] *E.g.*, $\Delta H = -160.3 \pm 2.9 = 0.8822(\Delta H_2) + 0.1178(\Delta H_3)$. [b] $\Delta H_f°(CF_4)$ and $\Delta H_f°(CO_2)$ as in text. [c] Based on $\Delta H = -246.84 \pm 0.07$ kcal mol^{-1} for C_2F_4(s, polymer) + $2F_2(g) \rightarrow 2CF_4(g)$; see J. L. Wood, R. J. Lagow, and J. L. Margrave, *J. Chem. Eng. Data*, **12**, 255 (1967). Using $\Delta H = 247.92 \pm 0.07$ kcal mol^{-1} for this reaction[9a] lowers $\Delta H_f°(COF_2)$ to -152 ± 15 kcal mol^{-1}. [d] From the heat of conversion[3] $\Delta H = -20.6 \pm 6.0$ kcal mol^{-1} for $C_2F_4(g) \rightarrow {}^2/_3C_3F_6(g)$. [e] Based upon $\Delta H = -25.15 \pm$ (?) for the conversion of $C_2F_4(g) \rightarrow {}^1/_2C_4F_8(g)$; see B. Atkinson and A. B. Trenwith, *J. Chem. Soc.*, 2082 (1953). Duus[3] gave $\Delta H = -24.7 \pm 6.8$ kcal mol^{-1}, which yields $\Delta H_f°(c$-$C_4F_8) = -359.4 \pm 17.6$ kcal mol^{-1} and $\Delta H_f°(COF_2) = -152 \pm 57$ kcal mol^{-1}. [f] Conversely, if $\Delta H_f°(COF_2) = -153$ kcal mol^{-1} is adopted, the data are consistent with $\Delta H_f°(C_2F_4) = -155$ kcal mol^{-1}. [g] See ref 5.

when all three gases were present in the initial mixture, runs 17 (1202°K) and 5 (1314°K), the mass action ratio was observed to increase. It is probable that the catalytic reaction sites are effectively blocked at lower temperatures, so that the reaction is not able to move toward equilibrium. At 1273°K (run 8, Figure 1) RL[1] were able to approach the equilibrium position from the reverse direction with initial mixtures of CO_2 and CF_4, but at lower temperatures, runs 7 and 8 in Table I, we were not successful.

The third-law analysis of all the acceptable data at about 1200°K and above (RL's experiments[1] 4–8 and runs 4, 5, 17–19 in Table I) yields $\Delta H_1°(298°K) = -10.9 \pm 2.2$ (probable error) kcal mol^{-1}. We have

$$\Delta H_f°(COF_2(g), 298°K) = -{}^1/_2\{\Delta H_1°(298°K) - \Delta H_f°(CF_4(g), 298°K) - \Delta H_f°(CO_2(g), 298°K)\}$$

Taking[9] $\Delta H_f°(CF_4(g), 298°K) = -223.0 \pm 0.5$ kcal mol^{-1} and $\Delta H_f°(CO_2(g), 298°K)$[5] $= -94.054 \pm 0.011$ kcal mol^{-1}, a value for $\Delta H_f°(COF_2(g), 298°K) = -153.1 \pm 1.4$ kcal mol^{-1} is obtained. The value derived from the heat of hydrolysis experiment is given in the JANAF tables[5] as -151.7 ± 2 kcal mol^{-1}; this is subject to the uncertainty in $\Delta H_f°(HF(aq))$.[9,10] Adjusting $\Delta H_f°(HF(aq))$[9,10] SWS[6] gave $\Delta H_f°(COF_2(g), 298°K) = -153.2 \pm 0.20$ kcal mol^{-1}. These error limits are probably unrealistically small.

Duus[3] reported thermochemical data on the reactions

$$C_2F_4 + O_2 \longrightarrow CO_2 + CF_4 \quad (2)$$

and

$$C_2F_4 + O_2 \longrightarrow 2COF_2 \quad (3)$$

and the corresponding reaction pairs with tetrafluoroethylene polymer, hexafluoropropylene, and perfluorocyclobutane. The fraction of fluorocarbon converted to COF_2 is ~12% in each case, except for the Teflon, where it is 20%. From the data we may obtain values for $\Delta H_f°(COF_2)$. The computations are summarized in Table II. Due to the small percentage conversion to COF_2 the calculations are very sensitive to the heat terms involved, and the limits of error are large. Interestingly enough, however, the average value is -153 kcal mol^{-1}.

Although we have been unable significantly to improve upon the data of RL[1] obtained over 30 years ago, the results do substantiate the value for $\Delta H_f°(COF_2)$ obtained from the hydrolysis experiment,[4-6] and a value of $\Delta H_f°(COF_2(g), 298°K) = -153$ kcal mol^{-1} is indicated, as recommended by SWS.[11]

Acknowledgments. The support of this work by the Defense Research Board of Canada, under Grant 9530/13, is gratefully acknowledged. G. O. P. wishes to thank the National Science Foundation for support. We also wish to thank a referee for helpful comments.

(9) (a) E. S. Domalski and G. T. Armstrong, *J. Res. Nat. Bur. Stand., Sect. A*, **71**, 105 (1967); (b) E. Greenberg and W. N. Hubbard, *J. Phys. Chem.*, **72**, 222 (1968); (c) J. W. Coomber and E. Whittle, *Trans. Faraday Soc.*, **63**, 1394 (1967).

(10) J. D. Cox and D. Harrop, *Trans. Faraday Soc.*, **61**, 1328 (1965).

(11) See ref 6a, p 217.

Specific Rates in the Acid Dissociation–Ion Recombination Equilibrium of Dilute Aqueous Hydrazoic Acid at 25°

by James J. Auborn, Percy Warrick, Jr., and Edward M. Eyring*

Department of Chemistry, University of Utah, Salt Lake City, Utah 84112 *(Received March 19, 1971)*

Publication costs assisted by the Air Force Office of Scientific Research

Azide ion is often used in rate studies of both ligand substitution and redox reactions. For instance, a comparison of azide with thiocyanate as bridging groups in redox reactions of transition metal ions has shown

that several such reactions proceed by an inner coordination sphere mechanism.[1] If an attempt were made to determine experimentally the probably[2] large specific rate for a reaction such as

$$Cu(H_2O)_6^{2+} + N_3^- \longrightarrow Cu(H_2O)_5N_3^+ + H_2O \quad (1)$$

it would be useful to know the rate constants for the competing equilibrium

$$HN_3 \underset{k_{13}}{\overset{k_{31}}{\rightleftharpoons}} H^+ + N_3^- \quad (2)$$

for which[3]

$$K_a = k_{31}/k_{13} = [H^+][N_3^-]/[HN_3] = 10^{-4.72} \quad (3)$$

in water at 25° and ionic strength $\mu = 0$.

We report below values of k_{13} and k_{31} in equilibrium 2 that we have determined by the dissociation field effect relaxation method.[4] The equilibrium 2 is coupled to that of the spectrophotometrically observable acid–base indicator bromocresol green (3,3′,5,5′-tetrabromo-*m*-cresolsulfonphthalein) the kinetics of which have been reported elsewhere.[5] The indicator acid dissociation–ion recombination, hydrazoic acid dissociation–ion recombination, and proton exchange between the indicator and hydrazoic acid are all taken into account in the complete coupled mechanism

$$\begin{array}{ccc} In^{2-} + H^+ + N_3^- & & \\ \;\;k_{12}\big\downarrow\big\uparrow k_{21} & & k_{13}\big\downarrow\big\uparrow k_{31} \\ HIn^- + N_3^- & \underset{k_{32}}{\overset{k_{23}}{\rightleftharpoons}} & In^{2-} + HN_3 \end{array} \quad (4)$$

Here In^{2-} and HIn^- represent the bromocresol green dianion and anion; $k_{12} = 5.4 \times 10^{10}\ M^{-1}\ sec^{-1}$ and $k_{21} = 7.5 \times 10^5\ sec^{-1}$ are the previously determined indicator ion recombination and acid dissociation rate constants.[5] The proton exchange rate constants k_{23} and k_{32} are both estimated at about $3 \times 10^8\ M^{-1}\ sec^{-1}$ from the small difference in pK_a between hydrazoic acid and the indicator using Eigen's data on proton exchange between various proton donors and acceptors.[6] A knowledge of the hydrazoic acid equilibrium constant (3), the previously determined bromocresol green kinetics,[5] and the proton exchange terms[6] allows the evaluation of the hydrazoic acid ion recombination rate constant k_{13} from the following

$$k_{13} = \frac{\tau^{-1}[\tau^{-1} - (\alpha_{11} + \epsilon_a + \epsilon_i)] + \alpha_{11}\epsilon_i + \alpha_{12}\epsilon_a}{c_{22}[\tau^{-1} - (\alpha_{11} + \epsilon_a)] + c_{21}(\alpha_{12} - \epsilon_i)} \quad (5)$$

where

$$\alpha_{11} = ([H^+] + [In^{2-}])k_{12} + k_{21} = ([H^+] + [In^{2-}] + K_i)k_{12} \quad (6)$$

$$\alpha_{12} = [In^{2-}]k_{12} \quad (7)$$

$$\alpha_{21} = [N_3^-]k_{13} \equiv c_{21}k_{13} \quad (8)$$

$$\alpha_{22} = ([H^+] + [N_3^-])k_{12} + k_{31} \equiv ([H^+] + [N_3^-] + K_a)k_{13} \equiv c_{22}k_{13} \quad (9)$$

$$\epsilon_i = [HIn^-]k_{23} + [In^{2-}]k_{32} \quad (10)$$

$$\epsilon_a = [N_3^-]k_{23} + [HN_3]k_{32} \quad (11)$$

Either one of the two experimentally observed relaxation times, τ, may be used in (5). We chose to use the faster of the two relaxations because it could be more reliably measured. The detailed mathematical analysis and the apparatus are both described elsewhere.[5,7]

Our kinetic data are assembled in Table I. Solutions were prepared by quantitative dilution of stock solutions made up by weight from Matheson Coleman and Bell sodium azide (recrystallized three times from water) and Matheson Coleman and Bell bromocresol green (recrystallized from glacial acetic acid). The pH was adjusted to the indicated value by addition of small amounts of HCl. Thus values of pH reported in Table I for constant concentrations of hydrazoic acid and bromocresol green were varied intentionally. The pH was checked before and after kinetic experiments and remained constant within ±0.02 pH unit. The k_{13} values reported in Table I are calculated by eq 5. The dominant term in the numerator is $\tau^{-1} - \alpha_{11}$. As can be seen from eq 6 and Table I, α_{11} is the calculated reciprocal relaxation time of bromocresol green under the same conditions and is nearly as large as τ^{-1} for the coupled systems. Since both τ^{-1} and α_{11} are each subject to errors of about 10%, the difference between them can show larger errors. This is seen in the variation in k_{13} reported in Table I. For this reason, we must take an average of several separate determinations and estimate a standard deviation of ±27% for our results. The average hydrazoic acid ion recombination rate constant, determined in this manner, is $k_{13} = 6.0 \pm 1.6 \times 10^{10}\ M^{-1}\ sec^{-1}$. When taken with the equilibrium constant (3), this yields a dissociation rate constant $k_{31} = 1.15 \times 10^6\ sec^{-1}$. These results are consistent with previous results found for other simple inorganic acids; *i.e.*, $k_{13} = 1 \times 10^{11}\ M^{-1}\ sec^{-1}$ for HF,[8] $k_{13} = 7.5 \times 10^{10}\ M^{-1}\ sec^{-1}$ for H_2S,[8] and $k_{13} = 7.2 \times 10^{10}\ M^{-1}\ sec^{-1}$ for acetic acid.[5] The hydrazoic acid result is also consistent with preliminary unpublished measurements on aqueous

(1) N. Sutin, *Annu. Rev. Phys. Chem.*, **17**, 119 (1966).

(2) M. Eigen, W. Kruse, G. Maass, and L. DeMaeyer, *Progr. React. Kinet.*, **2**, 285 (1964).

(3) L. G. Sillen, *Chem. Soc. Spec. Publ.*, **17**, 160 (1964).

(4) M. Eigen and L. DeMaeyer, "Technique of Organic Chemistry," Vol. VIII, Part II, S. L. Freiss, E. S. Lewis, and A. Weissberger, Ed., Interscience, New York, N. Y., 1963, Chapter 18.

(5) J. J. Auborn, P. Warrick, Jr., and E. M. Eyring, *J. Phys. Chem.*, **75**, 2488 (1971).

(6) M. Eigen, *Angew. Chem. Int. Ed. Engl.*, **3**, 1 (1964).

(7) S. L. Olsen, R. L. Silver, L. P. Holmes, J. J. Auborn, P. Warrick, Jr., and E. M. Eyring, *Rev. Sci. Instrum.*, in press.

(8) M. Eigen and K. Kustin, *J. Amer. Chem. Soc.*, **82**, 5952 (1960).

Table I: Dissociation Field Effect Relaxation Data for a Coupled Aqueous Hydrazoic Acid–Bromocresol Green System at 25°

C_a,[a] 10^{-6} M	C_i,[b] 10^{-6} M	pH[c]	τ^{-1},[d] 10^6 sec^{-1}	α_{11},[e] 10^6 sec^{-1}	k_{13},[f] 10^{10} M^{-1} sec^{-1}
50	50	4.25	7.75	4.18	8.64
50	50	4.60	3.82	2.91	4.37
50	50	4.05	7.50	5.78	6.34
10	50	4.32	4.98	3.79	7.06
10	50	4.75	3.24	3.02	4.86
25	25	4.79	3.03	2.14	5.36
25	25	4.32	4.19	1.91	8.04
25	25	4.54	3.49	2.62	5.62
100	50	4.54	4.46	3.04	4.04

[a] Total molar concentration of hydrazoic acid. [b] Total molar concentration of bromocresol green. [c] Average of pH measured in the sample cell before and after DFE experiments. [d] Faster of two experimental reciprocal relaxation times, average of four experiments. [e] Calculated reciprocal relaxation time $([H^+] + [In^{2-}] + K_i)k_{12}$ of bromocresol green under the same conditions using $K_i = 1.26 \times 10^{-5}$ M and $k_{12} = 5.4 \times 10^{10}$ M^{-1} sec^{-1}. [f] Specific rate of reaction $H^+ + N_3^- \xrightarrow{k_{13}} NH_3$ calculated from these data.

hydrazoic acid made in this laboratory with a conductometric dissociation field effect apparatus. The somewhat lower value of k_{13} for N_3^- than for the spherically symmetric F^- ion could indicate that not all directions of approach of the H^+ ion to the linear N_3^- ion are equally favorable for reaction.

Acknowledgment. The authors wish to acknowledge preliminary conductometric experiments by Dr. David L. Cole and to thank Professor K. Kustin for having suggested this problem. This work has been sponsored by AFOSR (SRC)-OAR, USAF, Grant No. 69-1717-F.

Molecular Complexes in the Vapor of Sodium Bromide and Zinc Bromide Mixtures

by Douglas W. Schaaf and N. W. Gregory*

Department of Chemistry, University of Washington, Seattle, Washington 98105 *(Received February 16, 1971)*

Publication costs assisted by the National Science Foundation

The equilibrium vapors above a number of alkali halide–metal halide systems have been shown to contain molecules in which both metal and alkali metal atoms are present. Of particular interest in relation to the present work is evidence for formation of molecules of the form $(NaCl)_x(ZnCl_2)_y$, found in transpiration studies by Rice and Gregory[1] and in mass spectrometric studies by Bloom, O'Grady, Anthony, and Reinsborough.[2] The latter work indicates that $Na_2Zn_2Cl_6$ is an important constituent, whereas the former suggests, from the observed dependence of the apparent pressure of the complex, derived from the sodium content of the vapor, on the pressure of $ZnCl_2$ in equilibrium with solid sodium chloride, that molecules containing more than one zinc atom are not present in significant amounts. The experimental conditions of the two studies were somewhat different: the transpiration work was done over the range 495–550° with an argon carrier gas at *ca.* 1000 Torr containing various partial pressures of zinc chloride equilibrating with solid sodium chloride; the mass spectrometric results were obtained from vapor issuing from a cell in which a condensed mixture of $ZnCl_2$ and NaCl (42–51 mol % of $ZnCl_2$) was dispersed on alumina powder and heated in the range 250–450°. In the mass spectrometric work the partial pressures of $ZnCl_2$ are expected to be relatively higher (in relation to sodium chloride) than in the transpiration studies which may enhance the contribution of $Na_2Zn_2Cl_6$; however, the apparent heats of formation derived for $NaZnCl_3(g)$ from the two studies are widely divergent (−18 as compared with −41 kcal/mol for formation from NaCl(g) and $ZnCl_2(g)$). We wish to report results of a related transpiration study of the NaBr–$ZnBr_2$ system.

Experimental Section

The experimental method was virtually identical with that described earlier in the work on the chloride system.[1,3] Very similar results were obtained. Data are presented in Table I.[4] The partial pressures derived for the various components of the equilibrium vapor were independent of flow rates between 15 and 50 cm^3 min^{-1}. The argon was made to flow either first over a sample of pure $ZnBr_2$, in a compartment adjacent to the main reactor and heated by a separate furnace to introduce the desired partial pressure of $ZnBr_2$, and then over a sample of NaBr(s) (method 1), or directly over heated NaBr–$ZnBr_2$ mixtures (method 2). Condensed mixtures used in method 2 had a mole fraction of NaBr *ca.* 0.9; it was assumed that NaBr(s) remained at unit activity in both types of experiment, analogous to the behavior indicated by the phase diagram for the chloride system.[5] In method 2 a liquid complex phase, assumed in equilibrium with NaBr(s), was present. The phase diagram for the bromide system does not appear to have been reported.

(1) D. W. Rice and N. W. Gregory, *J. Phys. Chem.*, **72**, 4524 (1968).

(2) H. Bloom, B. V. O'Grady, R. G. Anthony, and V. C. Reinsborough, *Aust. J. Chem.*, **23**, 843 (1970).

(3) D. W. Rice, Doctoral Dissertation, University of Washington, Seattle, Wash., 1968.

(4) Table I will appear immediately following this article in the microfilm edition of this volume of the journal. Single copies may be obtained from the Reprint Department, ACS Publications, 1155 Sixteenth Street, N. W., Washington, D. C. 20036. Remit $3.00 for photocopy or $2.00 for microfiche.

(5) N. Nikonowa, S. P. Pawlenko, and A. G. Bergman, *Bull. Acad. Sci. URSS, Cl. Sci. Chim.*, 391 (1941).

Starting samples of $ZnBr_2$ (Alfa Inorganics, reagent grade) and NaBr (Baker and Adamson, reagent grade) were vacuum dried; the $ZnBr_2$ was vacuum sublimed prior to use. Apparent ideal gas partial pressures in the equilibrium vapors were calculated from the relative numbers of moles of Zn, Na, and Ar found in the condensed vapor. The total zinc transported was determined by EDTA complexometric analysis;[6] a Beckman DU flame photometer was employed to determine the quantity of sodium. The pressure of argon was determined manometrically and the number of moles of argon

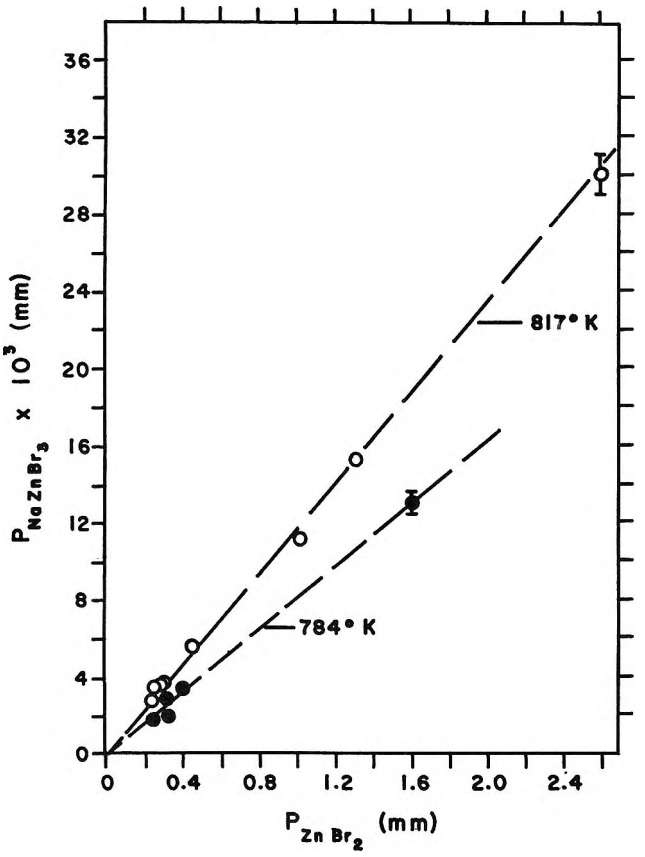

Figure 1. Pressure of $NaZnBr_3(g)$ *vs.* the pressure of $ZnBr_2(g)$. Pressures of $ZnBr_2$ lower than those necessary to form a NaBr–$ZnBr_2$ condensed phase: ●, 784 ± 1.5°K; ○, 817 ± 1.5°K. Pressures of $ZnBr_2$ above NaBr–$ZnBr_2$ condensed phase in equilibrium with NaBr(s): ◐, 784 ± 1.5°K; ◑, 817 ± 1.5°K.

flowing through the reactor during a given experiment was determined by measuring the pressure of the quantity collected after expansion into a calibrated volume. The contribution to the total number of moles of sodium expected from the vapor pressure of sodium bromide was predicted from the data of Cogin and Kimball[7] with allowance for the presence of dimer from the data of Guion, Hengstenberg, and Blander.[8] This contribution ranged from a negligible amount at the lowest temperatures to about 20% at the highest temperatures; see Table I.

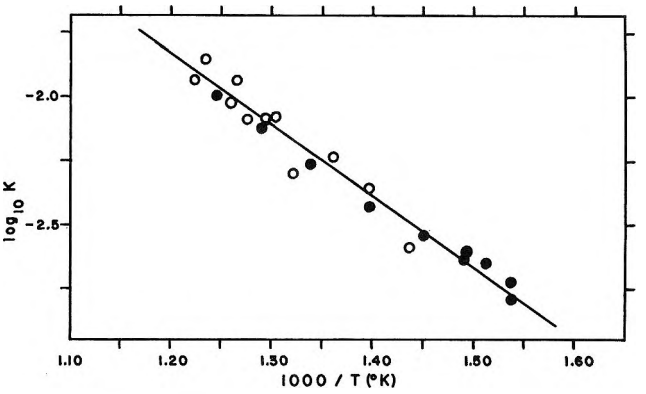

Figure 2. Transpiration results for the assumed equilibrium $NaBr(s) + ZnBr_2(g) = NaZnBr_3(g)$: apparent equilibrium constant, $K = P_{NaZnBr_3}/P_{ZnBr_2}$; ○, method 1; ●, method 2.

Results and Discussion

Apparent equilibrium constants were calculated for the reaction

$$x\text{NaBr(s)} + x\text{ZnBr}_2\text{(g)} \longrightarrow (\text{NaZnBr}_3)_x \qquad (1)$$

The value of x was assumed to be unity when it was found, Figure 1, that a plot of the apparent pressure of $NaZnBr_3$ *vs.* the pressure of $ZnBr_2$ was linear. The absence of any noticeable curvature in these lines suggests that species with more than one zinc atom are not of major importance in the equilibrium vapor. This behavior is similar to that found earlier in the chloride system.[1] The transpiration results do not provide evidence concerning the relative importance of species such as Na_2ZnBr_4, Na_3ZnBr_5, etc., since the activity of NaBr was not varied; however, these "higher polymers" are not expected to be present at significant concentrations, particularly in view of the low partial pressure of the sodium halide. The equilibrium constants listed in Table I are the values derived from the data when $NaZnBr_3(g)$ was assumed the only complex species. A log K *vs.* $1/T$ plot is shown in Figure 2; the associated least-squares linear line shown corresponds to the equation

$$\log K = (-2786 \pm 300)T^{-1} + 1.503 \pm 0.425$$

Values of the equilibrium constants at 784 and 817°K, respectively, were taken as the slopes of the respective lines in Figure 1. The value at 810°K was taken as the numerical average of the values in Table I because the small variation in $ZnBr_2$ pressures precluded a meaningful plot of data at this temperature. These averaged constants were weighted in the least-squares treatment to reflect the number of runs represented. The closed

(6) A. I. Vogel, "A Textbook of Quantitative Inorganic Analysis," Wiley, New York, N. Y., 1963, p 433.

(7) G. E. Cogin and G. E. Kimball, *J. Chem. Phys.*, **16**, 1035 (1948).

(8) J. Guion, D. Hengstenberg, and M. Blander, *J. Phys. Chem.*, **72**, 4620 (1968).

circles, Figure 2, represent results when argon was passed over the preformed mixtures of NaBr and $ZnBr_2$ (method 2). As a set they appear more consistent than the open circles (method 1). It may be reasonable to anticipate that the approach to equilibrium by decomposition of the condensed mixture is more rapid than by interaction of vapor with the solid phase, although no evidence for a systematic dependence of the results of method 1 on flow rate was apparent. The apparent enthalpy and entropy changes for (1), derived by a least-squares treatment (using all points), at the mean temperature of 740°K are 12.7 kcal mol^{-1} and 6.9 cal mol^{-1} deg^{-1}, respectively; these values are quite similar to those found in the chloride system.

The properties derived from the transpiration data for the "mixed metal dimer" molecules $NaZnX_3(g)$ (X = Br, Cl), when compared with those of $(NaX)_2$ and $(ZnX_2)_2$, are reasonably close to what might be expected for a random exchange without serious modification in bond energies.[9-11] This is not true of the mass spectrometric value for the relative enthalpy of the chloride. It is to be emphasized that the transpiration data provide no direct verification of the molecular form of the complex, however.

Acknowledgment. We are pleased to acknowledge financial support from the National Science Foundation, Grant NSF GP 6608x.

(9) "JANAF Thermochemical Tables," revised ed, The Dow Chemical Co. Midland, Mich., 1963.

(10) S. Datz, W. T. Smith, and E. H. Taylor, *J. Chem. Phys.*, **34**, 558 (1961).

(11) F. J. Keneshea and D. Cubiccotti, *ibid.*, **40**, 19 (1964).

COMMUNICATIONS TO THE EDITOR

Formation of Ozonide Ions in γ-Irradiated Aqueous Solutions of Alkali Hydroxides

Publication costs borne completely by The Journal of Physical Chemistry

Sir: In a recent communication Nazhat and Weiss claimed to have observed a phenomenon of considerable significance to the theory of trapped and solvated electrons.[1] They exposed 1 *M* aqueous solutions of the alkali metal hydroxides to ^{60}Co γ radiation at 77°K, and, after various annealing and bleaching procedures, they detected esr spectra comprising hyperfine features characteristic of the various alkali metal cations used. The data reported[1] are included in Table I. They postulated that the unpaired electrons are trapped in expanded orbitals on the hydrated alkali metal cations. These results, if correctly interpreted, constitute a major piece of evidence in the topic of solvated electrons, since such centers have long been one of the major models used to interpret the properties of metal solutions,[2] although no firm evidence for their formation in water or ammonia has been forthcoming prior to this work.[1]

Before using these results for theoretical purposes, we felt it wise to repeat the work, particularly since no esr spectra were actually presented, and various phrases[1] such as "to some extent characteristic of the alkali metal nuclei" and "the number of hyperfine lines corresponds roughly to the nuclear spin" made us somewhat cautious.

We have used a wide range of solutions and bleaching and annealing procedures but have completely failed to detect any features that could possibly be associated with hyperfine coupling to alkali metal

Table I: Esr Data Obtained from γ-Irradiated Aqueous Solutions of Alkali Metal Hydroxides after Annealing, Together with Data for O_3^-

Matrix	g_{av}	a, G	Ref
$NaOH-H_2O$	2.0056	14.8	1
$KOH-H_2O$	2.0060	10.0	1
$CsOH-H_2O$	2.0048	14.1	1

Matrix	g_{11}	g_{22}	g_{33}	Ref
LiOH, NaOH, KOH in O_2O or H_2O	2.004	2.018	2.011	*a*
NaO_3	2.0025	2.0174	2.0104	*b*
$NaBrO_3$	2.006	2.022	2.022	*c*
$KClO_3$	2.0026	2.018	2.016	*d*
$KrBrO_3$	2.003	2.0165	2.011	*e*

[a] Present work, ±0.001. [b] P. W. Atkins, J. A. Brivati, N. Keen, M. C. R. Symons, and P. A. Trevalion, *J. Chem. Soc.*, 4785 (1962). [c] T. Anderson, J. R. Bzberg, and K. J. Olsen, *J. Phys. Chem.*, **71**, 4129 (1967). [d] R. S. Eachus and M. C. R. Symons, *J. Chem. Soc. A*, 2433 (1968). [e] A. Begum, S. Subramanian, and M. C. R. Symons, *ibid.*, *A*, 918 (1970).

(1) N. B. Nazhat and J. J. Weiss, *J. Phys. Chem.*, **74**, 4298 (1970).

(2) M. C. R. Symons, *Quart. Rev., Chem. Soc.*, 99 (1959); P. W. Atkins and M. C. R. Symons, "The Structure of Inorganic Radicals," Elsevier, Amsterdam, 1967.

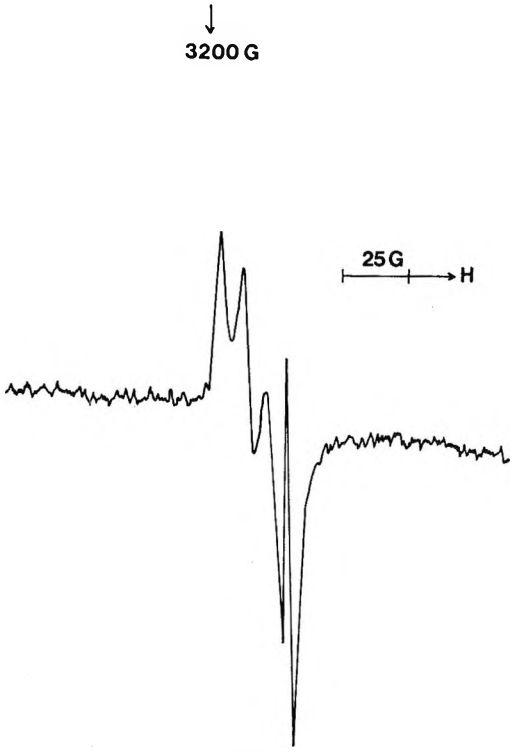

Figure 1. First-derivative esr spectrum for γ-irradiated 1 *M* KOH in D_2O after thermal annealing and recooling to 77°K.

nuclei. We have, however, detected a fairly long-lived radical having three g-value features at 77°K which average to a single feature on warming, together with a weak single line which appears just below the free-spin region. Under some circumstances these features, taken together, could be mistaken for a quartet, having $a_{iso} \doteqdot 11$ G (Figure 1). It seems possible that the species identified previously as electrons associated with hydrated sodium or potassium ions could in fact have been these species. This is ruled out for the following reasons. (i) The lines are independent of the nature of the cation. (ii) On warming, the low-field features merge to give a single, isotropic line at $g = 2.010$. (iii) The relative intensities of the lines are a function of the annealing temperature, there being, clearly, two species involved.

The principal values of the g tensor for the low-field species are close to those for the ozonode ion, O_3^-, in a variety of different environments (Table I). It is formed as the species usually described as O^- [3] decays, a possible route being $O^- + O_2 \rightarrow O_3^-$. The ozonode ion is known to be relatively stable,[4] which would account for its thermal stability in these glasses.

While we cannot identify the second species detected in our spectra, since it has only a single line in the free-spin region, it seems reasonable to assume that it is an impurity radical, such as CO_3^- or CO_2^- formed from carbonate impurity.

(3) M. J. Blandamer, L. Shields, and M. C. R. Symons, *Nature (London)*, 199, 902 (1963); *J. Chem. Soc.*, 4352 (1964).

(4) A. D. McLachlan, M. C. R. Symons, and M. G. Townsend, *ibid.*, 952 (1959).

DEPARTMENT OF CHEMISTRY
THE UNIVERSITY
LEICESTER, LE1 7RH, ENGLAND

K. V. S. RAO
M. C. R. SYMONS*

RECEIVED APRIL 29, 1971

Reply to "Formation of Ozonide Ions in γ-Irradiated Aqueous Solutions of Alkali Hydroxides"

Publication costs borne completely by The Journal of Physical Chemistry

Sir: Rao and Symons have rightly remarked that we were somewhat careful in the wording of the interpretation of our esr spectra. Because, although we found a difference between the NaOH and CsOH ices, these spectra, as we have stated, show an unsymmetrical pattern which suggests a superposition of the spectra of two or possibly more species, this makes any straightforward interpretation difficult; we were in fact, influenced in our interpretation by the work of Hart.[1] It would appear that Rao and Symons have confirmed some of our observations but do not agree with our interpretation. While it is thus possible that O_3^- may make some contribution to the spectra, it seems rather unlikely that the spectra which we have observed are essentially affected by adventitious impurities, as these authors suggest.

(1) C. Gopinathan, E. J. Hart, and K. H. Schmidt, *J. Phys. Chem.*, 74, 4169 (1970).

SCHOOL OF CHEMISTRY
THE UNIVERSITY
NEWCASTLE UPON TYNE, NE1 7RU
ENGLAND

N. B. NAZHAT
J. J. WEISS*

RECEIVED MAY 24, 1971

Extrapolation Procedures for Evaluation of Individual Partial Gram Ionic Volumes

Publication costs assisted by the Chemistry Department, University of Ottawa

Sir: In a recent comprehensive review[1] on determination of absolute partial gram ionic volumes,[2] $\bar{V}_i^0$, Panckhurst has asserted that a method recently proposed[3] for derivation of individual $\bar{V}_i^0$ based on extrapolation of partial molal volumes of homologous symmetrical tetraalkylammonium (TAA) salts to zero

(1) M. H. Panckhurst, *Rev. Pure Appl. Chem.*, 19, 45 (1969).

(2) J. E. Desnoyers and C. Jolicoeur, "Modern Aspects of Electrochemistry," Vol. 5, J. O'M. Bockris and B. E. Conway, Ed., Plenum Press, New York, N. Y. 1969, Chapter 1.

(3) B. E. Conway, J. E. Desnoyers, and R. E. Verrall, *Trans. Faraday Soc.*, 62, 2738 (1966).

cation molecular weight is arbitrary and that other related extrapolations give results for $\bar{V}_-^0$, the volume of the coanion, differing by up to the very large figure of 45 ml (g-ion)$^{-1}$ from the value derived in ref 3. The method criticized[3] gave, however, a value within 0.5 ml (g-ion)$^{-1}$ (for Br^-) of that derived by the completely different procedure of Zana and Yeager[4] based on ultrasonic vibration potentials.[5] The evaluation of individual ionic properties is now a matter of considerable interest in relation to the specific properties which ions exhibit in aqueous solution and individual ionic behavior is of importance in both physical chemistry and biophysics. The basis of the assertion of arbitrariness of the method under discussion[3] therefore requires further examination.

In this note we show that the conclusions of Panckhurst[1] about the arbitrariness of extrapolation procedures and the differences of resulting intercepts for the coanion volume are largely unfounded, being based (a) on an inappropriate choice of one of the functions to be extrapolated and (b) on failure to take into account that if the method is to give an approximately correct value for $\bar{V}_i^0$ for the coanion, the function chosen for the extrapolation must be selected with due consideration of the significance of the intercept which is derived. We shall not be concerned here with examining further[3] the reasons for the small but significant deviations of the $\bar{V}^0$ data (principally the $\bar{V}^0$ for Et_4N^+ salts) from the straight-line plots as a function of molecular weight[3] or number of C atoms in the ion.[6] Three reasons for such deviations were discussed previously.[3] We are concerned here with demonstrating that one of the extrapolations of Panckhurst must give a very different intercept which is not in fact at all related to $\bar{V}_-^0$, so that the impression he gave of the unreliability of the extrapolation procedure is misleading. In order to show the origin of Panckhurst's incorrect conclusion, it is necessary to examine the physical and algebraic bases of various extrapolation procedures which he discussed.[1]

Physical and Algebraic Bases of Extrapolation Procedures. The method we suggested[3] is based on the principle that the partial molal volumes of an homologous series of nonelectrostricting salts can be extrapolated to zero value of a parameter characterizing the size of the cation, so that the intercept on the volume axis is the partial molal volume contribution due to the coanion, $\bar{V}_-^0$. This approach is justified by the following considerations. The volume of the salt in solution is $\bar{V}_+^0 + \bar{V}_-^0$, and $\bar{V}_+^0$ can be broken down into the following terms

$$\bar{V}_+^0 = V_{in(+)} + V_{e(+)} + V_{s(+)}$$

where $V_{in(+)}$ is the effective intrinsic volume of the ion[7] and is always positive, $V_{e(+)}$ arises from the electrostriction of the solvent (always negative), and $V_{s(+)}$ is a structural contribution to the volume due to the inclusion of the ion in a cavity in the solvent (negative volume contribution) and to any reaction upon the solvent structure to produce an increase in "ice-like" character (positive volume contribution) locally about the ion. The series of TAA salts come closest to the requirement that $V_{e(+)}$ is 0 since the field at the periphery of such ions is negligible in terms of that required to cause significant electrostriction.[8,9] There is strong evidence[2] that TAA ions increase the local structure of the solvent water (positive contribution to $V_{s(+)}$ and increase of the solvent lattice relaxation times[10]). However, the overall sign of the structural contribution in $\bar{V}$ for hydrophobic solutes is generally negative[11,12] since they can usually be accommodated in their solvent cages with an overall economy of space. There is therefore some compensation between these two structural contributions in $V_{(s)+}$. As a result, $V_{(s)+}$ is probably small compared with $V_{in(+)}$ but should in any case vary progressively with the size of the ion. The $V_{in(+)}$ may hence be expected to be the principal term of the partial gram ionic volumes of the homologous series of TAA ions. This is borne out by the experimental results.[2,10] The dependence of $V_{in(+)}$ on the nature of the TAA ion may now be examined.

The molecular weight of a tetraalkylammonium (TAA) salt $R_4N^+A^-$, *i.e.*, $(C_nH_{2n+1})_4N^+A^-$ is given for the anion and cation by

$$M_+ + M_- = 4[nM_C + (2n + 1)M_H] + M_N + M_- \quad (1)$$

where M's are the atomic or molecular weights of the indicated species. It is reasonable to assume the usual proportionality between the molecular volume and the numbers of various types of atoms in given isoelectronic situations; *i.e.*, an equation, similar to (1), can be written for the cations as

$$\bar{k}_+V_+ = 4nV_Ck_C + 4(2n + 1)V_Hk_H + V_Nk_N \quad (2)$$

where the proportionality constants k_C, k_H, and k_N have the dimensions and significance of effective atomic densities and $\bar{k}_+$ is a mean density[13] of the cation.

(4) R. Zana and E. Yeager, *J. Phys. Chem.*, **70**, 954 (1966); **71**, 521 (1967).

(5) P. Debye, *J. Chem. Phys.*, **1**, 13 (1933).

(6) R. E. Verrall and B. E. Conway, *J. Phys. Chem.*, **70**, 3962 (1966).

(7) B. E. Conway, J. E. Desnoyers, and A. C. Smith, *Phil. Trans. Roy. Soc. London, Ser. A*, **256**, 389 (1964).

(8) J. E. Desnoyers, R. E. Verrall, and B. E. Conway, *J. Chem. Phys.*, **43**, 243 (1965).

(9) J. Padova, *ibid.*, **39**, 1552 (1963).

(10) H. G. Hertz, B. Lindman, and V. Siepe, *Ber. Bunsenges. Phys., Chem.*, **73**, 542 (1969).

(11) F. J. Millero and W. Drost-Hansen, *J. Phys. Chem.*, **72**, 1758 (1968).

(12) M. E. Friedman and H. A. Scheraga, *ibid.*, **69**, 3795 (1965).

(13) Since this note was submitted, King[14] has further considered the question of individual ionic $\bar{V}^0$ and discussed the matter in terms of mean ionic density.

(14) E. J. King, *J. Phys. Chem.*, **74**, 4590 (1970).

Since the C and N atoms are in the same state of sp^3 hybridization and both involve p shell valence electrons, the volume contribution and k values will be similar so that eq 2 can be factorized to a good approximation as

$$V_+ = \frac{1}{\bar{k}_+}[k_C V_C(4n + 1) + (8n + 4)k_H V_H] \quad (3)$$

$$= \frac{1}{\bar{k}_+}[k_C V_C(4n + 1) + (4n + 1)2k_H V_H] + 2k_H V_H/\bar{k}_+ \quad (4)$$

Hence, the volume of the cation can be expressed as a linear function of the total number $4n + 1$ of backbone chain atoms in it. It is evident that as $4n + 1 \rightarrow 0$, *i.e.*, for zero number of chain (C and N) atoms in the cation, the plot of the experimental quantity $\bar{V}_+^0 + \bar{V}_-^0$ for homologous salts in the TAA series will give a linear relation with an intercept of $\bar{V}_-^0 + 2k_H V_H/\bar{k}_+$ for 2 H atoms, the second term having a value approximately equal to 2 ($\bar{k}_+ \doteqdot 1$, *cf.* ref 3 and below).

Although the above treatment shows that an extrapolation based on numbers of atoms (eq 4), as employed by Verrall and Conway,[6] can be rigorously justified, with TAA salts having the normal isotopic composition, $\bar{V}_{salt}^0$ can also be directly plotted against molecular weight,[4] giving a linear relation. Although the deviations of $\bar{V}^1{}_{salt}^0$ from this addivity relation are significant enough[3] to be detected in precise measurements, the important and perhaps remarkable result is that the additivity is so good on the basis of this or any other function. In fact, the results must be plotted on a large-scale graph for the deviations to be seen. In terms of the molecular weight M_+ of the cation, the additivity implies that

$$\bar{V}_+^0 = \frac{1}{\bar{k}_+}M_+ + \text{constant} \quad (5)$$

with $\bar{k}_+$ independent of M_+, as shown, to a very good approximation, by the experimental results.[3]

Millero[15] has recently supported the method at present under discussion and reexamined the method of Zana and Yeager[4] for obtaining absolute $\bar{V}_i^0$ from ultrasonic vibration potentials and showed that Panckhurst's[1] arguments for rejecting that method are also unsound. He calculated that the maximum error introduced in using apparent molal volumes at finite concentration would be 0.6 cm^3 mol^{-1} which is within the uncertainty quoted by Zana and Yeager. On this basis, a scale of absolute $\bar{V}_+^0$ values can be obtained which is similar to our own values and corresponds to $1/\bar{k}_+ = 1.12$ cm^3 g^{-1} and a zero value of the constant in eq 5.

If, as argued above, $\bar{V}_+^0 \doteqdot V_{in(+)}$ and the atomic volumes are additive, *i.e.*

$$\bar{V}_+^0 = 4nV_C + 4(2n + 1)V_H + V_N \quad (6)$$

then $\bar{V}_+^0$ can also be expressed as f$(4n + 1)$ or f$(n + 1)$, *viz.*

$$\bar{V}_+^0 = (4n + 1)(V_C + 2V_H) + V_N - V_C + 2V_H \text{ (}cf.\text{ eq 4)} \quad (7)$$

or

$$\bar{V}_+^0 = (n + 1)(4V_C + 8V_H) - 4(V_C + V_H) + V_N \quad (8)$$

which give intercepts of $V_N - V_C + 2V_H$ and $V_N - 4(V_C + V_H)$, respectively, when $\bar{V}_+^0$ is plotted against $4n + 1$ or $n + 1$ (Figure 1). With the value of $1/\bar{k}_+$ quoted above, these intercepts have finite values given by

$$V_N - V_C + 2V_H = (1/\bar{k}_+)(M_N - M_C + 2M_H) = 4.5 \text{ ml mol}^{-1}$$

$$V_N - 4(V_C + V_H) = (1/\bar{k}_+)(M_N - 4M_C - 4M_H) = -42.5 \text{ ml mol}^{-1}$$

or if $\bar{V}_{salt}^0$ data are plotted, the intercepts are the above values plus $\bar{V}_-^0$ (Figure 1).

The latter corresponds to Panckhurst's intercept for the "$n + 1$" plot. The main purpose of the present note is therefore to demonstrate that the method proposed by Panckhurst of plotting the partial molal volume of the salt against the number of carbon plus nitrogen atoms *per chain*, *i.e.*, $n + 1$, to obtain the coanion $\bar{V}_-^0$ does not provide a satisfactory basis for extrapolation at all; this is evident from eq 8 which shows that such an extrapolation would give $V_N - 4(V_C + V_H) + \bar{V}_-^0$ which differs from $\bar{V}_-^0$ by *ca.* -42.5 ml mol^{-1}. Hence the lack of agreement between "$\bar{V}_-^0$" derived by extrapolations based on cation molecular weight, total number of atoms of the cation, and number of carbon and nitrogen atoms per chain cannot be used by Panckhurst as an argument for casting doubt on the validity of the principle involved in the previously published procedure. The present comparison of methods of extrapolation shows that choice of the method is not arbitrary but must be made by selecting the procedure with the soundest physical basis. Previously discussed[3] deviations from strict additivity in the original data are not the subject of this note and do not invalidate the basis of our criticism of Panckhurst's extrapolations, particularly that as a function of $n + 1$.

Interesting conclusions can be drawn from the present comparison of extrapolation methods. The fact that $\bar{V}_+^0$(abs) of TAA ions are a linear function of M_+ passing almost through the origin is a strong indication $\bar{V}_+^0$ is very nearly a measure of $V_{in(+)}$, *i.e.*, the volume the TAA ions would have if $V_{e(+)}$ and $V_{s(+)}$ were zero.

(15) F. J. Millero, "Structure and Transport Processes in Water and Aqueous Solutions," R. A. Horne, Ed., Interscience, New York, N. Y., 1970, Chapter 15.

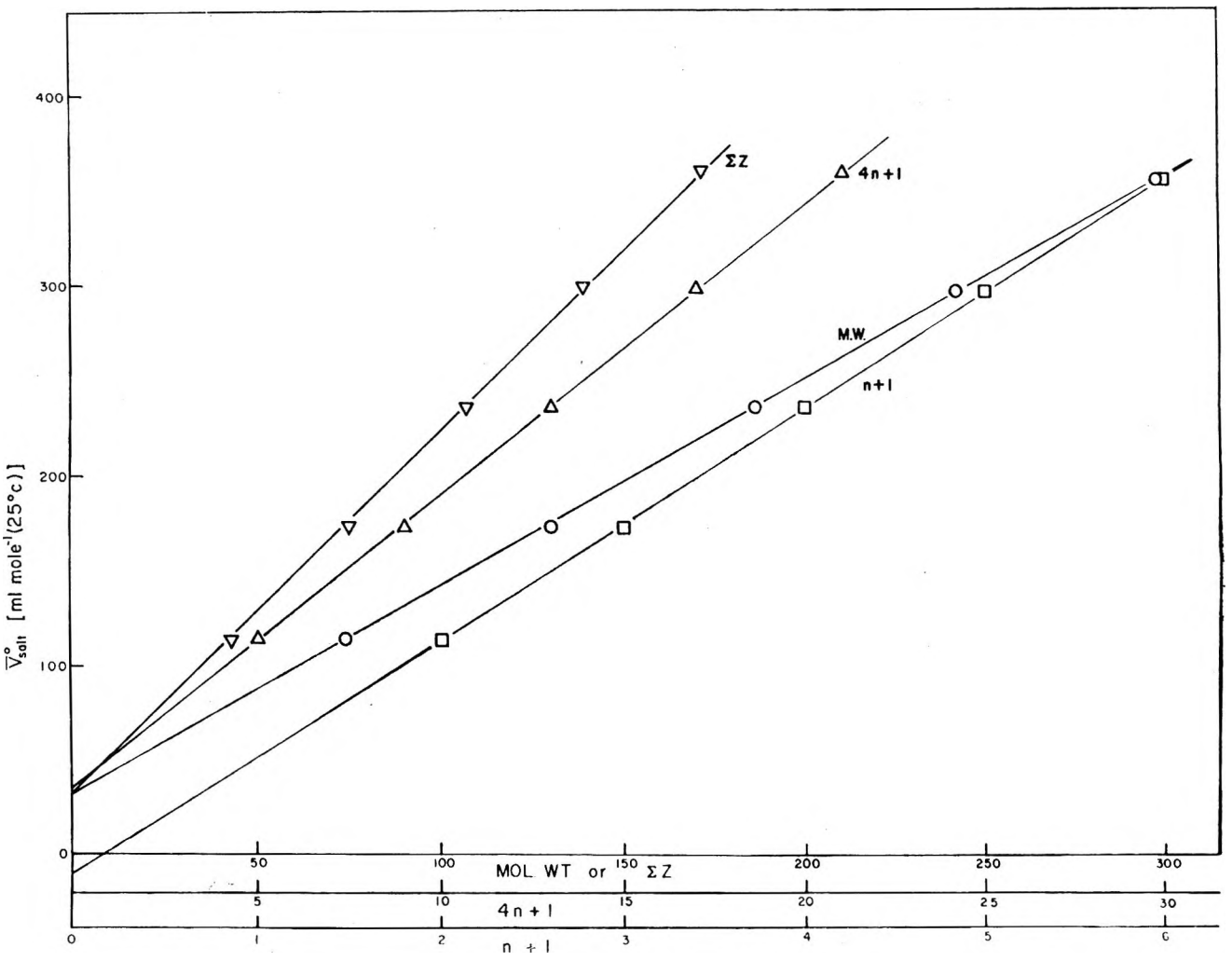

Figure 1. The partial molal volumes of bromide salts of tetraalkylammonium ions as a function of (a) molecular weight (M.W.), (b) total number of carbon and nitrogen atoms ($4n + 1$), (c) number of carbon and nitrogen atoms per chain ($n + 1$), and (d) total atomic number (ΣZ) of the cation.

Therefore in terms of volumes, the TAA ions form a nearly ideal solution. On the other hand, with other thermodynamic and kinetic functions there will not be any compensation between different structural interaction terms and a linear relation with molecular weight would not be expected.[16] This is in fact observed for B viscosity coefficients and ionic equivalent conductivities. Even though they are related to the size of the ion in water, the quantities B or $(4/3)\pi r_s^3$, where r_s is the Stokes radius, are not linear in M_+. For similar reasons, $\bar{V}_+^0$ of TAA ions in nonaqueous solvents, in solvent mixtures, or even in water at quite different temperatures are not,[16] or would not necessarily be, linear in M_+.

Finally, Panckhurst argued that the derived intercept in the extrapolation procedure should contain a "volume contribution from a positive charge having zero value of the particular molecular property" on which the extrapolation is based. This view seems to arise from a misunderstanding of the basis of the method. A series of salts is chosen which are not hydrated in the conventional sense, *e.g.*, without electrostriction. The extrapolation applies, as we have pointed out,[3] to only those real TAA ions which fulfill such a condition. Obviously, if NH_4^+ or limitingly $\oplus$ is included in the series,[2,6] there will be a negative contribution to the volume due to the electrostriction around this small, hydrophilic ion. Similar effects occur with $MeNH_3^+$, $Me_2NH_2^+$, and Me_3NH^+ ions.[6] This is observed in the original plot[2,6] and is expected; it does not affect the actual line used for extrapolation since this must be based only on $\bar{V}^0$ data for the *completely alkyl-coordinated* N^+ *ions, i.e.*, in the TAA salts where the positive charge is shielded from direct interaction with the water solvent.

Acknowledgments. Discussions with Dr. A. K. Covington (The University, Newcastle-upon-Tyne, England) and Dr. L. H. Laliberté (University of Ottawa) are gratefully acknowledged. We are in-

(16) D. Novak, M.Sc. Thesis, University of Ottawa, 1970, in course of publication.

debted to Dr. F. J. Millero for making his review manuscript available to us prior to publication.

DEPARTMENT OF CHEMISTRY
UNIVERSITY OF OTTAWA
OTTAWA 2, ONTARIO, CANADA
B. E. CONWAY*

DEPARTMENT OF CHEMISTRY
UNIVERSITY OF SHERBROOKE
SHERBROOKE, QUEBEC, CANADA
J. E. DESNOYERS

DEPARTMENT OF CHEMISTRY
UNIVERSITY OF SASKATCHEWAN
SASKATOON, SASKATCHEWAN, CANADA
R. E. VERRALL

RECEIVED APRIL 23, 1970

Reply to "Extrapolation Procedures for Evaluation of Individual Partial Gram Ionic Volumes"

Publication costs borne completely by The Journal of Physical Chemistry

Sir: In the preceding communication[1] Conway, Desnoyers, and Verral (CDV) reexamined the Conway, Verral, and Desnoyers[2] (CVD) method for obtaining individual (absolute) partial molar ionic volumes at infinite dilution, following my comments[3] on the method. One of my comments[3] was that the method depends on obtaining a linear relation between volumes for TAA salts and some molecular property which can be extrapolated to zero along the series. While the choice of molecular weight for this property is plausible (*i.e.*, as an empirical method), it was shown[3] that other functions gave as good a linear extrapolation and it was remarked that there is no apparent way of choosing between the widely differing intercept obtained. CDV[1] have now attempted to differentiate between these intercepts by assuming that, for TAA ions, the effective intrinsic volume of the ion is the principal term in the partial molar volume of these ions, that there is a direct proportionality between molecular volume and the numbers and types of atoms in the ions, that the volumes and atomic densities of carbon and nitrogen atoms are the same, and that $\bar{k}_+$ (the mean density of the ions) is constant for the ions in the series. Each of these assumptions can be questioned but, accepting them as a first approximation, I agree that CDV have now shown[1] that the major differences between intercepts in the various plots against numbers of atoms per chain or per ion arise from various combinations of atom volumes. In particular the intercept in the "$n + 1$" plot will include, as a first approximation, atom volumes represented by $V_N - 4(V_C + V_H)$, in addition to the volume of the coanion (see eq 8 of CDV[1]).

The important question which must now be considered is whether this justification has helped in assigning absolute partial molar ionic volumes and whether the original[2] extrapolation against molecular weight is justified. Whether $\bar{V}_-{}^0$ can be obtained using equations such as (4) in CDV[1] (ignoring the assumptions above) depends on a knowledge of the contribution of terms such as $2k_H V_H/\bar{k}_+$ to the intercept. One way of establishing this contribution is by comparison with some other method (as done by CDV[1]), such as that of Zana and Yeager.[4] This in itself implies that the method is not an independent one. Estimates of k_H and V_H could of course be made but a more fundamental uncertainty is the constancy of $\bar{k}_+$ for the ions considered by CDV.[1] The reciprocal of $\bar{k}_+$ appears as the slope of plots against numbers of atoms functions and against molecular weight if eq 5 in CDV[1] is accepted. $\bar{k}_+$ is directly related to the b parameter in the unnumbered table in CDV.[2] b is not constant from ion to ion (CDV[2] discussed possible reasons for this) meaning that all of the plots considered[1-3] are not strictly linear. This of course must show up as an uncertainty in the various intercepts. For example, a recalculation of the original CDV[2] extrapolation of $\bar{V}_s{}^0$ against molecular weight gives an intercept, using a linear least-squares analysis, of 23.6 ± 2.5 cm^3 mol^{-1}, where the uncertainty is the standard error. This intercept is interpreted as $\bar{V}^0(Cl^-)$ and CVD gave,[2] for the same extrapolation, $\bar{V}^0(Cl^-) = 23.6 \pm 0.2$ cm^3 mol^{-1}, stating that the limits correspond to "least squares uncertainty in the intercepts based on the linear plots." They did not say what least-squares uncertainty is intended but commented that the total uncertainty in $\bar{V}^0(X^-)$ would not exceed 0.5 cm^3 when the variation of b is taken into account. Their error estimates are optimistic and individual points deviate from the best straight line by up to 2 cm^3 mol^{-1}, or ten times the experimental precision. In my opinion a standard error uncertainty of 2.5 cm^3 mol^{-1}, arising from nonlinearity, considerably reduces the usefulness of the CVD method[2] for the particular ions considered. As noted by CDV[1], King[5] has recently used a method based on packing densities which has similarities to the methods discussed by CDV.[1] King[5] used a considerably wider range of ions and noted that the tetraethylammonium ion (one of those used by CVD) is significantly out of line compared with similar ions.

My second comment[3] on the CVD method,[2] as discussed by CDV,[1] was that the intercept should contain "a volume contribution from a positive charge having zero value of the particular molecular property" against which the volumes are extrapolated. This

(1) B. E. Conway, J. E. Desnoyers, and R. E. Verrall, *J. Phys. Chem.*, **75**, 3031 (1971).

(2) B. E. Conway, R. E. Verrall, and J. E. Desnoyers, *Trans. Faraday Soc.*, **62**, 2738 (1966).

(3) M. H. Panckhurst, *Rev. Pure Appl. Chem.*, **19**, 45 (1969).

(4) R. Zana and E. Yeager, *J. Phys. Chem.*, **70**, 954 (1966); **71**, 521 (1967).

(5) E. J. King, *ibid.*, **74**, 4590 (1970).

comment was badly worded and CDV[1] are correct in pointing out that this cannot refer to limiting $\oplus$. What I had in mind, and still maintain, is that the intercept may still contain some unknown contribution from $V_{e(+)}$ and/or $V_{s(s)+}$[1] which has not been extrapolated to zero. This is another way of saying that $V_{in(+)}$ may not be the only term in $\bar{V}_+^0$ and that, in particular, the CDV[1] argument that $V_{s(+)}$ "is probably small compared with $V_{in(+)}$ but should in any case vary progressively with the size of the ion" may not be correct. This can be demonstrated from the b values in the unnumbered table in CVD[2]. These b values are specific volumes per methylene group and give, when multiplied by the molar mass of four methylene groups, the added volume from ion to ion in the series. From the methyl ion to the ethyl ion this added volume is 59.8 ± 0.2 cm^3, from ethyl to n-propyl, 65.4 ± 0.1 cm^3, and from n-propyl to n-butyl it is 61.7 ± 0.3 cm^3, where the limits are estimates from the precision of the experimental data. These figures should all be the same if the CDV[1] assumptions are correct. If $V_{in(+)}$ does vary regularly from ion to ion, then evidently there is some contribution from $V_{e(+)}$ and/or $V_{s(+)}$ and it is possible that this contribution does not extrapolate out to zero. It is likely[6] that the absolute partial molar volume of the proton at infinite dilution in water at 25° lies in the region of 0 to −5 cm^3 mol^{-1}. For the above reasons it remains my opinion that the CVD[2] procedure cannot significantly narrow this range.

CDV[1] made the further points that the Zana and Yeager[4] method gives a value for absolute volumes within 0.5 cm^3 mol^{-1} of their own,[2] thus supporting the CVD values, and that Millero[6] claimed to have shown that my comments[3] on the ultrasonic vibration potentials method[4] are unsound. The following are comments I made on the Zana and Yeager ultrasonic vibration potentials method.[4] Experimental partial molar volumes and transport numbers at infinite dilution were used in the calculations where apparent molar volumes and transport numbers at the concentration under consideration should have been used; apparent molar volumes at finite concentration are not, in general, additive; the potential measurements were made at 22° but other quantities used in the analysis are for 25°; the theoretical formula used for vibration potentials is an approximate one applicable to "moderately dilute solutions"; and the quantity[4] ϕ/a, which in many cases is concentration dependent, is weighted toward higher concentrations.

Zana and Yeager[4] carried out measurements on some salts to 1 N and on most to 0.3 N. In view of their weighting procedure it is reasonable to consider the above points at 0.3 N, as has been done for some of them by Millero.[6]

Considering the use of partial molar volumes at infinite dilution instead of apparent molar volumes at finite concentrations Millero[6] pointed out that the simple alkali metal halides follow the limiting law ($\phi_V - \phi_V^0 = 1.868C^{1/2}$) closely in dilute solutions. For these salts at 0.3 N $\phi_V - \phi_V^0$ is therefore about 1.0 cm^3 mol^{-1} (Millero gave 0.6 cm^3 mol^{-1}, possibly through multiplying 1.868 by C instead of $C^{1/2}$). For 2:1 salts the difference is much larger, although not as large as the 3.8 cm^3 mol^{-1} calculated from the simple formula (see plots in papers by Dunn[7]). To this effect should be added the effect of nonadditivity of apparent molar volumes which Millero[6] gave as about 0.4 cm^3 mol^{-1} for the alkali metal halides at 0.3 N.

The effect of variation of transport numbers with concentration varies from salt to salt. For 1:1 salts with transport numbers near 0.5 there is little variation with concentration but for salts such as NaCl (t_+ = 0.396 at infinite dilution) variation with concentration is significant[8] and for NaCl leads to a change in the calculated value for V_+ of about 0.7 cm^3 mol^{-1}. Variation of transport numbers with concentration for higher valence type salts is usually greater than for 1:1 salts.[8]

The temperature variation of ϕ_V^0 around room temperature is of the order of 0.1 cm^3 mol^{-1} deg^{-1}. The volumes used in interpreting the Zana and Yeager measurements[4] at 22° should therefore differ from those at 25° by about 0.3 cm^3 mol^{-1}.

The Zana and Yeager[4] method certainly offers the possibility of determining absolute partial molar volumes but, in its present state of development and interpretation, it has an experimental precision which leads to an uncertainty of 2 cm^3 mol^{-1} in absolute volumes and uses an approximate formula which may not accurately describe the situation at the concentrations used. I am not competent to judge this latter point but it is still my opinion, considering the experimental uncertainty together with the other uncertainties mentioned above, that the Zana and Yeager method (as presently developed) does not do more than support the claim[6] that $\bar{V}_H^0$ is probably in the range 0 to −5 cm^3 mol^{-1} and does not justify the CVD extrapolation[2] against molecular weight.

Acknowledgment. I am grateful to Dr. F. J. Millero for making his review available before publication.

(6) F. J. Millero, "Structure and Transport Processes in Water and Aqueous Solutions," R. A. Horne, Ed., Interscience, New York, N. Y., 1970, Chapter 15.

(7) L. A. Dunn, *Trans. Faraday Soc.*, 62, 2348 (1966); 64, 2951 (1968).

(8) M. Spiro, "Technique of Organic Chemistry," Vol. 1, A. Weissberger, Ed., Interscience, New York, N. Y., and London, 1960, Part IV.

DEPARTMENT OF CHEMISTRY
UNIVERSITY OF OTAGO
DUNEDIN, NEW ZEALAND

M. H. PANCKHURST

RECEIVED MAY 25, 1970

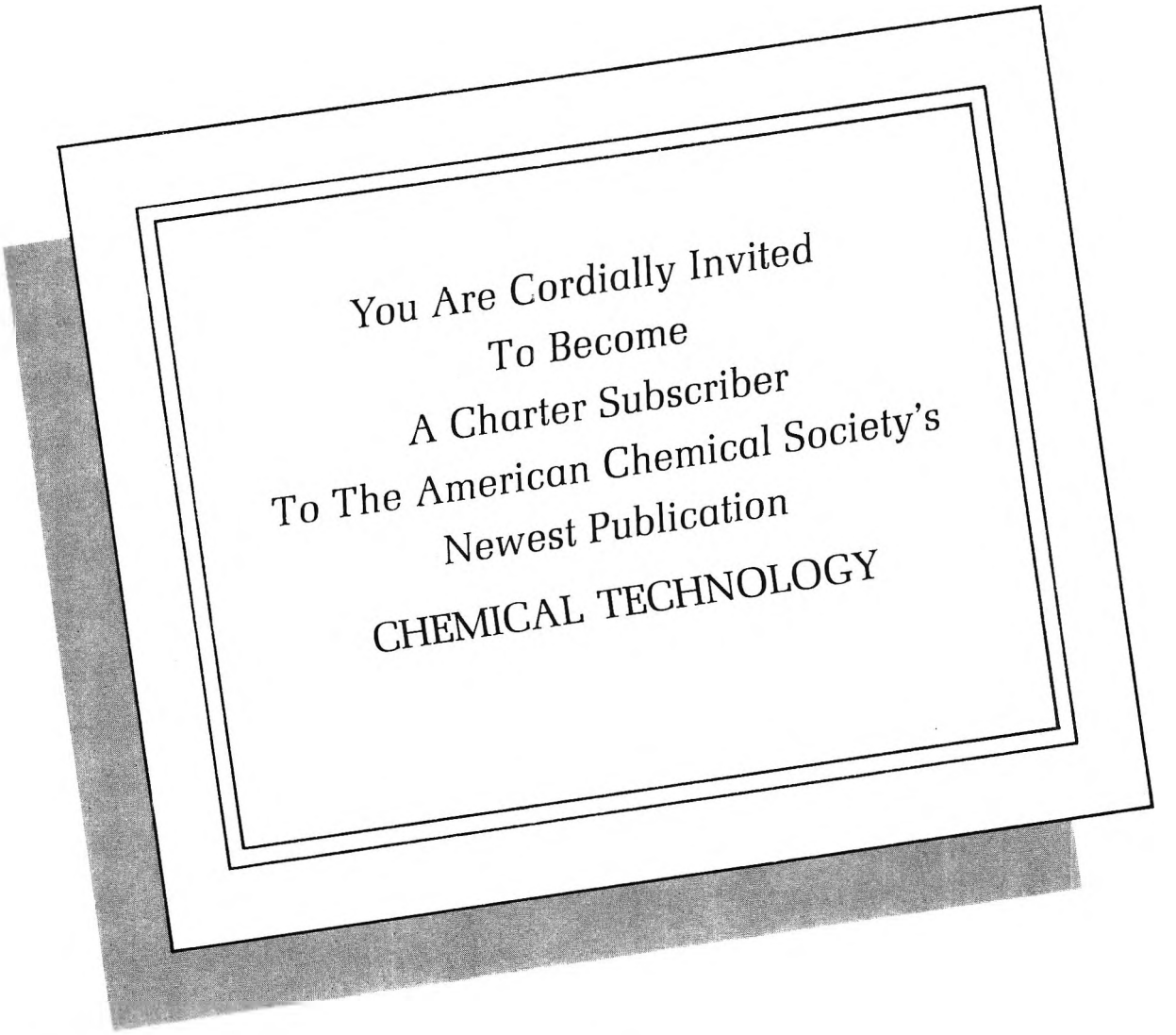

Cutting across all disciplines, the new monthly publication CHEMICAL TECHNOLOGY is written expressly for those charged with industrial innovation. Chemists and chemical engineers in industry will welcome its pragmatic approach.

Designed to be a highly readable, current awareness magazine, CHEMICAL TECHNOLOGY is a valuable addition to existing ACS publications.

Its articles range over areas of immediate interest, while monthly features deal with many facets of industrial life through interviews, articles, stories and anecdotes.

To start CHEMICAL TECHNOLOGY on its way to you, just complete and return the form at the right. You'll get a new outlook on the world of industrial chemistry.

American Chemical Society
1155-16th Street, N.W., Washington, D.C. 20036

Please start my one-year subscription to CHEMICAL TECHNOLOGY at the rate I have checked below.

Nonmember Rate:	U.S.	Canada, PUAS	Other Nations
	☐ $18.00	☐ $20.50	☐ $21.50

Name _____

Position _____
(Specify title, please)

Address: ☐ Home
☐ Business _____

City _____

State/Country _____ Zip _____

Your employer _____

Nature of your employer's business: ☐ Manufacturing or processing ☐ Other _____
(Please indicate)

If manufacturer, type of products produced _____

I2A

PHYSICAL CHEMISTRY

An Advanced Treatise

edited by HENRY EYRING, Department of Chemistry and Metallurgy, University of Utah, Salt Lake City, Utah, **DOUGLAS HENDERSON,** IBM Research Laboratories, San Jose, California, **and WILHELM JOST,** Institut fur Physikalische Chemie der Universitat Gottingen, Gottingen, Germany

Volume 1/**THERMODYNAMICS**

edited by WILHELM JOST

CONTENTS: R. HAASE: Survey of Fundamental Laws. A. SANFELD: Equilibrium, Stability, and Displacements. A. SANFELD: Irreversible Processes. A. SANFELD: Thermodynamics of Surfaces. R. HAASE: Thermodynamic Properties of Gases, Liquids, and Solids. E. U. FRANCK: Gas-Liquid and Gas-Solid Equilibria at High Pressures, Critical Curves, and Miscibility Gaps. HERBERT STENSCHKE: Thermodynamics of Matter in Gravitational, Electric, and Magnetic Fields. J. WILKS: The Third Law of Thermodynamics. MAX KLEIN: Practical Treatment of Coupled Gas Equilibrium. H. KREMPL: Equilibria at Very High Temperatures. ROBERT H. WENTORF, Jr.: High Pressure Phenomena. S. M. BLINDER: Caratheodory's Formulation of the Second Law. Author Index-Subject Index.

1971, 672 pp., $29.50
Subscription price: $25.50

Volume 8/**LIQUID STATE**

Part A

edited by DOUGLAS HENDERSON

CONTENTS: ROBERT L. SCOTT: Introduction. SOW-HSIN CHEN: Structure of Liquids. F. H. FRANCIS: Computer Calculations for Model Systems. R. J. BAXTER: Distribution Functions. MU SHIK JHON and HENRY EYRING: The Significant Structure Theory of Liquids. DOUGLAS HENDERSON and J. A. BARKER: Perturbation Theories. Author Index-Subject Index.

November 1971, about 427 pp., $23.00
Subscription price: $19.55

Part B

edited by DOUGLAS HENDERSON and PETER J. LEONARD:

CONTENTS: DOUGLAS HENDERSON: Liquid Mixtures. D. TER HARR: Liquid Helium. BRUCE J. BERNE: Time Dependent Properties of Condensed Media. JOHN STEPHENSON: Critical Phenomena: Static Aspects. H. EUGENE STANLEY, GERALD PAUL, and SAVA MILOSEVIC: Introduction to Dynamic Critical Phenomena in Fluid Systems. Author Index-Subject Index.

November 1971, about 467 pp., $25.00
Subscription price: $21.25

** Subscription prices for individual volumes valid only on orders for the complete set received before the publication of the last volume.*

STATISTICAL PHYSICS

by A. ISIHARA, State University of New York, Buffalo

CONTENTS: PRINCIPLES AND ELEMENTARY APPLICATIONS. Kinetic Theory. Principles of Statistical Mechanics. Partition Functions. Ideal Bosons and Fermions. CLASSICAL INTERACTING SYSTEMS: Linked Cluster Expansion. Distribution Functions. Brownian Motion. Lattice Statistics. Phenomena Near Critical Temperature. QUANTUM INTERACTING SYSTEMS: Propagator Methods for the Partition Functions. Propagator Methods for Distribution Functions. Transport Phenomena in Degenerate Systems. Irreversibility and Transport Coefficients. Second Quantization. Green's Functions. Subject Index.

1971, 453 pp., $18.50

SOLID ACIDS AND BASES

Their Catalytic Properties

by KOZO TANABE, Department of Chemistry, Faculty of Science, Hokkaido University, Sapporo, Japan

CONTENTS: SOLID ACIDS AND BASES: DETERMINATION OF ACIDIC PROPERTIES ON SOLID SURFACES: Acid Strength. Amount of Acid. Bronsted and Lewis Acid Sites. Relationship Between Acid Strength and Acid Amount. DETERMINATION OF BASIC PROPERTIES ON SOLID SURFACES: Basic Strength. Amount of Base. ACID AND BASE CENTRES: THEIR STRUCTURE AND ACID-BASE PROPERTIES: Metal Oxides and Sulfides. Mixed Metal Oxides. Natural Clays (Zeolites, etc). Metal Sulfates and Phosphates. Others. CORRELATION BETWEEN ACID-BASE PROPERTIES AND CATALYTIC ACTIVITY AND SELECTIVITY: Solid Acid Catalysis. Solid Base Catalysis. Solid Acid-Base Bifunctional Catalysis. CONCLUSION AND FUTURE PROBLEMS: Author Index-Subject Index-Catalyst Index.

1971, 175 pp., $11.50
This book is co-published with Kodansha, Tokyo

GROUP THEORY AND ITS APPLICATIONS

Volume 2

edited by ERNEST M. LOEBL, Polytechnic Institute of Brooklyn, Brooklyn, N.Y.

The current volume contains chapters on unitary groups, "accidental" degeneracy, dynamical groups in atomic and molecular physics, computer methods in group theory, and Galilei groups. Each chapter has been written by a specialist whose aim is to bring the newcomers to the field up to the frontiers of research, while introducing the expert to new research developments.

CONTENTS: W. J. HOLMAN, III, and L. C. BIEDENHARN: The Representations and tensor Operators of the Unitary Groups, **U(n)**. HAROLD V. McINTOSH: Symmetry and Degeneracy. CARL E. WULFMAN: Dynamical Groups in Atomic and Molecular Physics. STIG FLODMARK and ESKO BLOKKER: Symmetry Adaptation of Physical States by Means of Computers. JEAN-MARC LEVY-LEBLOND: Galilei Group and Galilean Invariance. Author Index-Subject Index.

September 1971, 328 pp., $18.50

CRYSTAL CHEMISTRY AND SEMICONDUCTION

In Transition Metal Binary Compounds

by JACQUES P. SUCHET, Institut fur Anorganische Chemie Stuttgart, Germany (on leave from Centre National de la Recherche Scientifique, Paris, France)

Provides the chemist and physicochemist with a detailed introduction of the problems of semiconduction in transition metals and rare earth compounds. The book provides the knowledge of crystal chemistry and crystal physics that is necessary for understanding past work on the mixed valency oxides and presents investigations of the conduction process in crystals containing "magnetic" atoms—i.e. transition metal or rare earth atoms. About half the book consists of a bibliographical digest that represents a thorough and specialized guide to the literature of the last twenty years. The book also includes useful theoretical bases on bonding and electrical conduction and discussions of actual problems and possible applications of magnetic semiconductor materials.

1971, 400 pp., $22.00

ACADEMIC PRESS NEW YORK AND LONDON
111 FIFTH AVENUE, NEW YORK, N.Y. 10003